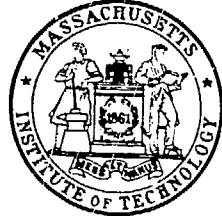


## DISCLAIMER

This report was prepared as an account of work sponsored by an agency of the United States Government. Neither the United States Government nor any agency thereof, nor any of their employees, makes any warranty, express or implied, or assumes any legal liability or responsibility for the accuracy, completeness, or usefulness of any information, apparatus, product, or process disclosed, or represents that its use would not infringe privately owned rights. Reference herein to any specific commercial product, process, or service by trade name, trademark, manufacturer, or otherwise does not necessarily constitute or imply its endorsement, recommendation, or favoring by the United States Government or any agency thereof. The views and opinions of authors expressed herein do not necessarily state or reflect those of the United States Government or any agency thereof.

BNL--51730

DE84 017247



# **PROCEEDINGS of the FIRST INTERNATIONAL SYMPOSIUM ON NEUTRON CAPTURE THERAPY**

**October 12-14, 1983**

**Ralph G. Fairchild and Gordon L. Brownell, Editors**

**Held at**  
**Massachusetts Institute of Technology**  
**Cambridge, Massachusetts, U.S.A.**

**Organized Jointly by**  
**Massachusetts Institute of Technology**  
**and**  
**Brookhaven National Laboratory**

**Sponsored by**  
**The United States Department of Energy**  
**and**  
**The National Science Foundation**  
**with additional support from**  
**Callery Chemical Company, Callery, Pennsylvania**  
**and**  
**Eagle-Picher Company, Miami, Oklahoma**

**NOTICE**

**PORTIONS OF THIS REPORT ARE ILLEGIBLE if**  
**has been reproduced from the best available**  
**copy to permit the broadest possible avail-**  
**ability.**

**MASTER**

**BROOKHAVEN NATIONAL LABORATORY**  
**UPTON, LONG ISLAND, NEW YORK 11973**



## **DISCLAIMER**

**This report was prepared as an account of work sponsored by an agency of the United States Government. Neither the United States Government nor any agency Thereof, nor any of their employees, makes any warranty, express or implied, or assumes any legal liability or responsibility for the accuracy, completeness, or usefulness of any information, apparatus, product, or process disclosed, or represents that its use would not infringe privately owned rights. Reference herein to any specific commercial product, process, or service by trade name, trademark, manufacturer, or otherwise does not necessarily constitute or imply its endorsement, recommendation, or favoring by the United States Government or any agency thereof. The views and opinions of authors expressed herein do not necessarily state or reflect those of the United States Government or any agency thereof.**

## **DISCLAIMER**

**Portions of this document may be illegible in electronic image products. Images are produced from the best available original document.**

## PREFACE

Renewed interest in Boron Neutron Capture Therapy is expressed by on-going clinical studies, by advances in physical and engineering knowledge, and by a rapidly increasing effort on the synthesis of boronated compounds.

This meeting was arranged jointly by MIT and BNL in order to illuminate progress in the synthesis and targeting of such compounds and to evaluate and document progress in radiobiological and dosimetric aspects of neutron capture therapy. It is hoped that this meeting will facilitate transfer of information between groups working in these fields, and encourage synergistic collaboration.

The meeting was sponsored by the United States Department of Energy and the National Science Foundation, with additional support from the Callery Chemical Company, Callery, Pennsylvania, and the Eagle-Picher Company, Miami, Oklahoma.

The proceedings were prepared for publication with the assistance of Ms. Margaret Dienes, technical editor, BNL.

### Cochairmen

G.L. Brownell and R.G. Fairchild

### Scientific Program Committee

R.G. Fairchild, Chairman, BNL  
D. Gabel, University of Bremen, FRG  
B. Larsson, University of Uppsala, Sweden  
H. Hatanaka, Teikyo University, Tokyo, Japan

### Local Organization Committee

G.L. Brownell, Chairman, MIT  
J. Kirsch, MIT  
R.G. Zamenhof, Tufts University  
C. Fitzgerald, MIT Office of Special Events

## CONTENTS

Preface. . . . .	iii
SESSIONS I and II. PHYSICS, DOSIMETRY, AND BORON ANALYSIS	
Chair: R.G. Zamenhof and K. Kanda	
1. Enhancement of Tumor Dose Via Beam Filtration and Dose Rate, and the Effects of These Parameters on Minimum Boron Content. . . . .	R.G. Fairchild and V.P. Bond 1
2. The Evaluation of Necessary Conditions for Neutron Capture Therapy Using Boronated Antibodies. . . . .	R.G. Zamenhof and G.R. Wellum 13
3. Filtered-Beam Dose Distributions for Boron Neutron Capture Therapy of Brain Tumors. . . . .	B.J. McGregor and B.J. Allen 14
4. Filtered Beams for Neutron Capture Therapy. . . . .	R.M. Brugger 26
5. Boron in Fast Neutron Therapy? Present Developments and Prospects. . . . .	B. Larsson 34
6. On the Possible Use of Spallation Sources in Neutron Capture Therapy; Proposed Measurements of Neutron Spectra at S.I.N. . . . .	J.F. Crawford and B. Larsson 35
7. Physics Studies on Neutron Field and Dosimetry for Neutron Capture Therapy in Japan. . . . .	K. Kanda, T. Kobayashi, O. Aizawa, H. Wakabayashi, and Y. Oka 44
8. Design Study of Facilities for Boron Neutron Capture Therapy. . . . .	Y. Oka and S. An 57
9. Mixed Dose Distributions of Fast Neutrons and Boron Neutron Captures for the Fast Neutron Beam from YAYOI. . . . .	H. Wakabayashi, K. Yosii, N. Sasuga, and H. Yanagi 67
10. A System for Simultaneous Monitoring of Thermal and Epithermal Neutron Flux During Boron Neutron Capture Therapy. . . . .	Y. Hayakawa, T. Inada, S. Harasawa, and H. Hatanaka 77
11. Preliminary Dosimetry Studies of the MIT Reactor (MITR-II) Medical Facility. . . . .	M. Ashtari, G. Brownell, and M. Forrest 88
12. In Vivo Measurement of Time Dependent Boron-10 Concentration in Tumor. . . . .	K. Kanda, T. Kobayashi, and K. Aoki 99
13. Boron-10 Analysis by Prompt-Gamma and Track-Etching Techniques. . . . .	R.G. Fairchild, D. Gabel, B.H. Laster, D.D. Greenberg, W. Kiszenick, and P.L. Micca 106
14. Remarks on the Optimization of Incident Neutron Energy for Neutron Capture Therapy. . . . .	K. Morstyn, B. Kawecka, and L.E. Feinendegen 114

SESSION III. RADIATION BIOLOGY  
Chair: B. Larsson

1. Boron-10 Dosage in Cell Nucleus for Neutron Capture Therapy--  
Boron Selective Dose Ratio. . . . . T. Kobayashi and K. Kanda 120
2. The Biological Effect of the  $^{10}\text{B}(\text{n},\alpha)^7\text{Li}$  Reaction and Its  
Simulation by Monte Carlo Calculations. . . . . D. Gabel,  
R.G. Fairchild, B. Larsson, K. Drescher, and W.R. Rowe 128
3. Effects of Deuterium Oxide and Cysteamine on the Acute Lethality  
of Head Irradiation. . . . K. Rosander, D.N. Slatkin, and R.D. Stoner 134

SESSION IV. TARGETING AND HISTOLOGICAL MICROANALYSIS OF BORON  
Chair: G.L. Brownell and Y. Mishima

SESSION V. SYNTHESIS AND BIOCHEMICAL PROPERTIES OF  
BORON-CONTAINING MOLECULES  
Chair: D. Gabel and A.H. Soloway

1. Chemical Overview of Boron Neutron Capture Therapy. . . . . A.H. Soloway, R.F. Barth, F. Alam, and W.E. Carey 207
2. Boron-10-Labeled Antibodies in Cancer Therapy. . . . . E. Mizusawa, A.J. Serino, M.F. Hawthorne, R.M. Sharkey, and D.M. Goldenberg 215
3. B-Decachloro-o-carborane Derivatives as Suitable Boron Carriers for the Preparation of Water-Soluble Boron-Conjugated Macromolecules. . . . . D. Gabel, R. Walczyna, F. Wellman, H. Riesenbergs, and I. Hocke 225
4. Boronation of Polyclonal and Monoclonal Antibodies for Neutron Capture. . . . . F. Alam, A.H. Soloway, R.F. Barth, C.W. Johnson, W.E. Carey, and W.H. Knoth 229
5. Coupling of Dextrans Conjugated with Boron to Gamma-Globulin: A Model for NCT. . J.J. Elmore Jr., D.C. Borg, P. Micca, and D. Gabel 237
6. Boron Analogs of  $\alpha$ -Amino Acids. . . . . B.F. Spielvogel, A.T. McPhail, I.H. Hall, R.G. Fairchild, and P.L. Micca 245
7. p-Borono-L-phenylalanine. . . . . J. Glass 255
8. Synthesis and Biological Activity of a Boron-Containing Pyrimidine Nucleoside. . . . . R.F. Schinazi, B.H. Lester, R.G. Fairchild, and W.H. Prusoff 260
9. The Distribution of Exogenous Porphyrins In Vivo; Implications for Neutron Capture Therapy. . R.G. Fairchild, D. Gabel, M. Hillman, and K. Watts 266
10. Boronated Anti-Estrogens for Boron Neutron Capture Therapy and Boron Neutron Capture Radiography. . . . . F. Wellmann and D. Gabel 276
11. Synthesis, Physical Properties, and Biological Activity of Estrogen Carboranes. . . . . H.E. Hadd 281
12. Recent Advances in the Synthesis of Boron-Containing Steroids and Porphyrins. . . . . S.B. Kahl 294

SESSION VI. PRECLINICAL BIOLOGICAL STUDIES  
Chair: L.E. Feinendegen

1. Pre-clinical Neutron Capture Therapy Trials at MIT Using  $\text{Na}_2\text{B}_{12}\text{H}_{11}\text{SH}$ . . . . . G.L. Brownell, J.E. Kirsch, J.C. Murphy, M. Ashtari, W.C. Schoene, C. Rumbaugh, and G.R. Wellum 304
2. Biological Studies of an Epithermal Beam for NCT with  $\text{Na}_2\text{B}_{12}\text{H}_{11}\text{SH}$ . . . . . D. Noonan and J.L. Russell Jr. 315
3. Testing Boron-Containing Estrogens on Human Breast Cancer Cells in a Neutron Beam. . . . . F. Sweet, M.-S. Kao, A. Williams, L. Khachatrian, B. Wessels, and J. Kirsch 323
4. Combined Action of Thermal Neutron Irradiation and Boron-10-Amino Acid Analogs on a Solid Experimental Tumor (E0771-C57 B1/6J). . . . . W. Porschen, J. Marx, H. Mühlensiepen, L. Feinendegen, F. Dallacker, H. Mückter, W. Müllners, and T. Böhmel 331
5. In Vitro and In Vivo Studies in Boron Neutron Capture Therapy of Malignant Melanoma. . . . . B.J. Allen 341
6. Cure of Malignant Melanoma by Single Thermal Neutron Capture Treatment Using Melanoma-Seeking Compounds:  $^{10}\text{B}/\text{Melanogenesis}$  Interaction to In Vitro/In Vivo Radiobiological Analysis to Preclinical Studies. . . . . Y. Mishima, M. Ichihashi, T. Nakanishi, M. Tsuji, M. Ueda, T. Nakagawa, and T. Suzuki 355
7. Neutron Capture Using Boronated Polyclonal and Monoclonal Antibodies. . . . . R.F. Barth, A.H. Soloway, F. Alam, W.E. Carey, C. Andrews, B. Holman, C.W. Johnson, J. Mohammed, J.W. Talnagi Jr., and Z. Steplewski 365

SESSION VII. CLINICAL  
Chair: W.H. Sweet

Enhancement of Tumor Dose via Neutron Beam Filtration and Dose Rate,  
and the Effects of These Parameters on Minimum Boron Content\*

R.G. Fairchild and V.P. Bond  
Brookhaven National Laboratory  
Upton, New York 11973

ABSTRACT

Calculations are made of the minimum boron content in tumor necessary for Neutron Capture Therapy. These estimations are made for various neutron beams, on the basis of therapeutic gain produced by effective dose (absorbed dose x relative biological effect). The effects of repair are evaluated, in anticipation of boronated biomolecules having selective and long-term binding to tumor cells, thus allowing protracted irradiations. Pure epithermal neutron beams (free of significant fast neutron and gamma contamination) are found to offer major advantages, particularly when the effects of repair are included. The various boron compounds being investigated for NCT are evaluated on the basis of necessary minimum boron content in tumor.

INTRODUCTION

Poor results in cancer therapy are due mainly to the limitation, by the presence of normal tissues within the radiation field, of the doses that can be delivered to tumor. The use of the  $^{10}\text{B}(\text{n},\alpha)^7\text{Li}$  reaction in radiotherapy produces radiations with a short range ( $\sim 1$  cell diameter) so that, in principle, it should be possible to keep the dose restricted to the tumor cells. In addition, the reaction products provide radiobiological advantages generally accorded to high-LET radiations. Initial clinical trials carried out between 1951 and 1961 failed. The poor results were attributed to two major problems: poor neutron penetration in tissue, and boron levels in blood higher than those in tumor. Viable tumor was found at depth following radiation doses that exceeded the tolerance of normal surface tissue (1).

The careful clinical studies carried out by Dr. H. Hatanaka have done much to stimulate interest again in NCT. Results with a thermal neutron beam and the "second-generation" compound  $\text{Na}_2\text{B}_{12}\text{H}_{11}\text{SH}$ , with a tumor-to-blood concentration ratio of about 1.5, show median survivals higher than those obtained with conventional techniques (2). Further improvements should result from the improved neutron penetration provided by epithermal reactor neutron beams which are now available (3). Also, recent studies have indicated that deuteration of tissues should significantly improve neutron densities at depth (4).

Major advances should be possible following the development of a boronated compound showing selective binding to tumor. Physiological targeting of boron to tumor cells would allow clearance of boron from normal tissues, if the boronated molecules have an assumed biological half-life (in

\*This work was supported by the U.S. Department of Energy under Contract DE-AC02-76CH0016.

tumor) of the order of days. The consequent improved  $^{10}\text{B}$  ratio (i.e., ratio of  $^{10}\text{B}$  concentration in tumor to that in normal tissue) should then provide conditions requisite for successful therapy. A number of biomolecules have been identified which may serve as vehicles for the transport of boron to tumors; these include chlorpromazine, thiouracil, porphyrins, amino acids, nucleosides, antibodies, steroids, and liposomes. A major activity emphasized at this meeting is the work being done on the synthesis and testing of boronated analogs of these compounds.

Success in this activity would lead to additional improvements in NCT. The long biological half-life of such molecules would relax requirements for intense neutron flux densities, thus allowing the use of alternative neutron sources such as heavily filtered beams with improved dosimetric characteristics. For example, scandium-filtered beams should be capable of delivering  $\sim 2$ -keV neutrons, which would have optimum penetration in tissue with a minimum of adventitious radiation.

Dosimetric aspects of NCT are well known. The major contributions of dose to normal (boron-free) tissues are due to gamma rays from the  $\text{H}(\text{n},\gamma)\text{D}$  reaction and protons from the  $^{14}\text{N}(\text{n},\text{p})^{14}\text{C}$  reaction. Further adventitious radiations are delivered by fast neutron and  $\gamma$  contaminations present in the incident beam. Experience has shown that contaminating  $\gamma$  rays can be effectively removed. Appropriately filtered beams may give good neutron penetration without significant fast neutron dose. Consequently, the remaining normal-tissue dose will be due mainly to low-LET  $\gamma$ 's from  $\text{H}(\text{n},\gamma)\text{D}$ , with a smaller component from the  $^{14}\text{N}(\text{n},\text{p})^{14}\text{C}$  reaction. In principle, it should be possible to reduce the former contribution by fractionating the doses to allow repair.

This paper describes the evaluation of therapeutic gain produced by various neutron beams, the effects of repair, and a determination of the minimum boron content necessary for NCT.

#### METHOD

In evaluating therapeutic efficacy, the determining factor is the ratio of tumor dose to maximum normal tissue dose, termed the "advantage factor" (AF) (5). Problems encountered in conventional radiotherapy stem mainly from the inability to obtain an AF greater than 1. Treatment volumes must be extended beyond bulk tumor in an effort to include unseen microscopic extensions of growth. The presence of normal tissues within the treatment volume then limits tumor dose to the normal-tissue tolerance dose. To the extent that misalignment of beam and tumor occurs during the usual course of  $\sim 30$  fractions over six weeks, the AF is less than 1.

It is generally considered that when tumor dose can be augmented by 10%, significant (observable) improvement in local control can be obtained. In the implementation and evaluation of a new therapeutic modality, it would perhaps be unwise to proceed unless a 20% increase in tumor dose could be expected, in order to ensure an observable response. Thus a criterion for embarking on the testing of a new modality would be that the  $\text{AF} \geq 1.2$ .

Advantage factors can be evaluated from absorbed dose distributions measured in anthropomorphic phantoms. The mixed-field components measured in a tissue-equivalent phantom head are given in Table 1 for an incident thermal and epithermal neutron beam which are representative of neutron sources in use

Table 1. Absorbed dose rate (rads/minute) in a tissue-equivalent anthropomorphic phantom\* (from Fairchild (6))

Depth in tissue, cm	Thermal neutron beam				Epithermal neutron beam			
	$\gamma$	N	H	$^{10}\text{B}$ (35 $\mu\text{g/g}$ )	$\gamma$	N	H	$^{10}\text{B}$ (35 $\mu\text{g/g}$ )
0	530	205	90	2925	50	3	183	42
1	530	150	70	2140	78	10	144	130
2	490	110	50	1500	88	13	111	193
3	415	75	40	1030	93	14	85	212
4	350	50	30	670	93	14	64	201
5	285	30	20	460	88	12	49	180
6	225	20	17	300	81	10	40	151
7	180	10	15	190	73	8	32	121
8	145	7	12	130	66	7	27	95
9	115	5	10	70	59	5	22	75
10	95	3	8	50	53	4	20	60

\*Medical Research Reactor, Brookhaven National Laboratory; reactor power 5 MW.  $\gamma$ , N, and H = dose from  $\text{H}(\text{n},\gamma)\text{D}$ ,  $^{14}\text{N}(\text{n},\text{p})^{14}\text{C}$ , and proton recoils.

or available for use in NCT today (6). Relative depth-flux distributions for such thermal and epithermal neutron beams are given in curves A and B respectively in Fig. 1 (normalized to 1 at 7 cm depth). The advantage of a distribution such as that produced by an epithermal beam (curve B) is that, during delivery of the required dose at depth, surface tissues are traversed by fewer thermal neutrons. As seen in Table 1, however, there is a significant fast neutron component in the epithermal beam. This beam is obtained by filtering out thermal neutrons from a  $1/\text{E}$  reactor spectrum with a Cd filter (3). Alternatively, it is possible to provide essentially monochromatic energy neutrons by using "pass-band" filters such as scandium, which transmits 2-keV neutrons with very small contaminations of  $\gamma$  rays and fast neutrons (7-9). The thermal neutron distribution for such a beam incident on a phantom head (8) is also shown in Fig. 1; the two distributions (from epithermal and 2-keV beams) are quite similar in shape, although the Sc-filtered beam is  $\sqrt{2}$  orders of magnitude lower in intensity ( $\text{~}10^8/\text{cm}^2\text{-sec}$ ) (9) because of the heavy filtration necessary to provide a relatively clean beam. In addition, curve B also represents the thermal neutron distribution in a phantom head reported for 37-eV and  $\sqrt{30}$ -keV beams (10,11). Thus, to a first approximation, it can be assumed that the thermal neutron distribution given by curve B in Fig. 1 represents that generated by any energy or mix of energies in the intermediate (epithermal) neutron energy region (between 0.5 eV and 10 keV).

The epithermal neutron energy region is of particular interest for NCT in that below  $\sqrt{10}$  keV it is thought that the proton recoils produced by scattered neutrons no longer have the energy required to produce ionizations

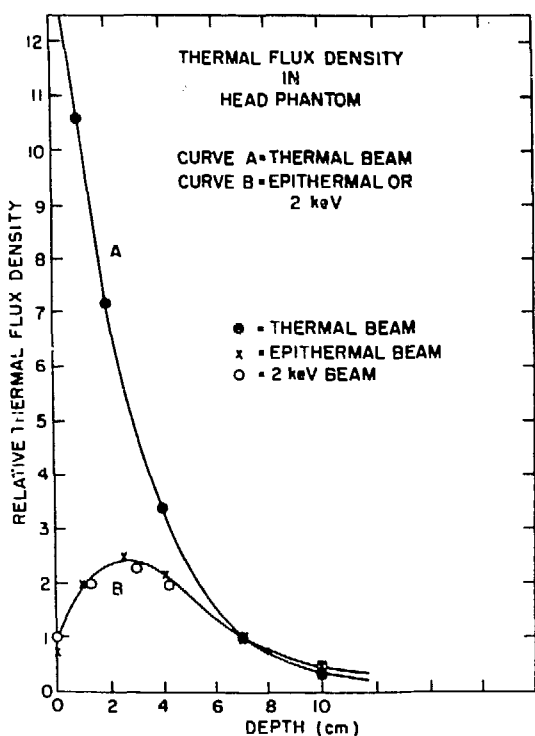


Fig. 1. Thermal neutron flux density generated in tissue-equivalent phantom head by a thermal and epithermal beam (3) and a 2-keV beam (8). Data normalized to 1 at 7 cm.

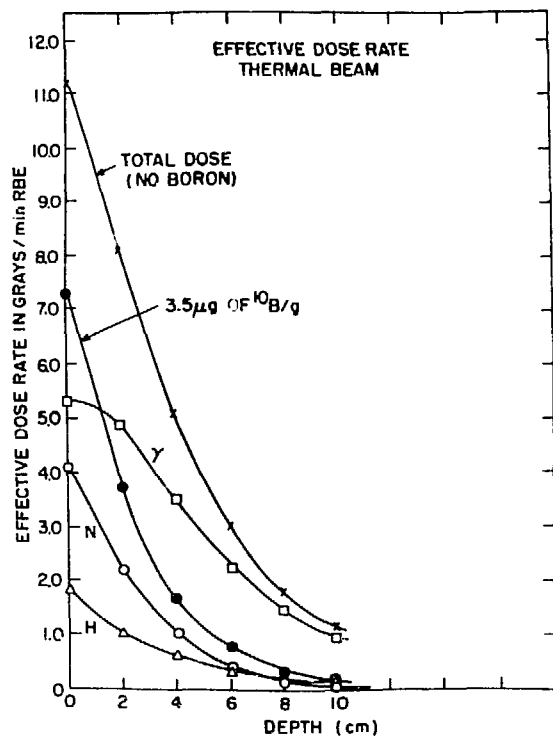


Fig. 2. Effective dose rate vs depth in an anthropomorphic phantom head for various components produced by an incident thermal beam. To obtain effective dose, absorbed dose values from Table 1 were multiplied by appropriate RBEs. RBE values were 2 for fast neutrons and the  $^{14}\text{N}(\text{n},\text{p})^{14}\text{C}$  reaction, and 2.5 for the  $^{10}\text{B}(\text{n},\alpha)^7\text{Li}$  reaction.

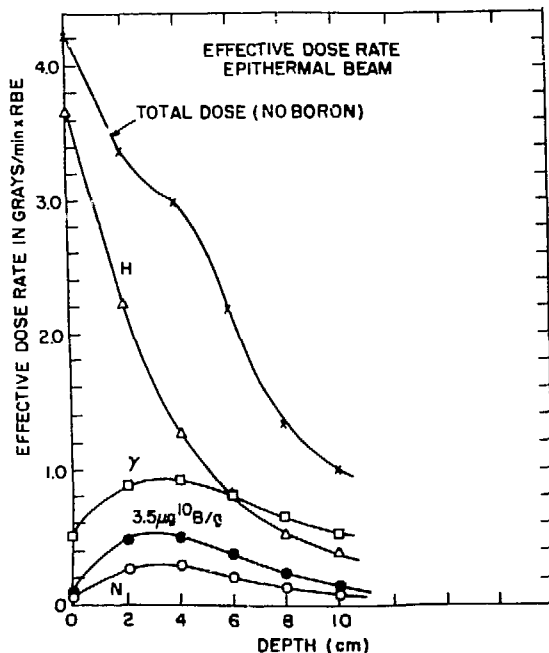


Fig. 3. Same as Fig. 2, but for an epithermal beam.

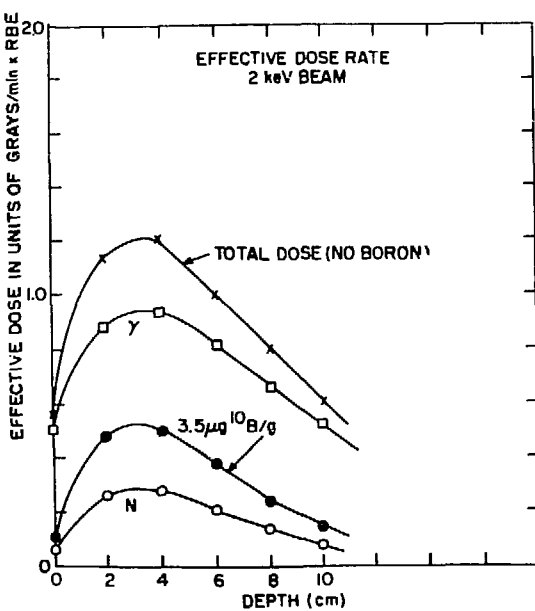


Fig. 4. Same as Fig. 2, but for a 2-keV beam (8).

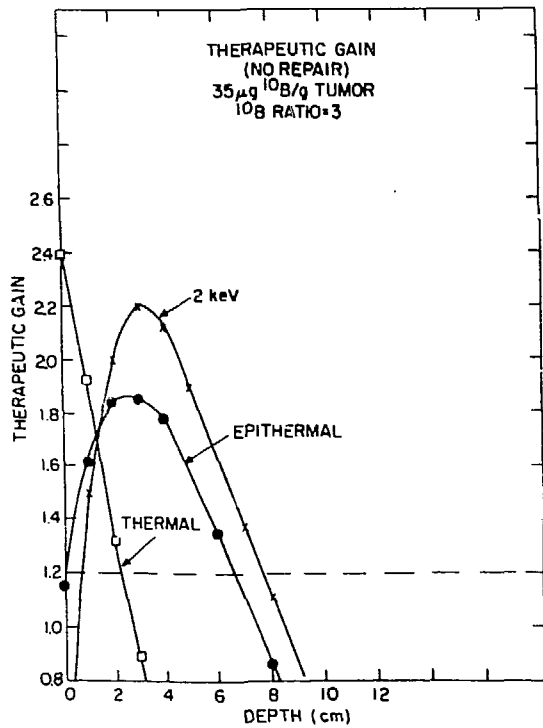


Fig. 5. Therapeutic gain (ratio of effective dose to tumor relative to the maximum effective dose to normal tissue) for thermal, epithermal, and 2-keV neutron beams as a function of depth in an anthropomorphic phantom head. Absolute  $^{10}\text{B}$  content in tumor was  $35 \mu\text{g}^{10}\text{B/g}$ , with a concentration ratio between tumor and normal tissue ( $^{10}\text{B}$  ratio) of 3.

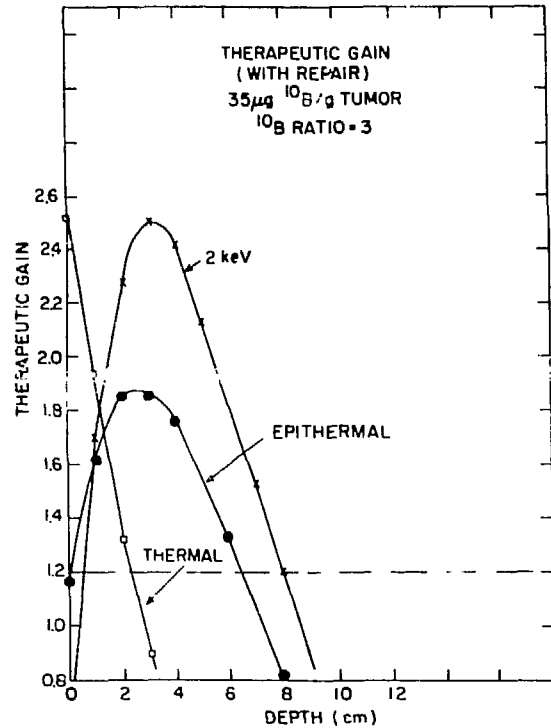


Fig. 6. Same as Fig. 5, but including repair.

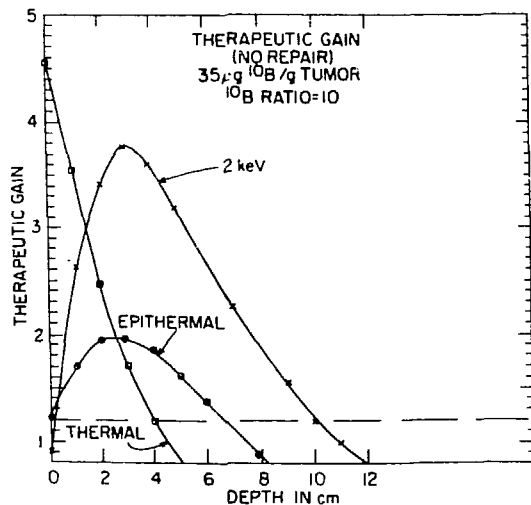


Fig. 7. Same as Fig. 5, but with a  $^{10}\text{B}$  ratio of 10.

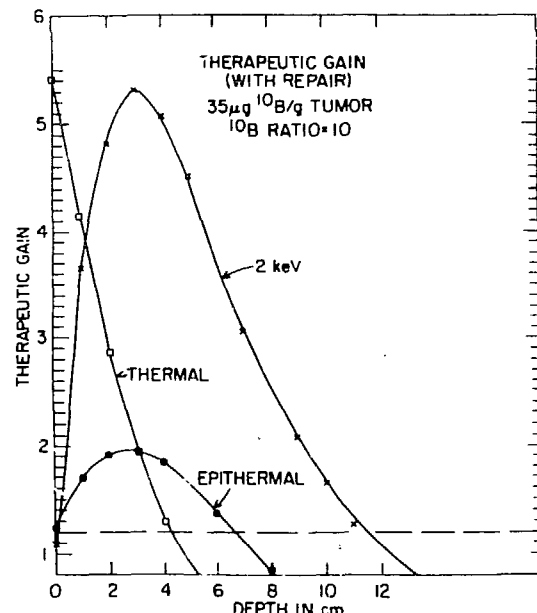


Fig. 8. Same as Fig. 6, but with a  $^{10}\text{B}$  ratio of 10.

(5,8). Energy will be dissipated mainly by heating, which is expected to produce little biological effect. Thus, say with 2-keV neutrons, there may be no contaminating radiation other than that from the  $^{14}\text{N}(\text{n},\text{p})^{14}\text{C}$  and  $\text{H}(\text{n},\gamma)\text{D}$  reactions unavoidably produced by thermal neutrons generated at depth.

Various radiobiological factors are thought to influence therapeutic outcome. These include the possible radio-resistance of hypoxic cells (oxygen gain factor) and the relative insensitivity of cells in  $G_0$  (the latent or non-proliferating pool) as well as the relative biological effect (RBE) as influenced by the linear energy transfer (LET). These factors are somewhat more nebulous than the parameter "absorbed dose" used to obtain the AF. The effects of RBE can, however, be incorporated in the evaluation, as they are fairly well known, and indeed must be accounted for in evaluating the biological effects of the  $^{10}\text{B}(\text{n},\alpha)^7\text{Li}$  reaction for clinical application. Recent measurements have indicated that the RBE for the  $^{10}\text{B}(\text{n},\alpha)^7\text{Li}$  and the  $^{14}\text{N}(\text{n},\text{p})^{14}\text{C}$  reaction are 2.3 and 1.9 respectively (12). Zamenhof has found a value of 2 for fast neutrons (10) encountered in NCT.

Rounding off gives a value of 2 for the RBE of fast neutrons and the  $^{14}\text{N}(\text{n},\text{p})^{14}\text{C}$  reaction, and a value of 2.5 for the  $^{10}\text{B}(\text{n},\alpha)^7\text{Li}$  reaction. These numbers will be used to obtain the biologically "effective dose" from absorbed dose; values of "effective dose" will then be used to evaluate possible therapeutic gain (TG). Given the criteria arrived at above, that the tumor dose should be 20% higher than maximum normal-tissue dose (i.e.,  $\underline{\text{TG}} \geq 1.2$ ) the minimum usable boron content can then be derived.

## RESULTS

The absorbed dose distributions for the various mixed-field components of a thermal beam given in Table 1 have been multiplied by the appropriate RBEs to get the "effective dose" distribution shown in Fig. 2. Similarly, an "effective dose" distribution for an incident epithermal neutron beam was obtained by using data in Table 1 (Fig. 3). The "effective dose" distribution for a scandium-filtered beam (Fig. 4) is idealized in that the thermalized neutron distribution generated in tissue was taken from Harvey and Mill (8) but the  $\gamma$  dose rate was obtained from measured values for the "epithermal" beam. This was done on the assumption that, since the thermal neutron depth-flux curve was similar, the  $\gamma$  dose would be also (in both cases there is negligible  $\gamma$  contamination in the incident beam (5, 9)). A major assumption is that the fast neutron dose is also negligible. This should follow from theoretical considerations, but remains to be verified. From the "effective dose" distributions in Figs. 2, 3, and 4 it is then possible to evaluate the therapeutic gain (TG), which is defined in the same way as the AF except that in this case the ratio of tumor dose to maximum normal-tissue dose is based on the parameter "absorbed dose x RBE."

The TG is a function of depth in tissue, absolute concentration of  $^{10}\text{B}$  in tumor, and  $^{10}\text{B}$  ratio (i.e., ratio of boron in tumor to that in normal tissue). For the sake of illustration, an absolute  $^{10}\text{B}$  concentration of 35  $\mu\text{g/g}$  was chosen in conjunction with a  $^{10}\text{B}$  ratio of 3, and the therapeutic gain was plotted as a function of the third parameter, depth, in Fig. 5, for a thermal, an epithermal, and a 2-keV beam. These parameters are similar to, but somewhat better than, those in use for NCT now in Japan (2,6).

If a protracted irradiation schedule similar to that in conventional therapy is used, it should be possible to increase normal tissue tolerance to low-LET radiation by a factor of 3. (It is assumed here that there is no significant repair for the other components.) This results from the repair of low-LET damage in conjunction with biofeedback producing regeneration of normal tissue, which is a well-known phenomenon. The TG has been plotted for each beam in Fig. 6 with the assumption of a fractionated regimen instead a single acute dose; thus the  $\gamma$  components given in Figs. 2, 3, and 4 have been reduced by 2/3. Protracted irradiation would be possible if the boronated compound's biological half-life were long enough, and indeed it might be necessary if alternative low intensity neutron sources (such as a Sc-filtered beam) were used. Thus Fig. 6 includes the effects of repair of low-LET damage. The effects of repair have little consequence with respect to TG for the thermal and epithermal neutron beams, but a significant improvement is seen for the 2-keV beam.

The parameters used in Figs. 5 and 6 are illustrative for boron compounds now in use for NCT. To illustrate the effect of the anticipated improvement in clearance of boron from normal tissues with use of boronated biomolecules that physiologically bind to tumor cells (6), curves analogous to those in Figs. 5 and 6 were constructed for a  $^{10}\text{B}$  ratio of 10: without repair (Fig. 7) and with repair (Fig. 8). From these data it is apparent that clearing boron from normal tissue is advantageous. Further major improvements are observed when the effects of repair are combined with the effects of using a 2-keV beam.

## DISCUSSION

### 2-keV Beam

The data provided in Figs. 2, 3, and 4 allow the derivation of therapeutic gain (TG) for any condition desired. The numerous variables involved ( $^{10}\text{B}$  ratio, concentration, depth in tissue, type of incident beam) make generalizations difficult. Nevertheless, it can be clearly seen from Figs. 5 to 8 that the deeper penetration of higher energy neutron beams is advantageous in that the TG maintains a usable value (i.e.  $\geq 1.2$ ) for significantly greater depths (6 to 11 cm vs  $\sqrt{2}$  to 4 cm for thermal beams). Furthermore, repair is seen to give significant advantages, particularly with relatively "pure" 2-keV beams which are not contaminated with over-riding high-LET contaminations. The major increase in TG demonstrated for the 2-keV beam in Fig. 8 ( $^{10}\text{B}$  ratio = 10; with repair) suggests that, upon the availability of boronated compounds with biological half-lives in tumor of the order of days, the development of such beams would be of prime importance.

### Minimum Boron Content

The selection of biomolecules to serve as vehicles for boron transport to tumor is complicated by the requirement for therapy of molar concentrations higher by a factor of  $\sqrt{10^4}$  to  $10^6$  than those needed for diagnostic techniques.

Thus the capacity of physiological pathways is likely to be exceeded before therapeutic levels are achieved. It then follows that in evaluating the potential of various molecules as influenced by binding-site densities, association constants, etc., a parameter of major importance is the minimum  $^{10}\text{B}$  concentration that will provide measurably improved tumor control. This parameter can be estimated, with reasonable assumptions. If it is assumed that (i) the TG must be  $\geq 1.2$ , and (ii) this value must obtain to a depth of 4 cm, then the minimum value for absolute  $^{10}\text{B}$  concentration can be derived. This is done by using the following equation to solve for the necessary dose from  $^{10}\text{B}$  at 4-cm depth:

$$D_N(4) + D_B(4) = 1.2 \{D_N(m) + D_B(m)/R\}$$

where

$D_N(x)$  = dose to boron-free tissue at depth  $x$ ,

$D_B(x)$  = dose to tissue from the minimum boron concentration at depth  $x$ ,

$R$  =  $^{10}\text{B}$  ratio,

$m$  = depth where maximum dose to normal tissues occurs, and

$D_B(m) = M D_B(4)$ , where  $M = D_B(m)/D_B(4)$  is obtained from Fig. 2, 3, or 4.

Data from the thermal beam, for example, with  $R = 10$ , give

$$5 + D_B(4) = 1.2 \{11.2 + (7.3/1.7) \cdot D_B(4)/10\} ,$$

$$D_B(4) = 17.5 .$$

The minimum boron content ( $\mu\text{g } ^{10}\text{B/g tumor}$ ) is then obtained:

$$17.5/1.7 \times 3.5 = 36 \mu\text{g/g} .$$

The minimum  $^{10}\text{B}$  concentration has been determined for  $^{10}\text{B}$  ratios of 3, 10, and  $\infty$ , for the various neutron beams described above (Table 2). With use of a rather optimistic  $^{10}\text{B}$  ratio of 10, the minimum  $^{10}\text{B}$  concentration is  $\sim 30 \mu\text{g } ^{10}\text{B/g tumor}$  for a thermal beam and  $\sim 15$  for an epithermal beam; if a beam analogous to a monochromatic 2-keV beam can be developed, the minimum value drops to  $\sim 2 \mu\text{g } ^{10}\text{B/g tumor}$ , and with repair, this can be halved.

The above values suggest minimum boron concentrations in tumor tissues requisite for improved cancer therapy; a uniform boron concentration (intra- and extracellular) has been assumed. Available evidence indicates that if the same boron concentrations are restricted to nuclear, cytoplasmic, or extracellular volumes, the necessary (local) boron concentrations will have to be higher by a factor of at least 2 to 4.

Table 2. Minimum  $^{10}\text{B}$  concentration

Beam	10 <sub>B</sub> Ratio					
	Without repair			With repair		
	3	10	$\infty$	3	10	$\infty$
Thermal	not possible	36	17	not possible	28	13
Epithermal	16	15	14	17	16	16
2-keV	2.8	1.9	1.7	1.4	0.94	0.83

#### Evaluation of Potential of Prospective Compounds

A number of biomolecules are under investigation as possible vehicles for boron transport. These compounds were chosen in part because there were indications that physiological pathways might be adequate, and because boronated analogs had, for one reason or another, been described in the literature (6). Boronated analogs of most of the seven classes of compounds discussed below have recently been synthesized and are currently being tested for efficacy in the NCT procedure, as reported in various papers in this Symposium. The potential of these compounds, based on necessary minimum boron content, is briefly reviewed.

Steroids. A number of reports describe boronated estrogens (13-15). In the review by Hechter and Schwartz (16), a total of  $4.5 \times 10^4$  estrogen receptor sites per cell was assumed (in MCF-7 cells, which had the highest receptor-site density of nine breast cancer cell lines evaluated). With the further assumption of a single carborane cage per steroid ligand, and a nuclear mass of 400 pg in which 80% of the receptor sites are concentrated, it then follows that the nuclear concentration of boron is 0.015  $\mu\text{g/g}$ . This projected boron content is too low to be useful. Hechter and Schwartz (16) suggest a number of ways to enhance this number, including the use of less specific binding sites.

Antibodies. Boronated antibodies are being synthesized by various groups (17-21). Current work indicates that up to  $10^3$  boron atoms per active antibody molecule should eventually be available, while studies of tumor-associated antibodies show antigen-site densities of  $\sqrt{10^6}$  sites per cell (22). Combining these parameters with a cell volume of  $1000 \mu^3$  (the approximate volume of a hamster V-79 cell) a boron concentration of 17  $\mu\text{g/g}$  is obtained (assuming uniform distribution throughout the cell). This boron concentration approaches the usable range with neutron beams now available, particularly if "cocktails" of various boronated monoclonal antibodies increase the available antigen-site densities. However, in view of the difficulties encountered in targeting therapeutic amounts of radio-labeled antibodies *in vivo*, it is unlikely that application of this technique will be simple.

Nucleosides. Schinazi et al. have synthesized a boronated analog of thymidine (DBDU) which shows evidence of biological activity (23). Mammalian cells are known to have  $\sim 6$  pg of DNA with  $5.5 \times 10^9$  base pairs, providing  $\sim 3.2 \times 10^9$  thymine bases available for substitution. Assuming a nuclear volume of  $100 \mu^3$  (100 pg), and 5% substitution of DBDU for thymidine (Tyd), the nuclear boron concentration would be  $27 \mu\text{g B/g}$  (6,24). Forty percent substitution of halogenated deoxyribonucleosides for Tyd has been obtained both in vitro and in vivo, while 5% replacement has been reported in human tumors (24). Thus, provided that DBDU proves to be an effective analog of Tyd, a therapeutic boron concentration should be possible.

Chlorpromazine (CPZ). Mishima and co-workers (25) have described the synthesis and testing of a boronated chlorpromazine (BCPZ). Other studies have shown that the total binding capacity of melanoma for CPZ (as well as other melanin-affinic agents) is  $\sim 0.8 \mu\text{mol per mg melanin}$ , and that it should be possible to deliver therapeutic amounts of BCPZ ( $\sim 30 \mu\text{g B/g}$ ), with multiple-dosing procedures (26).

Thiouracil (TU). The possibility of utilizing boronated thiouracil is being investigated by two groups (27,28). The total binding capacity of melanin for TU is  $\sim 7 \mu\text{mol TU per mg of synthesized melanin}$ . Studies with unboronated TU have shown that therapeutic amounts can be easily delivered with only  $\sim 10\%$  of the sites filled (28). (Assuming the boronated analog behaves the same way, the carrying capacity for 10% of the sites is  $\sim 30 \mu\text{g B/g}$ ). A major advantage of TU over CPZ is that it is taken up as a precursor to melanin synthesis, and thus shows no affinity to preformed melanin. While the boronation of uracil has been described by Schinazi (23), the successful synthesis of boronated TU has yet to be reported.

Amino Acids. Various boronated analogs of amino acids are being tested in Europe, Japan, and the United States (25, 29-31). Since proteins comprise  $\sim 15\%$  of tissue and have a rapid turnover, incorporation adequate for therapy would be expected; this has been verified with the unboronated amino acids glycine and phenylalanine (29). Studies by Mishima and co-workers with the compound p-borono-phenylalanine (BPA) have shown significant biological activity and incorporation in B-16 melanoma cells in vitro. In vivo studies have demonstrated uptakes of 10 to 30  $\mu\text{g B/g}$  of tumor, with tumor regression reported following neutron irradiation of both transplanted and spontaneous tumors (in hamster and swine, respectively) (25).

Porphyrins. The possibility of using boronated porphyrins has two distinct advantages. One is that, as opposed to the melanin-affinic molecules such as CPZ and TU (as well as perhaps BPA), porphyrins are apparently taken up equally well by all types of tumors. Second, uptake is robust, with a carrying capacity which is in principle  $\sim 10$  times that needed for therapy (32). Although the excess carrying capacity and general applicability make porphyrins unique among the various compounds being investigated, little effort has been directed toward synthesis of the many possible boronated analogs, and only two very preliminary reports are available (14, 32).

Most of the papers to be presented in this Symposium describe the synthesis and testing of new compounds for NCT. Some of these compounds have already demonstrated significant uptake and biological activity. It is to be hoped that at least one of these boronated molecules will be capable of providing the selective uptake in tumors which can then be used to demonstrate the

full potential inherent in the NCT procedure. Ultimately, it might be desirable to load tumors with boron via multiple physiological pathways; for example, the possibility exists that boronated analogs of antibodies, porphyrins, and nucleosides could be used to simultaneously target boron to various parts of tumor cells.

#### REFERENCES

1. W.H. Sweet. See paper VII-1 in this Symposium.
2. H. Hatanaka. See paper VII-3 in this Symposium.
3. R.G. Fairchild. *Phys. Med. Biol.* 10, 491-504, 1965.
4. W. Kiszenick, R.G. Fairchild, D.N. Slatkin, and G. Zubal. Increased neutron penetration in partially deuterated water: applications to neutron capture therapy. *Med. Phys.*, in press Jan.-Feb. 1984.
5. R.G. Fairchild and L.J. Goodman. *Phys. Med. Biol.* 11, 15-30, 1966.
6. R.G. Fairchild. Proc. Int. Symp. on Synthesis and Applications of Isotopically Labeled Compounds, Kansas City, June 1982, pp. 155-60. W.P. Duncan and A.B. Susan, Eds., Elsevier, Amsterdam, 1983.
7. R.C. Greenwood and R.E. Chrien. *Nucl. Instrum. Methods* 138, 125-43 (1976).
8. J.R. Harvey and A.J. Mill. 3rd Symp. on Neutron Dosimetry in Biology and Medicine, pp. 275-90. EUR 5848, 1978.
9. R.C. Block and R.M. Brugger. Filtered beams. Chap. 5 in *Neutron Physics and Nuclear Data in Science and Technology*, Vol. 2. Pergamon, Elmsford, NY, 1980.
10. R.G. Zamenhof, B.W. Murray, G.L. Brownell, G.R. Wellum, and E.I. Tolpin. *Med. Phys.* 2, 47-60, 1975.
11. D.J. Noonan, J.L. Russell, and R.M. Brugger. A filtered neutron beam approach to boron neutron capture therapy. Proc. 26th Annu. Mtg. Health Physics Soc., June 1981.
12. D. Gabel, R.G. Fairchild, H.G. Borner, and B. Larsson. The relative biological effectiveness in V79 Chinese hamster cells of the neutron capture reactions in boron and nitrogen. *Radiat. Res.*, in press, 1984.
13. H.E. Hadd and J.M. Kokosa. See paper V-11 in this Symposium.
14. S.B. Kahl. See paper V-12 in this Symposium.
15. F. Sweet et al. See paper VI-3 in this Symposium.
16. O. Hechter and I.L. Schwartz. See paper IV-8 in this Symposium.
17. E. Mizusawa et al. See paper V-2 in this Symposium.
18. D. Gabel et al. See paper V-3 in this Symposium.
19. F. Alam et al. See paper V-4 in this Symposium.
20. J.J. Elmore et al. See paper V-5 in this Symposium.
21. R.F. Barth et al. See paper VI-7 in this Symposium.
22. S. Ferrone et al. See paper IV-5 in this Symposium.
23. R. Schinazi et al. See paper V-8 in this Symposium.
24. R.G. Fairchild, A.B. Brill, and K.V. Ettinger. *Invest. Radiol.* 17, 407-16, 1982.
25. Y. Mishima et al. See paper VI-6 in this Symposium.
26. R.G. Fairchild, D. Greenberg, K.P. Watts, S. Packer, H.L. Atkins, P. Som, S.J. Hannon, A.B. Brill, I. Fand, and W. McNally. *Cancer Res.* 42, 556-62, 1982.

27. B.J. Allen. See paper VI-5 in this Symposium.
28. R.G. Fairchild, S. Packer, D. Greenberg, P. Som, A.B. Brill, I. Fand, and W.P. McNally. *Cancer Res.* 42, 5126-32, 1982.
29. B.F. Spielvogel et al. See paper V-6 in this Symposium.
30. J. Glass. See paper V-7 in this Symposium.
31. W. Porschen et al. See paper VI-4 in this Symposium.
32. R.G. Fairchild et al. See paper V-9 in this Symposium.

The Evaluation of Necessary Conditions for  
Neutron Capture Therapy Using Boronated  
Antibodies

Robert G. Zamenhof, Ph.D.

Medical Physics Division, Tufts-New England  
Medical Center, Boston, MA

Glyn R. Wellum, Ph.D.

New England Nuclear Corporation,  
Billerica, MA

**ABSTRACT\***

The application of "blood-brain-barrier" boronated compounds to neutron capture therapy, although demonstrating encouraging clinical results, does not permit large ( $>2-3$ ) macroscopic tumor-to-blood boron concentration ratios to be achieved. The concept of employing boronated antibodies, specifically targeted toward certain tumor types, to transport boron to the desired cellular sites is superficially attractive. To determine whether such an approach is practically realistic, we have carried out a modeling study to examine the interplay of various "physical" and "biochemical" variables, such as neutron flux-depth and dose-depth distributions, antibody-antigen association constant, antigen site density, number of boron atoms per antibody molecule, and the amount of boron present in the blood pool, in their impact on the "advantage depth" (a criterion for therapeutic efficacy). It is concluded that given the pharmacodynamic properties of potentially useful antibody preparations, significant improvements in therapeutic efficacy over the currently available "blood-brain-barrier" compounds are not likely to be readily achieved.

---

\*No complete manuscript submitted.

Filtered-Beam Dose Distributions for Boron  
Neutron Capture Therapy of Brain Tumours

B.J. McGregor

Nuclear Technology Division

and

B.J. Allen

Applied Physics Division

AAEC Research Establishment, Lucas Heights Research Laboratories  
Private Mail Bag, Sutherland 2232 NSW, Australia

ABSTRACT

The variation of RBE dose in brain tissue has been calculated as a function of depth for filtered reactor neutron beams from thermal to above 100 keV. Concentrations of  $^{10}\text{B}$  in the tumour greatly enhance the tumour dose relative to that for normal tissue. The optimum dose-depth distributions are obtained with a 6-keV neutron beam. In the brain tissue model for a tumour concentration of 40  $\mu\text{g } ^{10}\text{B/g}$ , the half-dose-depth is 7 cm, and the maximum useable depth is 10 cm for a tumour/tissue boron concentration of 10. For these conditions, an average tumour dose enhancement of  $\sqrt{3}$  is found.

1. INTRODUCTION

The principles of neutron capture therapy (NCT), although first enunciated in 1936 (1), have been slow in implementation. The first NCT trials utilised the  $^{10}\text{B}(\text{n},\alpha)^7\text{Li}$  reaction at the Massachusetts Institute of Technology reactor (2) (MITR), where boron doping of brain tumours was used with in vivo therapy by a thermal reactor beam. The large boron-10 capture cross section ensures a high production rate of  $\alpha$  and  $^7\text{Li}$  particles. The linear energy transfers of these particles are 150 and 175 keV  $\mu\text{m}^{-1}$ , and the ranges are 9 and 4.5  $\mu\text{m}$ , which is less than or of the order of one cell diameter.

The boron neutron capture therapy (BNCT) trials were not encouraging because of problems associated with the low boron tumour/blood ratio (less than unity), the poor penetration of thermal neutrons, and the high  $\gamma$  dose to the patient. The method lay dormant until 1973 when Hatanaka and Sano (3) reported an improved protocol. In subsequent years, some promising remissions from brain tumours have been obtained (4), although the method is less than satisfactory because of the limited penetration of the thermal neutron beam in tissue, i.e. half-dose-depth (HDD)  $\sqrt{2}$  cm. However, the thermal beam should be particularly suited to BNCT of advanced, primary melanoma (5).

An important requirement for BNCT is to devise a neutron beam with enhanced penetration so that higher doses can be given to the tumour with greater sparing of the skin and healthy tissue.

To this end, Frigerio (6) used cadmium to filter thermal neutrons ( $<0.5$  eV) from a well thermalised beam at the Argonne Research Reactor, and found a greatly improved penetration of the "epithermal" beam. Fairchild (7) measured cranial isodose distributions in a tissue-equivalent phantom for an epithermal

beam from the Brookhaven Medical Research Reactor. This beam contained a significant contamination of fast ( $>10$ -keV) neutrons.

A one-dimensional, discrete ordinate transport code (ANISN) was used by Zamenhof et al. (8) to calculate the dose-depth distribution in a brain model. In this study, the relative biological effectiveness (RBE) for photons, protons, and the  $^{10}\text{B}(\text{n},\alpha)^7\text{Li}$  reaction was taken to be  $\text{RBE}(\gamma) = 1.0$ ,  $\text{RBE}(\text{p}) = 2.0$  and  $\text{RBE}(\alpha,^7\text{Li}) = 3.7$ , the last value being taken from the experiments of Davis et al. (9).

It was noted that the neutron kerma ( $\text{cJ kg}^{-1}$ ) per unit neutron fluence has a minimum value in the 30 to 50-eV range. Kerma is the kinetic energy released in matter and is the sum of the kinetic energies ( $\Delta E$ ) of all charged particles produced by  $\text{n}$  and  $\gamma$  interactions in a mass ( $\Delta M$ ) of tissue. It is in this region that the energy transfer changes from primarily neutron capture in nitrogen ( $^{14}\text{N}(\text{n},\text{p})^{14}\text{C}$ ) below 10 eV to mainly proton recoils from neutron collisions with hydrogen nuclei ( $^1\text{H}(\text{n},\text{n})^1\text{H}$ ) above 200 eV. For this reason, Zamenhof et al. (8) calculated dose-depth distributions for thermal and 37-eV beams, the MITR therapy beam, and a  $^{252}\text{Cf}$  source. The last two cases included  $\text{D}_2\text{O}$  and  $^{10}\text{B}$  filtered beams, i.e. tailored beams.

Absorbed dose components were obtained for  $^1\text{H}(\text{n},\text{n})$ ,  $^{14}\text{N}(\text{n},\text{p})$ ,  $\text{H}(\text{n},\gamma)$  (i.e. included  $\gamma$ ), and 0 to 160  $\mu\text{g}$   $^{10}\text{B}/\text{g}$  tissue. The half RBE-dose-depth values (HDD) for 40  $\mu\text{g}$   $^{10}\text{B}/\text{g}$  tissue are given in Table 1.

Table 1. RBE Dose-depth Parameters (Zamenhof et al. (8))

	HDD (cm) ANISN	MUD (cm) ANISN	MUD (cm) Monte Carlo
Thermal	2.0	4.3	-
37-eV	4.2	8.2	-
MITR beam	2.2	4.3	3.5
$^{252}\text{Cf}$ tailored	5.3	6.3	4.2

The maximum useable depth (MUD) is that depth of tissue for which the total tumour dose equals the maximum normal tissue dose, wherever the latter occurs (i.e. the MUD is that depth where the tumour and maximum tissue doses are equal, or where the advantage factor  $\text{AF} = 1.0$ ). The MUD can then be used to compare beams for different tumour/blood  $^{10}\text{B}$  ratios, and for different absolute  $^{10}\text{B}$  concentrations in the tumour. Typical results for 40  $\mu\text{g}$   $^{10}\text{B}/\text{g}$  and tumour/blood ratio = 10 are given in Table 1. These results indicate the advantage of the 37-eV neutron beam for BNCT.

A multidimensional dosimetry calculation (10) using a Monte Carlo code gives somewhat lower values for MUD than ANISN for the MITR and tailored  $^{252}\text{Cf}$  beams (Table 1), and points to the need for a full dimensional calculation to obtain accurate dose-depth results.

The concept of a filtered beam was further extended by Mill and Harvey (11) to the 2-keV beam which could be obtained from a scandium filter (12). For the 2-keV beam, the peak fluence depth is 2.8 cm, and the half-flux depth

$HFD = 6.3$  cm. Taking a nominal flux of  $5 \times 10^{12}$  n cm $^{-2}$  s $^{-1}$  per unit lethargy for a typical high flux reactor, and compounding with transmission and geometric factors, Mill and Harvey (11) calculated a flux of  $\sqrt{7.4} \times 10^7$  n cm $^{-2}$  s $^{-1}$  for a scandium filter. For this flux and 30  $\mu\text{g}$   $^{10}\text{B}/\text{g}$  tissue, a mid-brain tumour dose of 70 cGy h $^{-1}$  would result. This is equivalent to 260 cGy h $^{-1}$  for photons, and could be acceptable for fractionated dose therapy.

Fairchild and Bond (13) compared experimental thermal, epithermal, and 2-keV relative thermal flux distributions as a function of depth. Half-flux depths (HFD) are given in Table 2. The peak flux of the BNL 2-keV beam (13) is  $9 \times 10^5$  n cm $^{-2}$  s $^{-1}$  at 2 cm tissue depth, two orders of magnitude down on the Mill and Harvey flux calculation. For the scandium-filtered 2-keV beam with 35  $\mu\text{g}$   $^{10}\text{B}/\text{g}$ , the HDD = 4.2 (absorbed dose), which is comparable to the 37-eV beam calculation of Zamenhof et al. (8).

Table 2. Half-flux and Dose Depths, from Fairchild and Bond (13)  
(Note that the epithermal beam contains a significant contamination  
of fast neutrons)

	HFD (cm)	HDD (cm)
Thermal	2	-
2-keV	4.2	4.2
Epithermal	6.2	-

The foregoing results point to the enhanced performance of the 37-eV, 2-keV, epithermal, and tailored  $^{252}\text{Cf}$  beams over that of the thermal beam. Whereas there is no practical beam filter at  $\sqrt{37}$  eV,  $^{238}\text{U}$ , Sc,  $^{56}\text{Fe}$ , and  $^{28}\text{Si}$  filters have been used at 186 eV and 2, 24, and 144 keV in neutron physics experiments. There is also the possibility of a copper filter at 7.5 keV. However, higher neutron energy beams, although achieving greater penetration, cause increasing RBE doses to healthy tissue. It is therefore timely to investigate the relative performance of these filters to determine the RBE dose-depth distribution so as to find the optimum beam for BNCT. In this paper, one-dimensional ANISN calculations are made for the complete set of filtered beams. Dose-depth distributions are obtained in each case  $^1\text{H}(n,\gamma)$ ,  $^{14}\text{N}(n,p)$  and  $^1\text{H}(n,n)^1\text{H}$ , and  $^{10}\text{B}(n,\alpha)^7\text{Li}$  energy transfer mechanisms.

Data are presented in graphs and tables, and advantage factors and maximum useable depths are found for a range of  $^{10}\text{B}$  tumour concentrations and tumour-to-tissue  $^{10}\text{B}$  ratios. Calculations are made for the brain tumour model.

## 2. ANISN CALCULATIONS

The one-dimensional discrete-ordinates transport code ANISN (14) was used for the calculation of comparative dose-depth distributions in the human brain. For these calculations, the scalp and skull are assumed to have been

removed. The code treats the effects of the transverse neutron and  $\gamma$ -ray leakage with an approximate buckling correction. However, the code is expected to be adequate for comparative dose calculations, as distinct from accurate dose distributions in the cranium. For this purpose, Monte Carlo calculations are required, and these will be reported separately. The ANISN code uses 42 group neutron and  $\gamma$ -ray coupled cross section data derived from ENDFB-IV. The group structure is virtually the same as that used by Zamenhof et al. (8) and is given in Table 8. It accounts for anisotropic scattering by a third-order Legendre polynomial expansion of the differential scattering cross section using the extended transport method.

The neutron and  $\gamma$ -ray spectra in successive layers of brain tissue are needed to determine the absorbed dose and biological dose equivalent in each volume element. The ANISN code accomplishes this by solving the one-dimensional, multigroup, time-independent Boltzmann transport equation, using the  $S_N$  variant of the discrete ordinates method.

The neutron and  $\gamma$ -ray fluences are converted to dose using the kerma factors for normal tissue tabulated by Zamenhof et al. (8) but modified for the brain composition given by Schaeffer (15) and listed in Table 3. A significant difference between brain and normal skin tissue composition is the important nitrogen proportion in the brain which is 1.9% rather than 3.5%. Table 8 shows the effect of the different compositions on kerma factors.

---

Table 3. ANISN Calculational Parameters

---

Cross section area  $13.9 \times 13.9 \text{ cm}^2$

	Element	Weight %
Brain composition	O	72.6
	C	15.1
	H	10.15
	N	1.9
	Cl	0.10
	Na	0.15

Density  $1.00 \text{ g cm}^{-3}$

Spatial resolution  $0.5 \text{ cm}$

Incident integrated neutron current  $10^{10} \text{ n cm}^{-2}$

---

Secondary charged particle equilibrium is required for the equivalence of kerma and absorbed dose. Heavy charged particles have ranges of  $<5 \text{ mm}$  for neutron energies below 16 MeV, and secondary electron ranges are generally  $<10 \text{ mm}$ . The equilibrium requirement can be relaxed if, as for  $\gamma$  rays, the second derivative of the kerma-depth distribution in tissue is not large (8).

### 3. RELATIVE BIOLOGICAL EFFECTIVENESS

A comparison of RBE dose for different neutron beams requires a knowledge of the relative biological effectiveness of the different energy transfer mechanisms. The quality factor (QF) is designed for chronic or low dose conditions as encountered in radiation protection, and is not suitable for use with the acute or high doses administered in therapy. The RBE is found from specific mammalian experiments with low survival end points. Whereas the RBE for hydrogen capture  $\gamma$  rays (2.2 MeV) can be taken to be 1, there is considerable uncertainty about the  $^{14}\text{N}(\text{n},\text{p})$  and the hydrogen elastic neutron scattering component, as well as the reaction products of the  $^{10}\text{B}(\text{n},\alpha)^7\text{Li}$  reaction.

#### RBE (protons)

At proton energies between 30 and 100 keV, the linear energy transfer to the medium ( $\text{LET}_\infty$ ) is at its maximum value of  $\sim 90 \text{ keV } \mu\text{m}^{-1}$ . Consequently, the RBE is also at its maximum value. For the  $^{14}\text{N}(\text{n},\text{p})$  reaction, the proton energy is 0.63 MeV, whereas for the neutron elastic collisions on hydrogen, the proton recoil energy is less than or comparable to the neutron energy.

The neutron RBE is determined from in vitro experiments and dose calculations, and varies markedly in the keV energy region depending on the biological end point used. Consensus indicates a broad maximum at RBE  $\sim 3$  at a 10% fraction for 100 to 600 keV, corresponding roughly to the broad peak in the effective  $\text{LET}_\infty$  calculation of Kellerer and Rossi (16). The few data available below 100 keV show an inverse relationship with energy (17).

In that our calculations are mostly for neutrons below 30 keV, we assume an RBE  $\sim 2$ , which is consistent with the thermal value. However, at higher energies, a larger value should be used. It is worth remarking on the paucity of data in this critical region.

#### RBE ( $\alpha, ^7\text{Li}$ )

Biological experiments for a variety of media and for survival, mutation, and chromosome aberration end points show a wide range of RBE values. For mammalian cells, values range from 1.05 (spleen-thymus weight) to 23 (chromosome aberrations in blood). The value consistently used in BNCT calculations is RBE = 3.7, reported by Davis et al. (9) on HeLa cells with 2 to 20  $\mu\text{g } ^{10}\text{B/g}$  concentrations.

An important factor in the  $^{10}\text{B}$  dose calculation is the boron selective dose ratio (BSDR), defined by Kobayashi and Kanda (18), which relates to the effectiveness of boron concentrations within the tumour cell. This would affect experimental RBE values, but at this stage the effect is unknown.

For the purposes of this paper, we have adopted the Davis et al. value of RBE = 3.7. Should this value be changed in the future, the tables for boron dose can be readily modified by the factor RBE/3.7.

The emission of a 478-keV  $\gamma$  ray from the  $^{10}\text{B}(\text{n},\alpha)^7\text{Li}$  reaction occurs in most (93.9%) boron-10 capture reactions. However, because the dose contribution of the  $\gamma$  ray is  $< 0.2\%$  of the total  $^{10}\text{B}$  dose to a volume element (8), it is ignored.

#### 4. RESULTS

The dose-depth distributions for standard tissue reported by Zamenhof et al. (8) for an incident flux of  $10^{10}$  neutron  $\text{cm}^{-2} \text{ s}^{-1}$  for thermal, 37-eV, and reactor beams were recalculated and, with the exception of the thermal and reactor beam results, good agreement was found. In these cases a value of half the incident neutron current of  $10^{10}$  neutron  $\text{cm}^{-2} \text{ s}^{-1}$  was needed to obtain the same dose distribution, suggesting different normalisations.

Dose distribution data are calculated for the thermal,  $\langle 37\text{-eV} \rangle$ ,  $\langle 186\text{-eV} \rangle$ ,  $\langle 2\text{-keV} \rangle$ ,  $\langle 24\text{-keV} \rangle$  and  $\langle 144\text{-keV} \rangle$  neutron energies, the brackets indicating average energies corresponding to possible reactor filters, with the exception of  $\langle 37\text{-eV} \rangle$ . This energy was chosen by Zamenhof et al. (8) because it lies at the broad minimum in the absorbed dose curve. Actual energy ranges for each neutron window are given in Table 4 together with the relevant filter parameters.

Table 4. Filtered-beam Parameters

Average energy (keV)	Energy range (keV)	Filter	Filter energy (keV)
Thermal	$\langle 0.15 \text{ eV} \rangle$	-	-
0.037	0.023-0.061	-	-
0.186	0.061-0.45	$^{238}\text{U}$	0.186
2.0	1.23-3.35	Sc	2.0
5.5	3.35-9.12	Cu	7.5
		Fe	14
24	9.12-67	Sb-Fe*	24
144	67-302	Si	144

\*Radioactive photo-neutron source.

The RBE dose-depth data for an incident current of  $10^{10}$  neutron  $\text{cm}^{-2} \text{ s}^{-1}$  are given in Table 5 for the sum of  $\text{H}(\text{n},\gamma)$ ,  $\text{H}(\text{n},\text{n})\text{H}$  and  $^{14}\text{N}(\text{n},\text{p})$ , and the  $^{10}\text{B}(\text{n},\alpha)^7\text{Li}$  components, the last being for a concentration of 1  $\mu\text{g}^{10}\text{B/g}$  tissue. From these data it is possible to calculate the RBE dose for any absolute concentration of  $^{10}\text{B}$  in the tumour, and for any tumour/brain tissue  $^{10}\text{B}$  concentration ratio. The RBE dose-depth distributions for 1  $\mu\text{g}^{10}\text{B/g}$  tissue and induced  $\gamma$  plus  $\text{p}$  dose are plotted in Figure 1, and the total dose-depth distribution for 40  $\mu\text{g}^{10}\text{B/g}$  tissue is shown in Figure 2.

It can be readily observed that beams in the eV to low keV energy region are the most suitable for BNCT of the brain. These beams give good dose-depth penetration and skin sparing, the  $\langle 6\text{-keV} \rangle$  beam offering the optimum skin sparing condition. This is not the case for the thermal beam, where the maximum dose is in the skin, nor for the 144-keV beam, where hydrogen recoil effects dominate the energy transfer within the first centimetre of tissue.

Table 5. Neutron-induced RBE Dose-Depth Distributions in Brain Tissue (cJ kg<sup>-1</sup>)  
 for 1  $\mu$ g  $^{10}\text{B}$ /g Tissue  
 (For incident integrated neutron current of  $10^{10}$  neutrons cm<sup>-2</sup>)

Depth (cm)	RBE											
	1.0 $\gamma$	2.0 P	3.7 $\alpha, ^7\text{Li}$	1.0 $\gamma$	2.0 P	3.7 $\alpha, ^7\text{Li}$	1.0 $\gamma$	2.0 P	3.7 $\alpha, ^7\text{Li}$	1.0 $\gamma_{\text{inc}}$	2.0 P	3.7 $\alpha, ^7\text{Li}$
<thermal>												
0.001-0.5	1.44	.98	.80	1.41	.36	.30	1.28	.33	.24	1.31		
0.5-1.0	1.63	1.01	.83	1.69	.61	.51	1.53	.54	.42	1.26		
1.5-2.0	1.55	.65	.53	2.05	.84	.70	1.87	.75	.61	1.15		
2.5-3.0	1.33	.42	.34	2.15	.83	.69	2.00	.77	.63	1.05		
3.5-4.0	1.11	.26	.22	2.05	.70	.58	1.95	.68	.55	0.96		
4.5-5.0	.91	.17	.137	1.84	.53	.44	1.78	.54	.44	0.88		
5.5-6.0	.74	.107	.087	1.59	.38	.32	1.56	.40	.33	0.80		
6.5-7.0	.60	.067	.055	1.34	.27	.22	1.33	.28	.23	0.73		
7.5-8.0	.49	.043	.035	1.11	.18	.15	1.12	.20	.16	0.67		
8.5-9.0	.41	.027	.022	.92	.12	.095	0.93	.131	.107	0.61		
9.5-10.0	.33	.017	.014	.75	.076	.062	0.76	.086	.070	0.56		
11.5-12.0	.23	.0065	.0053	.51	.031	.025	0.52	.036	.029	0.46		
14.5-15.0	.137	.0015	.0013	.30	.0076	.0062	0.30	.0090	.0074	0.35		
<2-keV>												
0.001-0.5	1.10	.64	.18	1.03	1.29	.17	.95	5.4	.14	.83	18.1	.110
0.5-1.0	1.30	.72	.33	1.23	1.22	.30	1.12	4.6	.25	1.11	16.2	.20
1.5-2.0	1.62	.75	.50	1.53	.96	.46	1.41	2.8	.40	1.34	11.1	.32
2.5-3.0	1.77	.72	.54	1.69	.79	.51	1.57	1.66	.46	1.47	7.1	.39
3.5-4.0	1.78	.64	.51	1.71	.66	.49	1.62	1.05	.46	1.50	4.4	.41
4.5-5.0	1.67	.53	.43	1.62	.54	.42	1.57	.71	.41	1.47	2.7	.39
5.5-6.0	1.50	.41	.33	1.47	.42	.33	1.45	.51	.34	1.37	1.65	.34
6.5-7.0	1.30	.30	.25	1.29	.31	.25	1.29	.36	.27	1.24	1.03	.29
7.5-8.0	1.10	.22	.18	1.10	.23	.18	1.12	.26	.20	1.10	.65	.23
8.5-9.0	.93	.15	.12	.93	.16	.13	.95	.18	.14	1.02	.42	.18
9.5-10.	.77	.10	.082	.77	.11	.087	.80	.13	.10	.88	.27	.133
11.5-12.0	.53	.043	.035	.53	.047	.039	.55	.057	.047	.63	.115	.069
14.5-15.0	.30	.011	.0093	.30	.013	.010	.32	.016	.013	.37	.032	.022

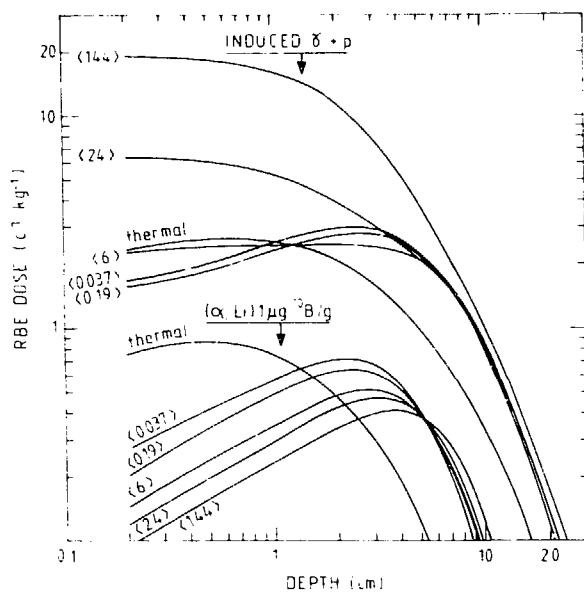


Fig. 1. RBE dose in  $\text{cJ kg}^{-1}$  (cSv) as a function of depth in brain tissue for (a)  $1 \mu\text{g} \text{ }^{10}\text{B/g}$  tissue, (b) induced  $\gamma$  and p components. Data are shown for thermal,  $<0.037>$ ,  $<0.19>$ ,  $<6>$ ,  $<24>$ , and  $<144>$  keV average neutron energies for an incident integrated current of  $10^{10} \text{ n cm}^{-2}$ .

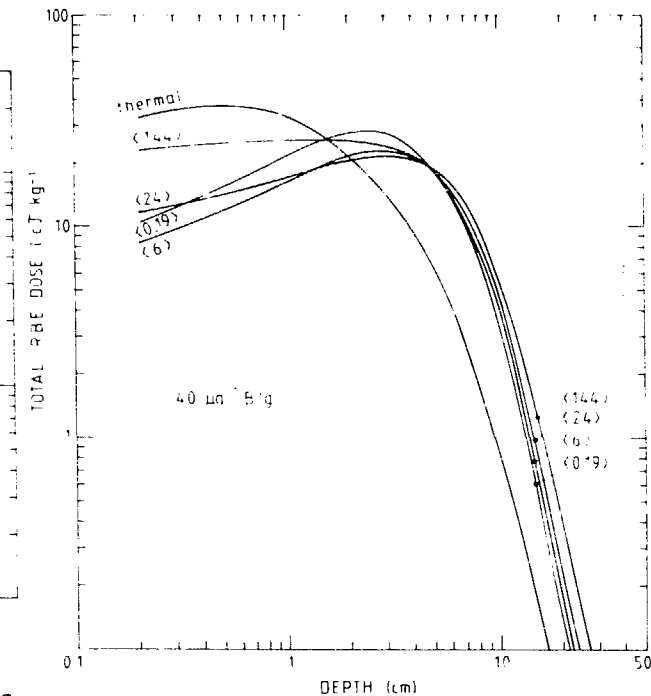


Fig. 2. Total RBE dose in  $\text{cJ kg}^{-1}$  (cSv) for  $40 \mu\text{g} \text{ }^{10}\text{B/g}$  and various average neutron energies as a function of brain depth. The  $<6>$  keV beam gives the best skin sparing. Incident integrated current is  $10^{10} \text{ n cm}^{-2}$ .

The advantage factor (AF) is the ratio of the tumour dose to the maximum tissue dose for a given beam filter, absolute  $^{10}\text{B}$  concentration, and relative tumour/tissue concentration. Advantage factors have been calculated for a likely therapy condition of  $40 \mu\text{g} \text{ }^{10}\text{B/g}$  and a tumour/tissue ratio of 10. These data are plotted for each filter in Figure 3.

Because of the blood-brain barrier (19), the normal brain tissue uptake of the boron compound is small, and Hatanaka (20) reports  $^{10}\text{B}$  concentrations in brain tissue of  $<1 \mu\text{g} \text{ }^{10}\text{B/g}$ . The main boron contamination, therefore, arises from the blood, but this comprises only 5% of the total brain mass (21). Thus, for a tumour/blood ratio of only 5, the average tumour/tissue  $^{10}\text{B}$  concentration is 100. However, local damage to capillaries may set the dose limit, rather than damage to normal brain cells, so we have assumed a tumour/tissue  $^{10}\text{B}$  ratio of 10 as being a likely condition.

The best advantage factors at 2 to 10 cm are achieved with the  $<0.19>$ ,  $<2>$ ,  $<6>$ , and  $<24>$  keV beam. If these beams could be realised, an advantage factor of 4 to 5 for 1 to 5-cm depth could be achieved for  $40 \mu\text{g} \text{ }^{10}\text{B/g}$  tumour with a tumour/tissue ratio of 10.

In cancer therapy, this advantage factor would be outstanding. Further, an advantage factor of  $>1$  would prevail to a depth of 10 cm, i.e. MUD = 10 cm.

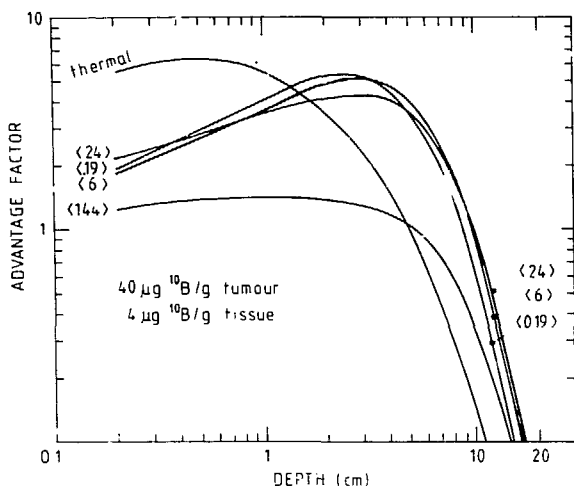


Fig. 3. Depth dependence of advantage factors for  $^{10}\text{B}$  concentrations of  $40 \mu\text{g/g}$  tumour and  $4 \mu\text{g/g}$  tissue. The  $\langle 0.19 \rangle$ ,  $\langle 6 \rangle$ , and  $\langle 24 \rangle$  keV beams show a factor of four enhancement over the thermal beam at 5 cm depth.

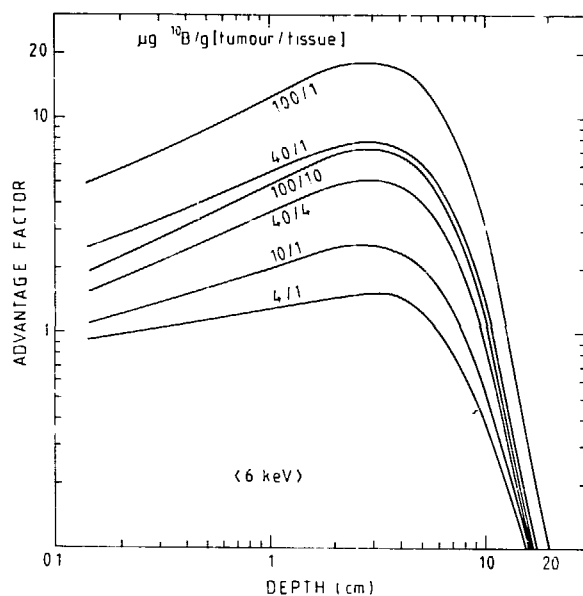


Fig. 4. Variation of advantage factors with absolute and relative  $^{10}\text{B}$  concentrations for the  $\langle 6 \rangle$  keV beam.

Advantage factors for various tumour/tissue concentrations are given in Table 6 and shown in Figure 4 for the  $\langle 6\text{-keV} \rangle$  beam. Above  $40 \mu\text{g}$  tumour/ $4 \mu\text{g}$  tissue, little gain is found in MUD. However, increases in absolute and relative concentrations will give very useful increases in advantage factors. For  $^{10}\text{B}$  concentrations of  $100 \mu\text{g/g}$  tumour and  $1 \mu\text{g/g}$  tissue, average advantage factors of more than 10 could be achieved. Average advantage factors  $\langle \text{AF} \rangle$  within the same useable depth are given in Table 7 for each beam for a range of tumour and tissue  $^{10}\text{B}$  concentrations. The  $\langle 6\text{-keV} \rangle$  beam has the best overall performance, marginally ahead of the  $\langle 0.19 \rangle$  and  $\langle 2 \rangle$  beams but markedly superior to the  $\langle 24 \rangle$  keV beam.

#### Incident $\gamma$ -ray component

The foregoing results have not included an incident  $\gamma$ -ray component in the neutron flux, which would be present in the real situation. The magnitude of the  $\gamma$ -ray flux per  $10^{10}$  neutron  $\text{cm}^{-2}$  could range from 0.05 cGy to 10 cGy, depending on the neutron and  $\gamma$ -ray shielding in the beam. For comparative purposes, we have included the  $\gamma$ -ray flux distribution of MITR, taken from Zamenhof et al. (9). The incident distribution is given in ANISN groups 31 to 42 in Table 8, and corresponds to a total incident  $\gamma$ -fluence of  $1.68 \times 10^9 \gamma \text{ cm}^{-2}$ , which is equal to a dose of  $1.3 \text{ cGy}$  at the surface, per  $10^{10} \text{ n cm}^{-2}$ . The dose-depth distribution resulting from this incident  $\gamma$ -ray flux is given in Table 5.

The effect of this incident  $\gamma$ -ray dose-depth distribution can be quite important at thermal energy for moderate boron concentrations. For  $40 \mu\text{g}$

Table 6. Advantage Factors for <6-keV> Beam (AF = tumour dose/max tissue dose)

μg $^{10}\text{B}/\text{g}$ :	Total dose ( $\text{cJ kg}^{-1}$ )					Advantage factor (AF)						
	1	4	10	40	100	Tumour:	4	10	40	40	100	100
Depth (cm)						Tissue:	1	1	1	4	10	1
0.001-0.5	2.49	3.00	4.02	9.12	19.3		1.00	1.3	3.1	2.0	2.5	6.5
0.5-1.0	2.74	3.64	5.44	14.4	32.4		1.22	1.8	4.8	3.2	4.3	10.8
1.5-2.0	2.95	4.33	7.09	20.9	48.5		1.4	2.4	7.0	4.6	6.4	16.1
2.5-3.0	2.99	4.52	7.58	22.9	53.5		1.5	2.5	7.7	5.1	7.1	17.9
3.5-4.0	2.86	4.33	7.27	22.0	51.4		1.5	2.4	7.4	4.9	6.8	17.2
4.5-5.0	2.58	3.84	6.36	19.0	44.2		1.3	2.1	6.4	4.2	5.8	14.8
5.5-6.0	2.22	3.21	5.19	15.1	34.9		1.07	1.7	5.1	3.3	4.6	11.7
6.5-7.0	1.85	2.60	4.10	11.6	26.6		.87	1.4	3.9	2.6	3.5	8.9
7.5-8.0	1.50	2.04	3.12	8.52	19.3		.68	1.0	2.8	1.9	2.5	6.5
8.5-9.0	1.21	1.60	2.38	6.28	14.1		.54	.80	2.1	1.4	1.9	4.7
9.5-10.0	0.97	1.22	1.75	4.36	9.58		.41	.59	1.46	.96	1.3	3.3
11.5-12.0	0.62	0.74	0.97	2.14	4.48		.25	.32	.72	.47	.59	1.5
14.5-15.0	0.33	0.36	0.42	0.72	1.32		.12	.14	.24	.16	.17	.44
MUD: 6.0 7.8 10.7 9.7 10.4 12.6												

Table 7. RBE Dose Parameters of Filtered Beams

(MUD is max useable depth in cm, for AF  $\geq 1$ ;  $\langle \text{AF} \rangle$  is average advantage factor within MUD)

Beam	μg $^{10}\text{B}/\text{g}$ in tumour: in tissue:	10		40		100	
		1	4	4	1	1	1
Thermal		4	2.2	6	3.5	8	10.2
<0.037>		7	1.9	8.5	3.4	11	10.6
<0.19>		7.5	1.9	9	3.2	12	9.9
<2>		8	1.9	9.5	3.3	13	10.2
<6>		8	1.8	9.7	3.2	13.5	10.0
<24>		5	1.2	10	2.8	11	4.9
<144>		1	1.0	5.5	1.3	9	1.7

Table 8. Neutron Fluence to KERMA and Photon Fluence to KERMA Factors  
 $(1.47 \cdot 7 \equiv 1.47 \times 10^{-7})$

Group	Neutrons			Gamma rays		
	Lower energy bound	Fluence to KERMA, erg(g particle cm <sup>2</sup> ) <sup>-1</sup>	Group	Lower energy bound	Fluence to KERMA, erg(g particle cm <sup>2</sup> ) <sup>-1</sup>	
		Brain	Tissue			
14	302	keV	1.47-7	31	10	MeV
15	183		1.08-7	32	8.0	
16	67.4		7.20-8	33	7.0	
17	24.8		3.60-8	34	6.0	
18	9.12		1.60-8	35	5.0	
19	3.35		5.60-9	36	4.0	
20	1.23	keV	2.20-9	37	3.0	
21	454	eV	7.55-10	38	2.0	
22	167		2.92-10	39	1.0	
23	61.4		1.31-10	40	0.51	
24	22.6		8.47-11	41	0.10	
25	8.32		8.10-11	42	0.01	
26	3.06		1.24-10			
27	1.125		1.94-10			
28	0.414		3.20-10			
29	0.152		4.98-10			
30	0.001		1.65-9			
			2.94-9			

tumour/4  $\mu$ g tissue, the MUD reduces by 20% and the  $\langle AF \rangle$  by 30% for a thermal beam. However, for the same concentrations, MUD and  $\langle AF \rangle$  are reduced by only 6% for the <6-keV> beam.

The dose-depth results for the low keV beams are most encouraging and require confirmation by detailed Monte Carlo calculations. It remains to be seen whether or not a therapeutic beam with sufficient intensity in the low keV energy range can be realised. However, if high boron concentration ratios can be attained (e.g. 100/1), a thermal beam can be effective up to 8-cm depth, if the  $\gamma$ -ray component is kept low.

#### REFERENCES

1. Locher, G.L. Biological and therapeutic possibilities of neutrons. Am. J. Roentgenol. 36(1936)1.
2. Sweet, W.H., Soloway, A.H., Wright, R.L. Evaluation of boron compounds for use in neutron capture therapy of brain tumours. J. Pharmacol. Exp. Ther. 137(1962)263.
3. Hatanaka, H., Sano, K. A revised boron neutron capture therapy for malignant brain tumours. Z. Neurol. 204(1973)309.

4. Hatanaka, H. Clinical experience of boron-10 slow neutron capture therapy. Presented at Int. Symp. on Synthesis and Application of Isotopically Labelled Compounds, June 1982, Kansas City.
5. Allen, B.J. Boron neutron capture therapy: A research program for glioblastoma and melanoma. Aust. Phys. Eng. Sci. Med. 6(1983).
6. Frigerio, N. Neutron penetration during neutron capture therapy. Phys. Med. Biol. 6(1962)541.
7. Fairchild, R.G. Epithermal neutron beam isodose charts in a phantom head. Radiology 85(1965)555.
8. Zamenhof, R.G., Murray, B.W., Brownell, G.L., Wellum, G.R., Tolpin, E.L. Boron neutron capture therapy for the treatment of cerebral gliomas: Theoretical evaluation. Med. Phys. 2(1975)47.
9. Davis, M.C., Little, J.B., Ayyangar, K., Reddy, A.R. Relative biological effectiveness of the  $^{10}\text{B}(\text{n},\alpha)^7\text{Li}$  reaction in HeLa cell. Radiat. Res. 43(1970)534.
10. Murray, B.M., Deutsch, O.L., Zamenhof, R.G., Pettigrew, R.I., Rydin, R.A., Brownell, G.L. New approaches to the dosimetry of boron neutron capture therapy at MIT-MGH. Symp. Biomedical Dosimetry, IAEA, Vienna (SM-193/48)(1975)179.
11. Mill, A.J., Harvey, J.R. Intermediate energy neutron production: A survey of existing techniques, a proposed source and its applications, EUR 6107 EN(June 1978)71.
12. Greenwood, R.C., Chrien, R.E. Filtered reactor beams for fast neutron capture  $\gamma$ -ray experiments. Nucl. Instrum. Methods 138(1976)125.
13. Fairchild, R.G., Bond, V.P. New compounds for neutron capture therapy and their significance. Private communication.
14. Engle, W.W. Union Carbide Corporation Report K-1673(1967).
15. Schaeffer, N.M. Reactor Shielding for Nuclear Engineers, USAEC Information Services (1973)614.
16. Kellerer, A.M., Rossi, H.H. The theory of dual radiation action. Curr. Top. Radiat. Res. Quart. 8(1972)85.
17. Kobayashi, T., Kanda, K. Analytical calculation of boron-10 dosage in cell nucleus for neutron capture therapy. Radiat. Res. 91(1982)77.
18. Key, M. Comparative effects of neutrons and x-rays on Chinese hamster cells. IAEA Symp. on Biophysical Aspects of Radiation Quality, Lucas Heights, March 1977, SM-145/14.
19. Sage, M.R. Blood brain barrier, AJNR 3(1982)127.
20. Hatanaka, H., Sweet, W.H. Slow neutron capture therapy for malignant tumours. Symp. Biomedical Dosimetry, IAEA, Vienna, (SM-193/79)(1975)147.
21. Betz, E. Phys. Rev. 3(1972)595.

## FILTERED BEAMS FOR NEUTRON CAPTURE THERAPY

Robert M. Brugger  
Research Reactor Facility,  
Department of Physics and Department of Nuclear Engineering,  
University of Missouri, Columbia, MO 65211

### ABSTRACT

For Neutron Capture Therapy (NCT) one would like a beam of neutrons with greater than  $10^{10}$  n/cm<sup>2</sup>-sec with energies in the range from a few eV to a few keV, with a minimal number of slower and faster neutrons and a minimal number of gamma rays. One approach to producing such a beam is to filter the raw neutron flux from a reactor or an accelerator through filtering materials that preferentially pass the desired neutrons while rejecting the undesirable neutrons and gamma rays. The different kinds of filters that might be considered are discussed and estimates of how closely these might come to meeting the desired conditions are presented. Experience with such filters at the MURR is included.

I. Introduction: Neutron Capture Therapy (NCT) is one promising method for the treatment of certain cancers. In NCT a chemical, which is loaded with  $^{10}\text{B}$ , is injected into a patient and preferentially seeks out the cancer. The patient is next exposed to neutrons which react with the  $^{10}\text{B}$  producing high LET products which destroy the cancer cells. The three major developments that must be successfully achieved for NCT to move from promise to practice are: 1) identifying nontoxic chemical compounds that will deliver the  $^{10}\text{B}$  in large enough quantities to the tumor while being in low concentrations in healthy tissue, 2) engineering beams that will deliver high enough fluxes of the optimum energy neutrons to the cancer region while being low in flux of the undesirable energy neutrons and gamma rays and 3) developing microdosimetry methods that will clearly identify how well 1) and 2) are being achieved.

This paper focuses on a possible method for achieving the beam of neutrons. The desired beam for NCT is about  $10^{10}$  n/cm<sup>2</sup>-sec of neutrons within the energy range from about 1 eV to 30 keV, few neutrons with higher or lower energies and few gamma rays. Neutrons are not stable so they must be produced when needed. To produce a large enough source flux of neutrons will require either a reactor or an accelerator. After the reactor or accelerator has produced as high an intensity of the desired neutrons as possible, it is the purpose of the filter to pass the desired energy neutrons while rejecting the undesirable energy neutrons and gamma rays which are produced along with the desired neutrons in the nuclear reactions.

II. Why Neutrons from 1 eV to 30 keV: Reactors and accelerators produce neutrons that can span the energy range from about 15 MeV down to thermal energies. The number of neutrons in each decade depends on the reaction and the moderator surrounding the target or source. Figure 1 shows a typical spectrum from a light water moderated fission reactor. The fission reaction produces neutrons in a fission spectrum which is group 3 in the figure. The water moderator slows down the neutrons through the keV to eV range, which is called the 1/E spectrum (group 2). At thermal energies the neutrons come

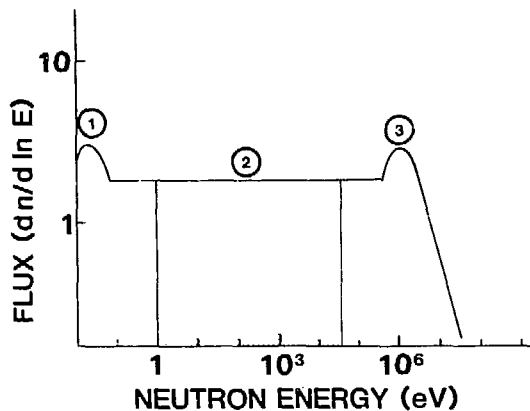


Figure 1: Typical spectrum from a light water moderated reactor: 1) thermal distribution, 2)  $1/E$  distribution, 3) fast fission distribution. The shaded area is 1 eV to 30 keV.

into equilibrium with the moderator to form the thermal spectrum (group 1). For an accelerator, the source is some nuclear reaction which produces neutrons in groups or bands above a few keV. A moderator around an accelerator source will produce a similar  $1/E$  group and a thermal group as are produced with a fission source. Thus the spectrum of neutrons from either a reactor or an accelerator that is moderated to produce some neutrons in the 1 eV to 30 keV range will be similar. In the rest of this paper the reactor spectrum will be used to discuss the filters.

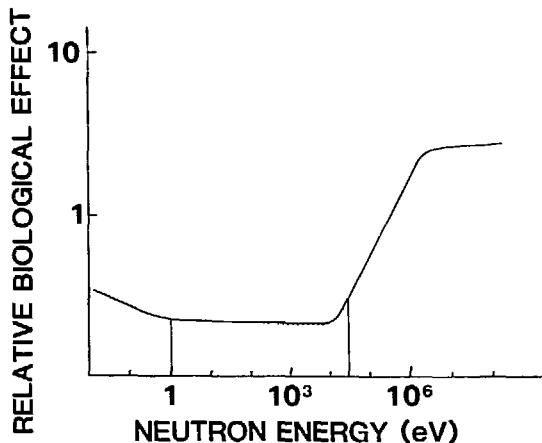


Figure 2: The general shape of the biological effect produced by neutrons in healthy tissue. The shaded area is 1 eV to 30 keV.

Figure 2 shows the general shape of the relative biological effect of neutrons of different energies. Above about 10 keV the biological effect increases and more healthy cells will be killed by these neutrons, so an upper limit of about 30 keV is set for the desired flux of neutrons. Neutrons below 1 eV interact quickly with  $^{10}\text{B}$  near the surface or skin which produces a high skin dose which is undesirable. Neutrons with energies greater than 1 eV will penetrate several centimeters into a body before being moderated to thermal at which energy they can be highly absorbed by  $^{10}\text{B}$ . Thus the desired band of neutrons that penetrate before thermalizing, that will not burn the skin and that cause modest effects from recoils to healthy tissue extends from about 1 eV to about 30 keV.

III. How Filters Work: Since neutrons are particles with a finite rest mass but no net charge, the interaction of neutrons with the material of a filter is essentially through nuclear reactions and the probability of such reactions is expressed as a cross section  $\sigma$ . If the neutrons of number  $I_0$  start from a source, and are directed through a filter of length  $x$ , and the number of nuclei/cc is  $n$ , then the number of neutrons  $I$  that arrive at the position of the patient is:

$$I = I_0 (\text{geometry effects}) \exp (-nx\sigma).$$

The geometrical effects will be considered in a later section. Cross sections for neutrons have been measured and graphs of these cross sections have been compiled<sup>1</sup>. A similar relation applies for the attenuation of gamma rays<sup>2</sup> but the  $n\sigma$  is replaced by a mass absorption coefficient  $\mu$ .

To act as a filter of neutrons, the cross section should be small for the energy band that one wants to pass and large for all other energies that should be stopped. Neutron cross sections have general features and these can be studied to select desirable filtering materials. Figure 3 shows a

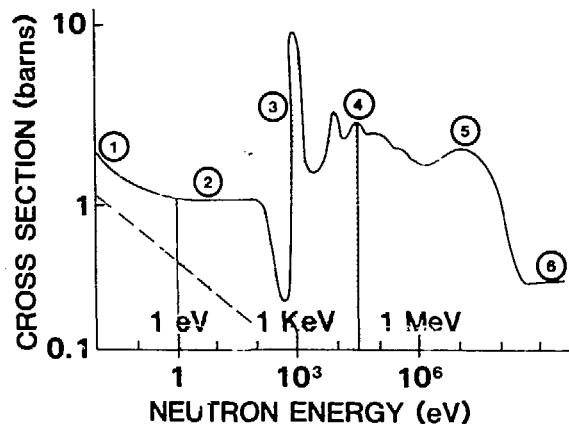


Figure 3: A generalized neutron cross section showing 2) the free atom region and 3) an S wave resonance region. The shaded area is the 1 eV to 30 keV band.

generalized cross section. Near thermal (range 1) the cross section increases because the neutrons experience the binding of each nuclei to its neighbor or the cross section increases because the  $1/v$  absorption cross section is large. Over the free atom cross section range (range 2), the atoms experience interaction with isolated nuclei. The neutrons can experience a resonance interaction (range 3) where the cross section is very large for small energy steps. For S wave resonances, interference may cause a dip before the resonance and this dip or window is used in some filters to pass a band of neutrons. In range 4 the resonances overlap each other and dips or windows seldom occur. Over the whole range of cross sections long-range oscillations are experienced because of optical type interference between the neutron and the nucleus. These oscillations can sometimes be used to advantage in filters. Neutron filters are designed to use the low cross section windows and regions to pass the desired neutrons and the high cross sections to stop the undesired neutrons.

IV. Present Neutron Filters: Table I lists<sup>3</sup> several filters that are being used or have been tried as neutron filters and that pass neutrons between 1 eV and 30 keV. The U, Sc and Fe filters are resonance window filters in which a strong resonance (for Sc two closely spaced resonances) with a deep minimum before the resonance acts as a window to pass neutrons. Besides the primary resonance and window, there are other higher energy S wave reson-

Table I  
Neutron Filters in the 1 ev to 30 keV range

Primary Filtering Material	Center of Neutron Energy Band (keV)	Band Width (keV)	Relative Intensity*
238U	0.186	0.0015	1
Sc	2	0.7	6
Fe	24	2	4
56Fe	24	2	12
Al/S	0.001-30	30	30

\*The relative intensities were estimated after studying the reported geometries, source fluxes and fluxes of each type of filter.

ances that also have windows and pass higher energy neutrons. Secondary filtering materials have been added to these filters to block these higher energy windows. For example Al and S are added to the Fe filters to block the windows above 24 keV.

The Fe filter at the MURR has been used for nuclear engineering experiments. The filter is in a tube 2.6 cm in diameter, while the sample position is 3.5 m from the source. The filter is a 50 cm length of Fe metal followed by 20 cm of Al and 5 cm of S. The flux of 24 keV neutrons at the sample position is about  $1.2 \times 10^6$  n/cm<sup>2</sup>-sec. The 24 keV neutrons are 92% of all neutrons in the beam and the measured flux of gamma rays is 44 mR/hr.

The geometrical arrangement of the source, filter and patient or sample partially determines how many neutrons will reach the patient. The flux  $\phi$  arriving at a patient is:

$$\phi = \phi_c \frac{A}{4\pi(d)^2}$$

where the isotropic flux at the source is  $\phi_0$ , the area of the source is A

and the distance between the source and the patient is  $d$ . The filtering material is placed between the source and the patient. The  $\phi$  can be optimized to some extent by using a larger  $A$  and a shorter  $d$ . Optimizing this Fe filtered beam by expanding the source area to the full face of the MURR and shortening the source to patient distance to 2 m would gain a factor of about 1000. Thus an iron filter might be designed for MURR from which the flux would be greater than  $10^9$  n/cm<sup>2</sup>-sec. In the <sup>56</sup>Fe filter<sup>5</sup>, the separated isotope is used instead of the element because the other isotopes of Fe cloud the 24 keV window of <sup>56</sup>Fe. Using the separated isotope instead of the element, the cross section at the window drops from one half barn for the element to 10 mb for the isotope <sup>56</sup>Fe. Thus a longer length of <sup>56</sup>Fe can be used as a filter without suffering a large attenuation at the primary window. This longer length produces more attenuation of neutrons at other windows, and more attenuation between windows and more attenuation of gamma rays. Unfortunately, large quantities of <sup>56</sup>Fe to make a filter are expensive. If <sup>56</sup>Fe could be obtained, a filter delivering  $3 \times 10^9$  n/cm<sup>2</sup>-sec might be achieved at MURR.

A Sc metal filter<sup>6</sup> has also been used at MURR and comparisons indicate that an optimized Sc filter would deliver more neutrons than an optimized elemental Fe filter. However, the cost of a large quantity of pure Sc metal to make a large area filter would be prohibitive (over one million dollars). Also the cost of separated isotopes to use as secondary filtering materials to remove neutrons above 30 keV would be prohibitive. A practical Sc filtered beam for NCT does not look possible.

In developing the <sup>238</sup>U filter<sup>7</sup> at MURR, secondary filtering materials were added to stop higher energy neutrons coming through other windows in the cross section. Neutrons that pass through higher energy windows appear to extend in energy to only a few keV. Since windows up to 30 keV are a help rather than a hindrance, a <sup>238</sup>U filter without secondary filtering material might pass more flux by a factor of 10 but still restrict the flux to energies less than 30 keV. The <sup>238</sup>U filter is very effective for stopping gamma rays and fast neutrons. Depleted uranium (0.2% U<sup>235</sup>) is relatively inexpensive and would increase the desired flux by about a factor of 2. Again optimizing by increasing the source size and shortening the distance for a <sup>238</sup>U filter at MURR might produce a beam of  $3 \times 10^9$  n/cm<sup>2</sup>-sec.

The Al/S filter is a mixture of resonance window effects and optical oscillation effects. Materials around mass number 30 have a lower cross section in the free atom range than in the Mev region. In addition strong S wave resonances occur near and above 30 keV. The difference in the cross sections below 30 keV compared to above 30 keV is not as great as one could hope for but still a filter of Al and S passes many neutrons below 30 keV while stopping most neutrons above 30 keV.

An Al/S filter<sup>8,9</sup> has been tested at MURR using the 2.5 cm diameter beam at beamport F and Figure 4 shows the calculated neutron spectrum and dose spectrum. A cut-off is observed near 30 keV. These spectra have been substantiated by measurements using Bonner sphere detectors<sup>10</sup>. Again considering an optimized beam of larger source and shorter distance, a flux of neutrons near  $10^{10}$  n/cm<sup>2</sup>-sec might be expected at MURR. From these comparisons of filters it appears that several are possible candidates to reach a flux of  $10^{10}$  n/cm<sup>2</sup>-sec at an intermediate neutron source like the MURR.

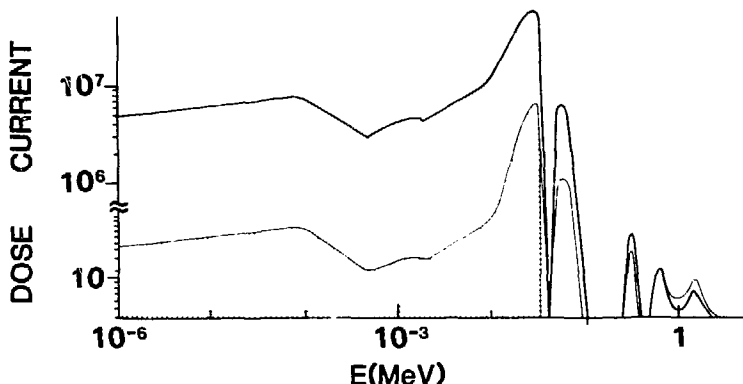


Figure 4: Calculated neutron current and neutron dose in an Al/S filtered beam.

V. Possible Improvements: Improvements of the filtered beams that might be considered include: increasing the reactor power, increasing the source area, shortening the distance between the source and the patient, increasing the  $1/E$  flux group from the source, improving the coupling between the source-reflector and the filter and optimizing the filtering materials' lengths. In most reactors the neutron flux is proportional to the power so an increase in power will produce an increase in flux. Since this is a possible option for a few reactors, but not for all, increasing the power will not be considered further in this paper.

Increasing the source area and shortening the distance between the source and the patient will increase the flux at the patient. The full face of the reactor core could be used as the source area if necessary, but some existing reactors will be restricted because of existing shielding. The source to patient distance should be made as short as possible while still leaving enough distance for adequate shielding around the filter. These two increases have already been taken into account in the "optimized" beam of the preceding section.

Most existing research reactors have been designed to give maximum fast flux ( $>0.8$  Mev) for radiation damage experiments or maximum thermal flux ( $<0.3$  eV) for isotope production or thermal neutron scattering experiments. Few reactors have been designed to maximize the  $1/E$  flux. The existing reactors should be examined to see if a change or modification of the reflector would yield more  $1/E$  flux. Such a modification would increase the 1 eV - 30 keV flux while not increasing the fast flux.

Closer coupling of the source and filter might yield increased flux. In the uncoupled case the source plus moderator produce a flux distribution like that of Figure 1. Here the filter passes only those neutrons from this spectrum that match the energies of the windows. In contrast, if the filtering material and the moderating material were the same, the neutrons might cascade down in energy till they reached a window, then the neutrons would fly out through the window of the moderator-filter. Thus all the neutrons from the source would become available to cascade down to the window.

The window in  $^{56}\text{Fe}$  is 2 keV wide, or 8% at the 24 keV of the resonance. In contrast neutrons experiencing elastic collisions in Fe have a maximum energy loss of 7%. Thus every neutron that moderates down to the window will experience an energy corresponding to the window; every neutron falls

into the window. About a hundred collisions will occur from fission down to 24 keV and the diffusive spreading of the source may be large before the neutrons have reached 24 keV and some neutrons will be lost to capture. However, this coupling might work and should be considered to increase the flux. Iron-56 would provide a more effective coupling than elemental Fe. In a similar manner, the Al might act as a filter-moderator for an Al/S filtered beam.

In reference 3 it is pointed out that two types of beam holes are available for filtered beams. The reentrant hole that looks at the reactor core has more fast neutron and gamma-ray components aimed through the filter at the patient. The tangential hole forces the neutrons to scatter at least once before starting toward the patient. The tangential hole arrangement reduces the flux of fast neutrons and gamma rays compared to i/E neutrons flying toward the patient. With a tangential beam port and scatterer, less filter is needed which saves some flux.

The only  $^{56}\text{Fe}$  filter is at BNL<sup>5</sup> where almost the entire U.S. supply of separate  $^{56}\text{Fe}$  is used (estimated cost \$400,000). This filter is very effective for passing most 24 keV neutrons while rejecting all others. However, to "optimize" an  $^{56}\text{Fe}$  filter by using a larger area would be prohibitive in cost. Filters of  $^{56}\text{Fe}$  with the very small cross section at the window are very appealing for more development if the cost could be overcome.

The "optimized" fluxes of the Fe, Al/S and U filters which are approaching  $10^{10} \text{ n/cm}^2\text{-sec}$  and their low cost indicate that these should be considered further to see if another factor of from 2 to 10 can be squeezed out in addition to improving on the fast neutron and gamma rejection. Adding a section of Ar to the Al/S filter may make it more effective.

Several other resonance window filters have been suggested but not yet tried. These are  $^{170}\text{Er}$ (60 eV),  $^{184}\text{W}$ (160 eV),  $^{68}\text{Zn}$ (400 eV),  $^{60}\text{Ni}$ (5 keV),  $^{58}\text{Ni}$ (13 keV) and  $^{64}\text{Zn}$ (2 keV). However, each of these uses expensive materials and will probably not be practical.

**VI. Conclusions:** With the intermediate power nuclear reactors, it appears that beams of  $10^{10} \text{ n/cm}^2\text{-sec}$  of 1 eV to 30 keV neutrons can be achieved by using filters and optimizing the beams. The filters that appear most promising are the Al plus S filter with the possible addition of Ar, the  $^{238}\text{U}$  filter with no secondary filtering material, the Fe filter coupled to the source as a moderator followed by Al and S secondary filters, and the Al/S filter with part of the Al coupled as a moderator to the source.

#### References

1. Gerber, D.T. and Kinsey, R.R., "Neutron Cross Sections, Vol. II, Curves", USDCE publication, BNL-325, 3rd ed. Vol II (1976).
2. Radiological Health Handbook, U.S. Dept. of Health, Education and Welfare (January 1970).
3. Block, R.C. and Brugger, R.M., Neutron Sources for Basic Physics and Applications, Chapter VIII, Vol 2, Pergamon Press 1983, S. Cierjacks ed.
4. Tsang, F.Y. and Brugger, R.M., Nucl. Inst. Meth. 134, 441 (1976).

5. Greenwood, R.C. and Chrien, R.E., Nucl. Inst. Meth. 138, 125 (1976).
6. Tsang, F.Y. and Brugger, R.M., Contr. Midwest Student Conf., Urbana, IL (1977).
7. Royer, R.B. and Brugger, R.M., Nucl. Inst. Meth. 145, 245 (1977).
8. Noonan, D.J., Russell, J.L. Jr., and Brugger, R.M., 26th Annual Meeting of the Health Physics Society, Louisville, KY June (1981).
9. Brugger, R.M., Miller, W.H., Sohl, J.D., Russell, J.L. Jr and Noonan, D.J., Proceeding of the ANS Meeting, San Francisco (Nov. 1981).
10. Sohl, J.D., "Experimental Benchmarking of the Bonner Sphere Spectrometer Using Filtered Neutron Beams". A thesis submitted to the Department of Nuclear Engineering, University of Missouri-Columbia (May 1982).
11. Harvey, J.R., and Mill, A.J., "The Status of a Proposed International Filtered Neutron Beam Project", Presented at the 4th Symposium on Neutron Dosimetry, G.S.F., Munich-Nuremberg, June 1-5, 1981.

## Boron in Fast Neutron Therapy? Present Developments and Prospects

Börje Larsson

Dept. of Physical Biology, The Gustaf Werner Institute, Uppsala, Sweden

Low energy neutrons present in tissue during fast neutron therapy may be used for dose enhancement in tumours that can be selectively loaded with boron. Since the probability of tumour control is a steep function of the dose, prospects of  $> 5\%$  selective increase of the biologically effective dose would provide a strong motive for such a supporting "neutron capture therapy" (NCT). Measurements reported in 1978 (Waterman et al., *Phys. Med. Biol.* **23** (1978) 592) indicated, indeed, that an uptake of  $35 \mu\text{g}^{10}\text{B/g}$  of tissue would produce  $2.5\text{--}11\%$  increase of the absorbed dose at  $8 \text{ cm}$  depth, on the central axis of beams with median energies of  $9.0\text{--}2.4 \text{ MeV}$ ,  $12 \times 12 \text{ cm}^2$ . The enhancement was dependent on the field configuration, and the point of measurement, but for a given beam it never seemed to vary by more than a factor 2, within a spherical target,  $6 \text{ cm}$  in diameter and centered on the beam axis.

With a view toward the high energies of fast neutrons available at modern apparatus, and the desire to give efficient capture dosage also to tumour cells near the edge of the field, uptakes of  $> 100 \mu\text{g}^{10}\text{B/g}$  of tumour ought to be strived for. Although such high concentrations may be within reach, it has so far been impossible to avoid, in the same time, untoward concentration of boron in the blood stream and normal tissues. As this problem would not be less in fast neutron therapy than in NCT, there is additional motive for the development of improved or new  $^{10}\text{B}$ -carriers. Although important progress has been made in preclinical or clinical studies with low-molecular compounds designed for NCT, there seems to be a long way to go before the results can be applied without risk in efficient NCT-assisted fast neutron therapy. The same is probably true for the foreseen new generation of boron compounds that ideally would show more selective accumulation in tumours, biological half-lives in the order of days, and a  $^{10}\text{B}$  ratio (concentration in tumour/normal tissue) of  $> 10$  (Fairchild and Bond, *In Proc. Int. Meeting on Stable Isotopes*, Kansas City, Mo, U.S.A., June 6-12, 1982).

With reference to the above observations, biological and pre-clinical studies are being initiated to facilitate later decisions about the possible introduction of boron compounds in fast neutron therapy. Measurements of neutron capture fluence should be done in clinically used fast neutron fields, in addition to currently used parameters. On the basis of such measurements, subtherapeutic amounts of  $^{10}\text{B}$ -carriers could soon be safely administrated, in case where the information obtained would be of diagnostic value. This would, for example, be very likely in studies with monoclonal antibodies labelled with  $^{10}\text{B}$  as well as with a radioactive marker, such as  $^{123}\text{I}$  or  $^{18}\text{F}$ . This combination would allow scintigraphic localization at the organ level, as well as neutron capture radiography of biopsy specimens, for determination of antibody behaviour at the cell and tissue levels. The knowledge obtained would permit detailed appreciation of the merits and pitfalls associated with the application of the studied carriers in the eventual therapeutic situation.

ON THE POSSIBLE USE OF SPALLATION SOURCES  
IN NEUTRON CAPTURE THERAPY;  
PROPOSED MEASUREMENTS OF NEUTRON SPECTRA AT S.I.N.

J.F.CRAWFORD, S.I.N.

and

B.LARSSON, UPPALA

The use of the powerful combination of epithermal neutrons and boron-10 loaded materials for radio-biology and radio-therapy was first proposed many years ago (Ref 1), and the idea has been used more recently (Ref 2). Hitherto, the amount of boron-10 which could in practice be put into the systems of interest has been severely limited. However, the recent development of monoclonal antibodies which can be loaded with very much more boron, possibly almost pure boron-10, and which will deliver the boron to specific sites, has revived interest in the technique. Antibody compounds now becoming available offer the promise of attaching 1000 or more boron-10 atoms to specific sites. One can therefore expect to be able to load target cells with at least 100 ppm of boron-10. This paper is concerned with the production of suitable neutron beams, and more particularly with the measurement of their energy spectra. Ref 3, an up-to-date summary, contains many useful references.

We describe here preparations for measurements of energy spectra and fluxes of epithermal neutrons from proposed test spallation sources in proton beams available at the Swiss Institute for Nuclear Research (S.I.N.). The method is based on conventional time-of-flight techniques and requires pulsing of the accelerator. Although no results can yet be presented, the plans seem to be of interest to illustrate the rationale and potentialities of the use of accelerators in Neutron Capture Therapy, as alternatives to nuclear fission reactors and other devices. Our intention is to develop an understanding of the properties of proton-induced neutron fields, and of the technological aspects of their utilization in biomedical applications of neutron capture in cell-seeking compounds loaded with boron-10. The work is done with a view to the ultimate use of proton accelerators in hospitals to provide facilities for pion or proton therapy, isotope production, N.C.T., etc.

For completeness, we list here various methods of generating neutrons:

Stripped deuteron beams

Specific nuclear reactions (e.g. low energy protons on scandium)

Transuranium neutron sources (e.g. californium-252)

Alpha emitters with converters (e.g. Am-Be)

Photon-induced reactions

Fusion-produced neutrons

Reactors

Spallation sources

We believe that spallation sources have great potential among these alternatives. This is the reason for our present interest in setting up experiments to study the production of filtered epithermal neutron beams by accelerated protons. Fig 1 (taken from Ref 4) shows the neutron yield (neutrons per incident proton and heat load per produced neutron) as a function of proton energy. The curves shown are calculated; however, some of them are well supported by measurement. It is worth pointing out that at less than 60 MeV, Beryllium becomes a more prolific source than lead. Because the neutrons are produced by a spallation process, and because they are moderated, their energy is not a strong function of proton energy.

Table I, derived from References 5 and 6, lists proton facilities that may be useful for the proposed experiments

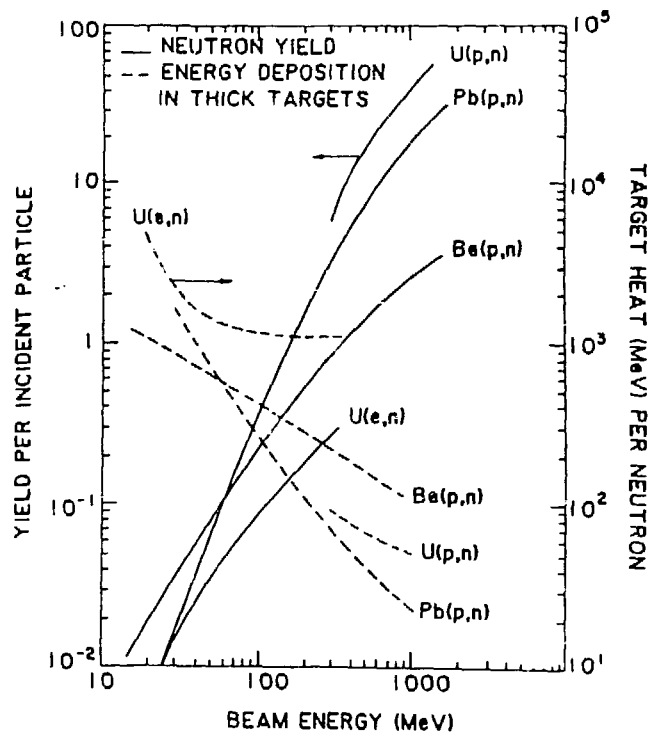


Figure 1 Comparison of neutron yields and energy deposition in various reactions in targets of thickness equal to the beam penetration

TABLE I - - USEABLE PROTON ACCELERATORS

NAME	LOCATION	ENERGY/CURRENT MeV/Microamp	NEUTRON FACTOR	STATUS
	Stellenbosch	100/100	37	1985
SIN	Villigen	600/150	1500	Running
		72/200	34	Running
		600/2000	20000	1984
		72/2000	300	1984
CERN SC	Geneva	600/3	30	Running
RCNP	Osaka	550/100	900	Design
Tohoku	Sendai	40/100	6	Running
	Moscow	1000/15	300	Design
	Munich	22/500	11	Running
LBL CP-42	Berkeley	60/200	21	Running
	Berkeley	42/200	12	Off-the-shelf
TRIUMF	Vancouver	500/100	700	Running
LAMPF	Los Alamos	800/>500	>7000	Running
MC-40	Uppsala	40/100 (goal)	6	Running
		200/10	16	1985
CYCLONE	Louvain	95/50	16	Running
	Orsay	200/7 (goal)	11	Running
JINR	Dubna	700/35	425	Running
SNS	Rutherford	800/200	3000	1984
EPNS	Argonne	450/10	60	Running

(spectral measurements in microampere beams, tests necessary to find optimized target-moderator-layout combinations). The "neutron factor" is simply the yield of neutrons per incident proton multiplied by the proton beam current in microamps. It measures the "neutron current" leaving the neutron production target. The integrated flux of neutrons after moderation and filtering will be less.

From the experience gained at the various centres listed, we note that there are three practical alternatives for hospital-based proton facilities with some potential for large-scale routine therapy with modalities tested so far: Many-hundred MeV accelerators (for pion therapy)  
Few-hundred MeV accelerators (for proton therapy)  
Small cyclotrons (for eye therapy and fast neutron therapy)

Amongst these, the small cyclotrons may be considered for combined fast-neutron and neutron capture therapy (cf Larsson's earlier communication) but, because of limited intensity, not yet for "pure" neutron capture therapy; they would be useable for radio-biological studies. Thus we are interested in studying the "many-hundred" and "few-hundred" MeV alternatives. It appears that the techniques for producing and investigating proton-induced neutron fields are similar at all these proton energies, and that in fact the S.I.N. facility at Villigen, Switzerland, offers the proper prerequisites for both types of experiment. For practical reasons we have chosen to propose experiments with the 72-MeV proton beam from the injector cyclotron. The proton beam (up to 200 microamps at 72 MeV in this case) is incident on a spallation source consisting of a target material (which can be Li, Be or something much heavier like Pb or U), surrounded by perhaps a metre of moderator (water, heavy water, Al, Fe, etc). Because of the differences in spallation properties as a function of proton energy, the target and moderator materials must be chosen in the light of the proton energy to be used, the neutron spectrum desired, etc. The epithermal neutrons are extracted through a hole perpendicular to the incident proton beam, but not necessarily in the same plane as it. Fig 2 shows a possible arrangement, based on the work of Atchison (Ref 7).

Protons are brought to rest in a lead target, which need be only a few cm long. Neutrons, produced with MeV energies, are moderated by the water to thermal or epithermal energies within a few cm, and within a few microseconds, the time depending on the final energy. Boron compounds are dissolved in the water to absorb unwanted thermalised neutrons. The beam pipe is adjustable in position, to test the effects of different thicknesses and layouts of the water moderator. Different moderator materials such as deuterium can be conveniently tested, as can various filter layouts. Once an optimal layout is

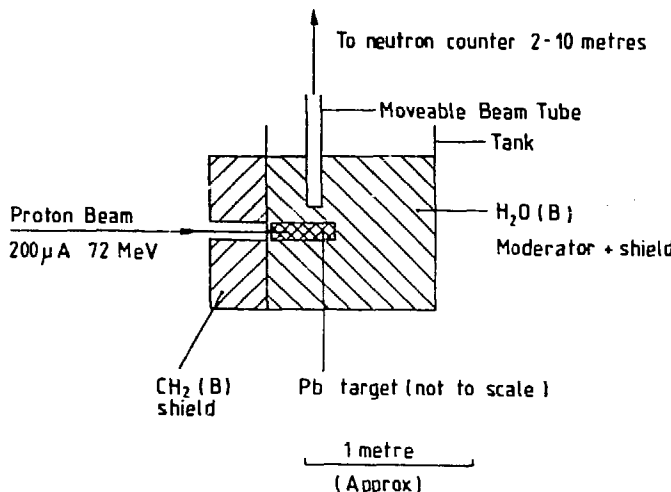


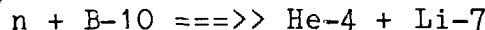
Figure 2

found, and this can be done without exact knowledge of how good it is, a final design can be made. The 200-microamp 72-MeV proton beam at present available would produce several times  $10^{14}$  neutrons per second in the lead. It should be possible to produce an intensity of several hundred thousand per sq cm-second at a distance of a few metres for radio-biology. The more powerful injector at present nearing completion will be able to deliver an order of magnitude more beam at the same energy.

The resulting neutron intensity and energy spectrum can be calculated by Monte Carlo techniques; however, there are uncertainties in such complex calculations, especially at the lower proton energies, and a direct experimental check is felt to be necessary. In principle, neutron beams can be measured by activation techniques, in which various materials are exposed to the beam and the resulting activities are measured. Given enough activatable materials, and enough information about their activation properties, it is possible to extract the properties of the epithermal neutron beam in an indirect and time-consuming way. The method described here is more direct. In essence it is the same as that of Bollinger and Thomas (Ref 8). The basic technique is to measure the time-of-flight of the neutron from the spallation source to a neutron detector. At reactors and other continuous sources, this can only be done by some kind of mechanical beam chopper arrangement, which can be awkward and expensive to build. However, an accelerator beam can in general be pulsed. At S.I.N. the pulse length can be as short as 500 nS fwhm, with a pulse repetition rate of a kHz or so. This is done electrostatically at a very early stage of acceleration,

where the protons have an energy of less than 100 keV. The time of emission of the neutrons can therefore be defined to a precision of  $\pm$  a few hundred nS. To complete the measurement, a neutron detector with corresponding time resolution and reasonable efficiency is needed.

Like most of the work under discussion at this Symposium, the detector is based on the reaction



with the release of 2.3-2.8 MeV as kinetic energy of the charged products. From a few millieV up to 500 keV, the cross-section for this reaction is approximately inversely proportional to the neutron velocity.

There is commercially available a liquid scintillator, NE 311 (Ref 9), which contains 5% of Boron by weight. If natural boron is used, then about 1% of the scintillator by weight is boron-10. The boron load can be enriched in boron-10, but for reasons discussed below, we do not believe that this is worth the substantial extra cost. The He and Li fragments come quickly to rest in the scintillator, emitting about 400 detectable photons as they do so. Because of saturation effects, this is about 50 times less than would be emitted by low LET radiation of the same energy. The light is detected by a pair of 5" PMTs. The tank itself is 3 x 3 x 30 cm; these dimensions give a good match to the 100 sq cm photocathode area of a 5" PMT. The walls of the counter are polished aluminium, the reflectivity of which is taken to be 70%. One can then estimate that if the neutron reaction takes place near the centre of the tank, each PMT should detect about 5 photo-electrons. Near a tube, the nearer tube detects about 8 photo-electrons, the farther about 2. For each detected event, amplitude and timing information from each tube can be recorded for later analysis. This information can be processed in various ways. Pulse height and/or shape can be used to suppress gamma background. To reduce tube noise, one can demand coincident signals in the two tubes. (Room background will not be affected by this technique.) In addition, the timing difference between the two tubes can be found. This will provide information on where in the counter the boron capture took place, and would provide a check that the counter was uniformly efficient everywhere.

Such a device can measure the time of occurrence of a boron fission accurate to a few nanoseconds. In addition, the neutron is calculated to take about 300 nS to be captured in the counter (Ref 8). This is a good match to the pulse length of the accelerators at S.I.N. Fig 3 shows, in the form of a nomogram, the energy, time-of-flight and flight path of neutrons. It will be seen that with a flight path of 10 metres, a repetition rate of 1 khz and a time resolution of  $\pm$  300 nS, neutrons between less than 1 eV and

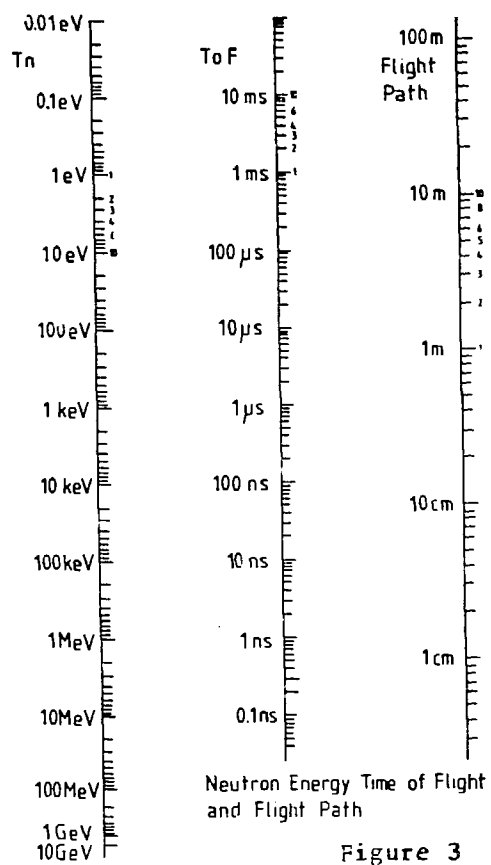


Figure 3

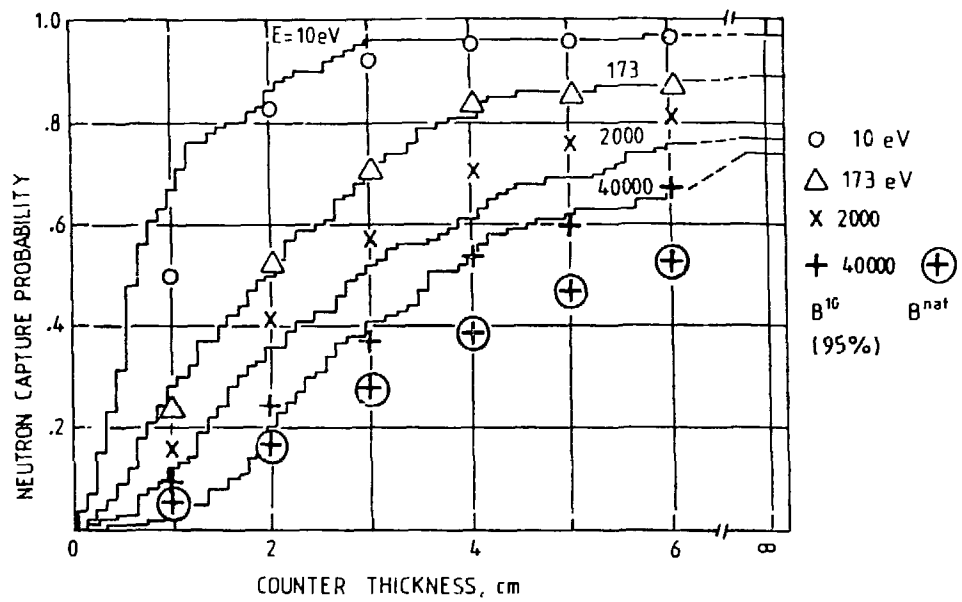


Figure 4

almost 1 MeV can conveniently be measured. Higher energies would require longer flight paths; lower, a longer repetition time. Because of practical limits on timing and flight paths, this performance could not be achieved with a mechanical chopper.

The efficiency of a counter of this kind can be calculated by Monte Carlo techniques. Such calculations were first done by Bollinger and Thomas in 1957 (Ref 8). A repeat of their calculation with better knowledge of cross-sections etc., and with much better statistics, shows good agreement (Fig 4). The figure shows for the most part estimates for a counter containing 95% boron-10. Some data are also given for natural boron. As can be deduced from the behaviour of the absorption cross-section, the natural material responds in the same way as pure boron-10 would to neutrons of about 18 times the energy. For the highest energy calculated, 40 keV, a 3-cm-thick counter has an efficiency of over 25%. It is clear that the natural material, which is more than a factor 10 cheaper, is fully adequate for our purposes.

Needless to say, it is vital to understand the efficiency of the counter as a function of neutron energy. This can of course be calculated by the programs mentioned above. However, it is felt that a direct experimental check would be most desirable. This can be done in at least two ways: with two similar counters directly in tandem, one can study the different rates in the two counters as a function of neutron energy (or time-of-flight). The ratio of these rates can be calculated by the Monte Carlo program, and compared with the measured values. Roughly speaking, one is measuring the counter efficiency as a function of energy. To illustrate the principle, consider a neutron energy of 2 keV, corresponding to a time-of-flight of 17 microsec over a ten-metre path. Then the ratio of counting rates in the counters after this flight time is expected to be about 2:1.

An equivalent result can be achieved by installing in front of the counter different thicknesses of an absorbing material (e.g. boron-loaded polythene), the atomic composition of which is similar to that of the counter. One then studies the measured neutron rate as a function of absorber thickness and compares the measured values with Monte Carlo predictions. Thus, considering the same example, an absorber of the same thickness as the counter is expected to reduce its counting rate by half. In each case, the objective is to confirm by measurement the accuracy of the calculations, upon which the understanding of the counter efficiency chiefly depends. The choice between the two methods would be influenced by availability of beam time, equipment, etc.

An additional check on the overall performance of the source and detector can be made by taking data at different flight paths. If all is well, the resulting time spectra should scale in a simple way with the flight path. On the other hand, neutrons not coming directly from the source, gammas from neutron absorption, etc., will in general behave differently.

References:

- 1) G. I. Locher, Am. J. Roentgenol., Vol. 36, pp 1-13 (1936).
- 2) See for example: H. Watanaka et al., Acta Neurochirurgica Vol. 42, p 57 (1978), and reports at this Symposium.
- 3) "Neutron Sources for Basic Physics and Applications", an OECD/NEA report edited by S. Cierjacks. This is Vol 2 of the series "Neutron Physics and Nuclear Data in Science and Technology", published by Pergamon Press in 1983:  
539.7'213 QC793.5.N462 ISBN 0-08-029351-4
- 4) M. A. Lone et al., Atomic Energy of Canada report AECL-7839.
- 5) Cyclotrons 1978, John A. Martin, IEEE Trans Nucl Sci NS-26 No 2 (1979)
- 6) Ninth Int. Conf. on Cyclotrons and their Applications, Caen, 1981.
- 7) F. Atchison, S.I.N., unpublished.
- 8) L. M. Bollinger and G. E. Thomas, Rev. Sci. Instruments, Vol. 28, pp 489-496 (1957).
- 9) Available from Nuclear Enterprises, Sighthill, Edinburgh EH11 4BY, Scotland. Because NE 311 is inflammable and hygroscopic, appropriate precautions are necessary.

Physics Studies on Neutron Field and Dosimetry  
for Neutron Capture Therapy in Japan

Keiji Kanda, Tooru Kobayashi

Research Reactor Institute, Kyoto University  
Kumatori-cho, Sennan-gun, Osaka 590-04, Japan

Otohiko Aizawa

Atomic Energy Research Laboratory  
Musashi Institute of Technology  
Oozenji, Aso-ku, Kawasaki 215, Japan

Hiroaki Wakabayashi, Yoshiaki Oka  
Nuclear Engineering Research Laboratory  
University of Tokyo  
Tokai-mura, Naka-gun, Ibaraki 319-11, Japan

## 1. Introduction

In accordance with the requests of medical doctors, physics studies on neutron field and dosimetry for neutron capture therapy and its related study have developed very much in the past 15 years in Japan.

The existing reactors have been remodeled for biomedical purposes, and some new facilities are being planned. The associated studies for neutron capture therapy have also been done experimentally and theoretically.

This paper reviews these studies in a limited space, although it cannot cover all.

## 2. Remodeling of Existing Reactors

### 2.1 HTR

In 1968, the first irradiation for neutron capture therapy was performed using the Hitachi Training Reactor (HTR, 100 kW). (See Fig. 1). Since then, 13 patients were treated until 1974, and the reactor shut down in 1975. The physics study on the irradiation field in the HTR is reported in Reference (1).

### 2.2 KUR

The Kyoto University Research Reactor Institute (KURRI) group (K. Kanda, T. Kobayashi et al.) developed a low-gamma neutron field by adapting a bismuth scatterer (2,3), (see Fig. 2), and it was employed in the heavy water facility of Kyoto University Reactor (KUR, 5000 kW, see Fig. 3). They also showed the effectiveness of low-gamma-ray field on the depth dose from the viewpoint of relative boron accumulation effect (RBAE), as shown in Fig. 4. The thermal neutron flux and gamma-ray dose rate of the facility (4) are,

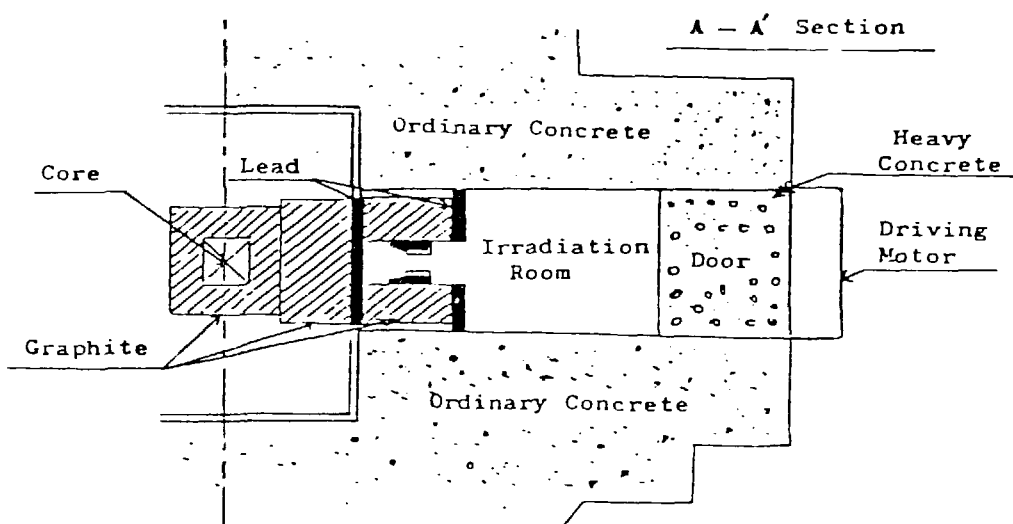
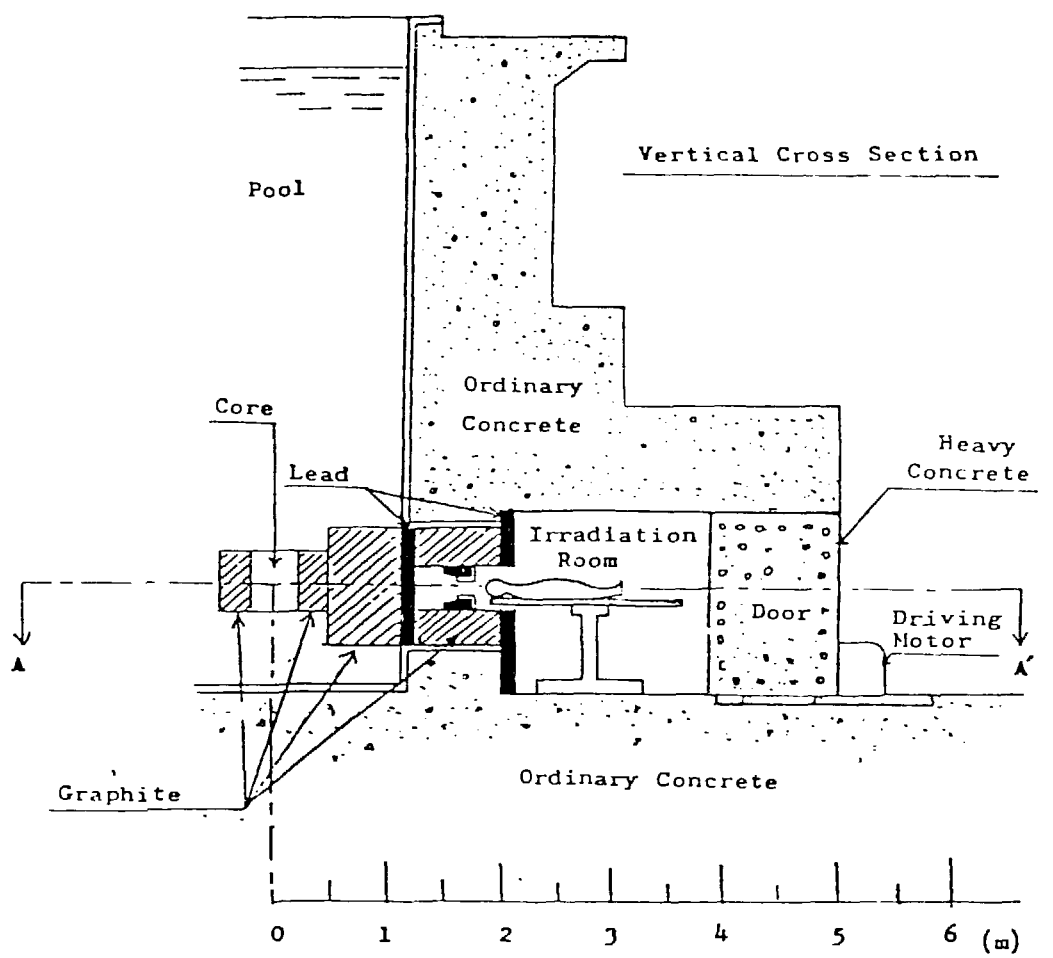


Fig.1 Irradiation room of HTR (1).

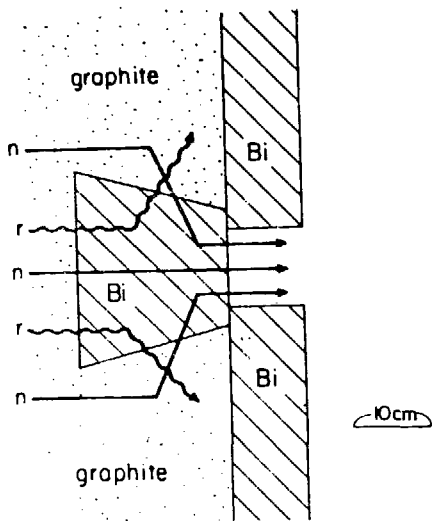


Fig.2 Basic principle of the bismuth scatterer method.

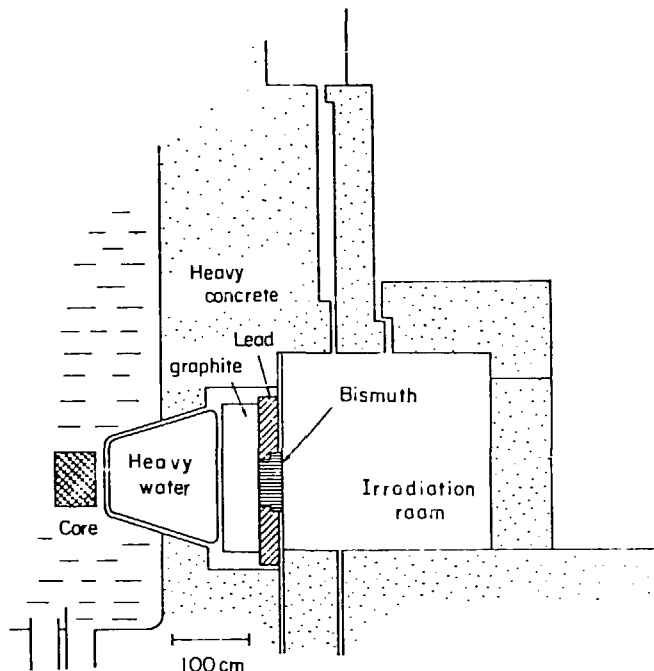


Fig.3 Heavy water facility of KUR (2).

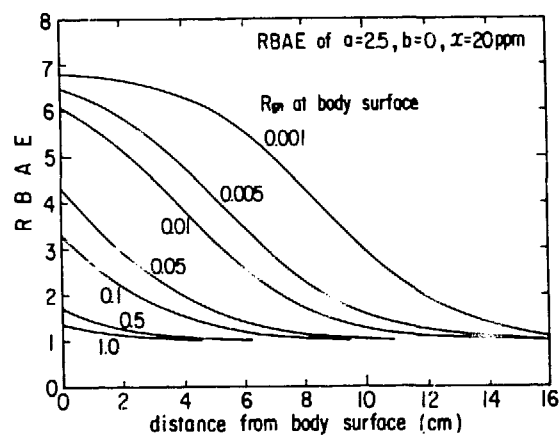


Fig.4 Change in RBAE with tissue depth for different initial gamma-to-neutron ratios.

$$RBAE = \frac{a}{a + 0.129b} + 0.294 \left( \frac{a + 0.129b}{a + 26.0b + 27.1Rgn} \right) x$$

where

a = RBE of heavy charged particles, i.e.,  $^{14}\text{N}(\text{n},\text{p})^{14}\text{C}$ ,  $^{10}\text{B}(\text{n},\alpha)^7\text{Li}$ ,

b = absorbed ratio of  $\gamma$  rays from  $\text{H}(\text{n},\gamma)\text{D}$  reactions in tissue,

Rgn = gamma-to-neutron ratio at body surface, and

x =  $^{10}\text{B}$  concentration (ppm).

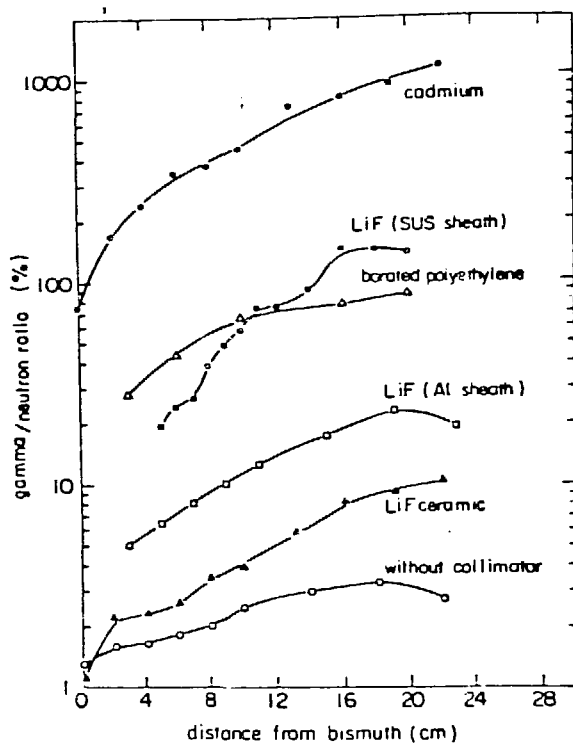


Fig.5 Gamma-to-neutron ratio for different collimating materials.

Neutron flux:  $\sim 3$  to  $5 \times 10^9$  n/cm<sup>2</sup> sec

Gamma-ray dose rate:  $\sim 60$  to  $90$  R/hr

$\gamma/n$  ratio in rad: 0.5%

The KUR is the only reactor of medium power used for joint study among university researches in Japan, so it is in continuous use and not suitable for clinical purposes. The prescheduled reactor operation program for six months prevents the interruption of the schedule by patients. It was used only once for clinical purposes, but is very crowded for fundamental experiments in biology and medicine.

New shielding materials using LiF, e.g. tile, flexible sheet and textile, were developed by KURRI, which do not yield secondary gamma rays and improve the  $\gamma/n$  ratio very much (5, 6, 7), as shown in Fig. 5. Table 1 shows their shielding ability for thermal neutrons. Figure 6 shows thermal neutron transmission for LiF fiber or textile. These materials enable us to make a low-gamma-ray irradiation box for small animals and cells, as shown in Figs. 7 and 8. The temperature in the box is controlled from  $-10^\circ\text{C}$  to  $50^\circ\text{C}$ , which is now commonly used by biologists.

Table 1 Thermal Neutron Shielding Ability for Various Materials

	Thickness (mm)	Density (g/cm <sup>3</sup> )	Neutron transmission
<b>LiF tile</b>			
natural	10	2.51	$2.51 \times 10^{-2}$
enriched	2	2.41	$1.52 \times 10^{-3}$
<b>Sheet</b>			
<sup>6</sup> LiF 40 w/o	5	1.36	$7.30 \times 10^{-3}$
B <sub>4</sub> C 40 w/o	5	1.36	$2.69 \times 10^{-4}$
<b>Textile</b>			
<sup>6</sup> LiF 40 w/o	13.0	*	$1.45 \times 10^{-2}$
B <sub>4</sub> C 40 w/o	12.5	*	$1.25 \times 10^{-2}$
BN 30 w/o	11.7	*	$3.40 \times 10^{-2}$

1) 0.49 g/cm<sup>3</sup>, 2) 0.43 g/cm<sup>3</sup>, 3) 0.47 g/cm<sup>3</sup>  
\* depends on weaving

### 2.3 MITR

The idea to use the bismuth scatterer and LiF tiles was applied to the thermal column of Musashi Institute of Technology Reactor (MITR, 100 kW TRIGA-II) (by O. Aizawa, K. Kanda et al.) shown in Figs. 9 and 10. As the distance between the core and irradiation post and the operation power were limited, the cavity effect on increasing neutron flux was also adapted (8).

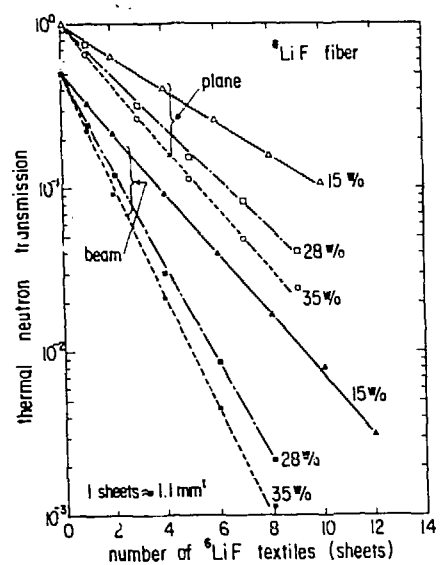


Fig.6 Transmission of thermal neutrons measured for  $^{6}\text{LiF}$  containing textile  
(beam = thermal neutrons from neutron guide tube; plane = thermal neutrons from thermal neutron column).

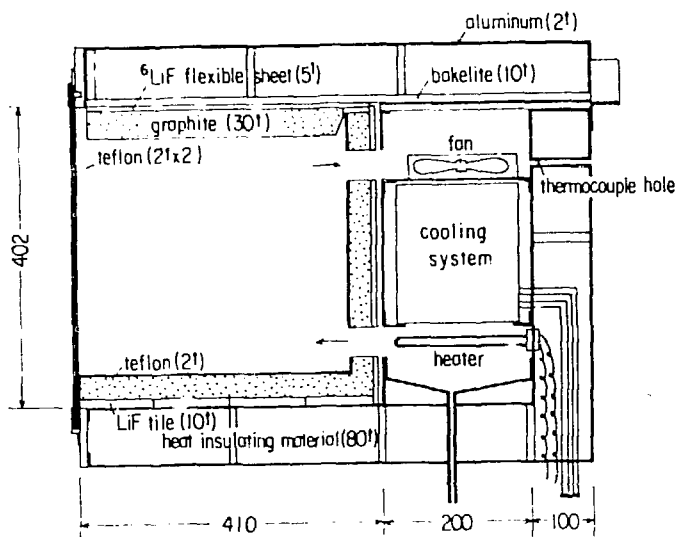


Fig.7 Biological irradiation box with thermo-control system for low-gamma-ray thermal neutrons.

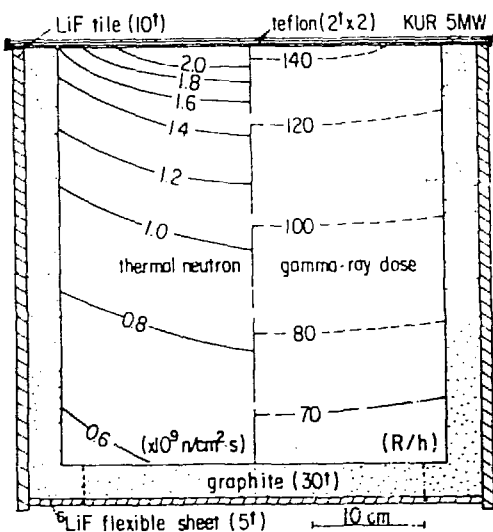


Fig.8 Distribution of thermal neutrons and gamma rays in the irradiation box.

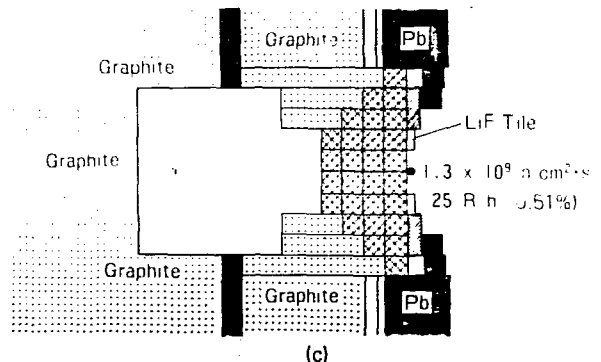


Fig.9 Fine adjustment of bismuth scatterer.

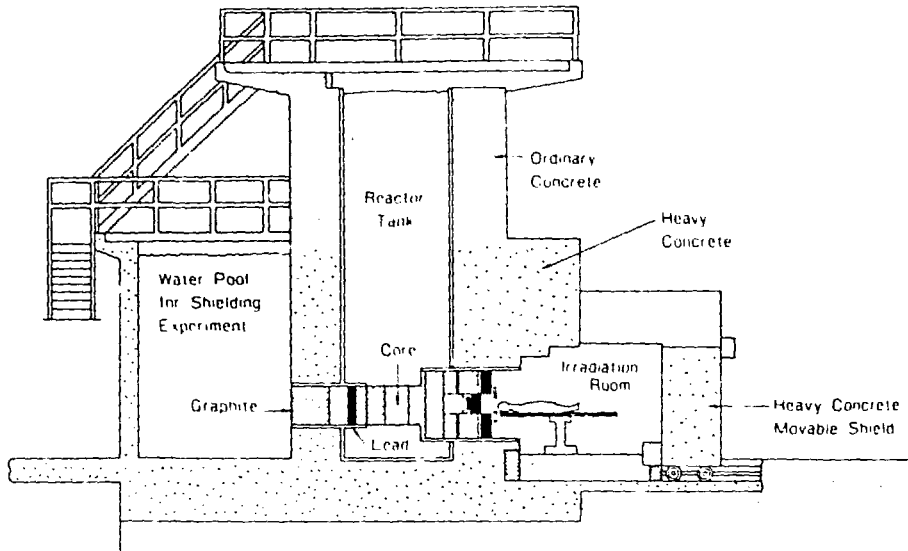


Fig.10 Cross-sectional view of modified MITR.

The thermal neutron flux and gamma-ray dose rate of the facility are,

Neutron flux:  $1.3 \times 10^9 \text{ n/cm}^2\text{-sec}$

Gamma-ray dose rate: 25 R/hr

$\gamma/n$  ratio in rad: 0.15%

The gamma-ray exposure rate distributions with and without a whole-body phantom are shown in Fig. 11.

The facility has been used for brain tumor treatment by Prof. Hatanaka and for other biological experiments.

#### 2.4 YAYOI

The University of Tokyo group (H. Wakabayashi et al.) tried to use the YAYOI (2 kW, fast neutron source reactor) for medical and biological purposes. As shown in Fig. 12, the beam is collimated between the shielding materials, such as polyethelene, borated paraffin and  $B_4C$  with rectangular holes. The irradiation post is 15 cm from the exit of the collimator or from the back surface of the heavy concrete shield (9, 10, 11). This facility has not yet been used for clinical purposes because of the intensity. It was used for measurements of RBE (12).

Another group of the University of Tokyo (S. An, Y. Oka et al.) including many researchers from other universities developed an epithermal

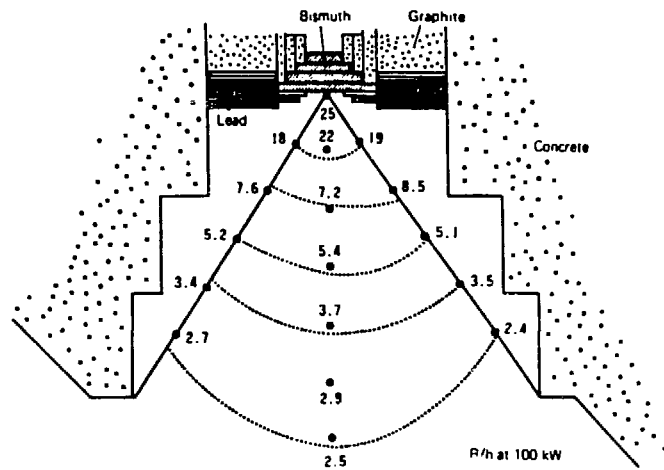


Fig.11  
Gamma-ray exposure rate distributions  
with and without a whole-body phantom.

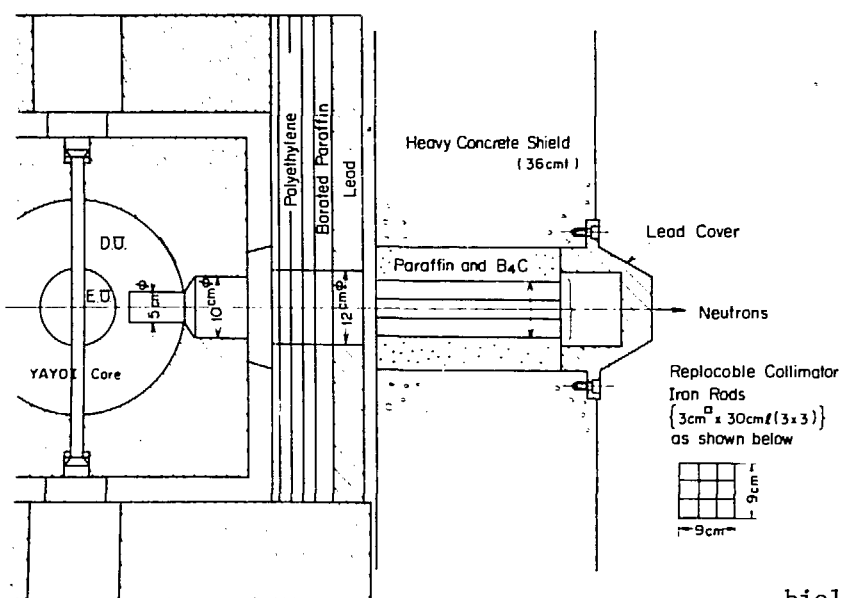
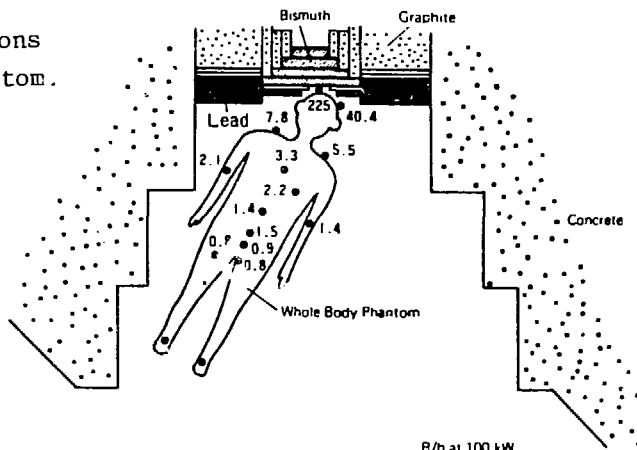


Fig.12  
Irradiation facility  
for medical and  
biological systems at YAYOI.

enriched neutron field for medical purposes using the YAYOI (13). Collimation of the neutron beam and shielding of the irradiation room were obtained with  $^6\text{LiF}$  flexible sheets and a laminated shield plate. The characteristics of the optimized field are as follows:  $\phi_{th} = 3.2 \times 10^8 \text{ n/cm}^2$  sec at a 2.4 cm depth in the head phantom, contaminating fast neutron and gamma-ray local doses are 990 and 357 rem during the required irradiation time, 2.6 hr. The configuration of the column is presented in Fig. 13.

## 2.5 UTR-Kinki

Kinki University group (Y. Honda, R. Miki et al.) remodeled the UTR-Kinki (1 W, twin core) for biological experiments using bismuth blocks and LiF tiles (14). Although the operating power is low, it has been used, for example, for mutation experiments at low dose rates.

## 3. Design of New Facilities for Biological and Medical Irradiations

A research group, including medical doctors, reactor engineers, physicists, chemists, zoologists, and radiation biologists, has been organized by S. An of the University of Tokyo to design a new facility to utilize the epithermal column in a 2 MW TRIGA reactor. The configuration of the epithermal neutron column is shown in Fig. 14 (15, 16).

KURRI has a plan to construct a research reactor of 30 MW, named the KUHFR, Kyoto University High Flux Reactor, to which a special facility for medical irradiation will be attached (17). As shown in Fig. 15, there is a clinical irradiation room in the basement besides a normal irradiation room for basic biology on the core floor.

In medical irradiation facilities heavy water has been commonly used as a moderator. The KURRI group developed a technique to evaluate the effect of  $(\gamma, n)$  reactions of heavy water on beam quality of a biological irradiation facility (18, 19). The reactions were treated as a kind of "up-scatter" in the ANISN-JR code. An example, applied to the KUR Heavy Water Facility, of the technique to calculate neutron flux distributions is shown in Fig. 16.

## 4. Neutron Flux Monitor and Boron Analysis

The absorbed dose in tissue mainly depends on neutron flux and boron concentration. The group of Y. Hayakawa (Tsukuba University) developed a small simultaneous monitoring system of thermal neutron flux, as shown in Fig. 17 (20). It has been used to estimate neutron dose in actual treatment.

The KURRI group developed a microanalysis system of ppm-order boron-10 concentration in tissue for neutron capture therapy by prompt gamma-ray spectrometry (21, 22) as shown in Fig. 18. It was applied to measure the time-dependent boron-10 concentration *in vivo* in tumor of hamsters (23).

## 5. Concentration of Boron-10 Dosage

Two groups at National Institute of Radiological Science (NIRS) and KURRI independently proposed the calculation methods on absorbed dose by heavy charged particles caused by  $^{10}\text{B}(n,\alpha)^7\text{Li}$  reactions in tissue, which made the advantage of selectivity clear (24, 25). The former model is based on

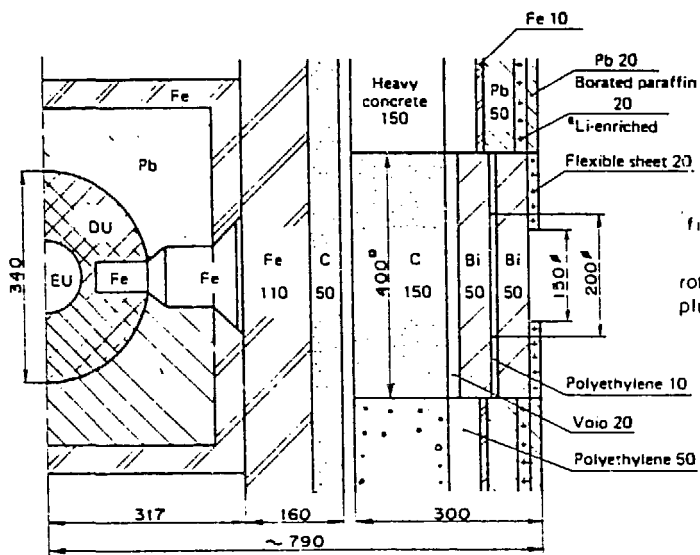


Fig.13  
Epithermal neutron column  
in YAYOI.

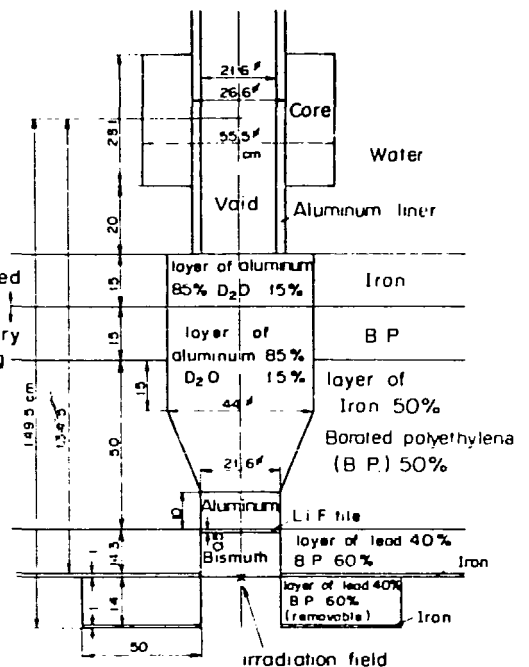


Fig.14  
Configuration of the epithermal  
neutron column in a TRIGA reactor.

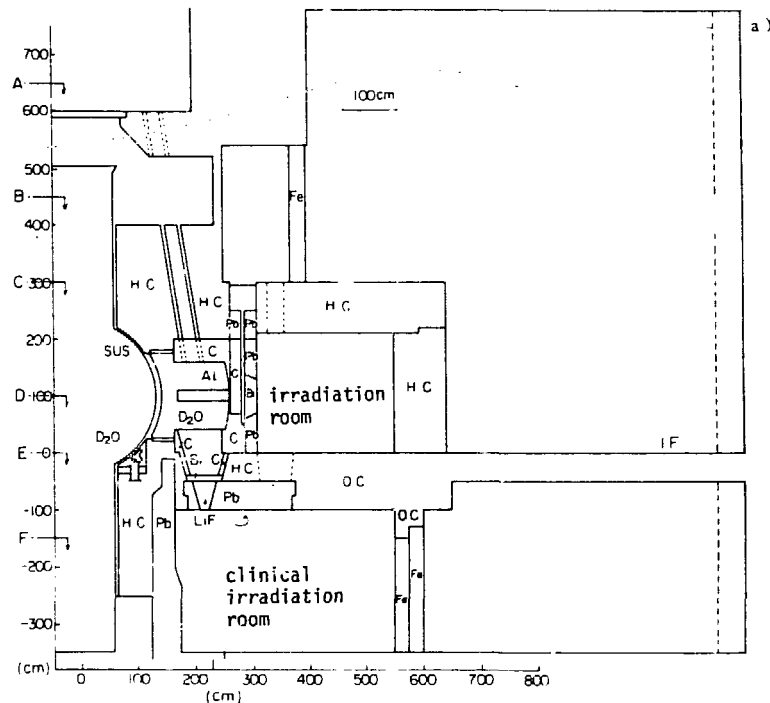


Fig.15 Cross-sectional view of medical and biological irradiation facility at KUHFR.

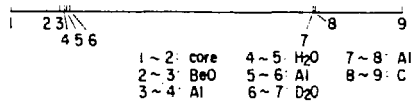
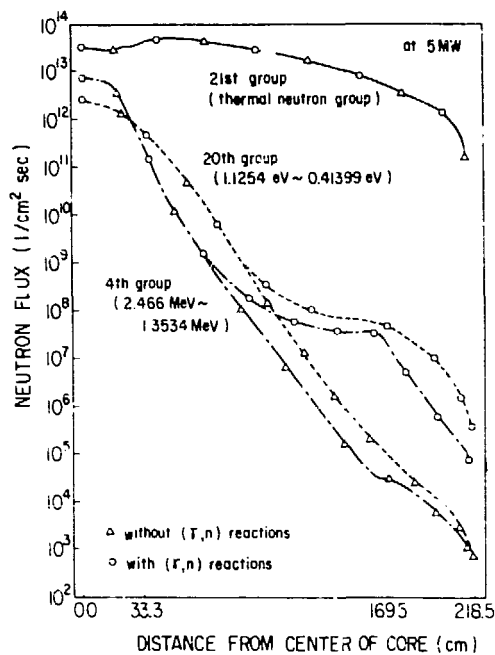


Fig.16 Neutron flux distributions at KUR heavy water facility with and without  $(n,\gamma)$  reactions.

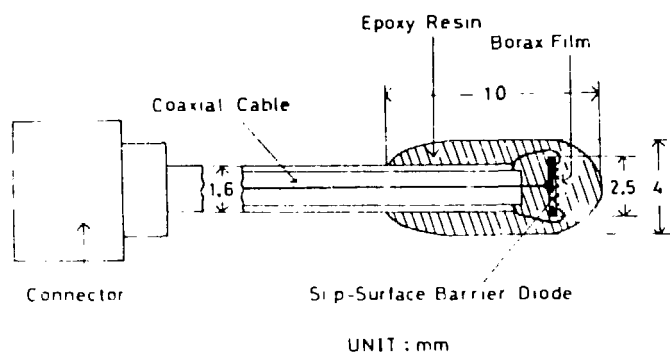


Fig.17  
Cross-sectional drawing of the neutron detector.

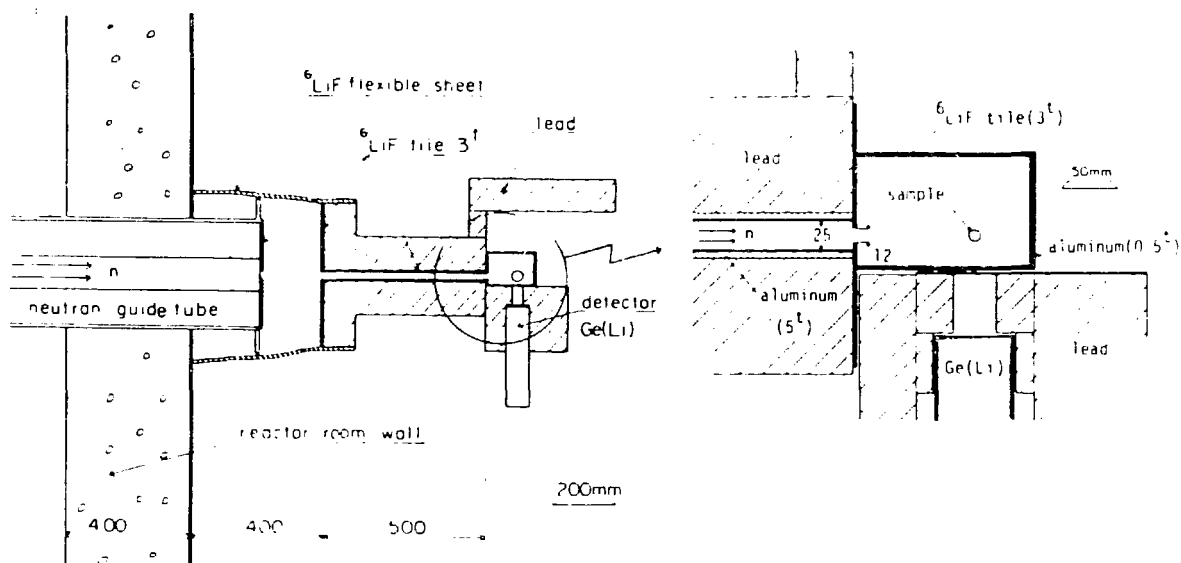


Fig.18 Measuring system of  $^{10}\text{B}(n,\gamma)^7\text{Li}^*$  prompt gamma rays attached to the neutron guide tube of KUR.

a cerebral vascular wall, while the latter model is based on cell level. Figure 19 shows the cell model of  $^{10}\text{B}(\text{n},\alpha)^7\text{Li}$  reactions. Figure 20 shows the surviving fraction versus thermal neutron fluence.

All the above studies except for NIRS were supported by Grant-in-Aid from the Ministry of Education, Science and Culture, and encouraged by Prof. H. Hatanaka of Teikyo University Hospital and Prof. Y. Mishima of Kobe University School of Medicine.

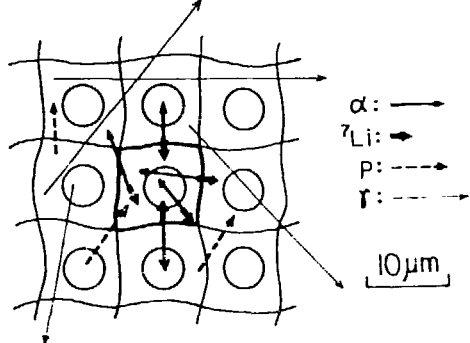


Fig.19 Cell model

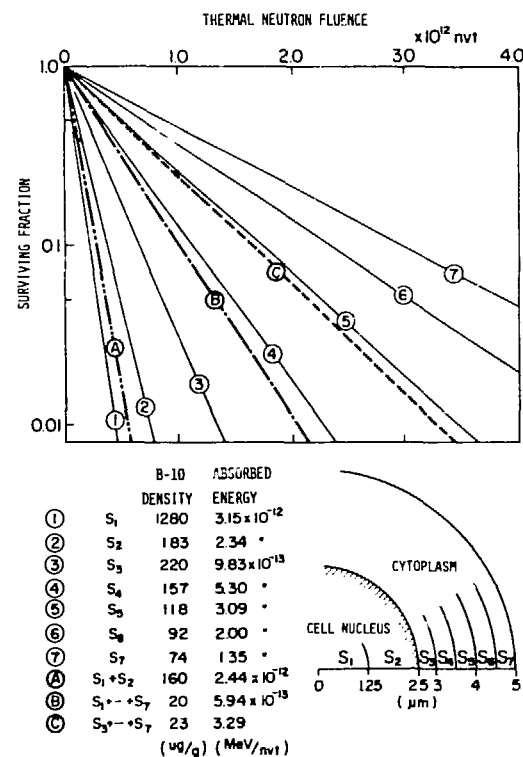


Fig.20 Effect of  $^{10}\text{B}$  distribution in cell on survival fraction (average  $^{10}\text{B}$  concentration : 20  $\mu\text{g}$ ).

#### References

- (1) M. Taguchi, Reactor neutron application for brain tumor therapy in Japan, Japan-Argentine Technology Transfer Forum on "Nuclear Development Technology" (April 1979)
- (2) K. Kanda, T. Kobayashi, K. Ono, T. Sato, Y. Ueno, Y. Mishima, H. Hatanaka, Y. Nishiwaki, Elimination of gamma rays from a thermal neutron field for medical and biological irradiation purposes, Biomedical Dosimetry, IAEA, 205 (1975)

- (3) K. Kanda, Development of neutron field for medical irradiation purposes, J. At. Energy Soc. Japan, 17, 552 (1975)
- (4) K. Kanda, K. Kobayashi, S. Okamoto, T. Shibata, Thermal neutron standard field with a Maxwellian distribution using the KUR heavy water facility, Nucl. Instr. Meth., 148, 535 (1978)
- (5) K. Kanda, T. Kobayashi, O. Aizawa, Reactor neutron field for boron neutron capture therapy of cancers, IAEA-SR-77-31 (1981)
- (6) K. Kanda, Lithium fluoride tile and sheet for neutron shield, J. At. Energy Soc. Japan 20, 37 (1978)
- (7) K. Kanda, T. Kobayashi, M. Takeuchi, S. Ouchi, Development of neutron shielding material using LiF, 6th Int'l. Conf. Radiat. Shield. 12-9 (Tokyo, 1983)
- (8) O. Aizawa, K. Kanda, T. Nozaki, T. Matsumoto, Remodeling and dosimetry on the neutron irradiation facility of the Musashi Institute of Technology Reactor for boron neutron capture therapy, Nucl. Technol., 48, 150 (1980)
- (9) H. Wakabayashi, K. Yoshii, N. Sasuga, H. Yanagi, Radiation field for fission neutron source reactor "YAYOI", J. Nucl. Sci. Technol., 19, 555 (1982)
- (10) H. Wakabayashi and S. An, A conceptual design of neutron tumor therapy reactor facility with YAYOI based fast neutron source reactor, J. Facul. Eng. Univ. Tokyo, 37, (1), 123 (1983)
- (11) H. Wakabayashi, K. Yoshii, N. Sasuga, T. Inada, K. Kawachi, T. Kanai, A. Ito, Dose rate characterization of the biomedical irradiation facility of fast neutron source reactor "YAYOI", J. Facul. Eng. Univ. Tokyo, in press
- (12) H. Wakabayashi, S. Suzuki, A. Ito, Measurement of relative biological effectiveness (RBE) for the radiation beam from neutron source reactor YAYOI, to be published in Radiat. Res.
- (13) S. An, A. Furuhashi, Y. Oka, M. Akiyama, H. Kuga, H. Tanaka, Development studies regarding the construction of epithermal enriched neutron field for medical purposes at the University of Tokyo YAYOI Fast Reactor, Nucl. Technol., 48, 204 (1980)
- (14) Y. Honda et al., Biological irradiation facilities of UTR-Kinki with low dose rate and low dose, to be submitted to J. At. Energy Soc. Japan
- (15) Y. Oka, S. An, Conceptual design of a nuclear reactor facility for medical and biological purposes, J. Facul. Eng. Univ. Tokyo, 34, (2), 15 1981
- (16) Y. Oka, I. Yanagisawa, A design study of the neutron irradiation facility for boron neutron capture therapy, Nucl. Technol., 55, 642 (1981)
- (17) T. Kobayashi, K. Kanda, Design of medical irradiation facility attached to the Kyoto University High Flux Reactor, KUHFR, to be submitted to KURRI-TR
- (18) K. Aoki, S. Shiroya, T. Kobayashi, K. Kanda, T. Shibata, Technique to calculate the effect of ( $\gamma$ , n) reactions of heavy water moderator on beam quality of biomedical irradiation facility, Annu. Rep. Res. Reactor Inst. Kyoto Univ. 15, 27 (1982)

- (19) K. Aoki, K. Kanda, Evaluation of effect of  $(\gamma, n)$  reactions of heavy water moderator in biomedical irradiation facility, *J. Nucl. Sci. Technol.*, in press
- (20) Y. Hayakawa, S. Harasawa, A. Nakamoto, K. Amano, H. Hatanaka, J. Egawa, Simultaneous monitoring system of thermal neutron flux for boron neutron capture therapy, *Radiat. Res.*, 75, 243 (1981)
- (21) T. Kobayashi, K. Kanda, T. Ebisawa, T. Akiyoshi, Development of microanalysis system of  $^{10}\text{B}$  in tissue for neutron capture therapy by prompt  $\gamma$ -ray spectrometry, *Annu. Rep. Res. Reactor Inst. Kyoto Univ.*, 14, 75 (1981)
- (22) T. Kobayashi, K. Kanda, Microanalysis system of ppm-order  $^{10}\text{B}$  concentrations in tissue for neutron capture therapy by prompt gamma-ray spectrometry, *Nucl. Instr. Meth.*, 204, 525 (1983)
- (23) T. Hamada, K. Aoki, T. Kobayashi, K. Kanda, The in vivo measurement of the time-dependent  $^{10}\text{B}$  movement in tumor of hamsters, *Annu. Rep. Res. Reactor Inst. Kyoto Univ.*, in press
- (24) K. Kitao, A method for calculating the absorbed dose near interface from  $^{10}\text{B}$   $(n, \alpha)\text{Li}$  reaction, *Radiat. Res.*, 61, 304 (1975)
- (25) T. Kobayashi, K. Kanda, Analytical calculation of boron-10 dosage in cell nucleus for neutron capture therapy, *Radiat. Res.*, 91, 77 (1982)

## Design Study of Facilities for Boron Neutron Capture Therapy

Yoshiaki Oka and Shigehiro An  
Nuclear Engineering Research Laboratory,  
Faculty of Engineering, University of Tokyo,  
Tokai-mura, Ibaraki, 319-11, Japan

### RESEARCH GROUP ON BNCT IN JAPAN (1975-1979)

One of the authors, S. An, organized a research group on boron neutron capture therapy (BNCT) during 1975 to 1979 with financial aid from the Ministry of Education, Science and Culture, Grant-in-Aid for Developmental Scientific Research No. 189007(1975-77) and No. 389001(1978-79). The group consisted of medical doctors (H. Hatanaka, K. Sano, T. Minobe, Y. Mishima, H. Mogami, K. Kitamura, J. Egawa, Y. Iino, and T. Watanabe), reactor engineers and physicists (S. An, Y. Oka, A. Furuhashi, H. Wakabayashi, A. Sekiguchi, K. Kanda, T. Shibata, K. Sumita, T. Sato, Y. Murata, M. Hattori, S. Harasawa, M. Saito, K. Kitao, T. Nozaki, R. Miki, M. Hachiya, M. Taguchi, S. Arai, and S. Sakamoto), chemists (M. Okamoto, H. Kakihana, and S. Sumimoto), a veterinarian (A. Takeuchi), and a radiation biologist (Y. Ueno). Therapy and development of irradiation fields were two major objectives of the group. Some of the studies were partly supported financially, for example (a) clinical trials at Musashi Institute of Technology reactor by H. Hatanaka, (b) a study of epithermal neutron field and design of a reactor facility for BNCT, which were performed at the University of Tokyo, (c) remodeling of the Musashi Institute of Technology reactor for BNCT, (d) research on thermal neutron fields for BNCT at Kyoto University Research Reactor Institute, (e) study of simultaneous monitoring of thermal neutron fluence rate during therapy, etc. Meetings were held frequently. The results of the researches were summarized in two Japanese reports (1,2). It was concluded in 1976 that a nuclear reactor facility was required for developing BNCT and related research. Conceptual design of the facility was performed according to consultation among the group members (3-5).

### OPTIMUM NEUTRON ENERGY FOR BNCT

The authors concentrated on study of an epithermal neutron field for BNCT. Irradiation with epithermal neutrons shows deeper penetration in tissue than with thermal neutrons (6). Fast neutron and gamma-ray contamination should be minimized, while epithermal neutron level is kept high enough for the therapy.

Optimum neutron energy for BNCT was studied using a two-dimensional discrete ordinates transport code TWOTRAN-II. The group constants used were neutron (13 groups) and gamma-ray (3 groups) coupled cross sections based on ENDF/B-IV and PUPOP4 libraries. Neutron KERMA factors were calculated from the data in ICRU Report No. 13. The dose conversion factors of the  $^{10}\text{B}$  reaction were calculated based on the Q values and the absorption cross sections (7). A head model of a man was used for the calculation. It was fashioned as

a cylinder of dimensions 16.6 cm in diameter and 23 cm in height. The neutron beam was uniformly incident on the bottom face of the model. The tissue composition was approximated by Rossi fluid. The neutron and gamma-ray distributions in the phantom were calculated for varying energy of incident neutrons. The dose rates of neutrons and gamma rays were figured out based on the distributions. The dose rates by the  $^{10}\text{B}(\text{n},\alpha)^7\text{Li}$  reaction were also calculated by assuming that 30  $\mu\text{g}$  and 10  $\mu\text{g}$  of  $^{10}\text{B}$  were contained in tumor and capillary respectively.

The dose-depth distributions for irradiation by fast neutrons (3.3 to 0.82 MeV) are presented in Fig. 1. This figure shows that fast neutrons are not suitable for BNCT because of the low  $^{10}\text{B}$  dose rate. The dose-depth distribution for thermal neutrons is presented in Fig. 2. Although the  $^{10}\text{B}$  dose is very high, the dose distribution decreases very rapidly in the phantom. The dose-depth distribution for epithermal neutrons (130 to 29 eV) is shown in Fig. 3. Maximum dose is observed in the phantom, and the attenuation is not so rapid. It can be seen from these figures that epithermal neutrons are most suitable for BNCT.

The concept of maximum usable depth (MUD) has been used for evaluation of the dose-depth distributions. It is defined as the depth in tissue where the total dose to  $^{10}\text{B}$ -loaded tumor equals the limit of the dose to normal tissue with a given  $^{10}\text{B}$  concentration. In this study the limit was assumed to be 0.4 times the maximum dose level of normal tissue loaded with 10  $\mu\text{g}$   $^{10}\text{B}$  per gram of tissue. The concentration of  $^{10}\text{B}$  in tumor was assumed to be 30  $\mu\text{g}/\text{g}$  of tissue. That is, the maximum dose limit of normal tissue loaded with 10  $\mu\text{g}$  of  $^{10}\text{B}$  was assumed to be 5000 rad, while the lower limit to destroy tumor loaded with 30  $\mu\text{g}$  of  $^{10}\text{B}$  was assumed to be 2000 rad. The values of MUD for irradiation with monoenergetic neutron beams having the energy of each group are summarized in Fig. 4 together with the values of the neutron dose at the brain surface, when the total dose reaches 20 Gy (2000 rad) at the MUD. The figure shows that epithermal neutrons having energies between 10 eV and 0.5 keV are suitable for the present purpose. Maximum usable depth is 7 cm for epithermal neutrons and 5 cm for thermal neutrons.

#### DESIGN OF EPITHERMAL AND THERMAL NEUTRON COLUMNS

Various kinds of neutron sources were evaluated for BNCT with epithermal neutrons. The results were summarized in a Japanese report (8). A thermal reactor was thought to be superior to an intermediate energy nuclear reactor and a  $^{252}\text{Cf}$  source, because of the limited experience with intermediate reactors, and the cost and availability problems of  $^{252}\text{Cf}$ . An annular core TRIGA reactor was chosen as a source. The neutrons leaking downward through the central hole are convenient for treating patients. It was also thought that the beam contains rather less fast neutrons than a direct beam from the core. In order to obtain epithermal neutrons, the neutrons from the core should be moderated by putting moderation materials or spectrum shifters in the central hole and below the core. The ratios of the leakage neutron fluxes with and without moderation materials in the core are presented in Fig. 5. The figure shows the characteristics of various moderating materials. The horizontal axis of the figure shows neutron energy. The first group is for fast neutrons and the 13th is for thermal neutrons. Fast neutrons should be

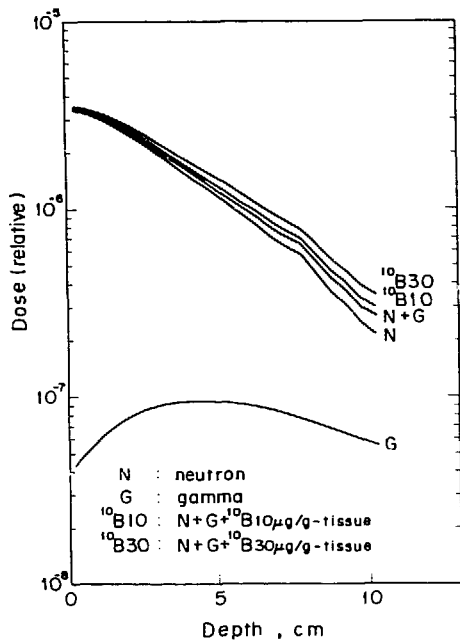


Fig. 1. Calculated dose distribution in the head irradiated by fast neutrons (3.3 to 0.82 MeV).

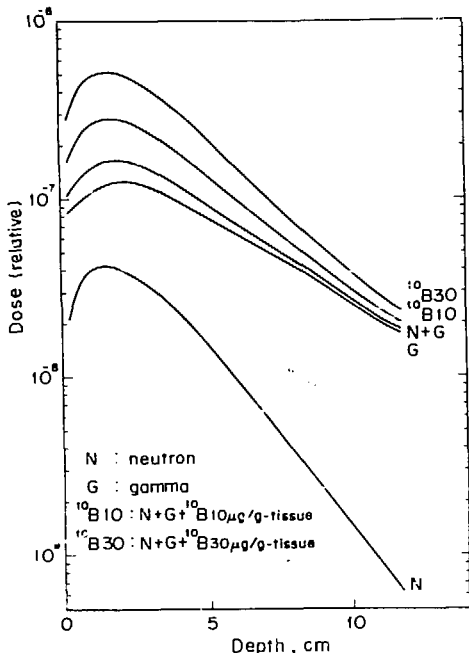


Fig. 3. Calculated dose distribution in the head irradiated by epithermal neutrons (130, 50, 29 eV).

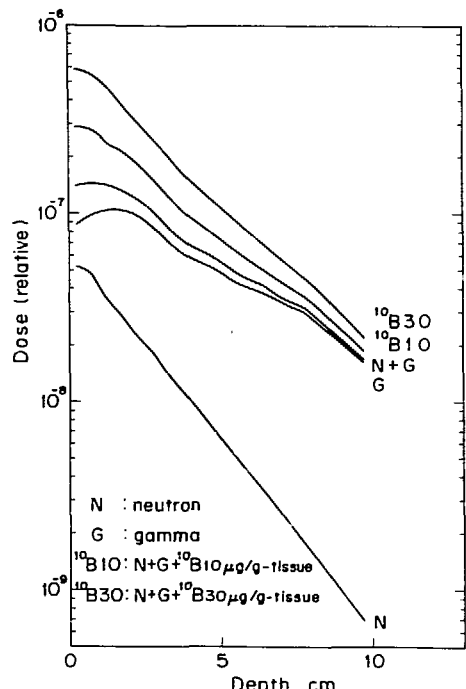


Fig. 2. Calculated dose distribution in the head irradiated by thermal neutrons (0.4 to 0.001 eV).

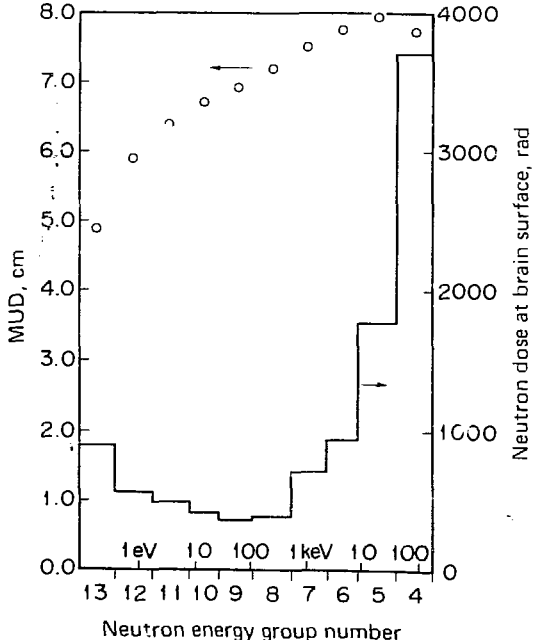


Fig. 4. MUD and neutron dose for irradiation with monoenergetic neutron beams.

attenuated as much as possible without attenuating epithermal neutrons. The figure shows that a combination of aluminum and heavy water is effective for the purpose. The leakage neutrons still contain a large fast component. The materials should be used as thick layers under the central hole of the core. The optimum volume ratio of heavy water to aluminum was studied. The ratios of group fluxes through a 77.5-cm-thick mixture of aluminum and heavy water are presented in Fig. 6. The results are normalized to the ninth group flux for each case, and the values of the fluxes are also presented. The figure shows that the neutron spectrum is greatly improved by adding 10% of heavy water to aluminum, while the addition of a higher percentage of heavy water decreases intensity. A mixture of aluminum with 10 to 20% heavy water is suitable for the present purpose.

After extensive study of configuration of layers, shielding against gamma rays and thermal neutrons in the beam, and also biological shielding surrounding the moderating layers, we obtained a final configuration of the epithermal neutron column, which is shown in Fig. 7. The details of the optimization study are presented in Ref. 3. The volume fractions of the moderating layer are aluminum 85% and heavy water 15%. LiF tiles are used for removing thermal neutrons. A 15-cm-thick bismuth layer is used for decreasing gamma rays. The shield surrounding the column consists of iron, borated polyethylene, and

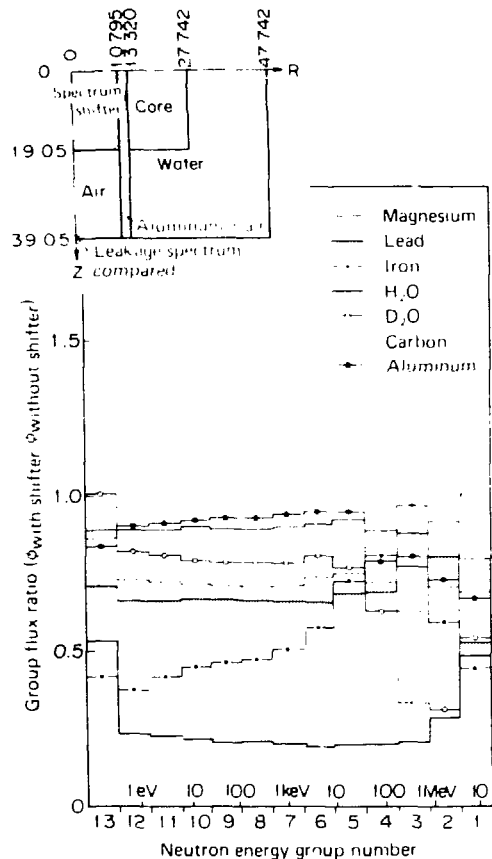


Fig. 5. Effect of various spectrum shifters on leakage neutron spectrum.

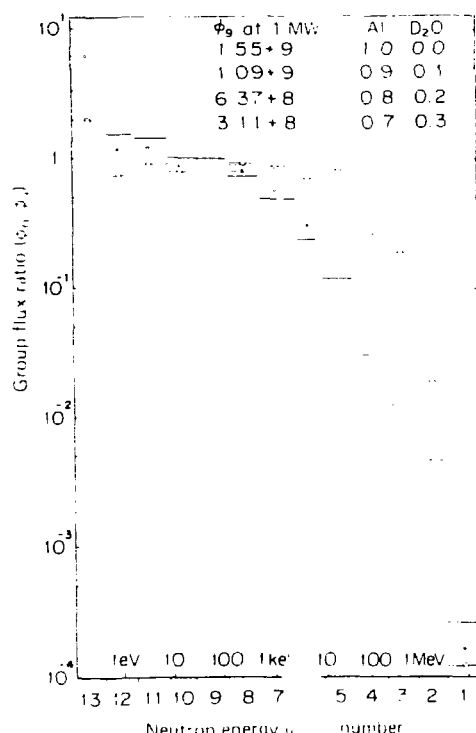


Fig. 6. Effect of the volume ratios of aluminum and heavy water on the transmitted neutron spectrum through a 77.5-cm-thick mixture.

lead. The dose-depth distribution in the phantom head irradiated at the column is shown in Fig. 8. The profile shows maximum dose at 1.5-cm depth. The MUD is about 7 cm. The fast neutron component is only  $30 \text{ rad h}^{-1} \text{ MW}^{-1}$ . The dose rate of the  $^{10}\text{B}$ -containing tissue is  $680 \text{ rad h}^{-1} \text{ MW}^{-1}$ . The irradiation time for BNCT is about 7 hours at a power of 2 MW. Relative biological effectiveness (RBE) is not considered in this study because it is difficult to assign definite RBE values for the beam of the present study. If RBE is considered, the irradiation time is 3 hours at 2 MW and MUD is again about 7 cm. Here the assigned values of RBE are 1.0 for gamma rays, 2.0 for neutrons, and 3.7 for the  $^{10}\text{B}(\text{n},\alpha)^7\text{Li}$  reaction.

Thermal neutrons are superior to epithermal neutrons for the treatment of shallow seated tumors. Some calculations were performed for the design of a thermal neutron column. The results are shown in Fig. 9. Heavy water is used as thermalization material. The dose-depth distribution in the head is shown in Fig. 10. MUD is about 5 cm. The time for the therapy is 1.3 hours at 2 MW. If RBE is considered, the time becomes 30 minutes. A void region in the column is supplied for maintaining neutron intensity because the total length of the column should be the same as that of the epithermal neutron column if they are built into one rotary plug. The length can be less if a thermal neutron column is built alone. The key issue of optimization would be effective attenuation of fast neutrons without decreasing intensity of low energy neutrons. If both the heavy water zone and the layer of aluminum and heavy water in Fig. 9 are replaced with graphite, the fast neutron dose at the surface of the head phantom during therapy becomes about ten times the present value. If one wants to use graphite as a thermalization material for BNCT, fast neutron contamination should be screened out. A two-dimensional Sn calculation would be a very powerful tool for designing and evaluating an irradiation field.

#### DESIGN OF A REACTOR FACILITY FOR BNCT

A reactor building was designed according to the above results. A cross-sectional view is shown in Fig. 11. There are one vertical and two horizontal irradiation rooms. The column between the core and the vertical irradiation room consists of a rotary plug and a fixed part to support the reactor core. The epithermal column, the thermal column, and a shield are set in every 120 degree sector of the rotary plug. When treatment is not being performed, the shield is set below the core, and the background dose level of the room becomes very low. One of the horizontal irradiation rooms is for thermal neutron therapy and the other is for epithermal neutron therapy. Surgical operation and monitoring of patients can be performed in the neighboring rooms. Design of a whole reactor facility was also performed. The facility consists mainly of the reactor, a hospital, and a research building. All kinds of research on neutron capture therapy can be performed at the facility.

#### EXPERIMENTAL STUDY OF EPITHERMAL NEUTRON FIELD AT YAYOI

The epithermal neutron field was studied experimentally at the fast neutron source reactor, YAYOI, of the University of Tokyo (9). A neutron beam

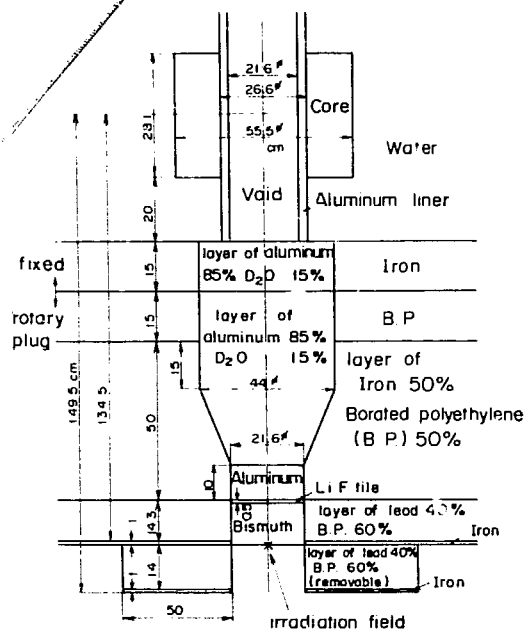


Fig. 7. Configuration of epithermal neutron column.

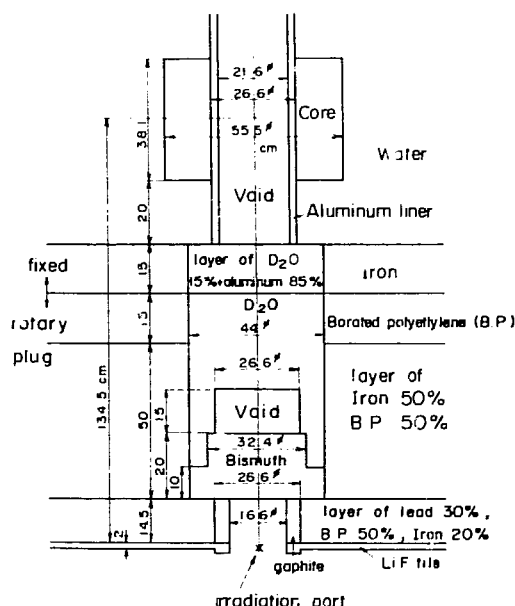


Fig. 9. Configuration of thermal neutron column.

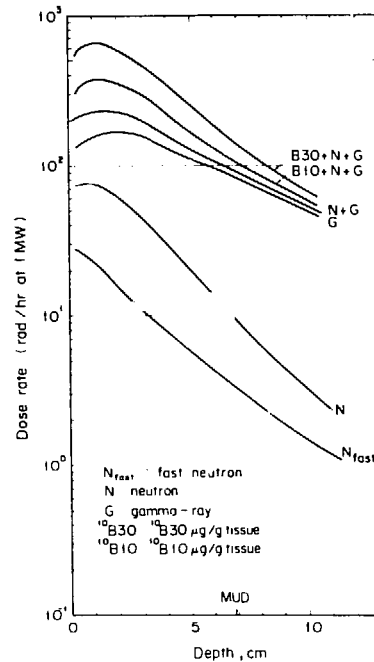


Fig. 8. Dose-depth distribution in the phantom head irradiated at the epithermal neutron column.

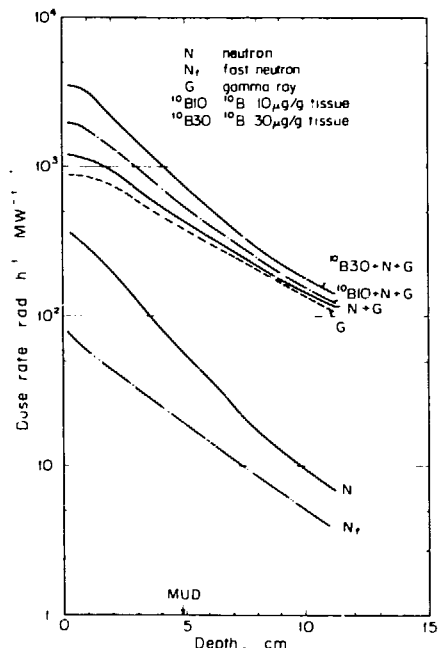


Fig. 10. Dose-depth distribution in the phantom head irradiated at the thermal neutron column.

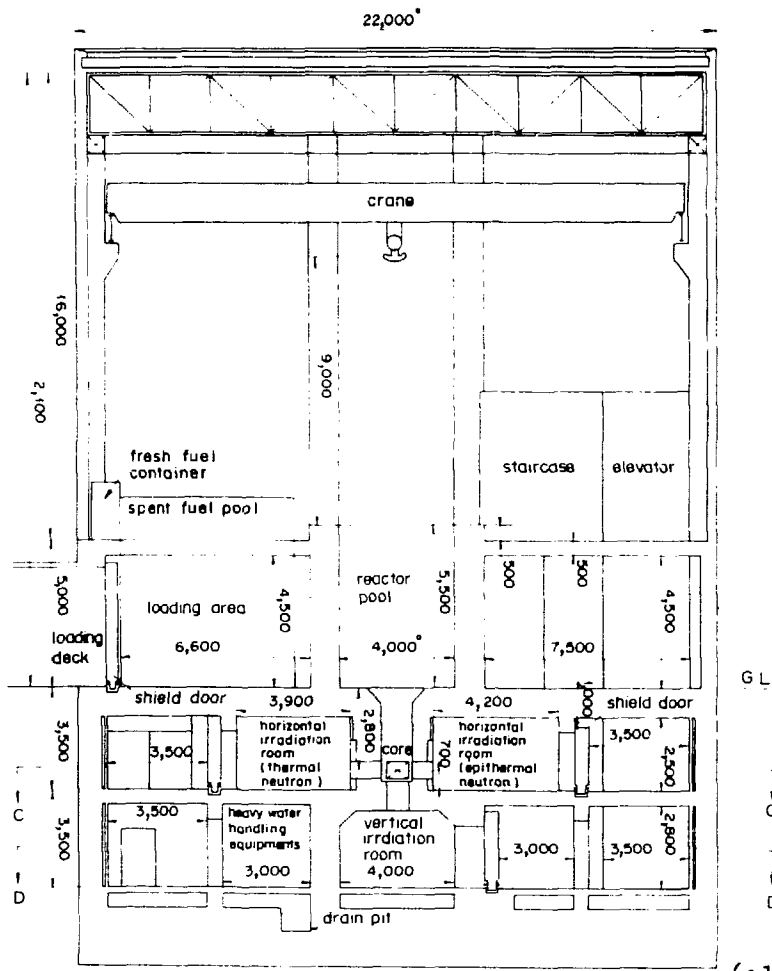


Fig. 11. Reactor building (elevation) (dimensions in mm.).

column was constructed for the study. Depth-flux curves in a head phantom were measured with combinations of iron, graphite, polyethylene, lead, and bismuth layers in the column. Combinations and thickness were optimized in order to obtain high thermal neutron fluence ( $3 \times 10^{12}$  nvt) at a 2.4-cm depth in the phantom under tolerable contamination of fast neutrons and gamma rays. The optimized configuration is shown in Fig. 12. Characterization of the irradiation field was performed by using a tissue-equivalent ionization chamber, a LET counter, gold foils, a rem counter, and TLDs (10,11). Fast neutron dose was found to be still high, but source intensity, or reactor power of YAYOI, is too low to add more layers under the limit of irradiation time. The maximum power level of YAYOI is only 2 kW. The authors are not satisfied with the field as an epithermal neutron field, but it has been used for basic research. Irradiations of beagles and mice were performed at the column. The effect of collimator size on the neutron intensity in the head phantom was studied. The thermal neutron flux in the phantom greatly increases with the diameter of the LiF collimator (11). This characteristic should be incorporated in procedures used during BNCT.

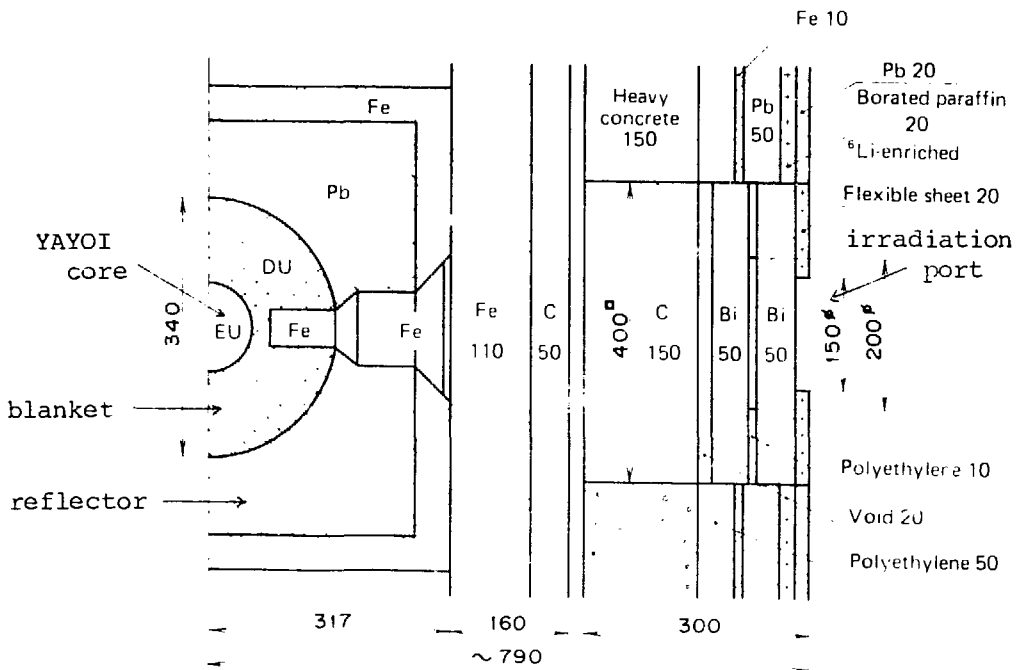


Fig. 12. Neutron column of YAYOI for biomedical research (elevation) (dimensions in mm).

#### CALCULATION FOR A $^{45}\text{Sc}$ 2-keV NEUTRON FILTER

Design of a beam filtered by  $^{45}\text{Sc}$  for BNCT and biological research was studied by calculation (12). The calculational method was similar to that for the epithermal neutron column study. DOT 3.5 was used instead of TWOTRAN-II. ANISN was used for a one-dimensional parametric survey. There were no evaluated cross sections of  $^{45}\text{Sc}$  for transport calculations. One of the authors, Y. Oka, had to evaluate neutron nuclear data on  $^{45}\text{Sc}$  (13). The evaluated data were included in a Japanese evaluated nuclear data library, JENDL-2. Group constants of  $^{45}\text{Sc}$  for transport calculation was prepared from the data by using the RADHEAT-V3 code system (14). Account was taken of group structure at 2 keV in order to represent the cross section minimum of  $^{45}\text{Sc}$ . An extensive parametric survey was performed. YAYOI was modeled as a neutron source. The result showed that (a) a mixture of aluminum and heavy water effectively decreases fast neutrons; (b) a layer of 2-cm-thick cobalt is good for removing leakage neutrons through higher resonance windows of  $^{45}\text{Sc}$ ; (c) the optimum scandium filter length is about 90 cm. A model for two-dimensional calculation is shown in Fig. 13. The relation between filter radius and transmitted neutron flux, dose, and purity was studied using the model. Purity is the percentage of 2-keV component in the total dose or flux. The result at 2-kW reactor power level is shown in Fig. 14. Intensity of the beam increases with the filter radius, while the "dose purity" decreases. Regrettably the intensity of the dose is too low for medical and biological re-

search. Furthermore, gamma rays were not taken into account for the above calculation. When they were taken into account, the dose purity, percent of 2-keV neutron dose in the total dose, became only 3%. This is due to capture gamma rays from  $^{45}\text{Sc}$ . The secondary gamma-ray production data were taken from the POPOP-4 library. The data whose identification number is 210101 were used. These were the only gamma-ray production data on  $^{45}\text{Sc}$  that we found. Extensive calculation was performed in order to improve dose purity and beam intensity. The final model for two-dimensional calculation is shown in Fig.

15. A LiF tile was used to decrease thermal neutron leakage to the scandium zone. A manganese reflector was used to increase 2-keV neutrons. Lead was used to decrease gamma rays. The dose purity at the beam exit becomes 57%, but the intensity of the 2-keV dose decreases to  $3.75 \times 10^{-3} \text{ rad h}^{-1}$  at 2 kW. The result is far from satisfactory for medical and biological research. Calculation for a scandium filter using a TRIGA reactor as a source was also performed. The best result showed 43% dose purity and  $2.5 \times 10^{-2} \text{ rad h}^{-1}$  of 2-keV neutron dose at 100-kW level. The result is still unsatisfactory for the purpose.

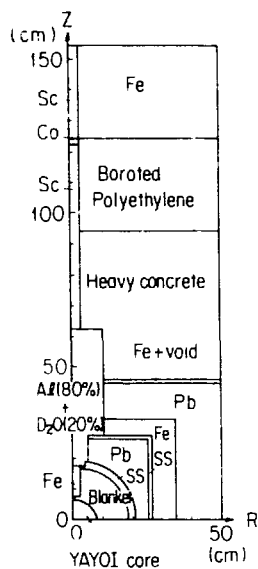


Fig. 13. Calculational model of a filtered beam column using  $^{45}\text{Sc}$ .

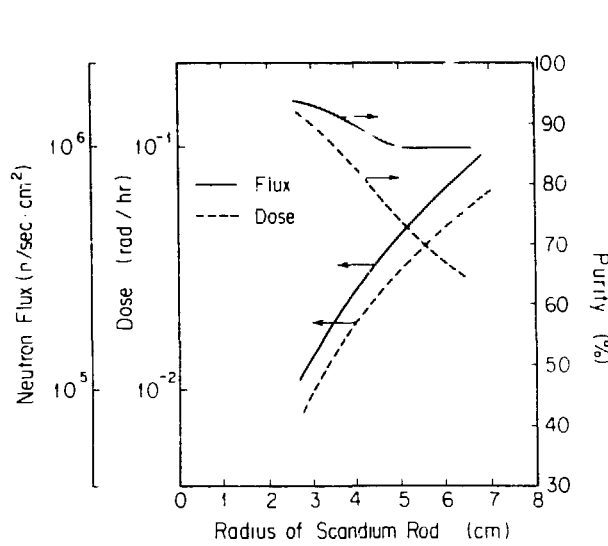


Fig. 14. Relation between scandium filter radius and 2-keV neutron flux, dose, and purity at the beam exit.

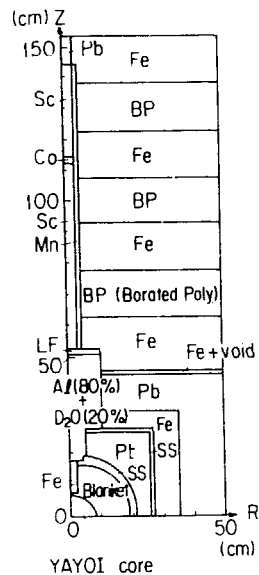


Fig. 15. Final calculational model of a filtered beam column using  $^{45}\text{Sc}$ .

## SUMMARY

1. A research group on BNCT which was organized by one of the authors, S. An, during 1975 to 1979 had great success in clinical trials and development of irradiation fields.
2. Calculated dose-depth distribution in a head shows that optimum neutron energy for BNCT is between 10 eV and 500 eV.

3. Layers of aluminum and heavy water whose volume ratio is 85/15 are effective in decreasing fast neutrons while maintaining a high epithermal neutron level.
4. Conceptual design of epithermal and thermal neutron columns and a reactor facility based on an annular core TRIGA reactor is completed. Heavy water is far superior to graphite as thermalization material for BNCT. Two-dimensional discrete ordinates transport calculation is a powerful tool for design and evaluation of an irradiation field.
5. Calculation for a  $^{45}\text{Sc}$  2-keV neutron filter for biomedical research reveals the problems of weak beam intensity and a high level of capture gamma rays from scandium.

#### REFERENCES

1. UTNL-R-0058, Nuclear Engineering Research Lab., U. of Tokyo, (1978) (in Japanese).
2. UTNL-R-0081 (1980) (in Japanese).
3. Y. Oka et al., Nucl. Technol. 55, 642 (1981).
4. Y. Oka et al., J. Fac. Engineering, U. of Tokyo (B) 36, No. 2, 15 (1981).
5. UTNL-R-0093 (1980) (in Japanese).
6. R.G. Fairchild, Phys. Med. Biol. 10, 491 (1965).
7. R.G. Zamenhof et al., Med. Phys. 2 47 (1975).
8. UTNL-R-0076 (1979) (in Japanese).
9. S. An et al., Nucl. Technol. 48, 204 (1980).
10. UTNL-R-0084 (1979) (in Japanese).
11. UTNL-R-0095, p. 6 (1979) (in Japanese).
12. Y. Oka et al., UTNL-R-0148 (1983) (in Japanese).
13. Y. Oka et al., JAERI-M-9981 (1982).
14. Y. Oka et al., Nucl. Sci. Eng. 73, 259 (1980).

## Mixed Dose Distributions of Fast Neutrons and Boron Neutron Captures for the Fast Neutron Beam from YAYOI

Hiroaki Wakabayashi, Koji Yosii, Norihiko Sasuga, and Hideharu Yanagi  
Nuclear Engineering Research Laboratory, Faculty of Engineering,  
The University of Tokyo, Shirakata Tokai-mura, Ibaraki, Japan

### 1. INTRODUCTION

In our efforts to develop boron neutron capture therapy (BNCT), thermal neutron based research and therapy have been conducted with some success. Thermal neutrons, however, are rather limited in penetration into tissue, and therefore deep-seated tumors are outside the scope of BNCT. Thermal neutrons, furthermore, tend to produce a captured photon background; the smaller this portion, the better for BNCT. Doctors are, thus, requesting a specific medical reactor which can provide intense intermediate neutrons. Neutrons, born as fast fission neutrons, undergo moderation into thermal neutrons through intermediate energy regions in moderating media. Without a specifically designed powerful intermediate neutron source reactor, it is usually difficult to form a usable intermediate neutron flux with little photon contamination for deep-seated tumor BNCT.

A new approach between fast neutron therapy and BNCT may be valuable to the extent it is feasible.

### II. A NEW APPROACH (1)

A fast neutron source reactor, a low powered research reactor based on a highly enriched uranium metal core (YAYOI for example), can alleviate the weak points of thermal reactor based BNCT. With the use of such a fast neutron beam as a radiation source into tissue, a better dose distribution with less photon contamination can be obtained.

Fast neutrons have nearly 0.9 MeV as an average initial energy after inelastic collisions in the core and, thus, are expected to have far greater penetration than thermal neutrons. Fast neutrons, though deficient in selectivity for BNCT, can be introduced directly into a central part of a bulky tumor, where slowing down and diffusion processes are expected to form a thermal neutron flux most desirable for BNCT with a boron distribution pronounced at the infiltrated periphery of a bulky tumor. In this way, a boosting of dose can be accomplished.

With this in mind, extensive measurements of neutron fluxes and doses (fast and thermal neutrons and photons) were done for both a water phantom and a body phantom. Preferable dose intensity and profiles were found which seem applicable for fast neutron therapy with a boost provided by BNCT.

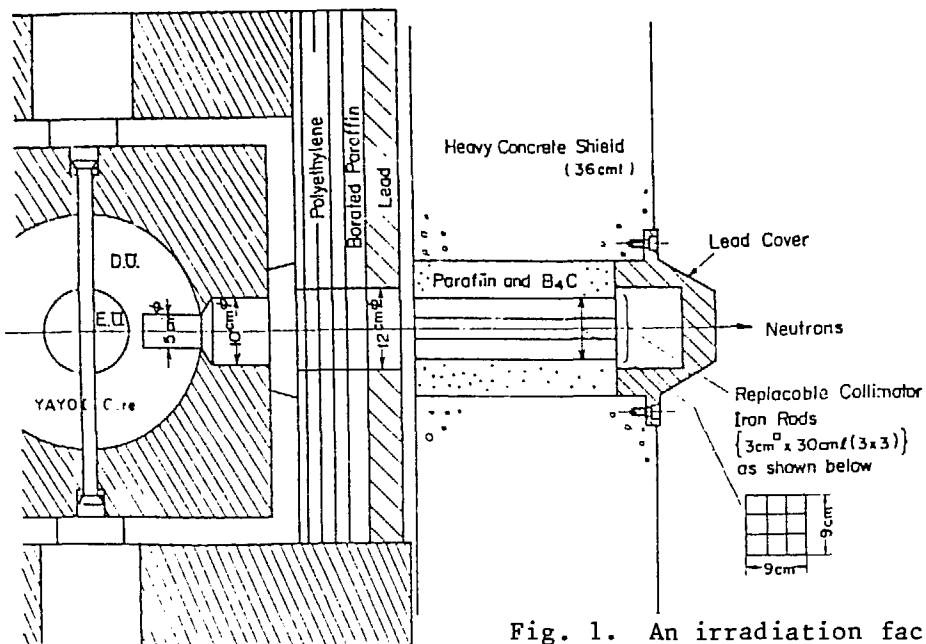


Fig. 1. An irradiation facility for medical and biological systems at YAYOI.

### III. YAYOI AND ITS BIOMEDICAL FACILITY

YAYOI (2) is a 2-kW rated fast neutron source reactor fueled with 28 kg Eu (93%). The maximum flux at the core center is  $10^{12}$  n/cm<sup>2</sup>·sec with an average neutron energy of nearly 900 keV. An irradiation facility (Figure 1) was devised to study irradiation effects on biomedical systems at a distance of 1 m from the core center.

The beam is collimated between the shielding materials, such as polyethylene, borated paraffin, lead, heavy concrete, and a special collimator made of paraffin and B<sub>4</sub>C with rectangular holes (the shape can be varied from 3x3 cm<sup>2</sup> up to 9x9 cm<sup>2</sup> for wider and irregular collimations by use of 9 replaceable iron rods of 3x3 cm square). The irradiation front is 15 cm from the exit of the collimator or from the back surface of the heavy concrete shield, which serves as a biological shield for the whole body of a patient.

### IV. DOSE RATE DISTRIBUTION IN AND AROUND WATER AND BODY PHANTOM

#### a. Dose Rate Distribution in Water Phantom

Placing a 30-cm cubic water phantom at a distance of 15 cm away from the exit of 3x3 cm<sup>2</sup> and 9x9 cm<sup>2</sup> collimators, fast neutron and photon dose rate (D<sub>f</sub>, D<sub>G</sub>) distributions were measured both axially and laterally by paired ionization chambers (shown in Figure 2). In a similar manner, but using gold foils with and without cadmium cover and taking the difference, thermal neutron flux distribution was measured.



0                    3cm  
 Center Line  
 $\sim 16 \text{ mm}^2$   
 Ionization Volume  
 $\sim 3 \text{ cc}$

1) Tissue Equivalent Chamber For Total Dose (TE Plastic + TE Gas)  
 $R_T = 0.97 D_n + 1.04 D_g \quad 0.611 \text{ v/rad}$  (for  $\text{CO}^{60}$ )

2) Carbon Chamber For Gamma Dose (Graphite-Teflon +  $\text{CO}_2$  Gas)  
 $R_C = 0.008 D_n + 1.04 D_g \quad 0.932 \text{ v/rad}$  (for  $\text{CO}^{60}$ )

Fig. 2. Gas-flow type paired ionization chambers.

In order to estimate absorbed doses, all units were converted into units of Gy/min, with the following values as KERMA factors:

Thermal neutrons ( $D_{th}$ )       $0.0149 \times 10^{-11} \text{ Gy/fluence}$

Fast neutrons ( $D_f$ )       $2.37 \times 10^{-11} \text{ Gy/fluence}$  (for 1-MeV neutrons)

Boron ( $n,\alpha$ ) reaction ( $D_B$ )       $7.27 \times 10^{-14} \text{ Gy/thermal fluence}/\mu\text{g/g}$

Here  $\mu\text{g/g}$  is the boron-10 concentration in tissue. Also, to convert Gy/fluence into Sv/min, RBE values of 2 and 3.7 were assumed for the neutron and boron reactions respectively. These values were all taken from Zamenhof et al. (3) with the conversion units 1 rad =  $10^{-2}$  Gy and 1 rem =  $10^{-2}$  Sv respectively. Epithermal neutron dose contribution can be neglected because it is only a fraction of thermal neutron dose and seemed small enough to be excluded for this case.

The results are shown in Figure 3-1 in units of Gy/min/2kW and in Figures 3-2, 4-1, 4-2, and 4-3 in units of Sv/min/2kW.

#### a-1. Axial dose rate distribution (Figures 3-1, 3-2)

Axial absorbed doses decrease either exponentially ( $D_f$ ) or with a peak at a depth of 2 to 3 cm ( $D_G$ ,  $D_B$ ,  $D_{th}$ ) in the water phantom (Figure 3-1). Note the similar order of magnitude of  $D_B$  and  $D_f$  at a depth of  $\sqrt{10}$  cm. This can be seen as a boosting of the fast neutron dose.

RBE doses of axial distribution are summarized in Figure 3-2 for collimators of  $3 \times 3 \text{ cm}^2$  and  $9 \times 9 \text{ cm}^2$ . Other various configurations with 9 steel rods of  $3 \times 3 \text{ cm}^2$  can be constructed by superpositions of the data for the  $3 \times 3 \text{ cm}^2$  case. From the therapeutic point of view, this RBE dose is more amenable to comparison than absorbed dose. A brief explanation follows, with the  $9 \times 9 \text{ cm}^2$  case as a specific example.

The fast neutron RBE decreases almost exponentially from 1.2 Sv/min/2kW with a half-value depth (HVD) of 3.3 cm, while the photon RBE dose makes a peak of 0.1 Sv/min/2kW at  $\sqrt{3}$  cm and then decreases exponentially. The total axial dose, at the point of entrance to the tissue, is characterized primarily by the fast neutron dose with less of a boron reaction dose contribution.

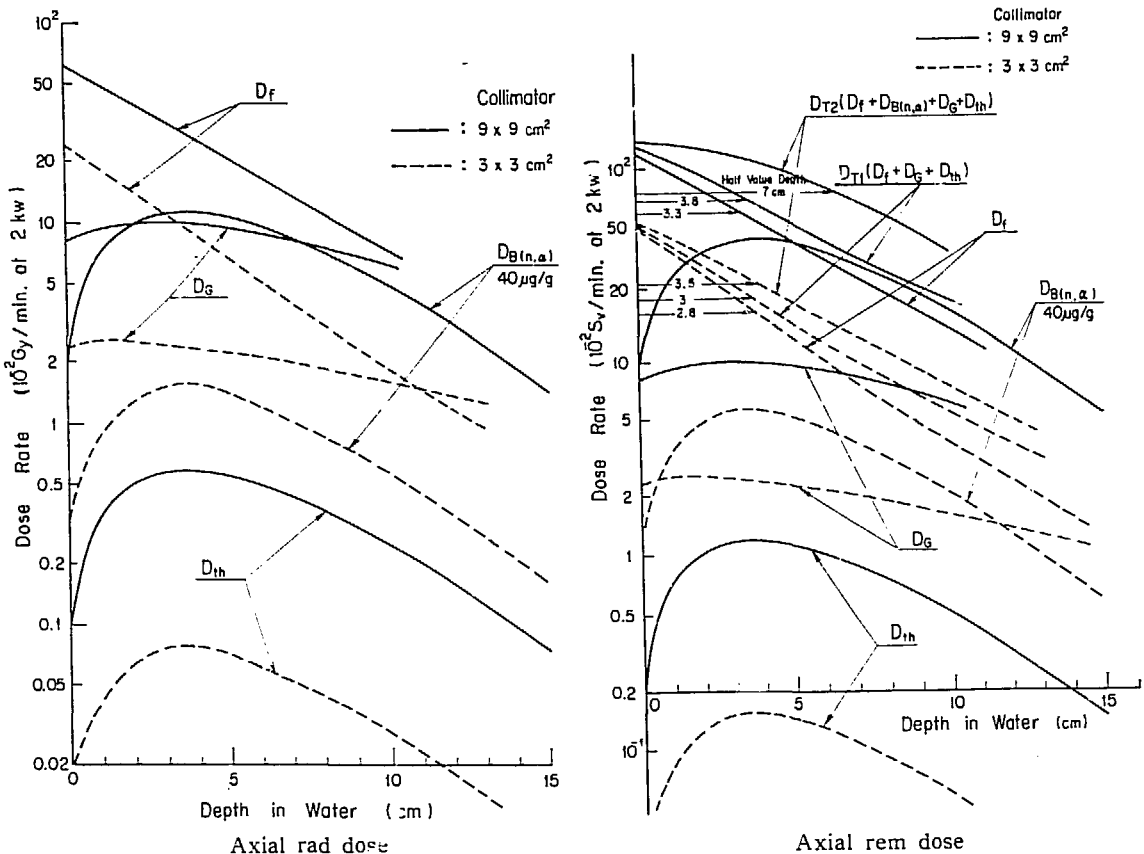


Fig. 3-1,2. Boron boosted therapy dose in water phantom for YAYOI collimated fast neutron beam.

Assuming a uniform boron compound distribution in tissue, the RBE dose due to the  $^{10}\text{B}(\text{n},\alpha)^7\text{Li}$  reaction was calculated, taking as a reference a boron concentration of 40  $\mu\text{g/g}$  tissue. Its distribution, similar to that of thermal neutrons, is about 36 times more intense and exceeds the fast neutron RBE dose in the area beyond 5.3 cm in depth. It makes a peak of 0.43  $\text{Sv}/\text{min}/2\text{kW}$  at a depth of 4 cm. This accounts for the remarkable extension of HVD from 3.8 cm ( $D_{T1}$ ) to 7 cm ( $D_{T2}$ ) and is certainly a therapeutically interesting advantage of this method because it almost corresponds to neutrons of an average energy of 6 MeV (16 MeV D on  $^9\text{Be}$ ) such as those at Hammersmith Hospital and at the Institute of Medical Science, University of Tokyo (4,5).

#### a-2. Lateral RBE dose rate distribution (Figures 4-1, 4-2, 4-3)

Lateral RBE dose distributions at depths of 1, 4, and 8 cm are all shown in Figure 4. HVD for  $D_{\xi}$  is about 14 cm through the collimator width of 9 cm. This broadening is due to directional spread rather than to the scattering effect of radiation in the medium.

The lateral boron reaction dose distributions, with a HVW of about 16 cm, are broader than those of fast neutrons.

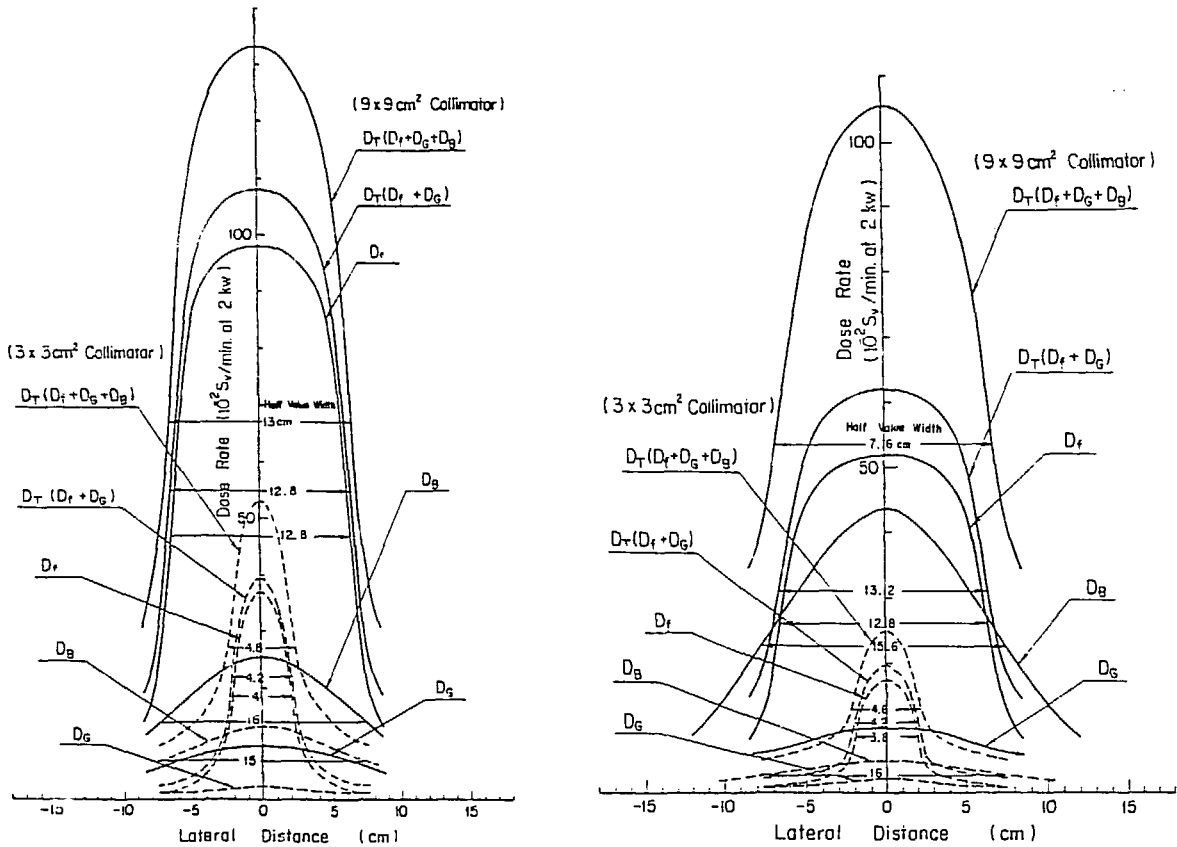


Fig. 4-1,2. Boron boosted dose in water phantom.

As far as thermal neutron and, similarly, boron reaction doses are concerned, collimation within tissue is almost impossible, thus their distributions within tissue are determined by fast neutrons as the source, and consequently a more intense dose is obtainable to the extent that the presence of fast neutrons can be permitted. Photon dose shows a broader distribution along the lateral distance, corresponding to the thermal neutron capture distribution as a photon source.

At a depth of 1 cm in the phantom, the fast neutron component is far more dominant than any other. Obviously the total RBE dose here is intense enough to be applicable for therapy purposes even at a radical distance of 8 cm ( $>0.1 \text{ Sv/min}$ ) (Figure 4-1).

At a depth of 4 cm and a radial distance of 7 cm in the phantom, the boron reaction dose almost equals that of the fast neutron (Figure 4-2), and the total RBE dose still remains around 0.5 Sv/min.

At a depth of 8 cm of phantom, the boron reaction RBE dose exceeds everywhere the fast neutron dose (Figure 4-3). The total RBE dose at both lateral and radial distances of 8 cm is still 0.24 Sv/min. These distributions are quite favorable, specifically for a tumor therapy conceptually depicted in Figures 5 and 6, which will be discussed later.

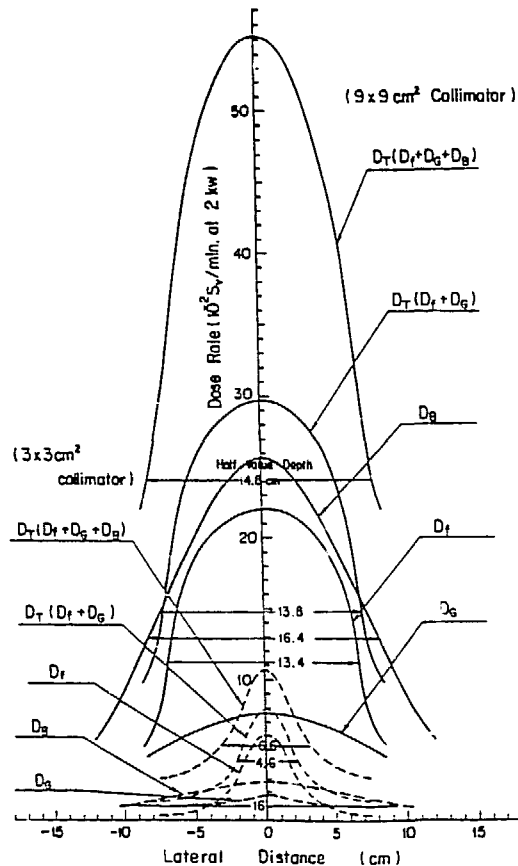


Fig. 4-3. Lateral rem dose, depth 8 cm.

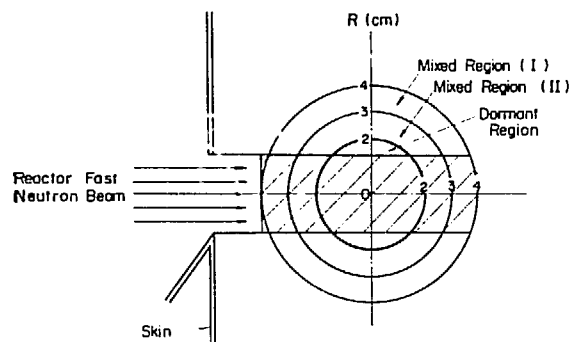


Fig. 5. Tumor irradiation by fast neutron beam with help of BNCT.

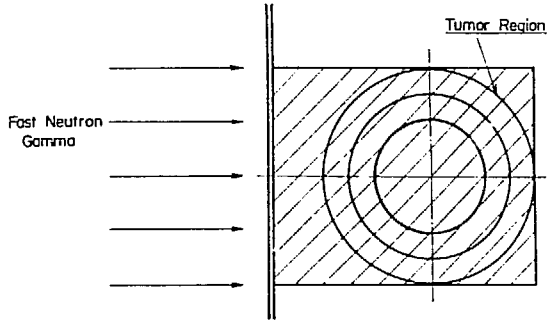


Fig. 6. Conventional tumor irradiation by fast neutron and/or  $\gamma$ -radiation without skin sparing.

Thus, the measurements conducted have shown that it is possible to get a favorable distribution of doses in tissue from a therapy point of view for certain applications.

#### b. Dose Rate Distribution In and Around Body Phantom

In order to evaluate the dose distributions in an actual case, a body phantom (BP) of polyester plastic (65 kg and 170 cm tall) was positioned with the chest back surface as the reference point, assuming, for example, a bulky lung tumor situated on the beam axis. Figures 7 and 8 show the axial and the radial (on the surface) distributions of the thermal and fast neutron flux and photon dose rate, referenced to the data on the water phantom (WP), making use of indium ( $E_n > 1.3$  MeV), gold, and TLD (BeO) respectively.

It was found that the axial distributions of photon dose rate in the two phantoms are very similar, while thermal neutron flux in the body phantom is flatter than in the water phantom and some 30% lower. This tendency should be taken into account for a therapy application.

The slight difference for thermal neutrons reflects a lower density of the body phantom at the chest, which accounts also for a similar tendency for the fast neutron dose distributions, as seen here for  $D_n$  (WP) and  $\phi_f$  (BP).

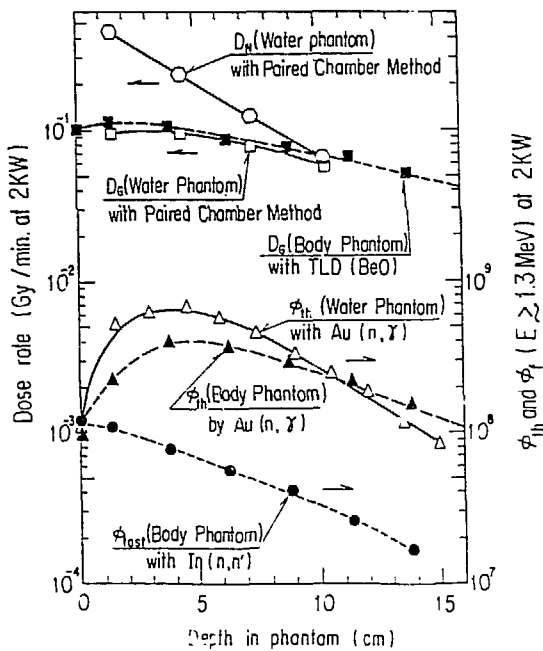


Fig. 7. Axial dose rate distribution in water phantom (30 cm cube) and body phantom (65 kg, 170 cm) (YAYOI Operation position B).

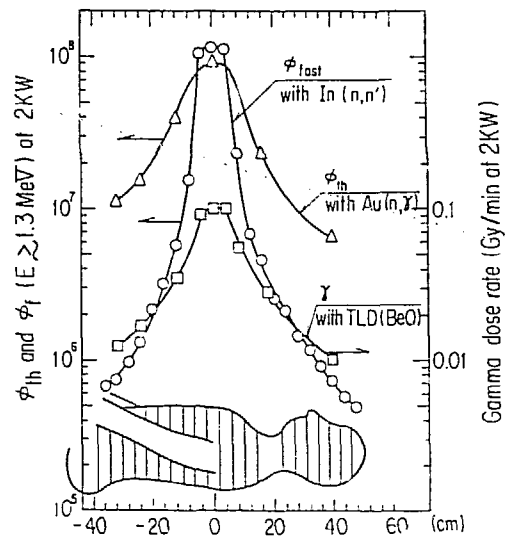


Fig. 8. Neutron flux and dose rate distribution on the axis of body phantom (65 kg, 170 cm) back surface (YAYOI Operation position B).

### c. Distribution of Radiation Dose Over Other Parts of Body

In our effort to pursue radiation therapy, the evaluation of unfavorable side effects of radiation exposure is important. Figure 9 shows some dose rates for a 1-Gy administration at a depth of 1.5 cm into the chest from the back surface: the reference point. The dose distributions for several spe-

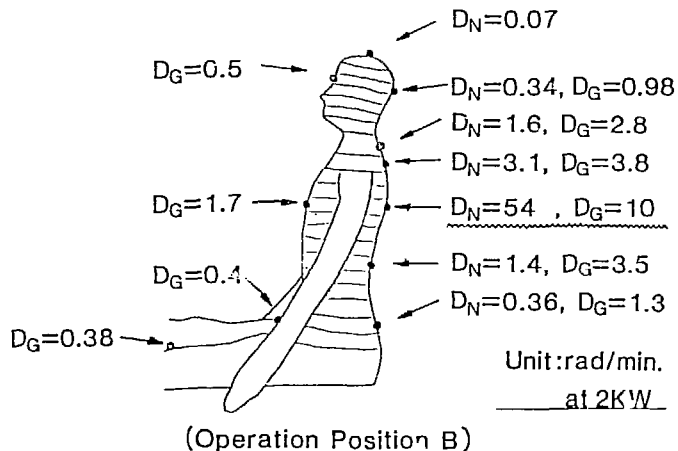


Fig. 9. Estimation of whole-body radiation dose.

cific parts are summarized in Table 1, referenced to the ICRU 26 (Jan. 1977) criteria. A dose of 0.03 Sv seems relatively high for the dose limitation of 0.05 Sv/yr for the marrow, indicating a need for more collimation and/or radiation shielding for this type of application.

Table 1. REM dose to be delivered at various critical organs for 1-Gy dose at chest: 1.5 cm depth from the back surface, compared with ICRP criteria.

Critical organ	REM dose $10^{-2}$ Sv	ICRP criteria $10^{-2}$ Sv/year	Comment
Bone marrow (the ilium)	3.4	5	Most critical
Genital gland	0.7	5	
Thyroid gland	6.2	30	
Leg joint	0.68	75	

## V. DISCUSSION

### a. Dose Rate Distribution

Favorable dose distributions for BNCT-enhanced fast neutron therapy were found at the YAYOI facility at the University of Tokyo research reactor (Tokai-mura, Ibaraki, Japan) for therapy of bulky tumors with a radius as large as 4 cm. Actually such a tumor has a stratified configuration, as shown in Figure 5. The region is schematically divided into three parts. Mixed Region (I) refers to the part where normal tissue is dominant, with sufficient oxygen, and thermal neutrons are preferably allowed, while Dormant Region refers to the part where tumor tissue is dominant, with deficient oxygen, and the fast neutrons can be allowed. Mixed Region (II) lies in between and can help in the moderation of fast neutrons. Thus the advantage of BNCT can be maintained, sparing the normal tissues located at the tumor periphery as well as the relevant skin, as shown in this figure.

The advantage of this method seems obvious compared with the situation in Figure 6, which shows conventional tumor irradiation by fast neutrons and/or photons without skin sparing. This situation is essentially nothing but total destruction of both tumor and nearby normal tissues altogether.

On the other hand, the fast neutron beam from a fission reactor has a higher LET ( $\sim 100$  keV/ $\mu$ ) than other higher energy neutrons on average, and seems more favorable in terms of radiation therapy of surface tumors in light of its limited penetration.

### b. BNCT Enhanced Fission Neutron Therapy

BNCT with thermal neutrons has been somewhat successful in its application only to brain tumors, while cyclotron fast neutrons ( $E_n = 7$  to 21 MeV) from the TAMVEC cyclotron ( $E = 16$  to 50 MeV) did not always show promising results for brain tumors (6), probably because of more damaging higher RBE effects on normal tissue than on tumor. Quite recently, however, significantly good results were reported with  $^{252}\text{Cf}$  neutron brachytherapy for hemispheric malignant glioma (7). In these cases, fast neutron doses of 2.5 Gy at 1 cm and 0.83 Gy at 2 cm from the applicator plus  $\sim 60$  Gy of  $^{60}\text{Co}$  photon of whole brain irradiation were administered. The increase in performance status in nine of ten patients and the decrease in mass size seen on the CT scan suggested that local response and tumor shrinkage occur after neutron implant therapy plus radiotherapy. As in this case, fission energy fast neutrons may, for some cases, be serviceable. The YAYOI fast neutron beam can also be used to deliver 2.5 Gy of fast neutron dose for some five minutes at a depth of 1 cm from the entrance of the tissue. Conversely, if high LET radiation is effective, BNCT with  $^{252}\text{Cf}$  fast neutrons may be effective and worth examining, and it deserves attention.

The development of a dedicated facility for a fast neutron source reactor for this specific purpose (8) has been described.

## VI. CONCLUSION

Fast fission neutron therapy enhanced by BNCT would be possible by employing a fast neutron source reactor like YAYOI. In this paper, experimental results obtained in a cubic water phantom (30 cm on a side) are shown, and some of them ( $9 \times 9 \text{ cm}^2$  case) seem interesting for therapy purposes. These data were compared with anthropomorphic phantom data, and  $\sim 30\%$  decreases of thermal flux, compared at the peak, were found. This should be taken into consideration when irradiating patients.

## ACKNOWLEDGMENTS

This work was done as a research project in the joint use program of the YAYOI facility 1977-1980. In this regard the authors are indebted to Profs. S. An and A. Furuhashi (now at Power Reactor and Nuclear Fuel Development Corp.) of the University of Tokyo for their guidance and advice. Many comments made by Prof. H. Hatanaka (Teikyo University) proved invaluable in the undertaking of this work. Thanks are due to Prof. T. Inada of the University of Tsukuba and Dr. A. Ito of the Institute of Medical Science, University of Tokyo, for their support and stimulating discussions of dosimetry methods and data analysis. Finally, the authors are indebted to Mr. R. Zielinski of the University of Tokyo (a graduate student from Massachusetts Institute of Technology) for his assistance in the editing of a part of this paper.

#### REFERENCES

1. H. Wakabayashi, K. 'cr' .1, N. Sasuga, and H. Yanagi, Radiation field for fission neutron enhanced boron neutron capture therapy employing fast neutron source reactor YAYOI, *J. Nucl. Sci. Tech.* 19(7), 505-62 (1982).
2. H. Wakabayashi, I. Saito, T. Tamura, and S. An, Operational experiences of fast neutron source reactor YAYOI as pulsed fast reactor, *J. Nucl. Sci. Tech.* 18(7), 545-7 (1981).
3. R.G. Zamenhof, B.W. Murray, G.L. Brownell, G.R. Wellum, and E.I. Tolpin, Boron neutron capture therapy for the treatment of cerebral gliomas. (I). Theoretical evaluation of the efficacy of various neutron beams, *Med. Phys.* 2, 47-60 (1975).
4. J.T. Breunen, Fast neutrons for radiation therapy, *Radiol. Clinics N. Am.* 7(2), 365-74 (1969).
5. H. Wakabayashi, S. Suzuki, and A. Ito, Measurement of relative biological effectiveness (RBE) for the radiation beam from neutron source reactor YAYOI, *J. Radiat. Res.* 24, in press (1983).
6. J.B. Smathers, Private communication (1972).
7. Y. Maruyama, H.W. Chim, A.B. Young, J.L. Beach, J. Bean, and P. Tibbs, Work in progress: neutron brachytherapy for hemispheric malignant glioma, *Radiology* 145(1), 171-4 (1982).
8. H. Wakabayashi and S. An, A conceptual design of neutron tumor therapy reactor facility with a YAYOI based fast neutron source reactor, *J. Fac. Eng. U. Tokyo.* (B), 37(1), 123-33 (1983).

A System for Simultaneous Monitoring of Thermal and Epithermal Neutron Flux  
during Boron Neutron Capture Therapy

Yoshinori Hayakawa and Tetsuo Inada

Institute of Basic Medical Sciences, University of Tsukuba,  
Niihari-gun, Ibaraki 305, Japan

Susumu Harasawa

Institute of Atomic Energy, Rikkyo University,  
Yokosuka, Kanagawa 240-01, Japan

and

Hiroshi Hatanaka

Department of Neurosurgery, Teikyo University, Itabashi, Tokyo 173, Japan

The absorbed doses in the tumor and in the brain of a patient treated by boron neutron capture therapy are determined by the neutron fluence and the concentration of boron-10 in the tumor and in the blood. In the past we used a gold foil activation method to determine the neutron fluence. This method has the drawback that the exact neutron fluence can be determined only after the irradiation is over. We developed in 1977 a system for simultaneous monitoring of thermal neutron flux during irradiation of the patient. Although we reported this in 1978, further advances have been made. We also report briefly on the measurement of boron-10 concentration in tissues.

The neutron intensity in the brain is influenced by many factors, such as the distance between the patient's head and the irradiation port, the size of the irradiation field, and the depth of the tumor. We developed a small detector for simultaneous monitoring which can be implanted into the brain of the patient.

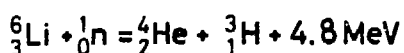


Fig. 1. Two kinds of nuclear reactions. The upper one is utilized for boron neutron capture therapy, the lower for simultaneous monitoring of slow neutrons.

In Figure 1, two kinds of nuclear reactions are shown. The upper one is the reaction used for boron neutron capture therapy. In 94% of cases this reaction accompanies prompt gamma rays of 0.48 MeV. The prompt gamma rays can be utilized for quick *in vitro* assay of boron-10 concentration in the tissue (Kanda et al., Fairchild et al., this Conference). The lower reaction has a considerably higher released energy than the upper one. The released energy is completely transferred to the heavy charged particles, namely alpha particles and tritium. The cross sections of the two nuclear reactions have similar dependence on neutron energy, being inversely proportional to the velocity of the neutrons.

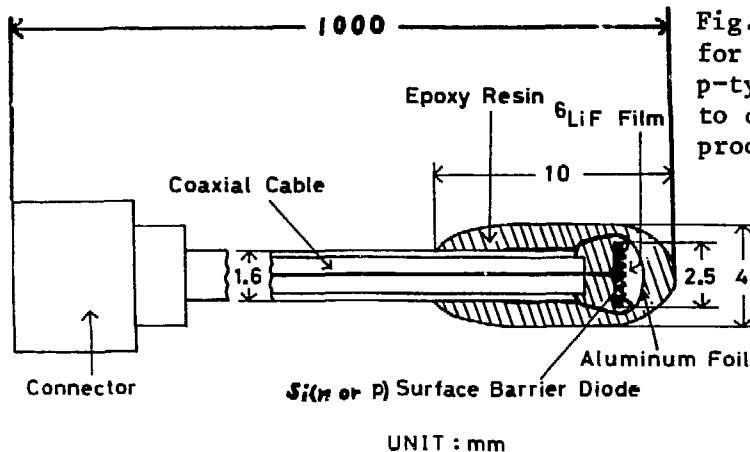


Fig. 2. The simultaneous detector for slow neutrons. Si n-type and p-type surface barrier diode is used to detect heavy charged particles produced by  $^{6}\text{Li}(\text{n},\alpha)^{3}\text{H}$  reaction.

Figure 2 shows, schematically, the simultaneous neutron detector we have developed. This neutron detector is made of a silicone surface barrier diode with a lithium-6 fluoride film attached to its surface to form a thin radiation-sensitive layer. The sensitive layer is  $<20\text{ }\mu\text{m}$  without bias voltage applied. When neutrons impinge on the detector, lithium-6 nuclei capture the neutrons, yielding alpha particles and tritium nuclei. These heavy charged particles are completely stopped within the radiation-sensitive layer, producing big pulses. On the other hand, the contaminating gamma rays produce high energy electrons with low LET. These electrons lose only a small part of their energy within the thin radiation-sensitive layer, producing small pulses. The neutron-sensitive part is 4 mm in diameter, and the cable is 1.6 mm in diameter.

Figure 3 is a photograph of the detector, with a scale in centimeters. As can be seen, the detector is quite small. Usually the neutron-sensitive part is covered by a thin rubber tube to protect the detector from water and other fluids.

Figure 4 is a block diagram of the monitoring system. The neutron detector produces signal pulses. The pulses are amplified and analysed by a multichannel analyzer at PHA mode. The pulse-height distribution is printed. The amplified pulses are discriminated by a single-channel analyzer, and, through a ratemeter, the counting rate is recorded continuously.

Figure 5 shows the pulse-height distribution of the pulses. The abscissa is the pulse height, that is, the channel number. The ordinate is the counting rate. Two major peaks are apparent. The higher peak is due to tritium nuclei, the lower to alpha particles. These two peaks are well separated from small noise pulses due to pile-up of electron pulses produced by gamma rays.

Figure 6 shows the proportionality between the neutron flux (the abscissa) and the signal counting rate (the ordinate). The proportionality is very good, which means that no dead-time correction is necessary. The flux is changed by changing the thermal output power of the reactor.

Figure 7 shows the stability of the detection system. The abscissa is the irradiation time in minutes, and the ordinate is the counting rate. It can be seen that the stability is very good. The neutron fluence rate was  $1.4 \times 10^9 \text{ n/cm}^2\text{-sec.}$

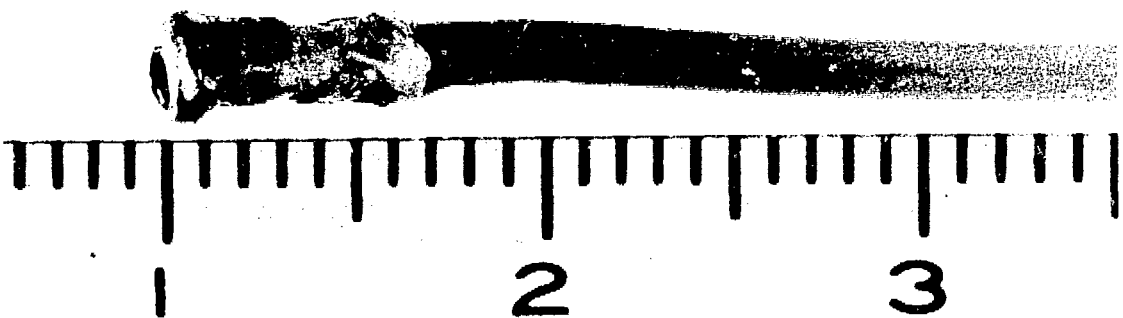


Fig. 3. Radiation-sensitive Si surface barrier diode used to monitor slow neutrons.

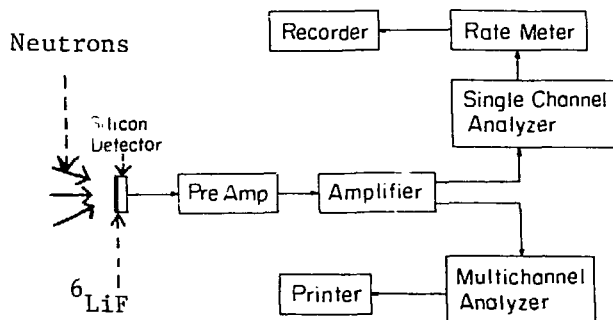


Fig. 4. Block diagram of the monitoring system for slow neutrons.

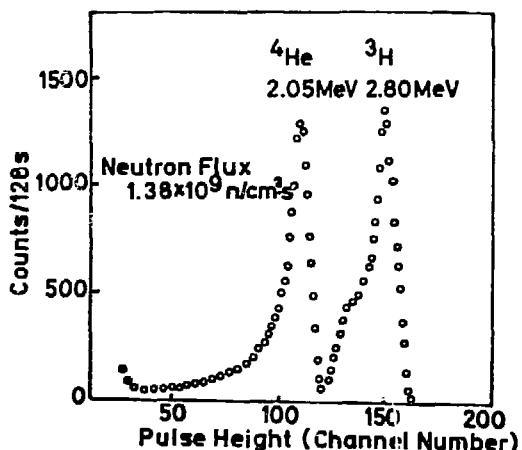


Fig. 5. Pulse-height distribution of the signals from the simultaneous slow neutron detector.

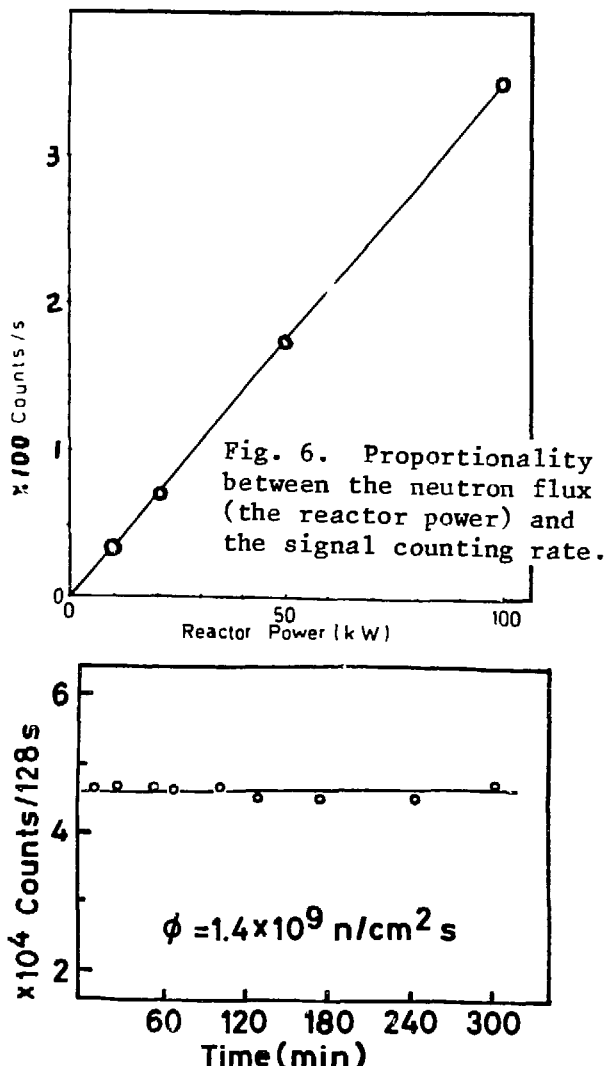


Fig. 6. Proportionality between the neutron flux (the reactor power) and the signal counting rate.

Figure 8 shows, schematically, the irradiation setup. It shows a nuclear reactor from which thermal neutrons are generated. The neutrons impinge on the operated patient's head. A simultaneous neutron detector is inserted into the hole created by removal of the tumor mass. Another detector is placed at the surface of the brain to determine the maximum dose delivered to the brain.

Figure 9 shows the actual application of the simultaneous neutron monitors. The inserted neutron detector has its neutron-sensitive part covered by a thin rubber tube to make it waterproof. A neutron shield, containing boron-10, prevents thermal neutrons from reaching the scalp. This is needed because human skin takes up boron-10 compounds. We use either boron-containing or lithium-6-containing plastic helmets or sheets.

Figure 10 shows the simultaneous neutron detector placed on the surface of a surgical drape which covers the patient's head in order to prevent bacterial contamination.

Figure 11 shows schematically the irradiation of a patient's brain. It shows a reactor and a patient lying on the bed. The irradiation room has a shield door made of concrete. The patient is anesthetized by remote control.

Figure 12 is a photograph taken just before the irradiation of a patient, who lies with the head apposed to the irradiation port, which has a collimator made of lithium fluoride ceramic. Also seen are a monitoring TV camera, preamplifiers for the neutron detectors, and two thin black cables for the neutron detectors, attached to the preamplifiers. One detector is put on the surface of the brain and another inserted in the cavity created by removal of the tumor mass.

Figure 13 shows data for a brain tumor treatment during which the neutron flux changed because of critical swelling of the brain matter. The abscissa is the duration of irradiation of the patient (in minutes), and the ordinate is the counting rate of the detector on the surface of the brain, with the right-hand ordinate showing the corresponding neutron flux. During the irradiation, we observed a slight increase of neutron intensity of 4.5%. This may be interpreted as having been caused by protrusion of the patient's brain through the craniotomy hole. The protrusion was estimated to be about 5 mm. The neurosurgeon (Hiroshi Hatanaka) took it for acute swelling of the brain caused by acute swelling of the tumor. The physicians therefore applied a hyperventilation maneuver to the patient, initiated at the time indicated by arrow A, which controlled the swelling of the brain. At the time indicated by arrow B, the reactor was shut off.

The detector seems to be useful for future epithermal neutron irradiation, since the dependences of the boron-10 reaction and the lithium-6 reaction cross sections on neutron energy are the same. The detector will monitor the "effective" neutron flux in future epithermal neutron irradiations in boron neutron capture therapy.

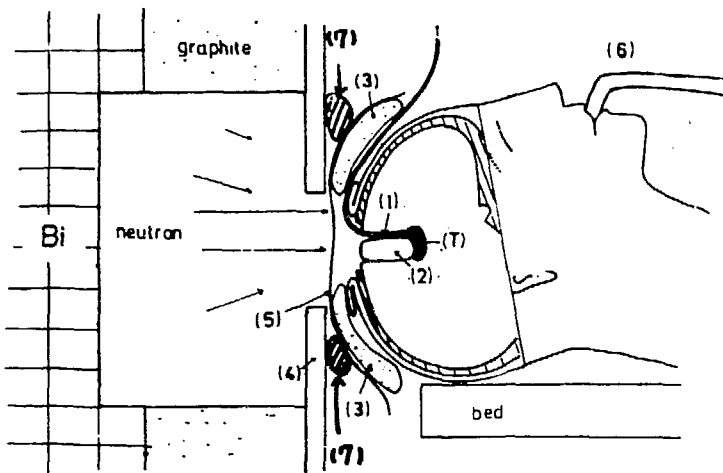


Fig. 8. Irradiation setup of patient. (1) Simultaneous slow neutron detector, (2) plastic hollow ball, (3) helmet containing  $^{6}\text{LiF}$  powder for shielding scalp from thermal neutrons, (4) thermal neutron collimator containing  $^{6}\text{LiF}$  powder, (5) surgical drape to prevent bacterial infection, (6) intracranial tube for remote anesthesia, (7) wax shielding containing borax to reduce leakage of thermal neutrons from gap between neutron collimator and helmet. The shield reduces total-body dose to patient.



Fig. 9. Actual application of the simultaneous detector for slow neutrons. Detector inserted into tumor bed is indicated by arrow. Plastic hollow ball is seen near detector. Black sheet around craniotomized head is shielding containing  $^{10}\text{B}$  to shield against thermal neutrons.



Fig. 10. Simultaneous detector for slow neutrons, attached to surface of surgical drape, monitors the neutron fluence permissible for brain surface.

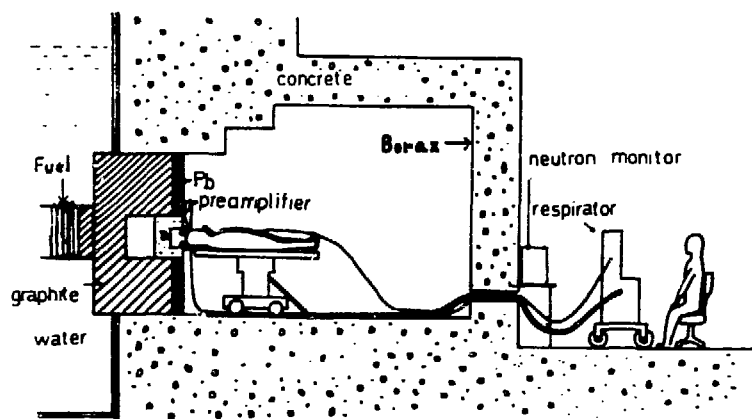


Fig. 11. Schematic drawing of patient irradiation.

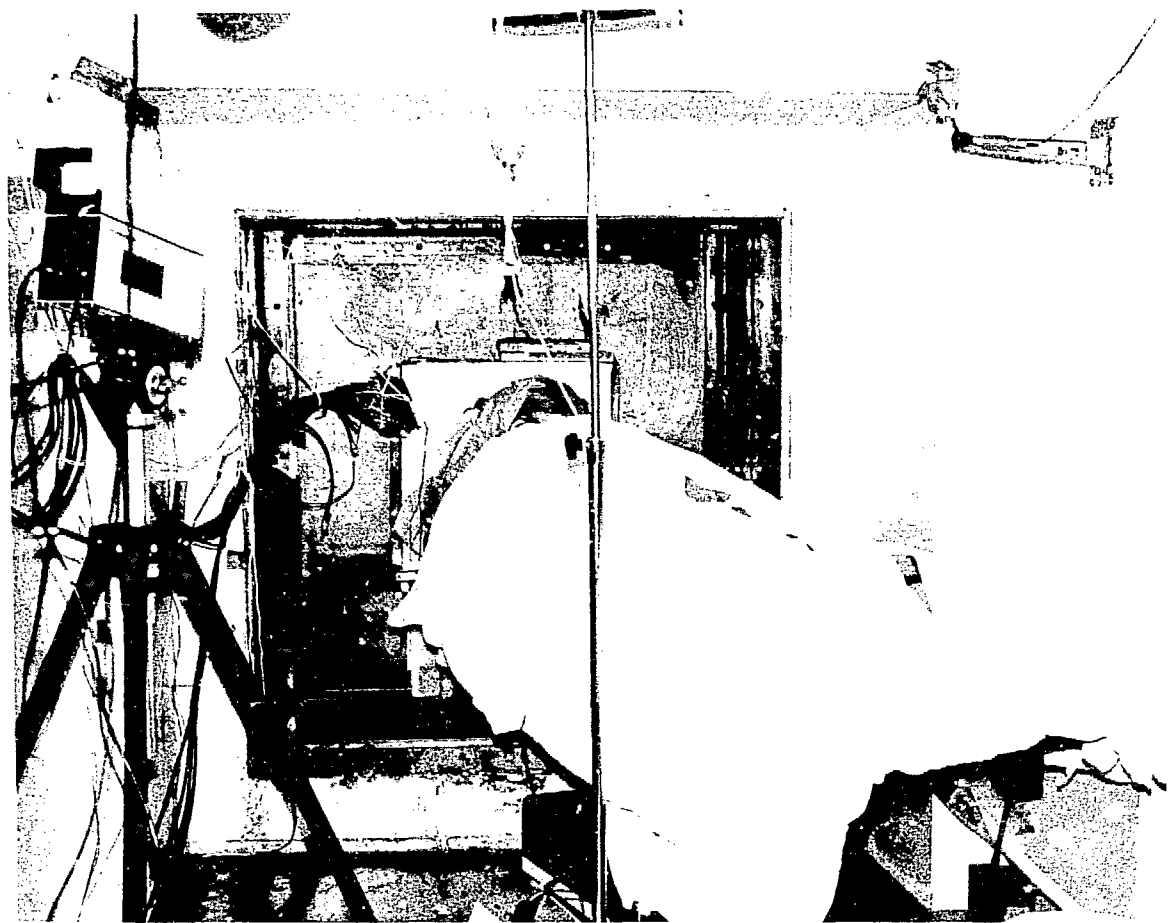


Fig. 12. Patient just before neutron irradiation. Preamplifiers for the neutron detectors and two thin cables of the simultaneous detectors for slow neutrons can be seen.

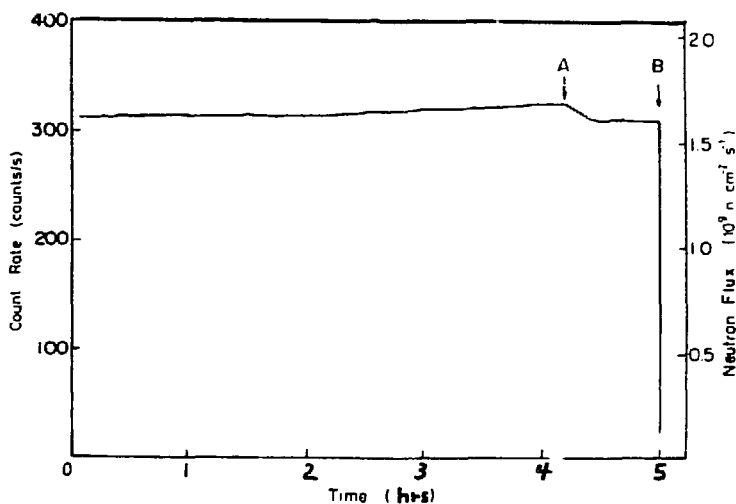


Fig. 13. Critical swelling of brain matter observed by simultaneous neutron monitoring system, with detector at surface of brain. Note the steady rise in count rate. Hyperventilation was achieved at A; reactor was shut off at B.

I would like to mention a quick in vitro assay of boron-10 concentration in the tissue and blood, which detects the prompt gamma rays from a specimen irradiated by a thermal neutron beam of known flux. We conducted the following experiment at the Rikkyo University reactor (Figure 14). The reactor is the same type as the one at Musashi Institute of Technology, a Trigger Mark II type (General Atomic Co. Ltd). The gamma rays from the reactor core are minimal at the beam ports. We put in the sample containing boron-10, and we detect the prompt gamma rays by a germanium-lithium drift detector.

Figure 15 shows the germanium detector shielded by lithium-6 fluoride ceramics to prevent activation of the detector by thermal neutrons.

Figure 16 shows the experimental setup. The beam port is collimated by a lead block with a hole. A sample holder made of quartz glass contains blood. The neutron flux at the position of the sample is  $3.7 \times 10^6$  n/cm<sup>2</sup>-sec, when the reactor thermal output power is at its maximum (100 kW). The sample is accurately positioned by a holder made of transparent plastic.

Figure 17 is a picture taken from a viewpoint nearly perpendicular to that of Figure 16. It shows the lead collimator behind which the germanium detector is located.

Figure 18 shows the pulse-height distribution of detected gamma rays emitted from pure water samples containing various concentrations of boron-10. The prompt gamma-ray reaction from boron-10 can be discriminated from other peaks because of the wider peak width ascribed to Doppler broadening.

Figure 19 shows the linear relationship between the counting rate of prompt gamma rays and the boron-10 concentration. Prompt gamma rays were observed even in the case of pure water containing no boron-10. This was attributed to ambient boron-10 contamination.

Figure 20 shows the pulse-height distribution of gamma rays from the blood of a patient. The blood sample was taken just prior to the irradiation. The prompt gamma rays emitted by boron-10 reaction are prominent. From the counting rate and the calibration curve shown in Figure 19 the concentration of boron-10 in this sample is determined to be 18  $\mu$ g boron-10 per gram of blood. The error was estimated to be  $\pm 5\%$ . The measuring time was 16 minutes. The accuracy and the measurement time seem to be sufficient for clinical purposes.

#### ACKNOWLEDGMENTS

The authors are grateful to Professor S. An (University of Tokyo) and Professor T. Sato (Musashi Institute of Technology) for their constant encouragement.

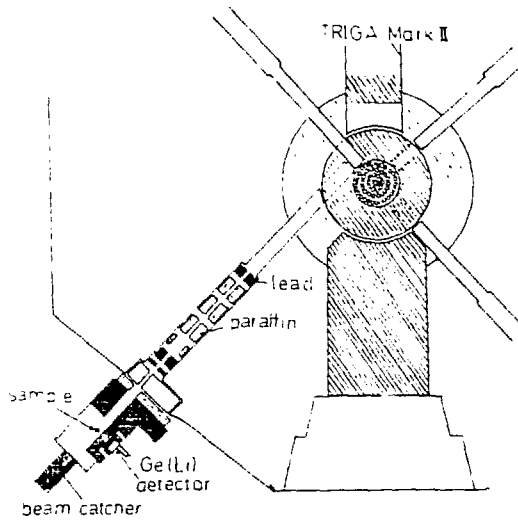


Fig. 14. Cross-sectional drawing of the Rikkyo University Reactor, showing collimator, position of Ge(Li) gamma-ray detector, and sample to be measured. Setup for quick *in vitro* assay of  $^{10}\text{B}$  concentration in tissue.

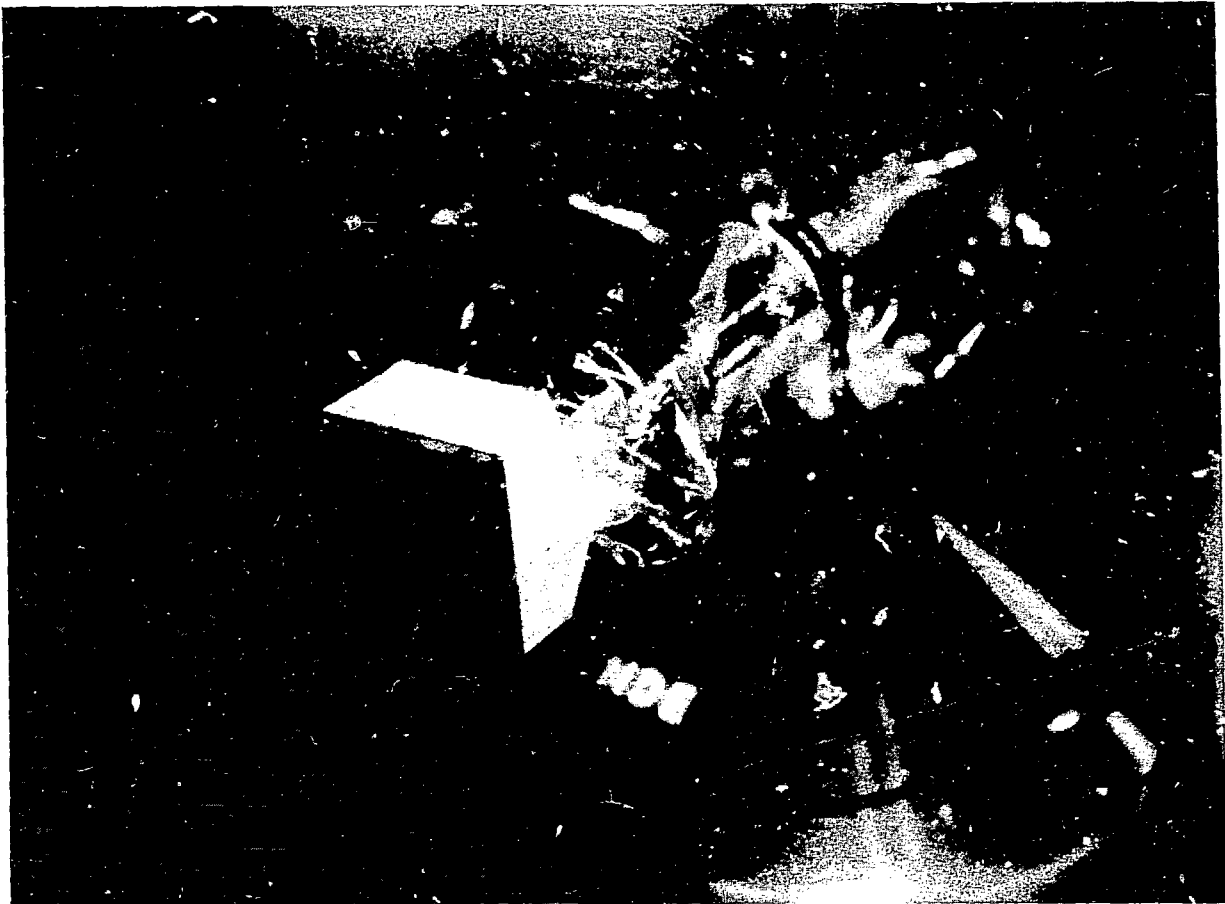


Fig. 15. Ge(Li) gamma-ray detector shielded from thermal neutrons by  $^{6}\text{LiF}$  ceramic tiles.

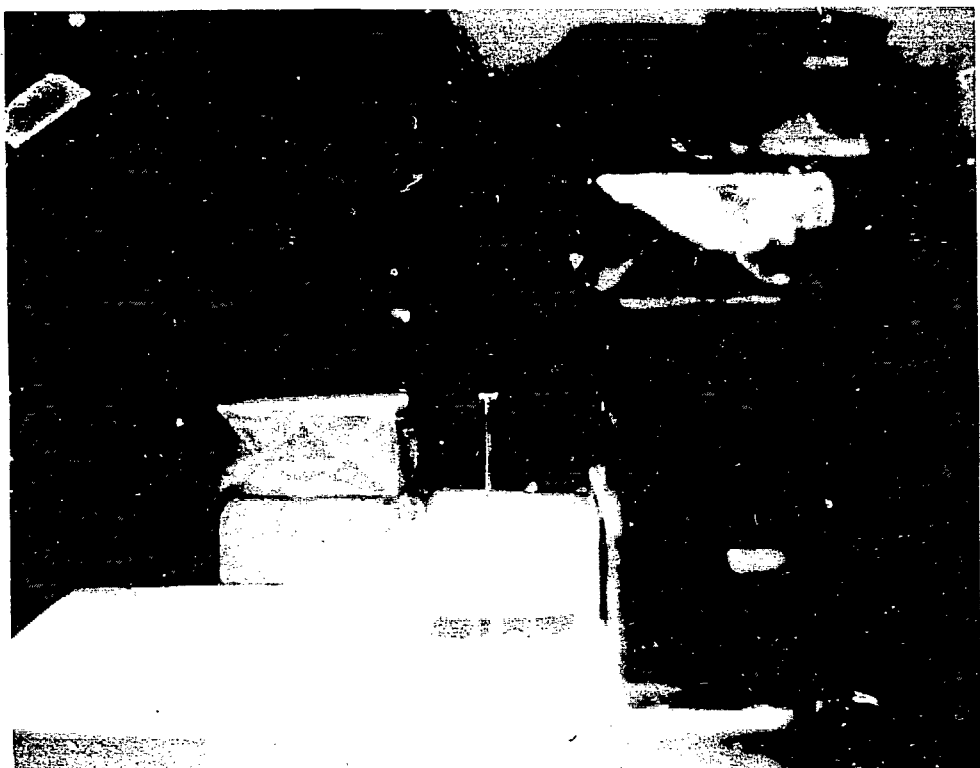


Fig. 16. Experimental setup for quick in vitro assay of  $^{10}\text{B}$  concentration in blood.

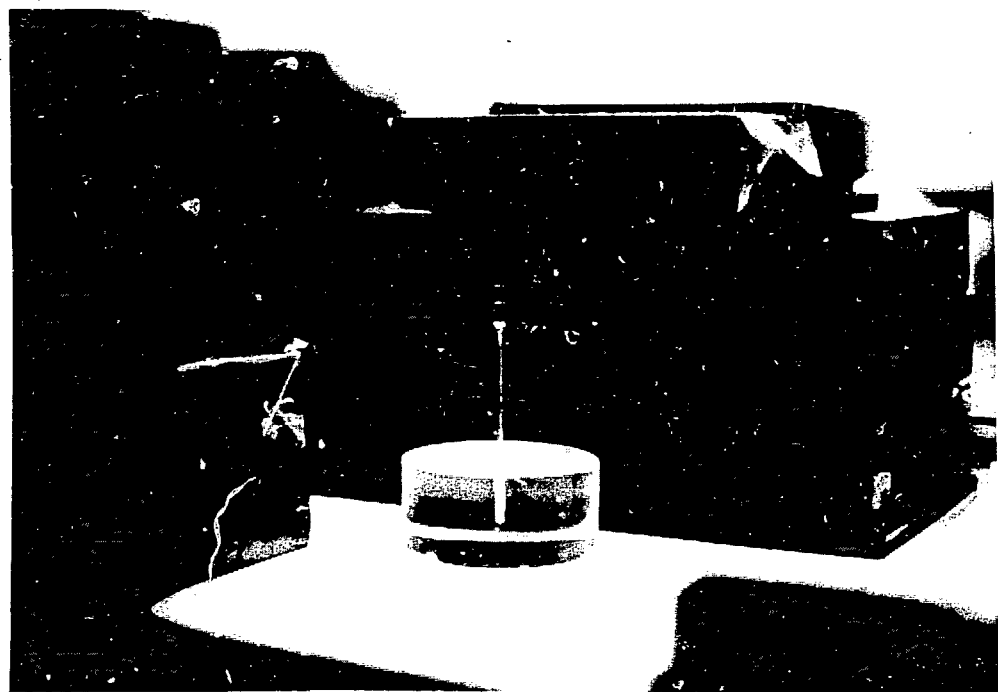
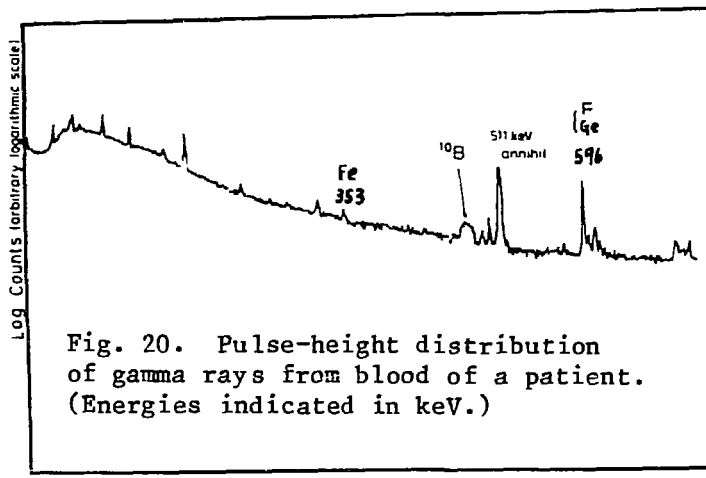
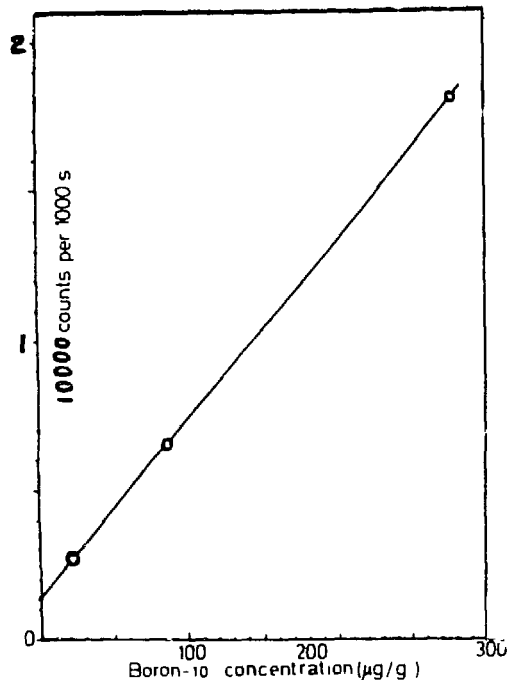
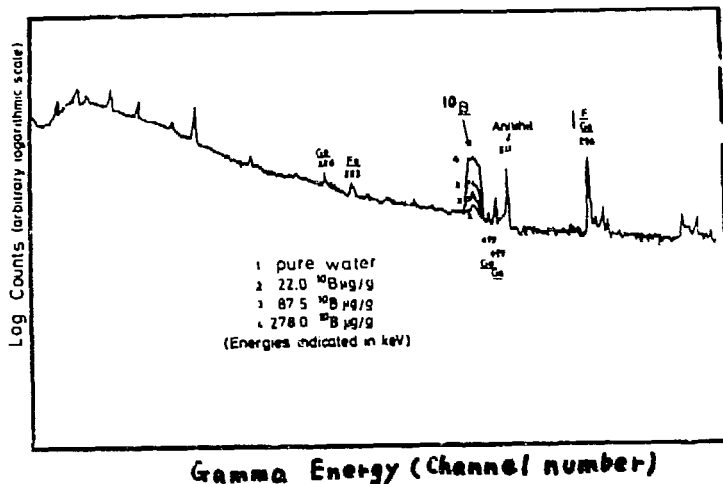


Fig. 17. View perpendicular to Fig. 16, showing lead collimator.



#### REFERENCES

1. Y. Hayakawa, S. Harasawa, A. Nakamoto, K. Amano, H. Hatanaka, and J. Egawa, Simultaneous monitoring system of thermal neutron flux for boron neutron capture therapy. *Radiat. Res.* 75 243-51 (1978).
2. S. Harasawa, A. Nakamoto, Y. Hayakawa, J. Egawa, O. Aizawa, T. Nozaki, T. Minobe, and H. Hatanaka, Improved monitoring system of neutron flux during boron neutron capture therapy. *Radiat. Res.* 88 187-93 (1981).
3. S. Harasawa, Y. Hayakawa, T. Nozaki, O. Aizawa, and H. Hatanaka, Dosimetry in boron neutron capture therapy. In Biomedical Dosimetry: Physical Aspects, Instrumentation, Calibration, pp. 173-86, IAEA-SM-249/20, International Atomic Energy Agency, Vienna, 1981.

PRELIMINARY DOSIMETRY STUDIES OF THE MIT REACTOR (MITR-II)  
MEDICAL FACILITY

Manzar Ashtari, University of Kentucky, Lexington, KY 40536  
Gordon Brownell, Mass. Institute of Tech., Cambridge, MA 02139  
Mark Forrest, Brigham and Women's Hospital, Boston, MA 02115

INTRODUCTION

Boron Neutron Capture Therapy (BNCT) is a technique that exploits the  $^{10}\text{B}(\text{n},\alpha)^7\text{Li}$  reaction in boron loaded tissue exposed to an intense flux of thermal neutrons. The emitted high energy charged particles, alpha particles and lithium-7 recoils, release large amounts of energy within a single cell or its immediate neighbor, causing irreparable damage to the cell. Since the range of the resulting charged particles is small, on the order of 8-10 microns, their distribution in tissue is expected to be restricted to the region of the boron loaded tissue, where the cells will be selectively destroyed.

The dosimetry of BNCT requires a variety of diverse experimental procedures, for the following reasons. First, a wide variety of radiation components is involved. These include thermal, epithermal and fast neutrons, externally incident gamma rays, neutron induced gamma rays and heavy charged particles from the  $^{10}\text{B}(\text{n},\alpha)^7\text{Li}$  and the  $^{14}\text{N}(\text{n},\text{p})^{14}\text{C}$  reactions. Second, since the different radiation components exhibit different relative biological effects, the dose evaluation must account for each dose component separately so that the total biological effect can be determined. From the experimental point of view, the separation of doses creates a problem because most dosimetry equipment responds to both neutrons and gamma rays.

A conventional method in mixed field dosimetry involves the use of two ionization chambers with different relative neutron sensitivities (Rossi-56). A tissue equivalent ionization chamber flushed with a tissue equivalent gas (TE), has approximately the same sensitivity to gamma rays as to neutrons, while a graphite walled chamber (GG) flushed with  $\text{CO}_2$  gas is primarily sensitive to gamma rays. To use these chambers to unfold the components of a mixed radiation beam such as MITR-II medical facility, the relative sensitivity of the chambers, TE and GG, to neutrons and gamma rays must be known. These sensitivity factors can be determined theoretically or experimentally.

Owing to extensive therapy studies with fast neutrons around the world, fast neutron and gamma sensitivity factors for TE and GG chambers have received considerable attention. Because the thermal neutron dose components of fast neutron beams are very small the response of these chambers to thermal neutrons has received very little attention in the literature. Unlike most neutron therapy modalities, BNCT calls for a radiation beam, such as MITR-II medical facility, which is primarily composed of thermal neutrons. Therefore a series of experiments

was planned to evaluate the thermal neutron sensitivity of the TE and GG chambers to thermal neutrons (Ashtari-82).

Using the above chambers and their associated sensitivities to the fast and thermal neutrons and gamma rays, along with a polyethylene phantom providing variable depth (simulating the human head) a combination of experiments was performed to unfold the components of the radiation beams in question.

These experiments focused on the comparison of the dose components and depth distribution of the two beams: A soft beam with a cadmium ratio of 250-300 and a rather harder beam with a cadmium ratio of 30. The harder beam was obtained by draining the  $D_2O$  tank of the medical facility (see Fig. 1). This was done in order to obtain a beam with an improved depth dose distribution. The more superior beam was chosen for future studies of BNCT.

#### IRRADIATION FACILITY

The irradiation facility used in the course of this work was the medical therapy facility at the Massachusetts Institute of Technology Reactor (MITR-II). The medical therapy facility is a surgical operating room that is located directly beneath the reactor. A penetration in the room ceiling allows a beam of either thermal or epithermal neutrons to be admitted.

The therapy beam is controlled by four shutters. These shutters are the  $D_2O$  blister tank, the  $H_2O$  tank, the boral shutter and the lead shutter. The medical facility arrangement is shown in Fig. 1.

The  $D_2O$  blister tank, which can be drained, controls the energy spectrum of the beam. The  $H_2O$  shutter is used to attenuate the neutron beam. A 1/2 inch moveable plate of boral, and a 9 inch thick slab of lead, are located in the ceiling and comprise the secondary shutter system.

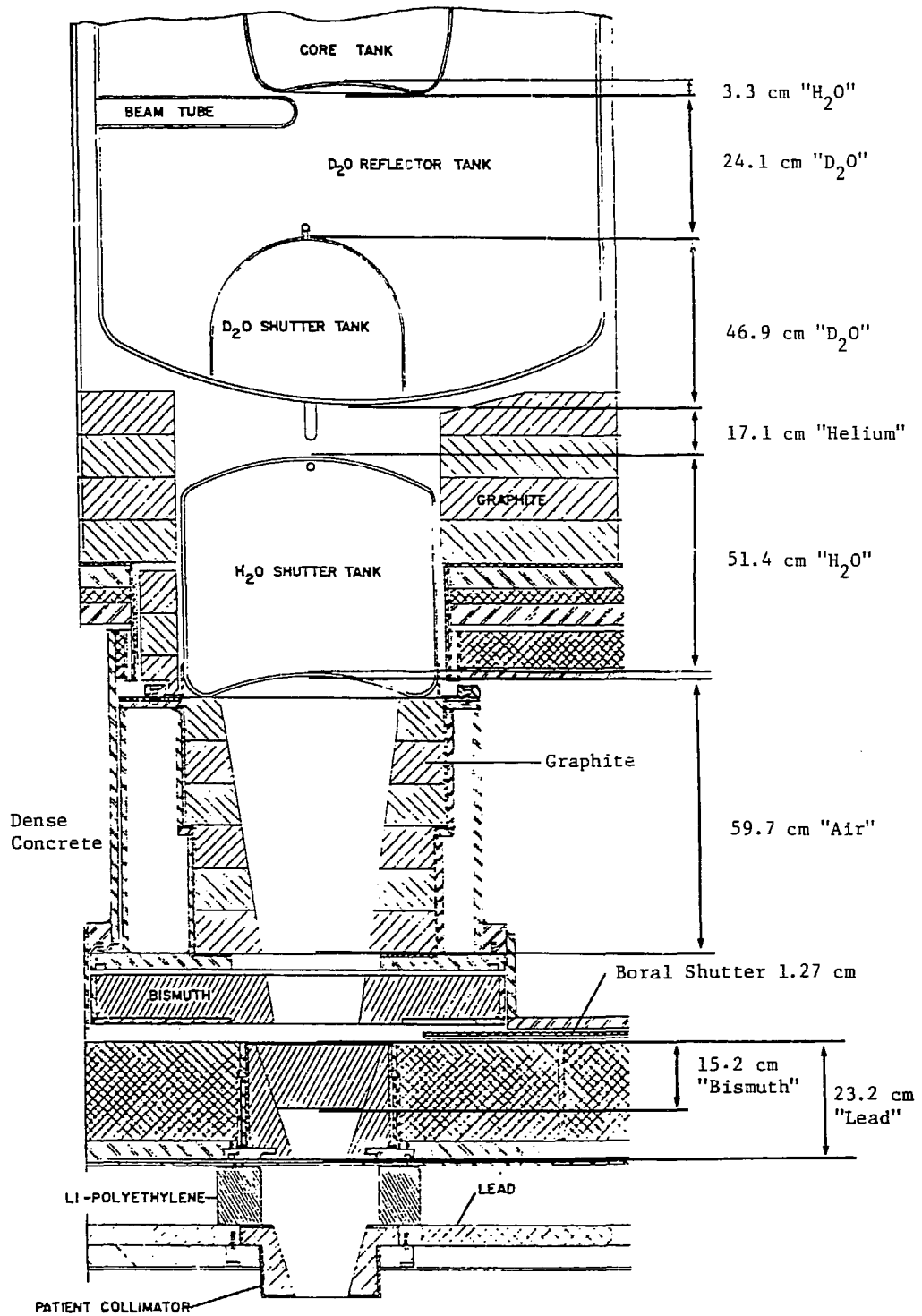
Experiments are normally set up in the medical therapy room while the reactor is operating at full power. This is done by first verifying that all four shutters are closed, setting up the experiment, evacuating all personnel from the medical room, and then closing the room's shielded door. The appropriate shutters are then opened for the desired time.

Additional absorbers and/or special collimators can be inserted in the beam. This was done to focus the beam on a small target. Polyethylene blocks are normally placed about the target so that the remaining portions of the therapy room will be shielded from neutron radiation.

#### IONIZATION CHAMBERS

The neutron insensitive ionization chamber we used was a high purity graphite chamber with a central electrode made of graphite (EG&G model IC-18G); it was constructed in such a way that  $CO_2$  gas could flow through the chamber. The neutron sensitive chamber was made of A-150 tissue equivalent plastic and filled with a tissue equivalent gas (see Table 1). This chamber and the graphite chamber, which had identical shapes,

FIG. 1



CROSS SECTION OF MITR-II MEDICAL FACILITY SHOWING THE D<sub>2</sub>O, H<sub>2</sub>O, LEAD AND BORAL SHUTTERS

were used as a pair. The physical characteristics of both are presented in Table 2.

Both chambers were calibrated in November 1981 (Far West Technology, Inc., Goleta, California), with a Co-60 source of 7 R/min. The flow rate for calibration and during all experiments for both chambers was 5 cc/min.

TABLE 1 ELEMENTAL COMPOSITION OF TISSUE EQUIVALENT GAS (AAPM-80)

ELEMENT	% BY WEIGHT
H	10.2
C	45.6
N	3.5
O	40.7

TABLE 2 PHYSICAL CHARACTERISTICS OF THE (TE) and (GG) CHAMBERS

CHAMBER MODEL	WALL MATERIAL	WALL THICK. (cm)	CHAMBER VOL. (cc)	CALIBRATION (R/coulomb)		
				Air	TE	CO <sub>2</sub>
IC-18	A-150 TE plastic	0.163	0.1	2.5 E+10	2.18 E+10	--
IC-18G	graphite	0.139	0.2	1.96 E+10	--	1.25 E+10

METHODS

It is possible to investigate the response of an ionization chamber to thermal neutrons by using a filter that absorbs all the thermal neutrons. Such a filter must have a high capture cross section but must not produce secondary radiation. Li-6 compounds are the best candidates for such a purpose. The response of the chamber to the mixed beam with and without the filter may be compared to determine its sensitivity to thermal neutrons.

A Li-6 enriched LiF epoxy filter was made and measurements with and without the filter were performed for both the graphite and tissue equivalent chambers. The results are summarized in Table 3. It is apparent from the table that the response of both chambers to thermal neutrons was high.

TABLE 3 EXPERIMENTAL RESULTS OF TE/TE AND GG/CO<sub>2</sub> CHAMBER READINGS USING Li-6 ENRICHED EPOXY FILTER

CHAMBER/GAS	NO FILTER		Li-6 FILTER
	AVERAGE CHAMBER READING (coulombs)	CORRECTED FOR γ ATTENUATION	
TE/TE	3.2 E-10	1.39 E-10	1.45 E-10
GG/CO <sub>2</sub>	3.6 E-10	2.20 E-10	2.29 E-10

Since the capture cross section of carbon and oxygen is very small, on the order of millibarns, these elements do not account for the thermal neutron response. Therefore, the response of the graphite chamber to thermal neutrons suggests that a secondary activated source of gamma rays was generated in the

presence of thermal neutrons. Therefore, to estimate the direct contribution of thermal neutrons to the chamber response, this interfering source of radiation had to be eliminated. Various sources were explored, such as the filtering, stem activation, and gamma rays produced in the shielding material around the chamber.

A new filter--a 1.5cm thick graphite holder filled with Li-6 enriched LiF powder--was tested with the graphite chamber with CO<sub>2</sub> gas. The experiment gave similar results to those obtained with the epoxy filter.

Aluminum stem activation was tested in a separate experiment. A plastic bag was filled with Li-6 enriched LiF powder and wrapped around the aluminum stem. Measurements were made with and without the stem covered. The stem activation contributed only 8% of the response and therefore was not a major activation source, contrary to what had been suspected.

Finally a small aperture collimator was used to reduce the streaming of neutrons into the surrounding material and to test the response of the graphite chamber to the activation gamma rays originating from polyethylene blocks around the chamber. A decrease of only 3% in the graphite chamber response with Li-6 filter, after correction for attenuation, confirmed that the main source of the unwanted radiation was from the shielding material. A refined experiment was then planned to keep the production of this background radiation as low as possible.

The neutron beam was thus confined to the chamber, and streaming into the medium was sharply reduced. Materials used in this study were chosen with extreme care. For example, the material that supports the chamber under the beam should not produce gamma rays with intense beams of thermal neutrons, it is almost impossible to fulfill this criterion unless pure Li-6 metal (the only element that does not produce capture gamma rays) is used. Unfortunately, lithium metal, which is highly reactive and explosive, is extremely difficult to work with. Therefore, another element with a very small capture cross section was chosen. Graphite, with its extremely low cross section (3.6 millibarn) and durability, was found to be the best choice for the chamber holder. A piece of graphite, machined into the shape of a pipe, housed the chamber so that only the active part of the chamber could be exposed.

To restrict the beam primarily to the active portion of the chamber, the holder was completely surrounded with plastic bags filled with Li-6 enriched LiF powder. The bags were wrapped around all but the top part of the chamber holder. The holder was then placed in a box filled with natural LiF powder to further absorb the thermal neutrons before they escaped from the medium (Fig. 2). A hole with the same diameter of the graphite holder was made in the top part of the box to expose the chamber. A Li-6 enriched filter disk with a small hole

(2.2 cm in diameter--the same as in the box and graphite holder) was used to stop thermal neutrons from reaching the chamber when the three holes (those of the graphite holder, box, and filter) were not aligned, as it is shown in Fig. 3C.

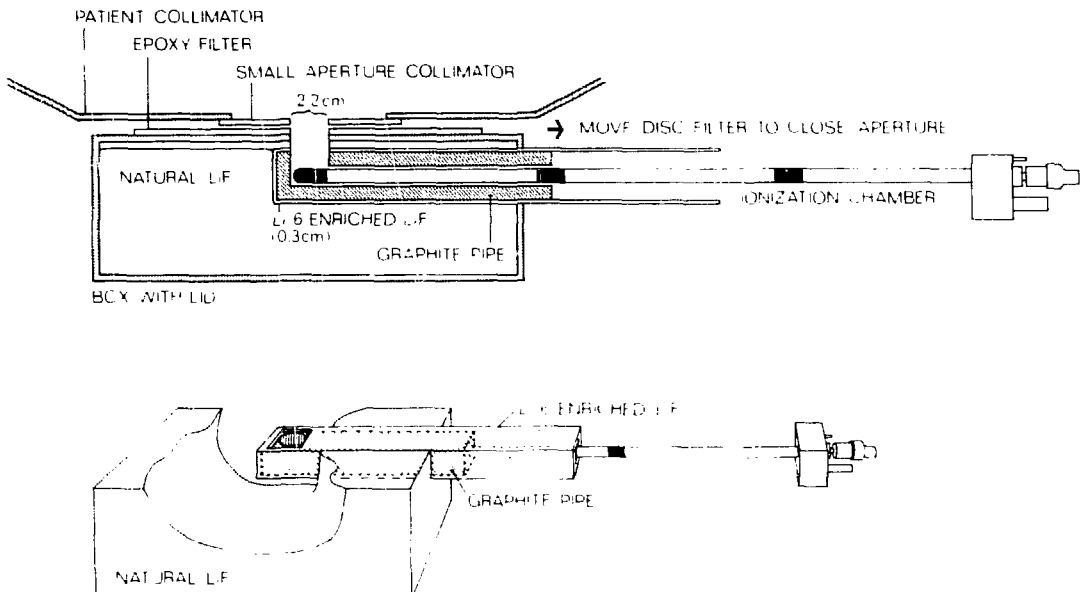


FIG. 2 SYSTEM PLACED UNDER THE REACTOR BEAM SUCH THAT ALL THE OPENINGS OF THE GRAPHITE PIPE, EPOXY FILTER AND THE COLLIMATOR ARE ALIGNED.

The entire system was then placed under the beam using a small collimator with a hole the same diameter as those in the graphite holder. When all the holes were aligned, the chamber's active portion and the part of the graphite holder that housed the active volume were the only materials exposed to the beam (Figs. 3A and 3B). Thermal neutrons not coming from the beam were absorbed and the production of unwanted gamma rays was prevented. To determine the effect of thermal neutrons in the beam on the chamber, the filter disk was pulled back along the box surface to cover the hole (Fig. 3C). This was done with great care so as not to disturb the alignment of the beam and the chamber.

Having determined the response of the chambers to thermal neutrons, the dual ionization chambers and the gold foils were used to unfold the components of the beam for the two cases where the  $D_2O$  blister tank was empty or full. To evaluate the depth dose distribution of the various radiation components of the beam, we constructed a polyethylene head phantom, 17.8 cm. in diameter and 19.8 cm. in height. The phantom was made from a solid piece of polyethylene with 1.27 cm. diameter holes drilled through it, and extending to the center of the phantom. The first hole was made 0.75 cm beneath the surface and the rest were spaced 1.75 cm apart (measured center to center) as de-

picted in Fig. 4.

The dose distribution in the phantom was determined by first placing the chamber on the surface of the phantom. The system was then aligned under the 7.6 cm. diameter collimator. The water, lead, and boral shutters were opened, and the phantom was irradiated with mixed neutron and gamma radiations. The current was integrated over one minute (as measured by the electrometer) for both positive and negative polarity and repeated three times for each case. Subsequent to this measurement, the  $D_2O$  blister tank was emptied and an identical set of measurements was recorded so that the responses of the chamber in the absence of the  $D_2O$  could be compared.

Next, all shutters were closed, and 12 minutes later (the time needed for the  $D_2O$  tank to fill) the chamber was placed in the first hole, 0.75 cm within the phantom. The remaining holes were blocked with polyethylene rods. During this maneuver special care was taken to maintain the original position of the phantom under the beam. The experimental procedures followed were identical to those for the previous position. The same experiment was carried out for positions 2, 3, 5, 7, 9, and 11, which correspond to phantom depths of 2.50, 4.25, 7.75, 11.25, 14.75, and 18.25 centimeters (Fig. 4). Detailed data were obtained for the graphite and tissue equivalent chambers when the  $D_2O$  tank was empty as well as full. In order to unfold the components of the beam in the above experiments, the chamber's response to thermal neutrons was excluded from the total chamber reading depending on the magnitude of the corresponding thermal flux at that position. Since the thermal neutron flux drops considerably with depth in the phantom, gold foils were used to evaluate the corresponding thermal neutron flux at each depth. After the ion chamber readings were corrected for thermal neutron contribution, the fast neutron sensitivity factors for the GG chamber and for the TE chamber were used in the following simultaneous equations (AAPM-80) to calculate the doses from fast neutrons and gamma rays for each experimental condition:

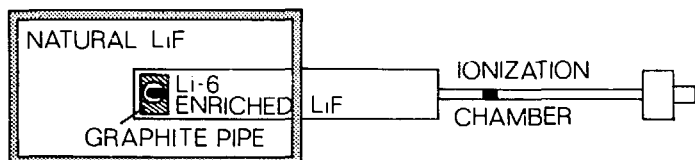
$$R_T = k_T D_N + h_T D_G$$
$$R_U = k_U D_N + h_U D_G$$

where the "h" and "k" are sensitivity factors due to gamma rays and fast neutrons respectively. Subscript T stands for neutron sensitive device and U is for the neutron insensitive,  $D_N$  and  $D_G$  are the fast neutron dose and gamma dose in rads.

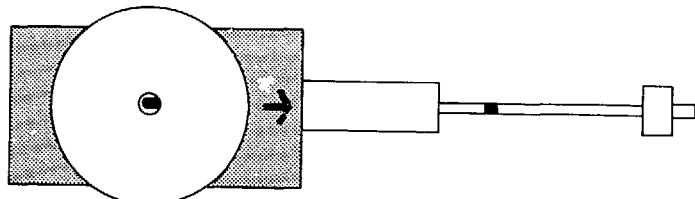
The thermal neutron doses were calculated by using the measured thermal neutron fluence and a KERMA-to-fluence factor of  $1.48 \times 10^{-11} \text{ rad-cm}^2/\text{n}$  (Zamenhof-75).

The incident gamma dose component was evaluated by placing the graphite chamber at various locations within the phantom while thermal neutrons were absorbed immediately at the beam exit. This procedure eliminated the formation of neutron induced gamma rays and left only the incident gamma component.

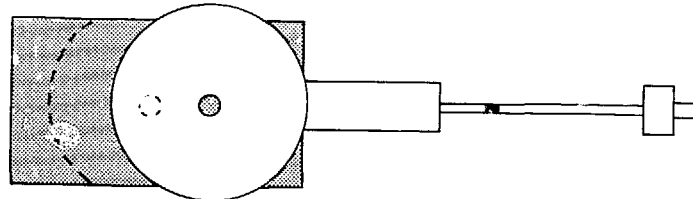
FIG. 3



(A) PLACEMENT OF THE IONIZATION CHAMBER IN THE GRAPHITE PIPE AND THE LiF BOX

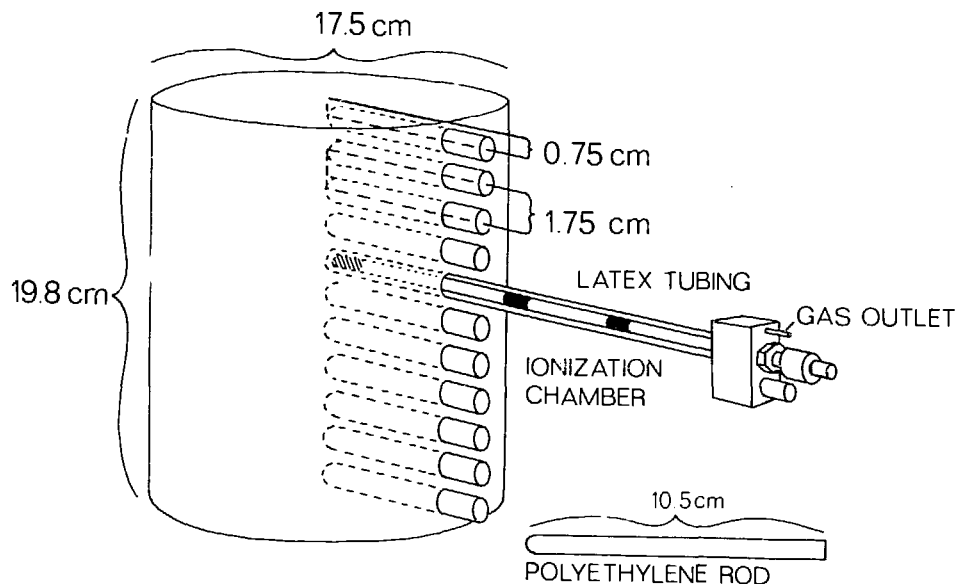


(B) A Li-6 FILTER WITH A CENTRAL OPENING WAS MADE TO FOCUS THE BEAM ON THE ACTIVE VOLUME OF THE CHAMBER



(C) MOVEMENT OF THE Li-6 FILTER ALONG THE BOX BLOCKING THE THERMAL NEUTRONS FROM REACHING THE CHAMBER

FIG. 4



POLYETHYLENE PHANTOM USED IN THE EXPERIMENTS WITH THE IONIZATION CHAMBER

The chamber response was corrected for attenuation of gamma rays by the filter.

#### RESULTS AND CONCLUSIONS

The first part of our results showed a thermal neutron response of  $1.59 \times 10^{-23}$  coulombs- $\text{cm}^2/\text{n}$  for the graphite chamber and  $4.8 \times 10^{-22}$  coulombs- $\text{cm}^2/\text{n}$  for the tissue equivalent chamber. These numbers correspond to .02% and 15% of the total response of the graphite and tissue equivalent chambers, respectively. The higher TE chamber response is due to  $^{14}\text{N}(n,p)^{14}\text{C}$  reaction in the TE gas of the TE chamber. The experimental results are summarized in Table 4.

TABLE 4 THERMAL NEUTRON RESPONSE FOR GG/CO<sub>2</sub> and TE/TE CHAMBERS

CHAMBER/ GAS	FLUX (n/cm <sup>2</sup> -sec)	NO FILTER	Li-6	READING
			FILTER*	DUE TO Nth (coulombs)
GG/CO <sub>2</sub>	$1.05 \times 10^9$	$3.90 \times 10^{-10}$	$3.89 \times 10^{-10}$	$.01 \times 10^{-10}$
TE/TE	$1.69 \times 10^9$	$3.25 \times 10^{-10}$	$2.76 \times 10^{-10}$	$.049 \times 10^{-10}$

\*Chamber Readings were corrected for attenuation of gamma rays

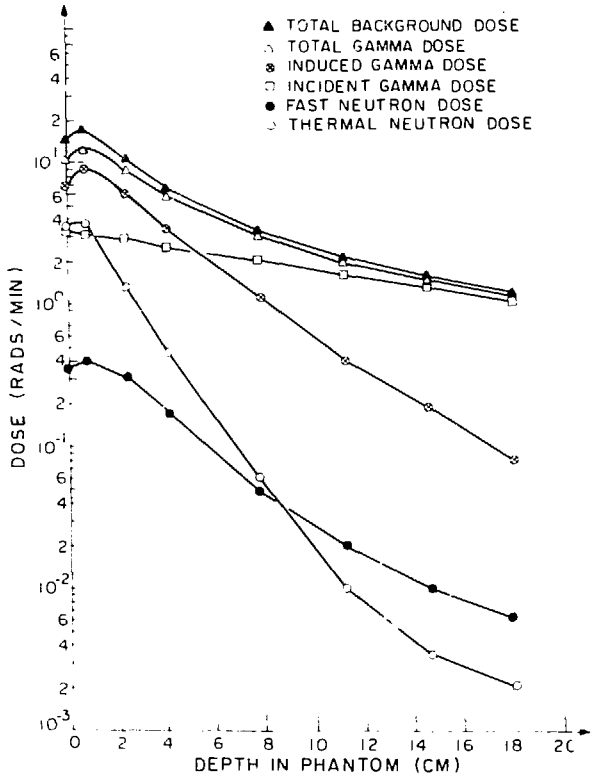
Figures 5 and 6 show the distributions of different dose components versus depth for the D<sub>2</sub>O tank full and empty. The top curves (solid triangles) in both graphs are the total background dose which is the sum of total gamma (incident and induced) and thermal and fast neutron doses. The open triangles are the total gamma dose which is the major component of the background dose, particularly when the D<sub>2</sub>O tank is full. When the D<sub>2</sub>O tank is empty, the fast neutron dose (solid circles) plays an important role as well. The induced gamma dose (crossed circles) is greater than the incident gamma dose up to about four to five centimeters deep inside the phantom. Hence, the induced gamma dose is important near the surface (comprising 67% of the total gamma dose) and the incident gamma dose (open squares) is the major gamma component at deeper locations within the phantom. The fast neutron dose (solid circles) at the surface is 17% higher than the thermal neutron dose when the D<sub>2</sub>O tank is empty and a factor of ten lower than thermal neutron dose when the tank is filled.

Finally, the thermal neutron dose component (open circles) is lower than the fast neutron component at all depths when the D<sub>2</sub>O shutter is open. When the shutter is closed, the thermal neutron component is greater, closer to the surface. At depths below 9 cm, however, the fast neutron dose remains higher.

A comparison of the magnitude of the surface dose of each dose component in Figs. 5 and 6 shows that in the absence of the D<sub>2</sub>O the thermal neutron dose increased by a factor of 2.16 and the total gamma dose was elevated by a similar ratio 2.15. The fast neutron dose, however, increased 25 fold. Despite this high increase the fast neutron dose comprised only 23% of the total dose. The major background dose component was the total gamma dose. This dose, in turn, was mostly from the induced

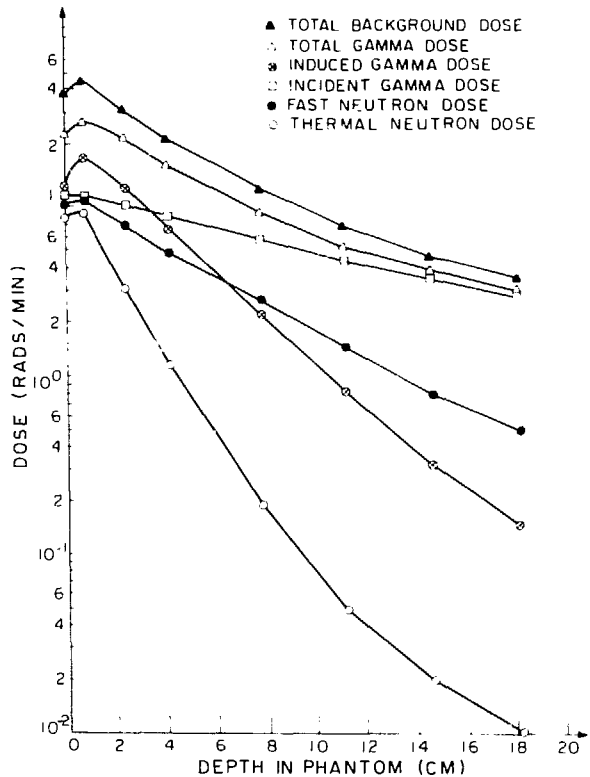
gamma rays at the surface (where thermal flux is high) and incident (core related) gamma rays at depth. Total gamma dose produces 57% of the total background dose. The remaining 20% results from thermal neutron dose not related to boron capture.

FIG. 5



ABSORBED DOSE VS. DEPTH IN POLYETHYLENE HEAD PHANTOM WITH  $D_2O$  TANK CLOSED (7.5 Cm Diameter Collimator) REACTOR POWER 4.6 MW

FIG. 6



ABSORBED DOSE VS. DEPTH IN POLYETHYLENE HEAD PHANTOM WITH  $D_2O$  TANK OPEN (7.5 Cm Diameter Collimator) REACTOR POWER 4.6 MW

When  $D_2O$  was present a greater percentage of the total background dose resulted from the total gamma dose (75%). Induced gamma rays comprised 66% of this dose and the remaining 34% resulted from incident gamma rays. The fast neutron contribution in this case was only 0.2% of the total dose.

It was concluded from these experiments that the beam obtained by draining the  $D_2O$  tank is superior because it results in more thermal neutrons, better depth penetration and shorter irradiation times.

We have seen that the dose from the reaction of the thermal neutrons with the boron compounds contributes a major part of the total dose. Determination of this dose, however, requires accurate information regarding the thermal neutron flux and the B-10 concentration in blood and/or tissue. Measurement of the thermal flux is possible with an accuracy of 10%. The prin-

cipal remaining problem in BNCT therefore is the determination of the B-10 concentration at the time of therapy. To date there has been no adequate technique of an on-line boron assay. Future clinical trials cannot be performed until such a technique is developed.

Another impediment to clinical trials is the lack of detailed information on the neutron spectrum of the MITR-II medical beam. This information and the development of an on-line boron assay are strongly recommended as the next step in Boron Neutron Capture Therapy.

#### REFRENCES

(AAPM-80) American Association of Physicists in Medicine. Protocol for neutron beam dosimetry. AAPM report no. 7 New York: American Institute of Physics (1980).

(Ashtari-82) Ashtari, M. Biological and physical studies of boron neutron capture therapy PhD thesis, Massachusetts Institute of Technology (1982).

(Rossi-56) Rossi, H. and Failla, G. Tissue equivalent ionization chambers. Nucleonics 14:32 (1956).

(Zamenhof-75) Zamenhof, R. G., Murray, B. W., Brownell, G. L., Wellum, G. R., and Eugene, I. T. Boron neutron capture therapy for treatment of cerebral gliomas; I: Theoretical evaluation of the efficacy of various neutron beams. Med. Phys. 2:2 (1975).

#### ACKNOWLEDGMENTS

Special thanks to the staff of the MIT Nuclear Reactor Laboratory especially John Bernard. The financial support of the National Institute of Health is greatly acknowledged.

# In Vivo Measurement of Time Dependent Boron-10 Concentration in Tumor

Keiji Kanda, Tooru Kobayashi and Kazuhiko Aoki

Research Reactor Institute, Kyoto University  
Kumatori-cho, Sennan-gun, Osaka, 590-04, Japan

## 1. Introduction

For boron neutron capture therapy, neutron irradiation doses depend greatly on  $^{10}\text{B}$ , which is pre-injected into the tumor in concentrations of ppm order (1-4). Therefore, to estimate the clinical effect and to decide the irradiation time, it is indispensable to know the  $^{10}\text{B}$  concentrations in the tumor just before neutron irradiations. The goal of the present study was to measure the  $^{10}\text{B}$  concentrations in tissue under the conditions that (i) samples should be alive after the measurements and (ii) the measuring time should be less than one hour with use of about a 1 g sample. We used the method of prompt gamma rays from  $^{10}\text{B}(\text{n},\alpha)^7\text{Li}^*$  reactions, because it had the possibility to be applied to the direct measurements of  $^{10}\text{B}$  concentrations of tumors in patients without any pretreatments and without great damage.

We have developed a system to detect neutron-induced prompt gamma rays by using the combination of the KUR thermal neutron guide tube,  $^6\text{LiF}$  tile neutron shield (5,6) and a  $\text{Ge}(\text{Li})$  detector. This system has a very low background of gamma rays for  $(\text{n},\gamma)$  measurements.

For the normalization of the neutron irradiation condition for known and unknown samples, prompt gamma rays from the  $\text{H}(\text{n},\gamma)\text{D}$  reactions were used. This treatment has many advantages for measuring homogeneous samples. By these improvements, we succeeded in measuring  $^{10}\text{B}$  concentrations of ppm order in 1 g of tissue accurately, reproducibly, and in a short time for neutron capture therapy.

## 2. Experiment

### 2.1. Neutron guide tube and neutron shielding material

The neutron guide tube is an apparatus which draws out neutrons of long wavelength to a distant point from the reactor core, so that pure thermal neutrons are available with very low contamination of gamma rays, epithermal and fast neutrons. The neutron guide tube of KUR has a guide part of 9.9 m and a neutron beam size of 10 (width) x 74 (height) mm<sup>2</sup>. The fluence rate of thermal neutrons is  $2 \times 10^6$  n/cm<sup>2</sup>.sec with a gamma-ray contamination of about 1 mR/h at an operating power of 5 MW. Fig. 1 shows the measuring system.

$^6\text{LiF}$  tiles were utilized as neutron shielding material near the sample, because of its small secondary gamma-ray production. Table 1 shows the features of the neutron shielding materials, i.e.  $\text{B}_4\text{C}$ , Cd metal and  $\text{LiF}$ . The number of capture gamma rays from  $\text{LiF}$  tiles developed by our group is extremely low compared with  $\text{B}_4\text{C}$  and Cd metal. Moreover, the number of gamma rays from  $\text{LiF}$  tiles of enriched  $^6\text{Li}$  is much less than that from natural  $\text{Li}$ .

${}^6\text{LiF}$  tiles made the equipment compact in size, which resulted in a small distance between the sample and the Ge(Li) detector, and so a high geometrical efficiency was obtained.

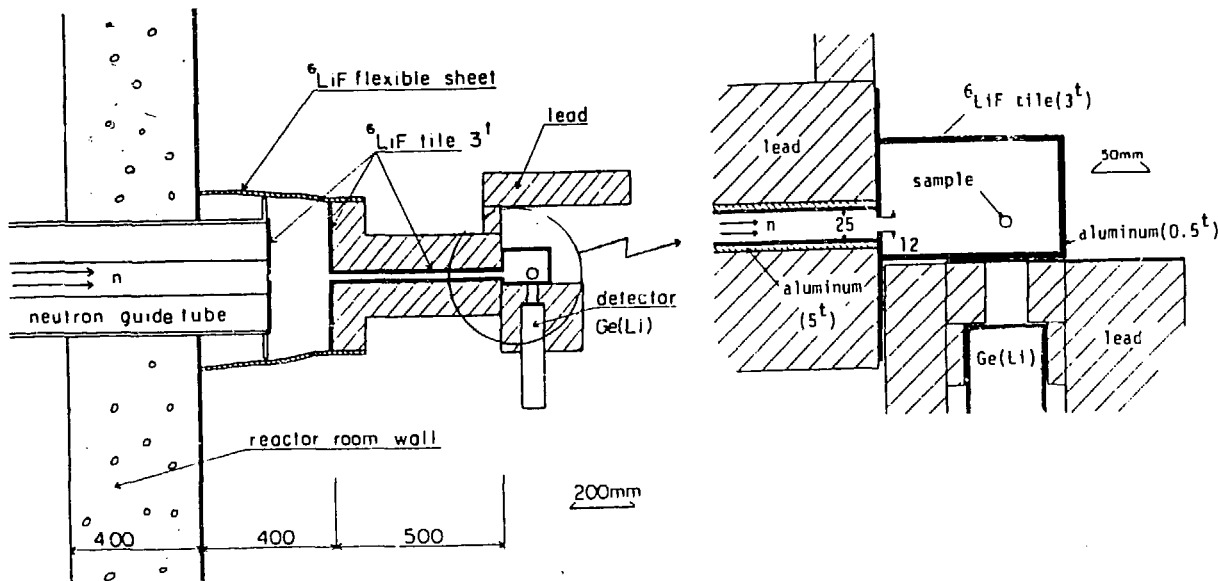


Fig. 1. Measuring system of  ${}^{10}\text{B}(n,\alpha){}^7\text{Li}^*$  prompt gamma rays attached to the neutron guide tube of KUR.

Table 1. Released energy of gamma rays per thermal neutron capture.

Material	Gamma-ray energy <sup>a)</sup> per capture (MeV)	Relative value	Comment
${}^6\text{LiF}$	$3.793 \times 10^{-4}$	1	
Nat. LiF	$4.381 \times 10^{-3}$	11.5	${}^6\text{Li}$ 7.4%
Nat. $\text{B}_4\text{C}$	$4.465 \times 10^{-1}$	1180	mainly from ${}^{10}\text{B}$
Nat. Cd	9.04	23800	mainly from ${}^{113}\text{Cd}$

<sup>a)</sup> Formula  $\sum_i \sigma_i f_i E_i / \sum_i \sigma_i f_i$ , where  $\sigma_i$ : microscopic cross section (b),  $f_i$ : fraction ratio in element,  $E_i$ : released gamma-ray energy (MeV). (Refer to Table of isotopes, 7th ed.)

## 2.2. Gamma-ray spectrometry

The energy resolution of the Ge(Li) detector system for gamma rays was 2.3 KeV at 1.33 MeV. The gamma-ray spectrum was measured directly in the 0-2.3 MeV range without the anti-Compton technique. When the S/N ratio is low, it can be improved by using the anti-Compton technique, but this usually results in a lower counting efficiency than the direct measurement. For the present purpose, we gave a high priority to getting a high counting efficiency for a short-time measurement.

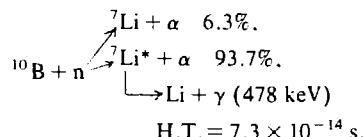
## 2.3. Samples

The standard samples with various  $^{10}\text{B}$  concentrations 0.01-100 ppm were made by diluting the JIS standard solution of 1000 ppm ( $\approx 100 \text{ ppm } ^{10}\text{B}$ ) with distilled water. The uncertainty of the  $^{10}\text{B}$  concentration for the 0.01 ppm standard sample was less than 1 %. We used the standard samples to check the detection limit of this measuring system. In addition, standard tissue samples were prepared into which known amounts of  $^{10}\text{B}$  in boric acid were added.

As sample case material, we can use pure Teflon  $(\text{C}_2\text{F}_4)_n$  which does not contain  $^{10}\text{B}$  and H, but we can not use ordinary aluminum because of its impurity of 10-100 ppm  $^{10}\text{B}$ . The Teflon sample cases used were 10 mm in outer diameter, 0.5 mm in thickness and 30 mm in length.

## 3. Determination of $^{10}\text{B}$ concentrations

The concentrations of boron and hydrogen can be assumed to be homogeneous in the tissue, so that prompt gamma rays emitted from hydrogen can be used for the normalization. In the thermal neutron energy region, cross sections of both  $^{10}\text{B}(\text{n},\alpha)^7\text{Li}^*$  and  $\text{H}(\text{n},\gamma)\text{D}$  have the  $1/\nu$  characteristic, and the branching ratio of  $^7\text{Li}^*$  is constant as follows:



We can find that at any point in the sample, the ratio of gamma rays emitted from the  $^{10}\text{B}(\text{n},\alpha)^7\text{Li}^*$  reaction to that from the  $\text{H}(\text{n},\gamma)\text{D}$  reaction is independent of thermal neutron irradiation conditions, i.e. neutron fluence rate, neutron energy spectrum and neutron distribution, as long as the distribution of  $^{10}\text{B}$  and H in the samples is homogeneous. Therefore, the ratio of gamma-ray counts of  $^{10}\text{B}(\text{n},\alpha)^7\text{Li}^*$  to that of  $\text{H}(\text{n},\gamma)\text{D}$  counted by a Ge(Li) detector is proportional to the atomic number ratio of  $^{10}\text{B}/\text{H}$  in the samples.

The  $^{10}\text{B}$  concentration in an unknown sample can be determined by comparison with known sample data. The relationship is as follows:

$$C_x = C_0 R_x A_x / R_0 A_0 \quad (1)$$

where

$C$ :  $^{10}\text{B}$  concentration of an unknown sample,  
 $C_x$ :  $^{10}\text{B}$  concentration of the known sample,  
 $R_x$ : counting ratio of prompt gamma rays from  $^{10}\text{B}$  to those from H for an unknown sample,  
 $R_0$ : counting ratio of prompt gamma rays from  $^{10}\text{B}$  to those from H for the known sample,  
 $A$ : concentrations of H in an unknown sample,  
 $A_x$ : concentrations of H in the known sample. Usually,  $A_0 = A_x$ .

The present method has the following advantages:

- 1) Thermal neutron irradiation conditions, i.e. neutron fluence rate, neutron distribution and neutron energy spectrum in the sample, are not affected.
- 2) Counting efficiency of the Ge(Li) detector is not affected.
- 3) Quantity and dimension of sample are not restricted.
- 4) Distance between the Ge(Li) detector and the sample irradiation position is flexible.

The quantity of the sample is not essential in this method, but it relates to the statistical error of the gamma-ray counting, so that the quantity of the sample is important for practical measurements.

#### 4. Results

Fig. 2 shows an example of a gamma-ray energy spectrum from  $^{10}\text{B}(n,\alpha)^7\text{Li}^*$  reactions for various  $^{10}\text{B}$  standard solutions of 1 g, measured by the Ge(Li) detector. Because of the Doppler effect of  $^7\text{Li}^*$  movement, gamma rays emitted from  $^7\text{Li}^*$  have a broad spectrum which looks a little broader than 10 KeV. While prompt gamma rays from  $(n,\gamma)$  reactions have steep peaks,  $^{10}\text{B}(n,\alpha)^7\text{Li}^*$  prompt gamma rays can be distinguished from the others by using the difference of the energy spectrum shape. Practically, we achieved the measurement of a swine melanoma sample of ppm order  $^{10}\text{B}$  without interference by gamma rays of 475 KeV from  $^{23}\text{Na}(n,\gamma)^{24}\text{Na}$  reactions (see Fig. 3).

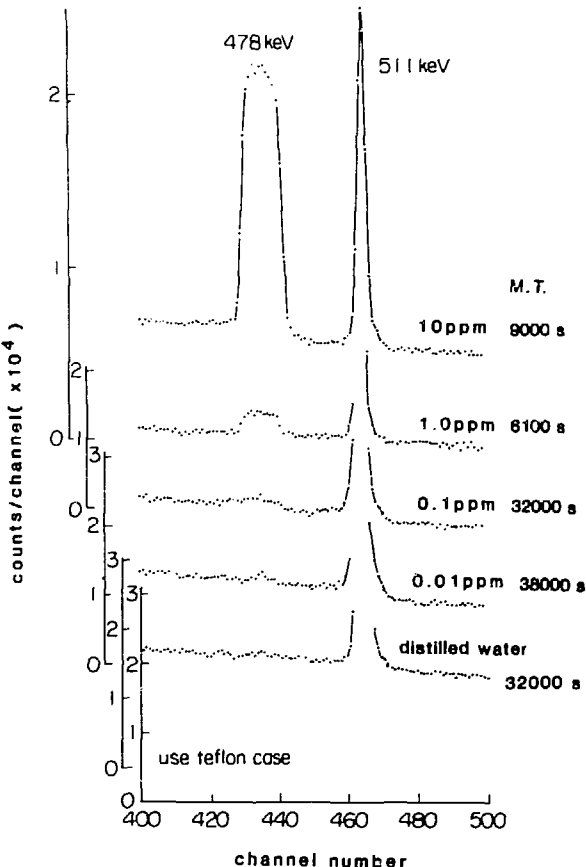


Fig. 2. Part of gamma-ray energy spectrum measured by Ge(Li) detector near  $^{10}\text{B}(n,\alpha)^7\text{Li}^*$  prompt gamma rays for various  $^{10}\text{B}$  concentrations.

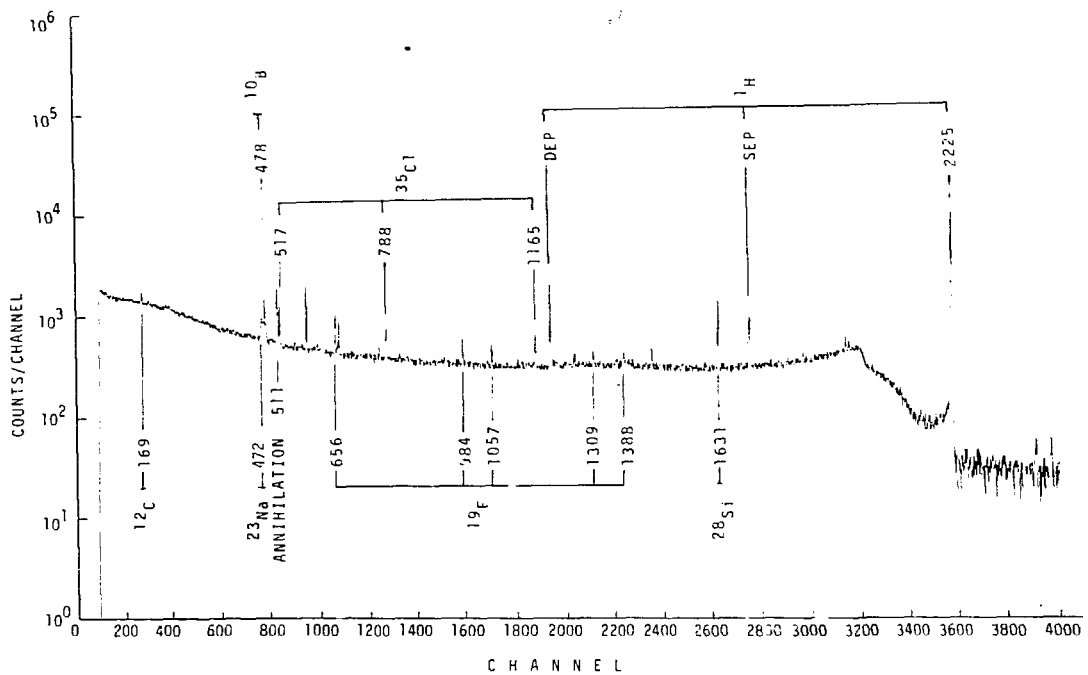


Fig. 3. Total gamma-ray energy spectrum measured by Ge(Li) detector for swine melanoma sample of 1 g containing 2 - 3 ppm  $^{10}\text{B}$ .

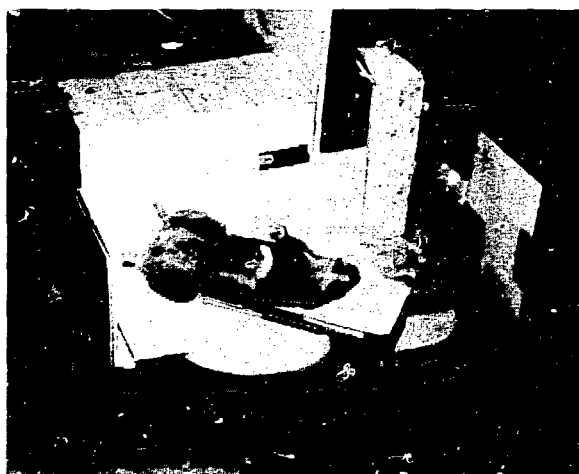


Photo. 1.

View of the time-dependent  $^{10}\text{B}$  measurement in hamster.

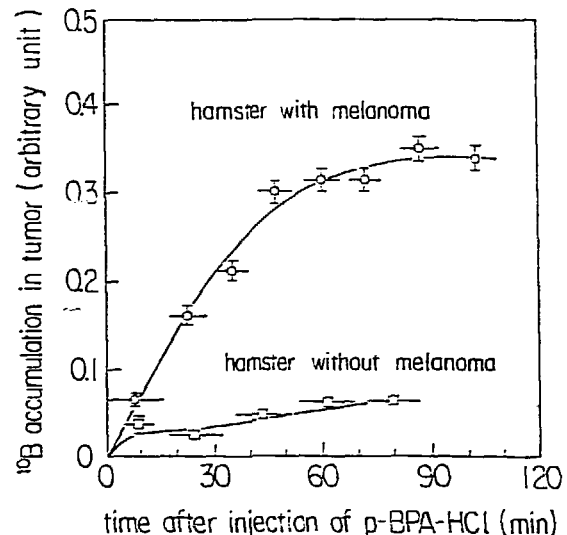


Fig. 4. Time-dependency of the  $^{10}\text{B}$  accumulation in tumor.

## 5. Discussion and application

For practical use, the terms such as  $C_0, R_0, A_0$  and  $A_x$  in eq.(1) can be determined previously with sufficient accuracy compared with  $R_x$ . So we considered that the error of  $C_x$  depends mainly on the relative standard deviation of  $R_x$ . A semi-empirical equation between the deviation of  $R_x$  and measuring time in this system,  $\sigma(X, t)$ , is derived from data on  $10^4$  ppm standard solution for 9000 sec as follows:

$$\sigma(X, t) = \frac{1}{\sqrt{t}} \left( \frac{\sqrt{2.03 \cdot X + 23.6}}{2.03 \cdot X} + \frac{\sqrt{44.8 + 1.68}}{44.8} \right)$$

where  $X$ :  $^{10}\text{B}$  concentration (ppm),  $t$ : measuring time (sec).

$^{10}\text{B}$  concentrations of 10 ppm, which are usually used for this therapy, can be measured in less than 30 sec with 10 % accuracy.

This method has been applied for the measurement of time-dependent boron concentrations in melanoma-bearing hamsters. (see Photo. 1) Figure 4 shows the results, in which the difference of  $^{10}\text{B}$  concentration in hamsters with and without melanoma is clearly observed.

### Acknowledgements

The authors would like to acknowledge the invaluable suggestions of Prof. Y. Mishima of Kobe University Hospital and Prof. H. Hatanaka of Teikyo University Hospital.

They also wish to thank Prof. S. Okamoto, Mr. T. Akiyoshi and Mr. T. Ebisawa of Kyoto University Research Reactor Institute (KURRI) for their advice on gamma-ray spectrometry. They also thank Mr. S. Shiroya and Mr. T. Hamada of KURRI for their support of the experiments.

This study was partially supported by a Grant-in-Aid from Ministry of Education, Science and Culture.

### References

- (1) Y. Mishima and T. Shimakage, Thermal neutron capture therapy for malignant melanoma using  $^{10}\text{B}$ -dopa and  $^{10}\text{B}_{12}\text{-chlorpromazine}$  compounds., *Pigm. Cell.*, 2, 394 (1976)
- (2) H. Hatanaka and W. H. Sweet, Slow neutron capture therapy for malignant tumors : its history and recent development, *Biomedical Dosimetry*, IAEA, 147 (1975)
- (3) K. Kanda, T. Kobayashi, K. Ono, T. Sato, T. Shibata, Y. Ueno, Y. Mishima, H. Hatanaka, and Y. Nishiwaki, Elimination of gamma rays from a thermal neutron field for medical and biological irradiation purposes, *ibid* 205 (1975)

- (4) T. Kobayashi and K. Kanda, Analytical calculation of boron-10 dosage in cell nucleus for neutron capture therapy, *Radiat. Res.*, 91, 77 (1982)
- (5) K. Kanda, Lithium fluoride tile and sheet for neutron field, *J. At. Energy Soc. Japan.* 20, 37 (1978)
- (6) T. Kobayashi and K. Kanda, Development of LiF tile neutron shield and measurement of tritium release from it, *KURRI-TR-198* (1980)
- (7) S. Okamoto et al., KUR neutron guide tube, *Kyoto Univ. Res. Reactor Inst.* (1975)
- (8) T. Hamada, K. Aoki, T. Kobayashi and K. Kanda, The in vivo measurement of the time dependent  $^{10}\text{B}$  movement in tumor of hamsters, *Annu. Rep. Res. Reactor Inst. Kyoto Univ.*, in press.
- (9) T. Kobayashi and K. Kanda, Microanalysis of ppm-order  $^{10}\text{B}$  concentrations in tissue for neutron capture therapy by prompt gamma-ray spectrometry, *Proceeding of 7th ICRR*, D4-15 (1983); *Nucl. Instr. Methods* 204, 523-31 (1983).

## Boron-10 Analysis by Prompt-Gamma and Track-Etching Techniques

R.G. Fairchild,<sup>1</sup> D. Gabel,<sup>1,2</sup> B.H. Laster,<sup>1</sup>, D. Greenberg,<sup>1</sup>  
W. Kiszenick,<sup>3</sup> and P.L. Micca<sup>1</sup>

<sup>1</sup>Medical Dept., Brookhaven National Laboratory, Upton, NY 11973

<sup>2</sup>Chemistry Dept., University of Bremen, Bremen, FRG

<sup>3</sup>Polytechnic Institute of Brooklyn, Brooklyn, NY 11201

### ABSTRACT

In order to predict the efficacy of boronated compounds for neutron capture therapy (NCT) it is mandatory that the boron concentration in tissues be known. Various techniques for measurement of trace amounts of boron (1 to 100 ppm) are available, including various wet chemical and physical procedures. Experience has shown that, with the polyhedral boron cages in particular, the usual colorimetric and spark emission spectroscopic methods are not reliable. Although compounds may be traced with radiolabels, direct physical detection of boron by non-destructive methods is clearly preferable.

Boron analysis via detection of the prompt  $\gamma$  ray from the  $^{10}\text{B}(\text{n},\alpha)^7\text{Li}$  reaction has been shown to be a reliable technique. Two prompt- $\gamma$  facilities developed at BNL are described. One, at the 60-MW High Flux Beam Reactor (HFBR), uses sophisticated beam extraction techniques to enhance neutron intensity and reduce fast neutron and  $\gamma$  contamination. The other was constructed at Brookhaven's 5-MW Medical Research Reactor (MRR) and uses conventional shielding to provide an "on-line" boron analysis facility adjacent to beams designed for neutron capture therapy (NCT), thus satisfying one of the requisite for clinical application of this procedure.

Technical restrictions attendant upon the synthesis and testing of boronated biomolecules often require the measurement of trace amounts of boron in extremely small (mg) samples. A track-etching technique capable of detecting ng amounts of boron is described. Thus it is possible to measure the boron content in small amounts (mg samples) of antibodies, or boron uptake in cells grown in tissue culture.

### INTRODUCTION

Technical difficulties associated with the synthesis of boronated biomolecules make it necessary to measure the boron content of these compounds at various stages in their production. In addition, the many variables involved in evaluating biological effects from the  $^{10}\text{B}(\text{n},\alpha)^7\text{Li}$  reaction make it necessary to have accurate information about boron content in tissues during the time course of experimentation. Perhaps most important of all, there is a firm consensus among those who have been or are involved in clinical application of NCT, that knowledge of boron concentration in tissue immediately prior to irradiation of humans is mandatory (1-4).

It is the common experience of many of those participating in this Symposium that conventional microanalytical techniques for boron analyses are unsatisfactory. Wet chemical colorimetric procedures often employed are time consuming, taking many hours, to days (5). In particular, we have found that the latter methods do not produce consistent results with the polyhedral borane and carborane cages commonly incorporated in experimental compounds; this inconsistency is probably due to incomplete breakdown of the cages (6). Spark emission spectroscopic techniques are equally unreliable, perhaps because of the low vaporization point of the boron cage compounds. Conventional radiolabels have been used as tracers in order to circumvent problems encountered in boron microanalysis; however, the potential lability of the tag as well as of boron itself appear to introduce unwarranted complications.

Boron analysis via detection of the prompt  $\gamma$  ray from the  $^{10}\text{B}(\text{n},\alpha)^7\text{Li}$  reaction has been reported by others (7,8), and is used in Japan for investigation of NCT (9,10). This method of quantification is independent of the chemical form of boron. Another major advantage of this procedure is that it is non-destructive; no observable damage is produced following the relatively low exposures to thermal neutron beams. Consequently, for example, borated monoclonal antibodies may be evaluated for boron content, and then used for biological experiments.

Two prompt- $\gamma$  facilities have been developed at BNL; one of these is at the 60-MW HFBR, and uses sophisticated (and therefore expensive) beam extraction devices to enhance neutron intensity while minimizing fast neutron and  $\gamma$  contamination. The second facility was constructed at the 5-MW MRR, with conventional techniques, in order to make possible "on-line" boron analysis immediately prior to possible clinical trials of NCT at the therapy beam ports of the MRR. Both facilities have similar sensitivities ( $\sim 200$  counts/min per  $\mu\text{g}$   $^{10}\text{B}$ ), and can detect at least  $1 \mu\text{g}$   $^{10}\text{B}$  per gram tissue in a few minutes.

Biochemical techniques used in the synthesis and analysis of boronated biomolecules typically produce extremely small quantities of natural boron for measurement. Various column chromatographic analyses produce multiple small samples; monoclonal antibodies are expensive even in mg amounts; typical cell culture experiments produce  $\sim 10^6$  cells ( $\sim 1 \text{ mg}$ ) per cell-culture flask. In response to these needs, a track-etching technique has been developed in which 0.5- $\mu\text{l}$ iter (0.5-mg) droplets containing  $\geq 0.1 \mu\text{g}$  of natural boron per ml can be detected ( $\sim 0.1 \text{ ng}$   $^{10}\text{B}$ ) (11).

## METHOD AND RESULTS

### Prompt- $\gamma$ Analysis

At Brookhaven's HFBR, various beam extraction techniques (Ni-plated glass wave guides; cold Bi filters) are used to produce "pencil" beams of pure thermal neutrons ( $\sim 2 \text{ cm}$  in diameter) which are free of significant contaminations of fast neutrons and  $\gamma$  rays. A stylized configuration of such a facility is shown in Fig. 1; in this geometry, background radiation was low; shielding around the 2x2-inch solid state detector (pure Ge or Ge(Li)) was

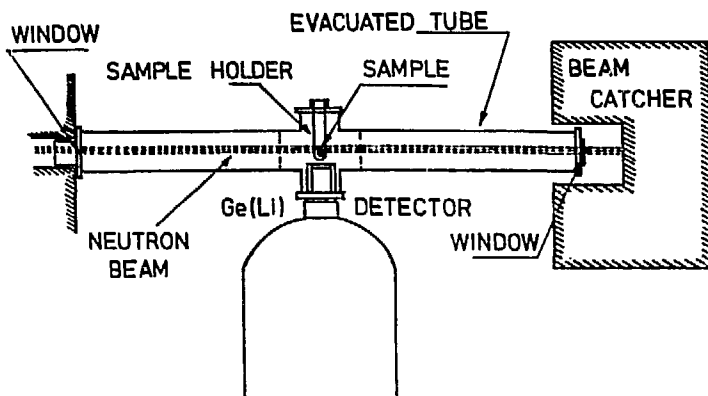


Fig. 1. Diagram of typical geometry used for prompt- $\gamma$  analysis of  $^{10}\text{B}$  at a pure thermal neutron beam from HFBR.

minimal, and the detector could be positioned within a few inches of the beam. Background was further reduced by absorbing thermal neutrons scattered off the sample with an enriched  $^{6}\text{Li}_2\text{CO}_3$  cylinder positioned coaxially with the beam and around the sample. Currently the H-1 beam at the HFBR is being used. The thermal neutron flux density is  $\sqrt{3} \times 10^7 \text{ n/cm}^2\text{-sec}$  at 60 MW; sensitivity is  $\sqrt{700}$  counts per  $\mu\text{g}$   $^{10}\text{B}$  per 200 sec, which is  $\sqrt{8\%}$  of background. Thus, for the usual 200-sec measurement, the error caused by background (1 SD)  $= 0.15 \mu\text{g}$   $^{10}\text{B}$ . All measurements are obtained from 1 g-samples of water or tissue in quartz test tubes. Typical spectra obtained from water and boron standards are shown in Fig. 2.

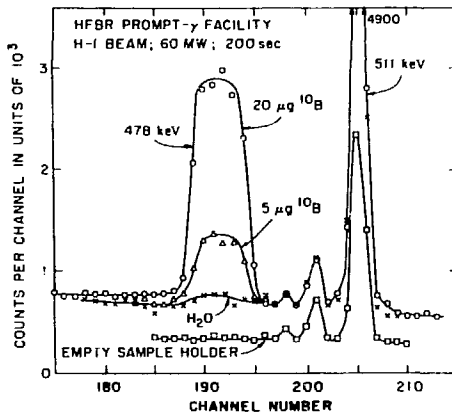


Fig. 2. Spectra obtained from the HFBR, showing background from water samples, and the response from  $^{10}\text{B}$  standards in  $\text{H}_2\text{O}$  used for calibration of unknown amounts of boron in various tissues.

Access to the H-1 beam of the HFBR is limited because of requirements of physics experiments. As noted above, problems encountered in clinical application of NCT have demonstrated the necessity of determining boron content of blood (and of tumor also, if possible) immediately prior to the irradiating of patients (and during the course of irradiation, if applicable). Consequently, an "on-line" facility for prompt- $\gamma$  analysis of boron has been constructed at the MRR radial tube (Fig. 3). In this apparatus, beam extraction, collimation, and shielding have been accomplished by using conventional (low-cost) materials available at any reactor facility. At a power of 2 MW, the flux density is  $\sqrt{8 \times 10^7}$  n/cm<sup>2</sup>-sec, and the sensitivity is  $\sqrt{500}$  counts per 200 sec (16-cm source-detector distance), which is  $\sqrt{4\%}$  of background. Thus at the MRR, background is twice that at the HFBR, and the sensitivity is somewhat less. Spectra from water and boron standards measured at the MRR are shown in Fig. 4.

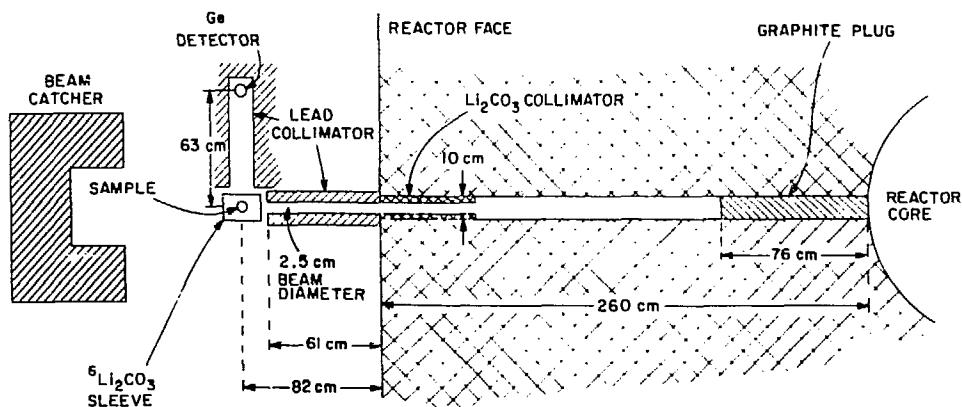


Fig. 3. Geometry of prompt- $\gamma$  apparatus at the MRR. Source-detector distance has been changed to  $\sqrt{16}$  cm.

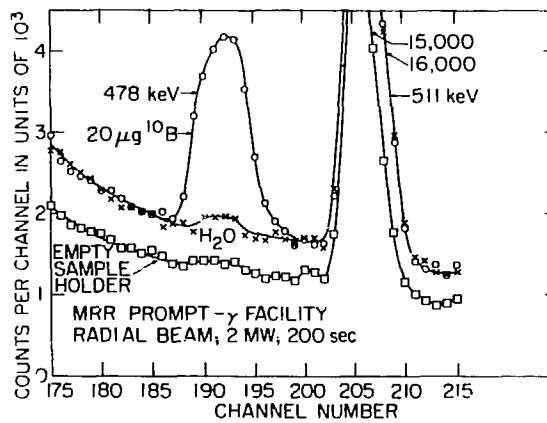


Fig. 4. Spectra obtained from the MRR, showing background from water, and the response from  $^{10}\text{B}$  standards in water.

### Boron Analysis by Track Etching

Prompt- $\gamma$  measurements are ideal for 1-g tissue samples. However, the sensitivity of the method is not adequate for many needs, such as 1-mg tissue samples obtained from tissue culture experiments. Therefore the technique developed by Gabel et al. (11) has been used for these smaller samples. In this procedure, 0.5- $\mu$ liter drops (0.5 mg) of the solution to be analyzed are deposited in cellulose nitrate track detectors (Kodak Pathé LR115 type 1; 6- $\mu$ -thick film on polyester sheets), and irradiated to  $\sim 6 \times 10^{12}$  n/cm<sup>2</sup>-sec (1 MW, 300 sec), at the patient port of the MRR. Standard solutions of natural boron are deposited on the film to construct a calibration curve, as shown in Fig. 5. Boron is mixed with F-10 cell medium plus fetal bovine serum (FBS), which serves as a matrix to hold the boron while drying. Relatively uniform fields of alpha tracks are obtained in this manner. Asymmetric deposition of boron is found if water is used as a solvent; the small crystals observed when phosphate buffered saline (PBS) + 1 mg protein/ml is used as the solvent (11) were also eliminated.

After irradiation, the film is developed in 10% NaOH at 60°C for 45 minutes. Tracks are then counted opto-electronically with a Zeiss microscope (4X objective with a green filter) interfaced with a Quantimet image analyzer. Fields obtained from drops with 1 and 10  $\mu$ g natural boron per ml are shown in Fig. 6 along with background fields. As can be seen from the calibration curve, the sensitivity extends below 0.1  $\mu$ g natural boron/ml (0.02  $\mu$ g  $^{10}B$ /ml), and, since 0.5-mg drops are used, the techniques can detect ng amounts of natural boron.

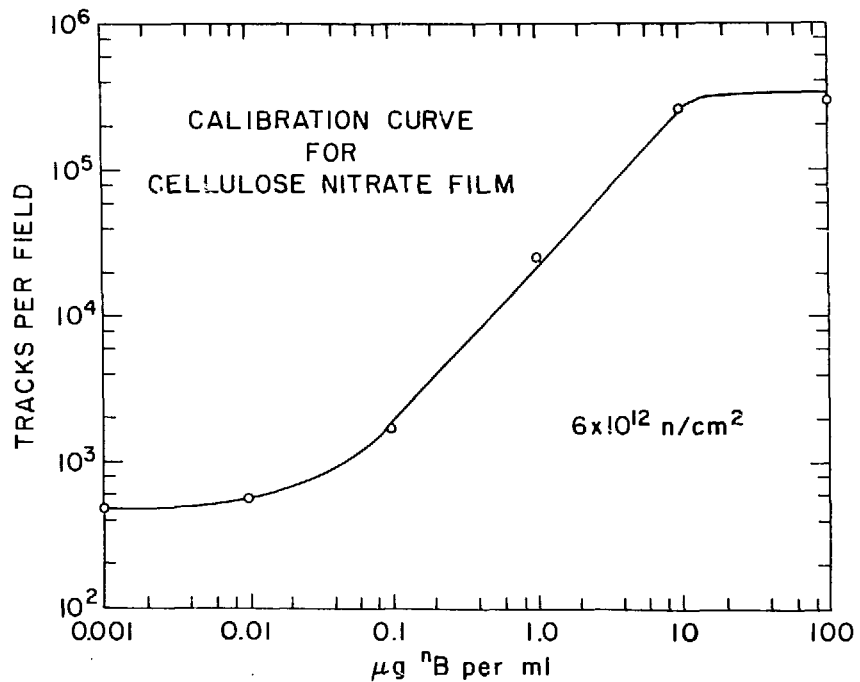


Fig. 5. Calibration curve obtained with 0.5- $\mu$ liter drops of standard solutions of natural boron.

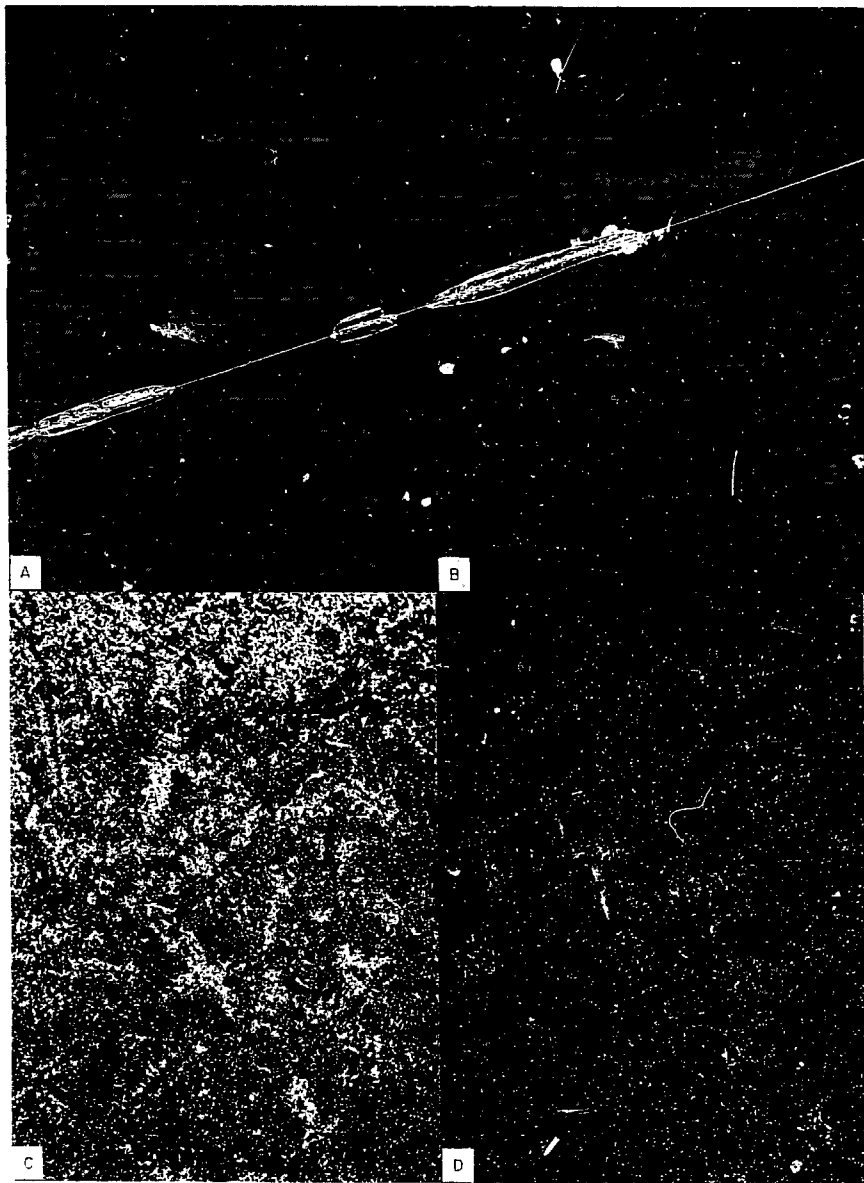


Fig. 6. Cellulose nitrate film irradiated to  $56 \times 10^{12}$  n/cm<sup>2</sup>-sec at the MRR. Field A = background; B = background from cell growth media used for suspension of boron standards; C = 10  $\mu$ g  $^{10}\text{B}$ /ml in 0.5- $\mu$ l drop; D = 1  $\mu$ g  $^{10}\text{B}$ /ml in 0.5- $\mu$ l drop.

#### DISCUSSION

Endogenous boron levels in humans are  $\sim 0.1$   $\mu$ g  $^{10}\text{B}$ /g (in blood, for example; ref. 12). The lowest level of  $^{10}\text{B}$  considered to be useful for therapy is  $\sim 1$   $\mu$ g  $^{10}\text{B}$ /g tumor (13). These levels define the limits of sensitivity of interest for prompt- $\gamma$  analysis of boron in tissue samples. As described

above, the two prompt- $\gamma$  facilities at BNL provide this capability, with the additional sensitivity at the HFBR used for tissue analysis of low boron concentration often obtained with trial compounds synthesized with natural boron.

Since the response from 1  $\mu\text{g}$  of  $^{10}\text{B}$  is only a few percent of background, background subtraction is of great importance. In particular, the prompt  $\gamma$  from Na (472 keV) interferes with B analysis and must be corrected for, to obtain accurate results. Table 1 summarizes Na and H contents in human tissues. If sample size or exposure time is monitored by the hydrogen capture  $\gamma$  ray (at 2.2 meV), then care must be taken to account for varying contents of H in different tissues. Most importantly, Na content is seen to vary from 8 to 18%, and thus will be responsible for significantly different backgrounds. We have taken multiple readings of various "blank" tissue samples from our mouse and rat tumor models, and have found that background must be corrected according to tissue type as well as sample size. For example, the background produced by Na varies from the equivalent of  $\sqrt{0.5} \mu\text{g }^{10}\text{B/g}$  of muscle to  $\sqrt{1.1} \mu\text{g }^{10}\text{B/g}$  for blood or tumor.

Although the relative background obtained at the MRR prompt- $\gamma$  facility is  $\sqrt{2}$  times that at the HFBR, the sensitivity and background is such that the analysis of 1  $\mu\text{g }^{10}\text{B/g}$  tissue is possible in a single 200-sec run. Consequently it has been possible to develop an "on-line" capability for boron analysis which will make possible the determination of boron content in blood immediately prior to (and during, if desired) irradiation of humans for NCT. Thus, one of the prime requisites for future clinical trials has been met. Furthermore, only conventional shielding materials were used, so that any reactor facility considering NCT in humans can construct a similar facility.

Table 1. Percent by Weight of H and Na in Human Tissues, from Snyder (12)

Tissue	Wt in g	$\text{H}^+$		$\text{Na}^+$	
		g/tissue	Wt %	g/tissue	Wt %
Brain	1,400	150	10.7	2.5	0.18
Blood	5,500	550	10.0	10	0.18
Small intestine	640	67	10.5	0.64	0.10
Liver	1,800	180	10	1.8	0.10
Muscle	28,000	2800	10	21	0.08
Pancreas	100	9.7	9.7	0.14	0.14
Lung	1,000	99	9.9	1.8	0.18
Parenchyma	570	55		1.0	
Blood	430	44		0.8	
Spleen	180	18	10	0.22	0.12

Probably the most difficult way to evaluate a boron compound for potential efficacy in NCT is to try to measure tumor control in animal tumor models following NCT. This necessitates multiple animals at multiple dose points, with concomitant experiments on controls in the neutron field as well as in x-ray beams. The development of information about the boron content necessary for successful NCT and about the potential effects due to variation in microdistribution (13-15) significantly reduces the necessity for such time-consuming and expensive experiments. The basic information is available from the boron content of tissues measured as described above.

Some basic parameters are more easily obtained from in vitro experiments in cell cultures. The biological activity of boronated antibodies and the binding of melanin affinic molecules as well as that of steroid and nucleoside analogs may all fit into this category. Again, a simple boron analysis on a cell culture of  $\sim 10^6$  cells ( $\sim 1$  mg) is much simpler than the determination of meaningful survival curves in mixed fields of neutrons and  $\gamma$  rays (again accompanied by the appropriate controls). The track-etching techniques described above provide the capability for this type of analysis, as cells may be lysed and deposited on film for appropriate analysis.

Additionally, needle biopsies may be obtained from tumor immediately prior to NCT, for boron analysis by track etching. The whole procedure could be completed within 1 hr, thus providing a most important parameter for determining the requisite exposure time for tumor control.

#### REFERENCES

1. W. Sweet, Paper VII-1, this Symposium.
2. K. Kanda and T. Kobayashi, Paper I-12, this Symposium.
3. M. Ashtari and G. Brownell, Paper I-11, this Symposium.
4. Y. Hayakawa, T. Inada, S. Harasawa, and H. Hatanaka, Paper I-10, this Symposium.
5. A. Kaezmarcyk, J. Messer, and C.E. Pierce. Anal. Chem. 43, 271-2 (1971).
6. D. Slatkin (Brookhaven National Laboratory), personal communication; paper in preparation (1984).
7. M.P. Fally, D.L. Anderson, W.H. Zoller, and G.E. Cordon. Anal. Chem. 51, 2209-21 (1979).
8. E.S. Gladney, B.T. Jurney, and D.B. Curtis. Anal. Chem. 48, 2139-42 (1975).
9. T. Kobayashi and K. Kanda. Nucl. Instr. Methods 204, 523-31 (1983).
10. K. Kanda and T. Kobayashi, Paper I-12, this Symposium.
11. D. Gabel, I. Hocke, and W. Elsen. Phys. Med. Biol. (1983) in press.
12. W.S. Snyder, Chairman, Report of the Task Group on Reference Man, ICRP Report No. 23. Published for ICRP by Pergamon Press, New York, 1975.
13. R.G. Fairchild and V.P. Bond, Paper I-1, this Symposium.
14. D. Gabel et al., Paper III-2, this Symposium.
15. T. Kobayashi and K. Kanda, Paper III-1, this Symposium.

Remarks on the Optimization of Incident Neutron Energy  
for Neutron Capture Therapy

K. Morstyn\* , B.Kawecka\* , L.E.Feinendegen

Institute of Medicine, Nuclear Research Center Jülich GmbH.

D-5170 Jülich, Federal Republic of Germany

Introduction

Many clinical and laboratory trials of specific tumor destruction by neutron capture products were performed since the exoenergetic reaction  $^{10}\text{B}(\text{n},\alpha)^7\text{Li}$  had first been suggested for this purpose /1/. Most of them were not as successful as one might have expected from the fundamental idea of producing the destructive energy selectively within the target volume.

Apart from the crucial biochemical problem with specific loading of tumor cells with absorbing nuclei ( $^{10}\text{B}$  or  $^6\text{Li}$ ), the proper choice of incident neutron energy seems to be of essential importance. Thermal neutron beams have mostly been applied till now /2,3/, even though superiority of epithermal /4,5/ or even intermediate /6,7/ neutrons has already been suggested \*\* . In spite of some comparative studies of slow neutron beams from different assemblies /7,9/, quantitative optimization of the incident neutron energy for the sake of neutron capture therapy has not yet been performed.

Method

In the calculations presented here we concentrated on the case of a deep-sited tumor, represented by a 1-cm diameter bo-

---

\*On leave from the Inst.of Physics and Nucl.Techn. AGH, Krakow, Poland.

\*\* The use of  $^{10}\text{B}$  was also proposed for enhancing conventional fast neutron therapy by making use of neutrons slowed-down within the patient's body /8/.

ron-loaded core centrally located within the ICRU sphere /10/ (a standard 30-cm diameter tissue-like phantom of a human body). Neutrons of varying energy were assumed to impinge isocentrially onto the phantom surface. Space-energy distributions of scattered neutrons and neutron-induced gamma radiations were calculated by solving the stationary transport equation in the multigroup discrete-ordinates numerical approach. The one-dimensional ANISN transport code /11/ and the DLC-31 multigroup data set /12/ (37 neutron and 21 photon groups, derived from the DNA  $\approx$  1 ENDF/B-IV cross-section libraries) were applied for this purpose. The depth distributions of the absorbed dose were then calculated in the kerma approximation with the use of recent fluence-to-kerma conversion factors /13/. The partial contributions of different secondaries to the absorbed dose were also calculated.

### Results

Fig. 1 presents the relative contribution of the  $^{10}\text{B}(n,\alpha)^7\text{Li}$  reaction to the absorbed dose in the tumor location vs. incident neutron energy for the case of 50  $\mu\text{g/g}$  of  $^{10}\text{B}$  in the target. Contributions of photons and other secondaries (mainly protons) are also given. It is evident that the short-range neutron capture products dominate only in some limited energy interval (approximately 0.05 - 2 MeV in this case). For lower neutron energies, gamma rays from the radiative capture on hydrogen nuclei become most important, whereas above 2 MeV recoil protons from elastic scattering play a dominant role.

A similar tendency was observed for a wide range of boron concentrations within the tumor volume, the effect being proportional to the  $^{10}\text{B}$  content up to about 200  $\mu\text{g/g}$ . Therefore, below this concentration, the relative dose increment (referring to the case with no boron in the target volume) may be presented per unit  $^{10}\text{B}$  uptake, as it is done in Fig. 2, both in terms of

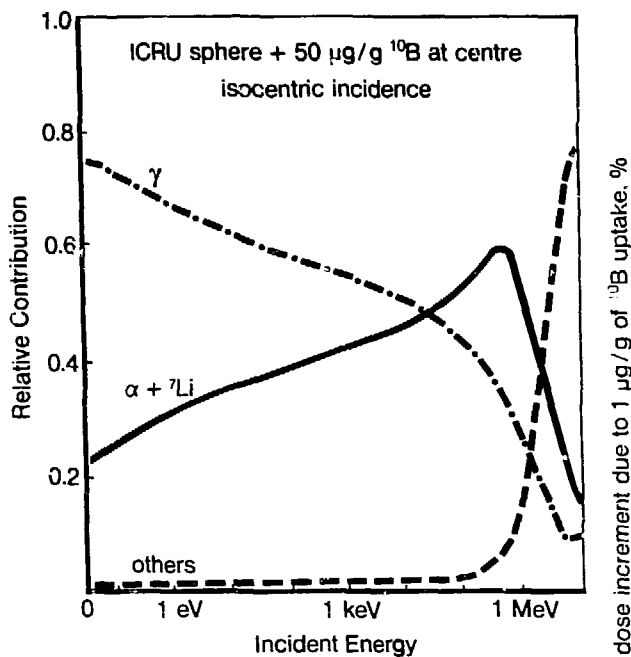


Fig. 1. Relative contributions to the absorbed dose in the central core (1-cm diameter, 50  $\mu\text{g/g}$   $^{10}\text{B}$ ) of the ICRU sphere irradiated isocentrically with neutrons of varying energy.

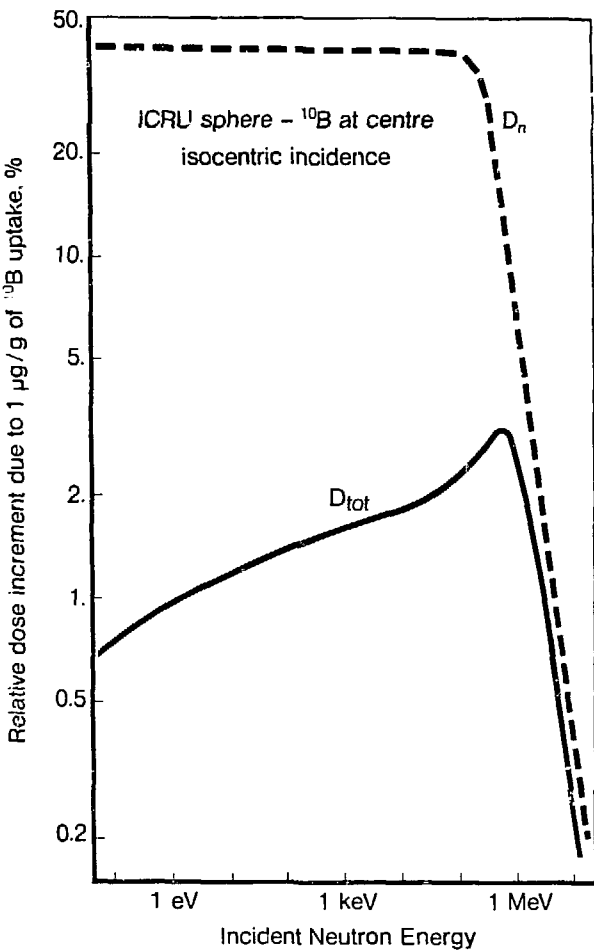


Fig. 2. Total and neutron dose increment due to 1  $\mu\text{g/g}$  uptake of  $^{10}\text{B}$  at the center of ICRU sphere.

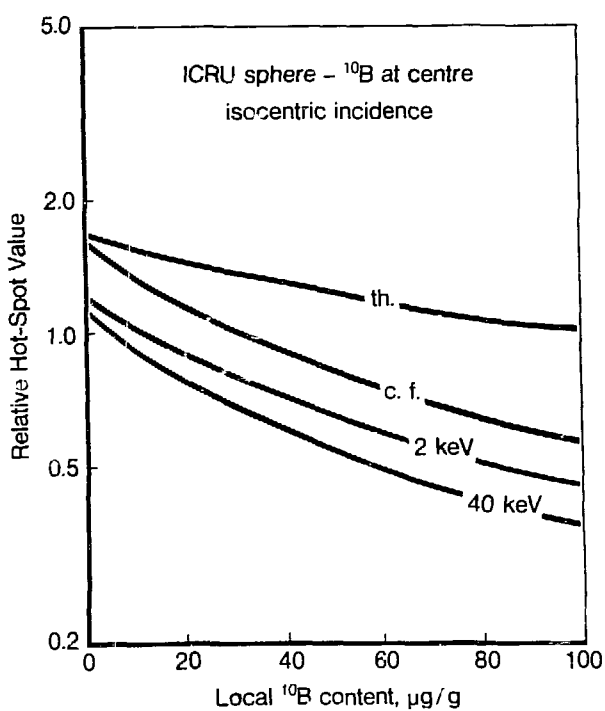


Fig. 3. Relative hot-spot value vs.  $^{10}\text{B}$  content in 1-cm diameter core of ICRU sphere isocentrically irradiated with different neutron beams (th.: thermal neutrons; c. f.: fission neutrons from a converting plate;  $\bar{E} = 1$  MeV).

total dose and of neutron dose separately. The comparison of the two curves implies that the sharp maximum for the total dose (at ca. 500 keV), indicating the most appropriate incident neutron energy, is caused mainly by the  $^1\text{H}(n,\gamma)^2\text{H}$  reaction. It has to be emphasized, however, that this "most appropriate energy" must not be considered as the absolute optimum. The problem strongly depends on target positioning, and for lower tumor depths the maximum will obviously occur at somewhat lower energies, but still in the intermediate neutron energy range. The  $D_n$  curve in Fig. 2 reflects the hypothetic situation of the absence of secondary gamma radiation. This case is obviously unrealistic, but it depicts the way in which significant enhancement of treatment efficiency may be expected, i.e. by partial elimination of gamma-ray production. This can be achieved e.g. by deuteration of irradiated tissues /14/ or by introduction of heavy water into body cavities close to the tumor (e.g. in the treatment of bladder carcinoma).

It is also useful to analyze the magnitude and localization of the "hot spot", i.e. the local dose maximum apart from the desired central maximum at the boron-loaded target. The minimum ratio of these two maxima may be considered as another criterion of optimization. In Fig. 3 the relative hot-spot values for some selected neutron beams are presented vs. varying  $^{10}\text{B}$  content in the tumor. In this case the results do not strongly depend on geometrical factors and the optimum at about 40 keV seems to have some more general meaning, because the hot spot is usually located outside the range of field disturbances caused by boron in the target volume and just reflects the dose build-up due to  $(n,n)$ ,  $(n,p)$  and  $(n,\gamma)$  interactions.

## Conclusions

Optimization of incident neutron energy is an important question for the development of neutron capture therapy. This is a complex multiparameter problem of which only some principal dosimetric aspects were dealt with in this paper. Further research is obviously required - at present even the optimization criteria are not clearly defined. However, from the above-presented preliminary numerical analysis it can be derived that the energy spread-out due to the  $^1\text{H}(n,\gamma)^2\text{H}$  reaction can be significantly reduced by shifting the applied neutron beams towards the intermediate energy range. Moreover, it seems that, due to the negligible radiative capture of neutrons by deuterium nuclei, introduction of heavy water into internal body cavities in the tumor vicinity should also improve treatment efficiency in some selected clinical cases.

## References

1. H.J. Taylor and H.Goldhaber, *Nature* 135, 341(1935)
2. G.L. Brownell et al.: *Boron Capture Therapy*, in "Modern Trends in Radiotherapy", Butterworths, London 1967, pp.132-144
3. H. Hatanaka and W.H.Sweet: *Slow Neutron Capture Therapy for Malignant Tumors - Its History and Recent Development*, in "Biomedical Dosimetry", IAEA-STI/PUB/401, Vienna 1975, pp. 147-178
4. R.G.Fairchild, *Phys.Med.Biol.* 10, 491(1965) & 11, 15(1966)
5. Y. Oka et al., *Nucl.Techn.* 48, 204(1980) & 55, 642(1981)
6. N.A. Frigerio: *Neutron Capture and Conversion Therapy with Intermediate Range Neutron*, in ANL-7136, Argonne 1965, pp.175-182
7. A.J. Mill and J.R.Harvey: *Intermediate Energy Neutron Production; A survey of Existing Techniques; A Proposed Source and its Applications*, CEGB Rep.RD/B/N4324, EUR6107 EN, Gloucestershire 1978
8. F.M.Waterman et al., *Phys.Med.Biol.* 23, 592(1978)

9. R.G. Zamenhof et al., *Med. Phys.* 2, 47(1975)
10. ICRU Rep.19, Washington 1971
11. W.W.Engle Jr.: ANISN. A One-Dimensional Discrete Ordinates Transport Code with Anisotropic Scattering, USAEC Rep.K-1693, Oak Ridge 1967 (upd. 1973)
12. RSIC Data Library Collection, pack. DLC-31(DPL1/FEWG1), descr. in ORNL/TM-4840, Oak Ridge 1977
13. ICRU Rep.26, Washington 1977
14. D.N.Slatkin et al., *Phys.Med.Biol.* 28, 1447(1983)

Boron-10 Dosage in Cell Nucleus for Neutron Capture Therapy  
— Boron Selective Dose Ratio

Tooru Kobayashi and Keiji Kanda

Research Reactor Institute, Kyoto University  
Kumatori-cho, Sennan-gun, Osaka, 590-04, Japan

## 1 Introduction

Neutron capture therapy utilizes high-LET particles of short range such as  $\alpha$  particles and  ${}^7\text{Li}$  nuclei produced by neutron reactions with  ${}^{10}\text{B}$ ,  ${}^6\text{Li}$ , etc. The advantage of the therapy is the selective destruction by neutron reactions of only the tumor into which  ${}^{10}\text{B}$  compound has been injected and not the normal tissue. The range of the local destruction covers cells containing  ${}^{10}\text{B}$  and their adjacent cells, since the range of  $\alpha$  particles is almost the same as a typical cell diameter of 10  $\mu\text{m}$ .

Medical colleagues asked us to estimate the absorbed dose in a cell nucleus when  ${}^{10}\text{B}$  is injected only into the cytoplasm and not into the cell nucleus because the cell nucleus is thought to contain the key of life. For ordinary radiation therapy, such as X rays, gamma rays, or electron beams, the average absorbed dose over the order of millimeters is sufficient to estimate a therapeutic effect. For neutron capture therapy, however, the therapeutic effect is sensitive to variations in the absorbed dose distribution within a cell (see Fig. 1).

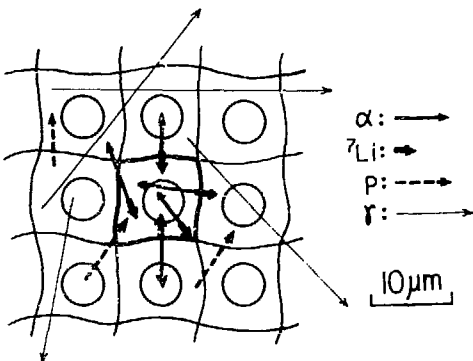


Fig. 1 The principle of selective therapeutic effect for boron neutron capture therapy. Main reactions in tissue are  ${}^{10}\text{B}(\text{n},\alpha){}^7\text{Li}$ ,  ${}^{14}\text{N}(\text{n},\text{p}){}^{14}\text{C}$ , and  $\text{H}(\text{n},\gamma)\text{D}$ .

For neutron capture therapy, calculations of absorbed dose of heavy charged particles from the  ${}^{10}\text{B}(\text{n},\alpha){}^7\text{Li}$  reaction in tissue have been made by Davis et al.(1) and Kitao(2). Their calculations were motivated by the success of boron neutron capture therapy for brain tumors by Hatanaka(3).

One of the keys of boron neutron capture therapy is the selective concentration of boron in tumors. For brain tumors the so-called blood-brain barrier(3) is utilized to concentrate the boron in tumors. On the other hand, melanin synthesis is utilized for malignant melanoma. The melanin is not synthesized in the cell nucleus(4) so boron is concentrated only in the cytoplasm. In other words, boron is not uniformly concentrated in tumor. We made a new model(5) to estimate the absorbed dose in a cell nucleus when the  $^{10}\text{B}$  concentration is different in the cell nucleus and cytoplasm. The model can estimate an interference effect between parts with and without  $^{10}\text{B}$  concentrations, which are located together within the range of the charged particles.

The shape of a cell nucleus is assumed to be spherical for easier analytical treatment. The range-LET relation of heavy charged particles in tissue is approximated by a definite linear equation, according to Kellerer's approximation of tracks(6), and was calculated from the tabulated data of Northcliffe and Schilling for water(7).

## 2 Calculation model for physical damage in the cell nucleus

For the analytical calculation the following is assumed :

- 1) The cell consists of a cell nucleus and cytoplasm. A spherical cell nucleus is located at the center of a cell and is surrounded by cytoplasm.
- 2) Tissue consists of equal-sized cells which are located regularly in it.
- 3) The movement of the particles is isotropic.
- 4) The path of the particles is a straight line.
- 5) The particle production rate in cells is spherically symmetric around the center of each cell nucleus.
- 6) The range-LET relation is the same in both a cell nucleus and cytoplasm.
- 7) The range-LET relation is expressed by a linear equation.

By using this calculation, the following four physical effects are obtained as average expected values :

- 1) absorbed energy in cell nucleus,
- 2) number of particles hitting and/or passing through cell nucleus,
- 3) integrated particle track length in a cell nucleus,
- 4) absorbed energy distribution in the cell structure.

The following five parameters were used : i) cell nucleus radius, ii) distance between cell nuclei, iii) particle range, iv) differential energy loss : range-LET relation, and v) particle production distribution in cell.

## 3 Calculated results of a typical cell and tissue

We studied the absorbed energy in cell nucleus (AECN) as an example in this paper. The assumptions made in calculations for a typical cell and tissue are shown in Table 1. In Table 2, nuclear reaction data with thermal neutrons are shown for C, H, O, and N in normal tissue and for  $^{10}\text{B}$  injected

Table 1 Assumption in Calculation suggested by Mishima

Cell nucleus radius	2.5 $\mu\text{m}$
Cell radius	5.0 $\mu\text{m}$
Tissue structure	Close packed
Elemental composition of tissue	$(\text{C}_2\text{H}_{40}\text{O}_{18}\text{N})_n^a$
Thermal neutron fluence	$10^{13}$ nvt
$^{10}\text{B}$ concentration	homo
Cell nucleus	20 ppm
Cytoplasm	20 ppm
	hetero <sup>b</sup>
	0 ppm
	22 ppm

<sup>a</sup> Refer to ICRP Report 26.

<sup>b</sup> Average concentration was 20 ppm in cell.

Table 2 Expected Reactions Caused by Thermal Neutrons in Tissue

Element	Natural Abundance (%)	Reaction	Thermal neutron cross section		Released energy per reaction (MeV)
			Microscopic $\sigma$ (barn) <sup>a</sup>	Macroscopic $\Sigma$ ( $\text{cm}^{-1}$ ) <sup>b</sup>	
$^1\text{H}$	99.985	$^1\text{H}(n,\gamma)^2\text{H}$	0.332	$1.99 \times 10^{-2}$	2.22
$^2\text{H}$	0.0145	$^2\text{H}(n,\gamma)^3\text{H}$	0.0005	$4.34 \times 10^{-9}$	6.25
$^{12}\text{C}$	98.892	$^{12}\text{C}(n,\gamma)^{13}\text{C}$	0.0034	$2.52 \times 10^{-5}$	4.95
$^{13}\text{C}$	1.11	$^{13}\text{C}(n,\gamma)^{14}\text{C}$	0.0009	$7.48 \times 10^{-8}$	8.15
$^{14}\text{N}$	99.635	$^{14}\text{N}(n,p)^{14}\text{C}$	1.81	$2.70 \times 10^{-3}$	0.63
$^{15}\text{N}$	0.365	$^{15}\text{N}(n,\gamma)^{16}\text{N}$	0.000024	$1.31 \times 10^{-10}$	2.48
$^{16}\text{O}$	99.759	$^{16}\text{O}(n,\gamma)^{17}\text{O}$	0.00018	$4.84 \times 10^{-6}$	4.14
$^{17}\text{O}$	0.037	$^{17}\text{O}(n,\alpha)^{14}\text{C}$	0.24	$2.39 \times 10^{-6}$	1.82
$^{18}\text{O}$	0.204	$^{18}\text{O}(n,\gamma)^{19}\text{O}$	0.00021	$1.15 \times 10^{-8}$	3.95
$^{10}\text{B}$	19.61		3837		2.79
		$^{10}\text{B}(n,\alpha)^7\text{Li}^*$	(93.7%) <sup>c</sup>	$4.33 \times 10^{-3}$	( $\gamma = 0.478$ )
		$^{10}\text{B}(n,\alpha)^7\text{Li}$	(6.3%)	$2.91 \times 10^{-4}$	(no $\gamma$ )

Table 3 Energy and Range of Charged Particles Produced in Tissue

Reaction	Released energy (MeV)	Particle energy (MeV)	Particle range <sup>a</sup> in water ( $\mu\text{m}$ )
$^{14}\text{N}(n,p)^{14}\text{C}$	0.63	$p = 0.59$ $^{14}\text{C} = 0.04$	10.8 0.2
$^{17}\text{O}(n,\alpha)^{14}\text{C}$	1.82	$\alpha = 1.42$ $^{14}\text{C} = 0.40$	8.7 1.5
$^{10}\text{B}(n,\alpha)^7\text{Li}$	2.79	$\alpha = 1.78$ $^7\text{Li} = 1.01$	10.2 5.5
$^{10}\text{B}(n,\alpha\gamma)^7\text{Li}$	2.79 ( $\gamma = 0.478$ )	$\alpha = 1.47$ $^7\text{Li} = 0.84$	8.8 4.8

for neutron capture therapy. Table 3 shows initial kinetic energy and range in water for the particles.

For the range-LET relation in tissue for protons,  $\alpha$  particles, and  $^{7}\text{Li}$  nuclei we used data in water of Northcliffe and Schilling. These are shown by a numerical table, but we made figures from them to show the shape of the range-LET relation. Arrows in Fig. 2 show the starting point of the particle produced from each nuclear reaction. The range-LET approximation of protons produced from  $^{14}\text{N}(\text{n},\text{p})^{14}\text{C}$  reaction is assumed to be  $\text{LET} = \text{constant}$ . For the other particles produced from the reaction of  $^{14}\text{N}(\text{n},\text{p})^{14}\text{C}$ ,  $^{17}\text{O}(\text{n},\alpha)^{14}\text{C}$ ,  $^{10}\text{B}(\text{n},\alpha\gamma)^{7}\text{Li}$  and  $^{10}\text{B}(\text{n},\alpha)^{7}\text{Li}$ , they are assumed to be  $\text{LET} \propto 1 - X$  (where  $X$  is fraction of range expended).

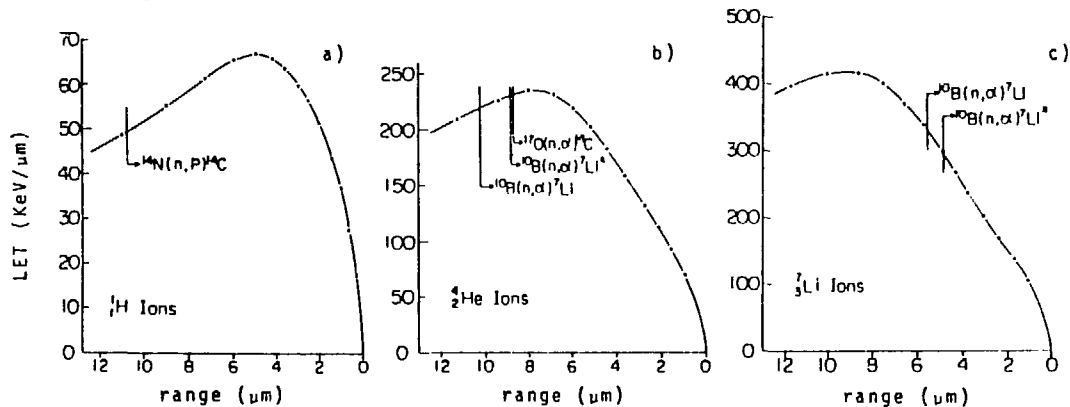


Fig. 2 Range vs LET in water for (a) H ions, (b)  $^{3}\text{He}$  ions, and (c)  $^{7}\text{Li}$  ions.

Table 4 shows the calculated results of AECN and percentage interference of AECN by other cell nuclei. From Table 4, we can find that the localized dose effect, which is the most remarkable feature of neutron capture therapy, is based mainly on protons,  $\alpha$  particles and  $^{7}\text{Li}$  nuclei produced from  $^{14}\text{N}(\text{n},\text{p})^{14}\text{C}$  and  $^{10}\text{B}(\text{n},\alpha\gamma)^{7}\text{Li}$  reactions.

In this case, the interference of 12 adjacent cell nuclei for AECN is less than 2%. However, the ratio of AECN without particle production in each cell nucleus to that with homogeneous particle production throughout the tissue is  $4.40/7.09 = 0.619$ , so that for estimating absorbed dose of neutron irradiations, it is very important to know whether  $^{10}\text{B}$  is in the cell nucleus.

#### 4 Boron Selective Dose Ratio : BSDR

We already defined boron accumulation effect(8), BAE, which represents the ratio of absorbed energy in  $^{10}\text{B}$ -containing tissue to that in  $^{10}\text{B}$ -free tissue. The BAE was calculated by the concept of KERMA and includes absorbed energy from gamma rays which are essentially mixed in the thermal neutron field from a nuclear reactor and from  $(\text{n},\gamma)$  reactions in tissue. The BAE clarifies the importance of a thermal neutron field with low gamma-ray contamination for effective neutron capture therapy.

Table 4 Results of Calculations with Assumptions of Table 1

Reaction	Particle	Absorbed energy (MeV)	Interference (%)	Comment
$^{14}\text{N}(n,p)^{14}\text{C}$	$p$	1.04	1.11	$^{14}\text{N}$ and $^{17}\text{O}$ exist homogeneously in tissue
	$^{14}\text{C}$	0.0704		
$^{17}\text{O}(n,\alpha)^{14}\text{C}$	$\alpha$	0.00222	1.11	$^{10}\text{B}$ exists homogeneously in tissue
	$^{14}\text{C}$	0.000626		
Total			1.11	
$^{10}\text{B}(n,\alpha\gamma)^7\text{Li}$	$\alpha$	4.18	-0.72	$^{10}\text{B}$ exists homogeneously in tissue
	$^7\text{Li}$	2.39		
$^{10}\text{B}(n,\alpha)^7\text{Li}$	$\alpha$	0.329	0	$^{10}\text{B}$ exists only in cytoplasm
	$^7\text{Li}$	0.186		
Total		7.09		
$^{10}\text{B}(n,\alpha\gamma)^7\text{Li}$	$\alpha$	2.91	-1.64	$^{10}\text{B}$ exists only in cytoplasm
	$^7\text{Li}$	1.15		
$^{10}\text{B}(n,\alpha)^7\text{Li}$	$\alpha$	0.242	0	
	$^7\text{Li}$	0.0994		
Total		4.40		

 Table 5 Calculations of BSDR for Various  $^{10}\text{B}$  Distributions in Cells

Class	Radius of region containing $^{10}\text{B}$ ( $\mu\text{m}$ )	$^{10}\text{B}$ concentration of region (ppm)	BSDR	Average $^{10}\text{B}$ concentration (ppm) at $\text{BSDR} = 2$
$S_1$	0-1.25	$64.00 \cdot c^a$	$1 + 1.42 \cdot c$	0.70
$S_2$	1.25-2.5	$9.14 \cdot c$	$1 + 1.05 \cdot c$	0.95
$S_3$	2.5-3.0	$10.99 \cdot c$	$1 + 0.443 \cdot c$	2.26
$S_4$	3.0-3.5	$7.87 \cdot c$	$1 + 0.239 \cdot c$	4.18
$S_5$	3.5-4.0	$5.92 \cdot c$	$1 + 0.139 \cdot c$	7.19
$S_6$	4.0-4.5	$4.61 \cdot c$	$1 + 0.0901 \cdot c$	11.1
$S_7$	4.5-5.0	$3.69 \cdot c$	$1 + 0.0608 \cdot c$	16.4
$S_1+S_2$	0-2.5	$8.00 \cdot c$	$1 + 1.10 \cdot c$	0.91
$S_3+---+S_7$	2.5-5.0	$1.14 \cdot c$	$1 + 0.148 \cdot c$	6.75
$S_1+---+S_7$	0-5.0	$1.00 \cdot c$	$1 + 0.268 \cdot c$	3.73

<sup>a</sup>  $c$  = average  $^{10}\text{B}$  concentrations in cell (ppm).

From the present calculation, we define the boron selective dose ratio (BSDR) for quantitative treatment of the selective therapeutic effect at the cell level.

Absorbed energy in cell nucleus from heavy charged particles in tissue containing  $^{10}\text{B}$

$$\text{BSDR} = \frac{\text{Absorbed energy in cell nucleus from heavy charged particles in tissue containing } ^{10}\text{B}}{\text{Absorbed energy in cell nucleus from heavy charged particles in normal tissue}}$$

Table 5 shows that BSDR depends on the  $^{10}\text{B}$  distribution in a cell. We found that BSDR was much influenced by the  $^{10}\text{B}$  distribution in a cell. Accordingly, for estimating absorbed dose in a cell nucleus due to neutron irradiation, it is very important to know the  $^{10}\text{B}$  distribution in a cell. BSDR, which is strongly related to the  $^{10}\text{B}$  concentration and its distribution in a cell, is a very useful scale for representing the selective therapeutic effect of neutron capture therapy.

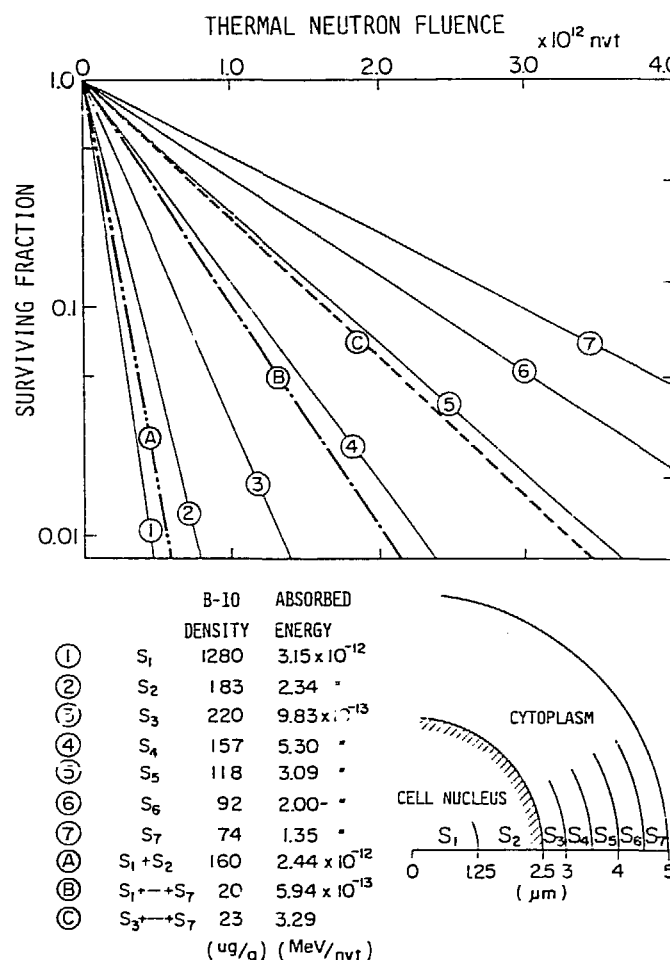


Fig. 3 Effect of  $^{10}\text{B}$  distribution in cell on survival fraction (average  $^{10}\text{B}$  concentration : 20  $\mu\text{g}$ )

The relation between thermal neutron fluence and survival fraction is known from many experiments and can be expressed by a single exponential line which has good reproducibility for cells not containing  $^{10}\text{B}$ . For cells containing  $^{10}\text{B}$ , a variety of survival curves are observed even though the average concentration of  $^{10}\text{B}$  over the cell samples is the same. Figure 3 shows a theoretical estimation of the variability based on the distribution of  $^{10}\text{B}$  in the cell.

## 5 Discussion

We can say that the BSDR is one of the useful ways to quantify the selective therapeutic effect in neutron capture therapy as well to develop the microanalysis system for  $^{10}\text{B}$  concentration(9). Also, the BSDR, which includes the effects of both  $^{10}\text{B}$  concentration and its distribution, can give a new viewpoint for the development of boron compounds for neutron capture therapy; i.e., the former goal for boron compounds was to inject more  $^{10}\text{B}$  in the tumor, but a new viewpoint will be to inject more  $^{10}\text{B}$  at more effective points in the tumor cell.

In the present paper, BSDR is defined as physical damage from absorbed energy in the cell nucleus; however, we can define other BSDRs for other targets, such as cell membrane, lysosome, and DNA, by using other types of physical damage or hit number or track length. These BSDRs will also be useful.

Here we have not mentioned gamma rays, because (i) their LET is small, (ii) their PBE is small, (iii) their range is long, and (iv) their total local energy absorption is small compared with heavy charged particles.

The authors express their gratitude to Professor Y. Mishima of Kobe University Hospital and Professor H. Hatanaka of Teikyo University Hospital for their valuable suggestions. They thank Professor M. Ishida of Kyoto University Research Reactor Institute (KURRI) for his advice on radiation biology. The calculation method was discussed with Dr. K. Kitao of National Institute of Radiological Science and Mr. Shiroya of KURRI. This work was supported by a Grant-in-Aid from the Ministry of Education, Science and Culture.

## REFERENCES

- (1) M. A. Davis, J. B. Little, K. M. M. S. Ayyanger, and A. R. Reddy, Relative biological effectiveness of the  $^{10}\text{B}$  ( $n,\alpha$ )  $^7\text{Li}$  reaction in HeLa. *Radiat. Res.*, 43, 534-553 (1970).
- (2) K. Kitao, A method for calculating the absorbed dose near interface from  $^{10}\text{B}$  ( $n,\alpha$ )  $^7\text{Li}$  reaction. *Radiat. Res.*, 61, 304-315 (1975).
- (3) H. Hatanaka and K. Sano, A revised boron-neutron capture therapy for malignant brain tumors : I. Experience on terminally ill patients after Co-60 radiotherapy. *Z. Neurol.*, 204, 309-332 (1973).
- (4) Y. Mishima and T. Shimakage, Thermal neutron capture treatment of malignant melanoma using  $^{10}\text{B}$ -dopa and  $^{11}\text{B}$ -chlorpromazine compounds. *Pigm. Cell.*, 2, 394-406 (1976).

- (5) T. Kobayashi and K. Kanda, Analytical calculation of boron-10 dosage in cell nucleus for neutron capture therapy. *Radiat. Res.*, 91 77-94 (1982).
- (6) A. M. Kellerer, A survey of approaches to radiation biophysics. In *Proceedings, Fifth Symposium on Microdosimetry, Verbania-Pallanza* (J. Booz, H. G. Ebert, and B. G. R. Smith, Eds.), pp. 409-442. Commission of the European Communities, Luxembourg, 1976. (EUR 5452 d-e-f).
- (7) L. C. Northcliffe and R. F. Schilling, Range and stopping-power tables for heavy ions. *Nucl. Data Tables A* 7, 233-463 (1970).
- (8) K. Kanda, T. Kobayashi, K. Ono, T. Sato, T. Shibata, Y. Ueno, Y. Mishima, H. Hatanaka and Y. Nishiwaki, Elimination of gamma rays from a thermal neutron field for medical and biological irradiation purposes. In *Biomedical Dosimetry*, 205-223. IAEA 1975.
- (9) T. Kobayashi and K. Kanda, Microanalysis system of ppm-order  $^{10}\text{B}$  concentrations in tissue for neutron capture therapy by prompt gamma-ray spectrometry. *Nucl. Instr. Meth.*, 204, 525-531 (1983).

The Biological Effect of the  $^{10}\text{B}(\text{n},\alpha)^7\text{Li}$  Reaction and Its  
Simulation by Monte Carlo Calculations

Detlef Gabel

Department of Chemistry, University of Bremen, FRG

Ralph G. Fairchild

Medical Department, Brookhaven National Laboratory, Upton, NY

Börje Larsson

Gustaf Werner Institute, Uppsala University, Uppsala, Sweden

Karsten Drescher

Department of Mathematics, University of Bremen, FRG

and

Wanda R. Rowe

Medical Department, Brookhaven National Laboratory, Upton, NY

There is considerable discrepancy in the literature regarding the relative biological effectiveness (RBE) of the  $^{10}\text{B}(\text{n},\alpha)^7\text{Li}$  neutron capture reaction. Whereas data obtained *in vivo* indicate values of about 2 (1,7-9), a value of 3.7 has been obtained for HeLa cells grown in culture (2). In view of the importance of this value for the implementation of successful boron neutron capture therapy, we have redetermined the RBE value for cells in culture (3).

V79 Chinese hamster cells were grown for two days in media containing different concentrations of boric acid (natural isotopic abundance). They were detached with a trypsin solution containing the same concentration of boric acid, suspended in phosphate buffered saline, again with the same boron content, and exposed to the thermal neutron beam at the patient port of the Medical Research Reactor at Brookhaven National Laboratory. At a reactor power of 1 MW, the neutron fluence rate inside the irradiation vessel was  $5.45 \times 10^9$  neutrons/cm<sup>2</sup>-sec. After irradiation, the cells were seeded out to form colonies. Survival of cells was recorded as percentage of clones formed compared with non-irradiated controls.

The dose D of the boron neutron capture reaction was calculated from  $D = 8.43 \times 10^{-6} \times \phi \times F$ , where  $\phi$  is the fluence and F the fraction by weight of boron. The dose rates for the boron reaction were between 7.7 and 46 rad/min. The dose rates for gamma and fast neutrons were 9.2 and 9.0 rad/min respectively; that for the  $^{14}\text{N}(\text{n},\text{p})^{14}\text{C}$  reaction was 2.6 rad/min, assuming a nitrogen content of 1.7% by weight.

Figure 1 shows survival curves for different amounts of boric acid present. Straight lines were fitted to the experimental points, excluding the points for zero dose. When the inverse of the slopes is plotted against the amount of boron present, a straight line is obtained. This indicates that there is, in the dose rate interval investigated, no noticeable dose rate effect. Doses could therefore be treated

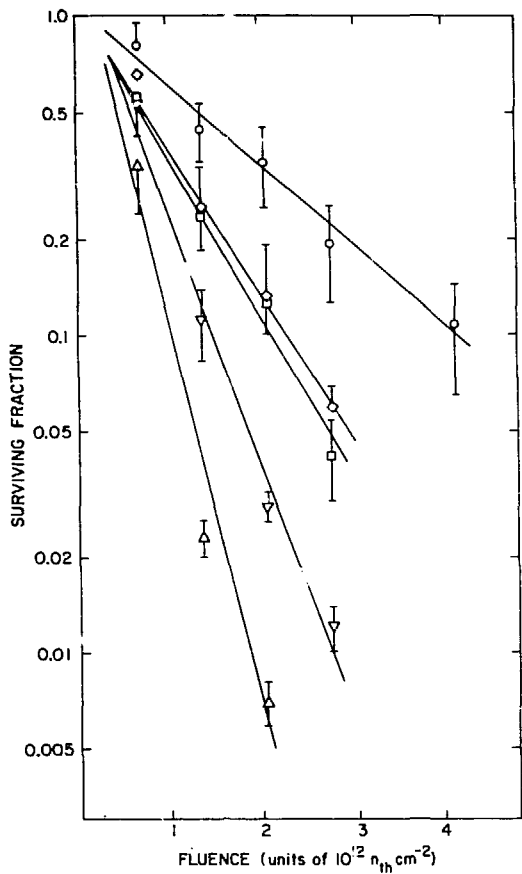


Figure 1. Survival curves for irradiation of V79 Chinese hamster cells at BNL with thermal neutrons in the presence of boric acid. The  $^{10}\text{B}$  concentrations, in  $\mu\text{g}/\text{ml}$ , were zero ( $\circ$ ), 2.8 ( $\bullet$ ), 5.6 ( $\square$ ), 11.2 ( $\nabla$ ), and 16.8 ( $\Delta$ ). Cells were irradiated in suspension. Colonies of 50 or more cells that had formed after plating and incubation for 8 days were counted. The mean  $\pm$  S.D. of quintuplicate experiments, each consisting of 5 dishes per data point, is shown. From Gabel et al. (3).

as additive. The  $D_0$  value of the  $^{10}\text{B}(n,\alpha)^7\text{Li}$  reaction could therefore be determined from all the data of Fig. 1, and was found to be 66 rad, with an estimated error of 10%. By using the  $D_0$  value of 150 rad determined (between 10 and 0.1% survival) for these cells when exposed to 250-kVp x-rays, an extrapolated RBE value of 2.3 is obtained.

This value is in agreement with previously reported values in animal systems (1,7-9). It is in disagreement with the value of 3.7 measured previously for cells in culture (2). In the calculations leading to the value of 3.7, it was assumed that the boron-containing growth medium, which was poured off the plated cells just prior to irradiation, was removed completely. Then, boron neutron capture events could occur only within the cells, depositing some of their energy outside the cells. In our hands, removal of culture medium from dishes left behind a film of liquid 30 to 40  $\mu\text{m}$  thick which would contain boron and thus would invalidate the above assumption.

Because of the short range and the high LET of the particles from the boron neutron capture reaction, a significant effect on radiation damage might be expected from the relative distribution of boron with respect to the cell nucleus (2,5,6). The dose of 66 rad obtained here for  $D_0$  represents, on the average, less than two neutron capture events in the volume of one cell. It was therefore thought that a calculation of the average dose delivered to the cells would not be adequate to describe the observed radiation damage. We have therefore developed a computer program which generates neutron capture events in isolated cells by Monte Carlo simulation.

Events were modeled as ensembles of tracks of two identical particles emerging back-to-back (see Fig. 2), with a combined range of 13.6  $\mu\text{m}$ . The origin of each track in space, as well as the track direction, was generated randomly. The density of tracks could be adjusted to a given average dose. The summed lengths of all parts of the tracks entering or passing a spherical volume representing the nucleus of the cell and their variations were recorded. Subsets of these values were obtained according to whether the tracks originated in the nucleus, in the cytoplasm, or outside the cell.

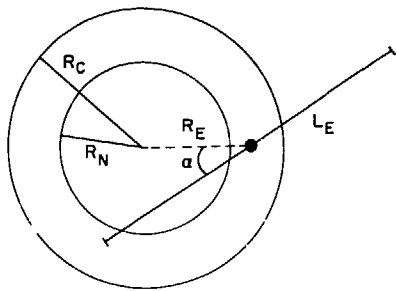


Figure 2. Monte Carlo simulation for boron neutron capture reactions. The values for  $R_E$  and  $\alpha$  were chosen such that a random isotropic distribution in space of track origins and directions was generated.

$R_N$ ,  $R_C$ : RADII OF NUCLEUS AND CELL

$L_E$ : LENGTH OF PARTICLE TRACK

The result of a typical simulation is shown in Fig. 3. The diameters of cell and cell nucleus were 13.0 and 7.6  $\mu\text{m}$ , respectively, corresponding to the values measured for the V79 Chinese hamster cells used in the RBE measurements here. The probability of occurrence of a track length sum in the nucleus shorter than, or equal to, the value given on the horizontal axis is plotted.

PROBABILITY DISTRIBUTION  
 INSIM=1000, RCELL= 6.50, ANUCL=3.80, R00=13.60, DOSE=160.001

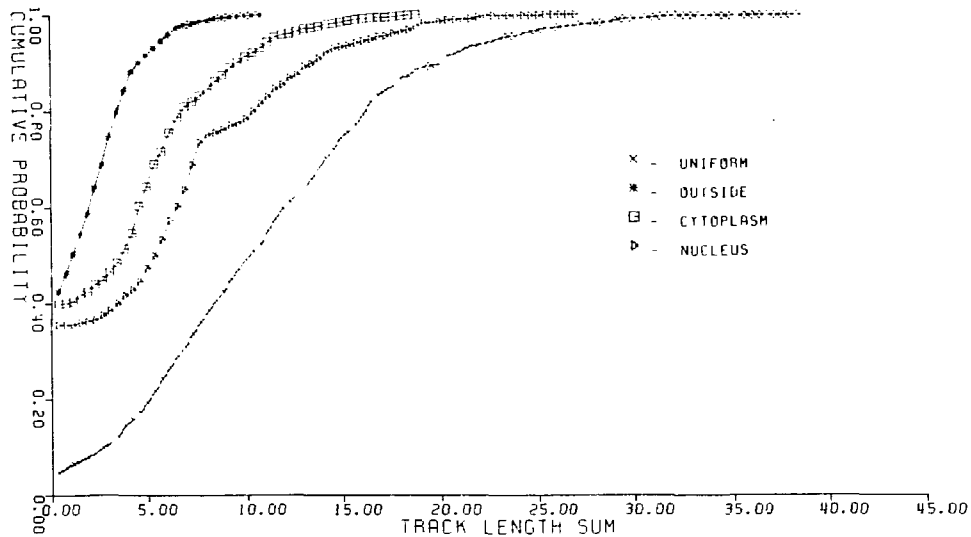


Figure 3. Probability of occurrence of track length sums. The probability of the track length sum in the nucleus is shown for a cell with a radius of 6.5  $\mu\text{m}$  and a nuclear radius of 3.8  $\mu\text{m}$ . 1000 events were simulated. With the average dose of 160 rads, this corresponds to 21,000 generated tracks.

For a mean dose of 160 rad, about 5% of the simulated events result in no track entering or passing through the nucleus, even when the distribution of the track origins is uniform. In 10% of the events, the accumulated track length in the nucleus is  $< 3 \mu\text{m}$ . With a mean dose due to the  $^{10}\text{B}(n,\alpha)^7\text{Li}$  reaction of 160 rad and a homogeneous boron distribution, the experimentally observed survival is 10%.

When the same average density of tracks originates only in the nucleus, a much larger fraction of simulated events (35%) results in no track in the nucleus (which here is equivalent to no capture event), as is the case with tracks originating only in the cytoplasm or outside the cell. For the latter case, 75% of the events resulted in a track length sum of  $< 3 \mu\text{m}$ , compared with 38% and 46% for the tracks originating in nucleus or cytoplasm.

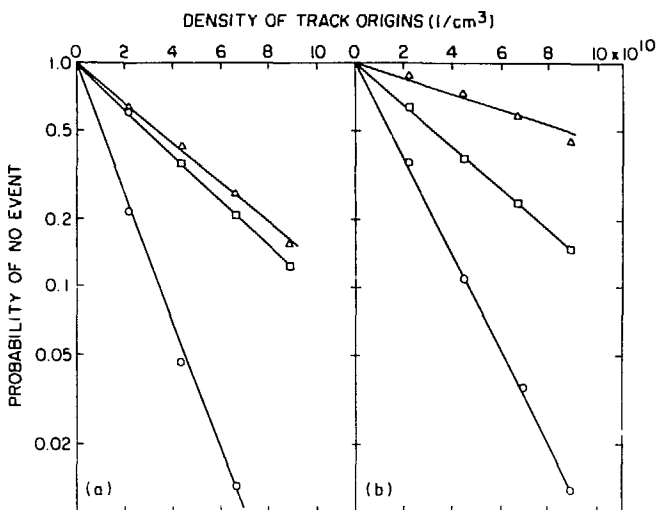


Figure 4. Probability of occurrence of track length sums as a fraction of track density for uniform distribution of track origins (o), tracks originating in the nucleus (□), and tracks originating outside the cell (Δ). Plots for a track length sum of (a) 0  $\mu\text{m}$  and (b) 3  $\mu\text{m}$ .

Figure 4 shows plots of probabilities of a given track length sum occurring vs density of tracks per volume element. These plots would represent survival curves, if the events inflicted lethal damage. Table 1 shows the track density ratios needed to obtain the same probability of no event for track length sums of 0 and 3  $\mu\text{m}$ . These values might be interpreted as RBE values.

Table 1. Track Density Ratios for Occurrence of Same Track Length Sums

Track length sum	Nucleus vs uniform	Outside vs uniform	Outside vs nucleus
0 $\mu\text{m}$	2.80	3.20	1.14
3 $\mu\text{m}$	2.31	6.23	2.70

Figure 4a shows the probabilities of a track length sum of zero  $\mu\text{m}$  (which is equivalent to no hit). In order to obtain the same probability of hit, about three times the density of tracks needed in uniform distribution has to be achieved when tracks originate only outside the cell or only in the nucleus.

Figure 4b shows that, in order to obtain the same probability of a track length sum of 3  $\mu\text{m}$ , 2.3 times the track density of uniform distribution is needed for events occurring only in the nucleus, but 6.2 times this density is needed when tracks originate outside the cell.

(It should be borne in mind that the density of tracks applies to that volume in which the tracks originate; the

number of tracks simulated in the nucleus is therefore <5% of the number simulated with a uniform distribution. For a constant neutron fluence, the density of track origins would translate directly into the local boron concentration.)

These simulations indicate that the average dose delivered in different geometries may not always be a good reflection of the biological effects to be expected. They raise the question as to what track length of a high LET particle is sufficient for cell death. The simulations performed here suggest a value of around 3  $\mu$ m. By confining boron to the outside of cells, using boron-conjugated macromolecules (4), this might be answered experimentally.

Here, we have not taken into account the variation of energy transfer from the particles along their paths. We thought, however, that only quantitative changes in the results of the above simulations might be found if this were taken into account.

#### ACKNOWLEDGMENTS

This work has been financially supported by the Deutsche Forschungsgemeinschaft and the Fonds der Chemischen Industrie (D.G.), the Swedish Natural Science Research Council, the Swedish Cancer Society and the Centre de la Recherche Scientifique (B.L.), and the U.S. Department of Energy under contract No. DE-AC-02-76CH00016 (R.G.F.).

#### REFERENCES

1. Bond, V.P., Easterday, O.D., Stickley, E.E., and Robertson, J.S. (1956) Radiology 67, 650-663.
2. Davis, M.A., Little, J.B., Ayyangar, K.M.M.S., and Reddy, A.R. (1970) Radiat. Res. 43, 534-553.
3. Gabel, D., Fairchild, R.G., Larsson, B., and Borner, H.G. (1983) Radiat. Res., in press.
4. Gabel, D. and Walczyna, R. (1982) Z. Naturforsch 37c, 1038-1039.
5. Kitao, K. (1975) Radiat. Res. 61, 304-315.
6. Kobayashi, R. and Kanda, K. (1982) Radiat. Res. 91, 77-94.
7. Robertson, J.S., Bond, V.P., Cronkite, E.P., Easterday, O.D., and Lippincott, S.W. (1957) Fed. Proc. 16, 107.
8. Stchrer, J.B., Harris, P.S., Furchner, J.E., and Laugham, W.H. (1957) Radiat. Res. 6, 188-288.
9. Yamamoto, Y.L. (1961) Yokohama Med. Bull. 12, 4-22.

EFFECTS OF DEUTERIUM OXIDE AND CYSTEAMINE ON THE ACUTE  
LETHALITY OF HEAD IRRADIATION

K. Rosander,\* D.N. Slatkin and R.D. Stoner  
Medical Department, Brookhaven National Laboratory, Upton, New York, USA

In radiation therapy of human tumors it is desirable to deliver the lowest possible dose to associated normal tissues. For boron neutron capture therapy (BNCT), one possible approach to this problem would be to deuterate tissue water.<sup>1,2,3</sup> Transient partial deuteration of body water would increase neutron penetration to a tumor and thereby also permit lower radiation doses to superficial normal tissues. Body water deuteration in the 20 to 40 atom % D range would reduce superficial tissue doses by about 30% for a given dose to a 6-cm-deep tumor.<sup>4</sup> In BNCT, partial deuteration of tissues would also reduce superfluous prompt gamma radiation from the hydrogen neutron capture reaction.

Deuterium oxide modifies BNCT dosimetry physically<sup>5</sup> and exerts a radiation-protective effect against low LET whole-body radiation without diminishing the lethality of whole-body high LET radiation from the  $^{10}\text{B}(\text{n},\alpha)^7\text{Li}$  reaction.<sup>1,2,6</sup> Experiments reported here were performed to ascertain the effects of deuterium oxide on the lethality of high LET and of low LET radiation directed primarily to the brain.

The heads of partially deuterated and normal mice were irradiated by x rays (low LET) or by charged particles from the  $^{10}\text{B}(\text{n},\alpha)^7\text{Li}$  reaction (high LET) at two dose levels which caused the acute central nervous system (CNS) radiation lethality syndrome<sup>7</sup> in less than and in more than one-half of exposed animals, respectively. Since cysteamine, another chemical radiation-protective agent, is known to lessen strand breakage in brain endothelial cell DNA caused by up to  $1.8 \times 10^3$  rad of low LET radiation directed primarily to the heads of rats,<sup>8</sup> parallel experiments were performed on deuterated and normal mice treated with a radiation-protective dose of cysteamine (150  $\mu\text{g}$  per gram of body weight) given intraperitoneally about 15 to 20 min prior to irradiation. Mice were deuterated by replacing acidified drinking water (2 ml concentrated HCl per liter) with similarly acidified, partially deuterated ( $50 \pm 1$  atom % D) water during the 13-day time interval which preceded irradiation. Body water levels of deuterium on the day of irradiation are estimated<sup>9</sup> to be about 32 atom %.

Neutron irradiations were carried out at the Brookhaven National Laboratory Medical Research Reactor operated at a power level of 3 MW. Mice were bred and treated in accordance with the regulations of the American Association for the Accreditation of Laboratory Animal Care. About 20 min before the start of exposure to neutrons, 8 to 12-wk-old female Swiss albino mice<sup>2</sup> were injected intraperitoneally with 96%  $^{10}\text{B}$ -enriched boric acid dissolved in water at a concentration of 37.98 mg/ml. The volume of solution injected, 0.02 ml per gram of whole-body weight, delivered 120  $\mu\text{g}$   $^{10}\text{B}$  per gram of body weight to each mouse. About 10 to 15 min before neutron

---

\*Present address: Gustaf Werner Institute, Uppsala University, Box 531, 751 21 Uppsala, Sweden

irradiation, each group of eight mice was anesthetized by a series of eight intraperitoneal injections of 7.5 mg/ml sodium pentobarbital (0.01 ml per gram of body weight). Mice were then confined to plastic tubes<sup>2</sup> in an irradiation holder where their bodies were partially shielded from slow neutrons by lithium carbonate powder (Fig. 1a,b). The head of each mouse projected 12 mm beyond the irradiation holder toward the reactor and touched the 25.4 x 25.4 cm bismuth face plate of the irradiation port. Four deuterated and four nondeuterated mice were irradiated for either 900 sec or 1050 sec. Slow neutron fluxes measured by unshielded gold foils were about 4.8 x 10<sup>10</sup> n/cm<sup>2</sup>-sec at mouse head surfaces. Dose rates from gamma photons, from fast neutron contamination of the slow neutron radiation field, and from the <sup>14</sup>N(n,p)<sup>14</sup>C reaction were approximately 2.5, 1.2, and 1.3 rad/sec, respectively.<sup>2</sup>

Low LET radiation was delivered to the head of each mouse by a General Electric Company "Maxitron 250" x-ray generator. Eight mice (4 deuterated and 4 nondeuterated) were irradiated for either 1200 sec or 1350 sec in a slowly rotating mouse holder (Fig. 1c,d) under sodium pentobarbital anesthesia with mouse bodies shielded by a 1/4-inch-thick lead plate. The x-ray generator was operated at 250 kV, 30 mA with 0.5 mm Cu and 1.0 mm Al filtration. The brain of each mouse was about 12 cm below the anode of the x-ray generator. The upper surface of the lead plate was 9.5 cm below the anode.

It is apparent from published data that the average post-irradiation survival time (D days) following acute x-irradiation (r rad) of the mouse head can be approximated by the equation

$$D = 2r^{-2.65} \times 10^{12}$$

if r is in the 30,000 to 70,000 rad range.<sup>7</sup> For example, 30,000 rad or more of low LET radiation to the head is expected to cause death by the CNS radiation lethality syndrome within three days after irradiation. Other experiments indicate that post-irradiation survival times within three days after irradiation are almost never associated with the gastrointestinal or the hematopoietic radiation lethality syndrome.<sup>2</sup> Death within three days after acute irradiation of the head was used as the measure of CNS radiation lethality in this study. Typical signs of the CNS radiation lethality syndrome were observed, including convulsions, opisthotonus, anorexia, pilo-erection, and immobility without diarrhea.

The results of these experiments are summarized in Table 1, which shows fractions of groups of mice that died within three days after head irradiation under several experimental conditions. Radiation doses to cerebrovascular tissues from the <sup>10</sup>B(n,α)<sup>7</sup>Li reaction, R rad, can be estimated from<sup>2</sup>

$$R = 8.83 FN \times 10^{-6}$$

where F is the weight fraction of <sup>10</sup>B in blood, and N is the slow neutron fluence (cm<sup>-2</sup>) at the point of interest in the mouse brain. It is apparent from Table 1 that deuterium oxide, unlike cysteamine, enhances CNS lethality caused by low-LET or by high LET radiation directed primarily toward the head.

Table 2 is a brief summary of our present knowledge concerning the influence of deuterium oxide and of cysteamine on the hematopoietic

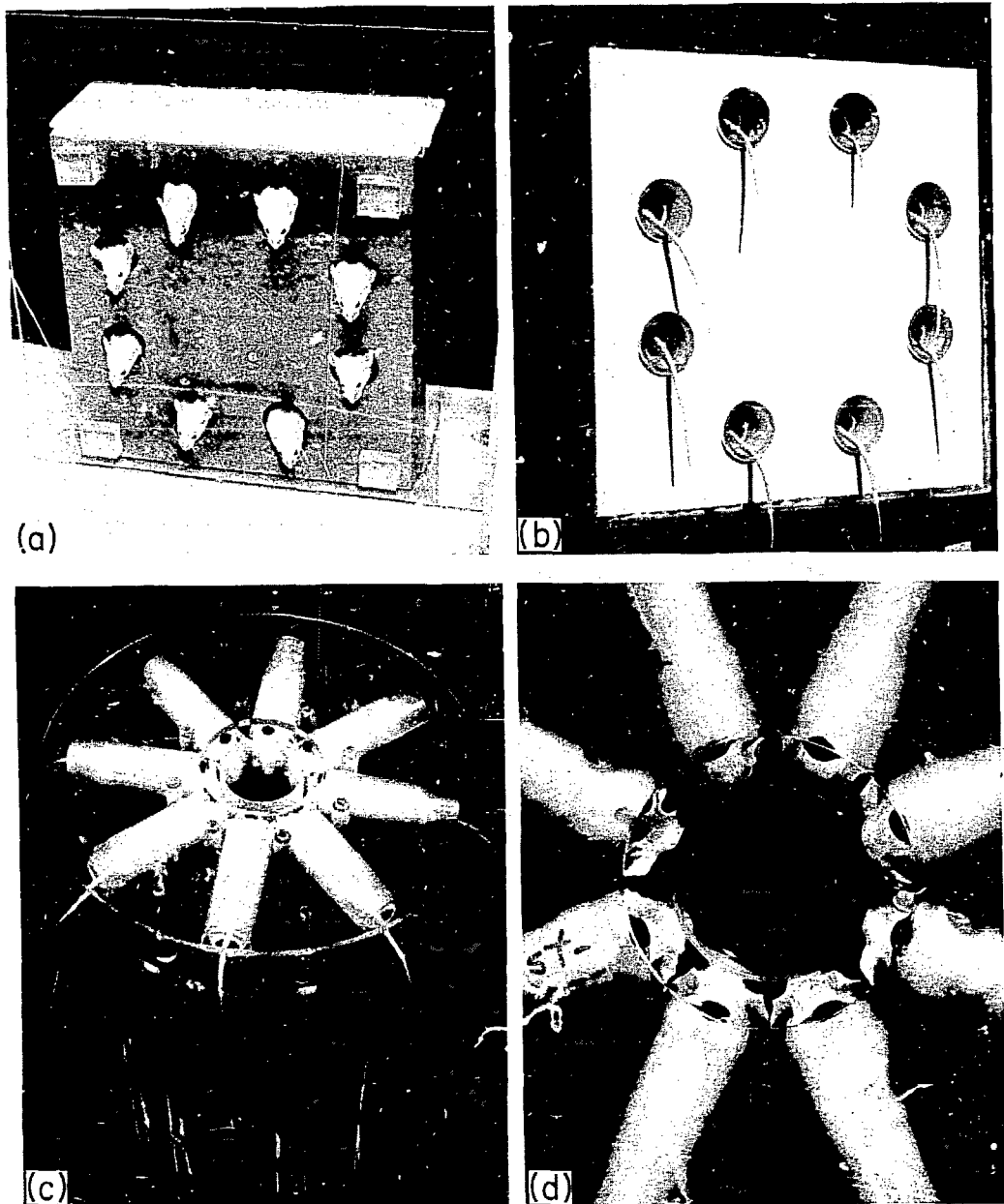


Fig. 1. Reactor irradiation holder for eight mice; front (a) and rear (b) views. X-irradiation holder for eight mice; general (c) and close-up (d) views. The lead body shield has been removed from the x-irradiation holder to show the one-inch-diameter plastic tubes in which anesthetized mice were confined during irradiation.

Table 1. Fractions of mice that died within 3 days after acute irradiation of the head.

	D <sub>2</sub> O	Control	Cysteamine	Control
<sup>10</sup> B(n,α) <sup>7</sup> Li: Incident Slow Neutron Fluence (cm <sup>-2</sup> )				
	4.3 × 10 <sup>13</sup> 5.0 × 10 <sup>13</sup>	19/24 23/24	11/24 14/24	5/24 5/20
x-ray: Brain Surface Dose (rad)				
	4.5 × 10 <sup>4</sup> 5.1 × 10 <sup>4</sup>	20/32 26/36	4/36 10/36	5/56 22/56

Table 2. Effects of cysteamine (MEA) and deuterium oxide (D<sub>2</sub>O) on the hematopoietic (BM), gastrointestinal (GI), and central nervous system (CNS) radiation lethality syndromes. Entries marked with asterisks are based on data from this study.

	BM	GI	CNS
			enhancement*
<sup>10</sup> B(n,α) <sup>7</sup> Li, D <sub>2</sub> O	untested	equivocal enhancement <sup>2</sup>	
<sup>10</sup> B(n,α) <sup>7</sup> Li, MEA	untested	untested	equivocal protection*
x-ray, D <sub>2</sub> O	protection <sup>1,2,6</sup>	untested	enhancement*
x-ray, MEA	protection <sup>10</sup>	protection <sup>11</sup>	equivocal protection*

(BM),<sup>1,2,6,10</sup> gastrointestinal (GI),<sup>2,11</sup> and central nervous system (CNS) radiation lethality syndromes. Entries marked with asterisks are based on data from this study. Radiation doses required to induce the CNS radiation lethality syndrome in mice are 5 to 10 times higher than doses generally used for radiotherapy of human brain tumors. The mechanism of the observed deuterium oxide-mediated enhancement of nearly lethal doses of radiation to the central nervous system is unknown. Whether deuterium oxide would enhance or reduce the effects of radiotherapeutic doses of radiation on mammalian CNS tissues is also unknown.

#### ACKNOWLEDGMENTS

We thank P. Micca, D. Greenberg, and J. Ryan for technical assistance. We thank E.N. Carter, S. Sajnacki, T. Holmquist, and other members of the Safety and Environmental Protection Division and of the Reactor Division of Brookhaven National Laboratory for their help. We acknowledge helpful discussions with B. Larsson. We thank R.G. Fairchild for assistance in radiation dosimetry. We thank L. Wasson and J. Webster for secretarial services. This work was performed mainly under Contract No. DE-AC02-76CH00016 with the U.S. Department of Energy. Accordingly, the U.S. Government retains a non-exclusive, royalty-free license to publish or reproduce the published form of this contribution, or allow others to do so, for U.S. Government purposes. K. Rosander acknowledges support in part from the Faculty of Science, Uppsala University.

#### REFERENCES

1. J.A. Laissue, E. Bally, D.D. Joel, D.N. Slatkin and R.D. Stoner. Protection of mice from whole-body gamma radiation by deuteration of drinking water. *Radiat. Res.* 96, 59-64, 1983.
2. D.N. Slatkin, R.D. Stoner, A.M. Gremme, R.G. Fairchild and J.A. Laissue. Whole-body irradiation of deuterated mice by the  $^{10}\text{B}(\text{n},\alpha)^7\text{Li}$  reaction. *Proc. Natl. Acad. Sci. USA* 80, 3480-3484, 1983.
3. D.N. Slatkin, M.M. Levine and A. Aronson. The use of heavy water in boron neutron capture therapy of brain tumors. *Phys. Med. Biol.* 28 (12), in press, Dec. 1983.
4. W. Kiszenick, R.G. Fairchild, D.N. Slatkin and G. Zubal. Increased neutron penetration in partially deuterated water: Application to neutron capture therapy. *Med. Phys.*, in press.
5. E.J. Hart, W.R. McDonell and S. Gordon. The decomposition of light and heavy water boric acid solutions by nuclear reactor radiations. *Proc. Conf. Peaceful Uses of Atomic Energy*, Geneva, 1955, pp. 593-598.
6. M.W. Biggs, J.E. Eiselein and G. Wilcox. Observations on murine leukemia treated with deuterium and x-ray. *Cancer Res.* 23, 1059-1062, 1963.
7. B. Rajewsky, O. Heuse and K. Aurand. Bestrahlung von weissen Mäusen mit hohen Dosen von Röntgenstrahlen. *Strahlentherapie* 95, 513-522, 1954.

8. H. Cerdá and K. Rosander. DNA damage in irradiated endothelial cells of the rat cerebral cortex. Protective action of cysteamine in vivo. *Radiat. Res.* 95, 317-326, 1983.
9. J. J. Katz, H. L. Crespi, D. M. Czajka and A. J. Finkel. Course of deuteration and some physiological effects of deuterium in mice. *Am. J. Physiol.* 203, 907-913, 1962.
10. Z. M. Bacq. Chemical protection against ionizing radiation. Charles C. Thomas, Springfield, 1965.
11. J. M. Yuhas and J. B. Stoner. Chemoprotection against three modes of radiation death in the mouse. *Int. J. Radiat. Biol.* 15, 233-237, 1969.

# Histological Microanalysis of Boron with Cold Neutrons

Börje Larsson 1, Jörgen Carlsson 2, and Detlef Gabel 3

1 The Gustaf Werner Institute, University of Uppsala, Box 531,  
S-751 21 Uppsala, Sweden

2 National Defence Research Laboratory, FOA-4, S-901 82 Umeå, Sweden

3 Department of Chemistry, University of Bremen,  
Postfach 330 440, D-2800 Bremen 33, F.R.G.

## 1. Introduction

Here we consider the prerequisites for observing local "receptor" activity, in animals or patients, through injection of appropriately labelled macromolecular "ligands" for subsequent topographic analysis. At the organ level, the concentration pattern of the radioactive tags may be measured non-invasively, by "Positron Emission Tomography" (PET) or by "Single Photon Emission Computerized Tomography" (SPECT), while at the histological level, the analysis may be performed, at microscopic resolution, on biopsy and autopsy materials. The latter approach is the particular theme of this communication where the merits of stable boron-10 as a marker are studied in particular.

There is presently a search for efficient, safe and practically convenient methods for quantitative analysis of receptor activity *in vivo* in experimental physiology and clinical medicine. Important applications are foreseen, especially in studies of the behaviour, in the body, of proteins or glycoproteins, such as antibodies, toxins, hormones and growth factors. Specific macromolecular tracers with affinity for cellbound members of the immunoglobulin family (1) may also be developed.

The present state of development is illustrated by reference to studies of the traffic and targeting of labelled antibodies and antibody derivatives. The potentialities of a number of new tracer nuclides are first mentioned with a view also towards other macromolecules ( $M > 10,000$  dalton) that may be used to identify, localize and quantify receptor activities expressed by organized cells in their natural habitat.

The term "cell-seeking antibodies" is used to signify native or modified immunoglobulins as they have been prepared for observation of antigenic cell surface markers. The majority of the studies referred to have been concerned with 150,000 dalton IgG antibodies, the most common class of blood-borne immunoglobulins. The molecular structure of such antibodies is well known (2). Typically, it consists of two identical "heavy" protein chains (50,000 dalton), each in close association with a shorter carbohydrate chain, and two identical "light" protein chains (25,000 dalton). A similar ground structure is also seen in the less common IgD and IgE antibodies and also in the subunits of the larger, more complex antibodies (IgA and IgM).

The unfolded structure of IgG antibodies resembles the letter Y, in

which the two arms correspond to the "Fab" parts of the molecule and the stem is made up of the "Fc" part. The outermost domains of the Fab arms contain the antigen binding sites. These have to be spared from modification by the labelling chemistry. Major modification of the rest of the molecule, including enzymatic removal of the Fc part, is possible without losing the receptor affinity of the (Fab)<sub>2</sub> fragment, however. It is a general observation, in fact, that one or several labels can be attached to the antibody molecule, even to the (Fab)<sub>2</sub> fragment, with no or little change in the association constant. On the other hand, the solubility or transport characteristics of the antibody may be affected, by fragmentation or chemical modification.

Being produced in the specialized lymphocytes called B-cells, antibodies fulfil their natural roles in the immune defence of all vertebrates. Antibodies obtained in the conventional way, by fractionation of "antisera" from immunized animals, are "polyclonal" and directed towards many different determinants on the used antigen. "Monoclonal" antibodies, with affinity for a single determinant only, represent a homogeneous gene product from a single clone of B-cells. Monoclonal antibodies, "Mabs", for experiments or clinical applications are usually obtained in the form of murine IgG, from carefully selected clones of hybridoma cells. Spontaneous or induced hypersensitivity to murine immunoglobulin is thus a limiting factor in clinical applications of cell-seeking antibodies. The production of human monoclonal antibodies has not yet reached the desired efficiency.

## 2. Choice of label

Since our theme is quantitative analysis, only labels are treated that permit direct stoichiometric determination. So, however useful they may be in histochemistry and sometimes for observations *in vivo*, ligands loaded with fluorophors, enzymes or enzyme substrates, heavy metal colloids or microspheres are not considered here.

With these restrictions, we are left with radiometric approaches based on the observation of nuclear (or atomic) events in nuclides (or elements). The methods to be considered are thus based on parenteral injection of receptor ligands tagged with spontaneously radioactive nuclides, or with stable nuclides (or elements) that could be studied by radiation-induced nuclear (or atomic) reactions (Table 1). In the case of non-radioactive tags, no distinction is made, in the following, between nuclidic and elemental labels.

In autoradiography, where prolonged measurements are possible, fairly long-lived radionuclides (such as S-35 and I-125, less conveniently H-3) could be used without excessive saturation of the receptors. As an alternative, even non-radioactive labels with large cross-sections for nuclear neutron capture (B-10), or particle-induced X-ray emission (elemental Br, I) can be useful.

In measurements based on external scintigraphy the observation period has to be restricted to a few hours, at most. This sets an upper limit for the half-life of useful tracers. The success of PET or SPECT, in studies of receptor activity, is dependent on whether sufficiently high specific radioactivity can be obtained. Favourable conditions can be achieved, in practice, only by using radionuclides with half-lives shorter than one

TABLE 1: Radioactive nuclides, more or less useful as labels for large receptor ligands\*. The half-life of the radioactive nuclides and energies (with abundance) of emitted photons ( $\gamma, X$ ), negatrons ( $\beta^-, e^-$ ), positrons ( $\beta^+$ ), alpha particles ( $\alpha$ ), or nuclear fragments ( ${}^7\text{Li}$ ) are given, together with the theoretical specific activity  $S_{\text{max}}$ . This concept may be used also for the stable species  ${}^{10}\text{B}$ , and elemental I and Br, while they are giving off prompt radiation at exposure by a given fluence of "activating" particles (slow neutrons capture and PIXE, respectively, see text).

Nuclide (or element)	$T_{\frac{1}{2}}$ hr	$\gamma, X$ MeV	$\beta^+$ MeV	$\beta^-, e^-$ MeV	$\alpha$ or ${}^7\text{Li}$ MeV	$S_{\text{max}}$ Bq/mol
Boron 10	(stable)	-	-	-	Prompt $\alpha + {}^7\text{Li}$	$0 - \infty$
Iodine	(stable)	Prompt $X$	-	-	-	$0 - \infty$
Bromine	(stable)	Prompt $X, K, L$	-	-	-	$0 - \infty$
Carbon 11	0.34	- $K, L$	0.96 (100%)	-	-	$3.3 \cdot 10^{20}$
Bromine 75	1.70	< 0.62	1.70 (90%)	-	-	$6.9 \cdot 10^{19}$
Flourine 18	1.83	-	0.635 (97%)	-	-	$6.3 \cdot 10^{19}$
Sulphur 38	2.87	< 1.88	-	< 3.0	-	$4.0 \cdot 10^{19}$
Indium 109	4.3	< 0.91	0.79 (6%)	< 0.201	-	$2.7 \cdot 10^{19}$
Technetium 99m	6.0	< 0.14	-	< 0.119	-	$2.0 \cdot 10^{19}$
Selenium 73	7.1	< 0.36	1.30 (65%)	< 0.35	-	$1.6 \cdot 10^{19}$
Astatine 211	7.2	< 0.687	-	-	$5.87\alpha (41\%)^{**}$	$1.6 \cdot 10^{19}$
Iodine 123	13	< 0.159	-	< 0.127	-	$9.0 \cdot 10^{18}$
Bromine 76	16	< 3.57	3.6 (62%)	-	-	$7.5 \cdot 10^{18}$
Indium 111	67	< 0.25	-	< 0.24	-	$1.8 \cdot 10^{18}$
Iodine 131	193	< 0.723	-	< 0.806	-	$6.1 \cdot 10^{17}$
Iodine 125	1440	< 0.035	-	< 0.030	-	$8.1 \cdot 10^{16}$
Sulphur 35	2112	-	-	< 0.167	-	$5.3 \cdot 10^{16}$
Hydrogen 3	107748	-	-	0.030	-	$11.0 \cdot 10^{14}$

\* From B. Larsson, In Proceedings of the Third Symposium on Medical Application of Cyclotrons, Turku, Finland, June 13-16, 1983. (In press.)

\*\* 7.45 MeV  $\alpha$  from the  ${}^{209}\text{Po}$  daughter not included.

month, or preferably much less. This is easy to show theoretically, and is also directly evident from experience already gained with smaller receptor ligands containing shortlived radionuclides. PET studies of hormones, drugs or neurotransmitters, at typical receptor concentrations, require high specific activity ligands, in any case not less than ca.  $10^{16}$  Bq mol $^{-1}$ . For macromolecular ligands at lower receptor concentrations, the requirements are more severe, and specific activities of at least  $10^{18}$  Bq mol $^{-1}$  should be striven for. This corresponds to half-lives of one week or less, placing I-131 at the upper limit of the useful interval.

Except the case when receptors are directly exposed to the blood-stream, there is also a lower limit to the half-life of otherwise useful radionuclides, because macromolecular ligands require considerable time to reach target receptors at a distance from capillary vessels. It is very unlikely, for example, that C-11, with its half-life of 20.5 min, in spite of its theoretically excellent specific activity and chemical properties, would find important uses in PET studies of macromolecular ligands of parenchymatic or tumour cell receptors.

Prior to the experimental work with B-10, illustrated below, in some detail, we made a survey of the physical-chemical characteristics of known (established or potentially useful) nuclidic or elemental labels, applicable to in vivo studies of antibodies. It resulted in a list of 15 radioactive and 3 stable species that seem worthy of special consideration. They are here presented and discussed briefly, with reference to the maximum theoretical specific activity and other physical characteristics given in Table 1.

### 3. Radioactive labels for antibodies

First, the radionuclides listed in Table 1 are presented in some detail, with reference to typical conditions of application:

Carbon-11. All available information indicates that many hours, even a day or two, are required to permit efficient cell-seeking and blood clearance of injected antibodies. The half-life, 20.5 min, of the commonly used positron-emitter C-11 seems therefore too short to permit meaningful studies of antibody-receptor activity in vivo.

C-11 with its well-known merits in PET investigations (3), might nevertheless be useful for studies of antibody behaviour, within the first hours after administration. From previous experience, rapid covalent labelling should be possible by attachment or incorporation of suitable C-11 precursors. The theoretically very high specific activity would then permit studies, at low antibody concentration, of important phenomena, such as the roles of the liver and the reticulo-endothelial system in the clearing process. Of special interest would also be studies of the effects of "antibody scavengers" or of structural modification, on the antibody traffic in the recipient.

C-11 is the only nuclide mentioned here, which has to be used in proximity of the production unit, say within a distance covered by 1 hour transportation.

Bromine-75 and Fluorine-18. These positron-emitters share the potential usefulness of C-11, in PET studies of antibody traffic. Their short half-life, 1.7-1.8 hours, permits high specific activity, but would

be a limiting factor, in studies of the receptors. However, there is hope that the process of blood-clearance can be made more efficient, by modification of the antibody structure, as well as by artificial scavenging of circulating non-bound antibodies. This would, no doubt, make Br-75 and F-18 more interesting as labels. Covalent binding of bromine and fluorine to protein would be easy, in principle, but efficient and sufficiently rapid processes have to be devised.

Sulphur-38, Selenium-73 and Sulphur-35. Although physically inferior to Se-73, a positron emitter that might be used to great advantage in studies of antibody behaviour, S-38 would be very useful in the desirable study of differences between S- and Se-labelled antibodies by emission-tomographic techniques. Comparison of Se-73- and S-38-antibodies would be invaluable, before implementing the seemingly ideal combination Se-73 + S-35 in experimental and clinical practice.

Both S- and Se-labels may be used to substitute natural sulphur in Mabs, by feeding hybridoma cultures with high specific-activity methionine, for natural incorporation in newly synthesized immunoglobin. The still hypothetical monoclonal antibodies, from hybridoma cells fed simultaneously with Se-73-L-methionine and S-35-L-methionine, would be a seemingly optimized combination for concerted studies of Mabs by macroscopic and microscopic techniques. The half-life of Se-73 of 7.1 hours gives a theoretical maximum specific activity of  $1.6 \times 10^{19}$  Bq/mol and is still long enough to permit observations for more than 24 hours after injection. S-35 is a soft beta-emitter that has well proven its value in autoradiography, in general. Its theoretical maximum specific activity of  $5.3 \times 10^{16}$  Bq/mol would leave little more to desire.

The proposed biotechnical production of Se-73- and S-35-Mabs would stimulate the use of labelled antibodies for therapy. Such Mabs could be further loaded with more efficiently cell-killing nuclides (cf. B-10 and At-211), by methods developed for native immunoglobulins.

Indium-109 and Indium-111 have convenient radiophysical characteristics. In-109 is a positron and gamma emitter, with a half-life of 4.3 hours, near-ideal for emission tomography. In-111, with its half-life of 67 hours and convenient beta emission, is very useful for autoradiography and may also be exploited in SPECT based on labelled antibodies.

The labelling chemistry of indium is unfortunately not very favourable, as covalent binding seems impossible. Acceptable labelling efficiency and stability can be achieved by means of bifunctional chelating agents, however. An increasing use of In-111 is presently seen in experimental oncoimmunology. Occasional clinical applications have also been reported.

Technetium 99m. This nuclide which is so important in nuclear medicine has difficulties to find its place in diagnostics or experimental research with labelled antibodies. There is undoubtedly a need for intensified research on labelling with Tc-99m, before any definite conclusions can be made as to its potential usefulness in the present context.

Astatine-211. This is the only spontaneous alpha-emitter considered for labelling of Mabs. With a half-life of 7.2 hours, giving a theoretical maximum specific activity of  $1.6 \times 10^{19}$  Bq mol<sup>-1</sup>, At-211 appears ideal for high-resolution autoradiography as well as for therapeutic applications. Its iodine-like characteristics permit convenient labelling chemistry (4).

The supplementary use of gamma rays from At-211 for SPECT is in fact also possible. The challenge for intensified research on this very interesting nuclide is highly felt. A limiting factor is that production has to be made by accelerated ions of rather high energy, by exploitation of the reaction  $\text{Bi-209}(\alpha, 2n)\text{At-211}$ , for example.

Bromine-76. The bromine isotope Br-76 gains its merits from its chemical characteristic permitting convenient halogenation, and also by being a positron emitter. The half-life of 16 hours is very attractive, in our context, and gives a maximum theoretical specific activity of  $7.5 \times 10^{18}$  Bq mol $^{-1}$ . Br-75, in combination with I-125 for autoradiography, appears to be the most promising alternative, in PET studies, to the combination of Se-73 and S-35 considered above.

Iodine-123, Iodine-131 and Iodine-125. These iodine isotopes are well-known tools in nuclear biology and medicine. I-123 with its 13-hour half-life and favourable radiometric properties is in fact an ideal nuclide for SPECT with labelled Mabs. It may be favourably combined with I-125 which permits high-resolution autoradiography. For practical reasons, I-131 is presently the dominating isotope of iodine, in the literature on labelled antibodies, in spite of its low theoretical maximum specific activity,  $6.1 \times 10^{17}$  Bq/mol I-123, in combination with I-125 for autoradiography, appears to be the most obvious choice, in SPECT studies of labelled antibodies.

Hydrogen-3. Tritium, H-3, will probably keep its important place as a versatile label, also in immunology, and the study of the physiological fate of antibodies and other macromolecules. Its long half-life and correspondingly low specific activity prevents its use for the efficient autoradiographic study of receptor activity, however. The main role of tritium will probably be as a tracer in experimental studies based on liquid scintillation analysis of biopsy materials, specimens of body fluids, and model systems in vitro.

#### 4. Pairs of labels

An attractive possibility is the concerted use of chosen pairs of labels, in studies of macromolecules with affinity for cellular target receptors. Three pairs of radionuclides of great potential usefulness have been identified (5) and are here given in order of their apparent qualifications:

Se-73 + S-35, for PET + autoradiography

Br-76 + I-125, for PET + autoradiography

I-123 + I-125, for SPECT + autoradiography

The use of alpha-emitting At-211 or the nuclear neutron capture reaction  $\text{B-10}(n, \alpha)\text{Li-7}$  is recommended for further study, also from this point of view. As alternatives to autoradiography based on S-35 or I-125 the measurements of stable iodine, or bromine, by particle induced X-rays, in particular, offer another alternative to the use of radioactive labels (6).

Stable and radioactive labels used together could possibly facilitate

double labelling of single populations of antibody molecules. "Neutron capture radiography" based on the reaction  $B-10(n,\alpha)Li-7$  may in this way be combined with radioactive labels to achieve efficient and convenient combinations of PET or SPECT with autoradiography (6). In the following, present experiences with neutron capture radiography (NCR) based on boron-10 are illustrated (7).

##### 5. Boron-10 as a stable label for cell-seeking macromolecules

We have studied the prerequisites for use of the stable boron isotope B-10 as a tag for biomolecules *in vivo*. The technique used is related to the radiographic analysis of boron in tissue specimens reported by Mayr et al. (8). They seem to have been the first to use the well-known neutron capture reaction in B-10 for the analysis of a biological specimen, already at a time when only photographic emulsions were available for use as a detector. With the organic, homogeneous solid state detectors now available (9,10) for detection of the fragments appearing at neutron capture by B-10, the signal/background ratio is much more favourable than with the photographic techniques originally used. Low-background techniques with potential application in the analysis of B-10-tagged macromolecules have previously been described (11,12). Neutron capture radiograms of whole-body histological sections from tumour-bearing mice, given boron compounds used in neutron capture therapy, have been produced by Matsuoka et al. (13). Such techniques may be referred to by the term "Neutron Capture Radiography, NCR".

In this paper, NCR based on solid-state "alpha-track detectors" and a slow neutron beam, practically free from contaminating radiations, is presented as an alternative to "autoradiography" based on the radioactive nuclides presently used for the tracing of macromolecules in histological samples. Tracing of macromolecules by neutron capture techniques is now becoming possible, thanks to the development of boron compounds suitable for conjugation. Immunoglobulins, for example, have been labelled with about 5 % (by weight) boron with retained solubility (14). At sufficiently high concentration of the B-10 label in the tissue, the tracks of alpha and Li-7 ions that appear upon neutron capture in this nuclide dominate over parasitic tracks. The latter include those ascribed to naturally present B-10 and Li-6, or any other nuclide that produces alpha or alpha-like tracks upon neutron capture, as well as occasional "background" tracks in the detectors.

With a pure beam of slow neutrons there is also little deterioration of the detector material, even at the high neutron fluences necessary to achieve high detection sensitivity for B-10. For a given solid-state detector material, the limits of sensitivity are set by competing nuclear capture reactions in the specimen (cf. Table 2) and the detector, not by the nuclear recoils and nuclear reactions produced by contaminating fast neutrons. This is an important aspect that has been demonstrated in experiments aiming at analysis of environmental actinides with solid-state "fission-track detectors" (15).

The majority of the experiments on which this report is based were made with a "cold" neutron beam from the high-flux reactor at Institut Laue-Langevin (ILL). As shown previously, such a beam is the ideal tool for

**Table 2.** Neutron capture reactions induced by a thermal capture fluence equivalent of  $10^{12}$  neutrons  $\text{cm}^{-2}$  in 1 ng of  $(\text{C}_5\text{H}_{10}\text{O}_{18}\text{N})_n$  containing  $0.1 \mu\text{g g}^{-1}$  natural boron and  $0.01 \mu\text{g g}^{-1}$  natural lithium. Types and calculated number of capture events and nuclear fragments or recoils (particles) are given for reactions of significance in studies of  $^{10}\text{B}$ -labelled compounds by neutron capture radiography. Isotopic abundances and microscopic cross-sections are from *Table of Isotopes* 1978 ed. C.M. Lederer *et al.* 7th ed. (New York: Wiley). Particle characteristics and total energy carried are inferred from data found in Kobayashi T. and Kanda K., 1982, *Radiat. Res.*, **91**, 77-94.  $1 \text{ b} = 10^{-24} \text{ cm}^2$ . From reference (7). Courtesy *Physics in Medicine and Biology*.  
[© The Institute of Physics, London, England]

Reaction	$^1\text{H}(\text{n}, \gamma)^2\text{H}$	$^{14}\text{N}(\text{n}, \text{p})^{14}\text{C}$	$^{17}\text{O}(\text{n}, \alpha)^{14}\text{C}$	$^{10}\text{B}(\text{n}, \alpha)^7\text{Li}$	$^{10}\text{B}(\text{n}, \alpha\gamma)^{17}\text{Li}$	$^{6}\text{Li}(\text{n}, \alpha)^3\text{H}$
Isotopic abundance of target nuclide (atom per cent)	99.985	99.63	0.038	19.8	19.8	7.5
Mass of target element (ng)	0.100	0.0348	0.715	$1.00 \times 10^{-7}$	$1.00 \times 10^{-7}$	$1.00 \times 10^{-8}$
Number of target atoms	$6.0 \times 10^{13}$	$1.5 \times 10^{12}$	$1.02 \times 10^{10}$	$1.10 \times 10^6$	$1.10 \times 10^6$	$6.5 \times 10^4$
Microscopic cross-section (b)	0.332	1.82	0.235	242	3595	942
Number of events <sup>†</sup>	20.0	2.7	$2.5 \times 10^{-3}$	$2.7 \times 10^{-4}$	$4.0 \times 10^{-3}$	$6.6 \times 10^{-4}$
Particle, kinetic energy (MeV)	$^2\text{H}$ , 0.0013 C, 0.04	p, 0.59 $^{14}\text{C}$ , 0.40	$\alpha$ , 1.42 $^{14}\text{C}$ , 1.40	$\alpha$ , 1.78 $^7\text{Li}$ , 1.01	$\alpha$ , 1.48 $^7\text{Li}$ , 0.84	$\alpha$ , 2.05 $^3\text{H}$ , 2.73
Total energy carried (MeV)	0.026	1.70	0.0045	0.0008	0.0093	0.0003
Particle range in water ( $\mu\text{m}$ )	$^2\text{H}$ , <1 $^{14}\text{C}$ , <1	p, 10 $^{14}\text{C}$ , <1	$\alpha$ , 8 $^{14}\text{C}$ , <1	$\alpha$ , 10 $^7\text{Li}$ , 6	$\alpha$ , 8 $^7\text{Li}$ , 5	$\alpha$ , 11 $^3\text{H}$ , 45
Particle <sup>‡</sup> approximate linear energy transfer (keV $\mu\text{m}^{-1}$ )	—	p, 50	$\alpha$ , 220	$\alpha$ , 220 $^7\text{Li}$ , 340	$\alpha$ , 230 $^7\text{Li}$ , 300	$\alpha$ , 210 $^3\text{H}$ , 20

<sup>†</sup> In the text, these figures (background) are compared with the figure 2.4, i.e., the number of capture reactions in a 1 ng specimen considered to contain  $10 \mu\text{g}^{10}\text{B g}^{-1}$ , a typical concentration in a tracer experiment (signal).

<sup>‡</sup> Here only particles of  $> 1 \mu\text{m}$  range are given.

studies of nuclear neutron capture reactions in thin biological specimens (16,17). Being defined by a wavelength-selecting beam-guide it is practically free from contaminating fast or epithermal neutrons.

A variation of the NCR technique here described has been used for the analysis of Li-6 in the brain of rats (18). Also in that case the cold neutrons gave advantages over conventional thermal reactor neutrons, and our analytical programmes have been coordinated, as far as common technical problems and instrumentation are concerned (16). Here we restrict the account to aspects of relevance for the use of B-10 as a marker for large biomolecules, with a special view towards studies of B-10-loaded antibodies and other immunoreagents in experimental and clinical physiology.

#### 6. Prerequisites for the detection of macromolecules labelled with B-10

Among nuclides with sufficiently large cross-section for nuclear neutron capture to permit demonstration by high-sensitivity NCR, B-10 is unique, in the sense that it can be covalently bound to organic molecules. In the chemical combinations considered, e.g. 1,2-dicarbacloso-dodecaborane derivates, it seems also relatively innocuous from the toxicological point of view (19). Physical prerequisites for the use of the  $(n,\alpha)$ -reaction of B-10 for topographic analysis in cells or tissue specimens are proper detection techniques and a high and pure fluence of slow neutrons. The capacity of presently used detector systems has been studied experimentally, as illustrated below, in current biological studies (7). In this paragraph we deduce the prerequisites that determine the signal/background ratio, and the energy transferred to the detector-specimen sandwich by the ionic fragments that appear upon neutron capture in the specimen. In these considerations, we use a theoretical model representative for the experimental situation. It consists of 1 ng of tissue  $(C_5H_{40}O_{18}N)_n$  with 0.1  $\mu g$   $g^{-1}$  natural boron and 0.1  $\mu g$   $g^{-1}$  natural lithium charged with a superimposed B-10 of 10  $\mu g$   $g^{-1}$ , the "label".

The chosen levels of "contamination" with natural boron and lithium, respectively, seem representative for human soft tissue specimens (20). The level of labelling with enriched B-10 corresponds to a typical experiment (*vide infra*), in which macromolecular carriers, such as immunoglobulin, polylysine or dextran, are being used. With markers such as aminophenylborate-substituted carboxymethylcellulose (21) or decachlorocarborane, local concentrations of 10  $\mu g$  boron  $g^{-1}$  were easily obtained in the cellular or tissue specimens under study. Also bloodborne boric-acid-containing liposomes prepared from lecithin and cholesterol (22) were used in preliminary tests at a similar concentration. One ng of tissue corresponds to a typical mammalian cell ( $1000 \mu m^3$ ) of density  $1 g cm^{-3}$  and may also - with generous approximation - represent a mass element in an organic solid-state detector in contact with the specimen. The model object so chosen was supposed to be irradiated by a thermal capture fluence equivalent of  $10^{12}$  neutrons  $cm^{-2}$ , a value that is also typical for the experimental situation referred to below (cf. Fig. 1).

Analysis of boron by NCR is based on the fact that capture of slow neutrons in B-10 leads to isotropic emission of pairs of Li-7 and alpha particles in antiparallel directions. Along the near-linear trajectories of these particles, less than  $10 \mu m$  long in the condensed materials consid-

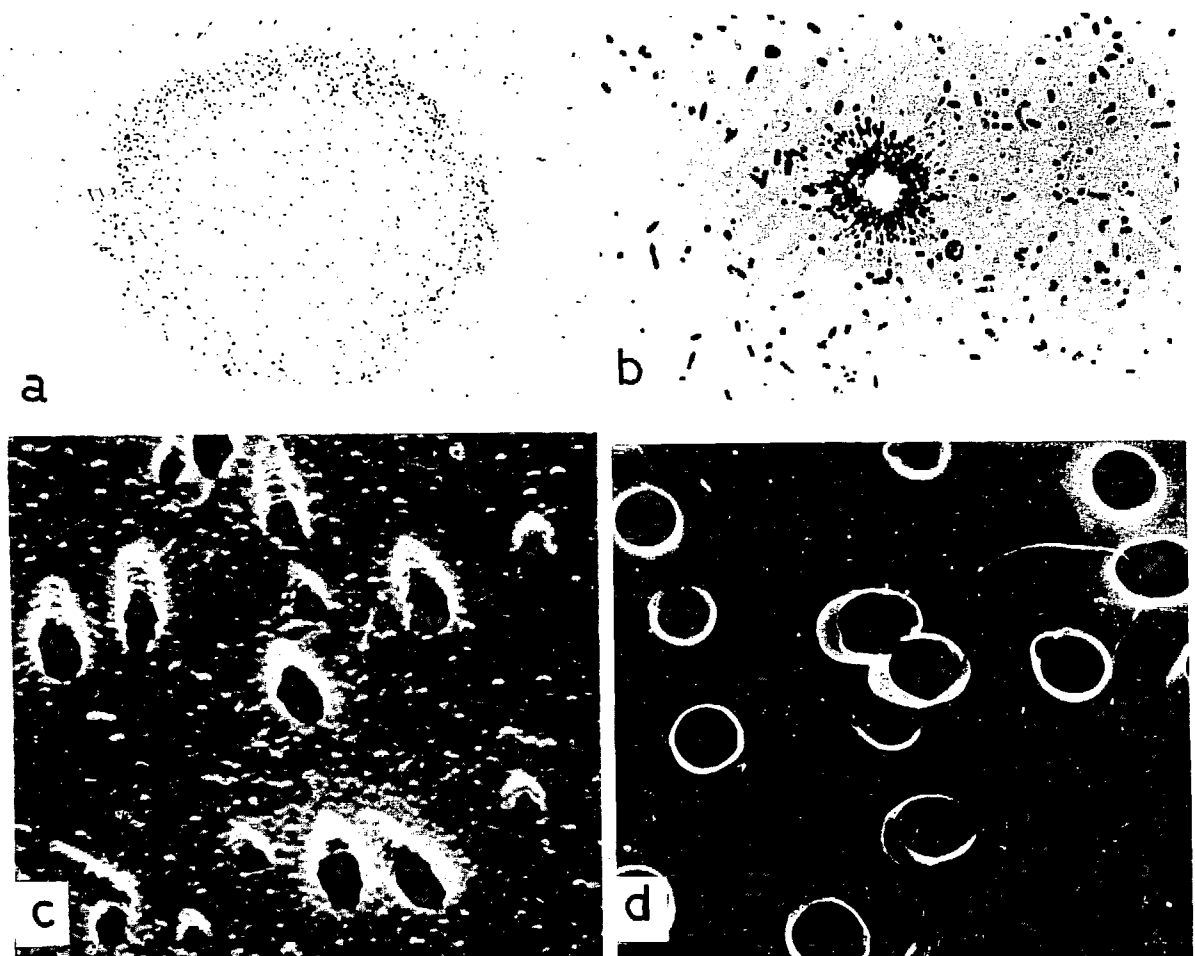


**Figure 1.** Examples of track structures produced via etching of cellulose nitrate detectors (LR115, Kodak-Pathé, Paris) after exposure to slow neutrons or to an attenuated, perpendicular flux of alpha particles. (a) From experiments on tumour spheroids, to demonstrate gradient of  $^{10}\text{B}$  after incubation in medium containing borate (x 50). (b) From experiments on rats given boron-loaded dextran intravenously, to demonstrate retention of this macromolecular preparation in the blood-stream. Tracks are confined to areas corresponding to a small artery (centre) and surrounding capillary vessel. Observe breakdown of detector at very high track density! (x 300). (c) Tracks similar to those of (a) and (b) as seen in the scanning electron microscope (SEM). The locations of capture events in  $^{10}\text{B}$  are clearly indicated by large hollow-structures, while smaller deficiencies may indicate neutron capture in  $^{14}\text{N}$  or  $^1\text{H}$  (x 5.000). (d) Tracks representing ca. 1 MeV alpha particles (x 5.000).

[© The Institute of Physics, London, England]

red, radiochemical changes occur so as to form "latent tracks". In the detector, these latent tracks can be "developed" into visible signals, i.e. the "signals" that can be studied in a microscope, visually or by automatic scanning techniques. The total energy liberated as kinetic energy of the reaction products (including, in 95 % of the events, a 0.46 MeV capture gamma ray) is 2.8 MeV. A value of 2.33 MeV for the average energy transferred by the ionic fragments per reaction would be accurate to about 1 %. The equivalent He-4 energy is 1.48 MeV, the Li-7 energy is 0.85 MeV and the corresponding ranges in water are ca. 8.9  $\mu\text{m}$  and ca. 4.8  $\mu\text{m}$ , respectively. In freeze-dried soft tissue the tracks are 5-10 times longer. With a thermal cross-section of the reaction  $\text{B-10}(n,\alpha)\text{Li-7}$  of 3837 barns, a B-10-concentration of 10  $\mu\text{g cm}^{-3}$  tissue, and a thermal capture fluence equivalent corresponding to  $10^{12}$  neutrons per  $\text{cm}^2$ , there would be, on the average, ca. 2.4 events in a volume element of  $1000 \mu\text{m}^3$ , the model chosen above for a mammalian cell.

The calculated types and numbers of significant neutron capture events obtained under the same conditions in H-1, N-14, O-17, B-10 and Li-6, i.e. the significant "background" events - in the absence of fast neutrons - are given in Table 2. In terms of He-4 (alpha) tracks, the signal/background ratio calculated would be  $2.4/0.0068 = 350$ . Since discrimination would be possible against all reactions except neutron capture in natural B-10 (and probably Li-6), the theoretical possible ratio is higher,  $2.4/0.0434 = 550$ . In reality the ratio would be inversely related to the natural boron content of the specimen. Useful experimental information would be possible to obtain, at signal levels one or two orders of magnitude lower than the values assumed in the above model, i.e. down to ca. 0.1 g B-10 per g tissue.

The only biogenic nuclides in animal tissues that have any thermal cross-sections of importance, in the present context, are H-1, N-14 and O-17 (Table 2). The hydrogen capture reaction  $\text{H-1}(n,\gamma)\text{H-2}$  produces very short recoils of deuterium ions which are both **harmless** from the point of view of absorbed radiation dose and easily discriminated in the etching procedure. Capture in N-14 contributes a significant amount of parasitic tracks through the reaction  $\text{N-14}(n,p)\text{C-14}$ . In natural as well as freeze-dried soft tissue, N-14 is present at a concentration of ca  $1.5 \times 10^{12}$  atoms per  $1000 \mu\text{m}^3$ . Its cross-section for thermal neutron capture, 1.82 barns, permits 2.7 events per  $1000 \mu\text{m}^3$  at a fluence of  $10^{12}$  nt / $\text{cm}^2$ . The tracks of the 0.586 MeV protons and 0.042 MeV C-14 ions can be easily discriminated thanks to their low linear energy transfer (LET) and short track length, respectively, but they contribute to the destruction of the detector and probably set the limits to the sensitivity of detection.

## 7. Boron-10 in tumour cell spheroids and experimental animals

### 7.1 Biological specimens

The problems encountered require supra-cellular, cellular or subcellular localization of B-10, with correspondingly increasing demands for spatial resolution, detection sensitivity, and high signal-background ratio. Special attention has been paid to localization of B-10 markers

- (1) in cultivated aggregated human tumour cells (spheroids)
- (2) in the central nervous system of the rat.

After incubation with or injection of chosen boron conjugates, for

varying lengths of time in vitro or in vivo, specimens were secured by deep-freezing of the studied systems and a corresponding control material. Cell spheroids and whole rats were rapidly frozen in cool propane, freeze-mounted and freeze-sectioned. Most of the radiographic studies so far have been made on freeze-dried 5-20  $\mu\text{m}$  thick sagittal sections prepared from the skull or the abdomen of adult rats.

### 7.2 Boron conjugates

Immunoglobulins, dextran and dextran derivatives, and human serum albumin have been used in the preparation of conjugates with markers such as decachloro-o-carborane (14) or amino-phenylborate-substituted carboxymethylcellulose (21). For comparison, and in order to further elucidate the behaviour of borate as an example of a small ligand, boric acid has also been used. For practical and economical reasons, all tests have been made so far with natural boron.

### 7.3 Solid-state detectors

In preliminary experiments, various detector materials were tested, including polycarbonate and CR-39. So far, the best results have been obtained with cellulose nitrate (CN) films, and for the purpose of illustrating the technique, all examples given in this paper are based on the use of 6 or 12  $\mu\text{m}$  CN (Kodak-Pathé LR 115 type I or II). During irradiation, the detector film and the freeze-dried tissue section were pressed tightly together in an evacuated bag of 0.1 mm thick polyethylene.

### 7.4 Neutron irradiation

Cold ( $\bar{\lambda} = 1.1 \text{ nm}$ ,  $E \leq 10 \text{ meV}$ ) neutrons were used at the high-flux reactor of ILL. The simple instrumentation described previously (16) was served by a short independent branch of the H 17 beam guide in the reactor hall. The "capture flux" was measured by gold foil activation to be equivalent to ca.  $5 \times 10^9$  thermal neutrons  $\text{cm}^{-2} \text{s}^{-1}$  and uniform within ca. 10 % over the circular beam cross section, 1.5 cm in diameter. Irradiation times were from some minutes to several hours.

### 7.5 Visualization of the tracks

The submicroscopic tracks of radiochemical changes produced by the He-4 and Li-7 ions in the solid-state detector have to be "developed" into structures visible in the microscope (Fig. 1) by chemical etching techniques. The procedures chosen have varied with the detector material. Mostly, for cellulose nitrate as well as for polycarbonate, we have used 2.25-6.25 N NaOH (Merck, p.a.) at  $60^\circ\text{C}$  for varying length of time, depending on the aim of each particular experiment. The developed tracks were easily seen by light or electron microscopy, depending on the length of the etching period. To facilitate the comparison of histological structure and track patterns we have adopted a system of two microscopes (Laborlux 12) integrated by an optical bridge system (Wild-Leitz, Zürich).

## 8. Results and discussion

A cold neutron beam, defined by a beam guide system, was found to be an ideal tool for studies of nuclear neutron capture in thin cell or tissue

specimens. Such a beam is practically free from particles that are able to cause chemical effects through direct transfer of kinetic energy to electrons or whole atoms in the target. Thus the effect of nuclear interaction can be easily observed, especially reactions in Li-6, B-10 and actinides, with large cross-sections for nuclear neutron capture. The use of cold neutrons also permits topographic analysis of such nuclides, at high sensitivity, by means of solid state track detector materials, a technique referred to by the term "neutron capture radiography" (NCR). In the case of B-10, antilinear emission of 1.47 MeV He-4 and 0.84 MeV Li-7 leaves distinct track structures in suitable chosen detector films.

The aim has been to optimize the experimental parameters for planned experiments with B-10-loaded antibodies and other immunoreagents. Various B-10-carriers have been used in model studies on cultivated cells, cell spheroids, and rats. NCR for B-10, based on cold neutrons, was found to be a very sensitive and quantitative method that may be considered an attractive alternative to corresponding methods that rely on the use of radioactive labels. The natural occurrence of boron and lithium is very low in animal tissues. The sensitivity of the method is in practice limited by the detector materials, that may break down at high exposure, i.e.  $10^{13}$  -  $10^{15}$  thermal neutron equivalents per  $\text{cm}^2$ , depending on the amount of N-14 present in the specimen and detector film. The spatial resolution is presently 3  $\mu\text{m}$  but may be improved considerably.

The rate of nuclear reactions or elastic collisions attributable to epithermal or fast neutrons, in or near the detector material, could be neglected since the cold neutrons were brought by a beam guide system to the targets. Reduction of these contaminating radiations to insignificant levels turns out to be an important prerequisite in radiographic applications (18), because the cross-section for fast neutron-induced recoil production in tissue nuclide is 1-5 barn. With the detector systems and boron concentrations used here, contamination by secondary protons or electrons (including beta decay, Compton or photo electrons) appears also insignificant, but the absorbed dose should be studied further since radiation damage to the detector may set the ultimate limits to the sensitivity of the method (15).

With the exception of a low number of tracks caused by environmental alpha radiation, parasitic high-LET tracks in the detector could be ascribed to neutron capture in natural or contaminating B-10, Li-6 or O-17, in the biological specimen itself or in the solid state detector. The frequency of such tracks should be low, however, compared to the frequency of "true signal" tracks, at the typical B-10-label concentration of 10  $\mu\text{g}$  B-10 g (Table 2).

The present features of the neutron capture radiography (NCR) technique, as it appears in its present version at ILL, are illustrated by four examples in Fig. 1. They may be summarized as follows:

(1) From the present study, and by corroborative studies with boron-doped silicon wafers, it can be concluded that the single tracks recorded represent the localization of single B-10 neutron capture events.

(2) The sensitivity of the method is high enough to permit pictorial representation of macromolecular distribution at ppm concentrations of B-10.

(3) The background situation is such that meaningful statistical studies based on single track B-10 analysis could be made at concentration levels down to 0.1  $\mu\text{g/g}$  or less, i.e. when the natural boron contents begins to introduce severe inherent limitations.

The present techniques might be improved considerably, aiming at increased signal to background ratios and expansion of the useful interval of measurement (in terms of the concentration of B-10 in histological specimens) or improved spatial resolution. The following steps are being considered in particular:

1. Reduction of background and radiation damage to the detectors by improved neutron beam characteristics, as already demonstrated here.
2. Reduction of background and radiation damage to the detector by choice of detectors without N-14.
3. Reduction of radiation damage to the detector by substitution of H-1 by H-2.
4. Reduction of background by use of B-10-starved cells and animals.
5. Decrease of background counts due to parasitic alpha tracks by introduction of multilayer sandwich techniques and track-source staining (7).

## 9. Conclusions

Neutron capture radiography (NCR) of cell preparations and tissue sections permits (i) single B-10-loaded macromolecules to be revealed, (ii) pictorial representation of macromolecular distributions at ppm levels of B-10, (iii) macromolecular tracing by statistical track analysis near natural concentrations of B-10, i.e. ca. 0.1  $\mu\text{g/g}$ , and (iv) spatial resolution of track sources by ca. 3  $\mu\text{m}$  or less.

The experimental results and theoretical considerations thus outlined indicate that high-sensitivity, low background B-10 autoradiography will be particularly important when human monoclonal antibodies will become available for experimental and clinical investigations in man. Such antibodies cannot be demonstrated by use of secondary antibody techniques. This would make B-10 labelling techniques and neutron capture radiography the only known practical alternative to presently used radioactive methods.

Provided a suitable source is available, use of neutron capture radiography is already possible, e.g. in studies of immune-body traffic in normal and tumour-bearing animals. With proper modifications to improve sensitivity and spatial resolution further, there is also a potential for the study of B-10-loaded macromolecules, in patients, by biopsy, as a substitute or supplement to existing radioactive methods.

We foresee the routine use of the techniques here summarized - with modifications introduced to improve sensitivity and spatial resolution - particularly in studies with monoclonal antibodies and other immune bodies for studies of immune-body traffic and targeting in tumour-bearing animals and in cancer patients. A most useful combination in applications requiring both emission tomography and microradiography would probably be selenium-73 + boron-10. Such techniques would be generally useful for gaining information on antibody behaviour in vivo, as well as in treatment planning for boron neutron capture therapy.

### Acknowledgements

This work was financially supported by the Deutsche Forschungsgemeinschaft, the Swedish Cancer Society, the Swedish Natural Science Council, and the Swedish Medical Association.

### References

1. WILLIAMS, A.F. and GAGNON, J., 1982, Science, 216, 696-703.
2. MARQUART M. and DEISENHOFER, J., 1982, Immunology Today, 3, 160-166.
3. TER-POGOSSIAN, M.M., RAICHT, M.E. and SOBEL, B.E., 1980, Scientific American, 243, 140-155.
4. SMIT, J.S., MYBURGH, J.A. and NEIRINCKX, R.D., 1973, Clin. exp. Immunol., 14, 107-116.
5. LARSSON B., 1983, In Proceedings of the Third Symposium on Medical Application of Cyclotrons, Turku, Finland, June 13-16 (In Press).
6. LINDH, U., 1982, Nucl. Instr. and Meth. 193, 343-347.
7. LARSSON, B., GABEL, D. and BÖRNER, H.G., Phys. Med. Biol. (In Press).
8. MAYR, G., BRUNER, H.D., and BRUCER, M., 1953, Nucleonics, 11, 21-25.
9. FLEISCHER, R.L., and PRICE, P.B., 1963, Science, 140, 1221-1222.
10. DEBEAUVAIS, M. and CUER, P., 1964, C.R. Acad. Sci., Paris, 254B, 1777-1778.
11. FAIRCHILD, R.G., TONNA, E.A., and SEIBOLD, C.T., 1967, Radiat. Res., 30, 774-787.
12. TSURUTA, T., and YAZAKI, M., 1977, J. Nucl. Sci. Technol., 14, 816-825.
13. MATSUOKA, O., HATANAKA, H., and MIYAMOTO, M., 1977, Acta pharmacol. toxicol., Copenhagen, 41, Suppl. I, 56-57.
14. GABEL, D., and WALCZYNA, R.B., 1982, Z. Naturforsch., 37c, 1038-1039.
15. SOHNIES, B., and DENNSCHLAG, H.O., 1982, Nucl. Instr. Meth., 197, 449-452.
16. LARSSON, B., BÖRNER, H.G., CARLSSON, J., FORSBERG, J., FOURCY, A., and THELLIER, M., 1982, in Progress in Radio-Oncology II, Eds. KÄRCHER, K.H., KOGELNIK, H.D., and REINARTZ, G., (New York: Raven) pp. 151-157.
17. GABEL, D., FAIRCHILD, R.G., LARSSON, B., and BÖRNER, H.G., 1983, Radiat. Res., Submitted for publication.
18. THELLIER, M., HEURTEAUX, C., and WISSOCQ, J.-C., 1980, Brain Res., 199, 175-196.
19. KLIEGEL, W., 1980, Ber in Biologie, Medizin und Pharmazie, (Berlin: Springer).
20. IYENGAR, G.V., KOLLMER, W.E., and BOWEN, H.J.M., 1978, The Elemental Composition of Human Tissues and Body Fluids, (Weinheim, New York, Verlag Chemie).
21. MALMQVIST, M., 1981, Personal communication.
22. ARVIDSON, G., 1982, Personal communication.

## Boron-10 Distribution in Rat Brain Tumors

Masamitsu Abe, M.D., D.Sc., Kazuyoshi Amano, M.D., D.Sc.,  
Katsutoshi Kitamura, M.D., D.Sc., Jun Tateishi, M.D., D.Sc.,  
and Hiroshi Hatanaka, M.D., D.Sc.

Departments of Neurosurgery and Neuropathology, Saga Medical  
School, Kyushu University, and Teikyo University, Japan

An ideal therapy for brain tumors would be one whereby all tumor tissue is selectively destroyed without causing damage to the functioning brain. For the boron neutron capture treatment to be "ideal", it must meet the minimum requirement that boron-10 be distributed within a tumor and only in the tumor. The distribution of  $\text{Na}_2^{10}\text{B}_{12}\text{H}_{11}\text{SH}$  that has been used for human brain tumor treatment was established in transplanted brain tumors by tritium-labeled autoradiography by Hatanaka, or by neutron-induced alpha-autoradiography by Matsuoka and others or by Amano. But boron-10 distribution in non-transplanted brain tumors had not yet been studied. The difference between transplanted tumor and non-transplanted tumor is quite significant with respect to the difference in susceptibility to boron penetration. I will report on boron-10 distribution in primary brain tumors of rats induced by ethylnitrosourea (ENU) as well as in transplanted rat brain tumors, and discuss the mechanism of the boron-10 accumulation in the tumor.

Two types of brain tumors were used for this experiment. One is a transplanted tumor which developed after intracerebral implantation of rat glioma cells of clone 6 strain, induced originally with N-nitrosomethylurea, and the other is a carcinogen-induced brain tumor which developed directly after transplacental injection of ethylnitrosourea. The term transplacental means that the mother of these rats had been injected with the carcinogen while the mother was still carrying them as fetuses in her uterus. The latter type of tumor may be regarded as mimicking spontaneously arising brain tumors, different from commonly used transplanted tumors.

Sodium mercaptoundecahydrododecaborate at 50 or 100  $\mu\text{g}$  boron-10/g body weight was injected intravenously into these tumor-bearing rats, and they were sacrificed at various time intervals between 1 and 48 hours. Frozen sections of the rat brains were mounted on cellulose nitrate film, and neutron-induced alpha-autoradiography, as described by Matsuoka and then by Amano, was performed.

Standard sections of known boron-10 concentrations were made, and the numbers of tracks were counted after neutron irradiation. The numbers of tracks were then plotted as a function of boron-10 concentration. The best-fitted curve was applied. Boron-10 concentration of each compartment in a tissue section was calculated from this standard curve.

### Boron-10 distribution in the normal rat brain

In the coronal section of the brain of the control rat to which boron-10 was administered, localized cloudiness of the track-etch picture

corresponds to the choroid plexus and subarachnoid blood vessels, showing some amount of boron-10 accumulated in these tissues.

In an autoradiography picture in which the alpha-tracks are superimposed on the brain slice, many rod-shaped tracks showing boron-10 accumulation are seen in the blood, vessel wall, and meninges. Only a small number of tracks are seen in the brain parenchyma.

Boron-10 concentration in the normal brain parenchyma was only 1  $\mu$ g boron-10/cm<sup>3</sup> or less. A slightly higher concentration was seen in the area postrema and infundibulum, which are the special regions devoid of the normal blood-brain barrier. Except for these regions, no areas of high concentration were found in the normal brain parenchyma.

#### Boron-10 distribution in the transplanted rat brain tumors

In sections, with etched alpha-tracks, of transplanted brain tumor 24 hours after injection, cloudiness indicating concentration of boron-10 is seen in the tumor. Inside the tumor, more boron-10 is found in the central necrotic focus; outside of the necrosis more boron-10 is found in the viable tumor tissue of the perimeter of the tumor than in the center.

This is one of the features of boron-10 distribution in transplanted brain tumors.

In a very large transplanted tumor with marked brain edema, boron-10 accumulated in the edematous brain as well as in the tumor. When the brain is in a state of edema such as this, boron-10 may reach brain tissue that surrounds the tumor.

#### Boron-10 distribution in the ENU-induced rat brain tumors

Incidence and classification of the ENU-induced tumors of the nervous system were tabulated. Several histologically distinguishable types of tumor developed and they varied in size. Multiple tumors in the same brain were not infrequent. Oligodendrogiomas, pleomorphic gliomas, and anaplastic gliomas frequently developed in the cerebral hemispheres, and they were used for this experiment.

In the section, with etched alpha-tracks, of ethylnitrosourea-induced brain tumors 12 hours after injection, there are four tumors seen in the brain. High concentration of boron-10 is noted in the large tumor, whereas its concentration in the small tumors is relatively low.

In sections, with etched alpha tracks, of ENU-induced brain tumors, one and a half hours after injection, and 18 hours after injection, a high concentration of boron-10 is noted in the large tumors, whereas its concentration in the small tumors is low. Boron-10 distribution in the former section is considerably localized in the tumor, whereas the distribution in the latter section extends outside the tumor.

A tabulation of tumor size, tumor histology, and boron-10 concentration in ENU-induced brain tumors and brain at different time intervals after injection showed that the boron-10 concentration is much higher in the large glioma than in the small gliomas. The regional difference of concent-

ration within gliomas varied from tumor to tumor. Concentration in the brain distant from the tumors was very low.

The factors affecting the boron-10 concentration in the gliomas

In the histological study of the gliomas, small gliomas induced by ENU were usually poorly vascularized similar to the vasculature of a low malignancy glioma.

Large gliomas had capillaries of markedly proliferated endothelial cells with formation of tufts resembling renal glomeruli, and sinusoidal capillaries, similar to those which are occasionally found in human malignant gliomas.

The vascular permeability of gliomas to Evans-blue and horseradish peroxidase (HRP)

Evans-blue, one of the typical protein-bound dyes, was administered intravenously to the tumor-bearing rats, and they were sacrificed at 24 or 48 hours after injection. Horseradish peroxidase was administered intravenously, and the rats were killed by perfusion fixation at 15 or 30 minutes after injection.

Coronal sections of the rat brain with ENU-induced tumors showed two gliomas. The large glioma stained strongly with Evans-blue, which permeated through the vessels, whereas the small glioma stained only faintly

And when horseradish peroxidase is administered intravenously, almost the entire contour of the large glioma with a large cyst is stained with reaction product, whereas the small glioma on the right side is not clearly stained.

In the histochemical study, penetration of horseradish peroxidase was marked around such abnormal vessels as glomeruloid vessels and sinusoidal vessels in the large gliomas, and it was negative in the small gliomas.

The results of the study on the vascular permeability to HRP in several rats with ENU-induced gliomas were tabulated. Degree of permeability varied considerably depending on the size and histological type of the tumors. As a rule, the permeability to HRP is marked in large gliomas and not clear in small gliomas.

These findings show that the distribution of intravenously injected boron-10 in gliomas is almost proportional to the vascularity and to the vascular permeability of the gliomas, as measured by Evans-blue or HRP.

In the microscopic picture of the tumor cells in the ENU-induced large glioma, with alpha-track etch, numerous tracks are seen in relation to the actual tumor cells.

Listing of the mean boron concentrations in the transplanted brain tumors and ENU-induced large gliomas after intravenous injection of  $10\mu\text{g}^{10}\text{B/g}$  showed that concentration gradually decreased with time and reached  $20\mu\text{g}^{10}\text{B/cm}^3$  at 10 hours after injection in the case of the transplanted tumors and 17 hours

after injection in the case of the ENU-induced large gliomas.

The tumor-to-blood ratio of boron-10 concentration increased with time after injection and reached unity at 12 hours after injection in the transplanted tumors and 7 hours after injection in the ENU-induced large gliomas. The tumor concentration at that time was  $18\mu\text{g}$  boron-10/ $\text{cm}^3$  in transplanted tumors and  $30\mu\text{g}$  boron-10/ $\text{cm}^3$  in ENU-induced large gliomas. The data presented so far suggest the following: uneven distribution of vasculature and uneven permeability in a tumor are likely to cause the uneven distribution of boron-10 in the tumor. Boron-10 concentration will be low if a low malignancy glioma exhibits poor vasculature. And where the brain is edematous around a tumor, the edematous brain tissue may be penetrated by boron-10 to some extent. In general, a high T/N ratio and high T/B ratio may well warrant an appreciable specific treatment of a brain tumor.

As far as the T/B ratio is concerned, this ratio has a secondary importance in comparison to the T/N ratio, because the radiation absorbed by the vascular wall is not really all of the radiation emitted within the vascular lumen, as Kitao had calculated. The absorbed dose by the capillary wall is said to be only one-third. Therefore, the T/B ratio does not have to be above unity. Clinical experience as reported by Hatanaka also supports this.

The alpha-autoradiographical results reported here on ethylnitrosourea-induced rat brain tumors which mimic spontaneously arising brain tumors are based on rodents which should have great species differences from human, and hence interpretation requires extreme care. Particularly, the results from the permeability experiment using Evans-blue or horseradish peroxidase were obtained by using protein-bound dye or protein itself; therefore, the results may well be different from human clinical practice where the boron compound is intraarterially infused. The intraarterial infusion probably enables the penetration of a large amount of boron compound into tumors in a protein-free form. The delicate maneuvering of the artery will alter a great deal the degree of blood vessel permeability. Unfortunately, animal studies up to the present cannot fully clarify these delicate differences.

We would like to conclude that this boron compound can penetrate rat brain tumors which mimic spontaneously arising brain tumors in the same way it penetrates transplanted brain tumors.

## Neutron-Induced Autoradiography of Human Brain Tumors

Kazuyoshi Amano, M.D., D.Sc.  
Teikyo University, Tokyo, Japan

The effectiveness of radiation in neutron capture therapy against tumors is quite different from that of other types of radiotherapy since neutron capture therapy is a concentration of micro-radiation in an extremely limited volume. If boron atoms are located outside the range of tumor cells, damage to tumor cells cannot be expected even with a favorable concentration of boron in the tumor tissue. On the other hand, a sufficient amount of boron in the tumor cells would lead to a favorable result regardless of the gross concentration in the tumor. Obviously, cytoidal effect depends largely on the location of boron atoms in relation to tumor cells.

Intratumoral localization of boron was studied by autoradiography to see whether the  $(n,\alpha)$  reaction took place effectively in brain tumor patients who had been actually treated by neutron capture therapy. Neutron-induced autoradiography is more conducive to localization of B-10 atoms than tritium labelling. In addition, direct observation of the passage in the tumor tissue of alpha particles released by the  $(n,\alpha)$  reaction confirms the actual deposition of energy in the tumor tissue. The superimposition technique that the author has developed made it possible to observe alpha particles (tracks) over the histological image (1,2).

### Materials and Methods

The brain tumor patient usually first undergoes craniotomy and partial removal of the tumor. In the meantime pathological diagnosis is confirmed. A week or two later, the nuclear reactor treatment is carried out. On the night before neutrnr irradiation, an isotonic solution of the boron compound, sodium mercaptoundecahydrododecaborate ( $\text{Na}_2\text{B}_{12}\text{H}_{11}\text{SH}$ ) is prepared and, after dilution with an equal volume of physiological saline, it is infused into the carotid or vertebral artery, depending on the location of the tumor. Usually about 50 mg B/kg body weight is administered. Then the patient is taken to the reactor on the following morning. The head is re-opened to avoid neutron exposure of the scalp. At this moment, the tumor specimens are obtained for autoradiographical study and immediately frozen in dry ice and acetone or iso-pentane and liquid nitrogen. The frozen specimen undergoes freeze-drying. It is embedded in epoxy resin and sliced into 3- $\mu\text{m}$ -thick sections by an ultramicrotome. The sections are mounted on the cellulose nitrate films without use of any liquid. They are taken to the reactor and exposed to thermal neutrons. After cooling, the samples are brought back to the laboratory and then the superimposition technique is applied to them.

The tissue sections are stained with toluidine blue. The plastic film is firmly fixed on the stage of a microscope (Nikon AFB). A photomicrograph of the histological image of the section is taken with the camera attached to the microscope. Then a drop of sodium hydroxide solution is applied to the section with a pipette. As the sodium hydroxide permeates the histological

section, it is discolored and damaged due to high alkalinity. The section is wiped off to obtain better sodium hydroxide permeation. Only etched pits become visible, and they are photographed again without advancing the film, resulting in a single photograph of double exposure. The result is the picture of the tracks precisely superimposed on the previous histological image, permitting one to exactly determine the relation of the alpha tracks to the tissue structures. Once the film or the glass slide is placed on a microscopic stage, it is not moved during the remaining procedures. Although **the result is slightly lacking in** good contrast owing to double exposure, there is little difficulty in histological identification.

Autoradiographical studies were carried out on three brain tumor patients who had been treated by neutron capture therapy.

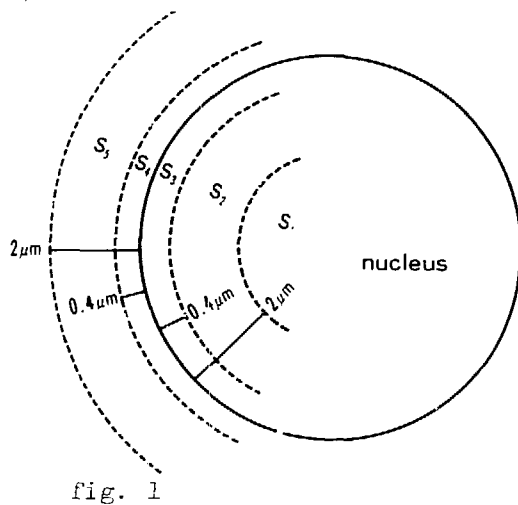
#### Results and Discussion

Case 1: 11 year-old girl. Fibrillary astrocytoma with abundant microcysts. 45.9 mg B/kg was administered 12 hours prior to tumor excision. Autoradiographs revealed the tracks in the cells. The tracks were scarcely seen in the microcysts. Eosinophilic hyaline granules also contained a comparable number of the tracks.

Case 2: 52 year-old female. Glioblastoma. 79.4 mg B/kg was given 15 hours prior to tumor excision via both right and left carotid arteries, as the tumor had occupied the bifrontal lobes through the corpus callosum. A great number of the tracks were found within the cells and appeared to be accumulated around and in the nuclei adjacent to the nuclear membrane.

Case 3: 42 year-old female. Anaplastic astrocytoma. 15 hours after administration of 60.7 mg B/kg. Most of the tracks were associated with the nuclei, situated in the perinuclear space with few tracks in the extracellular space.

In qualitative study, it was impressive that most of the tracks were associated with the nuclear membrane area. Hence, the distribution of these tracks in a tumor tissue was counted for numerical consideration. A tumor cell and its surrounding tissue was divided into five concentric circles (fig. 1).



- S<sub>1</sub>: The central core of the nucleus which is more than 2  $\mu$ m deep inside of the nuclear membrane of the tumor cell.
- S<sub>2</sub>: Between 2  $\mu$ m and 0.4  $\mu$ m deep inside the nuclear membrane.
- S<sub>3</sub>: Between the nuclear membrane itself and 0.4  $\mu$ m inside.
- S<sub>4</sub>: Between the nuclear membrane and 0.4  $\mu$ m outside of the membrane.
- S<sub>5</sub>: Between 0.4  $\mu$ m and 2  $\mu$ m outside of the nuclear membrane.

Beyond 2  $\mu\text{m}$  outside of the membrane there were few tracks. The tracks in these five sections were counted for a case of glioblastoma (table 1).  $S_3$  and  $S_4$  sections contained the largest number of tracks in the tumor cell (72.6 %).

Table 1. (fluence:  $1.4 \times 10^{13}$  nvt)

	intranuclear			extranuclear		
	$S_1$	$S_2$	$S_3$	$S_4$	$S_5$	total
tracks n = 50	16	42	132	160	52	402
%	4.0	10.4	32.8	39.8	12.9	
mean/cell	0.32	0.84	2.64	3.20	1.04	8.04
SD	$\pm 0.99$	$\pm 0.90$	$\pm 1.87$	$\pm 1.80$	$\pm 1.15$	$\pm 3.90$

The diameters of the tumor cell nuclei were measured on enlarged photographs, and the average diameter turned out to be 6.8  $\mu\text{m}$ . The density of the tracks in  $S_3 + S_4$  sections was obtained. The track density in  $S_3 + S_4$  was  $0.34/\mu\text{m}^2$  while the track density in the entire photograph was  $0.06/\mu\text{m}^2$ . The ratio was 5.7. This means that  $\text{In-10}$  concentration around the nuclear membrane was 5.7 times as high as the total tumor tissue.

Table 2 was obtained from the same glioblastoma case but from a different part of the tumor. Perinuclear sections  $S_3$  and  $S_4$  contained 75 % of all tracks. The track density in  $S_3 + S_4$  was  $0.035/\mu\text{m}^2$  and the track density in the entire photograph was  $0.007/\mu\text{m}^2$ . The track density in  $S_3$  and  $S_4$  was 5.0 times higher than the density in the whole tumor tissue.

Table 2. (fluence:  $1.8 \times 10^{12}$  nvt)

	intranuclear			extranuclear		
	$S_1$	$S_2$	$S_3$	$S_4$	$S_5$	total
tracks n = 34	1	3	11	16	5	36
%	2.8	8.3	30.6	44.4	13.9	
mean/cell	0.03	0.09	0.32	0.47	0.15	1.06
SD	$\pm 0.17$	$\pm 0.28$	$\pm 0.63$	$\pm 0.61$	$\pm 0.43$	$\pm 0.95$

Table 3 was obtained from a 42-year-old anaplastic astrocytoma case. The perinuclear  $S_3$  and  $S_4$  sections contained 78 % of all tracks, and the track density in  $S_3 + S_4$  ( $0.298/\mu\text{m}^2$ ) was 4.3 times higher than for the entire tumor tissue ( $0.069/\mu\text{m}^2$ ).

Table 3. (fluence:  $1.4 \times 10^{13}$  nvt)

	intranuclear			extranuclear		
	$S_1$	$S_2$	$S_3$	$S_4$	$S_5$	total
tracks n = 116	14	83	207	279	39	622
%	2.3	13.3	33.3	44.9	6.3	
mean/cell SD	0.13 ±0.40	0.72 ±0.87	1.78 ±1.42	2.44 ±1.50	0.34 ±0.63	5.36 ±2.43

Another slice of the tumor yielded slightly different values, and yet  $S_3$  and  $S_4$  contained 77.5 % of all tracks. The track density here in  $S_3 + S_4$  was 4.5 times higher than for the entire tumor slice (table 4).

Table 4. (fluence:  $7.9 \times 10^{12}$  nvt)

	intranuclear			extranuclear		
	$S_1$	$S_2$	$S_3$	$S_4$	$S_5$	total
tracks n = 100	9	33	132	117	30	321
%	2.8	10.3	41.1	36.4	9.3	
mean/cell SD	0.09 ±0.28	0.33 ±0.53	1.32 ±1.09	1.17 ±0.90	0.30 ±0.64	3.21 ±1.46

Although the number of cases is still very limited, the glioblastoma case showed a higher ratio of perinuclear track density than the astrocytoma case. A histological feature of glioblastoma, namely, its wider extracellular space than in the highly cellular astrocytoma, seems to have contributed to the higher ratio of perinuclear track counts to the track counts for the entire tumor tissue though it is premature to draw any conclusion.

An attempt was made to calculate B-10 concentration from the number of tracks obtained from 3- $\mu\text{m}$ -thick gelatin sections which contained a known amount of B-10 and which were irradiated with a known fluence of neutrons. After delivery of  $10^{12}$  neutrons nvt onto the 3- $\mu\text{m}$  gelatin sections, an average of 0.0022 tracks/ $\mu\text{m}^2$  with 10  $\mu\text{g/g}$  B-10 concentration was obtained (table 5).

Table 5. Track counts on 3- $\mu\text{m}$  thick gelatin sections ( $1 \times 10^{12}$  nvt)

B-10 concentration ( $\mu\text{g/g}$ )	number of tracks ( $\times 10^{-3}/\mu\text{m}^2$ )
10	2.22
20	4.42
30	6.92
60	12.84
80	17.28
100	22.01
10	average 2.20

By applying this calibration method, the calculated concentration for an entire tissue specimen of a fibrillary astrocytoma was 20.6  $\mu\text{g}$  B-10/g of tumor, 16.3 for a glioblastoma (at perinuclear zone 77  $\mu\text{g}$  B-10/g), and 23.9 for an anaplastic astrocytoma.

It was observed that the track count in or outside the nuclear membrane was at least 4 times as high as for the entire tumor tissue. This track counting method may well be applied to calculate the radiation dose and to determine the neutron exposure time for the therapy. As for the exact location of B-10 at the subcellular level, the tentative result is still insufficient. The information so far obtained, however, is enough to say that these tumor cell nuclei are being hit efficiently by these alpha particles in the course of the present regimen of boron neutron capture therapy.

#### References

- (1) K.Amano and W.H.Sweet, Nippon Acta Radiol. 33,267-272,1973
- (2) K.Amano, No To Shinkei 33,693-701,1981

IMPROVED METHODS OF NEUTRON-INDUCED  
TRACK ETCH AUTORADIOGRAPHY

John E. Kirsch and Gordon L. Brownell  
Massachusetts Institute of Technology, Cambridge, MA 02139

ABSTRACT

Knowledge of cellular  $^{10}\text{B}$  localization is necessary in order to assess the effectiveness of a compound for Neutron Capture Therapy. A high resolution neutron-induced track etch autoradiographic technique has been developed for this purpose and is described. Use of thin non-photographic polycarbonate films and an impermeable membrane between tissue sample and detector yields  $^{10}\text{B}$  cellular autoradiograms with low background, good cell morphology and staining, and clarity while maintaining tissue and detector contact throughout processing. Electron microscopic study of the three-dimensionality of the etched tracks for their use in subcellular autoradiography is also discussed.

INTRODUCTION

A definitive criterion for the therapeutic success of Neutron Capture Therapy lies in the development of a compound that has the capabilities of selectively delivering sufficient amounts of  $^{10}\text{B}$  to neoplastic tissue on a cellular basis while delivering negligibly low amounts to normal tissue. Furthermore, it has been quite evident that its cell retention and binding properties play a crucial role in attaining useful tumor-to-blood  $^{10}\text{B}$  ratios that would assure minimal  $^{10}\text{B}$  reaction dose to the normal vasculature upon thermal neutron irradiation [1-3].

Because the alpha particle and  $^{7}\text{Li}$  ion from the  $^{10}\text{B}(\text{n},\alpha)^{7}\text{Li}$  reaction have relatively low energies (1.47 MeV and 0.83 MeV respectively), their ranges in tissue are short and comparable to cellular dimensions. Therefore macroscopic dosimetric assessment must be replaced by a microscopic analysis that includes information of  $^{10}\text{B}$  localization that is also on a microscopic and cellular level. Several analytical and Monte Carlo studies have shown that microscopic differences of even subcellular boron delivery in tumor and healthy cells heavily influence the microdosimetry and subsequent radiobiological response of various cells and cell geometries [4-6]. Therefore, the demand exists for ways of directly localizing the boron at the highest levels of resolution in order to assess a compound for its effective use in neutron capture therapy.

Although they are useful, analytical and conventional autoradiographic methods are limited and must be complemented by a technique that directly localizes the  $^{10}\text{B}$  in the tissue down to cellular and subcellular levels. Analytical methods cannot provide the wealth of spatial information yielded by autoradiography. However, use of radiolabels such as  $^{3}\text{H}$  in conventional autoradiography also requires prior knowledge of the *in vivo* metabolic fate of the compound. Early studies carried out to directly localize  $^{10}\text{B}$  by thermal neutron irradiation and subsequent detection of its reaction products met

with limited success because of high background due to the response of the nuclear or photo-emulsions to competitive ( $n,\gamma$ ) and ( $n,p$ ) reactions [7-10].

In the recent past, nuclear track detection has been introduced as a means of detecting the alpha and lithium reaction ions. By replacing photographic emulsions with a non-photographic solid state organic polymer, such as cellulose nitrate or a polycarbonate, these ions can be detected without detecting lesser ionizing radiations such as thermal neutron reaction gammas, betas, and protons. Whole-body [11-13] and high resolution [14-17] boron localization has been carried out with such detecting mediums. Lithium distributions have also been studied with similar techniques [18-20].

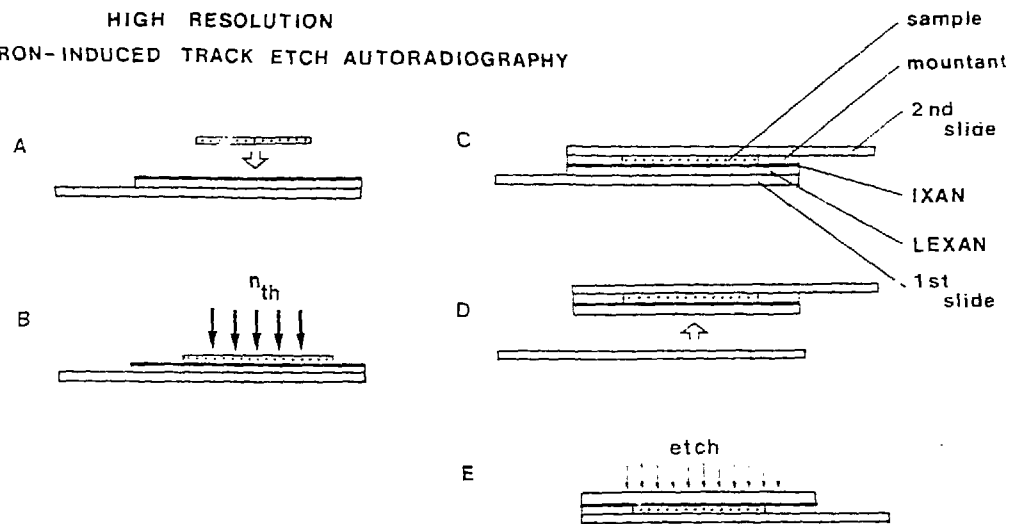
Nuclear track detection in solid state mediums has been used in numerous fields of research [21][22]. When a heavy charged particle traverses a dielectric medium, it deposits sufficient energy which alters the molecular structure of the solid usually manifested as chain breaks in polymers. Chemical resistivity in these damage trails is decreased, and when the surface is etched with an appropriate solution, a microscopic track or three-dimensional pit is formed at the weakened region. Coupling this method of detection with its application in boron or lithium localization is known as neutron-induced track etch autoradiography (NITEA).

A high resolution light microscopic method of NITEA has been developed for direct boron localization that allows the preservation of tissue and stain without separation of tissue and detector throughout processing and is presented here. Furthermore, preliminary work has been carried out on the electron microscopic level to assess the feasibility of utilizing the three-dimensional etched track profiles for electron microscopic subcellular autoradiography.

#### METHODS

The autoradiographic procedure for this NITEA technique is shown schematically in Figure 1.

FIGURE 1 -  
HIGH RESOLUTION  
NEUTRON-INDUCED TRACK ETCH AUTORADIOGRAPHY



The basic principle involves the use of extremely thin detector films. Upon thermal neutron irradiation, the reaction products have sufficient energy to traverse completely through the detector so that it can be etched from the outside. Inevitably, such thin films upon etching will produce holes at the site of the tracks. In order to prevent passage of caustic chemical etchant solutions through the etched holes to the tissue, an impermeable membrane is interposed between the tissue and detector. Therefore, high resolution is maintained, tissue morphology and stain is preserved, and tissue and detector remain intact for permanent documentation.

The solid state detector medium used is Lexan (tradename of General Electric Co., Pittsburgh, PA) bisphenol-A polycarbonate ( $C_{16}H_{14}O_3$ ) that is primarily insensitive to radiations less ionizing than low energy alpha particles. In order to produce uniform films of Lexan on the order of less than one micron in thickness, the polycarbonate is initially dissolved in dichloromethane ( $CH_2Cl_2$ ) at about 2% by weight. Complete dissolution occurs in about 12 hr. Clean microscope slides are coated with Lexan by drawing through the solution at a constant and slow rate according to the method described elsewhere [16]. Film thicknesses are measured initially by ellipsometry to obtain a standardization after which interference colors are used for rapid determination. These detector films are reproducible and uniform to within 10% variability provided the thickness is less than one micron. Desired thicknesses are controlled by both slide withdrawal rates and Lexan solution concentration.

Films of this extreme thinness will most assuredly produce holes from particle tracks that are etched and require an impermeable membrane to prevent passage of the etching solution to the tissue. IXAN-SGA (tradename of Solvay and Cie, Brussels, Belgium), a vinylidene chloride/vinyl chloride copolymer, is resistant to nearly all alkaline solutions (KOH and NaOH are commonly used etchants for polymers) and can be easily cast into films of thicknesses on the order of several thousand angstroms.

The recipe for preparing an IXAN solution is based on that of Keyser and Wijffels [23] originally described by Sawicki and Dazynkiewicz [24]. 9.7 gms of IXAN resin are slowly dissolved in 30 gms of butyl acetate. Once complete, which may take 24 hours, 57.9 gms of trichloroethylene are added. 0.8 gm of cyclohexanone and 1.6 gms of dibutyl phthalate are introduced as plasticizers and can be varied depending on the specific needs.

The impermeable film is cast according to methods described elsewhere [16] by placing one drop of the solution onto a filtered, degassed, distilled water bath at room temperature. The drop will spread to a maximum area and contract slightly until all of the solvents have evaporated. The Lexan coated microslides are then covered with this membrane and air dried in horizontal position overnight in a dust free environment. IXAN membrane thicknesses are measured first by ellipsometry and then by interference colors and are individually uniform to within 5%. Ellipsometry measurements have shown average thicknesses to be between 1500 and 2500 Å depending on the temperature and solution concentration used when they were cast.

Freeze-dried or conventional histologic tissue sections containing boron are mounted on the prepared slides and irradiated with thermal neutrons, after which the sections are stained (glass microslides are activated by neutron irradiation and normally require an interim prior to staining of several days to decay). If paraffin sections are used, hexane is employed to

remove the paraffin since xylene and other solvents that are normally used destroy the polymer films.

Once completed, the exposed stained tissue is mounted onto a second microslide with a glycerol-gelatin mountant (Sigma Chemical Co., St. Louis, MO), chilled by refrigeration for an hour and separated carefully from the original microslide. The second slide is then reversed and the exposed Lexan layer is etched at room temperature with an appropriate etchant solution. Many types of etchants can be used. However, the optimum was found to be 3 gms KOH dissolved in 9 gms H<sub>2</sub>O with 8 gms of ethanol added as an accelerator. This has been called the PEW etchant [25] and has a measured bulk surface etching rate of 0.52  $\mu$ ms/hr at 23°C for polycarbonates [16].

Etching is carried out for about 75 minutes yielding tracks on the average of 0.5 to 1 micron in diameter, easily visible by light microscopy. With typical thicknesses of the IXAN membrane being about 0.2  $\mu$ ms and the Lexan detector being about 0.8  $\mu$ ms prior to etching, the final combined IXAN and Lexan thickness after etching is about 0.3  $\mu$ ms. Since the depth of field in light microscopy is about 1  $\mu$ m, the tracks overlaying the tissue are simultaneously focused with the tissue morphology thereby eliminating any need for double exposures or overlapping of images.

## RESULTS

No conclusions concerning boron localization will be attempted with the following results due to the fact that the compound studied was water soluble and the tissues examined were not processed by freeze-drying. Results are presented only as a demonstration of the capabilities of this technique.

The tissue samples were obtained from 10-day-old pure bred beagles bearing 9-day-old transplanted tumors grown intracerebrally. The tumor type has been characterized as a sarcoma and was derived originally from the Rous sarcoma virus. The animals were intravenously administered the compound Na<sub>2</sub>B<sub>12</sub>H<sub>11</sub>SH at a dose of 30 mg<sup>10</sup>B/kg body weight and sacrificed by vascular perfusion after one hour. Complete coronal brain sections were formalin fixed, paraffin embedded and microtomed to about 5  $\mu$ ms in thickness, mounted on the Lexan/IXAN membrane-covered slide and prepared for irradiation.

Thermal neutron irradiation was carried out at the MITR-II 5 MWth research reactor at M.I.T. (Cambridge, MA). Two access ports were used. The blanket test facility (BTF) provides an average  $1.2 \times 10^9$  n/cm<sup>2</sup>-s flux with less than 2% variation over a radius at least 30 cms. The medical therapy beam port yields a higher flux of about  $3 \times 10^9$  n/cm<sup>2</sup>-s but remains uniform within 5% variation only over a radius about 4 cms. Flux determinations were accomplished by gold foil activation analysis. Thermal neutron exposure for the autoradiographic samples was typically  $10^{13}$  n/cm<sup>2</sup>.

Results are shown in Figures 2 through 4. In all NITEA micrographs, the average track diameter is 0.5-1.0  $\mu$ ms and the theoretical resolution is 0.6-0.8  $\mu$ ms. Figure 2 shows a typical region of tumor cells with heterogeneous boron uptake represented by the tracks overlaying the cells. Note the clarity and preservation of tissue and stain (Hematoxylin and eosin). The fact that the tissue was fixed and that the NITEA manifests a lack of tracks in extracellular spaces, is highly suggestive of at least partial cellular binding of the boron. Figure 3 is another typical NITEA micrograph of tumor tissue in the region of a blood vessel showing the expected lack of boron in

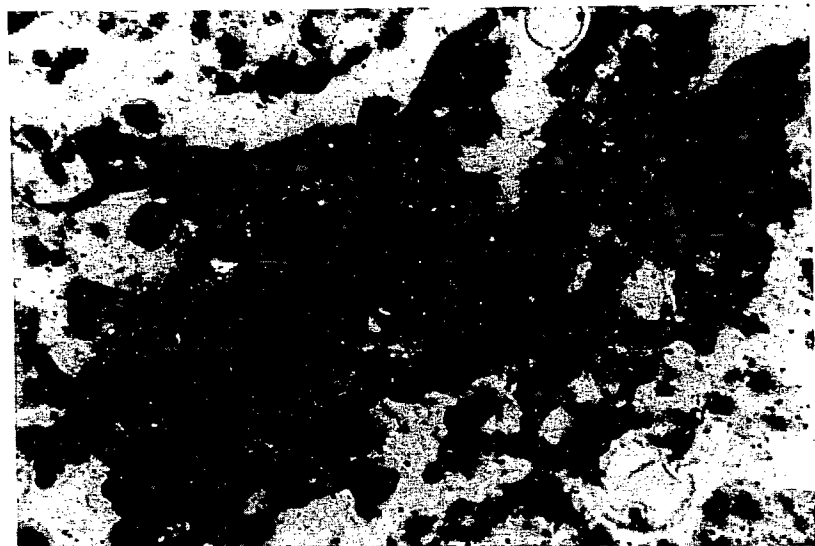


FIGURE 2 - High resolution NITEA micrograph of  $^{10}\text{B}$  localization in tumor cells ( $\sim 1500\text{x}$ ).



FIGURE 3 - High resolution NITEA micrograph of  $^{10}\text{B}$  localization in the region of tumor vasculature ( $\sim 1500\text{x}$ ).

the lumen since the animal was perfused and the blood was eliminated. Again, note the lack of tracks in extracellular spaces. Finally, the scanning electron micrograph shown in Figure 4 depicts the resolution capabilities of this technique. Clusters of tracks are seen around the regions of lighter background that represent individual tumor cells caused by the raised topology of the cells when overlayed by such thin detector films.

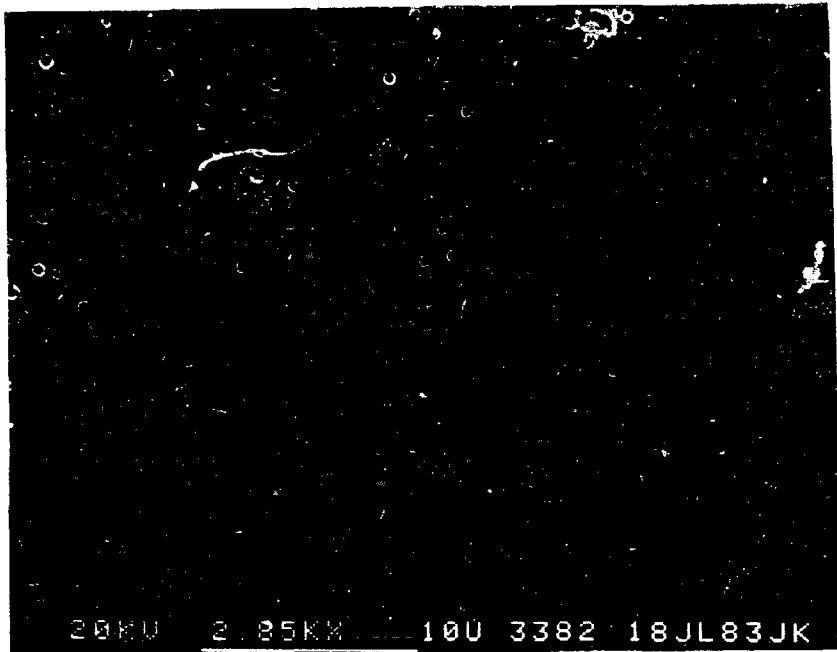


Figure 4 - Scanning electron micrograph of an NITEA of  $^{10}\text{B}$  etched tracks (holes) overlaying individual tumor cells (lighter background) (2850x).

#### ELECTRON MICROSCOPY

Accompanying the recent and rapid development of more complex and tumor-specific mechanisms of boron delivery such as monoclonal antibodies and estrogens is the demand for subcellular autoradiographic techniques. In principle, NITEA can be extended to this level with spatial resolution capabilities comparable to or better than that which is attainable by conventional radioisotopic methods. Unique to track etch methods is the three-dimensional information provided by the etched track [16,26,27]. With light microscopy, these details cannot be resolved and the use of electron microscopy must be introduced. Unlike developed silver grains where the history of the particle that sensitized the crystal is lost, a track retains all the characteristics of the particle that produced it. If this information can be extracted, such as

the angle of emission and energy of the ion, then in principle the origin of the reaction can be determined by geometrically extrapolating back along the path into the tissue where the reaction occurred.

Preliminary electron microscopy studies have been carried out to investigate the possibility of using etched track contours as a means of determining the particle's angle of trajectory and its energy when it entered the detector. Controlled experiments were performed with a well-collimated  $^{244}\text{Cm}$  alpha source. Particle energies were degraded by 3.1 cms of air to simulate the low energies of boron reaction alphas. Lexan polycarbonate sheets were irradiated at various angles of incidence and etched for 12 minutes with the PEW solution at  $60^\circ\text{C}$  (bulk etch rate for these conditions was measured to be  $9.2 \mu\text{ms}/\text{hr}$ ). Tracks were viewed by scanning electron microscopy and the results are shown in Figure 5. Note the change in ellipticity of the track contours. For an angle of  $45^\circ$ , it can be seen that the tracks are different in size owing not to variations in angle but variations in energy of the particle.

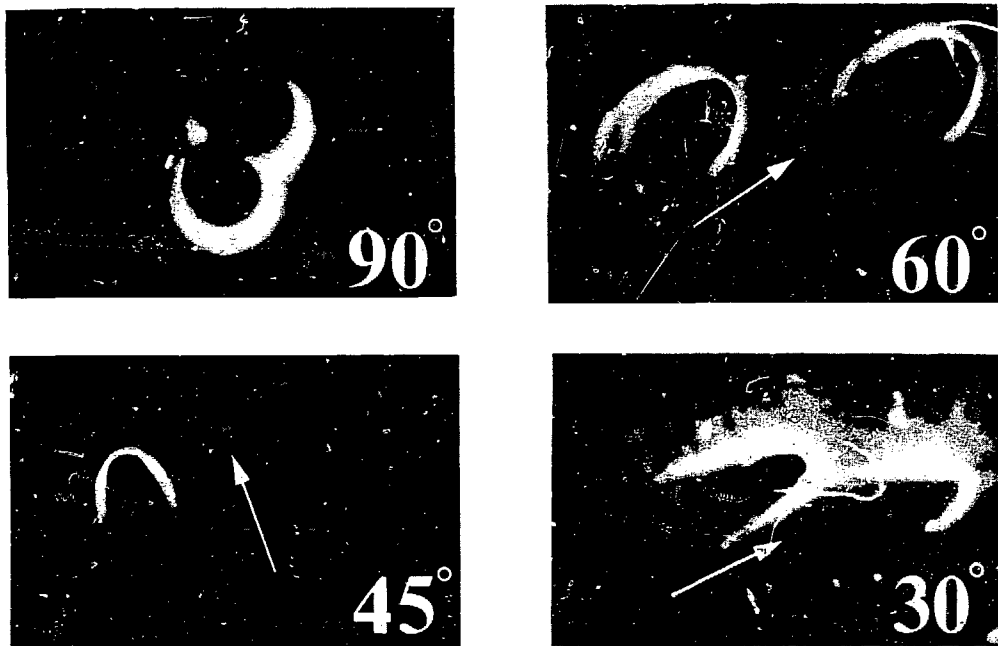


FIGURE 5 - Etched tracks of low energy alpha particles at various angles to the detector. Arrow denotes direction of incidence (12,900x).

It has been shown [16] that energy loss considerations and track etching principles can be coupled to formulate etched track evolution relations that can predict these shapes given the particle's energy and trajectory. A computer code has been implemented that simulates the tracks and an example is shown in Figure 6 that compares the simulated track and the experimental track of approximately the same particle and etching conditions. Note the similarities between the two.

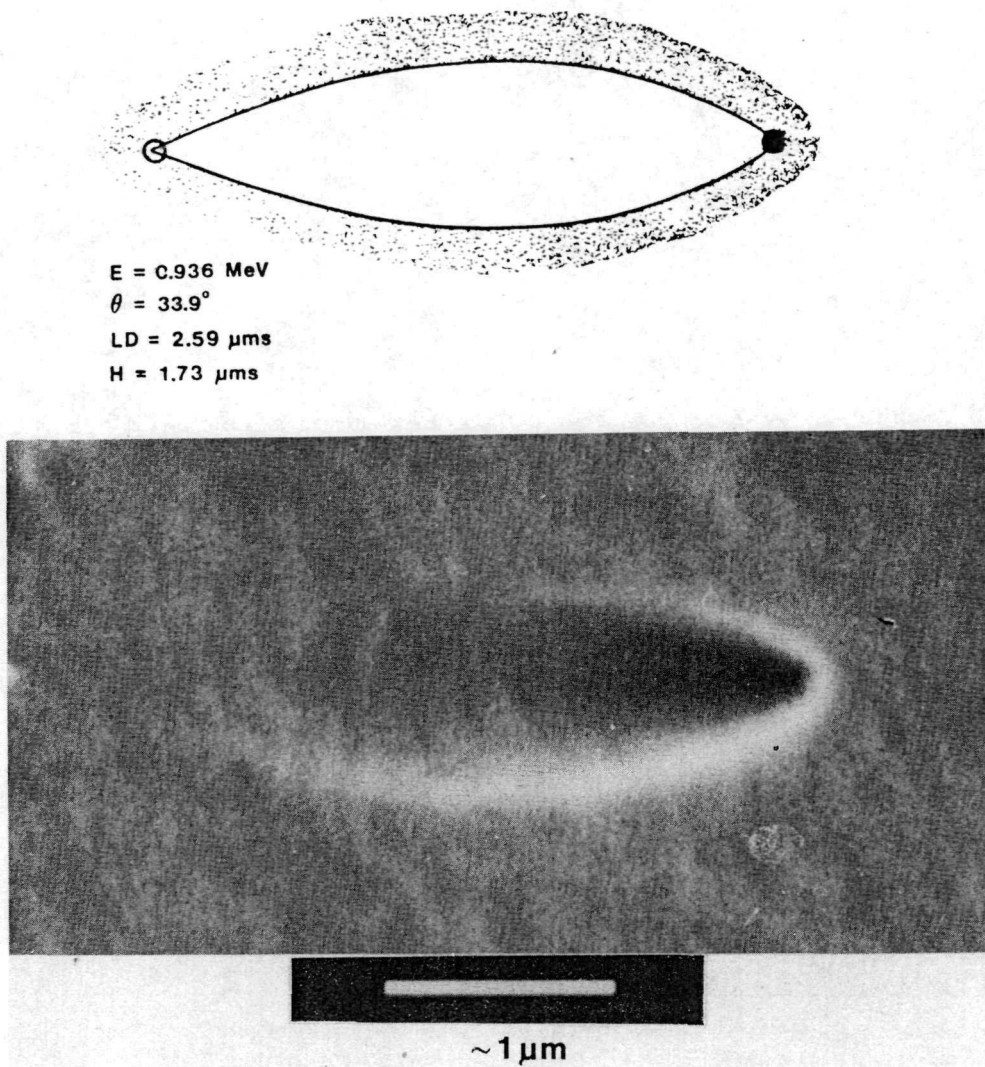


FIGURE 6 - Computer simulated alpha track (upper) and experimental alpha track (lower,  $E < 1 \text{ MeV}$ ,  $\theta = 30-35^\circ$ , total bulk etch length  $H = 1.73 \mu\text{m}$ ).

Conversely, another code is currently being developed to obtain the particle's energy and trajectory given its track shape as the input. If this can be accurately applied, digitized image processing can be employed to reconstruct the autoradiographic image by correcting the angular displacement (LD in Figure 6) of the track thus virtually eliminating geometrical considerations to within the limit of experimental error. Spatial resolution of this method should be well within the bounds of determining subcellular localization.

#### SUMMARY

It has been demonstrated that a thin film NITEA technique can yield high resolution cellular information to determine direct boron localization in cells for the evaluation of possible compounds to be used for neutron capture therapy. Tissue morphology and stain is preserved and documentation accomplished without double exposure of tissue and tracks. Furthermore, it has been shown that with the unique three-dimensionality of the tracks it is possible to extract information about the radiation that can lead to the establishment of its reaction origin within the tissue for its use in electron microscopic subcellular autoradiography. Finally, although this technique was developed for boron localization, its application can easily be adapted to localizing any spontaneous or induced charged particle emitting isotope.

This work was supported in part by NIH grant #CA19665.

#### REFERENCES

1. A.K. Asbury, R.G. Ojemann, S.L. Nielsen, W.H. Sweet, *J. Neuropath. Exp. Neurol.*, 31, pp. 278-303, (1972).
2. H. Hatanaka, W.H. Sweet, in Biomedical Dosimetry, IAEA-SM-193/79, pp.147-178, IAEA, Vienna, (1975).
3. G.L. Brownell, R.G. Zamenhof, B.W. Murray, G.R. Wellum, Chapt.18 in Therapy in Nuclear Medicine, R.P. Spencer (ed.), Grune and Stratton, New York, (1978).
4. K. Kitao, *Radiat. Res.*, 61, pp.304-315, (1975).
5. R.A. Rydin, O.L. Deutsch, B.W. Murray, *Phys. Med. Biol.*, 21, pp.134-138, (1976).
6. T. Kobayashi, K. Kanda, *Radiat. Res.*, 91, pp.77-94, (1982).
7. G. Mayr, H.D. Bruner, M. Brucer, *Nucleonics*, 11, pp.21-, (1953).
8. L.C. Edwards, *Int. J. Appl. Radiat. Isot.*, 1, pp.184-190, (1956).
9. R.G. Fairchild, E.A. Tonna, C.T. Seibold, *Radiat. Res.*, 30, pp.774-787, (1967).

10. R.G. Fairchild, E.A. Tonna, C.T. Seibold, R.F. Straub, *Radiat. Res.*, 36, pp.87-97, (1968).
11. O. Matsuoka, H. Hatanaka, M. Miyamoto, *Acta Pharm. Toxicol.*, 41, suppl. 1, pp.56-57, (1977).
12. M. Ashtari, J. Kirsch, W. Schoene, C. Rumbaugh, G.L. Brownell, in Synthesis and Applications of Isotopically Labeled Compounds, W.P. Duncan and A.B. Susan (eds.), Elsevier Scientific Publ., Amsterdam, (1983).
13. H. Hatanaka, K. Sano, *Z. Neurol.*, 204, pp.304-332, (1973).
14. K. Amano, W.H. Sweet, *Nippon Acta Radiol.*, 33, pp.267-272, (1973).
15. M. Abe, *Fukuoka Acta Medica*, 73, pp.250-271, (1982).
16. J.E. Kirsch, Ph.D. thesis, M.I.T., (1983).
17. J.E. Kirsch, *Med. Phys.*, 10, p.540, (1983).
18. M. Thellier, T. Stelz, J.C. Wissocq, *Biochim. Biophys. Acta*, 437, pp.604-627, (1976).
19. J.C. Wissocq, T. Stelz, C. Heurteaux, *J. Histochem. Cytochem.*, 27, pp.1462-1470, (1979).
20. M. Thellier, C. Heurteaux, J.C. Wissocq, *Brain Res.*, 199, pp.175-196, (1980).
21. R.L. Fleischer, P.B. Price, R.M. Walker, Nuclear Tracks in Solids, Univ. Cal. Press, Berkeley, CA, (1975).
22. H. Francois, N. Kurtz, J.P. Massue, M. Monnin, R. Schmitt, (eds.), Solid State Nuclear Track Detectors, Pergamon Press, N.Y., (1980).
23. A. Keyser, C. Wijffels, *Acta Histochem.*, suppl. 8, pp.359-367, (1968).
24. W. Sawicki, Z. Darzynkiewicz, *Folia Histochem. Cytochem.*, 1, pp.283-288, (1963).
25. G. Somogyi, *Nucl. Track Det.*, 1, pp.3-18, (1977).
26. G. Somogyi, *Nucl. Instr. Meth.*, 173, pp.21-42, (1980).
27. G. Somogyi, S.A. Szalay, *Nucl. Instr. Meth.*, 109, pp.211-222, (1973).

A human high molecular weight-melanoma associated antigen (HMW-MAA)  
defined by monoclonal antibodies: A useful marker to radioimage  
tumor lesions in patients with melanoma.

Soldano Ferrone  
Department of Microbiology and Immunology  
New York Medical College, Valhalla, NY 10595

Patrizio Giacomini and Pier Giorgio Natali  
Regina Elena Cancer Institute, Rome, Italy

Dirk Ruiter  
Universitair Medisch Centrum Leiden, The Netherlands

Gianluigi Burraggi  
National Cancer Institute, Milan, Italy

Lanfranco Callegaro, Umberto Rosa  
Sorin Biomedica, Saluggia, Italy

A variety of human melanoma associated antigens (MAA) have been identified with cell mediated immunity tests and with serological assays. In the latter ones, the sources of antibodies have been sera from patients with melanoma and from animals immunized to MAA and more recently monoclonal antibodies (for review, see 1-3). The high degree of specificity of these reagents has rekindled interest in the application of immunodiagnostic and immunotherapeutic approaches to melanoma.

By utilizing monoclonal antibodies we have characterized three types of membrane bound MAA which have distinct tissue distribution and structural properties (4-6). Among them the high molecular weight-MAA (HMW-MAA) appears to be a useful marker for radioimaging lesions in patients with melanoma and an appropriate target for immunotherapy. In this paper we will describe the properties of the HMW-MAA and we will summarize the results we have obtained in the imaging of melanoma lesions with radiolabelled monoclonal antibodies to the HMW-MAA.

Structural profile of the HMW-MAA

The HMW-MAA consists of two non covalently associated glycopolypeptides: one has an apparent molecular weight of 280 K and the other one has a molecular weight spanning from 300 K to 700 K. The latter heterogeneity appears to reflect different degrees of glycosylation of the polypeptide (7).

Pulse-chase biosynthetic studies of  $^{35}$ S-methionine labelled melanoma cells and analysis of the HMW-MAA synthesized by melanoma cells in presence of tunicamycin indicate a precursor/product biosynthetic relationship between the 280 K molecular weight component and the larger molecular weight component. This possibility is also supported by the

similarity of peptides generated from the two components of the HMW-MAA by digestion with *staphylococcus aureus* V-8 protease (7).

The HMW-MAA is highly susceptible to digestion by proteolytic enzymes: treatment of NP40 extracts of cultured melanoma cells with trypsin, chymotrypsin, pronase or *staphylococcus aureus* V-8 protease results in the generation of fragments with the molecular weight ranging from 70,000 to about 10,000. These fragments maintain their in vitro immunological reactivity (4,7,8).

#### Antigenic profile of the HMW-MAA

By utilizing splenocytes from mice immunized with cultured human melanoma cells we have developed (9) hybridomas producing monoclonal antibodies to the HMW-MAA. Inhibition binding assays with radiolabelled monoclonal antibodies (10) and analysis of the reactivity of fragments generated from the HMW-MAA by proteolysis with monoclonal antibodies (8) have identified 3 distinct and spatially distant antigenic determinants on the HMW-MAA. One is recognized by the monoclonal antibodies (MoAb) 138.13S, 225.28S, 473.54S and 653.40S, a second one is recognized by the MoAb 149.53 and M19.152 and a third one is recognized by the MoAb M23.35S, 730.25T and 763.24T.

The 3 determinants appear to be similar in their immunogenicity in xenogeneic combination, since immunization of mice with human melanoma cells results in the formation of a similar number of hybridomas secreting antibodies to the 3 determinants. Furthermore monoclonal antibodies to the 3 determinants have a similar affinity, i.e. higher than  $1 \times 10^{-9}$  moles/liter $^{-1}$ .

There is no evidence that the 3 determinants are immunogenic in autologous combinations, since antibodies reacting with the HMW-MAA have not been detected in patients with melanoma. However it cannot be excluded that the antibodies are formed but are not detected as they are complexed with the HMW-MAA which is in circulation. The three determinants recognized by our panel of monoclonal antibodies are monomorphic or have a high frequency as they have been detected on almost 90% of lesions removed from patients with melanoma. However the three determinants have a heterogenous distribution on the pool of HMW-MAA molecules synthesized by melanoma cells in long-term culture and expressed by surgically removed lesions (12-14). Whether this heterogeneity reflects the existence of various subpopulations of melanoma cells with different antigenic profile or different rate of synthesis of subpopulations of the HMW-MAA is not known.

The three determinants we have identified on the HMW-MAA appear to be protein in nature (7), since they are expressed on the HMW-MAA synthesized by cultured melanoma cells in presence of tunicamycin, an inhibitor of N-linked glycosylation, and on the HMW-MAA stripped of carbohydrates by treatment with endoglycosidases (8).

#### Tissue distribution of the HMW-MAA

Indirect immunofluorescence and immunoperoxidase staining of frozen sections of surgically removed normal, benign and malignant tissues and analysis with a double determinant immunoassay (DDIA) of NP40 extracts

of tissues have shown that the HMW-MAA has a restricted tissue distribution (11,12,14). It can be detected in melanomas (96 out of 107 lesions tested), nevi (42 out of 46 lesions tested) and skin carcinomas (16 out of 37 lesions tested). The HMW-MAA displays some heterogeneity in its expression among tumor cells within a lesion (Fig. 1), among autologous lesions removed from different sites from a given patient and among lesions removed from different patients (14,15). Representative results are shown in Figure 2, which also presents data about the level of HMW-MAA in various melanoma cell lines. The heterogeneity of the HMW-MAA is lower than that of other MAA we have identified with monoclonal antibodies (15).

The level of the HMW-MAA in surgically removed lesions does not correlate with their primary or metastatic nature, with their melanogenic potential and/or with their histopathological characteristics. On the other hand studies in progress suggest that the percentage of tumor cells stained by anti HMW-MAA and anti HLA monoclonal antibodies in metastatic lesions displays some relationship to the degree of malignancy of melanoma.

The density of each antigenic determinant recognized by the MoAb 149.55, 225.28S and 763.74T on cultured melanoma cells Colo 38 is higher than  $2 \times 10^6$  antigenic sites per cell, as determined by the amount of radiolabelled monoclonal antibody bound by the cultured melanoma cells under saturating conditions (Fig. 3). The incubation of melanoma cells Colo 38 with more than one monoclonal antibody to the HMW-MAA has an additive effect suggesting that the the number of antigen-antibody interactions on melanoma cell membranes *in vivo* may be increased by injecting mixtures of monoclonal antibodies to distinct determinants on the HMW-MAA.

The HMW-MAA is found in sera from patients with melanoma (14). Its level is not different from that in healthy donors and in patients with other types of malignancies. The ranges of the levels of the HMW-MAA in patients with melanoma are broader than in controls. The level of the HMW-MAA does not appear to correlate with the presence and level of circulating immunocomplexes, but tends to correlate with the extent of the disease. Treatment of patients with hyperthermia can change the serum level of the HMW-MAA, but without any characteristic pattern (14).

#### Modulation of the HMW-MAA

The HMW-MAA is not susceptible to antibody mediated modulation, since cultured melanoma cells incubated with varying amounts of monoclonal antibodies to a determinant of the HMW-MAA do not change in their ability to bind monoclonal antibodies to other determinants of the HMW-MAA. Modulation of the HMW-MAA does not occur even when cultured melanoma cells are incubated with monoclonal antibodies to the HMW-MAA and with antimouse Ig antibodies. Furthermore incubation of cultured melanoma cells with monoclonal antibodies to the HMW-MAA does not affect its shedding.

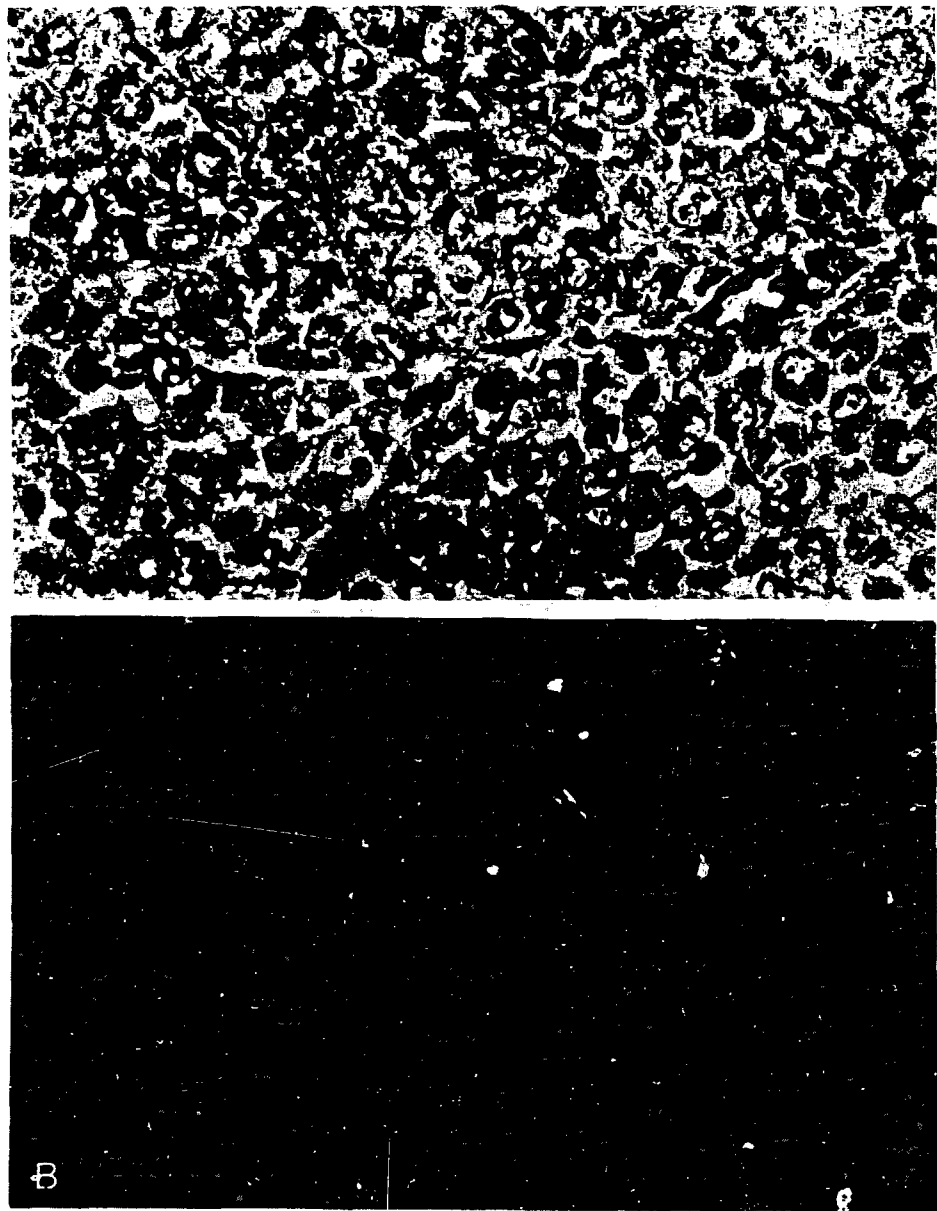


Figure 1. Phase contrast microscopy (panel A) and indirect immunofluorescence staining (panel B) with the anti HMW-MAA MoAb 225.28S of a metastatic melanoma lesion. The staining is heterogeneous in spite of the homogeneous histological features of melanoma cells. (A,B x640).

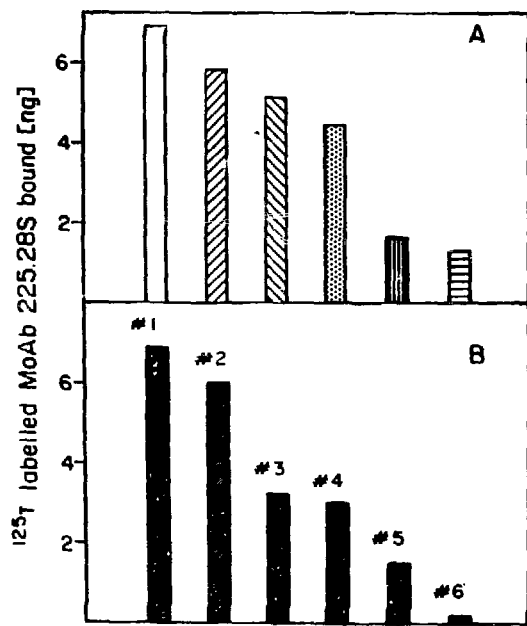


Figure 2. Level of the HMW-MAA in NP40 extracts of melanoma cell lines SKMel-93 (□), Colo 38 (▨), M21 (▨), HO-1 (▨), SKMel-37 (■) and BP-906 (▨) (panel A) and of 6 surgically removed melanoma lesions (panel B). The extracts were tested for their content of HMW-MAA utilizing a double determinant immunoassay performed as described elsewhere (12).

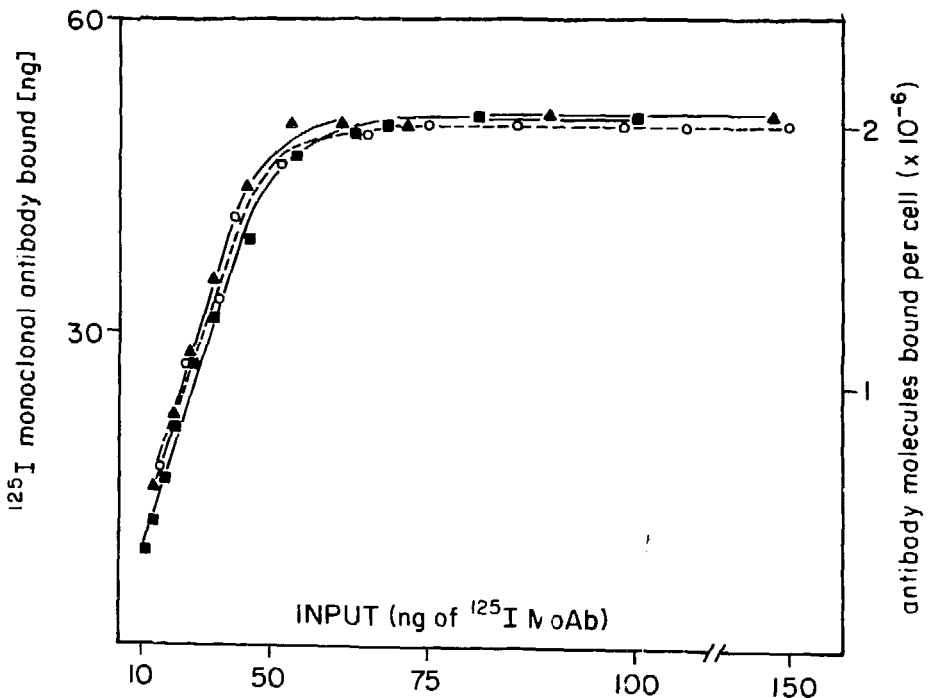


Figure 3. Binding under saturating conditions of  $^{125}\text{I}$  labelled MoAb 149.53 (■), 225.28S (▲) and 763.74T (○) to distinct determinants of the HMW-MAA by cultured melanoma cells Colo 38.

On the other hand components used for treatment of melanoma may modulate the expression and shedding of the HMW-MAA. Among them are interferons. Recombinant DNA  $\gamma$  interferon reduces the expression of the HMW-MAA in a dose related manner, while interferons  $\alpha$  and  $\beta$  do not affect it. The three types of interferon increase the shedding of the HMW-MAA (Fig. 4).

#### Imaging of lesions in patients with melanoma injected with radiolabelled monoclonal antibodies to the HMW-MAA

A total of 22 patients with melanoma have been thus far investigated utilizing the whole MoAb 225.28S or its Fab<sub>2</sub> fragments, which have been radiolabelled with either <sup>131</sup>I, <sup>123</sup>I, <sup>111</sup>In or <sup>99m</sup>Tc. Representative scans are shown in Figure 5 which presents the imaging of metastatic lesions in a foot and in a leg of two patients injected with <sup>99m</sup>Tc and <sup>111</sup>In-labelled Fab<sub>2</sub> fragments of the anti HMW-MAA MoAb 225.28S, respectively. The results obtained thus far are summarized in Table 1. Immunoscintigraphy yielded positive results in 12 of the 22 patients investigated. It is noteworthy that scanning could detect lesions with a diameter of at least 2 cm and that Fab<sub>2</sub> fragments gave significantly less nonspecific accumulation of radioactivity in the reticuloendothelium than the intact MoAb 225.28S.

#### Conclusions

The results we have presented indicate that through the use of monoclonal antibodies we have identified a MAA which appears to meet the criteria to be a useful marker for radioimaging and an appropriate target for immunotherapy. The HMW-MAA has a restricted tissue distribution, has a high density, displays a limited heterogeneity in its expression, and is not susceptible to antibody mediated modulation. Furthermore the monoclonal antibodies to the HMW-MAA we have developed have a high affinity. The positive results we have obtained by radioimaging lesions in patients with melanoma corroborate the *in vitro* findings. The latter studies have shown that even Fab<sub>2</sub> fragments of the anti HMW-MAA monoclonal antibodies do not eliminate completely non specific uptake by liver and spleen although they markedly reduce it. This non specific background may cause side effects when anti HMW-MAA monoclonal antibodies are used as carriers of toxic agents for selective destruction of lesions in patients with melanoma. To overcome this limitation experiments are in progress in collaboration with Drs. D.C. Borg and R.G. Fairchild and their associates at the Brookhaven National Laboratory, Upton, New York, to evaluate the usefulness of boronated anti HMW-MAA monoclonal antibodies to apply neutron capture therapy to melanoma.

#### Acknowledgments

This work was supported by the National Institute of Health grants CA 32609, CA 32634 and CA32920 and by the CNR grant "Controllo della Crescita Neoplastica" No. 830089096 by Progetto Finalizzato "Tecnologie biomediche e sanitarie: IIM-1". P.G. is supported by a fellowship from the Cancer Research Institute, New York. The authors wish to acknowledge the excellent secretarial assistance of Mrs. Edwina L. Jones.

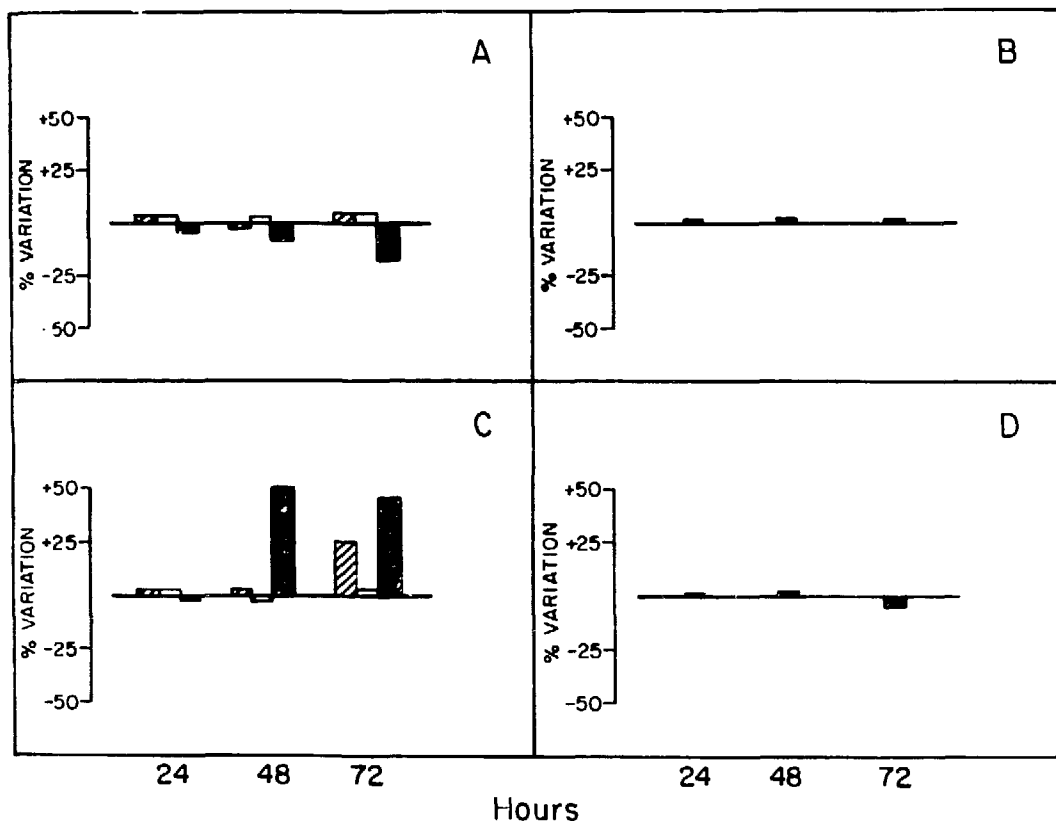
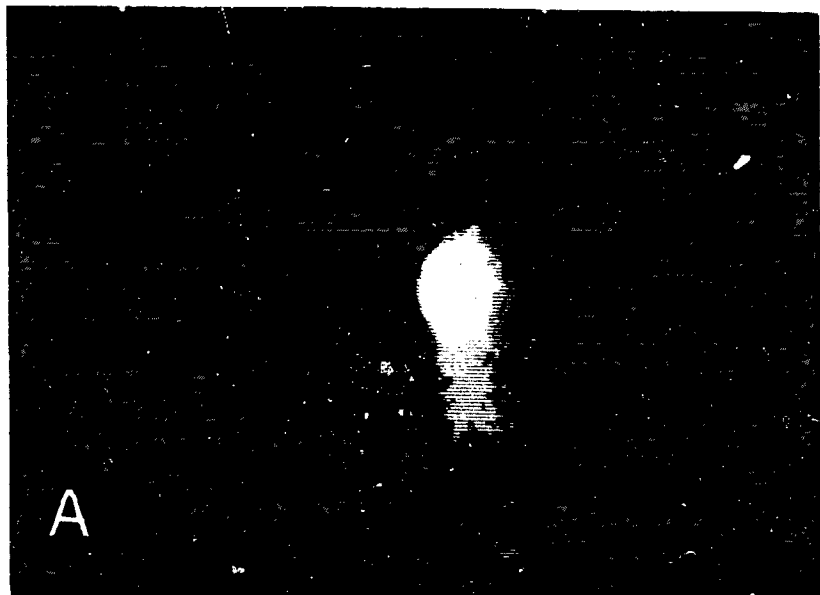


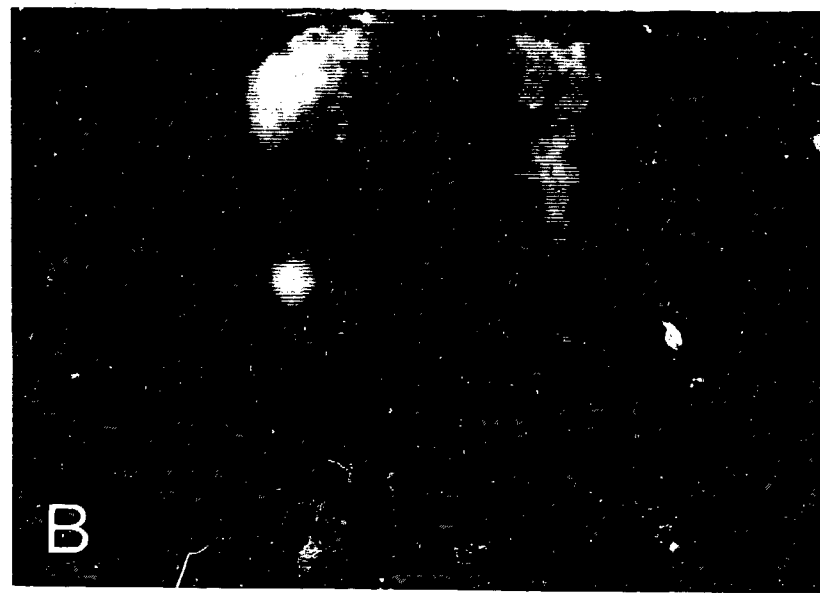
Figure 4. Effect of interferons (panels A and C) and of coating of melanoma cells with monoclonal antibodies (panels B and D) on the expression (panels A and B) and shedding (panels C and D) of the HMW-MAA.

A culture of melanoma cells Colo 38 was added with recombinant DNA  $\alpha$  (▨),  $\beta$  (□) and  $\gamma$  (■) interferons. At the indicated times cells and spent media were harvested and tested for their reactivity with  $^{125}\text{I}$  labelled anti HMW-MAA MoAb 225.28S in a binding assay and for their content of HMW-MAA in a double determinant immunoassay (DDIA) (12), respectively. Results are expressed as percentages of the values obtained with a cell culture incubated without interferon.

Melanoma cells Colo 38 were incubated with the anti HMW-MAA MoAb 225.28S for 2 hours at room temperature. These cells were washed and incubated at  $37^\circ\text{C}$  for up to 72 hours. At the indicated times cells and spent media were harvested and tested for the binding of  $^{125}\text{I}$ -labelled anti HMW-MAA MoAb 149.53, 225.28S and 763.74T and for their content of HMW-MAA in a DDIA, respectively. Results are expressed as percentages of the values obtained with melanoma cells Colo 38 coated with the MoAb 465.12S to an unrelated melanoma associated antigen.



A



B

Figure 5. Imaging of metastatic lesions in two patients with melanoma injected with  $^{99m}\text{Tc}$  (panel A) and  $^{111}\text{In}$  (panel B) labelled  $\text{Fab}_2$  fragments from the anti HMW-MAA MoAb 225.28S.

Table 1. Summary of the immunoscintigraphy studies performed in patients with melanoma with radiolabelled anti HMW-MAA MoAb 225.28S or its  $\text{Fab}_2$  fragments.

Reagent Patient no.	Antibody $\mu\text{g}$	Injected mCi	Specific activity*	Lesion size mCi/mg	Imaging
<u><math>^{131}\text{I}</math>-MoAb</u>					
PM 1	28	1.42	50.7	3.0	+
VB 2	14	0.75	53.6	0.7	-
CP 3	640	0.70	1.1	1.2	-
CM 4**	710	0.80	1.1	1.2	-
<u><math>^{131}\text{I}</math>-<math>\text{Fab}_2</math></u>					
SP 5	30	0.93	31.0	3.0	+
DL 6	20	1.02	51.0	6.0	+
GF 7	22	1.04	47.3	2.0	-
GG 8	18	1.03	57.2	8.0	+
<u><math>^{123}\text{I}</math>-<math>\text{Fab}_2</math></u>					
SR 9	200	2.40	12.0	4.0	+
DV 10	290	4.00	13.8	5.0	-
DG 11	210	3.37	16.0	6.0	+
PG 12	170	2.96	17.4	0.8	-
<u><math>^{99\text{m}}</math>Tc-<math>\text{Fab}_2</math></u>					
BG 13	110	4.48	40.7	5.0	+
PM 14	125	8.00	64.0	5.0	+
SW 15	200	8.00	40.0	6.0	-
VG 16	180	7.76	43.1	4.0	+
VL 17	180	8.50	47.2	2.0	-
<u><math>^{111}\text{In}</math>-<math>\text{Fab}_2</math></u>					
BE 18	32	1.61	50.3	4.0	+
MC 19	37	1.85	50.0	5.0	-
PE 20	40	2.00	50.0	2.0	+
CV 21	32	1.76	55.0	3.0	+
TM 22	38	1.90	50.0	2.0	-

\*At the time of injection

\*\*Histopathological analysis found the lesion to be benign

## References

1. Ferrone, S. and Pellegrino, M.A. In *Handbook of Cancer/Immunology* (H. Waters, ed.) Vol. 3, p. 291, Garland Publishing, New York, 1978.
2. Hellstrom, K.E., Hellstrom, I., Brown, J.P. *Springer Semin. Immunopathol.* 5, 127, 1982.
3. Lloyd, K.O. In *Basic and Clinical Tumor Immunology*, R. Herberman, Ed. Nijhoff, The Hague, The Netherlands 1984, in press.
4. Wilson, B.S., Imai, K., Natali, P.G. and Ferrone, S. *Int. J. Cancer* 28, 293, 1981.
5. Imai, K., Wilson, B.S., Bigotti, A., Natali, P.G. and Ferrone, S. *J. Natl. Cancer Inst.*, 68, /61, 1982.
6. Imai, K., Natali, P.G., Kay, N.E., Wilson, B.S. and Ferrone, S. *Cancer Immunol. Immunother.* 12, 159, 1982.
7. Wilson, B.S., Ruberto, G. & Ferrone, S. *Cancer Immunol. Immunother.* 14, 196, 1983.
8. Gold, A.M., Kantor, R.S., Giacomini, P., Ng, A.-K., Steinbach, G. and Ferrone, S., in press, 1983.
9. Imai, K., Ng., A.K. and Ferrone, S. *J. Natl. Cancer Inst.* 66, 489, 1981.
10. Ng, A.K., Giacomini, P., Kantor, R. and Ferrone, S. *Clin. Chem.* 28, 2347, 1982.
11. Natali, P.G., Imai, K., Wilson, B.S., Bigotti, A., Cavaliere, R., Pellegrino, M.A. and Ferrone, S., *J. Natl. Cancer Inst.* 67, 591, 1981.
12. Giacomini, P., Ng., A.K., Kantor, R.S., Natali, P.G. and Ferrone, S. *Cancer Res.* 43, 3586, 1983.
13. Wilson, B.S., Kay, N.E., Imai, K. and Ferrone, S. *Cancer Immunol. & Immunother.* 13, 69, 1982.
14. Giacomini, P., Veglia, F., Cordiali Fei, P., Rehle, T., Natali, P.G. and Ferrone, S. *Cancer Res.* in press, 1984.
15. Natali, P.G., Cavaliere, R., Bigotti, A., Nicotra, M.R., Russo, C., Ng, A.K., Giacomini, P. and Ferrone, S. *J. Immunol.* 130, 1462, 1983.

## Monoclonal Antibodies for the Localisation of Human Neoplasms in vitro and in vivo

Agamemnon A. Epenetos

Royal Postgraduate Medical School, Hammersmith Hospital, London,  
and The Imperial Cancer Research Fund Laboratories, London, UK.

### Abstract

Combinations of tumour associated monoclonal antibodies were used for the dissection of the phenotypic heterogeneity of neoplasms in an attempt to understand the neoplastic process at cellular level. Furthermore, combinations of tumour associated monoclonal antibodies proved helpful in problems of differential diagnosis in histopathological and cytological tissue samples. Also, immunoperoxidase screening on tissue sections was found to be an important step in the selection of appropriate antibodies for in vivo use.

Antibodies were radioiodinated ( $^{125}\text{I}$  and  $^{123}\text{I}$ ) and given parenterally to immunodeficient animals bearing human epithelial tumours such as colon xeno-grafts. External body scintigraphy showed tumour localisation in all the animals (smallest detectable tumour being 1 mm in diameter).

Based on the encouraging experimental data, clinical studies were commenced to study tumour targeting of  $^{123}\text{I}$  and  $^{131}\text{I}$  labelled monoclonal antibodies in ovarian cancer. The majority of tumour sites were radiolocalised (11 out of 15) and good tumour to non-tumour ratios were obtained (10:1 at 5 days). The absolute amounts of radiolabel targeted in tumour masses, however, were small, i.e. in the region of  $1-8 \times 10^{-3}$  per cent of the injected amount per gram of tissue.

These results indicate that although tumour associated monoclonal antibodies are potentially useful for in vivo diagnosis and therapy of neoplasia, significant improvements are required before these goals can be achieved.

### Introduction

Antibody guided radiolocalisation of tumours is not a new field (1) but this area received a great impetus with the advent of monoclonal antibodies (2). As it is well known, monoclonal antibodies have the advantage of specificity and reproducibility. No truly tumour specific antigens have been detected so far but several antigens have shown relative tumour specificity and appropriate monoclonal antibodies have been raised. A panel of monoclonal antibodies has hereby described which was found useful in the in vitro and in vivo localisation of human neoplasms.

### Methods

#### Monoclonal antibodies

AUAI This antibody is specific for an epithelial proliferating antigen and has a higher reactivity with neoplastic than normal epithelial cells as found (3) by testing in binding assays against cell lines and in sections using immunofluorescent and immunoperoxidase techniques.

HMFG2 This antibody is directed against a differentiation antigen found in delipidated human milk fat globule membranes as well as a wide range of carcinomas, particularly those of breast and ovary (4). They cross react with some normal epithelial structures such as sebaceous glands, sweat glands, exocrine pancreatic ducts and bile ducts.

Hi7E2 This antibody is directed against placental alkaline phosphatase (5). Placental alkaline phosphatase is found in normal term placenta as well as being expressed by some cancers such as testis, breast, ovary, stomach, pancreas. Using an immunoperoxidase technique, this antibody was found to be unreactive with normal tissues (other than term placenta) (5).

#### Immunoperoxidase technique

Fresh-frozen or formalin-fixed and paraffin-embedded sections of tumours and other organs were first dewaxed and then fixed in alcohol. Sections were tested against a panel of antibodies including negative control antibodies and without antibody to assess the non-specific background staining (3).

#### Radiolabelling of antibodies

Pure Iodine-123 (the Atomic Energy Research Establishment, Harwell) was supplied as "dry" sodium iodide. Iodine-125 and Iodine-131 were supplied by Amersham International, UK, in the usual fashion.

Antibodies were labelled with radioiodines using the iodogen technique as previously described (6) to a specific activity of 3-8 mCi/mg. Their immunoreactivity was tested in an Enzyme Linked Immunosorbent Assay (ELISA) system (6) and in a direct radioimmunoassay (RIA), including a competitive assay with unlabelled antibodies. Samples of radiolabelled antibodies were gel-filtered through a Sephadex G150 column (60 cm x 2.5 cm) to check for antibody aggregates. Radiolabelled antibodies were millipore-filtered and diluted in 1% human serum albumin (HSA) prior to patient administration.

#### Autoradiography

The selective localisation of injected antibodies in tumours was demonstrated by autoradiography (ARG). Tissue sections were fixed in alcohol and then ARGs were prepared using Ilford K<sup>5</sup> fluid emulsion. After drying in air, the sections were exposed for 7-30 days at 4°C. The sections were then developed, fixed and stained with haematoxylin for light microscopy.

#### Animals

Twenty nude (nu/nu) mice were tested. The mice were previously injected subcutaneously with 10<sup>6</sup>-10<sup>7</sup> HT29 cells (7).

#### Quantitation

Resected normal and neoplastic tissue sections were washed three times in phosphate buffered saline (PBS), dried and weighed prior to counting. A gamma

counter was used for simultaneous counting for  $^{125}\text{I}$  and  $^{131}\text{I}$ .

#### Patients

Ten women aged 35-82 years were studied. All patients had extensive disease, eight had both primary and metastatic disease and twelve had only metastatic disease at the time of scanning.

#### Scanning

Patients gave written informed consent to enter the study. Thyroid uptake of free and released  $^{123}\text{I}$  or  $^{131}\text{I}$  was blocked by potassium iodide 120 mg/day orally starting 24h before the injection and continuing for a week. Patients' skin was tested for hypersensitivity to mouse immunoglobulins. No reactions were recorded. Patients received 0.2-0.5 mg of antibody labelled with 1.0-2.0 mCi of  $^{123}\text{I}$  or  $^{131}\text{I}$  as an intravenous bolus in 2-3 ml PBS containing 1% HSA. Scans of total body and selected areas were taken from immediately up to 4<sup>th</sup> after injection when  $^{123}\text{I}$  was used and up to 5 days when  $^{131}\text{I}$  was used. Where indicated, patients had single photon emission computed tomography (SPECT).

#### Kinetic studies

Blood and urine samples were taken regularly to calculate the half-life of label in the vascular compartment and their rate of excretion.

#### Results

##### Immunoperoxidase data

The high reactivity of antibodies AUAI, HMFG2 and H17E2 with neoplastic tissues and the low reactivity with normal tissues was established by screening human tissues that were tested either fresh frozen or formalin fixed. An example is seen in Figure 1 where an ovarian cancer (top part of Figure) shows strong staining with HMFG2. Note, however, also weak but definite positive staining with normal ovarian glandular structures (bottom part of Figure). Similar staining was seen with antibody AUAI but antibody H17E2 produced negative reactions when tested against all types of normal tissues except the placenta (5).

##### Animal studies

Antibody AUAI labelled with  $^{123}\text{I}$  or  $^{125}\text{I}$  was used in the animal experiments together with a control antibody (8). Tumour localisation was achieved in all the animals and a typical scan is seen in Figure 2. A mouse with an HT29 tumour on its left leg was scanned at 20 min (view 4), 2h (view 13), 18h (view 50) and 48h (view 49) after an I.V. injection of AUAI labelled with  $^{123}\text{I}$ . As can be seen after 18h the tumour is clearly visible and this is not seen when a negative control antibody is used.

Specific antibody uptake in tumours ranged from 0.5% to 25% of the injected dose (mean 6% per gram of tumour). This level was reached between 4 and

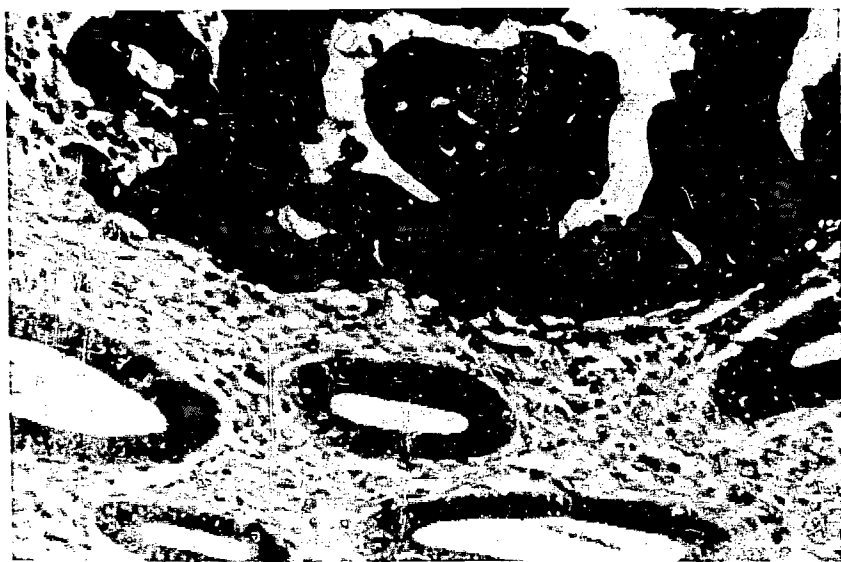


Fig. 1 A tissue section of ovarian cancer stained with antibody HMFG2. Note strongly positive reaction with cancer cells (top part of Fig.) but also weak positive reaction with normal ovarian tissues (bottom part of Fig.).



Fig. 2 Radioscans of a mouse with an I.M. HT29 tumour on its left leg taken at 20 min (view 4), 2h (view 13), 18h (view 50) and 48h (view 49) after injection of specific antibody AUAI labelled with  $^{123}\text{I}$ . Note clearly visible tumour at 18h and 48h.

18h after injection and remained relatively high for a long time, i.e. up to 65 days after injection.

Autoradiography performed on tumour masses (Figure 3) confirmed the presence of antibody and as can be noted dark grains are associated with the stroma of the tumours rather than the tumour cells. This may explain the remarkably long retention of radiolabel in the tumour masses. As will be seen, however, in the later human studies, the distribution of radiolabel is different with different antibodies.

#### Patient studies

Based on the encouraging animal studies, preliminary human studies were commenced and antibodies HMFG2 and H17E2 were studied in ovarian cancer. As can be seen from Figure 4 the majority of sites were detected by antibody guided scanning. The time of radiolocalisation by external scanning ranged from 10 mins to 18h. Successful radiolocalisation was not achieved in the first two patients because of technical difficulties such as poor iodination efficiency. However, in the following eight patients radiolocalisation was positive and in the last four patients it was confirmed by autoradiography of excised tumours (Figure 5).

Unlike antibody AUA1, antibody HMFG2 appeared to predominate in the luminal aspects of adenocarcinomas, which is consistent with previous experience of immunoperoxidase staining of tumours with these antibodies (4).

Figure 6 is a typical scan obtained 18h after injection of antibody HMFG2 labelled with  $^{123}\text{I}$ . As can be seen a large ovarian tumour is imaged (mid field of scan) but it is difficult to interpret uptake in the central part of the abdomen.

In view of the limitations of imaging the upper abdomen with antibody HMFG2, other antibodies were tested and H17E2, against placental alkaline phosphatase, was tried.

Figure 7 shows the early (8 min) 19h and 44h scan of patient after receiving H17E2 labelled with  $^{123}\text{I}$ . At 44h an area of uptake is seen in the left para-aortic region. A CT scan was then performed and this confirmed the presence of an abnormal lymph node 2 cm in diameter in the left para-aortic region (Figure 8).

Whenever possible, resected surgical normal and neoplastic tissues were counted for radioactivity.

Although good tumour to non-tumour ratios were obtained, i.e. approximately 10:1 at 5d after injection, the absolute amounts of radiolabel in tumour were disappointingly small, i.e. in the region of  $5-9 \times 10^{-3}$  per cent of the injected amount per gram of tumour and  $1-4 \times 10^{-4}$  per cent per gram of normal tissue.

#### Discussion

Our data show that successful imaging of tumour masses by external body scintigraphy using radioiodinated antibodies can be achieved. However, this technique needs considerable improvement before it can be widely used as a routine method in the investigations for malignant disease.

The absolute amount of radiolabel reaching the tumours is disappointingly small and this may be due to the instability of the label, i.e. dehalogenation



Fig. 3 ARG of HT29 tumour after administration of specific antibody AUAI labelled with  $^{125}\text{I}$ . Note dark outline of tumour islands at the outer "proliferating" edge of tumour.

$^{123}\text{I}$ - RADIOPRINTIMUNOSCINTIGRAPHY OF OVARIAN CANCER

Patient No.	Site	Result	
		Imaging	Autoradiography of excised tumour
1	Abdomen	-	
3	Chest	-	
	Abdomen	-	
	Lumbar spine	-	
7	Chest	+	
	Abdomen	+	
8	Chest	+	
	Abdomen	+	
11	Abdomen	+	
12	Abdomen	+	
13	Abdomen	+	+
	Pelvis	+	
16	Pelvis	+	+
17	Sacrum	+	+
18	Pelvis	+	+

11/15 sites positive

Fig. 4 Data on antibody guided scanning in the first 10 patients with ovarian cancer.

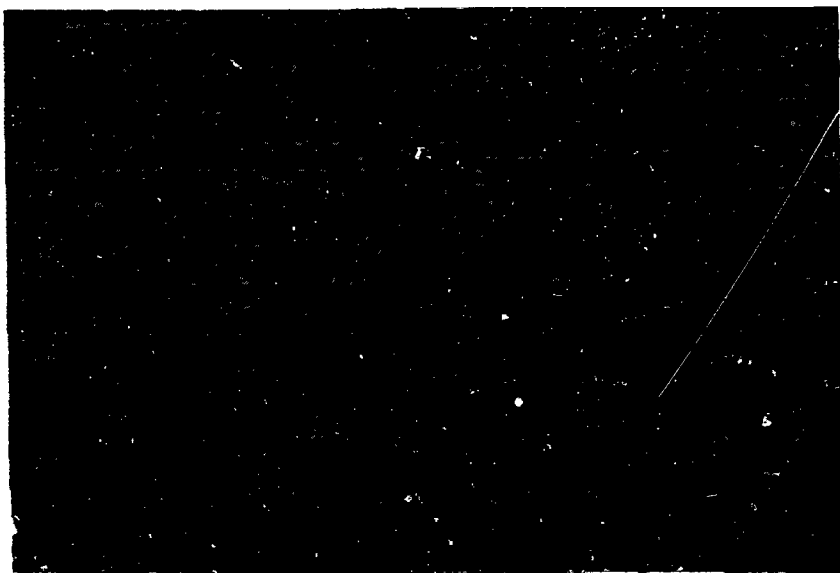


Fig. 5 ARG of an ovarian cancer after administration of specific antibody HMFG2 showing localisation of grains in the lumen of malignant tissues.

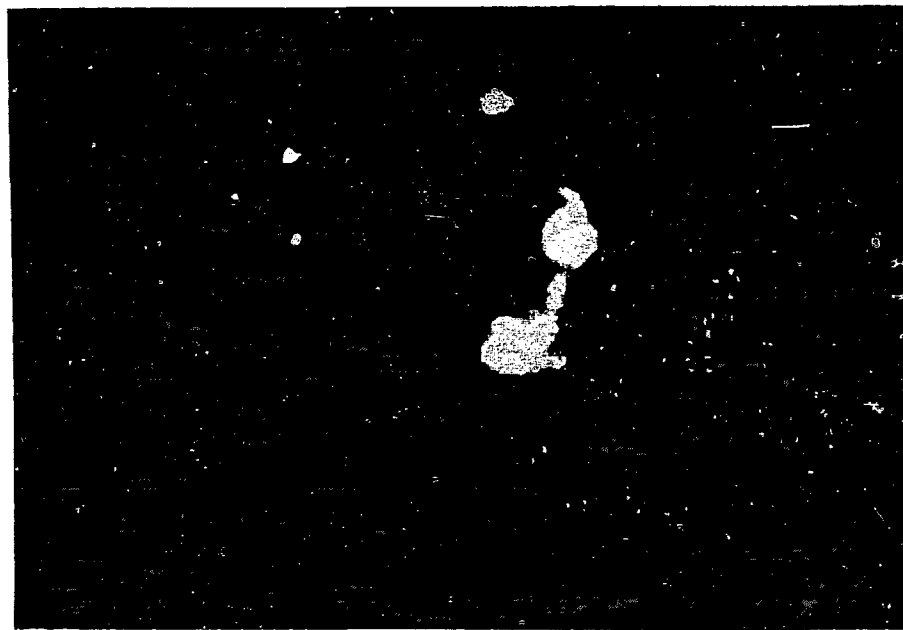


Fig. 6 This shows the antibody guided scan of a patient with ovarian cancer. Note uptake in tumour area (mid field of scan) but also uptake in the upper abdomen.

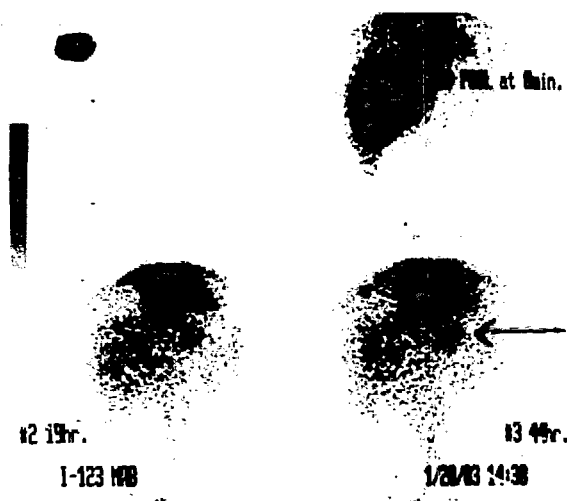


Fig. 7 Antibody scans (9 min, 19h, 44h) of a patient given HI7F2 labelled with  $^{123}\text{I}$ . Arrow shows abnormal spot in left paraaortic region.

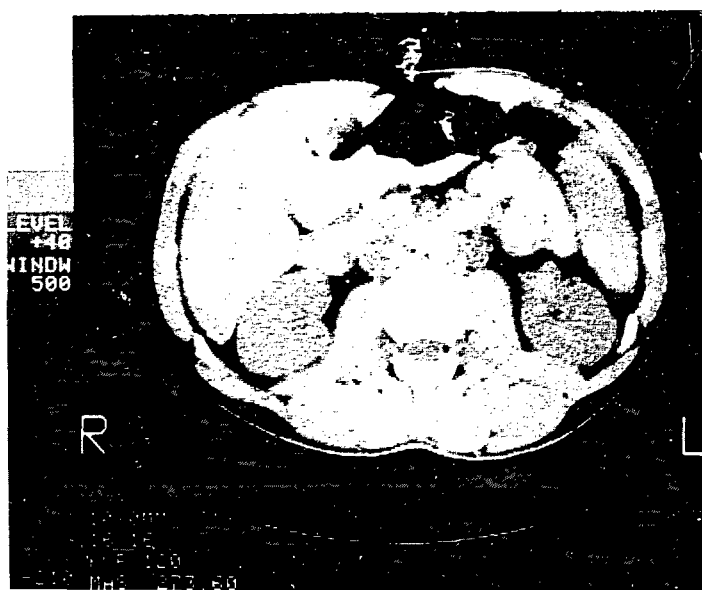


Fig. 8 CT scan of same patient confirming abnormal left sided paraaortic adenopathy.

in vivo may be a significant problem. Also, mouse immunoglobulins may be catabolised by humans efficiently and thus restricting the amounts reaching the tumours.

A great deal of knowledge is required on antigen-antibody interactions in vivo before the technique of radioimmunolocalisation can be advanced further. Nevertheless, the fact that antibodies can selectively localise to tumours has been a spur to therapeutic studies. If such an approach were to succeed it would, ironically, extinguish the imaging problem and the need for tumour localisation.

#### Acknowledgements

This work would not have been possible without the substantial and moral support received from the Imperial Cancer Research Fund, London, The Medical Research Council, UK, and The Royal Postgraduate Medical School, Hammersmith Hospital, London.

I thank Ann Freemantle for her secretarial and typing skills.

#### References

1. D. Pressman and L. Korngold, *Cancer*, 6, 619, 1953.
2. G. Kohler and C. Milstein, *Nature*, 256, 495, 1975.
3. J. Arklie, Ph.D. Thesis, University of Oxford, 1981.
4. J. Arklie, J. Taylor-Papadimitriou, W.F. Bodmer, M. Egan and R. Millis, *Int. J. Cancer*, 28, 23, 1981.
5. A.A. Epenetos, P. Travers, K. Gatter, D.Y. Mason, R.D.T. Oliver and W.F. Bodmer, *Br. J. Cancer* (in press).
6. A.A. Epenetos, K.E. Britton, S. Mather et al, *The Lancet*, ii, 999-1005, 1982.
7. J. Fogh, J. Fogh and T. Orfeo, *J.N.C.I.*, 59, 221, 1977.
8. A.A. Epenetos, C.C. Nimmon, J. Arklie et al, *Br. J. Cancer*, 46, 1, 1982.

## An Animal Model for Assessing Tumor Targeting\*

Karl Erik Hellström, Ingegerd Hellström,

Yoshinori Kohwi and Victor K. Lee

Oncogen, Seattle, Washington 98124 and Departments of Pathology  
and Microbiology/Immunology, University of Washington, Seattle, WA 98195

### ABSTRACT

Animal models have certain advantages over human experimentation when developing novel diagnostic and therapeutic procedures since experiments can be done more cheaply, are easier to control, and do not subject human beings to unnecessary risks. However, in order to be useful the animal models must resemble the situation in man as closely as possible. We have developed such a model, using rat antibodies to cell surface antigens that are most strongly expressed on chemically induced bladder carcinomas of mice.

### INTRODUCTION

A large variety of tumor-associated antigens has been identified by using monoclonal antibodies. Some of the most interesting antigens are those that are expressed more strongly by tumor cells of a particular histological type than by tumors of other types or by normal adult tissues (1-5). Although none of these antigens appear to be entirely tumor specific, several of them have sufficient degree of tumor specificity to be potentially useful as diagnostic markers and probably also as therapeutic targets. Another presentation from our group discusses three such antigens which are most strongly expressed in melanomas, and with which clinical trials are now performed (6).

Animal models can be of great use to work out the best diagnostic and therapeutic procedures with monoclonal antibodies, as long as the models closely reflect the situation in man. Chemically induced transitional cell carcinomas of the urinary bladder of mice and rats appear to meet the criteria of a good such model (7). We have recently prepared monoclonal rat antibodies to cell surface antigens that are most strongly expressed by mouse bladder carcinoma cells and shall discuss these antibodies and their potential usefulness for evaluating the targeting of tumors.

### THE MODEL

Tumors were induced by the insertion of 3-methylcholanthrene pellets into subcutaneously transplanted bladders of BALB/c mice, using a technique which has been described (8). Most of these tumors are transitional cell carcinomas but a few

---

\*This work has been supported by grants CA 14135 and 19148 from the National Institutes of Health. The work described in this article was performed when the authors were members of Fred Hutchinson Cancer Research Center, Seattle, Washington.

have an undifferentiated histology, resembling sarcomas (9). For the present study, we have used the transitional cell carcinomas except for a few cases when the undifferentiated, sarcoma-like tumors were studied for comparison. All tumors were maintained by serial transplantation in BALB/c mice and also cultured in vitro (9,10). They were regularly checked to make sure that their original morphology was being maintained.

Wistar Furth and Sprague-Dawley rats were immunized with bladder carcinomas, using a mixture of cultured transitional cell carcinomas and such tumors harvested directly from mice, and spleen cells from the immunized rats were hybridized with NS-1 mouse myeloma cells as described (9). Hybridoma supernatants were screened for production of antibodies binding preferentially to bladder carcinoma cells, using binding assays with cultured cells and immunohistological testing against frozen sections of tumor and normal tissues (10). The latter were carried out by a peroxidase anti-peroxidase technique as previously described (11).

Six hybridomas were selected, cloned and further tested (10). Tables 1 and 2 summarize the results on the three most interesting of the hybridomas, as assessed by immunohistological studies on frozen sections. As shown in the tables, one antibody, 6.10, reacted with mouse bladder carcinomas, induced by either 3-methylcholanthrene or [(4-5-nitro-furyl)-2-thiaozolyl formamide] (FANFT), and with epithelial cells from mouse embryos, but did not stain any of the other mouse tumors studied, nor a variety of adult mouse tissues. The two other antibodies, 3B12 and 8.3, bound most strongly to bladder carcinoma cells but also reacted with some normal epithelial cells, particularly the surface endothelial layer of normal bladder. In addition, they both bound to a transplanted mammary carcinoma.

## DISCUSSION

The antigens defined by the three antibodies we have described exemplify two types of antigens commonly detected in human neoplasms by using monoclonal antibodies, one that has a high degree of tumor specificity (as has antibody 6.10) and another that is tissue-type, rather than tumor-type, specific (antibodies 3B12 and 8.3). Since the antigens defined by the three antibodies are expressed in vivo, it should be possible to use the antibodies both for diagnostic studies by tumor imaging techniques and for targeting of anti-neoplastic agents to the tumor site. It may be an advantage that the three antibodies are of rat origin and hence foreign to the tumor-bearing host since the commonly used mouse antibodies are foreign to human patients. This characteristic should also make it possible to test the merits of a protocol which would use one optimal reagent for tumor targeting rather than the coupling of a tumor-targeting agent, boron, for example, to every single antibody preparation. According to this protocol, one would initially inject anti-tumor antibody (or a combination of several such antibodies). When the first antibody has attached to the tumor cells, we would then inject an antibody to the immunoglobulin first given (which should recognize the first antibody at the tumor cell surface). The second antibody would be the one that is coupled to the agent one wants to target to tumor, for example, to boron.

Table I. Expression of antigens defined by antibodies 3B12, 8.3 and 6.10 in frozen sections of tumor, as detected by immunohistology.\*

Tissue	No. of samples	3B12	8.3	6.10
<u>Bladder carcinoma</u>				
Primary (MCA)	2	++ to ++++	+ to ++	++
Transplanted (MCA)	4	+++ to ++++	++ to +++	+++
Transplanted (FANFT)	1	+++	++	++++
<u>Mammary carcinoma</u>				
Transplanted	1	++	+	-
<u>Melanoma</u>				
B16	1	-	-	-
<u>Sarcoma</u>				
Transplanted	3	-	-	-
<u>Lymphosarcoma</u>				
Transplanted	1	-	-	-

\* A peroxidase-antiperoxidase technique was used to demonstrate antigen expression in frozen sections of various tissues, as described under Materials and Methods. The degree of staining detected was graded from - (negative), through + (weakly positive) to ++++ (very strongly positive).

Table II. Expression of antigens defined by antibodies 3B12, 8.3 and 6.10 in frozen sections of normal tissues, as detected by immunohistology.

(See footnote to Table I)

Tissue	3B12	8.3	6.10	Remarks
<u>Normal adult mouse tissues</u>				
Bladder	+	+	-	Surface layer of epithelial cells
Kidney	-	-	-	
Heart	-	-	-	
Lung	-	-	-	
Liver	-	-	-	
Spleen	-	-	-	
Testicle	-	-	-	
Intestine	+	+	-	Epithelial cells of villi
<u>Mouse embryos</u> (10d, 16d, 19d)	+	+	+	Skin epithelium, periosteum stained +++ for antibody 6.10

## References

1. Hellström, K.E., Hellström, I., and Brown, J.P. Springer Seminars in Immunopathology Series, Mechanisms of Host Resistance in Cancer, R.W. Baldwin, ed., Springer-Verlag, 5: 127-146, 1982.
2. Burnol, T.F., and Reisfeld, R.A. Proc. Natl. Acad. Sci. USA 79: 1245-1249, 1982.
3. Koprowski, H., and Steplewski, Z. In: Monoclonal Antibodies and T-Cell Hybridomas, Res. Monographs in Immunology, No.3, Hammerling, Hammerling and Kearney, eds., Elsevier/North Holland Biomed. Press, Amersterdam Pps. 161-173, 1981.
4. Dippold, W.G., Lloyd, K.O., Li, L.T.C., Ikeda, H., Oettgen, H.F., and Old, L.J. Proc. Natl. Acad. Sci. USA 77: 6114-6118, 1980.
5. Imai, K., Wilson, B.S., Kay, N.E., and Ferrone, S. In: Monoclonal Antibodies and T Cell Hybridomas, Res. Monographs in Immunol., No. 3, Hammerling, Hammerling, and Kearney, eds., Elsevier/North Holland Biomed. Press, Amersterdam. Pps. 183-190, 1981.
6. Hellström, I., Hellström, K.E., Brown, J.P., Larson, S.M., Carrasquillo, J.A., and Goodman, G. See paper VII-2 in this Symposium.
7. Taranger, L.A., Chapman, W.H., Hellström, I., and Hellström, K.E. Science 176: 1337-1340, 1972.
8. Chapman, W.H. J. Urology, 88: 518-526, 1962.
9. Hellström, I., Rollins, N., Settle, S., Chapman, P., Chapman, W.H., and Hellström, K.E. Int. J. Cancer 29: 175-180, 1982.
10. Hellström I., Hellström, K.E., Rollins, N., Lee, V.L., and Nepom, G.T., submitted for publication.
11. Garrigues, H.J., Tilgen, W., Hellström, I., Franke, W., and Hellström, K.E. Int. J. Cancer 29: 511-515, 1982.

## Hormone Receptor Densities in Relation to $^{10}\text{B}$ Neutron Capture Therapy\*

Oscar Hechter

Northwestern University Medical Center, Chicago, IL 60611  
and

Irving L. Schwartz

Mt. Sinai Medical Center, New York, NY 10029

This presentation is a theoretical discussion of the possibility that "appropriate" steroid-carborane derivatives might be used to selectively deliver boron-10 ( $^{10}\text{B}$ ) to tumor cells with sex-hormone receptors in sufficient concentration for effective neutron capture therapy (NCT) of hormone-dependent mammary and prostatic cancer. This possibility arises and merits serious discussion because of the important independent contributions of Sweet (1) and Hadd (2) which served to demonstrate that estradiol coupled via the  $17\alpha$ -position to a single carborane cage (ten B atoms) retains the ability to interact with uterine estrogen receptor (ER) to produce the characteristic estrogenic uterotrophic effect. This borated-estradiol analog, which retains hormonal activity, is stable, is non-toxic (at least in short-term toxicity experiments), and is expected to accumulate selectively in cells with ER (whether malignant or normal), predominantly in the nucleus. Given these properties,  $17\alpha$ -carboranyl-estradiol has been proposed as a candidate for NCT of estrogen-dependent breast cancer. In principle, DHT ( $5\alpha$ -dihydrotestosterone), the active intracellular androgen of the prostate (cf. 3), if coupled (via  $17\alpha$ ) to a carborane cage, should likewise selectively accumulate in the nuclei of tumor and normal cells containing androgen receptor (AR); thus, carboranyl-DHT might be useful in NCT of androgen-dependent prostate cancer.

Granted that selective nuclear accumulation of  $^{10}\text{B}$  would indeed be achieved by administration of  $17\alpha$ -carboranyl derivatives of sex hormones, two basic questions arise. The first is: are the levels of ER and AR in malignant breast or prostatic epithelial cells sufficiently high to achieve the relatively high nuclear concentrations of  $^{10}\text{B}$  required for theoretically effective thermal neutron activation of the  $^{10}\text{B}(n,\alpha)^7\text{Li}$  reaction? For successful NCT of tumors, it is generally considered that 15 to 30  $\mu\text{g}$   $^{10}\text{B}$  per g tissue is required, with  $^{10}\text{B}$  ratios in tumor/normal tissue (and blood) of  $\sim 10:1$ . With a monochromatic beam of 2-keV neutrons, concentrations as low as 1 to 2  $\mu\text{g}$   $^{10}\text{B}$  per g tumor might be adequate (Fairchild and Bond, this Symposium). Geometrical considerations also will influence necessary boron content. The above numbers assume uniform boron content within the nucleus and cytoplasm and outside the cell. Restricted boron localization is discussed in detail by Kobayashi and Kanda and by Gabel, Fairchild, and Larsson (this Symposium).

The second question arises only if it should prove to be possible to define conditions such that a non-toxic borated steroid would deliver sufficient  $^{10}\text{B}$  to malignant cells with ER or AR so that irradiation with appropriate neutron beams would kill these cells. Would such successful NCT of hormone-dependent mammary or prostatic cancer be curative or merely another form of

---

\*Work supported in part by the Emma Gale Harris-Barlett Memorial Fund and the Life Sciences Foundation.

palliative treatment? If the latter, what potential benefits over other forms of palliative treatment are to be expected? Let us address the second question first.

#### SOME BASIC FACTS ABOUT MAMMARY AND PROSTATIC CANCER

Both these neoplasms, when first detected, are found to be comprised of heterogeneous clones of malignant cells which differ in growth rate and invasiveness, and in their dependence on circulating sex hormones (and their receptors) for growth and proliferation (cf. 4). One subset of these clones retains the specific sex hormone requirement exhibited by the parent normal cell; when these types of clones predominate, the tumor is termed "hormone-dependent." The sex steroid required for hormone-dependent prostatic neoplasms is DHT (derived predominantly from circulating testosterone); estradiol is the steroid required by hormone-dependent breast tumors. In addition to sex hormone-dependent clones, a second subset of malignant clones is found in both mammary and prostate cancer whose maintenance and proliferation does not depend on sex hormone support; when these clones predominate, the tumor is "hormone-independent."

Clonal heterogeneity is the underlying basis for success or failure of "endocrine therapy," in which a variety of ablative procedures and/or drugs are used to withdraw sex hormone support from hormone-dependent tumors. In advanced stages of breast and prostate cancer (with metastasis to distant sites, usually to bone), endocrine therapy produces objective remission in some but not all patients. Anti-androgen therapy in advanced prostate cancer results in objective remission in some 60 to 80% of treated patients (5) for a very variable duration (which may range from 6 months to 10 to 15 yr but is usually about 2 to 3 yr); thereafter "relapse" occurs. In advanced breast cancer, anti-estrogen therapy unfortunately results in remission in only about 25% of the treated patients (4), again for a variable duration (ranging from 6 months to many years but usually about 2 yr), after which relapse occurs. Relapse after endocrine therapy is due to the outgrowth of hormone-independent clones, initially few in number, which proliferate and cannot effectively be controlled by present chemotherapeutic procedures.

It is not known whether hormone-independent malignant cells arise from hormone-dependent clones which have mutated (whether in the primary tumor or in metastases, before or during endocrine therapy) or develop directly from normal epithelial cells which mutate. The question here relates to the issue of a unicellular vs multicellular origin of cancer (6). In either case, it is clear that in a large majority of patients with advanced prostatic cancer (perhaps as high as 80%), the tumor consists predominantly of androgen-dependent clones with AR, whereas a minority of patients with advanced breast cancer have tumors in which estrogen-dependent clones (with ER) predominate.

The relationship between the steroid receptor level in primary tumors and the response to subsequent endocrine therapy has been extensively investigated, particularly in breast cancer, to select the small fraction of patients likely to benefit from estrogen withdrawal (4). The results obtained clearly demonstrate that objective remission following anti-estrogen therapy is obtained in ~70% of patients with "ER-rich" primary tumors, but only in ~10% with "ER-poor" tumors. In prostate cancer, the evidence for a similar type of rela-

tionship between AR levels and a positive response to anti-androgen therapy is only suggestive (cf. 7,8).

Given these features, it may be predicted with some confidence that if an appropriate borated-steroid ligand for AR or ER (which may not necessarily be a 17 $\alpha$ -carboranyl sex hormone) could in fact deliver sufficient  $^{10}\text{B}$  (1 to 2  $\mu\text{g}$  per g nucleus) selectively to malignant cells, neutron irradiation of advanced breast or prostatic tumors would not remove all malignant cells. Such NCT would markedly and rapidly reduce tumor burden in a large majority of patients with advanced prostatic cancer, and a smaller fraction of patients with advanced breast cancer. Thus, for advanced cancer, this form of therapy would be "palliative," not "curative," since malignant cells which are "ER-poor" or "AR-poor" would survive, proliferate, and eventually kill the patient. However, significant benefits are to be expected in advanced disease with NCT. The major reduction in tumor burden, as well as the reduced heterogeneity of surviving malignant clones, might well be critical for increasing the effectiveness of other therapeutic modalities (e.g. immunotoxins, chemotherapy, etc.). There is also the possibility, in early stages of these cancers, that NCT might be curative. If all (or most) of the hormone-independent clones (HI-C) arise from hormone-dependent clones (HD-C), as in



then, depending on the dynamics of these cellular transformations, intervention with our hypothetical  $^{10}\text{B}$ -steroid at appropriate early stages opens the possibility of providing cancer "cure."

#### RECEPTOR CONCENTRATIONS IN TUMOR CELLS

Having pointed to possible benefits and limitations of NCT in prostatic and breast cancer, let us return to the original question:

Using a steroid ligand coupled to a single carborane cage, are the ER or AR concentrations in hormone-dependent tumor cells sufficient to provide  $^{10}\text{B}$  concentrations of 1 to 2  $\mu\text{g}$  per g nucleus which we shall assume are adequate for successful NCT?

The quantitative data required concerning receptor densities in prostate and breast tumors *in vivo* (or in cancer cell lines) are not available, for several reasons which will be briefly discussed: these relate to (i) general problems of methodology for steroid receptor assay, and (ii) special problems relating to receptor assay in malignant cells.

#### Some General Problems of Receptor Assay

The introduction of synthetic non-metabolizable steroid ligands (e.g. R-1881 for AR; R-2858 for ER; R-5020 for PR (progesterin receptor)) have removed certain problems associated with receptor assay (cf. 7-9); however, other general problems remain. One relates to the absence of a standardized procedure for collection and workup of surgical tissue samples; unoccupied receptors, which are very labile, may be destroyed during the (sometimes considerable) interval in tissue transit between surgery and subsequent workup (even when

the tissue is kept at low temperature). Receptors occupied with endogenous hormone are more stable, but other difficulties relate to their measurement. All of the published methods for assay of occupied receptors underestimate receptor number (9). The values reported for occupied AR, ER, or GR (glucocorticoid receptors) as measured by exchange assays thus represent only a fraction of the occupied receptor initially present in the tissue. Underestimation of receptor number is due to: loss of receptor binding sites during exchange incubation (due to proteases and other endogenous factors present in crude homogenate fractions, which inactivate binding sites) even at 0°C, and (ii) incomplete exchange of exogenous radioligand for endogenous hormone, this because of the very slow dissociation rate of hormone-receptor complexes at low temperature. In a collaborative study with Paul Robel and his associates (Lab Hormones, Bicêtre, France), we have recently described a combinatorial procedure which provided maximal stabilization of occupied AR in rat ventral prostate from mature animals (10); this involved "washout" of extracellular proteases and secretory products from tissue prior to homogenization; inclusion of a protease inhibitor (PMSF) and molybdate (a receptor stabilizing agent) in the exchange medium; and long-term incubation of homogenates at 0°C (96 hr). Using this "optimal" procedure, we were able to measure only ~50% of the AR sites initially present by  $^3\text{H}$ -R-1881 exchange (10). Other assay procedures, in which exchange was carried out for only 16 to 24 hr and no special attention was given to receptor stabilization, underestimated occupied receptors to an even greater extent. Thus, the receptor values reported for cancer samples obtained at surgery (as well as for cell lines) must be regarded with caution, and at best represent low approximations of the true receptor numbers.

#### Special Problems in Estimating Receptor Content in Malignant Cells

Surgical samples of primary tumors not only contain heterogenous clones of malignant cells but are contaminated to a variable degree with normal (epithelial and stromal) cells; since receptor content per unit cell may be variable, true receptor densities in heterogenous tumor cells are difficult to assess. Malignant cell lines grown in culture eliminate this particular difficulty but introduce another; the number and types of receptors in a cancer cell line may change dramatically during successive passages in culture, so that there may be little relationship to the situation which obtained *in vivo*. As a further problem, it is difficult to estimate receptor number per cell from the available receptor data, generally reported in units of fmol/g tissue or fmol/mg cytosolic protein. When data are expressed in units of fmol/mg DNA, and the DNA content of the cell is not reported (as is most often the case), accurate estimates of receptor content per cell are not possible. This is a serious problem with malignant cells, in which the DNA content is generally greater than in normal diploid somatic cells but varies in a broad band from less than diploid to tetraploid and beyond. Even if receptor concentrations per cell were known, morphometric measurements of nuclear volume are necessary to estimate receptor content per g nucleus.

Some of the difficulties described above are illustrated in the receptor data reported (11) for nine breast cancer lines grown in culture (Table 1); of the various receptors measured, only the values for nuclear ER are expressed

on a DNA basis, but the DNA content per unit cell was not reported. Occupied ER and potential  $^{10}\text{B}$  concentrations in the nucleus in these cell lines can be estimated only by introducing reasonable assumptions about nuclear volume and ploidy in these cell lines. Incidentally, it may be pointed out that in Table 1 the MCF-7 (SA) cells, which have the highest ER content in the series tested, were derived from MCF-7 (MRI) cells, which have about 1/5 the ER content of the (SA) cells.

Given the difficulties listed (as well as others not discussed), it is possible to give only a first-order approximation of the receptor concentrations, and the expected nuclear  $^{10}\text{B}$  concentrations, to be achieved in tumor cells using steroid ligands coupled to a single carborane cage.

Table 1. Receptor Content in Nine Breast Cancer Cell Lines (11)

Cell line	Nuclear ER (fmol/mg DNA)			Cytosol receptors (fmol/mg protein)			
	Unfilled	Filled	Total	ER	PR	GR	AR
BT-20	0	0	0	2	63	167	24
SW 163	0	0	0	2	61	220	4
HBL-100	0	0	0	4	96	920	0
MDA MB 231	0	0	0	56	0	386	0
MDA MB 175	0	125	125	0	39	96	0
MDA MB 361	298	11	309	3	175	82	140
T 47 D	125	268	393	3	1221	19	31
MCF-7 (MRI)	483	58	541	3	72	528	101
MCF-7 (SA)	2500	0	2500	93	300	770	24

#### NUCLEAR CONCENTRATIONS OF OCCUPIED RECEPTORS AND EXPECTED $^{10}\text{B}$ LEVELS

Three cases will be examined to determine whether normal or malignant cells treated with a steroid-ligand coupled to a single carborane cage have sufficient receptor density to provide 1  $\mu\text{g}/^{10}\text{B}$  per g nucleus. In all cases, the number of receptors per cell will be estimated from receptor number per unit DNA. We assume that when receptors are occupied, 80% of these receptor-complexes will be localized in the nucleus (12). There are reasonable morphometric measurements of nuclear volume in normal epithelial cells from the ventral prostate of mature rats (13); nuclear volume was  $400 \mu\text{m}^3$ . We shall assume that the nuclear volume in the malignant cells to be analyzed is either similar to or somewhat greater (50%) than this value. With these assumptions, it becomes possible to approximate  $^{10}\text{B}$  concentrations per g nucleus.

### a. Rat Ventral Prostate Epithelial Cells

Table 2 details how nuclear receptor content was estimated in rat prostate, which is comprised predominately of epithelial cells (stromal cells represent only 10 to 20% of the cells in rat ventral prostate). In Table 2, data are clearly differentiated from assumptions. The only assumption introduced in this calculation is that the density of a nucleus is about 1.0, equivalent to that of water; all other values are derived from experimental data. It will be seen that the corrected AR value of 13.4 pmol/mg DNA is equivalent to an intracellular AR concentration of 32 nM, with 173 pmol AR per g nucleus. The  $^{10}\text{B}$  expected in such a cell, where all AR is filled with a carboranyl-steroid ligand, would be 17 ng per g nucleus. A 60-fold increase in  $^{10}\text{B}$  would be required to achieve 1  $\mu\text{g}$  per g nucleus.

Table 2. Estimation of AR Concentrations in Normal Epithelial Cells of Ventral Prostate (Mature Rats)

Total AR detected by exchange (10)	6.7 pmol/mg DNA
Total AR (corrected) (10)	13.4 pmol/mg DNA
DNA content per cell (14)	6.4 pg
AR content per cell	$8.6 \times 10^{-5}$ fmol
AR content per nucleus	$6.9 \times 10^{-5}$ fmol
Morphometric volumes (13)	Cell = $3400 \mu\text{m}^3$ = $0.4 \times 10^{-6} \mu\text{l}$ Nucleus = $400 \mu\text{m}^3$ = $0.4 \times 10^{-6} \mu\text{l}$
Total aqueous volume in cell (80% of total vol)	= $2.7 \times 10^{-6} \mu\text{l}$
Concentration of AR in cell $(8.6 \times 10^{-5} \text{ fmol}/2.7 \times 10^{-6} \mu\text{l})$	= 32 fmol AR/ $\mu\text{l}$
Concentration of AR in nucleus $(6.9 \times 10^{-5} \text{ fmol}/0.4 \times 10^{-6} \mu\text{l})$	= 173 fmol/ $\mu\text{l}$
$^{10}\text{B}$ expected in nucleus	$1.73 \text{ nmol/g}$
	= 17.3 ng/g

### b. MCF-7 (SA) Breast Cancer Cell

This cell line, a widely used model for study of estrogen action at the cellular level, has the highest ER concentration per unit DNA among the nine breast cancer lines shown in Table 1. Table 3 shows the specific assumptions used to calculate ER content per nucleus. Despite the assumption that the ER is twice that actually reported, this calculation reveals that a 67-fold increase in ER would be necessary to achieve a value of 1  $\mu\text{g}$   $^{10}\text{B}/\text{g}$  nucleus.

### c. Primary Prostatic Cancer

The available evidence indicates that most (85 to 100%) primary carcinoma samples contain occupied AR with mean receptor number per unit DNA roughly

Table 3. Estimation of  $^{10}\text{B}$  Nuclear Concentrations Expected in MCF-7 (SA) Breast Cancer Cells Loaded with  $17\alpha$ -Carboranyl-estradiol

Total nuclear ER (11)	2.5 pmol/mg DNA
Total nuclear ER (arbitrarily "corrected")	5.0 pmol/mg DNA
DNA content per nucleus (ploidy assumed)	15 pg
ER content per cell	$7.5 \times 10^{-5}$ fmol
ER content per nucleus	$6.0 \times 10^{-5}$ fmol
Assume nuclear volume $400 \mu^3$ =	$0.4 \times 10^{-6} \mu\text{l}$
ER concentration in nucleus	
$(60 \times 10^{-6} \text{ fmol} / 0.4 \times 10^{-6} \mu\text{l}) = 150 \text{ fmol}/\mu\text{l}$	= 150 pmol/ml (or g)
$^{10}\text{B}$ expected in nucleus	1.5 nmol/g
	= 15 ng/g

equivalent to the AR values with normal or hyperplastic human prostate samples (8,15,16). In addition, PR has been detected in cytosol fractions of many prostatic cancer samples as well as in normal and hyperplastic prostate tissue (17). As expected, PR in prostate is unoccupied and found exclusively in the cytosol fraction. There is not sufficient data to compare PR levels in normal vs cancer tissue. GR has not been detected in cytosol fractions of either primary prostatic cancer or non-malignant prostate tissue (8); however, occupied nuclear GR was not examined. Moreover, GR occupied with cortisol (expected to be localized in the nucleus) would probably not be detected with the technics used. ER is present irregularly in prostatic cancer samples in low concentrations relative to either AR or PR (cf. 18,19).

In a collaborative study with Robel and associates (20), we have examined the receptor content of normal human prostate tissue, dissected from aged patients undergoing cystectomy for bladder cancer, relative to hyperplastic prostatic tissue, using the procedures previously described to maximize receptor stability. Although we did not measure prostatic cancer samples, we will assume for the sake of this discussion that the receptor values obtained in normal human prostate are similar to those found in primary prostatic cancer. The results obtained in normal human prostate are shown in Table 4, with and without correction for AR and ER degradation during incubation and for incomplete exchange.

If we assume that AR and PR are both present in the same malignant cell (which may not necessarily be so) and that all of these sites were filled by a carboranyl-steroid ligand with high affinity for both AR and PR, (of which R-1881 is only one of many examples (cf. 21)), then it is possible to obtain an approximate value for expected nuclear  $^{10}\text{B}$ , making reasonable assumptions about ploidy and nuclear volumes, as shown in Table 5.

#### d. Summary

The result of this analysis indicates that the concentrations of AR and PR in malignant prostatic cells or of ER in malignant mammary cells are too low to achieve nuclear  $^{10}\text{B}$  concentrations of 1  $\mu\text{g}$  per g of tumor by using a

Table 4. Steroid Receptors in Normal Prostate (pmol/mg DNA, mean  $\pm$  SEM) (20)

Zone	AR		PR		ER	
	Found	"Corr"*	Found	"Corr"	Found	"Corr"
Periurethral (inner)	1.7 $\pm$ 0.4 (5/5)	3.4	2.4 $\pm$ 0.7 (5/5)	2.4	0.1 $\pm$ 0.1 (2/5)	0.2
Peripheral (outer)	1.5 $\pm$ 0.5 (7/7)	3.0	1.7 $\pm$ 0.5 (5/7)	1.7	0.1 $\pm$ 0.1 (4/6)	0.2
Mean (frequency)	(12/12)	3.2	(10/12)	1.9	(6/11)	0.2

\*Based on assumption that exchange procedure measured only  $\sim$ 50% of receptor present.

AR: Incubation 72 h at 0 to 4° with  $^3$ H-R-1881 in presence of 5  $\mu$ M triamcinolone acetonide ( $\pm$ 100-fold excess radioinert R-1881).

PR: Incubation 16 h at 0 to 4° with  $^3$ H-R-5020 in presence of DHT (20 nM) and cortisol (500 nM) ( $\pm$ 100-fold excess R-5020).

ER: Incubation 72 h at 0 to 4° with  $^3$ H-estradiol in presence of DHT (20 nM) ( $\pm$ 100-fold excess DES).

Table 5. Estimate of Nuclear Concentrations of  $^{10}$ B in Prostatic Cancer Cells, Using a Carboranyl-steroid which Occupies Both AR and PR

Assume: Cancer cells have AR and PR concentrations present in normal prostate tissue: AR + PR = 5.1 pmol/mg DNA.

Assume: DNA in cancer cells is 2x that in normal diploid cells:  
20 pg DNA/nucleus.

Then AR + PR =  $102 \times 10^{-6}$  fmol/cell  
 $82 \times 10^{-6}$  fmol/nucleus.

Assume: Nuclear volume 400 to 600  $\mu$ m<sup>3</sup>, equivalent to 0.4 to 0.6 $\times 10^{-6}$   $\mu$ l.  
Nuclear concentration of AR + PR = 133 to 200 fmol/ $\mu$ l  
= 133 to 200 pmol/ml (or g).

$^{10}$ B nuclear concentration:

1.3 to 2.0 nmol/ml (or g) = 13 to 20 ng  $^{10}$ B/g nucleus.

steroid ligand coupled to a single carborane cage. In the case of ventral prostate of mature rats, where minimal assumptions were introduced to estimate nuclear  $^{10}$ B content, a 60-fold increase in  $^{10}$ B is required to achieve the nuclear levels required for therapeutically meaningful thermal neutron activation of the  $^{10}$ B(n, $\alpha$ ) $^7$ Li reaction in epithelial cells. Using generous assumptions about receptor levels in prostatic cancer samples (containing AR plus PR) or in the HCF-7 breast cancer line (containing ER), it was estimated that a 50- to 80-fold increase in nuclear  $^{10}$ B would be required to achieve levels of 1  $\mu$ g per g.

THE PROBLEM: HOW TO INCREASE  $^{10}\text{B}$  ACCUMULATION IN MALIGNANT PROSTATIC CELLS BY ABOUT TWO ORDERS OF MAGNITUDE?

Whether this is possible is problematic, but it is unlikely to be achieved solely by procedures which increase receptor content per cell or the boron content of a steroid ligand. However, a combinatorial strategy may be successful. Since NCT, if successful, would be expected to benefit a greater fraction of patients with prostate cancer than with breast cancer, let us consider some of the possibilities for increasing  $^{10}\text{B}$  in malignant prostatic cells with AR and PR, using a combinatorial approach.

1. It may be possible to couple two carborane cages to a single steroid ligand, retaining affinity for AR and PR, with translocation and nuclear accumulation of the occupied receptors. If it is possible,  $^{10}\text{B}$  would be increased 2-fold with this hypothetical borated steroid.

2. Our estimate of AR and PR in human prostate is based on data from aged men (>60 yr old). It is known that prostate AR levels in rats decrease with age and can be restored to levels found in young adults by administration of testosterone (22). Since the hypothetical  $^{10}\text{B}$ -steroid to be used should be an active androgen, AR levels might be increased 2- to 4-fold, with an additional 2- to 4-fold increase in  $^{10}\text{B}$ .

3. Finally, all steroid ligands bind to non-receptor proteins, as well as receptor proteins. Indeed, this is a major problem in steroid receptor assay. These low-affinity binding sites are present in great number relative to high-affinity receptors ( $K_D \approx 1 \text{ nM}$ ). Therefore it is possible that by using pharmacological concentrations of our hypothetical  $^{10}\text{B}$ -steroid, binding to non-receptor proteins present in cancer cells may increase  $^{10}\text{B}$  concentrations another 10-fold (perhaps greater), to a total of 80-fold, so that  $^{10}\text{B}$  levels of 1  $\mu\text{g}$  per g nucleus may be approached. If NCT can be successfully effective with the 10- to 20-fold reduction in  $^{10}\text{B}$  by the procedures suggested by Fairchild (this Symposium), namely, using fractionated doses of monoenergetic 2-keV neutrons, then the prospect of success of NCT for prostatic cancer becomes even more promising.

Based on these admittedly speculative considerations, a collaborative project has been established to study the potential of  $^{10}\text{B}$ -steroids for NCT of prostatic cancer, in which a majority of the afflicted patients have hormone-dependent tumors. In addition to Hechter and Schwartz, the group consists of P. Robel and E.E. Baulieu (Lab Hormones, Bicêtre, France) and R.G. Fairchild and V.P. Bond (Brookhaven National Laboratory). Roussel, Uclaf (Romainville, France) has agreed to synthesize the borated steroids for this project.

All members of our group recognize that the specific strategy suggested can be evaluated only by experimental analysis. However, we believe that an approach of this type merits serious investigation, since there is a reasonable possibility that  $^{10}\text{B}$  neutron capture may kill prostatic cancer clones containing AR and PR not only in early but also in advanced stages of prostatic cancer. At present it is not possible to predict whether or not our ideas about  $^{10}\text{B}$  neutron capture in prostatic cancer will be validated by hard experimental evidence. However, should this approach prove to be successful, radiotherapy for early stages of prostatic cancer in the future might well involve irradiation with epithermal neutron beams as well as with conventional megavoltage photons (with a corresponding reduction of radiation "side-

effects"). Beams of epithermal neutrons directed at pelvic lymph nodes or bones with metastases may markedly (and rapidly) reduce tumor volume with minimal toxic side-effects. Reduction in tumor volume as well as a reduced number of malignant clones, together with the new possibilities of immunological therapy, raise the prospect that curative procedures for prostatic cancer may become available during the next decade.

#### REFERENCES

1. Sweet, F. *Steroids* 37, 223-237, 1982.
2. Hadd, H., Brunsen, K.W., Kokosa, J.M. *Program 64th Ann. Meeting Endocrine Soc.* p 82, 1982.
3. Liao, S. in Biochemical Actions of Hormones Vol VI, pp 351-406 (G. Litwak, Ed) Academic Press, NY, 1977.
4. Jensen, E. *Cancer Chemotherapy* 3, 187-205, 1981.
5. Lee, C., Jesik, G., Uke, E., Talkowski, W., Grayhack, J.T. in Hormone Related Tumors (H. Nagagawa, K. Ake, Eds) pp 261-285, Springer-Verlag, Berlin, 1981.
6. Moolgavkar, S.H., Knudsen, A.G. *JNCL* 66, 1037-1052, 1981.
7. Raynaud, J.P., Bouton, M.M., Martin, P.M. in Steroid Receptors, Metabolism and Prostatic Cancer (F.H. Schroder, H.J. deVoogt, Eds) pp 165-181, *Excerpta Medica*, Amsterdam, 1980.
8. Ekman, P. *Ibid.* pp 208-224.
9. Robel, P. *Ann. Clin. Res.* 12, 216-222, 1980.
10. Hechter, O., Mechaber, D., Zwick, A., Campfield, L.A., Eychenne, B., Baulieu, E.E., Robel, P. *Arch. Biochem. Biophys.* 224, 49-68, 1983.
11. Horwitz, K.B., Zava, D.T., Thilager, A.K., Jensen, E.M., McGuire, W.L. *Cancer Res.* 38, 2434-2437, 1978.
12. Blondeau, J.P., Corpechot, C., LeGoascogne, C., Baulieu, E.E., Robel, P. *Vitam. Horm.* 33, 319-344, 1975.
13. Bruchovsky, N., Rennie, P.S., Vanson, A. *Biochim. Biophys. Acta* 394, 248-266, 1975.
14. Bruner-Lorand, J., Mechaber, D., Zwick, A., Hechter, O., Eychenne, B., Baulieu, E.E., Robel, P. *The Prostate*, in press.
15. Shain, S.A., Boesel, R.W., Lamen, D.L., Radwin, H.M. *J. Clin. Endocrinol. Metab.* 50, 704-711, 1980.
16. Barrack, E.R., Bujnovszky, P., Walsh, P.C. *Cancer Res.* 43, 1107-1116, 1983.
17. Gustafson, J.Å., Ekman, P., Pousette, Å., Snochowski, M., Höglberg, B. *Invest. Urol.* 15, 361-366, 1978.
18. Murphy, J.B., Emmott, R.C., Hicks, L., Walsh, P.C. *J. Clin. Endocrinol. Metab.* 50, 938-948, 1980.
19. Robel, P., Hechter, O. *Proc. Int. Cancer Congress* (Seattle, WA) Sept, 1982.
20. Robel, P., Eychenne, B., Picard-Groyer, M.T., Baulieu, E.E., Hechter, O. Submitted to *J. Clin. Endocrinol. Metab.*
21. Raynaud, J.P., Ojasoo, T., Bouton, M.M., Philibert, D. in Drug Design, Vol 8 (E.J. Ariens, Ed) pp 169-214, Academic Press, NY, 1979.
22. Boesel, R.W., Klipper, R., Shain, S.A. *Steroids* 35, 157-177, 1980.

## CHEMICAL OVERVIEW OF BORON NEUTRON CAPTURE THERAPY

Albert H. Soloway, Rolf F. Barth, Fazlul Alam and Walter E. Carey

College of Pharmacy and Departments of Pathology and Nuclear Engineering  
The Ohio State University, Columbus, Ohio 43210

The theoretical attractiveness of Neutron Capture Therapy (NCT) versus other radio- and chemotherapeutic approaches for the treatment of cancer is as appealing now as when first proposed by Locher (1). The concept of using two components, each relatively innocuous, whose interaction produces intense, ionizing radiation that is confined to single or adjacent cancer cells has obvious advantages. First and foremost, selective destruction may be achieved without adversely affecting nearby normal tissues. Second, and of equal importance, is the short mean free path of the heavy particles generated by NCT, and the limiting of ionizing radiation to a short distance from the point of neutron capture. Third, is the ability to vary each of the two components of the reaction independently from one another in order to achieve a cytocidal effect. Compared to conventional cancer chemotherapy, where toxic drugs are administered with little ability to control their distribution or deleterious effects on normal cells, one can readily appreciate the selectivity of NCT. Similarly, when ionizing radiation, such as externally directed, high energy particles, is used, the irradiated area usually has been predetermined. Consequently, there is little opportunity to limit the destructive events in normal tissues, once the process has been initiated.

Various nuclides that have a relatively high capture cross section for thermal neutrons are listed in Table 1. Some have been considered as potential candidates for NCT, and a few are normally radioactive, which would diminish their attractiveness. Others give rise to gamma rays as a product of the capture reaction, and therefore the ionizing radiation is not discretely confined to individual target cells. For still others, the ability to incorporate the particular nuclide into compounds that would be stable under physiological conditions is problematic. For these reasons, much of the chemical effort in NCT has focused on the fission reaction of boron-10:

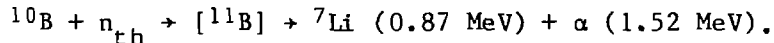


Table 1. Thermal Neutron Capture Cross Section Values in Barns of Potential Nuclides for Neutron Capture Therapy

Cross Section ( $\sigma$ )		Cross Section ( $\sigma$ )	
Nuclide	(barns)	Nuclide	(barns)
$^6\text{Li}$	953	$^{157}\text{Gd}$	240,000
$^{10}\text{B}$	3,837	$^{174}\text{Hf}$	400
$^{113}\text{Cd}$	20,000	$^{199}\text{Hg}$	2,000
$^{135}\text{Xe}^*$	2,720,000	$^{235}\text{U}^*$	678
$^{149}\text{Sm}$	41,500	$^{241}\text{Pu}^*$	1,375
$^{151}\text{Eu}$	5,900	$^{242}\text{Am}^*$	8,000
$^{155}\text{Gd}$	58,000		

\* Nuclides are radioactive

In this overview, we will touch on historical events, but more importantly we will focus on present work and future possibilities. In the early 1950's, chemists were, for the most part, not involved in NCT, and it was the physicists and clinicians who led the way. For this reason, boric acid and various borates, which were readily available, initially were screened in animals and ultimately were used clinically. Due to the interest of Dr. Sweet at the Massachusetts General Hospital and Dr. Farr at the Brookhaven National Laboratory, therapy largely was oriented towards patients with malignant brain tumors. These infiltrating neoplasms did not metastasize, were very lethal despite extensive surgery, and were unresponsive to conventional chemo- and radiotherapy. Concern, then, centered on determining which compounds would be excluded from normal brain tissue due to the blood-brain barrier, and which would achieve reasonable concentrations in brain tumors for specific time periods. A summary of tumor:brain boron ratios of various boronic acids and their physiochemical parameters are presented in Table 2. At that time significant progress in both the synthesis and structural determination of polyhedral boranes and carboranes was being made by Muetterties, Knoth and their collaborators at DuPont, by Heying and Schroeder at Olin, by Lipscomb at Harvard, by Kaczmarczyk at Tufts, by Hawthorne at U.C.L.A., and by Shore at Ohio State. Many compounds were extremely stable both chemically and physiologically. During the 1950's and early 60's some of these compounds, boronic/borinic acids and their derivatives and boron/nitrogen isosteres of various organic structures were screened in animals and ultimately evaluated in man. Of these, two compounds, p-carboxybenzene-boronic acid and sodium decahydrodecaborate, showed tumor localizing properties in mouse ependymoblastomas (Figure 1) and human glioblastomas (Figure 2).

Fig. 1. Tumor/Brain Boron Ratios in Mice

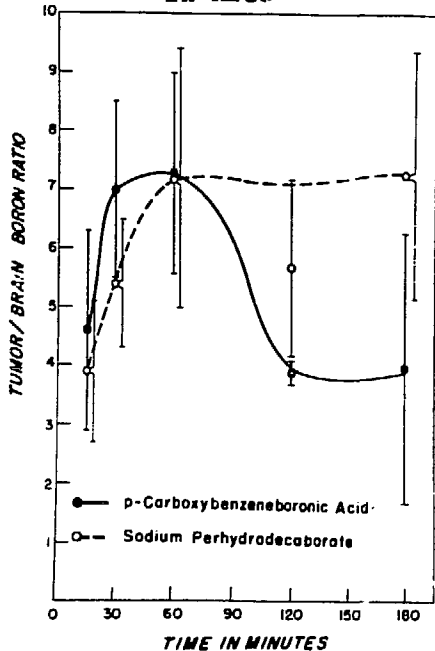


Fig. 2. Boron Concentrations in Human Brain Tumors

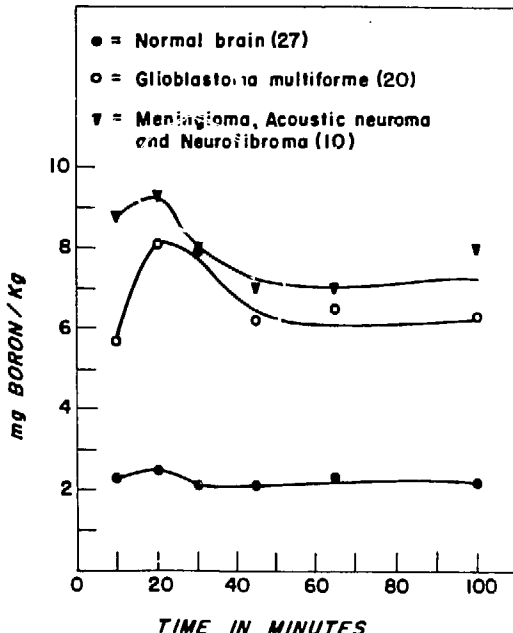


Table 2. Tumor/Brain Ratios of Various Boronic Acids

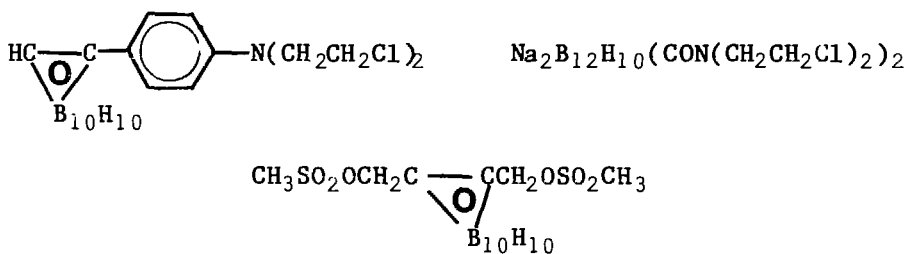
Substituted Benzeneboronic Acid X-Ph-B(OH) <sub>2</sub>	Aqueous/Benzene Partition Coefficients	Tumor/Brain Boron Ratios
4-Si(CH <sub>3</sub> ) <sub>3</sub>	0.03	0.1*
2,4,6-tri-CH <sub>3</sub>	0.4	0.2*
3-CF <sub>3</sub>	0.4	0.2*
2-CH <sub>2</sub> OH (anhydride)	0.6	---*
4-SCH <sub>3</sub>	0.7	0.2*
4-Br	0.8	0.2*
4-OC <sub>2</sub> H <sub>5</sub>	1	0.6
4-Cl	1	0.4
2-CH <sub>3</sub>	2	0.4
3-CH <sub>3</sub>	2	0.3
4-CH <sub>3</sub>	2	0.3
4-OCH <sub>3</sub>	3	0.7
4-F	3	0.3
4-H	6	0.7
2-NO <sub>2</sub>	7	0.6
3-NO <sub>2</sub>	12	0.4
3-NHCOOC <sub>2</sub> H <sub>5</sub>	14	0.6
4-CHO	29	0.6
3-CO <sub>2</sub> -4-CH <sub>2</sub>	29	0.5
3-NO <sub>2</sub> -4-COOH	51	2.5
3-NH <sub>2</sub> -4-CH <sub>3</sub>	67	0.9
4-COOH	67	4.8
3-NO <sub>2</sub> -5-NH <sub>2</sub>	170	1.8
4-B(OH) <sub>2</sub>	200	2.3
3-NH <sub>3</sub>	200	1.2
4-N(CH <sub>3</sub> ) <sub>2</sub>	200	1.4
3-NHCOC <sub>6</sub> H <sub>5</sub> -5-COOH	200	4.0
2-NO <sub>2</sub> -4-NH <sub>2</sub>	200	2.6
3-COOH	200	5.7
4-CH <sub>2</sub> CHCOO <sup>-</sup>   NH <sub>3</sub> <sup>+</sup>	200	8.5
3-OH	200	1.5
4-OH	200	1.6
2-NO <sub>2</sub> -4-COOH	200	7.7
3-NH <sub>2</sub> -4-COOH	200	6.4
3-NHCOCH <sub>2</sub> CH <sub>2</sub> COOH	200	6.9
3-NHCONH <sub>2</sub>	200	7.5
3,5-di-NH <sub>2</sub>	200	7.5
2-CH <sub>3</sub> -3,5-di-NH <sub>2</sub>	200	4.8
2-CH <sub>2</sub> -4-COOH	200	7.3

\*Animals died at low doses of the compound.

Boron-10 enriched compounds were prepared and a clinical trial was initiated in patients at the Massachusetts General Hospital. The failure to obtain a significant therapeutic effect in this study could be attributed to non-uniform distribution of the compounds in the tumor and uptake by surrounding normal brain tissue. Furthermore, blood levels were high and this resulted in exposure of the vessel walls to cytoidal doses of radiation, thereby producing necrosis of the vascular endothelium. Normal brain and tumor destruction, therefore, were directly attributable not only to the alpha irradiation but also to ischemic necrosis.

For this reason, studies were initiated to screen compounds that would leave the vascular compartment and become more selectively localized in malignant cells. Even prior to this, boron compounds were being synthesized with the objective that they might selectively be incorporated into more rapidly dividing neoplastic cells. The clinical failures provided additional impetus for these studies. Boron-containing anti-metabolites and other tumoristatic compounds were synthesized, including amino acids, purines, pyrimidines and various alkylating agents. A few examples of the types of compounds that were synthesized by one of us (A.H.S.) and evaluated biologically are presented in Figure 3.

Figure 3. Examples of Boron Compounds Evaluated Biologically



At the same time a number of polyhedral boranes, synthesized at DuPont, were evaluated in tumor-bearing mice for their ability to leave the vascular compartment and localize in tumors. Two compounds that displayed these properties were  $\text{Na}_2\text{B}_{12}\text{H}_{11}\text{SH}$  and  $\text{Na}_2\text{B}_{10}\text{Cl}_8(\text{SH})_2$  (2). These promising initial results in animals, summarized in Table 3, led Hatanaka (3) to use  $^{10}\text{B}$ -enriched  $\text{Na}_2\text{B}_{12}\text{H}_{11}\text{SH}$  for NCT in patients. Although this compound per se did not demonstrate a high degree of specificity for malignant cells, the basis for its selectivity is of significant interest and may aid in the design of new compounds that are more specific.

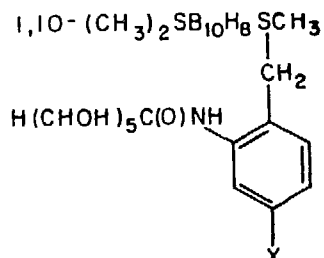
Table 3. Tumor and Blood Distribution of  $B_{12}H_{11}SH^{2-}$ 

Micrograms of Boron/g		Tumor:Blood Ratio
Tumor	Blood	
17.2	4.4	3.9
21.8	5.0	4.4
6.5	1.7	3.8
4.4	2.1	2.1
33.0	6.2	5.3
6.0	2.2	2.7
37.6	2.1	17.9
19.9	3.9	5.1
4.2	1.1	3.8
5.0	1.8	2.8
13.3	2.0	6.6
7.5	0.9	8.3
23.4	3.4	6.9
18.7	3.3	5.7
Average:		5.7

Dose: 35  $\mu$ g Boron/g mouse/dayTotal Dose: 175  $\mu$ g Boron/g

With the development of hybridoma technology and the production, isolation and purification of monoclonal antibodies directed against tumor-associated antigens, there has been resurgent interest in the potential use of antibodies for the specific delivery of tumoricidal agents. Antedating the era of monoclonal antibodies, initial studies by one of us (A.H.S.) focused on the question of whether polyclonal antibodies could be boronated with a sufficient amount of boron and yet retain their water solubility. Some of these compounds and the early results on their covalent attachment to antibody molecules are shown in Figure 4 and Table 4.

Fig. 4. Structures of the Protein-Binding Polyhedral Borane Derivatives



**1a**, X = NH<sub>2</sub>  
**b**, X = NCS  
**c**, X = CO<sub>2</sub>H

Table 4. Molar Concentrations of Boron and Protein and Their Mole Ratios in the Coupling Reaction Mixtures and in the Purified Conjugate

Compd	Reaction mixture		Conjugate	
	[Boron] <sup>a</sup> (M $\times 10^3$ )	[Protein] (M $\times 10^6$ )	[Boron: protein (molar ratio)]	[boron: protein (molar ratio)]
<b>1a</b>	3.96	6.50	610	26
	5.28	6.50	810	82
	7.92	6.50	1200	99
<b>1b</b>	3.90	6.50	600	410
	5.20	6.50	800	590
	7.80	6.50	1200	1100
<b>1c</b>	3.75	6.70	500	85
	5.00	6.70	750	120
	7.50	6.70	1100	260

<sup>a</sup> Calculated as gram-formula weights of the element per liter of solution.

High levels of binding are a necessary requirement, but clearly not the only one. Wellum, Zamenhof and Tolpin (4) have focused on two critical factors: 1) Antigen-antibody association constants ( $K_a$ ), and 2) antigen site densities. A high  $K_a$  is essential, if there is to be any potential for NCT using boronated antibodies. That in and of itself will not be sufficient if the antigen site density is low. Since the amount of boron delivered to the tumor cell will be proportional to the antigen site density, the most favorable conditions for NCT involve a high antigen site density. Calculations show that approximately  $10^9$  boron atoms per tumor cell will be required for a lethal  $n,\alpha$  reaction (5). Thus, with an antigen site density of  $10^6$  receptor sites per cell, 1,000 boron atoms will be needed per antibody molecule.

A fundamental question that must be answered is whether the boronated antibodies would retain their tumor-localizing properties, and whether all malignant cells express the relevant tumor-associated antigens. The more highly boronated the antibody, the greater its potential to deliver destructive alpha particles to target cells. At the same time, adding additional boron moieties increases the probability that the altered antibodies may show reduced  $K_a$ 's, by either directly or indirectly affecting the combining sites. Furthermore, boronation may be variable, and, for the following reasons, there may be a need to separate non- or lightly boronated molecules from heavily boronated ones. First, the boron groups are relatively low in molecular weight, perhaps less than 1,000. An increase of that order of magnitude to an antibody with a molecular weight in the range of 150,000 would be inconsequential. Thus, separation of the monoclonal antibodies from the non-boronated or lightly boronated antibodies might be difficult. Furthermore, the non-boronated antibodies might have higher  $K_a$ 's and preferentially bind to the tumor cells. On the other hand, the more highly boronated the species, the fewer the number of molecules that would be required to sustain a lethal  $n,\alpha$  reaction. Ideally, then, we would like to maximize the degree of boronation without reducing the affinity, avidity or tumor localizing properties of the antibodies. Since the non-boronated antibodies may be more effective in competing for antigen binding sites than their boronated counterparts, it may be desirable to separate out the boronated from the non-boronated antibodies. These problems might be obviated by linking a heavily boronated macromolecule to the antibody. For example, attachment of a boron polymer with a molecular weight of 30,000 to an antibody with a molecular weight of 150,000 would increase its weight by 20% with the addition of the first unit. Such an increase in molecular weight might considerably simplify the separation of non-boronated from boronated molecules. This also would fulfill the requirement of delivery of a critical number of boron atoms to each target cell. The synthesis of such a polymeric species containing protein-binding functional groups should be well within our capabilities. Our own preliminary data have shown that it is possible to link polyhedral boranes to antibody molecules, and to deliver a critical amount of boron-10 to sustain a lethal  $n,\alpha$  reaction (6). In concluding this section relative to boronated antibodies, it is fair to say that although monoclonal antibodies appear to offer great potential as the so-called "magic bullet", translating that potential into a practical thera-

peutic method for NCT still remains a challenge. On the other hand, significant problems have been encountered in the in vivo use of immunotoxins (7), but this has not detracted from their fundamental attractiveness as tumoricidal agents. Taken in its proper perspective, extraordinary advances have been made in the area of hybridoma technology over the past five years, and the potential for using monoclonal antibodies for targeting still remains great.

Not all of the recent work has focused solely on the incorporation of boron into antibodies and other macromolecules. Significant effort also has been directed towards the synthesis of boron analogues of amino acids, purines, pyrimidines and other nucleic acid precursors. The rationale for this is clear, namely, that rapidly dividing tumor cells might incorporate these analogues into cellular organelles or constituents. In addition, investigators have been concerned with the synthesis of boronated steroids, especially estrogens, for incorporation of boron into tumor cells that express these receptors. Such compounds ultimately might localize in the cell nucleus, thereby increasing their potential to sustain a lethal  $\alpha$  reaction. The key problem again is to achieve critical boron levels. Synthesis of boronated derivatives of compounds that have shown a clear predilection for tumor cells also is a very active research area. Among these are boron-labeled porphyrins, tetracyclines and the very interesting work using boronated chlorpromazine for targeting to melanoma cells (8). There are many alternatives, therefore, to develop boron compounds that might selectively localize in neoplastic cells. These compounds could be used together with antibodies to deliver the requisite amount of  $^{10}\text{B}$  to tumor target cells.

The stage, which we presently are at, is analogous to the state of cancer chemotherapy in the early 1950's. At that time single agents, many of which were relatively ineffective and are no longer used, were employed. Contrast this to the situation today, where combinations of more selectively tumoricidal drugs are used together with surgery and radiation to effectively treat cancer patients. Seen in this context, it would be most appropriate to ask the question "why shouldn't NCT be used in combination with other therapeutic modalities?" The key problems have been outlined in the preceding discussion. If they can be circumvented, then NCT may have an important role to play in cancer therapy in the next decade, and it might contribute to a further improvement in the survival rates for those tumors that currently are associated with high mortality. NCT can destroy tumor cells. The limitation has been the requirement to destroy every single tumor cell, but if NCT is combined with other therapeutic modalities it may well provide the basis for total eradication of the malignant cell population.

#### ACKNOWLEDGMENT

This work was supported in part by Department of Energy Contract DE-AC0282ER60040 and grant PDT-197 from the American Cancer Society.

#### REFERENCES

1. G.L. Locher, Am. J. Roentgenol., 36:1-13, 1936.
2. A.H. Soloway, H. H. Hatanaka and M.A. Davis, J. Med. Chem., 10:714-717, 1967.
3. H. Hatanaka, in "Synthesis and Applications of Isotopically Labeled Compounds" ed. W.P. Duncan and A.B. Susan, Elsevier, 1983, pp 167-174.
4. G.R. Wellum, R.G. Zamenhof and E.I. Tolpin, Int. J. Rad. Oncol., Biol. & Phys., 8:1339, 1982.
5. F. Alam, unpublished.
6. F. Alam, A.H. Soloway, R.F. Barth, C.W. Johnson and W.E. Carey. See paper V-4 in this symposium.
7. J. Ritz and S.F. Schlossman, Blood, 59:1-11, 1982.
8. M. Ichihashi, T. Nakanishi and Y. Mishima, J. Radiation Res., 19:52, 1978.

## Boron-10-Labeled Antibodies in Cancer Therapy

Eugene Mizusawa, Anthony J. Serino, M. Frederick Hawthorne  
University of California at Los Angeles, Los Angeles, CA 90024  
and

Robert M. Sharkey and David M. Goldenberg  
University of Medicine and Dentistry of New Jersey, Newark, NJ 07103

### ABSTRACT

The specific objectives of this study are to develop boron labeling methods which maximize the boron-10 content of antibodies against carcinoembryonic antigen (CEA) while minimizing antibody protein precipitation and to measure the selective tumor accretion of boron-10 by these boron-10-labeled, tumor localizing antibodies. The boron labeling of antiCEA IgG with *p*-[1,2-dicarba-clos-[1-<sup>3</sup>H]dodecaboran(12)-2-yl]-benzenediazonium ion ([<sup>3</sup>H]DBD) has been investigated and in *vivo* studies using hamsters bearing GW-39 tumors show that boron-10-labeled anti-CEA IgG retains selective localization in tumors. To further investigate the boron labeling of anti-CEA IgG, new boron containing compounds which can be used to conjugate antibodies have been synthesized, including those expected to have enhanced water solubilities.

### RESULTS AND DISCUSSION

More than 3 decades have passed since Bale suggested that boron conjugated to antitumor antibodies might provide a selective and effective method of cancer therapy. (1) Recent clinical studies have affirmed that a number of antitumor antibodies can accrete selectively in tumors containing the appropriate antigen target, and when these antibodies are labeled with a suitable radionuclide, tumor imaging (radioimmunodetection of cancer) is achieved (2-8). It thus became apparent to us that the conditions were favorable for a reexamination of the potential use of antitumor antibodies as a vehicle for delivering boron-10 to tumors as neutron-capture agents.

Radioactivity was used as the method of choice for the determination of the conjugation efficiency of [<sup>3</sup>H]DBD with purified anti-CEA IgG. (9) Consequently, 1-phenyl-1,2-dicarba clos-dodecaborane(12) was tritiated and converted to [1-<sup>3</sup>H]dodecaborane(12) as described in Figure 1. Two preparations of the tritiated aminophenyl derivative were carried out with <sup>3</sup>H<sub>2</sub>O biological grade, having specific activities of 0.1 and 5.0 Ci/ml. Diazotization of these samples, followed by quantitative azo-coupling to 2-naphthol, provided solutions of the highly colored azo derivative ( $\epsilon_{485} = 1.98 \times 10^4 \text{ M}^{-1}\text{cm}^{-1}$ ), which were simultaneously examined by absorbance measurements and <sup>3</sup>H radioassay.

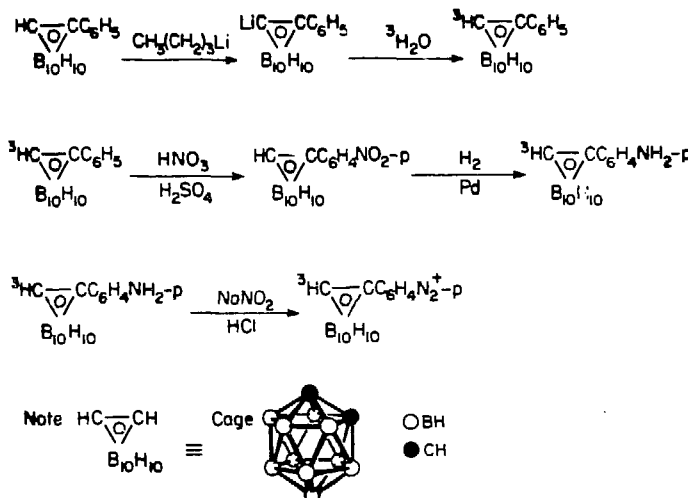


Figure 1.

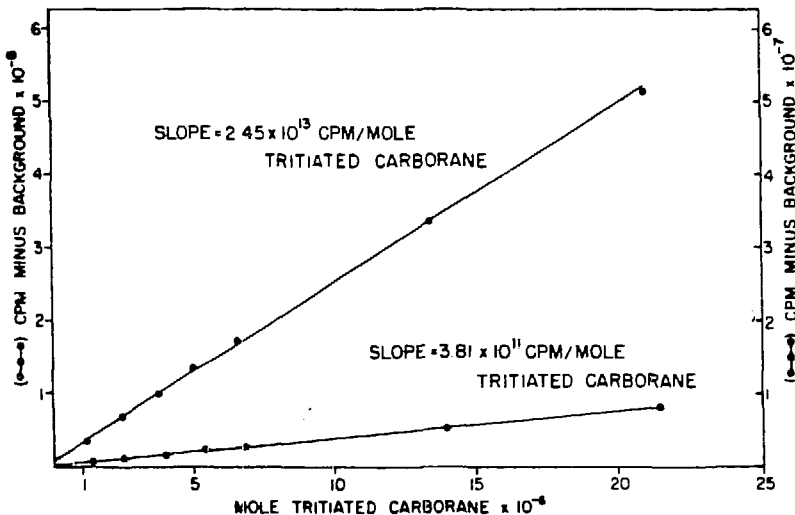


Figure 2. Determination of cpm per mol for two tritiated carborane preparations.

Because one carborane group is present in each molecule of the azo-coupling product, it was possible to determine the cpm of  $^3\text{H}$  per mol of  $[^3\text{H}]$ DBD from least-squares plots of absorbance vs. cpm corrected for the background value (Fig. 2). Values of  $3.81 \times 10^{11}$  and  $2.45 \times 10^{13}$  cpm of  $^3\text{H}$  per

mol of tritiated carborane substituent were obtained. The tritium assayed by this procedure was shown to be associated with only the [<sup>3</sup>H]DBD by comparative thin-layer chromatography of the 2-naphthol azo-coupling product against all possible contaminants. As expected, specific activity was found to be independent of [<sup>3</sup>H]DBD concentration. Therefore, it is only necessary to determine the specific activity of each 2-(*p*-aminophenyl)-1,2-dicarba-clos-[1-<sup>3</sup>H]dodecaborane(12) preparation once from a plot similar to that shown in Figure 2.

Table 1. Effect of [<sup>3</sup>H]DBD-to-antibody protein molar ratio on carborane labeling at pH 6.5 and 7.5

Molar ratio	pH	Carborane cage/antibody molecule <sup>a</sup>	Recovery of antibody protein, %
10:1	6.5	1.6	100
	7.5	2.6	77
20:1	6.5	4.4	82
	7.5	5.9	71
50:1	6.5	5.8	42
	7.5	13.7	33
100:1	6.5	10.8	10
	7.5	12.4	6

<sup>a</sup> mM carborane/mM antibody protein.

The results obtained with conjugation procedures using different molar ratios of [<sup>3</sup>H]DBD to anti-CEA IgG at different pH are given in Table 1. As many as fourteen carborane cages or 140 boron atoms can be covalently attached to each antibody molecule; however, as the number of carborane cages that are bound per antibody molecule increases, so does denaturation of antibody protein. Coupling conditions were also observed to affect the degree of antibody precipitation. Although the number of bonded carborane cages per antibody molecule was greater at pH 7.5 than at pH 6.5, the loss of antibody protein had also increased. Whether the loss of antibody protein was due to denaturation during the labeling procedure or to a decrease in the solubility of the carborane antibody conjugates is unknown.

Anti-CEA IgG was labeled with the [<sup>3</sup>H]DBD of higher specific activity in order to measure the recovery of immunoreactive antibody protein. The anti-CEA IgG was conjugated at pH 6.5 with molar ratios of [<sup>3</sup>H]DBD to antibody of 5:1, 10:1, 20:1, and 30:1. The conjugates obtained had 1.4, 3.6, 5.5, and 7.8 carborane cages per antibody molecule, respectively. There was no significant loss of antibody

protein with a molar ratio of 20:1 or less. The percentage of immunoreactivity with a CEA immunoabsorbent of the four carborane anti-CEA IgG conjugates was similar to that of the control radioiodinated antibody preparation.

Table 2. Immunoreactivity of carborane-conjugated and non-conjugated goat anti-CEA antibody

Sample	Percent of Radioactivity Bound	
	Kynar anti-goat IgG <sup>a</sup>	CEA immunoabsorbent
[ <sup>3</sup> H]DBD-goat anti-CEA	79	80
[ <sup>3</sup> H]DBD-normal goat IgG	79	8
<sup>131</sup> I-goat anti-CEA-[ <sup>3</sup> H]DBD	84	71
<sup>125</sup> I-normal goat IgG-[ <sup>3</sup> H]DBD	86	4
<sup>131</sup> I-goat anti-CEA	87	69
<sup>125</sup> I-normal goat IgG	81	5

<sup>a</sup> Values given for the Kynar assay reflect subtraction of non-specific binding of the samples to Kynar goat anti-rabbit IgG.

Since the *in vivo* distribution of [<sup>3</sup>H]DBD-anti-CEA conjugates could not be monitored by <sup>3</sup>H-activity due to the low specific activity, the [<sup>3</sup>H]DBD-IgG conjugates were radioiodinated. As shown in Table 2, antibody activity as determined by the binding of either the tritium or the iodine isotope to a CEA immunoabsorbent or Kynar donkey anti-goat IgG was similar, indicating that neither the [<sup>3</sup>H]DBD coupling nor the subsequent radioiodination of the conjugates influenced antibody activity.

Hamsters were injected intra musculature in both hind legs with 0.5 mL of a 20% suspension of freshly excised GW-39, a CEA-producing human colonic cancer xenograft (10). After allowing 6 days for tumor growth, the animals were injected inter peritoneal with either a mixture of <sup>131</sup>I-anti-CEA/<sup>125</sup>I-normal IgG or <sup>131</sup>I-anti-CEA antibody-[<sup>3</sup>H]DBD/<sup>125</sup>I-normal IgG[<sup>3</sup>H]DBD. Animals were sacrificed 1, 3 and 7 days post-injection. The tumors and organs were removed and counted for both <sup>131</sup>I and <sup>125</sup>I in a Packard Auto-Gamma Scintillation Spectrometer. Tissue distributions were calculated according to the following formulae: % injected dose per gram tissue = 100(cpm per gram tissue/total cpm injected); tumor/non-tumor ratio = cpm per gram tumor/cpm per gram non-tumor tissue; localization ratio = (cpm anti-CEA antibody per gram/cpm normal IgG per gram)/(cpm antibody injected/cpm normal IgG injected); localization index = localization ratio tumor/localization ratio blood.

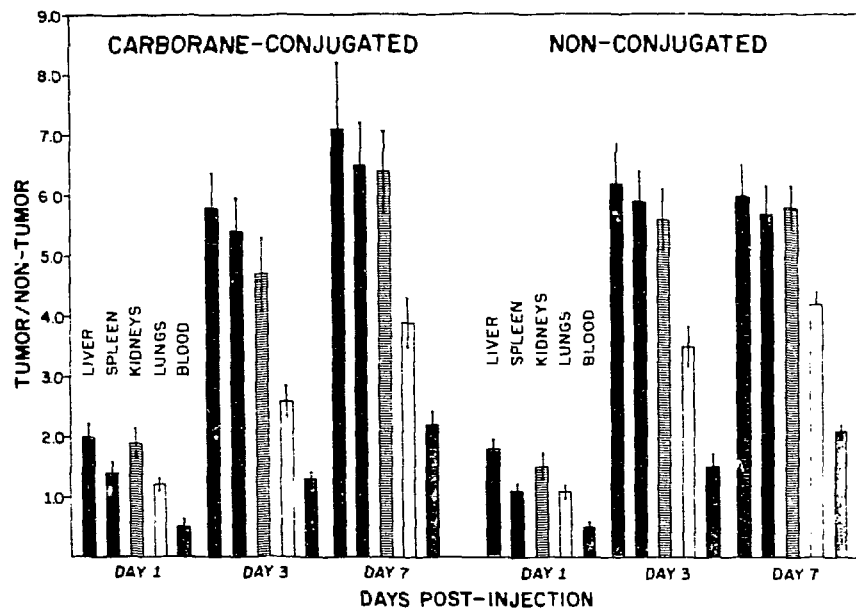


Figure 3. Graphical representation of carborane conjugated and non-conjugated IgG tumor/non-tumor ratios.

Figure 3 shows representative tissue distribution data from 1 of 2 separate *in vivo* localization experiments comparing non-conjugated anti-CEA antibody to carborane-conjugated antibody (carborane:IgG ratio = 3). The data illustrate that conjugation of carborane to the anti-CEA antibody did not appreciably alter the specific tumor localization properties of the antibody, nor was there any significant difference in the antibody distribution in the non-tumor tissues.

The conjugated and non-conjugated antibody as well as the normal IgG were all cleared from the circulation at the same rate (Fig. 4a), but the average percent of the conjugated antibody remaining in the circulation was generally observed to be slightly lower than the non-conjugated antibody. Maximum accretion of the antibody in the tumor was observed at day 3 for both samples (Fig. 4b). The average percent injected dose per gram tumor for the non-conjugated antibody was higher than for the conjugated antibody on day 3, but the difference was not statistically significant ( $p > 0.10$ ). Differences were evident in the amount of normal IgG in the blood and the tumor (Fig. 4a and 4b). Calculation of the localization index, a value that corrects for radioactivity differences in the blood (11), revealed that there was no significant difference between the conjugated and non-conjugated samples ( $5.4 \pm 0.48$  and  $4.9 \pm 0.17$  respectively). This suggests that the major factor contributing to the lower localization ratio of the non-conjugated sample was the slower clearance from the blood of the non-conjugated normal IgG.

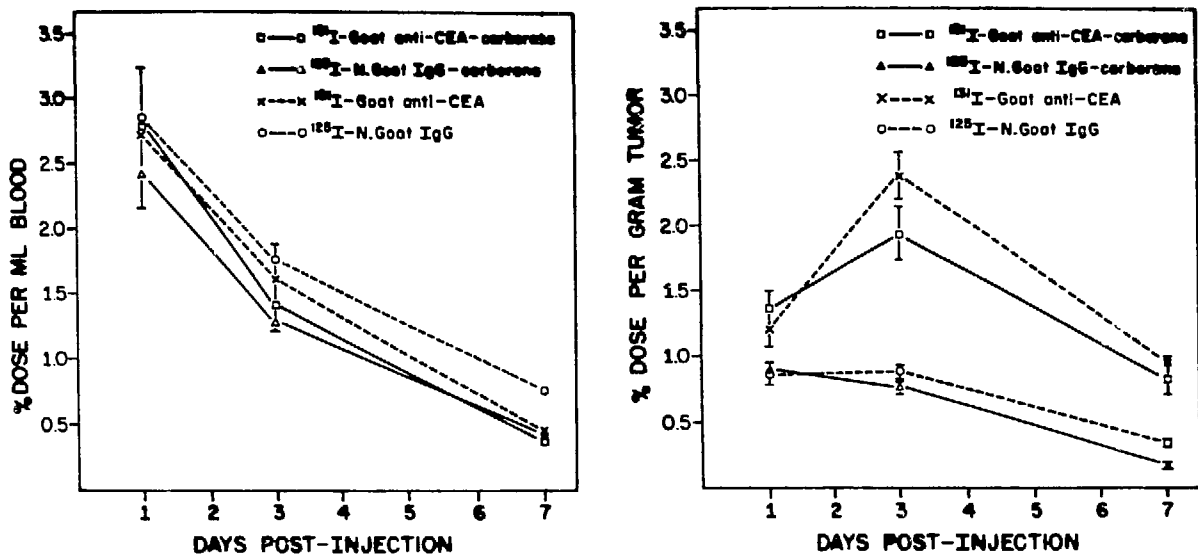


Figure 4. Blood clearance (a) and tumor localization (b) of radioiodinated, carborane-conjugated and non-conjugated goat anti-CEA antibody or normal goat IgG in GW-39 tumor-bearing hamsters. Values represent the means  $\pm$  S.E.; n = 5 animals, 2 tumors per animal.

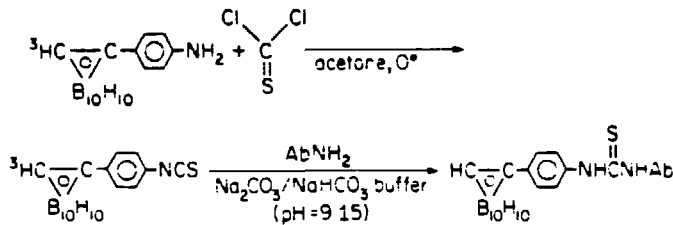
Table 3. In vitro stability of  $^3\text{H}$ -carborane-antibody conjugates

	Affinity Chromatography Percent $^3\text{H}$ -Bound
<u><math>^3\text{H}</math>-carborane-anti-CEA</u>	
Untreated	80.1
24hr/37° C hamster plasma	74.6
<u><math>^3\text{H}</math>-carborane-normal goat IgG</u>	
Untreated	8.1
24hr/37° C hamster plasma	6.2

$^3\text{H}$ -carborane-IgG(100  $\mu\text{l}$ ) was incubated for 24 hr/37° C in 1 ml of 0.01 M PO<sub>4</sub> buffered saline, pH = 7.2 (untreated) or 1 ml of normal hamster plasma. The samples were then passed over a CEA immunoabsorbent and the amount of  $^3\text{H}$ -activity was determined.

The plasma stability of the [<sup>3</sup>H]DBD-anti-CEA antibody was determined by affinity chromatography after incubation of the conjugated antibody in normal hamster plasma for 24 hr at 37° C. Table 3 shows the percentage of [<sup>3</sup>H]DBD-anti-CEA antibody bound to a CEA immunoadsorbent remained the same after incubation in plasma, indicating no loss in the amount of [<sup>3</sup>H]DBD from the coupled antibody.

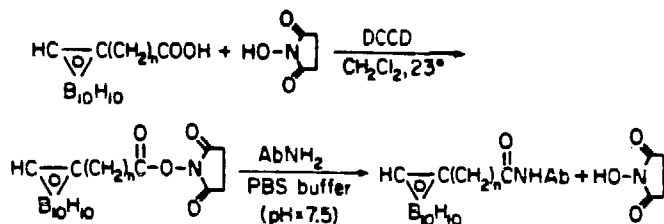
From the foregoing results, it is apparent that the carborane-conjugated anti-CEA antibodies retained immunoreactivity as well as their efficacy for selective accretion in the CEA-containing human colonic tumors, thus supporting the view that boron-10 can be transported to neoplasms selectively by being conjugated to antitumor antibodies. Indeed, the localization ratios and tumor/non-tumor ratios achieved with the boron labeled antibodies were not inferior to those obtained with non-conjugated antibodies to CEA. Nevertheless, it is as yet premature to conclude that the quantity of boron delivered to the tumors is sufficient to achieve their destruction by neutron-capture therapy, despite the fact that up to 30 boron-10 atoms can be conjugated to each antibody IgG molecule. Direct measurements of boron-10 content in the tissues as well as the cytotoxic effects of thermal neutrons are the objectives of current experiments.



note Ab = antibody

Figure 5.

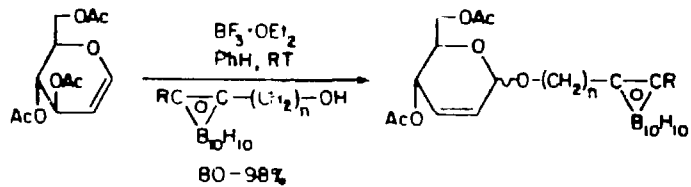
To further investigate the boron labeling of anti-CEA, new boron containing compounds that can be used to conjugate antibodies have been synthesized, including those expected to have enhanced water solubilities. Two compounds that employ different antibody conjugating procedures are the phenylisothiocyanate and N-succinimidyl ester derivatives of 1,2-dicarba-closo-dodecaborane(12). The phenylisothiocyanate derivative reacts with glycine methyl ester hydrochloride in sodium carbonate/bi-carbonate buffer (pH=9.15) and in the same manner can react with antibody primary amino groups to give the corresponding theioureas. (Fig. 5). The N-succinimidyl ester derivative can react with antibody primary amino groups in 0.1M PBS (pH=7.5) (Fig. 6). Boron labeling of antibody using these two reagents is presently being evaluated using anti-human serum albumin(anti-HSA) and HSA immunoadsorbent.



note: DCCD=dicyclohexylcarbodiimide

Figure 6.

The loss of antibody protein during boron-10 labeling may be due to the nature of the coupling procedure or may simply be a direct result of a decrease in solubility. In an effort to maximize boron content of antibody without precipitation, we have attempted to utilize the inherent solubility of carbohydrates to increase the overall solubility of boron-labeled antibody. We envisioned that the attachment of polyhydroxylic appendages to our antibody labeling reagents would allow us to better compromise unfavorable interactions between a relatively hydrophobic carborane cage and the aqueous environment which surrounds the carborane-labeled antibody.



R	n	d / β ratio ( <sup>1</sup> H NMR estimate)
H	1	9.5 : 0.5
H	2	9 : 1
CH <sub>3</sub>	2	9 : 1
H	3	7 : 3
CH <sub>3</sub>	3	7 : 3

Figure 7.

Along these lines, several routes to glycosyl carboranes have been investigated, resulting in the development of two effective methods for the attachment of a carbohydrate molecule to the carborane cage. A  $\text{BF}_3 \cdot \text{OEt}_2$  - catalyzed synthesis of O-glycosyl carboranes has proven to be a fast and efficient means to introduce a carborane moiety to the anomeric center of cyclic carbohydrates. Yields in the range of 60-98% have been routinely recorded in these reactions (Fig.7).

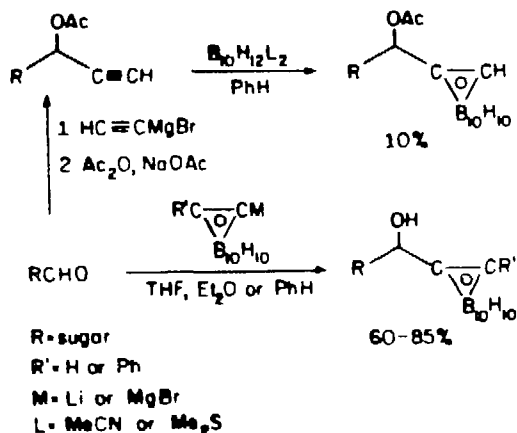


Figure 8.

The cage-forming reactions of acetylenic sugars with bis-ligand adducts of decaborane have also afforded glycosyl carboranes but the yields in these reactions were disappointingly low. Direct hydroxyalkylations of metallated  $\alpha$ -carboranes with aldehydic sugars were therefore studied and subsequently shown to afford the same products but in substantially better yields. Both cyclic and acyclic aldehydic carbohydrates were converted to glycosyl carboranes in yields of 60-85% (Fig. 8).

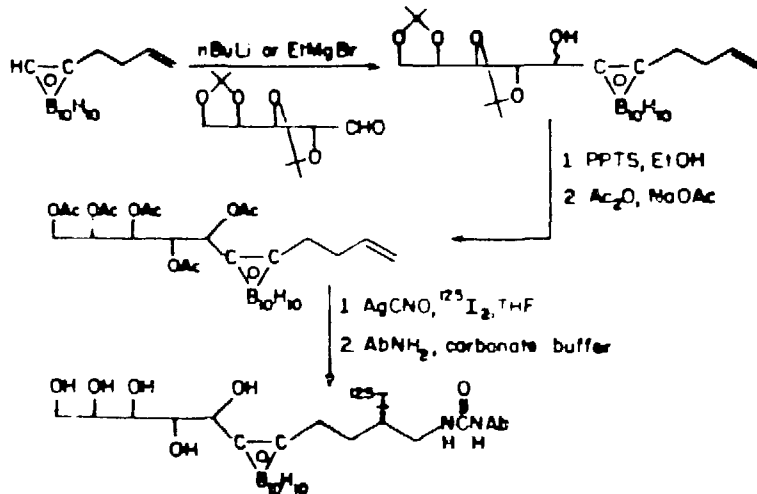


Figure 9.

In an illustrative reaction, the alkylation product shown in Figure 9 was converted to its pentaacetate by an acid hydrolysis of the ketals followed by acetylation with acetic anhydride. By invoking an iodoisocyanation reaction, developed some two decades ago by Hassner and co-

workers(12), this olefin was converted to an isomeric pair of iodoisocyanates, suitable for coupling to IgG through free amino groups on the peptide backbone. With the use of elemental iodine-125, radiolabeled carborane can be covalently attached to antibody and the efficiency of coupling, as well as its distribution in tissue, can be accurately assayed. The results of this study as well as the synthesis of other carbohydrate-modified reagents will be described in detail at a later date.

1. Bale, W.F. (1952) Proc. Natl. Cancer Conf. 2, 967-976.
2. Goldenberg, D.M., Deland, F.H., Kim, E.E., Bennett, S., Primus, F.J., van Nagell, J.R., Jr., Estes, N., Desimone, P. & Rayburn, P. (1978) N. Eng. J. Med. 298, 1384-1388.
3. Goldenberg, D.M., Kim, E.E., Deland, F.H., Bennett, S. & Primus, F.J. (1980) Cancer Res. 40, 2984-2992.
4. Goldenberg, D.M., Kim, E.E., Deland, F.H., Spremulli, E., Nelson, M.O., Gockerman, J.P., Primus, F.J., Corgan, R.L. & Alpert, E. (1980) Cancer 45, 2500-2505.
5. Goldenberg, D.M., Kim, E.E., Deland, F.H., van Nagell, J.R., Jr. & Javadpour, N. (1980) Science 208, 1284-1286.
6. Goldenberg, D.M. & Deland, F.H. (1982) J. Biol. Response Modifiers 1, 121-136.
7. Goldenberg, D.M., Kim, E.E., Bennett, S.J., Nelson, M.O. & Deland, F.H. (1983) Gastroenterol. 84, 524-532.
8. Goldenberg, D.M., Deland, F.H., Bennett, S.J., Primus, F.J., Nelson, M.O., Flanigan, R.C., McRoberts, J.W., Bruce, A.W. & Mahan, D.E. (1983) J. Am. Med. Assoc. 250, 630-635.
9. Mizusawa, E., Dahlman, H.L., Bennett, S.J., Goldenberg, D.M. & Hawthorne M.F. (1982) Proc. Natl. Acad. Sci. USA 79, 3011-3014.
10. Goldenberg, D.M., Witte, S. & Elster, K. (1966) Transplantation 4, 760-763.
11. Moshakis, V., McIlhinney, R.A.J., Raghavan, D. & Neville, A.M. (1981) Br. J. Cancer 44, 91-99.
12. Hassner, A., Lorber, M.E. & Heathcock, C. (1967) J. Org. Chem. 32, 540-549.

B-Decachloro-o-carborane Derivatives as Suitable Boron Carriers for the Preparation of Water-Soluble Boron-Conjugated Macromolecules

Detlef Gabel, Rita Walczyna,\* Folkert Wellmann, Horst Riesenber, and Ingrid Hocke

Department of Chemistry, University of Bremen, Postfach 330 440, D-2800 Bremen 33

The preparation of boron-containing macromolecules, especially immunoglobulins, for boron neutron capture therapy, has so far been rather unsuccessful, because of the increased water insolubility of heavily substituted proteins. For successful use in NCT, proteins would have to be substituted with 5% by weight of boron-10, in order to achieve therapeutically significant dose increases in the target organ.

By using polar boron compounds, some of the difficulties previously encountered (2-4) in the preparation of boron-conjugated immunoglobulins might be overcome. To this end, we have investigated the use of B-decachloro-o-carborane ( $B_{10}Cl_{10}C_2H_2$ ) for the preparation of water-soluble macromolecules.

This compound was first described by Zakharkin et al. (7). It is a strong CH-acid with a  $pK$  value of about 6.5. Its anionic form is easily soluble in water. It has been reported to react as a nucleophile under alkaline conditions. By reaction of the sodium salt of decachlorocarborane in ethanol under reflux, mono- and disubstituted alkyl, allyl, and benzyl derivatives have been obtained after reaction with the appropriate halide (5).

We found that decachlorocarborane reacts in ethanol with alkyl halides other than methyl or ethyl halides only under more extreme conditions. Then, a variety of side reactions might take place, including hydrogen halide elimination, which would lower the yield and complicate the work-up procedure.

The previously described reaction with benzyl bromide could easily be applied to other ring-substituted benzyl bromides (several of which have never been described before). Unless a great excess of the benzyl halide is reacted, only mono-substituted products are formed. The products are in both cases isolated from the reaction mixture after addition of water and acidification.

Interestingly, decachlorocarborane can undergo Michael addition to activated olefins. Under the strongly alkaline conditions used for reaction with alkyl halides, this reaction

---

\*Present Address: Institute of Chemistry, Gdansk University, ul. Sobieskiego, Gdansk, Poland

might occur to some extent or even be the predominant reaction.

Decachlorocarborane reacts very smoothly with epoxides. The products (obtained by nucleophilic attack on the most accessible carbon atom) are formed in good yield and with little contamination by side products. In contrast to the alkyl and benzyl substituted decachlorocarboranes, they can be recovered from the alkaline solution by filtration, as they have a tendency to precipitate without acidification. This might be due to an internal charge delocalization between the non-substituted carbon of the cage and the OH-group on the side chain.

An undesirable reaction apparently occurs between deca-chlorocarborane and sulfochlorides, leading to the corresponding sulfones. These seem to be hydrolytically unstable, so that during the work-up procedure the sulfone is converted to sulfonic acid and decachlorocarborane.

A summary of the compounds prepared is given in Table 1. In some cases, protecting groups had to be used to arrive at the described products. Some of these compounds would have to be activated prior to conjugation.

Problems are encountered in the purification and the characterization of decachlorocarborane-containing compounds.

The decachlorocarborane moiety gives rise to a pronounced tailing of the compounds in normal and reversed-phase chromatography. In reversed-phase chromatography, the adsorption coefficient increased with increasing concentration. It was therefore in general rather difficult to remove unreacted starting material from the desired product.

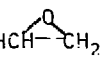
The weight fractions of decachlorocarborane compounds in boron and chlorine make NMR and elemental analyses difficult. Also, for NMR spectroscopy only a few solvents could be employed, as strong hydrogen bonding might be observed (6) with, e.g., dimethyl sulfoxide.

Mass spectroscopy of the compounds yielded an  $M^+$  peak only under very mild ionization conditions. With electron impact ionization, any side chain of the decachlorocarborane cage is split off, and the spectrum is dominated by the fragmentation products of the cage. Because of the natural isotope mixture of both boron and chlorine, characteristic fragmentation products of the side chains cannot be found.

The decachlorocarborane cage is stable in strong acidic solutions and moderately stable in strong alkaline solutions. It is not attacked by hydrogen on palladium or complex hydrides. These properties allow a relatively unrestricted use of protecting groups during synthesis.

The strong electron withdrawing character of the decachlorocarborane cage influences the reactivity of side chains attached to the cage carbon atoms. Thus, allyl-deca-chlorocarborane was not amenable for hydroboration,

Table 1. Decachloro-*o*-carborane (Decloc) Derivatives for Conjugation with Macromolecules

I	DECLOC-CH <sub>2</sub> CH <sub>2</sub> CO <sub>2</sub> H
II	DECLOC-CH <sub>2</sub> CH <sub>2</sub> CN
III	DECLOC-CH <sub>2</sub> CH <sub>2</sub> CH <sub>2</sub> NH <sub>2</sub>
IV	DECLOC-CH <sub>2</sub> -  -CO <sub>2</sub> H
V	DECLOC-CH <sub>2</sub> -  -CN
VI	DECLOC-CH <sub>2</sub> CHOHCH <sub>2</sub> 
VII	DECLOC-CH <sub>2</sub> CHOHCH <sub>2</sub> -O-  -NH <sub>2</sub>
VIII	DECLOC-CH <sub>2</sub> CHOHCH <sub>2</sub> -O-  -NCS
IX	DECLOC-CH <sub>2</sub> CHOHCH <sub>2</sub> OH
X	DECLOC-CH <sub>2</sub> CHOHCH <sub>2</sub> Cl

epoxidation, or halogen hydrin formation. The chlorohydrin (X in Table 1) could not be epoxidized in strongly alkaline solutions. The  $pK_a$ -value of the acid (I) is lowered to about 3.5.

The anionic form of the decachlorocarboranyl moiety of several of the compounds in Table 1 was found to interact strongly with positively charged compounds. Thus, an aqueous solution of compound I yielded a precipitate when added to a solution of 1-(3-diethylaminopropyl)-3-ethyl carbodiimide at pH 8.0. Compound X co-precipitated with poly-DL-lysine when mixed at pH 10.0.

Some of the compounds of Table 1 were conjugated to proteins and other macromolecules. When using high protein concentrations (10 mg/ml and higher), incorporation of compounds VI, VII, and VIII led to water soluble protein conjugates with up to 7% boron by weight. With lower protein concentrations, we usually obtained a lower boron content. With increasing amounts of boron compounds added, protein yields decreased, probably because of adsorption on the solid boron compound.

Anti-(human-IgM) antibodies from goat were borated with compound VI and subjected to affinity chromatography on IgM-Sepharose. Inactive protein (already present in the commercial starting preparation) was eluted first, whereas active material was retained and could subsequently be eluted with ammonium thiocyanate. The active protein was found to contain 2.5% boron by weight, corresponding to ~400 boron atoms per IgG molecule.

#### ACKNOWLEDGMENTS

This work was financially supported by the Deutsche Forschungsgemeinschaft, the Fonds der Chemischen Industrie, and the Otto Roehm Gedächtnisstiftung.

#### REFERENCES

1. D. Gabel and R. Walczyna (1982) Z. Naturforsch. 37c, 1038-1039.
2. M.F. Hawthorne, R. Wiersema, and M. Tagasuki (1972) J. Med. Chem. 15, 449-452.
3. E. Mizusawa, H.L. Dahlman, S.J. Bennett, D.M. Goldenberg, and M.F. Hawthorne (1982) Proc. Natl. Acad. Sci. U.S.A. 79, 3011-3014.
4. H.S. Wong, E.I. Tolpin, and W.N. Lipscomb (1974) J. Med. Chem. 17, 785-791.
5. L.I. Zakharkin and N.A. Ogorodnikova (1966) Bull. Acad. Sci. USSR, Div. Chem. Sci. 314-316.
6. L.I. Zakharkin and N.A. Ogorodnikova (1968) J. Organomet. Chem. 12, 13-22.
7. L.I. Zakharkin, V.I. Stanko, and A.I. Klimova (1964) Bull. Acad. Sci. USSR, Div. Chem. Sci. 314-317.

## Boronation of Polyclonal and Monoclonal Antibodies for Neutron Capture

Fazlul Alam, Albert H. Soloway, Rolf F. Barth, Carol W. Johnson, Walter E. Carey  
College of Pharmacy, Departments of Pathology and Nuclear Engineering,  
The Ohio State University, Columbus, Ohio 43210  
and  
Walter H. Knoth  
Central Research Department, Experimental Station,  
E.I. du Pont de Nemours and Company, Wilmington, Delaware 19898

### ABSTRACT

This study describes the synthesis of some derivatives of the closo-dodecahydrododecaborate anion ( $B_{12}H_{12}^{2-}$ ) that contain protein-binding groups and the linkage of such compounds to polyclonal antibodies directed against human thymocytes and monoclonal antibodies reactive with tumor-associated antigens. The protein-binding functions incorporated into these boron-containing compounds include the isocyanate, sulphydryl, carboxyl and N-hydroxysuccinimide ester groups. Using compounds containing single dodecaborate cages, more than  $10^3$  boron atoms have been incorporated per antibody molecule without causing antibody precipitation. However, antibodies boronated by this method exhibited marked decrease in their ability to bind to target cells. More than 80 sites on each antibody molecule had to be modified to incorporate  $10^3$  boron atoms by this method. To address this problem, and yet attain a high degree of boronation required to make this approach practical for BNCT, water-soluble macromolecules containing approximately 28% by weight boron, and up to 1500 boron atoms per molecule, were prepared by covalently linking  $B_{12}$  cages to  $\epsilon$ -NH<sub>2</sub> groups on poly-DL-lysine, but attempts to link these boronated macromolecules to the polyclonally derived antithymocyte globulin (ATG, The Upjohn Company) resulted in the precipitation of the antibody.

As an alternate approach, ATG boronated with  $B_{12}H_{11}NCO^{2-}$ , containing  $>10^3$  boron atoms per antibody molecule (and found to be drastically reduced in activity), was crosslinked to fresh ATG with glutaraldehyde.

As a next step, we decided to boronate a secondary protein with a protein-binding polyhedral borane instead of boronating the antibody directly, and then to link the boronated secondary protein to the antibody. For this purpose, BSA was exhaustively boronated with  $B_{12}H_{11}NCO^{2-}$  and the boronated BSA then crosslinked with the photosensitive heterobifunctional reagent N-hydroxysuccinimidyl-4-azidobenzoate (HSAB); preliminary results indicate that roughly 1400 boron atoms were conjugated per antibody molecule. Use of this heterobifunctional reagent enabled greater control over the crosslinking procedure than possible with glutaraldehyde, and simplified subsequent separation steps.

Biological studies with these boronated antibodies are being reported separately. Our current efforts are being focused on the preparation of macromolecules with higher boron content and optimizing the crosslinking of the boronated macromolecule to the antibody so as to achieve the highest number of boron atoms conjugated per antibody molecule with minimal loss of antibody affinity.

Boron neutron capture therapy (BNCT) for the treatment of cancer depends on the selective localization of boron-10 atoms on tumor cells. We are investigating the use of boron-loaded antibodies to tumor-associated antigens as the means for achieving that selective localization. The most attractive feature of this approach for BNCT is the possibility of attaining a high ratio of boron concentration in tumor (T) to that in blood (B). It has been shown by Zamenhof, Brownell and Tolpin (1) that the advantage depth and the selective radiation damage to neoplastic tissue by BNCT are very dependent on the T/B ratio. Calculations by Wellum, Zamenhof and Tolpin (2) indicate that boronated antibodies having a high antibody-antigen association constant would nearly saturate available antigen sites while yielding an optimally low blood boron concentration of 0.1 to 0.5  $\mu\text{g}^{10}\text{B/g}$  blood. At useful tumor boron concentrations ( $\text{T} > 10 \mu\text{g}^{10}\text{B/g tumor}$ ), a T/B ratio of up to 100 or more is theoretically achievable.

However, there are serious difficulties with this approach to BNCT, as outlined by Wellum, Zamenhof and Tolpin (2). A critical factor is the sheer number of boron atoms that must be delivered by antibody molecules to limited receptor sites on target cells (3). At a thermal neutron fluence of  $2.7 \times 10^{12}$  neutrons/cm<sup>2</sup>, which may be higher than the actual fluence deliverable at tumor sites,  $10^8$  boron-10 atoms will be required statistically in order to produce a single capture event. Therefore, for therapy to be effective, it is necessary that of the order of  $10^9$  boron-10 atoms be delivered to each tumor cell (which would be approximately  $20 \mu\text{g}^{10}\text{B/g tumor}$ ) for its destruction. With antigen site densities between  $10^5$  and  $10^6$  per tumor cell surface, roughly  $10^3$ - $10^4$   $^{10}\text{B}$  atoms per antibody molecule is necessary if this approach is to be practicable.

To determine if the use of boron-loaded antibody for BNCT would be at all feasible, our first goal is to demonstrate that adequate numbers of boron atoms could be delivered to target cells. For this purpose, in vitro studies with boronated antibodies were carried out in an attempt to produce a cytotoxic effect by neutron capture irradiation. We used two antibodies for these in vitro experiments. One is the polyclonally derived anti-thymocyte globulin (ATG) from the Upjohn Company, Kalamazoo, MI, and the other is the monoclonal antibody 17-1A directed against colorectal carcinoma (4) provided kindly by Dr. Zenon Steplewski of the Wistar Institute, Philadelphia, PA.

We have primarily used three protein-binding derivatives of the closo-dodecahydrododecaborate anion ( $\text{B}_{12}\text{H}_{12}^{2-}$ ) as boronating agents. Dicesium mercaptoundecahydro-closo-dodecaborate (5) ( $\text{Cs}_2\text{B}_{12}\text{H}_{11}\text{SH}$ ) was provided by Dr. G.R. Wellum of New England Nuclear Corporation, Billerica, MA, and radiolabeled with tritium at New England Nuclear by the Wilzbach method (6). This compound is of particular interest because it has been used in BNCT as the boron-10 enriched sodium salt, to treat cerebral glioma patients by Hatanaka with encouraging results (7). Dr. Hatanaka has recently provided us with a quantity of the boron-10 enriched material. The mechanism by which this particular anionic polyhedral borane localizes in tumor long enough to permit neutron irradiation is not yet clear. Nevertheless, it is distinctly different from the unsubstituted  $\text{B}_{12}\text{H}_{12}^{2-}$ , which does not exhibit such tumor localization. An early study by Soloway, Hatanaka and Davis (8) found that both  $\text{B}_{12}\text{H}_{11}\text{SH}^{2-}$  and the unsubstituted  $\text{B}_{12}\text{H}_{12}^{2-}$  are strongly bound to bovine serum albumin and remained bound even after exten-

sive dialysis. Only  $B_{12}H_{12}^{2-}$  was totally removed from the protein by passage through anion exchange resin. They suggested that  $B_{12}H_{11}SH^{2-}$  was probably covalently bound to the protein by the disulfide linkage. A later, more elaborate study by Nakagawa and Nagai (9) determined that the binding of  $B_{12}H_{12}^{2-}$  was solely ionic, while  $B_{12}H_{11}SH^{2-}$  was in part bound covalently. A disulfide linkage between the boron cage and BSA was proposed as suggested earlier (8). However, Nakagawa and Nagai stated in their report (9) that much of the data reported obtained were at best semiquantitative due in part to the boron analysis. In our experiments, we found that the reaction of ATG with a 100 to 300-fold molar excess of tritium-labeled  $B_{12}H_{11}SH^{2-}$  resulted in the incorporation of between 8 and 13 boron cages (96 to 156 boron atoms) per molecule of ATG. The boronated ATG was purified by sequential passage through Sephadex G-25 columns and the level of boron incorporation calculated from tritium activity and protein concentration assay (Bio-Rad Laboratories, Richmond, CA). Even after 1 month storage at 4°C, there was negligible loss (<2%) of  $B_{12}H_{11}SH^{2-}$  from the protein on gel filtration or  $(NH_4)_2SO_4$  precipitation, indicating the stability of the conjugation.

For comparison, a sample of  $Na_2B_{12}H_{12}$  was labeled with tritium under identical conditions. Surprisingly, a 150-fold higher specific tritium activity was obtained compared to the  $Cs_2B_{12}H_{11}SH$  sample. The reaction of the tritiated  $B_{12}H_{12}^{2-}$  with ATG resulted in the incorporation of only approximately 1.5 cage per ATG molecule, probably as a result of 'ionic binding'.

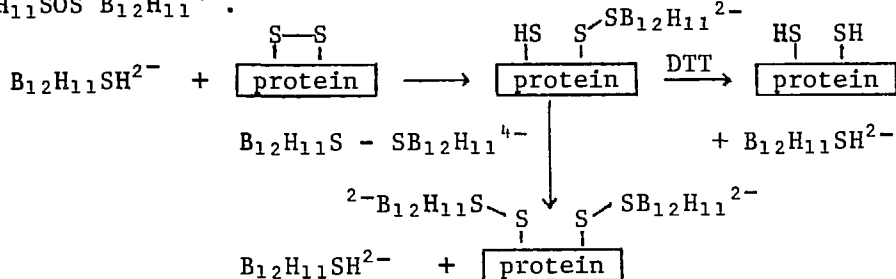
It does appear that  $B_{12}H_{11}SH^{2-}$  may indeed bind to proteins in the vascular supply or on the surface of the tumor cells. Such boronated proteins may be incorporated into the neoplasm via a pinocytotic mechanism and thereby a more selective localization is achieved.

These results are in agreement with the earlier reports (8,9) regarding the difference in protein-binding characteristics of  $B_{12}H_{12}^{2-}$  and  $B_{12}H_{11}SH^{2-}$ . The next step has been to provide confirmational evidence of a disulfide linkage in the binding of  $B_{12}H_{11}SH^{2-}$  to the gamma globulin. ATG boronated with  $B_{12}H_{11}SH^{2-}$  was treated with excess dithiothreitol (DTT), a bis-sulfhydryl compound used to reduce disulfide bonds. Within 24 hours at 4°C, roughly 80% of  $B_{12}H_{11}SH^{2-}$  was lost from the ATG, indicating that, indeed, most of the  $B_{12}H_{11}SH^{2-}$  binds to the protein by disulfide links.

The tritium-labeled  $B_{12}H_{11}SH^{2-}$  was recrystallized to constant specific activity before reacting with ATG. However, there are high-activity impurities, probably produced during tritiation, that co-crystallize with this salt; some of these are of sufficient size so that they appear in the void volume on gel filtration through Sephadex G-25 columns. A blank correction must be used in measuring the  $^3H$  activity of purified protein fractions in order to determine the number of  $B_{12}H_{11}SH^{2-}$  cages conjugated per molecule of antibody.

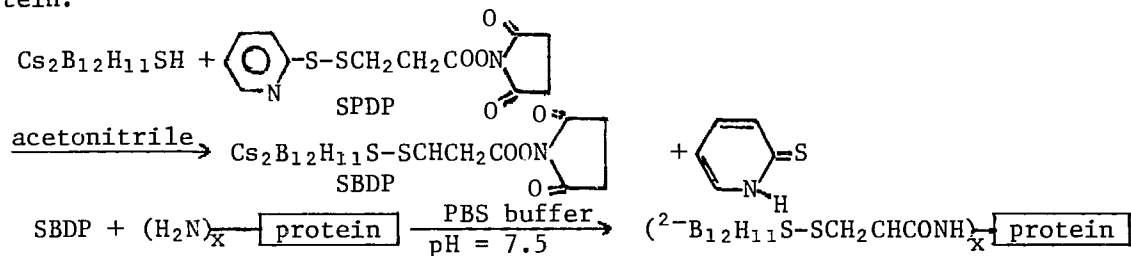
From reports that  $B_{12}H_{11}SH^{2-}$  appears to undergo change in the presence of oxygen, it is conceivable that oxidation products of  $B_{12}H_{11}SH^{2-}$  may be partially responsible for the incorporation of these anions into proteins (9). A likely oxidation product of  $B_{12}H_{11}SH^{2-}$  is  $\mu$ -disulfido-bis(undeca-hydro-closo-dodecaborate),  $B_{12}H_{11}S - SB_{12}H_{11}^{4-}$ . The tritium-labeled cesium salt of this anion was prepared by the oxidation of tritiated  $Cs_2B_{12}H_{11}SH$  with sodium iodosobenzoate (10). However, this anion did not significantly boronate ATG under conditions similar to those used for the boronation with  $B_{12}H_{11}SH^{2-}$ . It is possible that when it is present as an impurity in

$B_{12}H_{11}SH^{2-}$ , it may contribute substantially to the boronation as shown in the equations below. Other oxidation products of  $B_{12}H_{11}SH^{2-}$  are indeed possible boronating species which should be considered, including  $B_{12}H_{11}SOS B_{12}H_{11}^{4-}$ .



While the interaction of  $B_{12}H_{11}SH^{2-}$  with ATG provided some more insight into the nature of its binding with proteins and the mechanism by which it may localize in tumor cells, the level of boron incorporation (8-13 cages) into the antibody was not sufficient to pursue this method for the boronation of antibodies for BNCT.

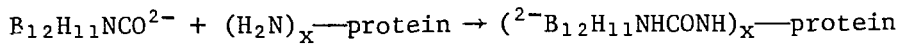
The next derivative of  $B_{12}H_{12}^{2-}$  that we studied for boronating antibodies is a novel heterobifunctional boronating agent that was prepared by the reaction of N-succinimidyl-3-(2-pyridyldithio)propionate (SPDP; Pharmacia Fine Chemicals, Piscataway, NJ) with  $Cs_2B_{12}H_{11}SH$  in dry acetonitrile (11). This reagent, N-succinimidyl-3-(undecahydro-closo-dodecaboranyldithio)propionate (SBDP in short) contains an active ester end group, which reacts rapidly with amino groups on proteins in aqueous buffers under very mild conditions, producing covalent linkage of the  $B_{12}$  cage to the protein.



The hydrolysis half-life of SBDP is 2-3 hours at room temperature and pH 7. Up to 20mM concentration of this reagent at 1300:1 molar ratio has been used with antibodies without causing antibody precipitation. The reaction of SBDP with ATG at 200:1 molar ratio for one hour at room temperature followed by continued reaction overnight at 4°C resulted in the incorporation of  $4.8 \times 10^2$  boron atoms per antibody molecule. A similar reaction of  $^{10}B$ -enriched SBDP with monoclonal antibody 17-1A at a mol ratio of 1300:1 resulted in the incorporation of  $1.3 \times 10^3$  boron-10 atoms per antibody molecule. Rather surprisingly, these heavily boronated antibodies still exhibited considerable, though reduced, binding to target cells. While this boronating agent appears to be a very convenient and suitable reagent for boronating antibodies for in vitro experiments, a disulfide linkage to the  $B_{12}$  cage makes such boronated antibodies susceptible to deboronation by in vivo disulfide cleavage. This could arise from the reaction of sulfhydryl groups in blood proteins or other sulfhydryl-containing biochemicals.

With these non-tritiated boron compounds, the boron contents of boronated antibodies were determined by prompt- $\gamma$  method (12). These analyses were carried out at the Brookhaven National Laboratory by Dr. R. G. Fairchild.

The third protein-binding polyhedral borane used in our studies, isocyanatoundecahydro-closo-dodecaborate ( $B_{12}H_{11}NCO^{2-}$ ) (13), was prepared by the action of  $NaN_3$  on monocarbonylundecahydro-closo-dodecaborate ( $B_{12}H_{11}CO^-$ ) in acetonitrile (14). This reagent reacts readily with primary amines resulting in spontaneous urea linkage.



The reaction of  $B_{12}H_{11}NCO^{2-}$  with ATG at more than 2000:1 mol ratio for one hour at room temperature followed by 3 days at  $4^\circ C$ , in PBS buffer at pH  $\sim 7.5$ , resulted in the incorporation of approximately 40 cages or 480 boron atoms per ATG molecule. Reaction at pH = 9 for a longer period increased the level of boron incorporation to  $1.1 \times 10^3$  boron atoms per ATG molecule. However, the antibody lost its activity in the process. In a similar experiment, the lectin Con-A was boronated to roughly 7% by weight boron with  $B_{12}H_{11}NCO^{2-}$ , but the lectin also lost its ability to bind to target cells. The levels of boron incorporated into antibody molecules with the three protein-binding polyhedral boranes,  $B_{12}H_{11}SH^{2-}$ , SBDP and  $B_{12}H_{11}NCO^{2-}$ , are listed in table I.

TABLE I. Summary of Boron-incorporation Into Antibodies

Antibody (A)	Boronating Agent (B)	Reaction mol ratio A:B	Analysis of purified boronated antibody		
			Protein concen- tration (mg/ml)	Boron concen- tration ( $\mu$ gB/ml)	Number of boron atoms per anti- body molecule
ATG	$B_{12}H_{11}SH^{2-}$	1:300	5.3	55	$1.5 \times 10^2$
ATG	SBDP	1:200	3.3	105	$4.8 \times 10^2$
ATG	$B_{12}H_{11}NCO^{2-}$	1:2000	3.0	218	$1.1 \times 10^3$
Monoclonal 17-1A	SBDP	1:1300	2.2	202	$1.3 \times 10^3$

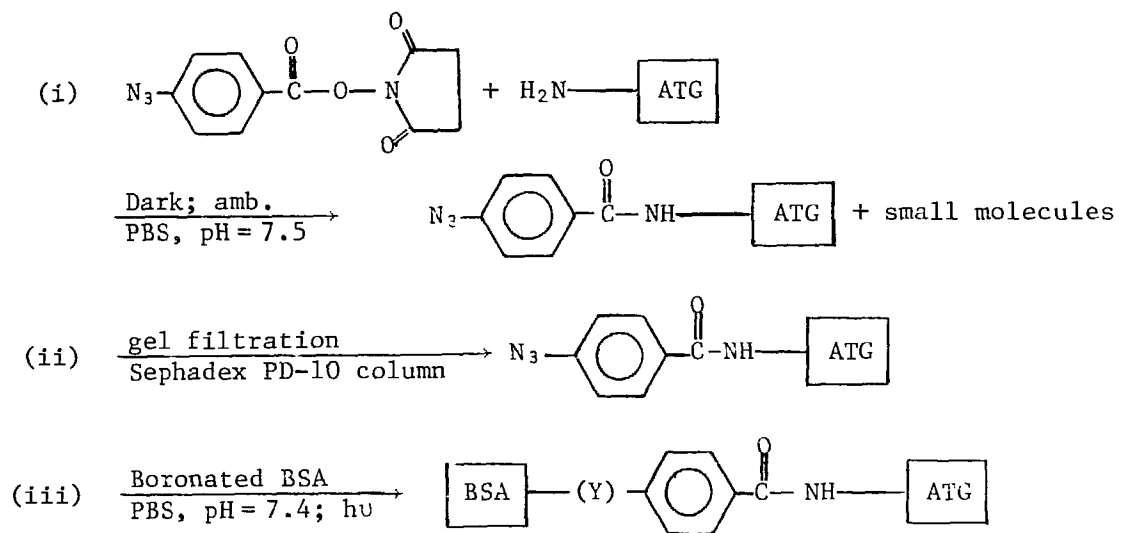
Both SBDP and  $B_{12}H_{11}NCO^{2-}$  appear to fulfill one of our objectives, namely, the incorporation of  $10^3$ - $10^4$  boron atoms per antibody molecule. However, with this method, many single  $B_{12}$  cages are attached to each antibody resulting in a considerable loss in the **affinity** of the antibody. In order to incorporate  $10^3$  boron atoms into an antibody molecule by this method, modification of more than 80 sites on the protein was necessary. Such an extensive number of sites prompted our efforts to prepare macromolecules containing  $\sim 10^3$  boron atoms, which could then be linked at one or several points on the antibody. The rationale is that, by chemically altering only a few sites on the antibody, there may be a minimum loss of antibody **activity**. There are other very significant advantages of this method. The number of boron atoms that may be linked by this method could easily reach  $10^4$  or higher. Since only a few discrete units, say with a 50,000 Dalton molecular weight, would be linked by

this method, inhomogeneity introduced into a monoclonal antibody (MCA) by the boronation process would be considerably reduced. Importantly as well, separation of non-boronated antibody molecules from the product mixture should be possible by gel filtration. The presence of non-boronated antibody or antibody containing few boron atoms in the boronated antibody preparation, may considerably reduce the effectiveness of this approach to BNCT, since these same molecules may bind to antigen sites on tumor cells preferentially over the heavily boronated antibody molecules.

For this purpose, water-soluble macromolecules containing 28% by weight boron and up to 1500 boron atoms were prepared by reacting  $B_{12}H_{11}NCO^{2-}$  with poly-DL-lysine. But in attaching such macromolecules to ATG, immediate precipitation occurred. However, boronation of ATG with  $B_{12}H_{11}NCO^{2-}$  had already been accomplished yielding  $1.1 \times 10^3$  boron atoms per molecule. To this inactive boronated species, fresh ATG was added and both proteins were then cross-linked with glutaraldehyde. Support for this approach stems from the work of Poznansky and Bhardwaj (15) who were able to crosslink an albumin- $\alpha$ -1,4-glucosidase polymer to antibody molecules raised against isolated rat hepatocytes via glutaraldehyde as the crosslinking agent. They found that the antibody conjugated with the albumin-enzyme polymer of roughly 300,000 Daltons achieved the same differential localization on hepatocytes as the unconjugated antibody. If a similar polymer containing 10% by weight boron were linked to an antibody, the result would be incorporation of 3000 boron atoms per antibody molecule. However, in our experiment, glutaraldehyde caused extensive precipitation of ATG. This crosslinking procedure is being modified to prevent such antibody precipitation.

As a logical extension, we decided to boronate a secondary protein with the protein-binding polyedral boranes instead of directly boronating the antibody itself. Crosslinking the boronated secondary protein to the antibody is the next step. We chose the readily available BSA as the secondary protein and boronated it with a large excess of  $B_{12}H_{11}NCO^{2-}$ . Approximately 4.2% by weight of boron was incorporated into BSA. To crosslink the boronated BSA to ATG, we decided on a more selective reagent than glutaraldehyde, namely, N-hydroxysuccinimidyl-4-azidobenzoate (HSAB), a photosensitive heterobifunctional reagent (16) (obtained from Pierce Chemical Company, Rockford, IL). It contains an N-hydroxysuccinimide active ester group at one end and an aromatic azide group at the other end. The product can be photoactivated to give a nitrene capable of reacting with  $NH_2$ ,  $OH$  and  $CH$  bonds on proteins.

Conjugation of boronated BSA to antithymocyte globulin was achieved stepwise. The antibody was first reacted with HSAB at 1:50 molar ratio for 30 minutes in a dark room with only a dim red light on, and then gel filtered through a Sephadex PD-10 column (Pharmacia Fine Chemicals, Piscataway, NJ). Excess HSAB was thereby removed. The boronated BSA was then added to the ATG solution and the light turned on for 30 minutes. After that period, the solution was stored for 5 hours at  $4^\circ C$ . This mixture was gel filtered through a Sephadex G-150 column to remove unbound BSA. Preliminary indications are that approximately  $1.4 \times 10^3$  boron atoms were incorporated per molecule of ATG. There was no significant loss of the ability of conjugated ATG to bind the target cell as determined by immunofluorescent assay. These preliminary results need to be confirmed by further purification and analysis of the conjugated antibody.



The advantages of using a heterobifunctional reagent to crosslink a boronated macromolecule to an antibody in a stepwise reaction are rather obvious. The particular scheme outlined above was designed to prevent crosslink of boronated BSA to another boronated BSA molecule; such a crosslink would occur if glutaraldehyde were used as the **crosslinking reagent**, and that would make it very difficult to separate unbound BSA from the antibody. Crosslinking of one antibody molecule to another is minimized by having an excess of the boronated BSA in the actual crosslinking step. Since excess of the crosslinking reagent was removed prior to that step by gel filtration, the possibility of forming extensive crosslinks to give aggregates (resulting in the precipitation of the antibody that was observed when glutaraldehyde was used as the crosslinking reagent) was avoided.

Work is currently underway to prepare secondary macromolecules of higher boron content that can be crosslinked to antibody molecules without causing antibody precipitation. The goal is to optimize the crosslinking procedure and subsequent purification of the conjugated antibody.

In conclusion, we have demonstrated that  $>10^3$  boron atoms can be incorporated per antibody molecule, in both polyclonal ATG as well as monoclonal 17-1A without a loss in aqueous solubility. Our results indicate that boronation of antibodies to that level using compounds containing single  $B_{12}$  cages can lead to a drastic reduction in antibody activity. Preliminary results suggest that it may be possible to overcome this problem by boronating a secondary macromolecule first and then crosslinking the boronated secondary macromolecule at a few points on the antibody molecule. In vitro biological studies have been carried out with these boronated antibody preparations and will be reported separately (17). Further in vitro and in vivo studies are clearly warranted in order to demonstrate the potential of these compounds for NCT.

#### ACKNOWLEDGMENTS

This work was supported in part by Department of Energy Contract DE-AC0282-ER 60040 and a grant PDT-197 from the American Cancer Society. We are grateful to Dr. R.G. Fairchild of Brookhaven National Laboratory, Upton, NY for providing prompt- $\gamma$  boron analysis, to Dr. G.R. Wellum of New England Nuclear Corporation, Billerica, MA for supplying dicesium mercaptoundecahydro-closo-dodecaborate and to Dr. H. Hatanaka of Teikyo University, Tokyo, Japan for supplying  $^{10}\text{B}$ -enriched dicesium mercaptoundecahydro-closo-dodecaborate. We thank Dr. Zenon Steplewski of the Wistar Institute, Philadelphia, PA for supplying the monoclonal antibody 17-1A and the Upjohn Company, Kalamazoo, MI for supplying antithymocyte globulin.

#### REFERENCES

1. R.G. Zamenhof, B.W. Murray, G.L. Brownell, G.R. Wellum and E.I. Tolpin, *Med. Phys.* 2:47, 1975.
2. G.R. Wellum, R.G. Zamenhof and E.I. Tolpin, *Int. J. Rad. Oncol. Biol. Phys.* 8:1339, 1982.
3. E.I. Tolpin, G.R. Wellum, F.C. Dohan, Jr., P.L. Kornblith and R.G. Zamenhof, *Oncology* 32:223, 1975.
4. Z. Steplewski and H. Kaprowski, *Anti-colorectal carcinoma monoclonal antibodies*. In *Hybridomas in Cancer Diagnosis and Treatment*. Ed. Mitchell and Oeltgen. Raven Press. New York 1983, pp. 207-211.
5. W.H. Knoth, J.C. Sauer, H.C. Miller and E.L. Muettterties, *J. Am. Chem. Soc.* 86:3973, 1964.
6. New England Nuclear catalog (1983) p. 8.
7. H. Hatanaka, K. Amano, S. Kamano, F. Tovarys, N. Machiyama, T. Matsui, H. Fankhauser, T. Hanamura, T. Nukada, T. Kurihara, N. Ito and K. Sano, Boron-neutron capture therapy vs. photon beam for malignant brain tumors - 12 hrs' experience. *Mod. Neurosurg.* 1:1981 (In press).
8. A.H. Soloway, H. Hatanaka and M.A. Davis, *J. Med. Chem.* 10:714, 1967.
9. T. Nakagawa and T. Nagai, *Chem. Pharm. Bull.* 24:2934, 1976.
10. G.R. Wellum, E.I. Tolpin, A.H. Soloway and A. Kaczmarczyk, *Inorg. Chem.* 16:2120, 1977.
11. F. Alam, A.H. Soloway, J.E. McGuire, R.F. Barth and W.E. Carey, Submitted.
12. R.G. Fairchild *et al.*, See paper I-13 in this Symposium.
13. F. Alam, A.H. Soloway, R.F. Barth, W.E. Carey and W.H. Knoth, in preparation.
14. W.H. Knoth, J.C. Sauer, J.H. Balthis, H.C. Miller and E.L. Muettterties, *J. Am. Chem. Soc.* 89:4842, 1967.
15. M.J. Poznansky and D. Bhardwaj, *Biochem. J.* 196:89, 1981.
16. R.E. Galardy, L.C. Craig, J.D. Jamieson and M.P. Printz, *J. Biol. Chem.* 249:3510, 1974.
17. R.F. Barth, A.H. Soloway, F. Alam, W.E. Carey, C. Andrews, B. Holman, C.W. Johnson, J. Mohammed, J. Talnagi, Jr., and Z. Steplewski, See paper VI-7 in this Symposium.

Wuf

## Coupling of Dextrans Conjugated with Boron to Gamma Globulin: A Model for NCT\*

J.J. Elmore, Jr., D.C. Borg, P. Micca and D. Gabel<sup>†</sup>

Medical Department, Brookhaven National Laboratory, Upton, N.Y. 11973 and

<sup>†</sup>Department of Chemistry, University of Bremen, Bremen, F.R.G.

This is a report on the progress of our research grant entitled "Boronated Dextran-Antibody Conjugates for Neutron Capture Therapy", on which we have been working since this past May. The rationale for our project is to meet more effectively the well-known primary requirement for treatment with boron-10 neutron capture therapy (NCT): namely, the selective localization of a sufficient amount of boron in or on cancer cells or other target cells. As is evident from earlier presentations, this is needed to ensure that the boron-10-enhanced radiation damage in the target tissue exceeds by a sufficient amount the combined effect on normal tissues of residual boron-10-dependent irradiation plus contaminating background radiation.

Monoclonal antibodies (MCA) to tumor-associated antigens are attractive targeting carriers for boron-10 in terms of the needed selective localization, as several previous papers have emphasized. However, to many investigators in this field, the densities of surface receptors on tumor cells have seemed marginal or deficient to achieve successful NCT. If one seeks the necessary radiotherapeutic ratios by increasing the numbers of boron atoms or carborane cages bound per MCA, then inactivation of the antibody can occur through loss of receptor specificity or avidity and/or by precipitation of the protein, as Hawthorne has pointed out (1).

Fairchild has calculated that for effective tumor therapy by boron neutron capture, the therapeutic gain or "advantage factor" should be at least 1.2 (2). Assuming a uniform distribution of boron-10 within the target and access to an epithermal neutron beam, such as we have at Brookhaven, a range of 14-17 micrograms of boron-10 per gram of target tissue (i.e., ppm) will be required, depending upon the relative uptake of boron by target and normal tissues and upon whether tissue repair is included or not (Table 1). If a scandium-filtered neutron beam is used, only about 1-3 ppm of boron-10 will be needed (Table 1).

On the other hand, most monoclonal antibodies bind to antigenic determinants on the cell surface, and in the absence of information to the contrary, it would be conservative to assume that there is no subsequent internalization by cells. Kobayashi and Kanda (3) and a preliminary evaluation by Gabel have shown that if boron remains on the cell surface, geometric factors reduce its efficacy by approximately three times over that expected from homogeneous distribution. Accounting for this leaves us the goal of reaching about 30-45 ppm of boron-10 for epithermal NCT or only 2-8 ppm if a scandium-filtered beam is available (Table 1).

To achieve the goals calculated by Fairchild while overcoming the limitations of antibody binding capacity, we have elected to use water-soluble dextrans as intermediate carriers. This permits each MCA molecule to target many atoms of boron-10 to the specified antigenic receptors while only 5 to 10 of the amino acid residues of the protein are conjugated by dextrans carrying boron-10. As a result, there should be little of the loss of receptor

\*This work was supported by PHS Grant No. CA32920, awarded by the National Cancer Institute, DHHS.

Table 1. Concentrations of Boron-10 Required in Target Tissues for Neutron Capture Therapy Compared with Concentrations Delivered by Boronated Dextran-Monoclonal Antibody Conjugates

CONDITIONS				MIN. PPM NEEDED ( $\mu$ g/g)	COMMENTS
Therapeutic Gain	Quality of neutron beam	Distribution of $^{10}\text{B}$ in target			
1.2	Epithermal	Uniform		14-17	From Bond & Fairchild: 1. Minimum advantage factor = 1.2 2. Calculated for 4-cm depth 3. Range due to conc. ratios = 3 to infinite; repair = + or - From Bond & Fairchild From Koyabayashi & Kanda; Gabel: 4. Geometry may reduce efficacy by 2-3 times
1.2	Scandium filtered Epithermal	Uniform		1-3	
1.2		Cell surface		30-45	
1.2	Scandium filtered	Cell surface		2-8	
Dext.: to:MCA ratio	M.W. of Dext.	$^{10}\text{B}$ :to Dext. ratio w/w; no.	Cell size diam. vol. ( $\mu\text{m}$ ); ( $\mu\text{m}^3$ )	Sites per cell	PPM PRE- DICTED
5	$4 \times 10^4$	5%; 200	12.4; 1000		
5	$4 \times 10^4$	5%; 200	12.4; 1000	$10^6$	
5	$4 \times 10^4$	5%; 200	12.4; 1000	$10^6$	17
3+	$4 \times 10^4$	5%; 200	12.4; 1000	$>= 10^7$	170
10?	$1 \times 10^5$ ?				109
10?	$1 \times 10^5$ ?	5%; 500	12.4; 1000	$>= 10^7$	850

specificity or affinity discussed by Soloway (4). Hurwitz and Arnon and their coworkers from Sela's group at the Weizmann Institute have bound many molecules of cytotoxic antibiotics to each molecule of antibody by way of dextran bridges with excellent retention of antibody specificity (5).

In the preceding presentation from the Ohio State group, Alam described the attachment of many boron atoms to polymers or to albumin (6). That approach is conceptually akin to our project, which utilizes well characterized, hydrophilic dextrans as intermediate carriers.

A secondary gain from the use of boronated dextran-antibody conjugates may be more efficient uptake of MCA's or their  $\text{F}(\text{ab}')_2$  fragments. Several enzymes and other proteins are stabilized against metabolic degradation when conjugated by dextrans (7,8). Hence, slowed clearance of antibody-dextran complexes from the blood may be expected.

As a first step in preparing MCA's or  $\text{F}(\text{ab}')_2$  fragments each carrying a thousand or more boron-10 atoms via dextran bridges, we have developed our chemical methodology by studying the reactions of chemically activated dextrans with human IgG, provided by Sigma as Cohn fraction II of gamma globulin. We shall report on the experimental progress only of the work employing periodate activation (9) to form reactive dialdehydes from some of the

glucose moieties of the dextran polymers.

On the one hand, these will form Schiff base complexes with the epsilon amino nitrogens of a few of the lysyl residues of antibodies under the right incubation conditions. On the other hand, Schiff base linkages can also form between aldehydes of the activated dextrans and appropriately boronated synthetic amines, which will thereby be bridged to the antibodies. As Detlef Gabel reported (10), his laboratory has already prepared an aliphatic amine and an aromatic amine each of which carries a decachlorocarbonane cage, so the stage is set to complete our first synthesis of a boronated dextran-antibody complex. The alternative cyanogen bromide activation of dextrans noted by our abstract is still in preliminary form, although it is already clear that dextrans can also be conjugated to proteins in this way (7). Hence, we cannot tell yet which type of activation will be preferable in the long run.

#### METHODS:

We now describe briefly our methods and results utilizing periodate activation of dextrans for conjugation to IgG. Because Schiff base formation is optimized at pH's below 6, we departed from the method employed by the Weizmann Institute group (5,11) and others (12) of coupling periodate-activated dextrans with antibodies at a pH of 8.5 or above. Hydrolysis of the Schiff base linkages and fragmentation of the dextrans probably occurred at those alkaline pH's, and this, in turn, may have given rise to some aggregated products (12). Our incubations were carried out at pH 6.0 or at pH 4.5.

First we activated with sodium periodate an aqueous solution of dextran of molecular weight about 40 kilodaltons. The periodate was present at a ratio one half that of the glucose residues of the dextran polymer, whose concentration was determined by an anthrone colorimetric reaction (13). Isolating the partially oxidized dextran by dialysis and lyophilization and then using the Prussian blue method of assaying aldehydes (14), about 16% of the glucose residues were found to contain dialdehyde. A second periodate oxidation afforded an additional 5% conversion of glucose residues to "free" aldehyde for a final yield of 21%.

At slightly acid pH cyanoborohydride has been reported to reduce labile Schiff bases to more stable secondary and tertiary amines without reducing aliphatic aldehydes (15), so on some runs sodium cyanoborohydride was added. Most reactions were terminated by reduction of the remaining free aldehyde groups with sodium borohydride at a pH of 9.0-9.5. Following anion exchange chromatography, the fractions were analyzed for dextran and for protein.

#### RESULTS:

Table 2 summarizes some typical reactions. The extent of conjugation of IgG by dextran is given on a weight-per-weight basis in the last column. The values shown represent averages of the fractions in the protein-containing peaks, unweighted for their protein contents, along with their standard deviations. We shall return to the significance of these values after examining briefly two representative chromatograms.

Figure 1 shows a chromatogram of a reaction carried out at pH 4.5. The elution profile contains two unreacted dextran peaks. The first, probably

Table 2. Coupling of periodate-oxidized dextrans with IgG

Reactions <sup>1</sup>				Product Analyses <sup>2</sup>	
Exp't	pH	Schiff's Bases Reduced by NaCNBH <sub>3</sub> ?	"Free" Aldehydes Reduced?	Protein Recovery (percent)	mg Dextran mg IgG
1	4.5	No	Yes	80	1.26 + 0.18
2	4.5	Yes	Yes	73	1.29 + 0.20 (low I) 1.03 + 0.07 (high I)
3	6.0	No	Yes	41	1.01 + 0.14
4a	6.0	Yes	Yes	81	1.37 + 0.11
b		Yes	Yes	87	1.21 + 0.06 (major) 1.17 + 0.23 (minor)
5	6.0	Yes	No	22	0.8 - 0.9

<sup>1</sup> Reaction conditions: IgG (4 mg/ml, Cohn Fraction II, human) was reacted with 21% oxidized dextran (20 mg/ml) in 0.1 M sodium acetate buffer, pH 4.5, or 0.1 M sodium phosphate buffer, pH 6.0. 1 M sodium cyanoborohydride was added to a final concentration of 0.06 M, when used (Yes in column 3); reaction time: 24-26 hours. Reactions with final reduction of aldehyde groups were terminated by addition of solid sodium carbonate to pH 9-9.5 followed by 5 M sodium borohydride to a final concentration of 0.15 M (Yes in column 4).

<sup>2</sup> Analyses: Reaction mixtures were desalted on G25 Sephadex equilibrated with 0.01 M tris base prior to anion exchange chromatography. Stepwise increases in ionic strength (I) to 1.0 M sodium chloride were used to elute unreacted dextran followed by dextran-IgG complexes. Ion exchangers were DEAE cellulose or DEAE BioGel A. Protein was determined by UV spectra and optical absorbance at 278 nm, using an optical density of 1.3 for one mg/ml at 1 cm pathlength. Total recovery (column 5) was obtained by integrating values from all fractions. Dextran was quantified by the anthrone reaction using as a standard 21% oxidized dextran with its "free" aldehyde groups reduced by sodium borohydride. The extent of conjugation of dextran with IgG is given on a weight-per-weight basis (Column 6). The values shown represent averages of the fractions in the protein-containing peaks, unweighted for their protein contents, along with their standard deviations.

uncharged, elutes at the lowest ionic strength, while the second appears at low ionic strength and presumably contains some charged groups at pH 8-9. However, neither peak has been further characterized.

Although the IgG of Cohn fraction II is not homogeneous, under the conditions used for this run essentially all the protein is eluted in one peak. Quantification of the dextran-to-protein weight ratio was ascertained for each fraction in the peak and is shown at the upper right. The important point to remember from Figure 1 is that there is no evidence for significant variation of the dextran binding ratio in different fractions, and the average value of 1.26 corresponds to 4 or 5 molecules of dextran per globulin.

Under the conditions of the reaction represented by Figure 2 the unconjugated, heterogeneous IgG elutes as three peaks in essentially the same locations as shown here for the gamma globulin conjugated with dextran. Because one of the unreacted dextran peaks overlaps the first protein peak

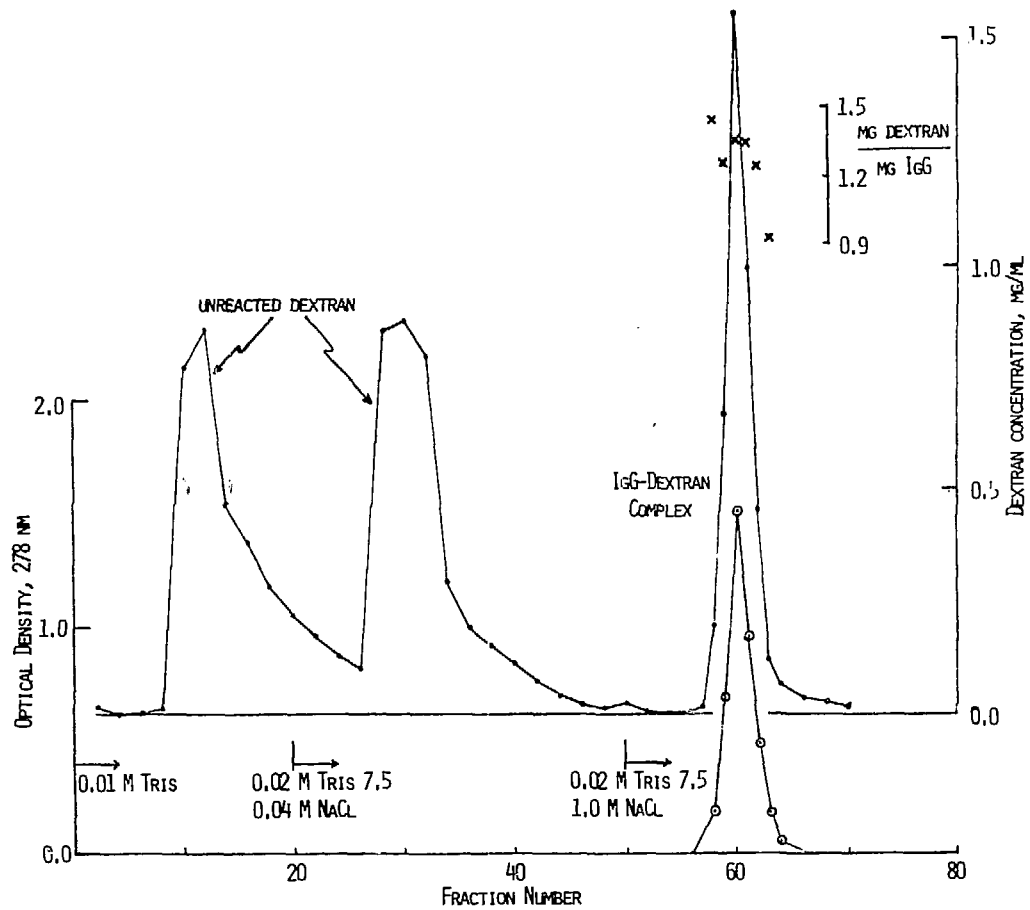


Figure 1. Anion exchange chromatography of a reaction of IgG with 21% oxidized dextran at pH 4.5 in the absence of sodium borohydride. Refer to Table 2 (experiment 1) for reaction conditions. Exchanger: DEAE cellulose;  $1.5 \times 10.4$  cm (diameter  $\times$  length); 1.8 ml per fraction. Dextran determinations are given by the upper trace with its ordinate at the right in units of mg/ml. Protein elution is represented by the lower trace with its ordinate on the left, in units of optical density at 278 nm.

that is eluted, no meaningful dextran-to-protein coefficients can be calculated for the corresponding fractions. However, the conclusion to be emphasized by this figure is that even for the minor, late-eluting protein fraction, the dextran-to-IgG ratios are not significantly different from those of the main peak, which correspond to about five molecules of dextran per immunoglobulin. In other words, all the IgG molecules appear to be conjugated with dextran to about the same extent. This is consistent with Figure 1 and with other runs not shown.

In experiment 5 (Table 2) IgG was conjugated with dextran and chromatographed with its "free" aldehyde groups still oxidized. Although these are recent data, and it is clear from the poor protein recovery noted in column

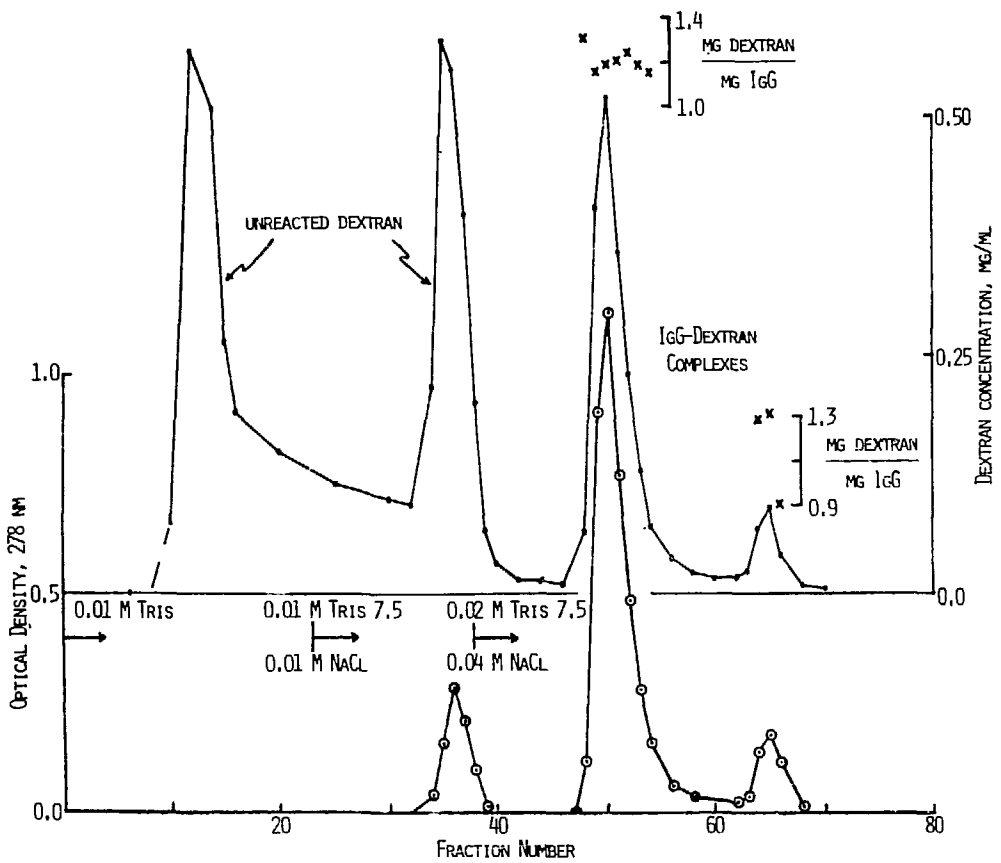


Figure 2. Anion exchange chromatography of a reaction of IgG with 21% oxidized dextran at pH 6.0 in the presence of sodium cyanoborohydride. Refer to Table 2 (experiment 4b) for reaction conditions. Exchanger: DEAE BioGel A; 1.5 x 11.4 cm (diameter x bed height); 1.8 ml per fraction. Dextran determinations are given by the upper trace with its ordinate at the right in units of mg/ml. Protein elution is represented by the lower trace with its ordinate on the left, in units of optical density at 278 nm.

five that we have yet to optimize chromatographic conditions, this preliminary experiment introduces an important extension of our work. It represents the case wherein dextran is conjugated to IgG but still carries many aldehyde moieties which are capable of further reaction to form bridging Schiff base linkages with boronated synthetic amines, such as the aliphatic and aromatic amines complexed to carborane cages that Detlef Gabel and his colleagues have already synthesized (10). Successful achievement of this step may afford boronated dextran-antibody globulin conjugates of the kind needed for NCT.

#### DISCUSSION:

We return now to the significance of the coefficients in the last column of Table 2. Assuming that the dextrans of 40-kilodalton molecular weight have not been fractionated significantly and that the mean weight of

the somewhat heterogeneous IgG is 153 kilodaltons, a dextran-to-IgG weight coefficient of one corresponds to an average of about 3.8 dextrans complexed to each gamma globulin. Thus a combining ratio of 5 requires a coefficient of 1.31, which is surpassed or nearly equaled by half of the runs terminated by reduction of the "free" aldehydes, as shown by experiments 1-4 in Table 2. Preliminary experiment 5 with IgG conjugated by dextran that is still highly activated for combination with amines carrying carborane cages clearly reflects suboptimal conditions, as noted before. But even so, the fraction of globulin that was recovered in that experiment was attached to more than 3 oxidized dextrans, on the average.

In summary, Table 2 indicates that about five dextrans of 40-kilodalton molecular weight can be bound per antibody. Gabel has already complexed dextrans with decachlorocarboranes to the extent of 5% boron by weight (16), so a projection of at least 1000 boron-10 atoms per lightly conjugated antibody is reasonable. If a characteristic cell volume is taken as 1000 cubic microns, which is typical of a V-79 Chinese hamster cell for example, then the boron-10 content per million antigenic sites per cell will be 17 ppm (Table 1). However, for the antimelanoma MCA's we plan to use, Ferrone has reported 3 million antigenic determinants per cell for each of the first three MCA's whose binding he has quantified (17), and two additional highly specific antibodies have been characterized recently. Hence a "therapeutic cocktail" of boronated dextran-conjugated derivatives of all five of his antimelanoma antibodies might be able to carry as much as 170 ppm of boron-10 to the target if, among the five antibodies, as many as 10 million binding sites are available (Table 1). This compares favorably with the 30 to 45 ppm of boron required for successful antibody-targeted NCT with epithermal neutrons and the 2 to 8 ppm required for scandium-filtered neutrons, and there is a comfortable margin for error.

In short, only the first stage of our project has yet been approached experimentally. Nevertheless, pessimistic projections regarding successful NCT with boronated MCA's appear unwarranted. The use of intermediate carriers to link a thousand or more boron-10 atoms to each antibody with only a handful of amino acid residues on the globulin being conjugated appears very promising for NCT in cases where there are a million or more antigenic sites per cell for the monoclonal antibodies that are available.

In closing, we emphasize that the concept of NCT is not limited to potential cancer treatment, despite the emphasis given to the goal by this symposium and even by this presentation. Extension of the principles developed here should permit NCT to achieve highly specific radiation inactivation of other cellular targets toward which appropriately selective antibodies can be developed, such as clones of cells involved in autoimmune diseases, transplant rejection, etc.

#### REFERENCES:

1. E. Mizusawa, A.J. Serino, M.F. Hawthorne, R.M. Sharkey and D.M. Goldenberg (1984). This symposium, paper V.2.
2. V.P. Bond and R.G. Fairchild (1984). This symposium, paper I.1.
3. T. Kobayashi and K. Kanda (1984). This symposium, paper III.1.
4. A.H. Solloway (1984). This symposium, paper V.1.

5. E. Hurwitz, R. Maron, A. Bernstein, M. Wilchek, M. Sela and R. Arnon (1978). *Int. J. Cancer* 21: 747-755.
6. F. Alam, A.H. Soloway, R.F. Barth, C.W. Johnson and W.E. Carey (1984). This symposium, paper V.4.
7. H.K. Blomhoff and T.B. Christensen (1983). *Biochim. Biophys. Acta* 743: 401-407.
8. J.J. Marshall (1978). *Trends in Biochem. Sci.* 3: 79-83.
9. I. Parikh, S. March, P. Cuatrecasas (1974). *Methods in Enzymology* 34: 77-102.
10. D. Gabel, R. Walczyna, F. Wellman, H. Riesenbergs and I. Hocke (1984). This symposium, paper V.4.
11. A. Bernstein, E. Hurwitz, R. Maron, R. Arnon, M. Sela and M. Wilchek (1978). *J. Natl. Cancer Inst.* 60: 379-384.
12. T.P. King, L. Kochoumian, K. Ishizaka, L.M. Lichtenstein and P.S. Norman (1975). *Arch. Biochem. Biophys.* 169: 464-473.
13. T.A. Scott, Jr., and E.H. Melvin (1953). *Anal. Chem.* 25: 1656-1661.
14. J.T. Park and M.J. Johnson (1949). *J. Biol. Chem.* 181: 149-151.
15. R.F. Borch, M.D. Bernstein and H.D. Durst (1971). *J. Amer. Chem. Soc.* 93: 2897-2904.
16. D. Gabel and R. Walczyna (1982). *Naturforsch.* 37c: 1038-1039.
17. S. Ferrone, P. Giacomini, P.G. Natali, G. Buraggi, Z. Callegaro and U. Rosa (1984). This symposium, paper IV.<sup>c</sup>.

## Boron Analogs of $\alpha$ -Amino Acids

Bernard F. Spielvogel and Andrew T. McPhail

Paul M. Gross Chemical Laboratory, Duke University, Durham, NC 27706

Iris H. Hall

School of Pharmacy, University of North Carolina, Chapel Hill, NC 27514

Ralph G. Fairchild and Peggy L. Micca

Brookhaven National Laboratory, Upton, NY 11973

We have been concerned with the synthesis, characterization, and definition of a class of novel isoelectronic and isostructural boron analogs of the  $\alpha$ -amino acids as shown in Table 1.

Table 1. Boron Analogs of  $\alpha$ -Amino Acids

Amino Acid	Boron Analog (Amine-carboxyborane)
Glycine, $\text{H}_3\text{NCH}_2\text{COO}^-$	$\text{H}_3\text{N}\cdot\text{BH}_2\text{COOH}$
Alanine, $\text{H}_3\text{NCH}(\text{CH}_3)\text{COO}^-$	$\text{H}_3\text{N}\cdot\text{BH}(\text{CH}_3)\text{COOH}$
Betaine, $(\text{CH}_3)_3\text{NCH}_2\text{COO}^-$	$(\text{CH}_3)_3\text{N}\cdot\text{BH}_2\text{COOH}$

We are generally interested in these boron amino acid analogs, their precursors and derivatives because of their potential biological activity in view of the enormous biological activities of the  $\alpha$ -amino acids.

Of specific interest is the use of these amino acid analogs in boron neutron capture therapy with a potential two-fold attack on tumors as suggested by Soloway (1). Thus, the boron amino acid analogs could serve as antimetabolites and inhibit tumor growth as well as possibly being selectively incorporated into the proteins of the neoplasm. This approach stimulated the synthesis of amino acid analogs of the boronic acid type by a number of investigators as described by Soloway. This paper presents a brief review of the preparation and characterization of some of the first examples of the analogs (shown in Table I) and related compounds and describes their antitumor activity. Brief mention is also made to other potent biological activity found for these compounds. Finally, the results of preliminary testing at Brookhaven as to the suitability of these analogs for use in BNCT will be presented. It should be noted that two of the boron amino acid analogs described herein have been used on a solid experimental tumor using BNCT as reported by Dr. W. Porshen in these Proceedings.

### Amine-Carboxyboranes, Boron Analogs of Amino Acids

The representative boron analogs shown in Table 1 are essentially substituted amine-boranes. At the start of this work the major questions concerning these analogs were the hydrolytic and oxidative stability of the B-H bonds, H<sub>2</sub> loss (and aminoborane formation) from those containing NH bonds such as H<sub>3</sub>N•BH<sub>2</sub>CO<sub>2</sub>H and lastly possible reduction of carbonyl by hydride transfer from boron to the carbonyl carbon.

As a general preparative route, we elected to focus our attention on the hydrolysis of the cyano group in amine-cyanoboranes.

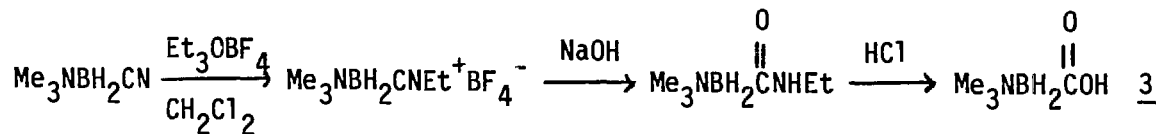


Adequate amounts of the precursor amine-cyanoboranes can be obtained by use of a general and convenient high-yield synthetic route developed by Spielvogel *et al.* for this class of compound (2, 3).



### Boron Analog of Betaine

To ascertain if the hydrolysis of the cyano group in amine-cyanoboranes would provide a feasible entry to amine-carboxyboranes, Me<sub>3</sub>N•BH<sub>2</sub>CN was selected as the initial substrate in order to avoid complications which might arise with amines containing N-H bonds. Initial attempts to hydrolyse Me<sub>3</sub>N•BH<sub>2</sub>CN directly with strong acid or base even under reflux conditions were found to give either unreacted Me<sub>3</sub>N•BH<sub>2</sub>CN or hydrolysis products of the B-H bond. However, alkylation of the cyano nitrogen with Et<sub>3</sub>O<sup>+</sup>BF<sub>4</sub><sup>-</sup> enhanced the susceptibility of the CN group to hydrolysis. Thus, reaction of the alkylated intermediate with 1.0M NaOH led to the N-ethylamide derivative (60% yield) which could then be converted into the desired carboxyborane by reaction with dil. HCl(aq.) (4). Alternatively, the alkylated intermediate could be reacted directly with water to form the carboxyborane in yields of up to 55% (5).



Trimethylamine-carboxyborane, Me<sub>3</sub>N•BH<sub>2</sub>COOH, the boron analog of betaine, is a white crystalline solid (m.p. 147 °C, dec.). It exhibits considerable hydrolytic stability with no detectable hydrolysis of aqueous solutions for a period of one month. About 25% hydrolysis occurs in 1N HCl in one week at room temperature. The compound exists in the solid state as discrete hydrogen bonded dimers (4).

### Boron Analog of Glycine and *N*-Methyl Glycines

Attempts to prepare  $H_3N \cdot BH_2CN$ , the precursor to  $H_3N \cdot BH_2COOH$ , the boron analog of glycine, according to eqn 2 were not successful. Our attempts to repeat a literature report (6) on the preparation of  $H_3N \cdot CH_2CN$  from  $Me_3N \cdot BH_2I$  with  $NaCN$  in liq  $NH_3$  resulted instead in the novel complex,  $[Na(H_3N \cdot BH_2CN)_6]^{+}I^{-}$ , whose structure was determined by single-crystal x-ray analysis (7). Pure  $H_3N \cdot BH_2CN$  could be obtained however by extraction with ether on an aqueous solution of the above  $NaI$  complex or by  $NH_3$  displacement on aniline-cyanoborane (8).

With the availability of  $H_3N \cdot BH_2CN$ , attempts were made to convert it into  $H_3N \cdot BH_2COOH$  by alkylation and hydrolysis but these were unsuccessful. An amine exchange reaction involving  $Me_3N \cdot BH_2COOH$  and liq.  $NH_3$  (ca. 1:10 w/w) in an evacuated stainless steel cylinder at room temperature for three weeks yielded 50-55% of crude  $H_3N \cdot BH_2COOH$  (9). Recrystallization from cold water gave pure product, m.p.  $116^{\circ}C$  (dec.). The structure was established by a single-crystal x-ray analysis. In the solid state,  $H_3N \cdot BH_2COOH$  exists as hydrogen bonded dimers which are associated further via interdimer  $N-H \cdots O$  hydrogen bonds. Hydrolysis of  $H_3N \cdot BH_2COOH$  occurs very slowly in pure  $H_2O$  with only trace decomposition in 3 h and several percent after several weeks. Only trace decomposition occurs in 1N  $NaOH$  after several days, but rapid hydrolysis takes place in 1N  $HCl$ .

By use of similar base-displacement reactions involving  $Me_3N \cdot BH_2COOH$  with, in turn,  $Me_2NH$  and  $MeNH_2$  in a steel cylinder,  $Me_2NH \cdot BH_2COOH$  and  $MeNH_2 \cdot BH_2COOH$  (the boron analog of sarcosine) were obtained in yields of up to 80% (10). These two derivatives exhibited hydrolytic stability similar to  $H_3N \cdot BH_2COOH$ . As found for  $H_3N \cdot BH_2CN$ , the carboxyboranes of  $Me_2NH$  and  $MeNH_2$  could not be prepared from the corresponding cyanoborane by the method of eqn 3.

The amine carboxyboranes  $Me_{3-n}^nH \cdot N \cdot BH_2COOH$  ( $n = 0-3$ ) have  $pK_1$  values in the range 8.14 - 8.38 and appear to be the weakest known simple carboxylic acids of zero net charge (11). The corresponding  $pK_1$  values for the methyl glycines are around 2. Thus, replacement of the carbon with boron results in a six-fold change in  $pK$ . There is no evidence for amine nitrogen deprotonation at  $pH < 11$  for the amine-carboxyboranes.

### Other Amine-Carboxyboranes, -Cyanoboranes, and -Carbamylboranes

Using the general methods described above, a variety of cyanoboranes have been prepared including bis adducts of TMED and en (3). Likewise, carboxyboranes of pyridine, N-methyl morpholine and TMED have been synthesized and characterized (3). Carbamylboranes of formula  $(CH_3)_x NH_3-x \cdot BH_2C(O)NHEt$  ( $x = 0-3$ ) have been synthesized and characterized (12). The latter serve as simple models of a boron amino acid peptide linkage. A number of dipeptides

containing a boron amino acid and a normal amino acid have been prepared in work yet to be published from our laboratories.

The derivative chemistry of amine-carboxyboranes appears to be vast. The only limitation we can foresee is possible instability of derivatives containing functional groups such as  $-\text{BH}_2\text{C}(\text{O})\text{Cl}$  (hydride transfer to carbonyl-carbon). There may well be a variation in the stability of such species  $[\text{R}_3\text{NBH}_2\text{C}(\text{O})\text{X}]$  similar to that which we have proposed for  $\text{H}_3\text{BC}(\text{O})\text{X}^-$  (13).

### Metal Complexes

In contrast to glycine and its mono- and di-N-methylated derivatives, no evidence up to pH 11 could be found for amine nitrogen deprotonation and chelation with  $\text{Zn}^{2+}$  or  $\text{Cu}^{2+}$  with the amine-carboxyboranes (11). The amine-carboxyboranes were found to bind only through the carboxylate group.

Stability constants for  $\text{Zn}^{2+}$  binding are comparable to that of  $\text{Zn}^{2+}$  with  $\text{NH}_3$ .

We have recently prepared a binuclear Cu(II) complex of formula  $\text{Cu}_2(\mu\text{Me}_3\text{NBH}_2\text{CO}_2)_4 \cdot 2\text{Me}_3\text{NBH}_2\text{CO}_2\text{H}$ . The structure of the complex reveals that the Cu...Cu intradimer distance is the shortest yet encountered in such copper(II) carboxylate bridged dimers and is the first recorded instance for this class of compound where it is less than that of  $2.56\text{\AA}$  in copper metal (14).

### Antitumor and Other Pharmacological Activity

The boron substituted  $\alpha$ -amino acids and related compounds described above have been found to possess antineoplastic, anti-inflammatory, antiarthritic and analgesic activity (5, 15). The antineoplastic activity was evident against the growth of Ehrlich and Lewis lung carcinoma, Walker 256 carcinosarcoma, and marginal activity was observed against B-16 melanoma and P-388 lymphocytic leukemia cells growth by dosages of from 2.5 to 20 mg/kg/day (5). The analogs were observed to suppress S-adenosyl methionine methyl transferase activity thus blocking methyl transfer to nucleic acids, nucleoproteins and the thymidylate synthetase enzyme.

Further studies with a binuclear copper (II) complex demonstrated that DNA polymerase  $\beta$  activity was inhibited as well as purine synthesis specifically at the sites of PRPP amidotransferase and dihydrofolate reductase (16). The boron analogs reduced the enzyme activity by a magnitude which would account for the DNA synthesis inhibition.

Sur (17) has reported that trimethylamine-carboxyborane encapsulated in positive liposomes gave an increase in life span of 89% at a much reduced dosage than the free drug in the Ehrlich ascites tumor model.

Several boron analogs of  $\alpha$ -amino acids produced hypolipidemic activity at 5-20 mg/kg/day reducing significantly both serum cholesterol and triglyceride levels (18). The regulatory enzyme of cholesterol synthesis,  $\beta$ -hydroxy- $\beta$ -methyl glutaryl CoA reductase, was suppressed by the boron analogs as well as early enzyme, acetyl CoA synthetase and ATP dependent citrate lyase activities in the synthetic pathway. Regulatory enzymes of fatty acid synthesis pathway also were inhibited by the agents.

The anti-inflammatory and antiarthritic activities of the boron derivatives are attributed to inhibition of hydrolytic enzyme activity of PMN's and liver cells, prostaglandin synthetase activity and oxidative phosphorylation processes. The boron derivatives proved to be more potent than commercial agents.

### Tissue Distribution of Radiolabeled Glycine

Since amino acids comprise  $\sim 15\%$  of tissue, and turnover is rapid, one would hope this physiological pathway would be adequate for delivery of therapeutic amounts of boron. Numerous studies indicate increased metabolism in various tumors, so that differential concentrations of amino acids between tumor and supporting normal tissues should be available. In particular, the work of Oldendorf has shown that, of the various amino acids, glycine has the slowest transport across the blood-brain barrier (19). Consequently glycine (and, therefore, perhaps boronated glycine) might demonstrate preferential uptake in brain tumors. In order to evaluate this possibility,  $^{14}\text{C}$ -glycine was administered in trace, medium, and high doses to BALB/c mice carrying Harding-Passey melanoma. Medium and high doses were obtained by using doses of 0.6 and 6.0 mg glycine per mouse, tagged with 20  $\mu\text{Ci}$  of  $^{14}\text{C}$ -glycine (0.16  $\mu\text{g}$  of radiolabeled glycine). The results of these studies are represented by the curves in Fig. 1, showing uptake of glycine in tumor, blood, and brain, at 1, 6, and 24 hr post-i.v. injection. Preferential uptake in tumor is observed; since the results were essentially the same for trace, medium, and high doses, it can be assumed that the physiological pathway was not saturated. At the high dose administered (6 mg/mouse) tumor uptake was  $\sim 5\%$  dose per g; if the boronated analog behaved in the same way, tumor content would be  $\sim 40\text{ }\mu\text{g B/g}$  tumor--a boron concentration clearly adequate for therapy (20).

### Tumor Uptake of Boronated Analogs of Glycine and Betaine

Studies with  $^{14}\text{C}$ -labeled glycine in our murine melanoma revealed a tumor/brain ratio of  $\sim 10$  and a tumor/blood ratio of  $\sim 5$ , as well as usable con-

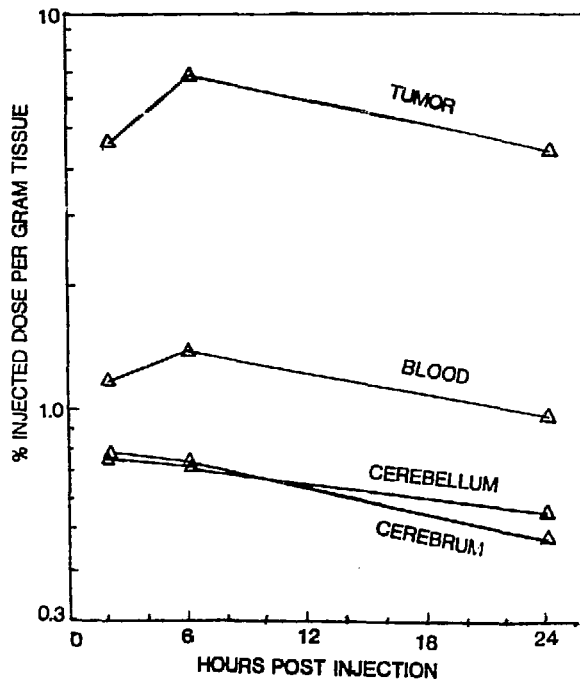


Fig. 1. Tissue distribution of  $^{14}\text{C}$ -glycine in BALB/c mice carrying Harding-Passey melanoma. These data are representative of concentrations measured following i.v. administration of trace, medium, and high doses of glycine (0.16  $\mu\text{g}$ , 0.6 mg, and 6.0 mg glycine per dose, respectively; 20  $\mu\text{Ci}$   $^{14}\text{C}$  glycine per dose).

centrations in tumor. Providing the boronated analog behaves similarly, the latter compound would be a significant improvement relative to  $\text{Na}_2\text{B}_{12}\text{H}_{11}\text{SH}$  currently in clinical use (tumor/brain ratio  $\approx 5$ ; tumor/blood ratio between 1 and 2). Following a synthesis similar to that described above, a boronated analog of glycine ( $\text{H}_3\text{NBH}_2\text{COOH}$ ) has been produced by the Callery Chemical Co., Callery, PA. Boron distribution studies in our murine melanoma with this compound, as well as with samples of the same compound synthesized by Spielvogel, have shown however that the boronated analog no longer behaves as an amino acid; usable concentrations and/or concentration ratios were not obtained (see Table 2). Boron contents of the various tissues shown in Table 2 were obtained following a single injection of compound sufficient to provide 40  $\mu\text{g}$  B per gram body weight.

The difference in behavior between glycine and the boronated analog is further illustrated by the thin-layer chromatogram shown in Fig. 2. The

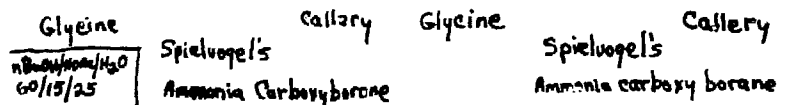


Fig. 2. Thin-layer chromatogram: black spots are glycine; oval spots are from ammonia carboxyborane.

Table 2. Tissue Distribution of Various Compounds in BALB/c Mice Carrying Harding Passey Melanoma\*

Compound	Hr post injection	Exp. No.**	Boron uptake, $\mu\text{g} \text{B}^7\text{B}$ per gram tissue									
			Blood	Brain	Tumor	Pancreas	Muscle	Gut	Spleen	Kidney	Lung	Liver
S-1 (glycine analog)	2	1	4	4.8	6.3							
"	"	2	4 8.1	9.4 6.9	12.4 5.8	10.5 4.5	8.1 7.2	13.6 6.3	10.3 3.1	16.0 8.2	9.6 3.4	10.6 4.2
"	"	4	10.5 6.2	10.2 6.8	16.9 11.7	7.3 6.6	9.3 12.2	11.6 8.7	9.7 8.5	18.0 13.7	9.3 7.5	8.6 8.6
"	"	3	8.6 8.8	8.0 7.6	11.2 16.2	16.8 14.9	19.9 13.4	11.1 11.9	16.3 11.9	18.9 18.2	13.5 9.2	11.4 9.3
"	"	5	12.1 10.5	9.8 9.3	15.8 12.6							
"	6	1	0 0	2.8 2.0	5.7 1.9	0 0	5 0	0 0	0 0	3.9 3.9	0 0	0 0
"	"	2	0 0	0 0	0 0							
"	"	4	0 0	2.8 2.5	3.7 1.5	0 0	0 0	0 0	0 0	2.7 3.4	0 0	0 0
"	"	3	3.5 3.75	6.0 6.1	7.0 8.0	7.0 4.4	10.0 6.1	7.0 7.0	4.7 6.4	9.7 11.7	6.1 5.7	5.4 6.2
"	"	5	1.8 2.25	4.9 2.9	5.3 4.5							
"	12	2	0 0	0 0	0 0							
"	"	3	0 0	0 0	0 0	0 0	0 0	0 0	0 0	0 0	0 0	0 0
"	24	1	0 0	0 0	0 0							
"	"	3	0 0	0 0	0 0							
S-6 (betaaine analog)	1		44.5 45.2	39.4 38.2	45.7 50.9							
"	6		12.2 12.4	12.2 12.5	17.5 14.2							
"	12		0 0	3.7 4.0	3.6 0							
"	24		0	0	0							
S-3	1		54.8 54.4	45.3 39.8	51.3 48.7							
"	12		0 0	0 0	3.8 2.8							

\*Animals were given a single i.p. injection (i.v. for Expt. No. 1 only) of compound dissolved in saline, sufficient to provide 40  $\mu\text{g}$  boron per gram body weight. Boron analysis done by colorimetric techniques.

\*\*Compound S-1, for Expts. 1, 2, 4, and 5 was obtained from Gallery Chemical Co.; for Expt. 3, from Dr. B. Spielvogel. All experiments were done with i.p. injection except for No. 1 which was i.v.

Table 3. Boronated Compounds Screened for Uptake in Harding-Passey Melanoma in BALB/c Mice

Compound	Formula	Solubility	Toxicity
S-1* ammonia-carboxyborane (glycine analog)	$\text{NH}_3\text{BH}_2\text{CO}_2\text{H}$	good	not toxic
S-6 trimethylamine-carboxyborane (betaine analog)	$\text{Me}_3\text{NBH}_2\text{CO}_2\text{H}$	good	not toxic
	0 "		
S-3	$\text{CH}_3\text{NH}_2\text{BH}_2\text{CNHC}_2\text{H}_5$	good	not toxic
S-2	$\text{Me}_3\text{NBH}_2\text{CN}$	good	toxic
S-4*	$\text{NH}_3\text{BH}_3$	good	toxic
S-5*	$\text{Me}_3\text{NBH}_3$	poor	toxic

\*Available commercially.

glycine standard and two samples of the ammonia carboxyborane were chromatographed on Eastman cellulose media and developed in  $\alpha$ -butanol:acetic acid:water = 60:15:25 (proportions by volume). The compounds were visualized with ninhydrin. The  $R_f$  of the two carboxyboranes are equal and differ from that of glycine, indicating differing solubilities.

In addition, a number of other carboxyboranes, amino boranes, and cyanoboranes, including a betaine analog, were evaluated, as indicated in Table 3. As with the boronated analog of glycine, there was no evidence of incorporation of these compounds in tumor (Table 2).

#### Discussion

In view of the selective accumulation in tumor demonstrated by glycine, the failure of the boronated analogs of glycine and betaine to be incorporated in tissue as amino acid analogs was disappointing. These findings are consistent with the data presented by Dr. Porschen, who tested these two compounds in the neutron capture therapy procedure in C57 mice carrying an adenocarcinoma (21). The tissue distribution of the boronated analogs of glycine and betaine was less specific for tumor than that of the compound  $\text{Na}_2\text{B}_{12}\text{H}_{11}\text{SH}$  in use clinically by Dr. Hatanaka (22,23). Thus it would not appear useful to pursue the testing of these compounds.

It is possible that the failure to show biological activity is a consequence of the presence of boron in the  $\alpha$ -carbon position, and that better analogs of amino acids will result when boron is located further from this biologically active position. Additional studies are underway to evaluate this possibility. Available evidence indicates that p-borono-phenylalanine demonstrates useful biological activity (24,25).

### References

1. A. H. Soloway, Progress in Boron Chemistry, 1, H. Steinberg and A. L. McCloskey, Eds., The MacMillan Company, New York, 1964, Chapter 4.
2. P. Wisian-Neilson, M. K. Das, and B. F. Spielvogel, Inorg. Chem., 17, 2327 (1978).
3. B. F. Spielvogel, P. Wisian-Neilson, and F. Harchelroad, Jr., J. Inorg. and Nucl. Chem., 41, 1223 (1979).
4. B. F. Spielvogel, T. Wojnowich, M. K. Das, A. T. McPhail, and K. D. Hargrave, J. Amer. Chem. Soc., 98, 5702 (1976).
5. H. Hall, C. O. Starnes, B. F. Spielvogel, P. Wisian-Neilson, M. K. Das, and L. Wojnowich, J. Pharm. Sci., 68, 685 (1979).
6. P. J. Bratt, M. P. Brown, and K. R. Seddon, J. Chem. Soc., Dalton Trans., 353 (1976).
7. K. D. Hargrave, A. T. McPhail, B. F. Spielvogel, and P. Wisian-Neilson, J. Chem. Soc., Dalton Trans., 2150 (1977).
8. A. T. McPhail, K. D. Onan, B. F. Spielvogel, and P. Wisian-Neilson, J. Chem. Research (S) 205 (M), 2601 (1978).
9. B. F. Spielvogel, M. K. Das, A. T. McPhail, K. D. Onan, and I. H. Hall, J. Amer. Chem. Soc., 102, 6343 (1980).
10. B. F. Spielvogel; "Boron Chemistry"; R. W. Parry, G. Kodama, Eds.; Pergamon: New York, N. Y., 1980, p. 119.
11. K. H. Scheller, R. B. Martin, B. F. Spielvogel, and A. T. McPhail, Inorganica Chimica Acta, 57 227 (1982).
12. B. F. Spielvogel, F. U. Ahmed, K. W. Morse, and A. T. McPhail, Inorg. Chem. 23, 0000 (1984).
13. B. F. Spielvogel, A. T. McPhail, J. A. Knight, C. G. Moreland, C. L. Gatchell, and K. W. Morse, Polyhedron, 2 1345 (1983).
14. B. F. Spielvogel, M. E. Sheitlin, G. E. Silvey, A. T. McPhail, Abstracts, p. 53, IMEBORON V, Swansea, U. K., July, 1983.
15. I. H. Hall, C. O. Starnes, A. T. McPhail, P. Wisian-Neilson, M. K. Das, F. Harchelroad, Jr., and B. F. Spielvogel, J. Pharm. Sci., 69, 1025 (1980).
16. I. H. Hall, B. F. Spielvogel, A. T. McPhail, J. Pharm. Sci., 73, 0000, (1984).
17. P. Sur, D. K. Roy, and M. K. Das, IRCS Medical Science, 9, 1066 (1981).
18. I. H. Hall, M. K. Das, F. Harchelroad, Jr., P. Wisian-Neilson, A. T. McPhail, and B. F. Spielvogel, J. Pharm. Sci., 70, 339 (1981).
19. W. H. Oldendorf, Amer. J. Physiol., 221, 1629 (1971).
20. R. G. Fairchild, Paper I-1, This Symposium.
21. W. Porschen, Paper VI-4, This Symposium.

22. R. G. Fairchild, Paper V-9, This Symposium.
23. H. Hatanaka, Paper VII-3, This Symposium.
24. Y. Mishima, Paper VI-6, This Symposium.
25. J. Glass, Paper V-7, This Symposium.

## p-Borono-L-phenylalanine

John Glass  
Mount Sinai School of Medicine, Fifth Ave. at 100th St., New York, NY 10029  
and  
Brookhaven National Laboratory, Upton, NY 11973

### INTRODUCTION

The synthesis of p-boronophenylalanine was reported by Snyder et al. (1) in 1957 with the suggestion that it might be useful in what is now called neutron capture therapy. The compound is of continuing interest in this context (2,3), and biological studies have so far been reported using the racemic amino acid (4,5). In preliminary studies on the selective uptake of p-boronophenylalanine into a transplantable melanoma of mice we found that favorable distributions of boron between tumor tissue and other tissues was obtained at relatively short times after i.p. injection of the amino acid derivative. Under these circumstances it seemed worthwhile to obtain the pure L isomer of the phenylalanine derivative and avoid excess boron backgrounds in the blood which might logically result from injection of the D isomer, which is unlikely to be metabolically active.

An enzymatic resolution of the stereoisomers of p-boronophenylalanine based on the selective hydrolysis of the L form of the ethyl esters by chymotrypsin has been reported (6). We preferred to develop a resolution based on the differential deacylation of N-acetyl-p-boronophenylalanine isomers for two reasons. (i) The acetyl derivative is an intermediate in the synthesis of the racemic amino acid (Figure 1), and its enzymatic hydrolysis shortens the synthetic route to the L amino acid by two steps (Figure 2). (ii) We plan to use the N-acetyl-p-boron-D-phenylalanine in further studies where the ethyl ester of the D amino acid would be a less satisfactory starting material.

With the proper ratios of substrate to enzyme, renal acylase smoothly converted N-acetyl-p-borono-d,1-phenylalanine to a mixture of p-borono-L-phenylalanine and N-acetyl-p-borono-D-phenylalanine. The L amino acid was isolated by an ion-exchange step followed by adsorption to a cross-linked dextran at pH 8.5 and desorption in 0.2 M acetic acid. The final adsorption to, and desorption from, cross-linked dextran serves as a convenient desalting procedure as well as a method for removing traces of tyrosine and phenylalanine from the product.

### EXPERIMENTAL

#### Preliminary Animal Experiments with Racemic p-Boronophenylalanine

To determine whether p-boronophenylalanine is concentrated by a representative experimental melanoma and to determine the time course of tumor concentration, mice (BALB/c) with Harding-Passey melanomas were each injected with 1.0 mL of a solution of p-borono-d,1-

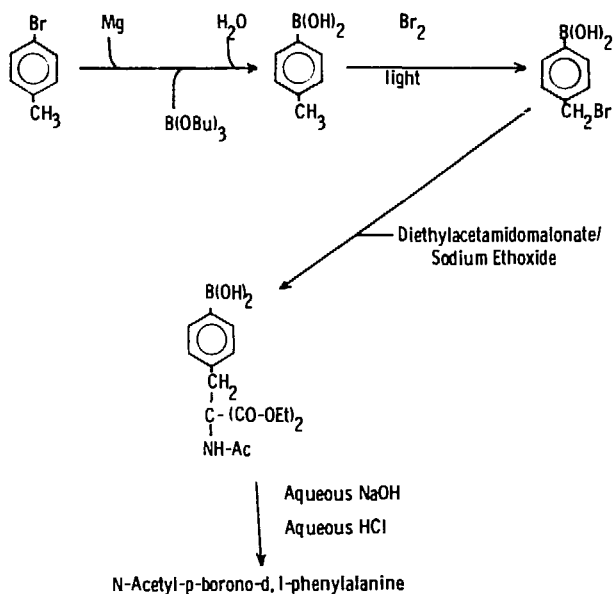


Figure 1. Synthetic route to N-acetyl-p-borono-d,L-phenylalanine by the method of Snyder et al. (1).

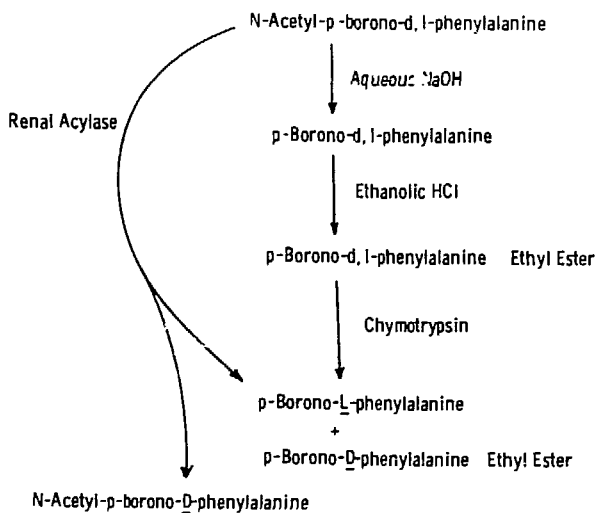


Figure 2. Alternative methods for enzymatic resolution of p-boronophenylalanine. The method involving chymotryptic action on ethyl esters was reported by Roberts et al. (6): the route using renal acylase treatment of N-acetyl derivatives is described here.

phenylalanine at 12.2 mg/mL in 0.1 M tris/HCl, pH 8.1. At 6 hr, 12 hr, and 24 hr (Expt. 1) or at 1 hr, 3 hr, and 6 hr (Expt. 2) animals (one animal for each time point in Expt. 1 and 3 animals for each time point in Expt. 2) were sacrificed, and selected tissues were analyzed for boron content. Boron analyses in Expt. 1 were done by a chemical/spectrophotometric method (7),

and boron analyses in Expt. 2 were done by a prompt-gamma neutron activation method (8). Results of both Expts. 1 and 2 are recorded in Table I.

Table I. Distributions of Boron in Mouse Tissues at Stated Intervals after Injection of Racemic p-Boronophenylalanine: Micrograms Boron/Gram Tissue

	Experiment 1			Experiment 2		
	6 hr	12 hr	24 hr	1 hr	3 hr	6 hr
Blood	4.1	<1	<1	15.5±8.3	21.5±4.3	7.4±1.6
Brain	7.7	"	"	6.3±1.9	13.6±3.5	9.7±3.4
Tumor	16.9	"	"	25.8±7.6	41.2±8.4	30.3±8.3
Muscle	5.6	"	"	15.3±4.2	12.2±4.4	6.6±1.7
Liver	4.1	"	"	21.9±4.4	8.5±1.0	3.3±1.9

Stereoselective Enzymatic Cleavage of N-Acetyl-p-borono-L-phenylalanine and Isolation of p-Borono-L-phenylalanine

The preliminary animal experiments with racemic p-borono-phenylalanine indicated that the amino acid was concentrated by tumor tissue and that the highest differential concentrations of boron were obtained at relatively short time intervals after injection of the amino acid. Under these conditions it was considered advantageous to resolve the stereoisomers and work with the pure p-borono-L-phenylalanine without background interference from the D isomer. For reasons outlined in the introduction of this paper, a resolution based on enzymatic hydrolysis of N-acetyl-p-borono-L-phenylalanine was chosen and developed.

N-Acetyl-p-borono-d,L-phenylalanine was dissolved at 0.01 M in 0.1 M sodium phosphate buffer (pH 7.5) containing 0.1 M ethylene glycol. Renal acylase I (Sigma #A 8376, 1200 U/mg) was added at a ratio of 1.6 g crude enzyme for each gram of substrate. At time intervals aliquots of the reaction mixture were withdrawn and diluted with 0.2 M sodium citrate buffer (pH 2.2). These samples were analyzed for ninhydrin-reactive materials by application to the short column of a Beckman-Spinco 120 amino acid analyzer (Figure 3). The analyzer system was calibrated with p-borono-d,L-phenylalanine. Enzyme protein in the enzymatic digest was precipitated by heating at 100° (boiling water bath) for about 10 minutes. Precipitated protein was removed by centrifugation.

The centrifugal supernatant solution was examined by thin-layer chromatography on silica gel G layers in 4:1:1 n-butanol: acetic acid: water with ninhydrin development. There was one ninhydrin-reactive spot which comigrated with racemic p-borono-phenylalanine. The product also comigrated with racemic p-borono-phenylalanine in a high voltage electrophoretogram at pH 3.5 and in an ion-exchange chromatography on the Beckman 120C amino acid analyzer (long column) in 0.2 M sodium citrate buffer, pH 4.25. In the latter chromato-

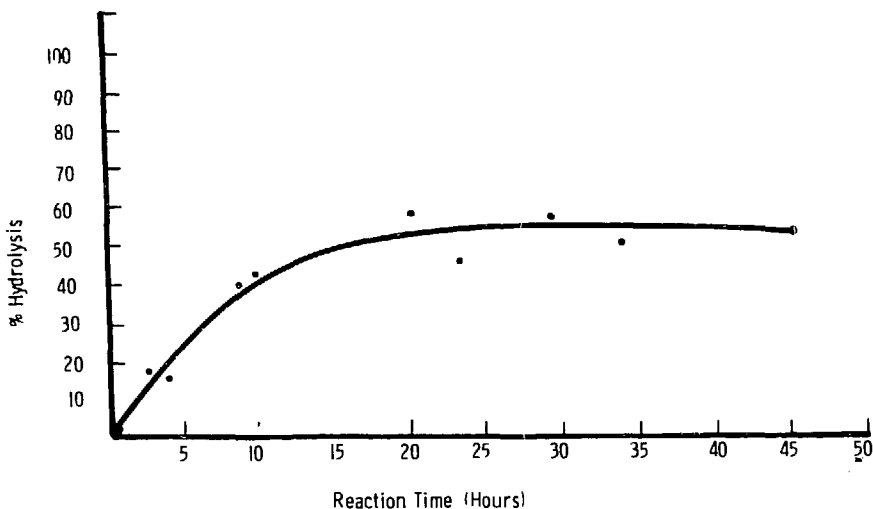


Figure 3. Time course of the action of renal acylase I on N-acetyl-p-boronono-d,L-phenylalanine as measured by the release of ninhydrin-reactive material. Note that the reaction proceeds to about 50% hydrolysis of the acetyl amino acid derivative, as would be expected for a stereospecific hydrolysis of only the L isomer.

graphic system the product eluted at approximately the position which cystine occupies in the same chromatographic system. The product peak is well separated from those corresponding to tyrosine and phenylalanine, which are expected by-products in the synthesis of p-boronophenylalanine. With heavy sample loading it appeared that there were traces of tyrosine, phenylalanine, and perhaps other amino acids in the crude enzymatic digest.

The centrifuged solution had its pH adjusted to about 2.5 with HCl, and it was passed through a column of Dowex 50Wx4 in the protonated form. The column was washed with 0.2 M sodium citrate (pH 2.2) and with water. The column eluate and wash solutions were checked by amino acid analysis in the long column system described above to be sure that the product was completely retained on the ion exchanger. The column was eluted with 0.2 M sodium phosphate (pH 8.0), and fractions of about 10 ml were collected. The pH of each eluted fraction was checked with a pH meter: the first few fractions were acidic, then the pH of the eluate rose to 8. The product began to elute from the column shortly after this pH change. The fractions containing the product were located by amino acid analysis in the long column system described above. These fractions were pooled and applied to a column of Sephadex G-25 (2 cm in diameter by 74 cm long) which had been equilibrated with 0.1 M disodium phosphate. The column was washed with 0.1 M disodium phosphate followed by 0.01 M disodium phosphate. The eluate and wash were free of boronophenylalanine but contained small amounts of phenylalanine, tyrosine, and other ninhydrin-reactive materials, as determined by ion-exchange chromatography in 0.2 M sodium citrate buffer (pH 4.25), as described above. The p-boron-L-phenylalanine was stripped from the Sephadex G-25 column with 0.2 M acetic acid. The product was crystallized from water and was then lyophilized from a dilute

acetic acid solution to obtain a fine powder which was convenient for redissolution.

When the column purification procedure described above was carried out starting with 100 to 200 mg of N-acetyl-p-borono-d,1-phenylalanine, the purification went smoothly with the product remaining in solution throughout. When a larger lot was processed (beginning with 1 g of racemic N-acetyl amino acid), product crystallized from solutions in the fraction collector after both the ion-exchange step and the desorption from Sephadex G-25. Since the solubility limit of the free amino acid is easily exceeded during the purification process, it is necessary to be careful that material is not lost by crystallization on the columns.

Animal experiments with p-borono-L-phenylalanine are now underway to determine proper dose levels and time courses for optimal loading of experimental mouse melanomas with boron for neutron capture therapy. Studies with other types of tumors which might be expected to concentrate the boron-containing amino acid derivative are also in progress.

#### ACKNOWLEDGMENTS

This work was supported by NIH grant GM 18752 and by the U.S. Department of Energy. The author is grateful to Peggy Micca and Dennis Greenberg of the Medical Department at Brookhaven National Laboratory for the measurements of tissue distributions of boron in mice after administration of p-borono-d,1-phenylalanine.

#### REFERENCES

1. Snyder, H.R., Reedy, A.J., and Lennarz, W. (1958) J. Am. Chem. Soc. 80: 835-838.
2. Soloway, A.H., Hatanaka, H., and Davis, M.A., (1967) J. Med. Chem. 10: 714:717.
3. Soloway, A.H., Wright, R.L., and Messer, J.R. (1961) J. Pharmacol. Exp. Ther. 134:117-122.
4. Ichihashi, M., Nakanishi, T., and Mishima, Y. (1982) J. Invest. Dermatol. 78:215-218.
5. Mishima, Y., Ichihashi, M., Nakanishi, T., and Tsuji, M. (1980) Kyoto daigaku Gemishiro Jikkensho (Tech Rep) KURRI-TR-195 28-32.
6. Roberts, D.C., Suda, K., Samanen, J., and Kemp, D.S. (1980) Tetrahedron Lett. 21:3435-3438.
7. Musser, J.R. and Peirce, C.E. (1971) Anal. Chem. 43:271-272.
8. Fairchild, R.G. and Gabel, D. See paper I-13 in this Symposium.

**Synthesis and Biological Activity  
of a Boron-Containing Pyrimidine Nucleoside**

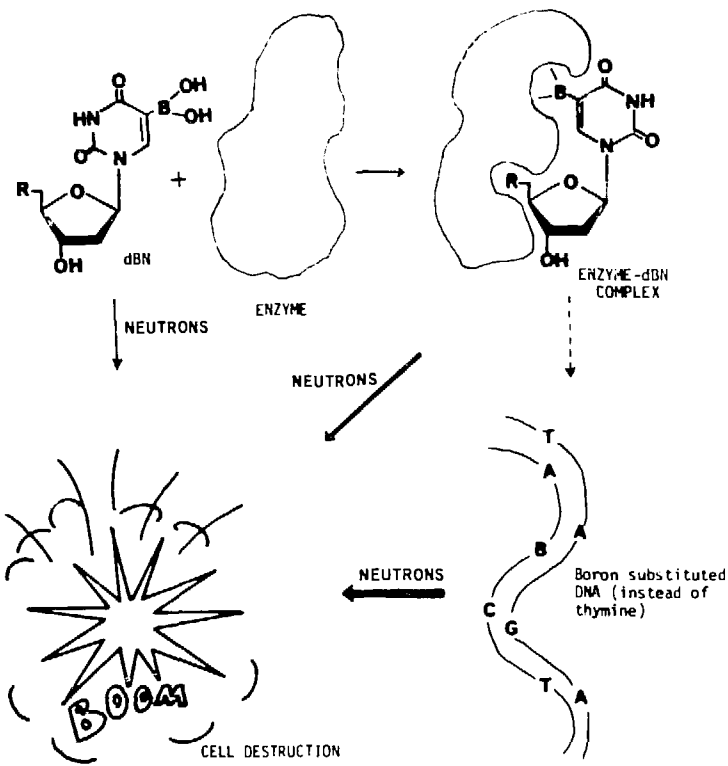
Raymond F. Schinazi  
Emory University School of Medicine and  
Veterans Administration Medical Center, Atlanta, GA 30303

Brenda H. Lester and Ralph G. Fairchild  
Brookhaven National Laboratory, Upton, NY 11973

William H. Prusoff  
Yale University School of Medicine, New Haven, CT 06510

The potential of purine and pyrimidine nucleoside analogs for the chemotherapy of viruses and cancers has been well recognized (1,2). These compounds behave as substitutes of natural components of nucleic acids and co-enzymes, and they have been extensively reviewed. Various boron heterocycles which resemble the bases of DNA have been tested for anti-cancer activity, but most of these have been found to be either hydrolytically and biologically unstable or too toxic. Others were inactive, probably because of deboronation or high polarity or, more likely, because these bases in contrast to the corresponding 2'-deoxyribonucleosides are poorly utilized for the biosynthesis of DNA. Soloway (3), Matteson et al (4), and Maitra (5) have discussed the difficulties involved in making purines and pyrimidines containing boron. Our approach was to synthesize a boron-containing nucleoside which closely resembles one of the naturally occurring pyrimidine nucleosides. This compound could (a) be taken up selectively by tumors and be preferentially trapped in the cell as the 5'-monophosphate--selectivity would be achieved if this drug is a better substrate for cancer cell thymidine kinase (TK) than normal cell TK; (b) act as an inhibitor of several enzymes known to be involved in pyrimidine nucleoside biosynthesis; (c) incorporate into the tumor cell DNA as counterfeit pyrimidine nucleotide; and (d) undergo a combination of a, b, and/or c. In addition, neutron irradiation of the cells containing this boron nucleoside could result in cell destruction at any of the steps described above (Figure 1).

At this Symposium, Kobayashi and Kanda as well as Gabel, Fairchild, and Larsson (papers III-1 and III-2) have presented data demonstrating that geometrical considerations dictate that the biological effectiveness of the  $^{10}\text{B}(\text{n},\alpha)^7\text{Li}$  reaction is at least twice as great when the site of interaction occurs in the cell nucleus rather than in the cytoplasm. We have estimated that if 5% of thymine bases in DNA are substituted by a pyrimidine nucleoside, the nuclear boron concentration would be 25  $\mu\text{g B/g}$ , which should be adequate for NCT. If this compound is to be used for the treatment of brain gliomas, further selectivity may be achieved, since--unlike brain tumors--tissues of the CNS do not synthesize significant amounts of DNA.



R = OH ENZYME = THYMIDINE KINASE  
 R =  $\text{OPO}_3^{2-}$  ENZYME = THYMIDYLATE KINASE  
 R =  $\text{OP}_2^{2-}$ <sub>6</sub> ENZYME = NUCLEOSIDE DIPHOSPHATE KINASE  
 R =  $\text{OP}_3^{2-}$ <sub>9</sub> ENZYME = DNA POLYMERASE

Figure 1

The synthesis of the first 5-boron-substituted pyrimidine nucleoside, 5-dihydroxyboryl-2'-deoxyuridine, 5-B(OH)<sub>2</sub>-dUrd or DBDU, was reported by us in 1978 (6). The syntheses of 5- and 6-dihydroxyboryluracil, which are isoelectronic and isostructural with orotic and iso-otic acid, respectively, were also reported in that note. DBDU was synthesized via a metal-halogen exchange at -50°C in tetrahydrofuran on 5-bromo-3',5'-bis-O-trimethylsilyl-2'-deoxyuridine using *n*-butyl lithium followed by boronation at -65°C with tri-*n*-butyl borate. Hydrolysis of the product followed by column chromatography and repeated recrystallization from methanol afforded the analytically pure compound in an overall 18% yield.

(mp 226-227°C dec.).  $^1\text{H-NMR}$   $[(\text{CD}_3)_2\text{SO}]$   $\delta$  2.12 (m, 2, 2'-H), 3.54 (m, 2, 5'-CH<sub>2</sub>), 3.80 (m, 1, 4'-H), 4.22 (bs, 1, 3'-H), 4.95 (t,  $J$  = 5.3 Hz, 1, 5'-OH), 5.28 (d,  $J$  = 3.5 Hz, 1, 3'-OH), 6.14 (t,  $J$  = 6.6 Hz, 1, 1'-H), 8.12 [s, 2, B(OH)<sub>2</sub>], 8.13 (s, 1, 6-H), 11.65 (s, 1, NH);  $^{11}\text{B-NMR}$  [DMSO; external standard  $\text{BF}_3$ -etherate]  $\delta$  - 41.84 (bs); UV 0.01 M HCl  $\lambda$  max 268 nm ( $\epsilon$  12,500),  $\lambda$  min 236 ( $\epsilon$  2,310); 0.01 M NaOH  $\lambda$  max 265 nm ( $\epsilon$  10,200),  $\lambda$  min 236 ( $\epsilon$  4,350); Anal. Calc. for  $\text{C}_9\text{H}_{13}\text{BN}_2\text{O}_7$ : C, 39.75; H, 4.78; B, 3.98; N, 10.30. Found: C, 40.04; H, 5.03; B, 4.01; N, 10.64. For  $^{13}\text{C-NMR}$  of DBDU relative to related pyrimidine nucleosides, see Table 1. Note that the peak for C-5 in DBDU is broad and is probably caused by the boron quadrupolar relaxation effect.

Table 1.  $^{13}\text{C-NMR}$  of boron nucleoside and related pyrimidine nucleosides.

Carbon atom	5-B(OH) <sub>2</sub> -dUrd(DBDU)	ppm <sup>a</sup>	dThd	dUrd	BrdUrd
C-4	167.14		165.07	162.98	158.53
C-2	152.24		151.76	150.28	149.13
C-6	150.06		137.50	140.31	139.68
C-5	102.08 (broad)		110.68	101.54	95.05
C-4'	88.26		88.60	87.30	86.98
C-1'	86.87		85.23	84.16	84.28
C-3'	71.70		71.83	70.30	69.38
C-5'	62.49		62.53	61.22	60.25
C-2'	40.55		40.60	39.59	37.66
Other	-	13.42(Me)	-	-	-

<sup>a</sup>In DMSO or DMSO/D<sub>2</sub>O/dioxane relative to TMS at 308°K. Measured on 360 MHz Brucker 270 HX spectrometer.

An important advantage of the route described above is that it can easily be modified to prepare <sup>10</sup>B-enriched compound (starting material <sup>10</sup>B-boric acid).

DBDU was tested against murine S-180 cells in vitro and was found to be inactive at a concentration of 200  $\mu\text{M}$ . However, this compound was not cytotoxic to Vero cells even at a concentration of 1600  $\mu\text{M}$ .

The drug inhibited herpes simplex virus replication in Vero cells (Figure 2) and this inhibition was prevented by thymidine but not by 2'-deoxyuridine, -cytidine, -guanosine, or -adenosine or by the corresponding ribonucleosides (Table 2).

DBDU is a competitive inhibitor of the phosphorylation of thymidine by the herpes thymidine kinase, with an inhibition constant of 63  $\mu\text{M}$ . The compound did not inhibit thymidylate synthetase, i.e. it did not interfere with the conversion of dUMP to dTMP (Dr. T. Kalman, private communication). These results suggest that DBDU is a good analog of thymidine and can affect the synthesis of certain viruses in cell culture. This antiviral effect is not secondary to cytotoxic effects of the drug.

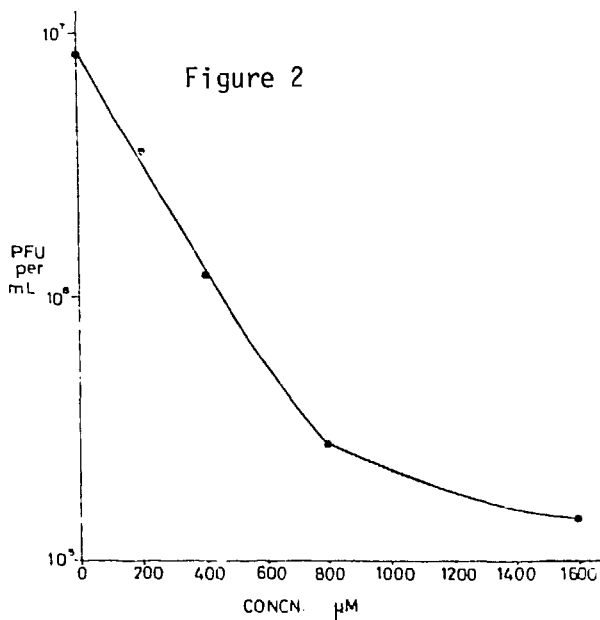


Table 2. Effect of various natural nucleosides on the inhibition of HSV-1 by 5-dihydroxyboryl-2'-deoxyuridine (800  $\mu$ M).

Nucleoside	% Inhibition
None	91
dThd (5 $\mu$ M)	69
dThd (25 $\mu$ M)	35
dThd (50 $\mu$ M)	21
dUrd (25 $\mu$ M)	91
dCyd (25 $\mu$ M)	91
dAdo (25 $\mu$ M)	91
C'uo (25 $\mu$ M)	91
Cyd (25 $\mu$ M)	91
Urd (25 $\mu$ M)	91
Ado (25 $\mu$ M)	91
Guo (25 $\mu$ M)	91

Because of these encouraging results, the compound was tested for its ability to sensitize V79 Chinese hamster cells to neutrons (Figure 3). Cells maintained in the presence of 1  $\mu$ M aminopterin, to block de novo pyrimidine biosynthesis, were pulsed for 12 hr with 50  $\mu$ M DBDU. The cells were harvested and washed 3 times with phosphate-buffered saline (pH 7.4). The cells ( $3 \times 10^5$  per ml) were then resuspended in growth medium and irradiated at the patient port of the Medical Research Reactor at Brookhaven National Laboratory for 2, 4, 6, 8, and 12 min. Control cells were maintained in the same pulsing medium but were provided dThd and no boronated nucleoside. Radiation damage was measured by a cloning assay (7).

The preliminary results showed that the surviving fractions were clearly reduced compared with those of control cells treated at the same neutron fluence. The relative biological effect (RBE) under these assay conditions was calculated to be 2 (Figure 3). We are currently repeating this experiment using different concentrations of DBDU and thymidine in the medium. In addition we are determining the amount of boronated nucleoside incorporated into the DNA of the hamster cells.

Obviously, this is merely a beginning. Large quantities of this compound will be needed for testing in animal models. Pharmacological, toxicological, and tissue distribution studies in animals will also be necessary. The results of these phase 1 studies will permit a toxicological evaluation of DBDU in humans prior to testing its potential for the treatment of various tumors by BNCT. The findings described above have stimulated us to synthesize--as candidates for BNCT--other nucleosides containing an endo- or exocyclic carbon-boron bond.

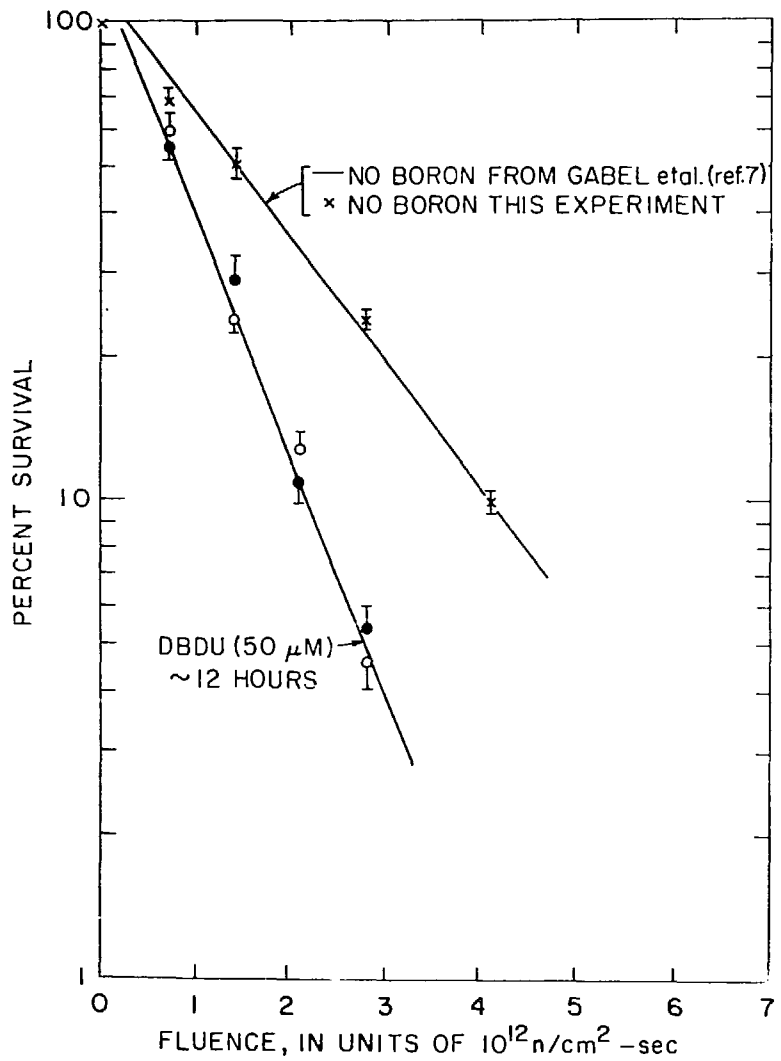


Figure 3

#### ACKNOWLEDGMENTS

RFS is supported by grants from the Veterans Administration and the NIH/NIAID (AI 18600). We wish to acknowledge the support of the Southern New England Field NMR Facility made possible by a grant from the Biotechnology Resources Program of the National Institutes of Health. The boron NMR spectra were obtained through the NSF regional NMR Center at the University of South Carolina (CHE 82-07445). This work was supported by U.S. Public Health Service Research Grant CA-05262. BL and RLF are supported by contract DE-AC02-76CH00016 from the U.S. Department of Energy with Associated Universities, Inc.

#### REFERENCES

1. Schinazi, R.F. and Prusoff, W.H. *Pediatric Clinics of North America*, 30, 77, 1983.
2. Prusoff, W.H. and Ward, D.C. *Biochem. Pharmacol.* 25, 1233, 1976.
3. Soloway, A.H., *J. Am. Chem. Soc.* 81, 3017, 1959.
4. Matteson, D.S., Biernbaum, M.S., Bechtold, R.A., Campbell, J.D. and Wilcsek, R.J. *J. Org. Chem.* 43, 950, 1959.
5. Maitra, A., *Indian J. Chem.* 16B, 85, 1978.
6. Schinazi, R.F. and Prusoff, W.H. *Tetrahedron Lett.* 50, 4981, 1978.
7. Gabel, D., Fairchild, R.G., Borner, H.G. and Larsson, B.: Accepted for publication, *Rad. Res.* (1984).

The Distribution of Exogenous Porphyrins In Vivo;  
Implications for Neutron Capture Therapy

Ralph G. Fairchild,<sup>1</sup> Detlef Gabel,<sup>1,2</sup> Manny Hillman,<sup>3</sup> and Karen Watts<sup>1</sup>

<sup>1</sup>Medical Dept., Brookhaven National Laboratory, Upton, NY 11973

<sup>2</sup>Dept. of Chemistry, University Bremen, Bremen, FRG

<sup>3</sup>Dept. of Applied Science, Brookhaven National Laboratory, Upton, NY 11973

ABSTRACT

Endogenous porphyrins (HpD) are already in clinical use for phototherapy, in which red light is used to stimulate a cytotoxic response in tumors. The evident success, at least with superficial cancers, gives biological evidence of selective concentrations of porphyrins in tumors adequate for therapy. We have investigated, in addition, the biodistribution of a synthetic porphyrin (tetraphenylporphinesulfonate, or TPPS) in seven different animal tumor models. Our data, as well as those of others, indicate abundant accumulations of TPPS in tumor. If boronated analogs behave in the same way, boron concentrations would be up to 10 times that needed for therapy. Thus, available data indicate that boronated porphyrins may provide the most direct route to adequate boron localization in neoplastic growth. Utilization of such porphyrin analogs in the neutron capture therapy (NCT) procedure is similar in concept to phototherapy currently being used clinically, with the distinct advantage of deeper tissue penetration produced by the activating neutrons. In addition, we would propose initial clinical testing of NCT in brain cancer, where the blood-brain barrier excludes porphyrins from normal brain.

INTRODUCTION

Systemic application of appropriate radiolabeled and/or cytotoxic tumor-seeking agents should in principle allow targeting to primary and metastatic neoplasms on a cellular level. However, drug uptake in non-target but competing cell pools often exceeds toxic levels before sufficient amounts are delivered to tumor. In addition, specific metabolic pathways often used in diagnosis generally have a low capacity so that at the large concentration of molecules necessary for therapy ( $\sim 10^4$  to  $10^6$  times that needed for diagnosis), effects of saturation are often found. Application of NCT can circumvent problems associated with high uptake in competing non-target cell pools, as the  $^{10}\text{B}(\text{n},\alpha)^7\text{Li}$  reaction is activated only within the radiation field. A comparison of this technique with other modes of particle therapy had indicated that NCT provides significant advantages (1). A major problem still remains in that it is difficult to obtain vehicles for boron transport which demonstrate both the tumor specificity and concentration requisite for NCT. The various compounds which have been used in NCT are shown in Table 1.

Initial clinical trials between 1951 and 1961 used the first-generation compounds, which showed no selective binding to tumor. These efforts failed to extend the life of patients. Clinical trials of NCT have been in progress since 1968 using the second-generation compound  $\text{Na}_2\text{B}_{12}\text{H}_{11}\text{SH}$ . With this mole-

Table 1  
Compounds Used in Neutron Capture Therapy

First generation	Second generation	Third generation
Sodium pentaborate $\text{Na}_2\text{B}_{10}\text{O}_{16}$	Sodium Mercaptoundeca-hydrododecaborate $\text{Na}_2\text{B}_{12}\text{H}_{11}\text{SH}$	Steroids Antibodies Nucleosides Chlorpromazine Thicuracil Amino acids Porphyrins
Paracarboxybenzene borsalic acid $\text{C}_7\text{H}_7\text{B}_2\text{O}_4$		
Sodium perhydrodecaborate $\text{Na}_2\text{B}_{10}\text{H}_{10}$		
Hydrated sodium borate (borax) $\text{Na}_2\text{B}_4\text{O}_7 \cdot 10\text{H}_2\text{O}$		

cule, the ratio of  $^{10}\text{B}$  in tumor to that in blood ( $^{10}\text{B}$  ratio) is  $\sqrt{1}$  to 2, vs 0.5 to 0.8 obtained with first-generation compounds (2-4). As of December 1983, 65 patients have been treated by Dr. Hatanaka, using a thermal neutron beam; the median survival time of these patients has been extended significantly (5).

While clinical results in Japan are encouraging with  $\text{Na}_2\text{B}_{12}\text{H}_{11}\text{SH}$ , it is our belief that the full potential of NCT lies in the development of boronated analogs of compounds such as those listed as third-generation compounds in Table 1; these biomolecules should allow localization of boron in tumors with a concomitant clearance from blood and other normal tissues within the treatment volume. Further, the long biological half-life of the newer compounds will allow a protracted or fractionated irradiation schedule, thus permitting selective repair in normal tissue and the use of lower intensity neutron beams with improved dosimetric characteristics, as indicated in the first paper of this Symposium (6).

Following the evaluation of these new compounds based on their potential to deliver the minimum necessary boron content ( $\sqrt{15}$  and 30  $\mu\text{g}$   $^{10}\text{B}/\text{g}$  tumor, for epithermal and thermal neutron beams currently available), it is evident that such boron concentrations will not be easily achieved; attainment of sufficient levels may require multiple-dosing procedures, or the use of a combination of boronated biomolecules (6). Consequently, those moieties having greater potential carrying capacity for boron may become increasingly important.

The early work by Winkelman (7,8) showed that, following a single injection of the synthetic porphyrin tetraphenylporphinesulfonate (TPPS) into rats carrying Walker carcinosarcoma (dose = 40 mg TPPS/kg body weight), robust amounts of TPPS were selectively concentrated in tumor with a biological half-life of the order of days ( $>100 \mu\text{g}$  TPPS/g tumor). Other studies (7,9) indicated that the concentration of porphyrins administered in a single dose can be increased by a factor of  $\sqrt{10}$  with proportionately higher amounts going to tumor. Various boronated analogs of such porphyrins have been described by

Haushalter, with boron contents approaching 50% by weight (10-12). If these analogs behave similarly to TPPS, boron concentration adequate for therapy will be easily obtained, with an "excess" carrying capacity of 1 order of magnitude.

The porphyrin ring is shown in Fig. 1. Natural porphyrins are water insoluble, with substitutions on the ring positions (beta-substituted porphyrins). Synthetic porphyrins with substitutions on the bridge carbon atoms constitute the meso-substituted porphyrins, and are water soluble. TPPS is one of the synthetic porphyrins, as indicated in Fig. 1, and was investigated following the work of Winkelman which indicated that TPPS showed better accumulation in tumor than did natural porphyrins (7-9).

The clinical use of hematoporphyrin derivatives (HpD) for phototherapy gives further evidence that porphyrin distributions in tumor and normal tissues may be adequate for NCT. (In phototherapy, red light is used to stimulate cytotoxic reactions in tissue sensitized with HpD.) Phototherapy has been shown to be effective for superficial tumors ( $\leq 1$  cm in depth) (13,14). Utilization of the NCT procedure would extend the treatment depth significantly because of the greater penetration in tissue of neutrons than of red light. As with phototherapy, care must be exercised to protect against damage from tissue photosensitization to ambient light.

Thus it is evident that porphyrins are unique among the biomolecules being studied for use as vehicles for boron transport to tumor; there is excess carrying capacity, and, in principle, they should be useful for any type of tumor. The data described in this paper were obtained to demonstrate these principles; the biodistribution of TPPS in seven different small animal tumor models was measured. In addition, preliminary work on the synthesis and testing of boronated analogs is briefly discussed.

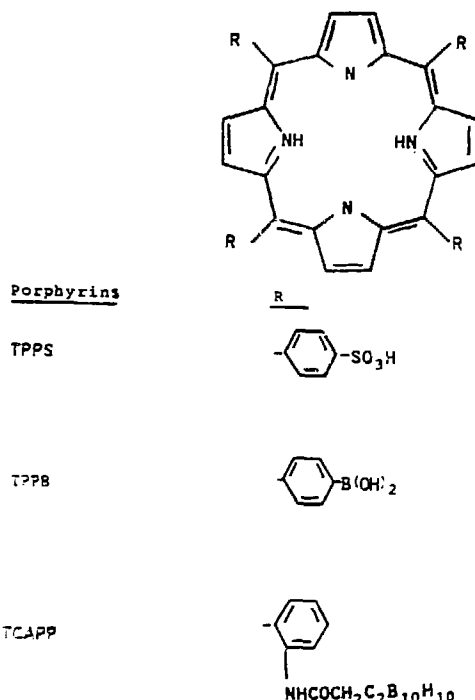


Fig. 1. The porphyrin ring, with substituents (R) in the meso-position, as described in the text.

## TISSUE ANALYSIS OF TPPS

Previous work has indicated that for  $^3\text{H}$ -TPPS and  $\text{TPP}^{35}\text{S}$ ,  $^3\text{H}$  and  $^{35}\text{S}$  are labile under conditions existing *in vivo*, and the presence of various metal ions chelated to the tetrapyrrole ring ( $^{57}\text{Co}$ ,  $^{99\text{m}}\text{Tc}$ ,  $^{109}\text{Pd}$ ) changes the apparent tissue distribution (7,15). Carbon-14 incorporated into the ring structure of TPPS is known to be a valid tag, but the synthesis is complex. Thus the spectrophotometric method of analysis described by Winkelmann (7) was used, in which the absorbance was measured at pH 2 in order to separate the response of exogenous (synthetic) porphyrin (TPPS) from that of endogenous (natural) porphyrins. Typical spectra are shown in Fig. 2 (obtained with a Cary Model 15 spectrometer); at basic pH, the absorbance spectrum from TPPS is superimposed on that from natural porphyrins (413 nm), whereas in acidic media the separation at 440 nm is good. Absorbance measurements used to evaluate TPPS content in these experiments were made with a Carl Zeiss PMQ II S spectrophotometer, at 440 nm. The background from endogenous porphyrins was subtracted by using standard curves constructed for each tissue by adding known amounts of TPPS to "control" tissues as described below (see Fig. 3).

TPPS was obtained commercially; 50 mg was dissolved in 1 cc of bacteriostatic saline, and administered intravenously (1.0 mg for mice, 10 mg for rats,

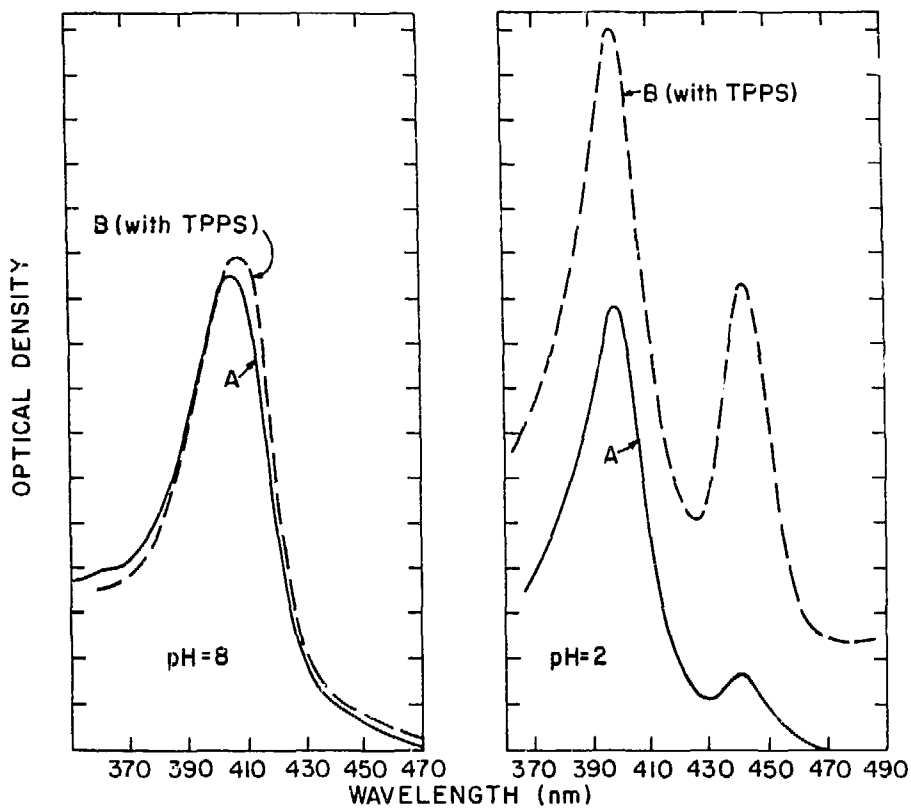


Fig. 2. Optical absorption measurements of hamster spleen tissue without TPPS (curve A) and with TPPS (curve B). For the latter, samples of spleen were obtained from a 140-g hamster that had received 10 mg of TPPS.

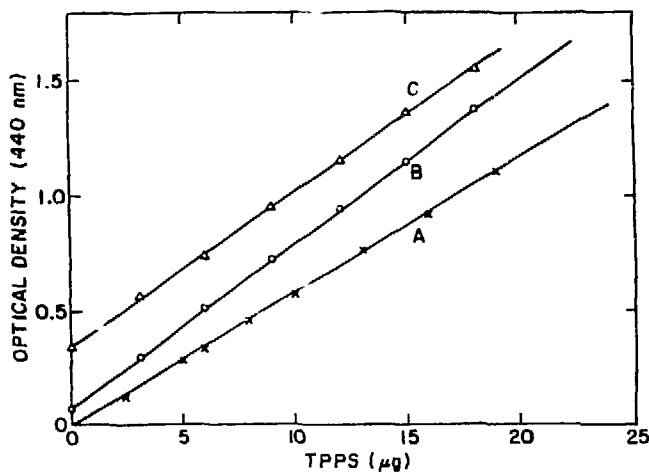


Fig. 3. Calibration curves for various tissues, used to subtract background due to endogenous porphyrins. Curve A was produced by adding known amounts of TPPS to 4.5 ml of MeOH:NH<sub>4</sub> (10:1) and 0.5 ml of 6 N HCl (no tissue). Curve B is representative of those obtained for muscle, liver, kidney, spleen, pancreas, heart, and lung. Curve C shows the higher background obtained for blood.

or  $\sim 40$  mg/kg). Winkelman had found that tumor uptake was greater (and more uniform) with i.v. administration than with i.p. injection (7). For analysis, tissue samples were taken (0.3 to 0.6 mg) and homogenized in 7.0 ml of 0.25 M glucose. One-ml aliquots of the homogenate were diluted with 2 ml H<sub>2</sub>O and 2 ml of 10% trichloroacetic acid, mixed, and centrifuged at 10,000 rpm for 10 min. The supernatant was removed, and 4.5 ml of MeOH:NH<sub>4</sub> (10:1) was added to each precipitate; the mixture was then filtered through pipets containing a glass-wool plug, and 0.5 ml 6 N HCl was added to each filtrate to bring the pH to 2. The acidified filtrates were spun at 3000 rpm for 5 min. For "unknowns" this clear solution was read at 440 nm, and then checked to ensure separation from endogenous porphyrins in a general absorption spectrum.

Calibration curves were obtained for each tissue by adding known amounts of TPPS (in steps of 3  $\mu$ g TPPS, from a freshly mixed stock solution of 100  $\mu$ g TPPS/cc) to the acidified (pH 2) filtrate obtained with tissues from an uninjected "control" animal. Standard curves were also made using clear solutions of 4.5 ml of MeOH:NH<sub>4</sub> (10:1) and 0.5 ml of 6 N HCl. The latter were used for the various tumors, as it was found that, except for blood, the background optical densities were low (see Fig. 3) and showed little variation between sample sizes varying from 0.3 to 0.6 mg. Calibration curves were found to be linear for TPPS concentrations up to  $>200$   $\mu$ g/g. For blood, background was dependent upon tissue volume; therefore, calibration curves were obtained for various samples from 0.3 to 0.6 ml. The amount of TPPS per gram tissue (wet weight) was obtained by correcting for the dilution factor of seven and for sample weight. The backgrounds obtained for various tissues ( $\sim 0.5$ -g samples, no added TPPS) are summarized in Table 2.

## RESULTS

The tissue distribution of TPPS was measured in seven different tumor models in small animals; the results are given in Table 3. Both mice and rats were given doses of  $\sim 40$  mg TPPS per kg body weight. As in the work of Winkelman with Walker carcinosarcoma (8), high uptake was found in tumor, and

Table 2  
Backgrounds from  $\sim 0.5$  g of Various Tissues (no added TPPS) at 440 nm

Tissue	Optical Density	Tissue	Optical Density
Blood	0.34	Skin	0.02
Brain	0.04	Muscle	0.07
Lung	0.05	Liver	0.03
Kidney	0.03	Pancreas	0.02
Heart	0.05	Spleen	0.06

significant uptake was observed also in liver, kidney, and spleen. Of primary importance is the finding that tumor uptake was high in all tumors studied, with TPPS concentration remaining high for periods of 1 day post injection (the longest time investigated here). Concentrations of TPPS in blood were difficult to measure reproducibly because of the high background from endogenous prophyrrins (see Fig. 3) but were similar to those in tumor.

Because of the unique potential of TPPS as a carrier for boron (concentrated in all tumors, with excess carrying capacity), preliminary efforts were made to synthesize boronated analogs. Tetraphenylporphine-p-boronic acid was prepared (TPPB), but proved to be insoluble. Dr. Haushalter kindly supplied us with a sample of one of his boronated porphyrins, tetra(1-carboranylacetamido-o-phenyl)porphyrin (TCAPP; see Fig. 1). This carboranyl porphyrin is not soluble in water, and so was degraded to the nido-hendecacarborane by reaction with KOH (see Fig. 4). The water-soluble compound was tested in BALB/c mice carrying Harding-Passey melanoma, at 12 hr post injection. No uptake was observed in tumors, but it was found that TCAPP was concentrated almost exclusively in the pancreas. Efforts are now under way to repeat these experiments.

#### DISCUSSION

The data summarized in Table 3 verify the high uptake and long biological half-life of TPPS in tumor reported by Winkelman. Further, the large variety of tumors investigated here would suggest that TPPS would be generally applica-

- 4

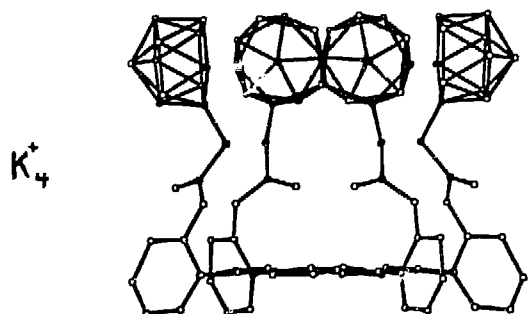


Fig. 4. Diagram of tetra(1-carboranylacetamido-o-phenyl)porphyrin (TCAPP) degraded to the nido-hendecacarborane by reaction with KOH.

**Table 3**  
**Tetraphenylporphine Sulfonate Content in Varicous Tissues**

<b>Amelanotic melanoma, BALB mice*</b>					
	1 hr	12 hr	27 hr		
	#1	#2	#1	#2	#1
Tumor	131	62	152	126	135
Kidney	103	167	325	265	335
Pancreas	19	18	93	23	45
Liver	56	79	81	70	109
Spleen	228	115	124	143	85
Lung	91	132	70	165	69
Heart	87	25	133	90	68
Muscle	85	95	37	5	11
Skin	140	76	46	67	27
Brain	17	21	24	19	

Melanotic Harding-			Walker carcinoma, EMT		
Passey	T-9 glioma, CDF rats,**	T-9 glioma, CDF rats,**	Sprague-Dawley	Sarcoma, BALB	Adeno-carcinoma
melanoma, CDF rats,**			rats	mice	C57 mouse
BALB mice* subcutaneous	intracranial				

	12 hr	24 hr	24 hr	24 hr	12 hr	12 hr
Tumor	184	136	45	83	100	111
Kidney	324	309	81	125	88	174
Pancreas	71	93	54	42	0.9	32
Liver	78	81	32	56	44	55
Spleen	80	91	73	64	42	83
Lung	135	260	59	22	73	106
Heart	96	61	0	17	20	12
Muscle	17	25	0	0	1.4	0
Skin	99	148	0	2.2	1.6	2.2
Brain		18	0	2.5	0.4	0

\*1 mg TPPS per mouse.  
 \*\*10 mg TPPS per rat.

ble (as a vehicle for boron transport) to all types of tumors. Competing uptake in such organs as spleen, liver and kidney would preclude use of radiolabeled TPPS for therapy, but would not hinder its application for NCT in situations where tissues with high uptake can be excluded from the treatment volume. In particular, the negligible amount of TPPS found in brain tissue would suggest that boronated analogs of TPPS would be ideal for the treatment of brain tumors such as glioblastoma. Levels of TPPS in blood were evidently similar to that in tumor in these experiments (data not presented here because of large errors introduced by the presence of endogenous porphyrins), but the work of Zanelli (15) indicates that tumor/blood ratios of 2 to 5 may be obtained at  $\sim$ 2 days post injection. Alternatively, exchange blood transfusions may be used to lower blood levels.

A major attribute of TPPS is the robust accumulation in tumor ( $\sim$ 100  $\mu$ g/g following a single dose of  $\sim$ 40 mg TPPS/kg body weight). In view of the possibility of making analogs with boron contents approaching 50% by weight (MW of TPP = 614), a single injection could deliver  $\sim$ 50  $\mu$ g  $^{10}$ B/g tumor. As noted above, minimum boron concentrations of from 15  $\mu$ g/g (epithermal neutrons) to 30  $\mu$ g/g (thermal neutrons) are needed for NCT. Indications are that higher TPPS concentrations would be available via larger initial doses or through multiple injections (7).

The potential advantages provided by TPPS may be illustrated by comparing the data in Table 3 for TPPS uptake in amelanotic and melanotic melanoma in BALB/c mice with boron concentration in the same tumor model from first- and second-generation compounds. Table 4 shows the time course of some first- and second-generation boron compounds, indicating the lack of specificity and binding. Some binding is seen for  $Na_2B_{12}H_{11}SH$  at 12 to 24 hr, although absolute boron concentration is small and not adequate for successful therapy as defined above. Injected doses used to obtain the data in Table 4 were similar to those employed with humans, on the basis of mg/kg body weight (4,5).

Boron content for the first- and second-generation compounds shows rapid wash-out at times  $\geq$ 6 hr. The remaining concentrations are well below the "equilibrium" value of 40  $\mu$ g/g (the "equilibrium" value of the total injected dose assuming uniform distribution throughout the body). Conversely, TPPS concentrations in tumor are well above the equilibrium value of 40  $\mu$ g TPPS/g, indicating physiological targeting and accumulation in tumor with a biological half-life of the order of days--ideal characteristics for a vehicle for boron transport to tumor.

Little is known about the mechanism which causes porphyrins to accumulate in tumors (14), although at least one investigator has concluded that porphyrins penetrate the cell membrane and are associated with cytoplasmic macromolecules (16). There appears to be a consensus that TPPS accumulates in tumor better than endogenous porphyrins and at least as well as any of the synthetic porphyrins (7-9,15,17).

The apparent abundance of chemical routes for the boronation of various porphyrins should enhance the chance of eventual success. For example, in addition to the various analogs described by Haushalter, analogs can be synthesized with borazine rings in place of the phenyl groups, and these might be better (18). In view of the relatively high level of carrying capacity and applicability of porphyrins, it is hoped that more effort will be devoted to this avenue of research.

Table 4

## Comparison of Temporal Distribution of Boron Compounds in BALB/c Mice Carrying Harding-Passey Melanoma

Compound	Tissue	Boron concentration ( $\mu\text{g/g}$ tissue) at various times post injection of 40 $\mu\text{g B/g}^*$				
		1 hr	2 hr	6 hr	12 hr	24 hr
$\text{Na}_2\text{B}_{10}\text{O}_{16}$ (Sodium pentaborate)	tumor	27	4	0	0	0
	brain	27	2	0	0	0
	blood	15	2	0	0	0
$\text{Na}_2\text{B}_4\text{O}_7 \cdot 10\text{H}_2\text{O}$ (Sodium borate)	tumor	33	7	0	0	0
	brain	21	6	0	0	0
	blood	31	6	0	0	0
$\text{Na}_2\text{B}_{12}\text{H}_{11}\text{SH}$ (Sulphydryl boron hydride)	tumor	19	6	4	3	
	brain	0	0	0	0	
	blood	32	5	0	0	

\*No significant difference has been found between i.p. or i.v. injection.  $\text{Na}_2\text{B}_{10}\text{O}_{16}$  and  $\text{Na}_2\text{B}_{12}\text{H}_{11}\text{SH}$  were given i.p., and  $\text{Na}_2\text{B}_4\text{O}_7 \cdot 10\text{H}_2\text{O}$  was administered i.v. Each value is the average from 2 or more animals.

## ACKNOWLEDGMENTS

The possibility of using boronated analogs of tetraphenylporphyrins was first suggested to us by Stephen J. Hannon (then at UCLA) in a personal communication (March 7, 1979). The original work at BNL, measuring TPPS uptake in hamsters, was done by T. X. Aufiero, a summer student from Haverford College, Haverford, PA, and summarized in an internal report (August 17, 1979).

## REFERENCES

1. R.G. Fairchild and V.P. Bond. A comparison of particle radiation therapy modalities. Proc. of Tokyo Medical Society Meeting on Neutron Capture Therapy, Tokyo, Jan. 1981, in press.
2. R.G. Fairchild. Proc. of Int. Symp. on Synthesis and Applications of Isotopically Labelled Compounds. Kansas City, MO, June 1982, pp. 155-60. W.P. Duncan and A.B. Susan, Eds., Elsevier, Amsterdam, 1983.
3. E.I. Tolpin, G.R. Wellum, F.C. Dohan, Jr., P.L. Kornblith, and R.G. Zamenhof. Oncology 32, 223-46 (1975).

4. H. Hatanaka. *J. Neurol.* 209, 81-94 (1975).
5. H. Hatanaka. See paper VIII-3 in this Symposium.
6. R.G. Fairchild and V.P. Bond. See paper I-1 in this Symposium.
7. J. Winkelmann. *Cancer Res.* 22, 589-96 (1962).
8. J. Winkelmann, G. Slater, and J. Grossman. *Cancer Res.* 27, 2060 (1967).
9. J. Winkelmann and D.S. Rasmussen-Taxdal. Quantitative determination of porphyrin uptake by tumor tissue following parenteral administration. *Bull. Johns Hopkins Hosp.* 107, 228-33 (1960).
10. R.C. Haushalter and R.W. Rudolph. *J. Am. Chem. Soc.* 100, 4628 (1978).
11. R.C. Haushalter and R.W. Rudolph. *J. Am. Soc.* 101, 7080 (1979).
12. R.C. Haushalter, W.M. Butler, and R.W. Rudolph. *J. Am. Chem. Soc.* 101, 2620 (1981).
13. T.J. Dougherty, J.E. Kaufman, A. Goldfarb, K.R. Weishaupt, D. Boyle, and A. Mittleman. *Cancer Res.* 38, 2628-35 (1978).
14. F. Hetzel. Proc. of 25th Ann. ASTR Meeting. *Int. J. Rad. Oncol. Biology-Physics* 9, 118 (1983).
15. G.D. Zanelli and A.C. Kaelin. *Brit. J. Radiol.* 54, 403-7 (1981).
16. C.J. Carrani. Studies on meso-tetra(p-sulfophenyl)porphine as a tumor localizing agent. Thesis, Texas A&M University, College Station, Texas.
17. T.S.T. Wang, R.A. Fawwaz, and P. Tomashefsky. Metalloporphyrin derivative: structure localization properties in radiopharmaceuticals. In *Structure-Activity Relationships*, pp. 225-50, R.P. Spencer, Ed., Grune and Stratton, New York, 1981.
18. R. Porter (Chemistry Dept., Cornell U., Ithaca, NY). Personal communication, July 27, 1981.

Boronated Anti-Estrogens for Boron Neutron Capture Therapy  
and Boron Neutron Capture Radiography

Folkert Wellmann and Detlef Gabel

Department of Chemistry, University of Bremen  
Postfach 330 440, D-2800 Bremen 33, F.R.G.

One of the main obstacles so far to a successful general means of boron-10 neutron capture therapy is the difficulty of finding suitable vehicles for boron which allow selective and quantitatively sufficient accumulation of boron in the tumor tissue.

In estrogen sensitive cells, estrogens bind to receptor proteins via van der Waals, electrostatic, and hydrogen bond interactions. The cytoplasmic estrogen-receptor complex is translocated to the cell nucleus, where it initiates a series of events eventually leading to cell growth and division. Estrogen receptors might therefore be suitable vehicles for transporting boron-containing estrogens to the cell nucleus, if it were possible to synthesize such compounds with retention of biological activity and physiological properties. The  $^4\text{He}$  and  $^7\text{Li}$  particles produced in the  $^{10}\text{B}(\text{n},\alpha)^7\text{Li}$  neutron capture reaction could in this case have a high probability of hitting the DNA and damaging it irreversibly (4,9).

To reduce radiation damage in surrounding tissue, sufficient clearance of administered boron compounds, especially from the blood, has to be achieved. The tumor-to-surroundings ratio, and especially the tumor-to-blood ratio, would therefore have to stay above a certain minimal level. In addition, irradiation with thermal neutrons leads to  $^1\text{H}(\text{n},\gamma)^2\text{H}$  and  $^{14}\text{N}(\text{n},\text{p})^{14}\text{C}$  capture reactions. There is, therefore, an upper limit for the total neutron dose delivered, demanding a certain minimal uptake of  $^{10}\text{B}$  in the cell. (It should be kept in mind that, although there are, as yet, no definite numerical estimates for the parameters mentioned, the existence of such limitations is undisputed.)

Jungblut et al. (8) have measured the time course of the concentrations of estrogens and estrogen receptors in the cell nucleus, following an estradiol pulse. A rapid and parallel increase of estradiol and receptor concentrations in the nucleus was found, followed by a decrease of both with a half-time of ~90 min. Whereas the nuclear receptor contents levelled off at about 10 000 receptors per nucleus, estradiol was eliminated exhaustively.

Similar results have been obtained by Horwitz and McGuire (6), using MCF-7 cells in culture. The nuclear receptor concentration increased rapidly, and then decreased with half-times similar to those observed by Jungblut et al. (8).

The short retention time in the nucleus seems characteristic for estrogens in general. It casts doubt on the usefulness of boronated estrogens in neutron capture therapy. In particular, sufficient blood clearance seems unobtainable, and this leads to high radiation damage in the surrounding tissue and vessels.

Anti-estrogens are capable of being taken up in the cell nucleus by the same receptors as estrogens. They do not seem, however, to trigger the same chain of events, thus being antagonists to estrogens (5).

Horwitz and McGuire (6) have investigated the nuclear receptor concentrations in MCF-7 cells also after administration of the anti-estrogens tamoxifen and nafoxidin. Tamoxifen led to slower receptor release from the nucleus, and nafoxidin caused all of the translocated receptors to stay in the nucleus for several hours. Such prolonged uptake in the nucleus would make sufficient blood clearance more likely.

We have therefore attempted the synthesis of boron-containing anti-estrogens, especially derivatives of the biologically active compound 6-hydroxy-2-phenyl-1-(p-2',3'-dihydroxypropoxy)phenyl-1,2,3,4-tetrahydronaphthalin, (U-23,469-M) (5,12), which is formed in vivo from the originally described 6-methoxy compound (11) (Fig. 1).

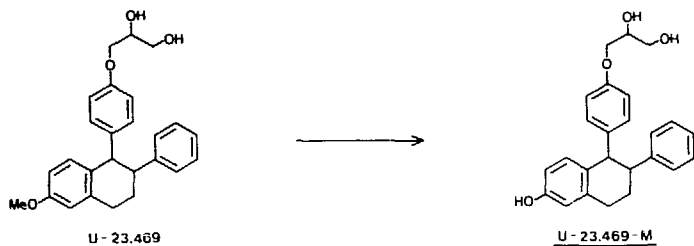


Fig. 1 Formulas of the anti-estrogens U-23,469 and U-23,469-M.

The phenol 6-methoxy-2-phenyl-1-(p-hydroxy)phenyl-1,2,3,4-tetrahydronaphthalin described in the literature (11) (Fig. 2) was reacted with epichlorohydrin to the 2',3'-epoxypropyl ether. The base-catalyzed addition of B-decachloro-o-carborane (3) yielded U-23,469-Decloc.\* Selective cleavage with  $\text{BBr}_3$  of the ether at position 6 of the tetrahydronaphthalin system yielded the desired derivative U-23,469-M-Decloc.

The homologous compound U-23,469-M-CHOH-Decloc, with an additional hydroxymethylene group in the side chain, can be obtained by reaction of the above phenol with 1-decachlorocarbonyl-2-hydroxy-3,4-epoxybutane and subsequent selective demethylation with  $\text{BBr}_3$ .

\*Decloc = decachloro-o-carborane.

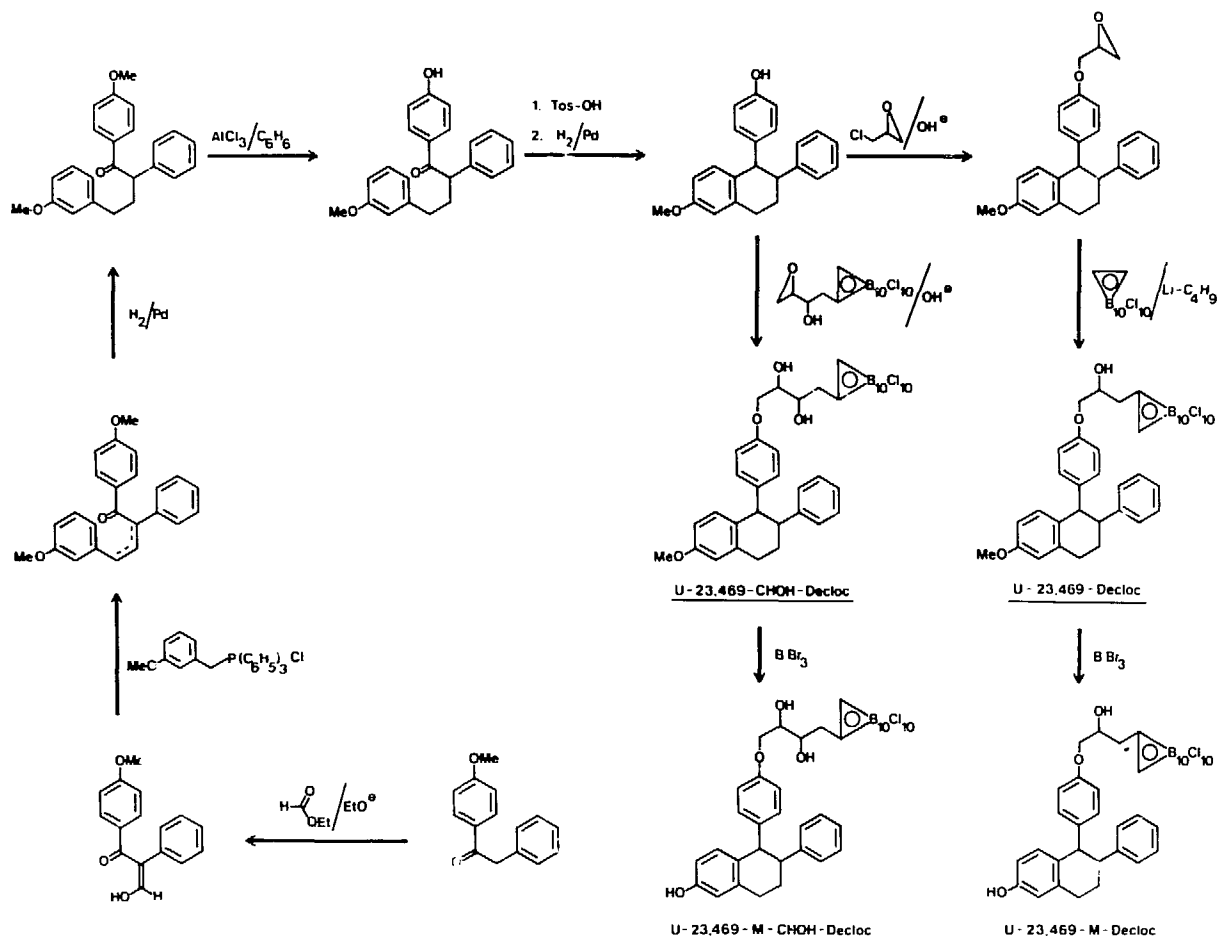


Fig. 2. Reaction scheme for the synthesis of U-23,469-M-Decloc.

By choosing more suitable protecting groups, these complications can be circumvented. In addition, as shown in Fig. 3, the number of necessary steps in the synthesis can be decreased. Thus, generation of the *p*-hydroxy function in the butanone derivative can be done at the same time as hydrogenation of the butane isomers, if benzyl or benzylloxycarbonyl groups are used as protecting groups. Masking of the 6-hydroxy group is better achieved with the ethoxycarbonyl group, which is resistant to acidic or hydrogenolytic cleavage. The masking group can be eliminated, after the introduction of decachlorocarboration, by treatment with strong alkali, and this yields the desired products nearly quantitatively.

In the course of the synthesis we found that the selective demethylation steps to 1-(*p*-hydroxy)phenyl-2-phenyl-4-(*m*-methoxy)phenylbutanone-1 and especially to U-23,469-M-

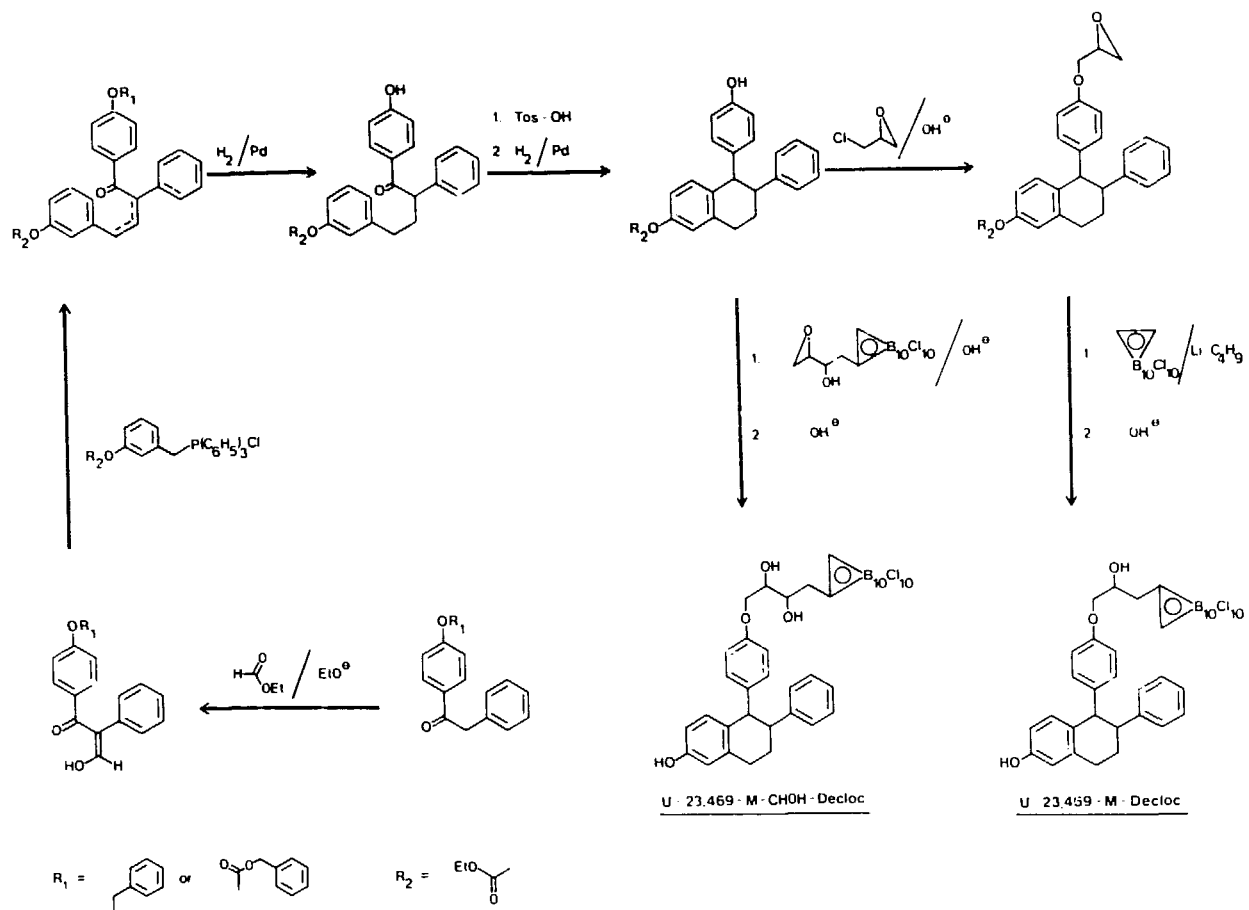


Fig. 3. Improved synthesis of U-23,469-M-Decloc and U-23,469-M-CHOH-Decloc.

Decloc and U-23,469-M-CHOH-Decloc, caused difficulties. In the latter two cases, the reaction mixtures contained, besides unreacted starting material, all three possible cleavage products. Their chromatographic separation was greatly hindered by the pronounced tailing of the decachlorocarbonyl compounds.

We found that the compound U-23,469-M-Decloc was taken up by ZR75-1 cells (1) in culture. Cells grown in RPMI medium supplemented with 10% fetal bovine serum were exposed to  $10^{-5}$  M of the anti-estrogen. After 30 min at  $37^\circ$ , the cells were washed three times with cold phosphate buffered saline, trypsinized, and centrifuged. An aliquot was taken for boron analysis (2). ZR75-30 cells (1) were treated correspondingly to serve as a control.

In the ZR75-1 cells, which contained estrogen receptor, the anti-estrogen accumulated to an amount of about  $10^5$  mole-

cules per cell, whereas in the ZR75-30 cells, which served as control, the boron content was not above the background level, which is about the same as the number of estrogen receptors found for these cells (7).

In view of the low receptor concentrations found in cells containing estrogen receptors, it might be doubtful that steroids and their antagonists will be applicable in boron neutron capture therapy (see also Hechter and Schwartz, in this Symposium). The compounds described here might, however, be useful in the *in vivo* measurement of receptor densities of material obtained, e.g., through needle biopsies, or in neutron capture radiography (10).

#### ACKNOWLEDGMENTS

We wish to thank Dr. P.W. Jungblut for helpful discussions. This work has been financially supported by the Deutsche Forschungsgemeinschaft and the Fonds der Chemischen Industrie.

#### REFERENCES

1. Engel, L.W., Young, N.A., Tralka, T.S., Lippman, M.E., O'Brien, S.J., and Joyce, M.J. (1978) *Cancer Res.* 38, 3352-3364.
2. Gabel, D., Hocke, I., and Elsen, W. (1983) *Phys. Med. Biol.*, in press.
3. Gabel, D. and Walczyna, R. (1982) *Z. Naturforsch.* 37c, 1038-1039.
4. Gabel, D. et al. See paper III-2 in this Symposium.
5. Hayes, J.R., Rorke, E.A., Robertson, D.W., Katzenellenbogen, B.S., and Katzenellenbogen, J.A. (1981) *Endocrinology* 108, 164-172.
6. Horwitz, K.B. and McGuire, W.L. (1978) *J. Biol. Chem.* 53, 8185-8191.
7. Horwitz, K.B., Zava, D.T., Thilajar, A.K., Jensen, E.M., and McGuire, W.L. (1978) *Cancer Res.* 38, 2434-2437.
8. Jungblut, P.W., Hughes, A., Kallweit, E., Maschler, I., Parl, F., Sierralta, W., Szendro, P.I., and Wagner, R.K. (1979) *J. Steroid Biochem.* 11, 273-278.
9. Kobayashi, T. and Kanda, K. (1982) *Radiat. Res.* 91, 77-94.
10. Larsson, B., Gabel, D., and Borner, H.G. (1983) *Phys. Med. Biol.*, in press.
11. Lednicker, D., Emmert, D.W., Lyster, S.C., and Duncan, G.W. (1969) *J. Med. Chem.* 12, 881-885.
12. Tatee, T., Carlson, K.E., Katzenellenbogen, J.A., Robertson, D.W., and Katzenellenbogen, B.S. (1979) *J. Med. Chem.* 22, 1509-1517.

Synthesis, Physical Properties, and Biological Activity of Estrogen Carboranes

Harry E. Hadd

Northwest Center for Medical Education, Gary, Indiana

ABSTRACT\*

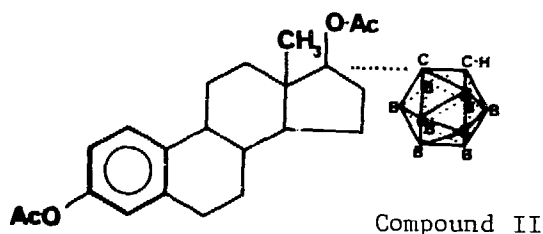
Herein is reported the synthesis and physical characterization of the first  $17\alpha$ -carborane-estradiol- $17\beta$ -acetate:  $(17\beta)$ - $17$ -[ $1,2$ -dicarba-dodecaboran( $12$ )- $1$ -yl] estra- $1,3,5(10)$ -triene- $3,17$ -diol monoacetate (III), for evaluation in boron neutron capture modalities (Pat. Appl., Harry E. Hadd for Indiana University Foundation, Jan. 12, 1983, no. 457,384).

A benzene solution of ethynylestradiol- $3,17\beta$ -diacetate was refluxed with acetonitrile and decaborane for 72 hrs, with TLC monitoring to determine the qualitative nature of the reaction mixture. It was observed that as  $\text{EE}_2\text{Ac}_2$  disappeared from the mixture, two areas of less polar steroid derivatives presented themselves. The least polar appeared to be  $\text{E}_2\text{-Ac-CBN}$  (I); the compound of intermediate polarity was  $\text{E}_2\text{-Ac}_2\text{-CBN}$  (II). Following the reaction semi-preparative HPLC on silica gel with the solvent methylene chloride/isooctane (7:3) was employed to separate and purify the two compounds. Physical Properties: (I) mp 182-5, crystallized from ethanol. MS:  $M^+$   $439\pm 3$ ;  $398\pm 4$ ; 282, 254, 228. Calc.  $\text{C}_{22}\text{H}_{34}\text{O}_2\text{B}_{10}$  + ( $438.622$ )- $\text{C}_2\text{H}_5\text{OH}$  (484.69); C 59.47, H 8.32, B 22.31; found C 59.87, H 8.44, B 22.40.

(II) mp 223-5, crystallized from methylene chloride/isooctane. MS:  $M^+$   $498\pm 3$ , ( $M^+-42$ ) 456 (boron complex 453-458),  $M^+-42-59$  397 (boron complex 398-401), 228, 213, 159 (boron complex 157-161). Calc.  $\text{C}_{24}\text{H}_{38}\text{B}_{10}\text{O}_4$  (498.624); C 57.77, H 7.65, B 21.65; found C 57.59, H 7.68, B 21.42.

(II) was heated under reflux with 1N HCl in ethanol to yield (III) the 17-monoacetate, mp 259-261 UV  $\lambda_{\text{max}}^{\text{MeOH}}$  280nm (MeOH)  $2.82 \times 10^3$ . Crystallized from MeOH. Calc.  $\text{C}_{22}\text{H}_{36}\text{O}_3\text{B}_{10}$ , B 23.68; found B 23.56. Other physico-chemical data:  $^1\text{Hnmr}$ ,  $^{13}\text{Cnmr}$ ,  $^{11}\text{B}$  nmr, IR, UV. X-ray crystallography of (II) confirmed the structural assignments. Uterotrophic bioassay using infantile mice showed that (III) maintained about 10-20% of the activity of estrone. The mp and ir of (II) purportedly synthesized by Sweet and Samant (Synth. & Applic. Isotop. Label. Cpd., Duncan & Susan, eds., pp 175-180, Elsevier, 1983) does not conform to  $\text{E}_2\text{-3,17Ac}_2\text{-17CBN}$  herein described.

Supported by a grant by the LCMCDA and NIH grant RR 01077.



\*Paper withdrawn after volume went to press.

## RECENT ADVANCES IN THE SYNTHESIS OF BORON-CONTAINING STEROIDS AND PORPHYRINS

Stephen B. Kahl

Department of Pharmaceutical Chemistry  
University of California, San Francisco, CA 94143

### Introduction

We are pleased to present recent work from UCSF on the synthesis of carboranyl steroids and carboranyl porphyrins. The steroidal compounds represent the most recent efforts in our six year old program in this area, while the porphyrins represent our initial synthetic attempts to attach carborane cages to porphyrins. Since this Symposium has also heard a number of stimulating papers presented in the area of boron analysis, some of our recently published work describing the development of a highly sensitive gas chromatographic-microwave induced plasma (GC-MIP) boron analysis is also presented

### Materials and Methods

Ortho-carborane was purchased from Dexsil Chemical Corp., steroids from Steraloids, Inc., and all other reagents from Aldrich. Carborane was sublimed prior to use and all reaction solvents were dried and distilled using accepted methods. Infrared spectra were obtained as KBr mulls on Perkin-Elmer 727B or 1310 infrared spectrophotometers. Ultraviolet-visible spectra of the porphyrins were recorded in acetone solution at approximately 0.1 mM concentration using a Cary 118C. Proton nmr spectra were obtained on either a Varian FT-80 or a home built 240 MHz spectrometer at the University of California, San Francisco. Low resolution electron impact mass spectra were obtained through the generosity of the NIH Regional Resource for Mass Spectrometry directed by Dr. A.L. Burlingame at UCSF. Elemental analyses were performed by either Galbraith Labs or the microanalytical laboratory at UC, Berkeley.

### 17 $\alpha$ -Carboranyl methyl-3-Methoxy-Estradiol (I)

Ten millimoles of lithium carborane were prepared by adding 6.25 ml of 1.6 M n-BuLi in hexane to a solution of 1.44 g orthocarborane in 10 ml dry benzene. The mixture was stirred at room temperature for 1  $\frac{1}{2}$  hours. The white precipitate was dissolved by the addition of a few ml of THF followed immediately by the dropwise addition of a solution of 0.598g (2 mmoles) of the oxirane, prepared by the method of Wall and coworkers,<sup>1</sup> in 30 ml of THF. The mixture was stirred at room temperature for 48 hours at which time TLC indicated no remaining oxirane. The mixture was acidified to pH 1 with 1N HCl and 50 ml of ether added. The organic layer was separated, washed with saturated aqueous NH<sub>4</sub>Cl (2X) and water (2X), and dried over MgSO<sub>4</sub>. Solvents were stripped to give an oil which was triturated with hexane to yield a gummy solid. This solid was recrystallized to yield 0.060g of a

fluffy white solid, m.p. 198-199°C (uncorrected). Anal. Calcd. for  $C_{22}H_{38}O_2B_{10}$ : C, 59.70; H, 8.65;  $\delta$ , 7.23. Found: C, 59.4; H, 8.88; O, 7.15. Pmr ( $CDCl_3$ ):  $\delta$  1.00 (C-18 methyl), 3.65 ( $-CH_2-$ carborane), 3.79 (3- $OCH_3$ ), 4.60 (carborane CH). IR (KBr): 3300  $cm^{-1}$  (OH), 3060 (carboranyl CH), 2920 (CH), 2870 ( $OCH_3$ ), 2580 (BH). Low resolution electron impact mass spectrum consisted of a parent ion peak at 442 with a base peak at m/e = 227.

#### 16 $\alpha$ -Carboranyl-3-Methoxy-Estradiol (II)

Ten millimoles of lithiocarborane, prepared by the method described above, were dissolved by the addition of a few ml dry ether. To this solution was added a solution of 2 mmoles of the 16 $\beta$ , 17 $\beta$ -epoxide prepared by the method of Ponsold.<sup>2</sup> Mixture was heated at reflux for 30 hours to produce an orange solution and a significant amount of light colored precipitate. TLC showed little or no starting steroidal material. The reaction was quenched by pouring into 100 ml of saturated aqueous  $NH_4Cl$ . Organic layer was separated, washed twice with water and dried over  $MgSO_4$ . Removal of solvents gave a dark colored semi-solid which, when triturated twice with hexane, yielded 0.82 g off-white powder. This material was purified by flash chromatography to give 0.80 g white solids, m.p. 165-169°C (uncorrected). Anal. Calc. for  $C_{21}H_{36}O_2B_{10}$ : C, 58.85; H, 8.47; O, 7.47. Found: C, 59.1; H, 8.57; O, 7.30. Pmr ( $CDCl_3$ ):  $\delta$  0.85 (C-18 methyl), 3.79 ( $-OCH_3$ ), 3.96 (carborane CH). IR (KBr): 3280  $cm^{-1}$  (OH), 3060 (carborane CH), 2920 (CH), 2870 ( $OCH_3$ ), 2580 (BH). LREI mass spectrum showed a parent ion peak at m/e = 428 with a base peak at m/e = 160.

#### Meso-ar-Tetra (c-Carboranylaminophenyl) Porphyrin (III)

Meso-tetra(o-aminophenyl) porphyrin (1.43 g, 2.12 mmoles), produced by the method of Collman and coworkers,<sup>3</sup> was dissolved in 120 ml of dry  $CH_2Cl_2$  with 2 ml dry pyridine added. To this was added a  $CH_2Cl_2$  solution of 12.7 mmoles (50% excess) of carborane carboxylic acid chloride, prepared from 2.39 g of acid and 2.64 g  $PCl_5$  by the method of Zakharkin.<sup>4</sup> The mixture was refluxed for 2 hours, then cooled to room temperature. Twenty ml each of water and dilute  $NH_3$  were added and the mixture stirred for 2 hours. To this was added 100 ml dilute NaOH. The organic layer was separated and washed with dil.  $NH_3$  (2X),  $H_2O$  (2X) and saturated aqueous NaCl. Following drying over  $MgSO_4$  the solvents were removed to give a crude product which was chromatographed on silica with 1:1  $CH_2Cl_2-Et_2O$  as the eluting solvent. The residue was recrystallized from ethanol to give 0.300 g dark purple crystals. Visible spectrum (acetone): 656 nm ( $\log \epsilon = 3.36$ ); 591 (3.62); 550 (3.61); 517 (4.11), 420 (5.18). IR (KBr): 3375  $cm^{-1}$ : (porphyrin NH), 3060 (carboranyl CH), 2580 (BH), 1700 (amide carbonyl). Pmr ( $CDCl_3$ ):  $\delta$  4.15 (carborane CH), 7.5 - 8.1 (phenyl rings); 5.50 - 8.58 (amide NH), 8.72 - 8.87 ( $\beta$ -pyrole).

#### Meso-ar-H<sub>2</sub> [P( $C_6H_4NHCOB_9H_{10}C_2$ .pipH)<sub>4</sub>] (IV)

The closed cage amide (III) was degraded by refluxing a solution of 100 g in 16 ml dry pyridine and 8 ml dry piperidine for 4 hours. The amines were

removed at reduced pressure to produce an iridescent purple solid which was washed with  $\text{Et}_2\text{O}$  to remove any remaining amines. The residue was dissolved in acetone and filtered. The filtrate was evaporated, redissolved in acetone, filtered and then evaporated. This product was stirred with  $\text{Et}_2\text{O}$ , filtered, air dried, and finally heated at 100°C under vacuum overnight to yield 0.117 g of an iridescent purple microcrystalline solid. Visible spectrum (acetone): 660 nm ( $\log \epsilon = 3.57$ ), 599 (3.61), 561 (3.79), 524 (4.08), 430 (5.28). IR (KBr):  $3380 \text{ cm}^{-1}$  (porphyrin NH), 2530 (BH), 1620 (amide carbonyl). Pmr (DMSO-d<sup>6</sup>): 1.4-1.7, 3.0 (pip<sup>+</sup>), 3.4 (carborane CH), 7.6, 7.9, 8.3 (phenyl rings), 8.15 (amide), 8.69 ( $\beta$ -pyrole).

22-Oxo-22[C1',C2'-dicarbaclosododecaboranyl]-23,24-bisnor-5-cholene-3-ol-acetate (V)

Compound V was prepared from the acid chloride and lithiocarborane as noted in reference 6.

Instrumentation

The GC-MIP instrumentation is shown schematically in Figure 5. The gas chromatograph was a Tracor model 550 modified by removal of the electron capture detector and replacement of all exposed metal parts with silanized glass or glass-lined metal parts. A 3 ft x 2 mm i.d. packed glass column of Permabond methyl silicone was utilized for the steroidal carborane analysis. Addition of a glass-lined metal splitting "tee" permitted a fixed ratio of the column effluent to be transferred to the FID-MIP interface. MIP-bound column effluent was solvent-vented and then mixed with inert carrier gas for transport into the Beenakker TM<sub>010</sub> cavity. Within this cavity the boron-containing compounds were excited by the microwave discharge. An optical bench, containing a focusing lens, an optical beam splitter and two monochromators, was placed at right angles to the microwave beam such that the emissions of both carbon and boron could be monitored. A more complete description of the instrumental details may be found in reference 5 and references cited therein.

**RESULTS AND DISCUSSION**

Steroids

Successful synthetic methodologies designed to form carbon-carbon bonds between steroids and carboranes through nucleophilic attack of C-metallocarboranes on electron-deficient carbon centers in steroids have been relatively difficult to achieve.<sup>6</sup> This has resulted in part from the rather weak nucleophilicity of the carborane anion and also in part because the tertiary alcoholate salt formed upon reaction of a C-metallocarborane and a ketone, an obvious synthetic pathway for steroids, is suspected of being unstable. Recently we have attempted to circumvent this problem by two methods, one of which has been successful, the other not.

Conversion of a steroidal ketone to a spiro oxirane with a sulfur ylide by the method of Wall<sup>1</sup> followed by reaction with monolithiocarborane yielded the alcohol as shown in Figure 1.

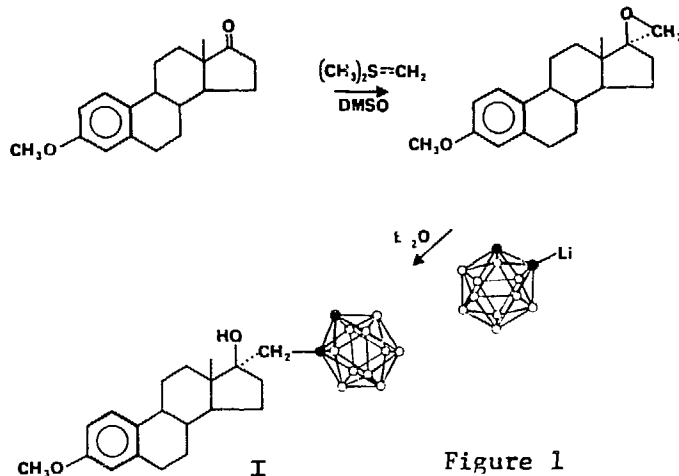


Figure 1

The yield in this process was quite low but no attempt was made to seek optimum reaction and work-up conditions. Thin layer chromatograms taken during the reaction suggested that the reaction was essentially complete. As a result of separating the electron-withdrawing cage from the alcoholic carbon by a methylene, the 17 $\alpha$ -carboranyl methyl compound I seems to be much more stable to base than the 17 $\alpha$ -carboranyl alcohols described previously by Sweet<sup>7</sup> and by Hadd<sup>8</sup>. The spectral properties of this compound are not particularly noteworthy except for two features. The position of the carborane CH at 4.60 is rather more deshielded than expected, since this resonance usually occurs in the 4.2-3.9 ppm range. This deshielding may be indicative of intra-molecular hydrogen bonding with the 17 $\beta$ -OH. The 18-methyl group also appears downfield of its expected position relative to both other estrogen derivatives and to other carboranyl steroids. Since the chemical shift of this group is quite sensitive to electronic effects, its position in I is possibly a reflection of the strong electron-withdrawing ability of the carborane cage.

Since we had shown that spiro-oxiranes could be opened with lithiocarborane, attempts were made to react more hindered oxiranes. Such a reaction is shown in Figure 2.

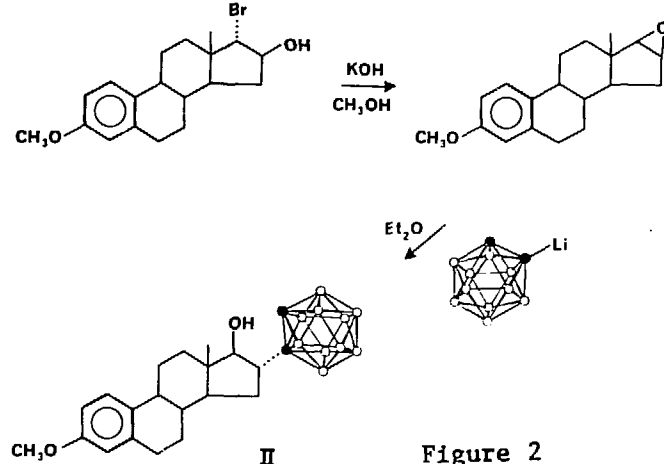


Figure 2

The  $16\beta$ ,  $17\beta$  epoxide shown could be cleaved by prolonged reflux with excess nucleophile, but similar attempts to open its  $16\alpha$ ,  $17\alpha$  isomer failed. This failure reflects the steric influence of the carborane cage since it must approach from the upper or  $\beta$ -face of the steroid and thus must be influenced by the  $18$ -methyl group.

We have tried for years to find conditions suitable for successful reaction of steroidal 17-ketones with metallocarboranes, but no avail. Our latest attempt was prompted by recent reports that crown ethers significantly enhance the nucleophilicity of some nucleophiles by tight complexation of the metal counter ion. When estrone-3-methyl ether was reacted with lithiocarborane in the presence of 18-crown-6, a lithium-specific crown ether, no alcoholic product could be isolated nor was there any indication of  $3^\circ$  alcoholate salt formation. Thus it appears that such reactions are not feasible.

Compound I is currently being examined by the Brookhaven group for binding to two lines of cultured breast cancer cells, one known to possess cytosolic estradiol binding protein, the other known to lack such receptors. We are also attempting to determine the receptor binding constants for both I and II and hope to report on these studies in the near future.

### Porphyrins

The rationale for the synthesis of boron-containing porphyrins is that both natural and synthetic porphyrins are known to be selectively taken up by a very wide variety of tumor tissues. Dougherty and others have pioneered the clinical examination of derivatives of hematoporphyrin in a form of photo-radiation therapy in which a solution of about 2.5 mg/kg of hematoporphyrin derivative is injected intravenously followed several hours later by irradiation of the tumor region by 630 nm light.<sup>10</sup> Significant clinical success has been observed with this treatment in melanotic and amelanotic melanoma, Kaposi's sarcoma, recurrent breast cancer, and cancers of the lung, brain, colon and rectum, to note but a few. Fairchild has noted that the synthetic porphyrin tetraphenylporphinesulfonate, TPPS, localizes in various mouse tumors at levels in the range of 150  $\mu\text{g/g}$  tumor with tumor/tissue ratios ranging from 3 to 9 depending on the organ examined.<sup>11</sup>

Our carboranyl porphyrin syntheses were based on similar work reported recently by the late Ralph Rudolph and coworkers.<sup>12</sup> The synthesis of the closed cage carboranyl porphyrin III proceeded as shown in Figure 3. The starting aminophenyl porphyrin was prepared by the method of Collman.<sup>3</sup>

This material consists of a mixture of four atropisomers and no attempt was made to separate them further before reaction with carborane carbonyl chloride. However, the column chromatographic purification method utilized almost certainly did affect such separation of the resultant amides. Normal yields for a reaction such as this would have been expected to be upwards of 80-85% yet we obtained only about a 10% yield. The  $\alpha\beta\alpha\beta$  atropisomer is the least polar and should move most rapidly using  $\text{CH}_2\text{Cl}_2\text{-Et}_2\text{O}$  (1:1) as the

eluent. Moreover, it should represent only about 12% of the total amide product. We now believe that only this atropisomer was isolated before halting the separation. Work is currently underway to isolate and characterize all four atropisomers.

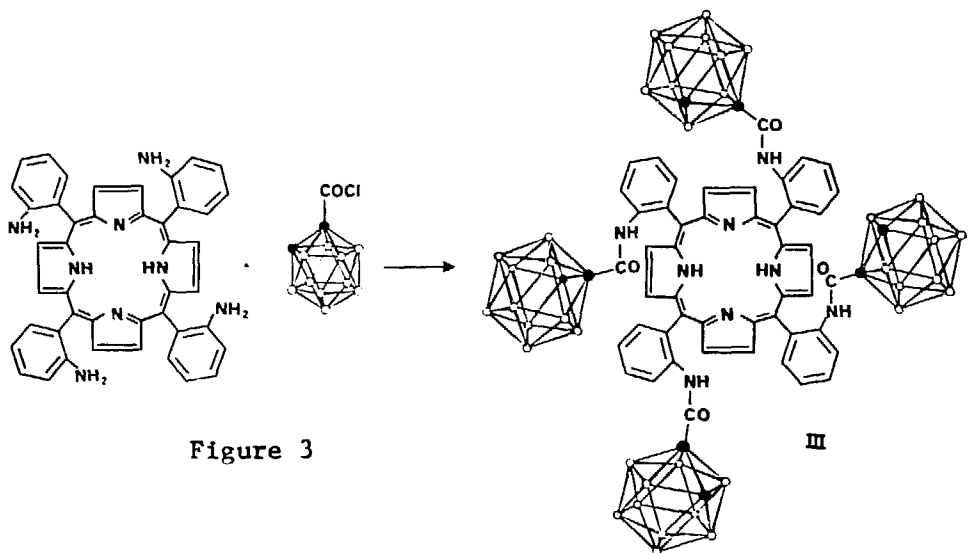


Figure 3

The spectral characteristics of porphyrin III are noteworthy. In the proton nmr the carboranyl CH appears as a broad singlet at 4.15 ppm in  $\text{CDCl}_3$ , the region predicted for a carboranyl amide. This differs significantly from the 4.5 ppm cited by Haushalter *et al.* for their analogous compound.<sup>12</sup> Theirs differs from III in that a methylene group is interspersed between the amide and the carborane cage, whereas in III no such separation exists. The nmr solvent for their compound was not reported, but if it was also  $\text{CDCl}_3$ , the carborane CH would have been expected to be in the 4.1 - 3.8 region or perhaps even more upfield. The visible spectrum of III shows four peaks plus the Soret band expected of a free-base porphyrin and in the etio pattern anticipated. The peaks are somewhat red-shifted (4-10 nm) from those of similar compounds, but small anomalies such as these have been reported previously for o-substituted tetraphenyl porphyrins.<sup>13</sup> The peak positions of para-substituted tetraphenyl porphyrins are known to show increasing bathochromic shifts relative to TPP with increasing electron-donating power of substituents.<sup>14</sup> Since the carborane cage is strongly electron-withdrawing, the carboranyl amido-function is expected to cause either a very small bathochromic shift or perhaps a hypsochromic shift.

The nido-carboranyl amidophenyl porphyrin IV was prepared in essentially quantitative yield as the piperidinium salt by refluxing III in a solution of piperidine in pyridine. This treatment removes one of the two equivalent cage boron atoms directly adjacent to both carbons and leaves an open faced, five membered ring, as shown in Figure 4. The visible and proton nmr spectra of this compound show some potentially very significant values. The

carboranyl CH peak in the pmr appears centered at 3.44 ppm, a shift of 0.71 ppm upfield of its close parent. This shift has been observed previously for similar nido-carboranes<sup>15</sup>, but is in sharp contrast to the lack of any such shift observed by Rudolph and coworkers for their compound.<sup>12</sup> They noted no change in the spectrum "except for the addition of broad piperidinium resonances at  $\delta$  3.38 and 1.64". Since their spectra are not reproduced we can only surmise that the broad peak at 3.38 was incorrectly assigned and actually represents the carborane CH. We also noted small but observable shifts at 240 MHz in the phenyl ring, amide, and  $\beta$ -pyrrole protons of IV as compared to III.

-4

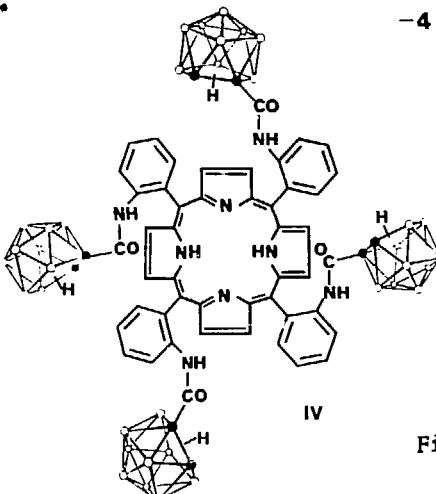


Figure 4

The visible spectrum of IV in acetone shows the expected *etio*-porphyrin pattern but is very significantly red-shifted from the spectrum of the *closo* compound III. The Soret band is found at 430 nm, one of the longest wavelengths yet reported for a free-base porphyrin and more representative of an acid dicationic porphyrin, although the spectral pattern clearly distinguishes it from such a dication. The four other peaks are red-shifted by 4-11 nm from those of the *closo* compound. Taken together, the visible spectra of III and IV are more typical of porphyrins with electron-donating substituents, such as alkyl groups, placed directly on the bridge carbons of the porphyrin framework. It should also be noted that the visible spectrum of IV differs significantly from that reported for the analogous open cage compound by Haushalter *et al.* who noted no differences between their *closo* and *nido* carboranyl porphyrins.<sup>12</sup>

It is interesting to speculate on the source of such a strong red shift. The phenyl ring planes in tetraphenyl porphyrins are oriented about 40° from the porphyrin plane in TPP, and in our compounds, with yet another bulky substituent located ortho to the porphyrin ring, these angles might be expected to be even greater. Such large dihedral angles would be expected to preclude conveyance of  $\pi$  resonance effects. Nevertheless, Meot-Ner and Adler have noted that substituent effects in para-substituted tetraphenyl porphines correlate best for a predominantly resonance contribution.<sup>14</sup> The closed cage compound III should exhibit spectral effects dominated by a strongly electron-withdrawing substituent, while those of the open cage

compound IV would be expected to exhibit a more substantial resonance contribution. Meot-Ner and Adler and others have noted a distinct blue shift when a direct steric interaction is present as in the case of simple ortho-substituted tetraphenylporphines. This observation suggests that the red shifts observed in our ortho-carboranyl amide compounds may actually be underestimating the extent of interaction of the cage with the  $\pi$  system, particularly in the case of the open cage compound. We are currently preparing the para-substituted isomers in order to explore further these intriguing observations.

Examination of the toxicological and tumor-seeking characteristics of the open cage degraded compound is currently underway in collaboration with Dr. Ralph Fairchild's group at Brookhaven. Compound IV as the piperidinium salt is not water soluble but can be made so by passing a solution in aqueous alcohol through a  $K^+$  cation exchange column. Results are not complete but to date two significant observations may be made. Firstly, the compound is not toxic at doses of  $\sim 2.5$  mg/kg in mice. This is significant because administration of the simple nido cage compound  $B_9C_2H_{12}^{-1}$  is toxic under these conditions. Secondly, as noted earlier by Dr. Fairchild, a Brookhaven prepared sample of the potassium salt of compound IV appeared to localize in the pancreas. This result, however preliminary, has clear implications, since the treatment of pancreatic cancer is currently one of the more intractable problems of cancer oncology. Further and more controlled studies in this area are underway.

#### Boron Analysis

In collaboration with Dr. Ira Krull of Northeastern University, we have developed and recently reported on a gas chromatographic microwave induced plasma boron analysis. The instrumentation is shown in Figure 5 and described in more detail in reference<sup>5</sup>. Because the column effluent from the GC was split with a fixed ratio splitter within the GC oven, both an FID and MIP chromatogram is recorded for each substance leaving the column. Furthermore, the optical beam splitting arrangement after the MIP discharge tube permitted recording of both carbon and boron emission chromatograms for each peak containing these elements. These arrangements allow us to make reasonable estimations as to the molecular structures detected. This is a clear advantage over colorimetric and prompt gamma methods of boron analysis which simply provide total boron content.

Figure 6 indicates the FID and MIP chromatograms one of our earliest steroidial carboranes (V). We have found that the boron MIP peak heights are linearly related to the amounts of carboranyl steroid injected with very high correlation coefficients. Calibration plots using boron peak height, boron peak area, carbon peak height, and carbon peak area are all linear over at least three orders of magnitude, from the low ng/injection of boron entering the plasma to the low  $\mu$ g/injection of boron into the MIP, with linear correlation coefficients of  $R > 0.99$ .

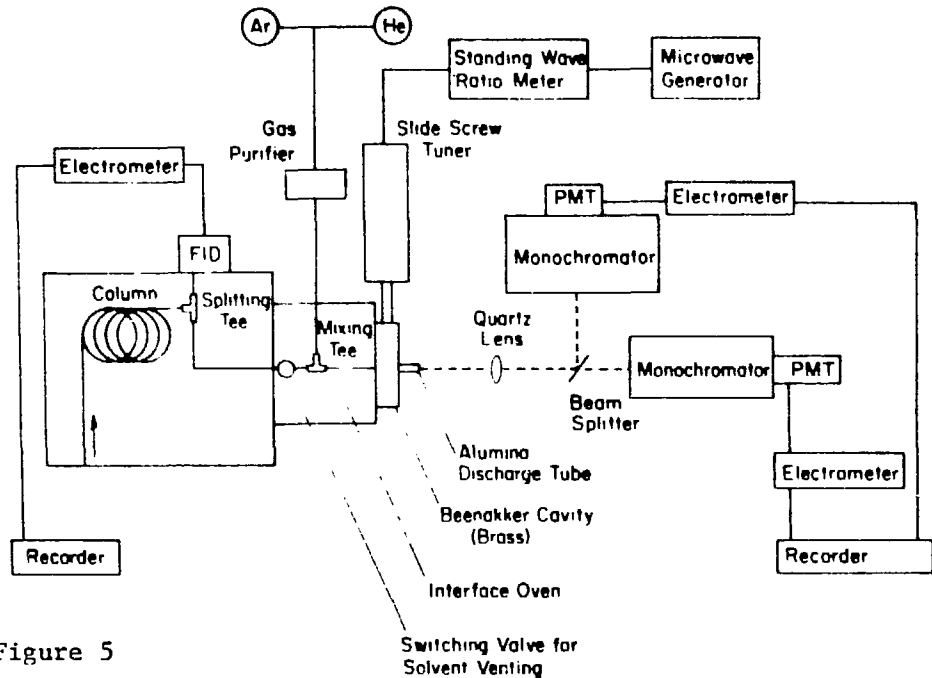


Figure 5

Switching Valve for Solvent Venting

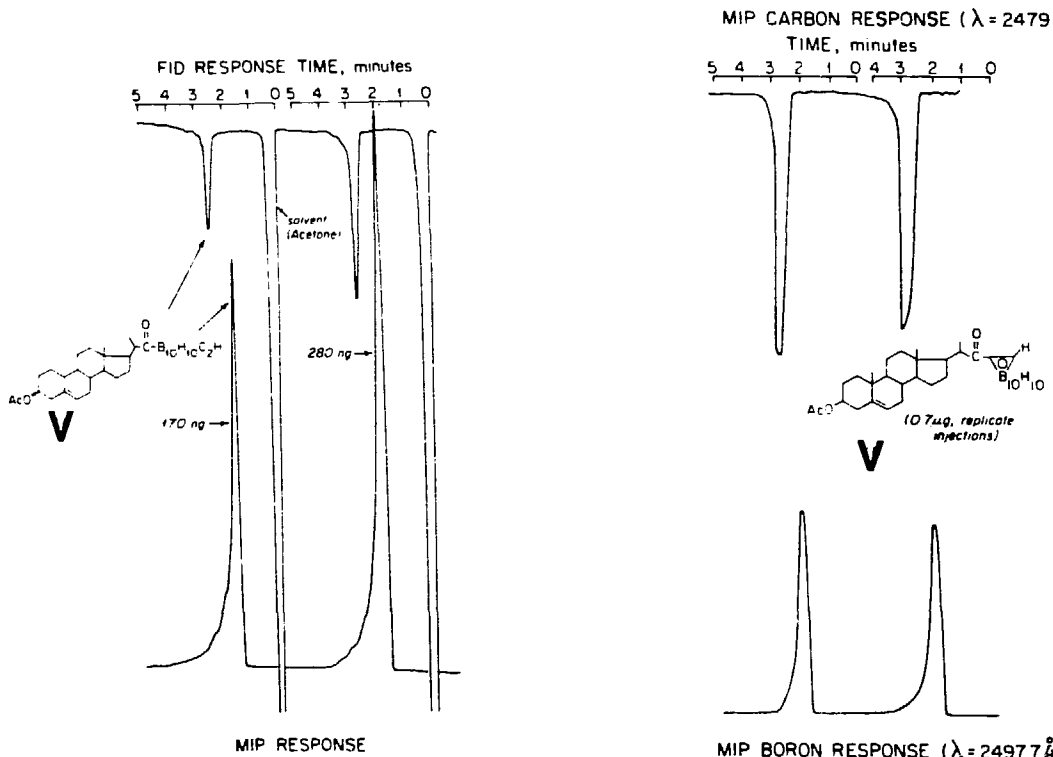


Figure 6

Figure 7

Figure 7 shows both the boron and carbon MIP chromatograms for compound V. We estimate the average minimum limits of detection for steroidal carboranes to be about 9 pg/sec of compound entering the plasma for the boron response and about 80 pg/sec for the carbon. These calculations take into account splitting ratios, transfer efficiencies, and the known ratio of boron content to total molecular weight of the injected carboranyl steroids.

Since the MIP responses to boron and carbon differ, boron/carbon ratios calculated simply on the basis of peak height or area are not expected to reflect the "known" values for a compound. We have found, however, that within a given class of compounds, they are reflective of the "known" values. That is, we can discriminate between steroidal carboranes having "known" C/B ratios of 2.4 and 2.2, for example. It is hoped that such elemental ratioing will be of benefit at such time as boron-containing compounds are utilized in humans. Overall methods for recovering such compounds from biological matrices or preparing such extracts for GC/MIP determinations are under development.

#### ACKNOWLEDGEMENTS

We wish to acknowledge the generous support of this work by the Department of Pharmaceutical Chemistry at University of California San Francisco.

#### REFERENCES

1. C.E. Cook, R.C. Carley and M.E. Wall, *J. Org. Chem.*, 33, 2789 (1968).
2. B. Schonecker, K. Ponsold and P. Neuland, *Z. Chem.*, 10, 221 (1970).
3. J.P. Collman, R.R. Gagne, C.A. Reed, T.R. Halbert, G. Lang and W.T. Robinson, *J. Am. Chem. Soc.* 97, 1427 (1975).
4. L.I. Zakharkin, Y.A. Chapovskii, V.A. Brattsev and V.I. Stanko, *Zh. Obsch. Khim.*, 36, 878 (1966).
5. I.S. Krull, S.W. Jordan, S.B. Kahl and S.B. Smith, Jr., *J. Chrom. Sci.*, 20, 489 (1982).
6. S.B. Kahl, Proceedings of the International Symposium on the Synthesis and Applications of Labeled Compounds, W.P. Duncan and A.B. Susan (eds.), Elsevier Scientific Publishing Co., 1983, pp. 181-186.
7. F. Sweet, in reference 6, pp. 175-180.
8. H.E. Hadd, this volume, paper V-11.
9. S.B. Kahl and M.F. Wiff, Abstracts of Semi-Annual Meeting of the American Chemical Society, Las Vegas, 1980, Medi. Abstr. 108.
10. T.J. Dougherty, Porphyrin Photosensitization, D. Kessel and T.J. Dougherty (eds.), Plenum Press, 1983.
11. R.G. Fairchild, *Int. J. Radiat. Oncology, Biology, and Physics*, 6, 1450 (1980).
12. R.C. Haushalter, W.M. Butler and R.W. Rudolph, *J. Am. Chem. Soc.*, 103, 2620 (1981).
13. J.B. Kim, J.J. Leonard and F.R. Longo, *J. Am. Chem. Soc.*, 94, 3986 (1972).
14. M. Meot-Ner and A.D. Adler, *J. Am. Chem. Soc.*, 97, 5107 (1975).
15. M. F. Hawthorne, D.C. Young, P.M. Garrett, D.A. Owens, G. Schwerin, F.N. Tebbe, and P.A. Wegner, *J. Am. Chem. Soc.*, 90, (1968).

PRE-CLINICAL NEUTRON CAPTURE THERAPY TRIALS  
AT M.I.T. USING  $\text{Na}_2\text{B}_{12}\text{H}_{11}\text{SH}$

G.L. Brownell, J.E. Kirsch, J.C. Murphy  
Massachusetts Institute of Technology, Cambridge, MA 02139

M. Ashtari  
University of Kentucky, Lexington, KY 40536

W.C. Schoene, C. Rumbaugh  
Brigham and Womens' Hospital, Boston, MA 02115  
and  
G.R. Wellum  
New England Nuclear Corporation, N. Billerica, MA 01862

#### ABSTRACT

Pre-clinical neutron capture therapy (NCT) trials with neonate beagles bearing transplanted cerebral tumors were carried out at the MITR-II research reactor medical therapy facility and are presented with a preliminary discussion of earlier studies conducted to determine the NCT dose tolerance to the normal canine brain. The boron compound administered,  $\text{Na}_2\text{B}_{12}\text{H}_{11}\text{SH}$  (92%  $^{10}\text{B}$  enriched), was incorporated in the tumor as a result of the breakdown of the physiological blood-brain barrier. Pre- and post-irradiation tumor growth was monitored by computerized axial tomography scanning aided with contrast enhancement. Clinical, radiological, and pathological assessments were performed, revealing positive, though episodic, results of therapy, and are described.

#### INTRODUCTION

The concept of neutron capture therapy (NCT) is unique to therapy. The characteristically infiltrating and highly invasive nature of high grade astrocytomas was an impetus to its early development. Unlike conventional treatment modalities, NCT exploits the short ranges and high energy losses from the  $^{10}\text{B}(\text{n},\alpha)^7\text{Li}$  reaction ions so that radiation dose is differentially delivered on a cellular level. In principle, such properties will lead to adequate insult for cell death of even isolated tumor cells while rendering surrounding healthy tissue intact, provided the boron selectivity is appropriate and the thermal neutron exposure is sufficient.

NCT remains a promising technique particularly in view of the fact that presently accepted treatments of certain tumors, especially high grade astrocytomas, continue to yield a poor prognosis. However, its clinical usefulness remains to be proven. Preliminary clinical results in Japan with cerebral neoplasms have been encouraging [1] as are pre-clinical trials for the treatment of malignant melanomas [2]. Furthermore, renewed interest in this therapeutic modality has led to investigations of new boron compounds and methods of boron delivery [3-5].

## PREVIOUS STUDIES ON NORMAL BRAIN TOLERANCE

Pre-clinical NCT trials have been conducted at the Massachusetts Institute of Technology (MIT) in order to gain further insight as to its therapeutic effectiveness. Early studies were aimed at determining maximum dose tolerance limits of NCT in the normal canine brain and vasculature [6]. It was evident from neuropathological findings of therapeutic trials conducted in 1959- 1961 that the primary cause of death resulted from unexpectedly large radiation doses to the endothelial lining of the vasculature due to high levels of boron in the blood [7]. Therefore with the presently accepted compound  $\text{Na}_2\text{B}_{12}\text{H}_{11}\text{SH}$  an attempt was made to determine the total dose level to the blood at the surface of the brain at which no acute or delayed radiation effects or other neuropathologic abnormalities would be found in canines.

These results showed that of all dogs receiving less than 3000 rads to the blood ( $^{10}\text{B}$ , fast neutron, induced proton, and gamma combined dose) no neuropathologic difference from a normal non-irradiated animal was found even after 9 months. One dog having received a total dose of 3620 rads exhibited a small number of vacuolated neurons, particularly the perkinje cells, but no major neuropathologic abnormalities. It was further found that an equivalent x-ray dose produced significant neurological damage.

These results demonstrated that radiation dose levels to blood in normal brain could be tolerated at the desired fluence and boron level for NCT. This was attributed to the fact that radiation doses to the brain tissue adjacent to the blood were significantly less due to low boron levels since the physiological blood-brain barrier prevents passage of the boron from the blood to the tissue. Furthermore, analytical and Monte Carlo calculations have shown that the NCT dose to the vasculature lining is considerably less than the dose delivered to the blood [8-10]. These preliminary trials seemed to have substantiated this fact.

The initial assessment of radiation effects to the normal brain by NCT led to our most recent investigations of the treatment of a transplanted cerebral tumor in neonate beagle dogs.

## PRE-CLINICAL NCT TRIALS

A transplanted cerebral tumor model was chosen for the NCT trials that was developed initially by the A.D. Little Co., Inc. [11] and later improved by us for our purposes. The original neoplasm was initiated by the intra-cerebral inoculation of a suspension of live Rous sarcoma virus (Schmidt-Ruppin strain) into a neonate beagle and was continued by cerebral transplantation of the tumor cells in subsequent neonates. Originally found to be a gliosarcoma, it has been most recently characterized as a sarcoma.

In order to obtain consistent and reproducible results for each specific trial, a single litter of 6 to 8 neonate pure-bred beagles were inoculated with the tumor cells by the use of a modified stereotaxic instrument. In this manner, consistent positioning of the transplanted cells was assured. The animals were anesthetized within 24 hours after birth and injected intracerebrally, laterally and anteriorly within the frontal lobe in order to avoid ventricular invasion of the tumor, and along a cranial suture line to prevent plugging of the injection needle. Successful tumor growth was nearly 100% and

the mean survival was found to be about 13 days post injection [11].

Tumor growth was periodically monitored beginning at about one week after injection of the cells by computerized axial tomography (CAT) scanning aided with Renografin-60 contrast enhancement medium. Animals with positively identified cerebral tumors were then randomly separated into a control and experimental group.

At 7 to 10 days post inoculation, the experimental group of neonates were subjected to NCT. The irradiation facility used was a well-collimated (1.8-cm-diameter), highly thermalized (Cd/Au ratio  $\sim 300$ ) vertical neutron beam located in the medical therapy room directly beneath the MITR-II research reactor core (4.9 MWth maximum operating power). Exposures were performed by remotely controlling a series of beam shutters shown in Figure 1. The three shutters - boral plate, lead plate, and  $H_2O$  tank - can be opened simultaneously and closed

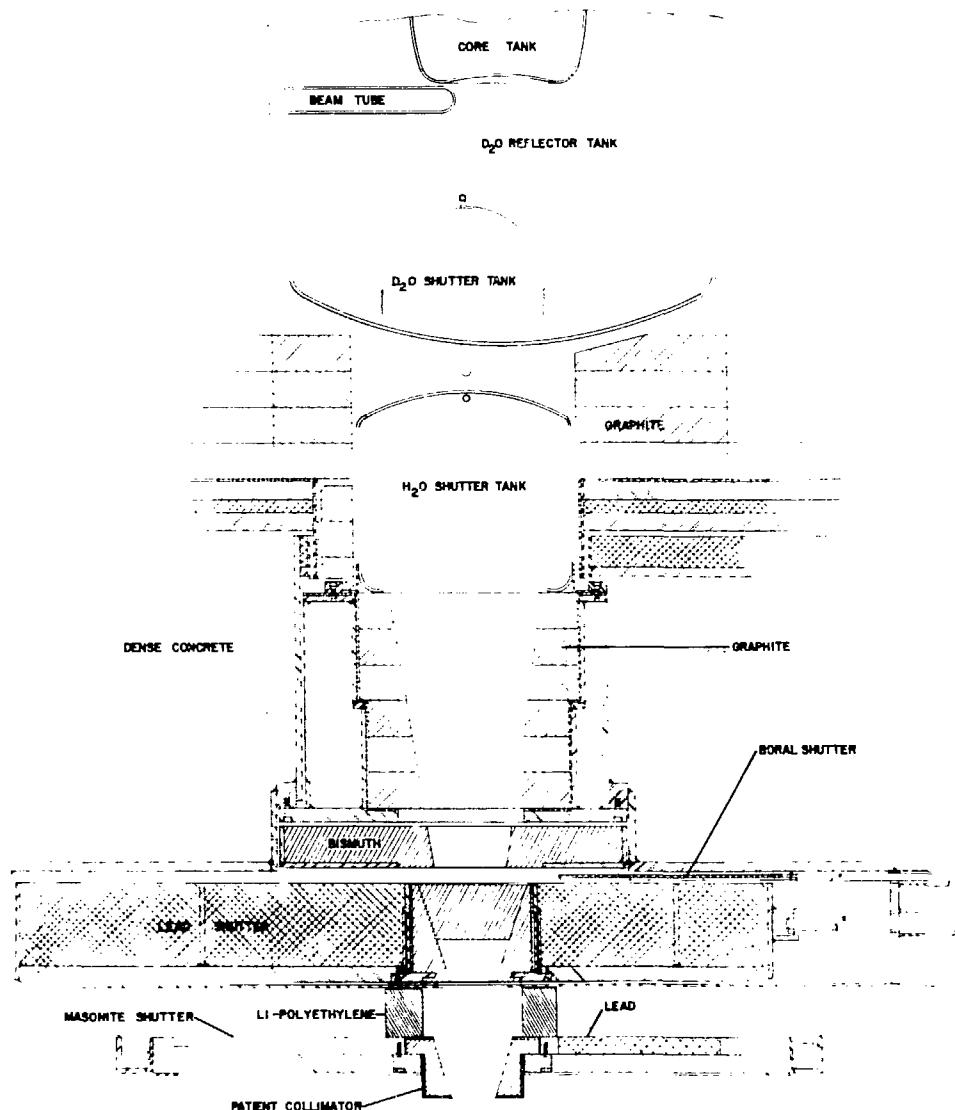


FIGURE 1 - MITR-II research reactor medical therapy facility and neutron beam shutter arrangement.

rapidly to allow immediate access to the room which was originally designed for NCT treatments. A fourth shutter is located in the reflector region and is composed of  $D_2O$ . The optional evacuation of this tank shifts the neutron spectrum to higher energies (beam hardening) allowing increased penetration for deep-seated tumors decreasing the Cd/Au ratio to about 50 and increasing the gamma dose by nearly a factor of two. Effects of energy modifications are discussed in detail elsewhere [12,13]. Thermal neutron flux with the  $D_2O$  tank full was measured by gold foil activation to be about  $2.5 \times 10^9 n/cm^2\text{-s}$  and with the  $D_2O$  tank empty, about  $8 \times 10^9 n/cm^2\text{-s}$ , both with the collimator in place and determined at full reactor power. In the majority of the animal trials performed, the  $D_2O$  tank shutter was evacuated to assure sufficient neutron irradiation of the tumor.

The medical therapy room thermal neutron beam imparts a background multi-component radiation dose both directly to tissue, and indirectly due to neutron activation of elemental constituents present in tissue. These components have been measured in tissue-equivalent and polyethylene phantoms at varying depths by the use of thermoluminescence dosimeters (TLD), gold-foil activation, and ionization chambers [12]. The results are shown in Figure 2 for the therapy conditions and a targeted surface neutron fluence of  $10^{13} n/cm^2$ . Note that theoretical augmented dose components for the  $^{10}B$  reaction have been added assuming 10, 30, and  $60 \mu g^{10}B/g$  concentrations.

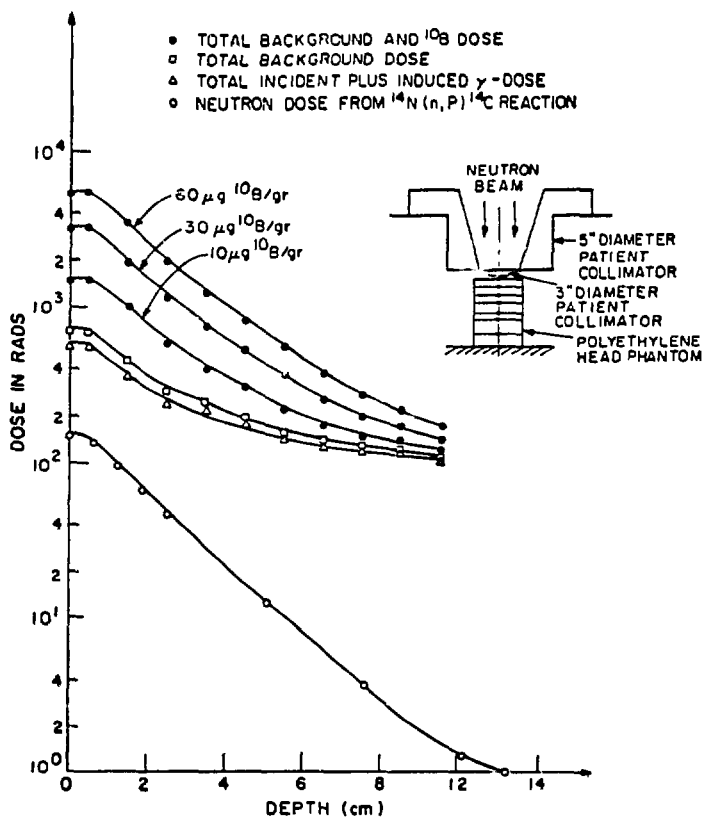


FIGURE 2 - Absorbed radiation dose vs. depth in a polyethylene head phantom with the  $D_2O$  tank shutter open and a surface fluence of  $10^{13} n/cm^2$ .

Typically one hour prior to therapy, the neonates were injected intravenously with the boron compound,  $\text{Na}_2\text{B}_{12}\text{H}_{11}\text{SH}$ , enriched to 92%  $^{10}\text{B}$ . All dogs were administered doses of 30  $\mu\text{g}^{10}\text{B}/\text{g}$  body weight. This compound is currently being used clinically in Japan [1] and selectively delivers  $^{10}\text{B}$  to cerebral tumors by means of the blood-brain barrier breakdown at the site of the tumor. Figure 3 demonstrates the typically large differential uptake of  $^{10}\text{B}$  by the tumor in the neonate beagle tumor model presently used. At left is a coronal brain section with a clearly visible tumor located in the upper right hemisphere. At right is the corresponding neutron-induced track etch autoradiogram of  $^{10}\text{B}$  localization [14].

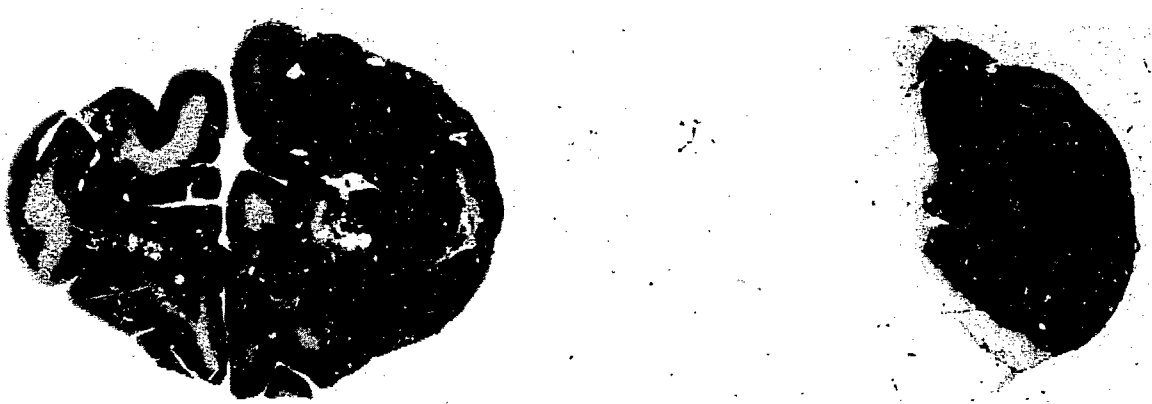


FIGURE 3 - Selective  $^{10}\text{B}$  uptake in intracerebral tumor.  
Coronal brain section (left) and corresponding  
neutron-induced track etch autoradiogram (right).

The compound was obtained commercially (Gallay Chemical Co., Gallay, PA) in the more stable form of a cesium salt. After testing for purity by thin layer chromatography [15], appropriate weights of the crystalline compound were dissolved in distilled water and applied to a cation exchange column to convert the solution to the sodium form. After dilution, the volume was adjusted to give an isotonic solution, the pH was adjusted as necessary to 7.4 and the solution was sterilized by 0.2 micron Millipore filtration.

In order to obtain experimental dosimetry measurements for each individual therapy trial, TLDs and gold foils were placed at various positions on the animal's body. Total surface dose to blood was determined by measuring the thermal neutron flux at the site of the tumor and calculating the  $^{10}\text{B}$  dose at this point. This was accomplished by sampling the blood just prior to and after irradiation and measuring the  $^{10}\text{B}$  concentrations by track etch detection methods [14]. It was found that boron levels in the blood did not change significantly over the course of irradiation. Therefore, an average concentration was taken as a representative value. The tumor dose was estimated from previous tumor/blood boron ratios.

The neonates were anesthetized and placed in formed styrofoam boats used as holders. The detectors were mounted and the animal then shielded by 1/8"

thick 25% boron rubber sheets everywhere except the site of irradiation. Additional shielding of  $^6\text{LiCO}_3$  powder packets was applied to the eyes. The irradiation was carried out to a targeted fluence of  $10^{13} \text{ n/cm}^2$  at the tumor surface which corresponded to roughly 20 to 30 minutes with the  $\text{D}_2\text{O}$  tank shutter emptied and the reactor at or near full power.

Immediately following treatment, blood was drawn and the animals returned to the litter. Tumor growth of both the control group and the treated group was monitored periodically thereafter by CAT scanning enhanced with contrast medium. Clinical observations were also documented. At the point of death or sacrifice, a dog from the other group would be sacrificed simultaneously so that comparative pathological evaluations could be carried out. Several neonates were kept alive for a long period of time ( $\sim 9$  months) to determine any delayed radiation effects due to NCT treatment.

#### DOSIMETRY

Radiation dose components were measured at the surface of the tumor site, neck, jaw, and back of each animal receiving treatment. Table 1 lists these for the three treated pups in one litter of neonates. Note the significantly lower doses delivered to parts of the body other than the tumor due to shielding. The relatively large gamma component was due to the fact that this particular series of dogs received exposures from the hardened neutron beam resulting from the evacuation of the  $\text{D}_2\text{O}$  shutter tank.

TABLE 1 - Radiation dose components of therapy to various body regions for litter F81-63. Thermal neutron exposure was conducted with beam hardening.

Pup ID	Average $^{10}\text{B}$ Concentration in Blood at the Time of Therapy (ugm/gm)	IR Time (min)	Location of the Detector	Neutron Fluence ( $\text{n/cm}^2$ )	Surface Neutron Dose to Blood (rads)	Surface $\gamma$ -Dose (rads)	Surface $^{10}\text{B}$ -Dose to Blood (rads)	Total Surface Dose to Blood (rads)
F81-63/1	56.6	35	Tumor	$1.10 \times 10^{13}$	163.9	1414.47	5568.64	7147.01
			Neck	$1.19 \times 10^{11}$	1.773	239.21	60.24	301.22
			Jaw	$5.21 \times 10^{10}$	.776	166.37	26.36	193.51
			Back	$1.06 \times 10^{10}$	.158	77.64	7.37	83.17
F81-63/3	54	35	Tumor	$1.10 \times 10^{13}$	163.9	1503.53	5322.24	6989.67
			Neck	$1.14 \times 10^{11}$	1.69	253.13	55.16	309.98
			Jaw	$6.11 \times 10^{10}$	.910	200.26	29.56	230.73
			Back	$1.06 \times 10^{10}$	.158	71.76	5.13	77.05
F81-63/5	58.5	35	Tumor	$1.09 \times 10^{13}$	162.41	1625.72	5713.34	7501.47
			Neck	$8.04 \times 10^{10}$	1.19	205.32	42.	248.51
			Jaw	$6.22 \times 10^{10}$	.927	165.83	32.60	199.16
			Back	$1.17 \times 10^{10}$	.13	86.74	6.13	93.

## RESULTS

The effectiveness of neutron capture therapy in this limited study of neonate tumors was not statistically demonstrated. However, dramatic results were observed in every case although long-term survival was achieved only episodically. The most consistent result of therapy was demonstrated by the contrast enhanced CAT scans monitoring the tumor growth. Figure 4 presents the scans of two treated and two untreated neonates several weeks after therapy treatment. Notice the significantly enhanced intracranial regions identifying the presence of viable tumor in the untreated animals located in the upper right hemisphere and the virtual absence of enhancement in the treated animals. (Note that the right appears on the left in these scans because of the orientation of the dogs.) Furthermore, the lateral ventricles indicated by the darker, lower density regions appear symmetrical in the treated and asymmetrical due to tumor presence in the untreated neonates. Enlargement of the ventricles was characteristic of all animals regardless of the therapy and was attributed to the presence or former presence of tumor growth. All four dogs were scanned with contrast medium on the same day and therefore at the same age.

Time sequential CAT scans showing the course of tumor growth after therapy also demonstrated a positive effect of NCT. Figure 5 depicts three sets of four scans taken progressing posteriorly in a control animal at three different times after the point of therapy: 2 days, 6 days, and 13 days. Tumor presence is quite evident. Figure 6 demonstrates the effect of treatment on tumor growth. Three sets of four scans are shown at the same times after therapy as for the animal in Figure 5. Note the initial presence of tumor at 2 days post-irradiation, and its gradual regression by 13 days. This contrasts sharply the tumor progression in the untreated animal shown in Figure 5.

Clinical differences between treated and control groups were less conclusive. Although the majority of the untreated animals followed a clinical course of weight loss, fluctuating growth rates, general weakness, and trembling, a significant number of treated animals had similar symptoms. 62.5% (10/16) controls and 46.7% (7/15) treated animals died or were sacrificed near

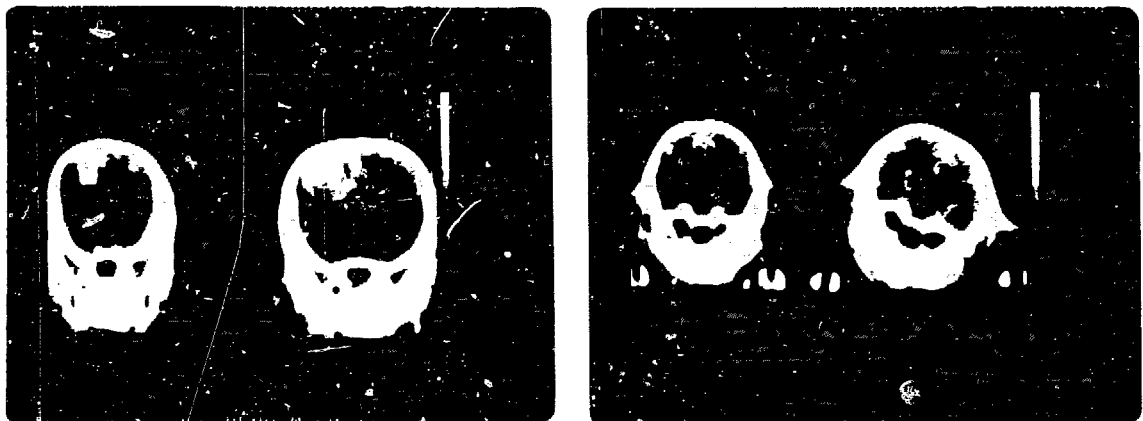


FIGURE 4 - Contrast enhanced coronal brain scans of two neonate beagle controls (left) and two treated by NCT (right).



FIGURE 5 - Time sequential CAT scans of tumor growth in an untreated neonate beagle (Top row: 2 days, Middle: 6 days, Bottom: 13 days after therapy date).

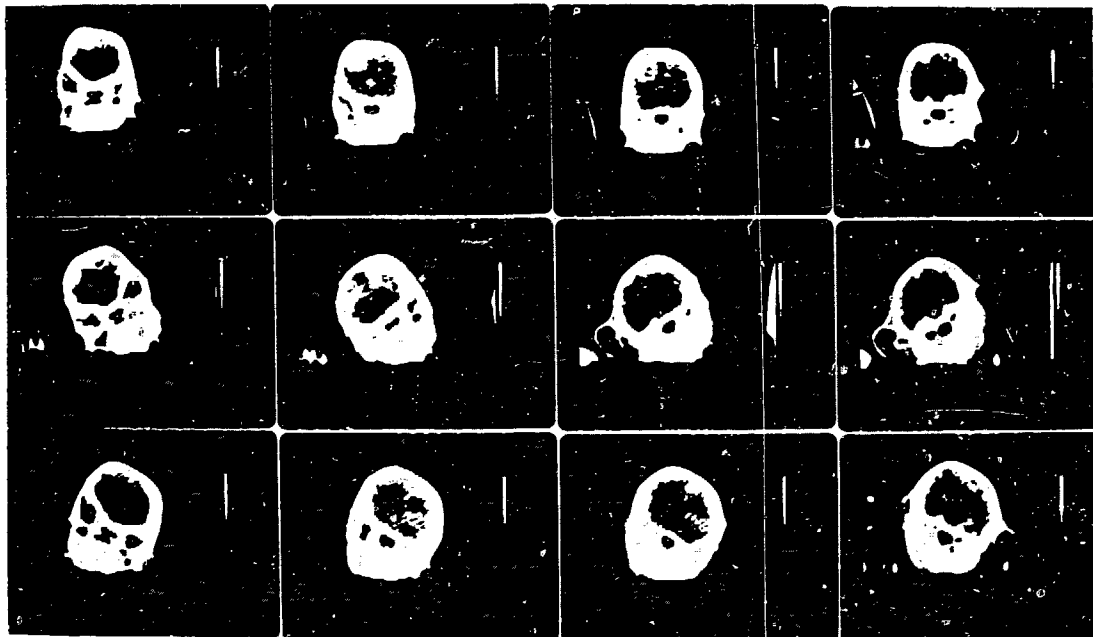


FIGURE 6 - Time sequential CAT scans of tumor growth in a treated neonate beagle (Top row: 2 days, Middle: 6 days, Bottom: 13 days after therapy).

the point of death. No conclusions or correlations could be drawn concerning any adverse effects of treatment on these clinical findings.

Firm conclusions from the pathological results were equally difficult to draw. Nevertheless, upon microscopic examination, 62.5% (10/16) of the untreated controls showed presence of viable tumor, whereas only 20% (3/15) of the treated dogs revealed the same result. Furthermore, 12.5% (2/16) showed no residual tumor without therapy versus 33.3% (5/15) with therapy. Long-term radiation effects could not be evaluated to any degree of certainty. Table 2 gives a summarized compilation of the results for untreated and treated dogs.

TABLE 2 - SUMMARY OF NCT TRIALS WITH  
NEONATE BEAGLES BEARING INTRACEREBRAL TUMORS

- UNTREATED -				- TREATED -				
PUP ID	LIFE-SPAN (days)	MODE OF DEATH	TUMOR HIS-TOLOGY	PUP ID	TOTAL DOSE (rads)	LIFE-SPAN (days)	MODE OF DEATH	
<u>WITH RESIDUAL TUMOR</u>				<u>WITH RESIDUAL TUMOR</u>				
F80-30/2	50	SAC-H*	NECRO*	F80-30/4	3750†	50	SAC-H	NECRO
F80-30/5	44	SAC-H	NECRO	F80-30/9	3370	44	SAC-H	NECRO
F81-13/3	16	SAC-I*	NECRO	F81-13/1	2400	51	SAC-H	NECRO
F81-13/4	51	SAC-H	N/A	F81-13/6	2300	29	SAC-H	NECRO
F81-27/2	9	DIED	VIABLE	F81-27/1	2900	22	DIED	NECRO
F81-27/3	13	DIED	VIABLE	F81-27/5	3200	20	DIED	VIABLE
F81-27/4	15	DIED	VIABLE	F81-38/3	3559	20	DIED	VIABLE
F81-27/6	14	DIED	VIABLE	F81-38/5	3627	16	DIED	VIABLE
F81-38/2	15	SAC-I	VIABLE	F81-63/1	7147	38	SAC-H	NECRO
F81-38/4	15	SAC-I	VIABLE	F81-63/3	6989	38	SAC-H	NECRO
F81-38/6	15	SAC-I	VIABLE	<u>WITHOUT RESIDUAL TUMOR</u>				
F81-38/8	18	SAC-I	VIABLE	F80-30/6	3690	>1 yr	SAC-H	---
F81-63/2	14	SAC-I	VIABLE	F81-13/2	2190	250	SAC-H	---
F81-63/6	37	SAC-H	VIABLE	F81-38/1	3577	20	DIED	---
<u>WITHOUT RESIDUAL TUMOR</u>				F81-38/7	3459	33	DIED	---
F81-13/5	250	SAC-H	---	F81-63/5	7501	23	SAC-I	---
F81-63/4	32	SAC-H	---					

\* SAC-H = Sacrificed/clinically healthy

SAC-I = Sacrificed/clinically ill

NECRO = Necrotic and/or calcified tumor tissue

† NOTE: Total dose was determined as the combined  $^{10}\text{B}$ , fast neutron, incident and induced gamma radiation dose delivered to the blood at the surface of the tumor. Since past studies have shown that at the time of treatment tumor/blood boron ratios were nearly unity, this dose was also assumed to be the dose to the tumor.

## DISCUSSION

The effectiveness of NCT in treating transplanted intracerebral tumors in neonate beagles with  $\text{Na}_2\text{B}_{12}\text{H}_{11}\text{SH}$  was not proven in this study. Positive therapeutic results were observed in episodic cases. One of the primary causes for the inconsistent results in these trials was the use of neonates. It was found that survival beyond a certain age (~ 2 weeks) without treatment would increase the probability of tumor regression due to the immunological response of the animals. Such occurrence of spontaneous regression made it difficult to assess the actual effect of therapy except in the very qualitative manner that was presented.

We have concluded that continuation of these pre-clinical studies with this animal model would not provide further insight into our understanding of the efficacy of NCT. The reasons for this are several-fold. The characterized tumor type, a sarcoma, is not representative of the tumors to be eventually treated in humans. Also, the invasiveness of the transplanted tumor is minimal and typically develops into a solid, well-delineated mass in contrast to the highly infiltrating, diffuse nature that is characteristic of high grade astrocytomas in humans. Therefore, refining the treatment and improving the results in this animal model would serve little purpose in contributing towards the ultimate aim of mounting preliminary clinical trials here in the United States.

However, the clear results of therapy in all dogs from CAT scans and the episodic results based on survival and pathology are encouraging. We believe that these results add to the body of biological results leading towards a resumption of clinical trials at the MITR-II. In our opinion, the successful demonstration of therapeutic effectiveness in any animal model, although highly desirable, does not guarantee clinical success. Such studies are required, however, to understand the problems encountered in clinical trials. For this purpose, limited studies using naturally occurring dog brain tumors may be essential.

The continuing efforts to pursue the research and development of fundamental chemical, biological, and physical aspects of NCT is vital. Efforts to develop new compounds, investigate more sophisticated mechanisms of boron delivery, expand the applications to other types of malignancies, and develop improved neutron beams will all contribute to the ultimate success of neutron capture therapy.

## ACKNOWLEDGEMENTS

We wish to acknowledge the MITR-II staff, the MIT Division of Comparative Medicine, and the Brigham and Womens' Hospital for their assistance in this study. We also wish to express thanks to Dr. William H. Sweet, Dr. Robert G. Zamenhof, and Ms. Janette Messer for providing valuable advice.

This work was supported by NIH grant #CA19665.

#### REFERENCES

- 1) H. Hatanaka, in Synthesis and Applications of Isotopically Labeled Compounds, W.P. Duncan and A.B. Susan (eds.), pp.167-174, Elsevier Scientific Publ. Co., Amsterdam, (1983).
- 2) M. Ichihashi, T. Nakanishi, Y. Mishima, J. Invest. Dermatol., 78, pp.215-218, (1982).
- 3) R.F. Barth, C.W. Johnson, W. Wei, W.E. Carey, A.H. Soloway, J. McGuire, Cancer Det. and Prevention, 5, pp.315-323, (1982).
- 4) E. Mizusawa, H.L. Dahlman, S.J. Bennett, D.M. Goldenberg, M.F. Hawthorne, Proc. Natl. Acad. Sci. USA, 79, pp.3011-3014, (1982).
- 5) F. Sweet, Steroids, 37, pp.223-238, (1981).
- 6) G.L. Brownell, R.G. Zamenhof, B.W. Murray, G.R. Wellum, Chapt. 18 in Therapy in Nuclear Medicine, R.P. Spencer (ed.), Grune and Stratton, N.Y., (1978).
- 7) A.K. Asbury, R.G. Ojemann, S.L. Nielsen, W.H. Sweet, J. Neuropath. Exptl. Neurol., 31, pp.278-303, (1972).
- 8) R.A. Rydin, O.L. Deutsch, B.W. Murray, Phys. Med. Biol., 21, pp.134-138, (1976).
- 9) K. Kitao, Radiat. Res., 61, pp.304-315, (1975).
- 10) T. Kobayashi, K. Kanda, Radiat. Res., 91, pp.77-94, (1982).
- 11) A.D.L. Ref. #77106, A.D. Little, Inc., Cambridge, MA, unpublished, (1974).
- 12) M. Ashtari, Ph.D. thesis, M.I.T., (1982).
- 13) R.G. Zamenhof, B.W. Murray, G.L. Brownell, G.R. Wellum, E.I. Tolpin, Med. Phys., 2, pp.47-60, (1975).
- 14) J.E. Kirsch, Ph.D., thesis, M.I.T., (1983).
- 15) G.R. Wellum, E.I. Tolpin, L.P. Andersen, R. Sneach, J. Chromatography, 103, pp.153, (1975).

Biological Studies of an Epithermal  
Beam for NCT with  $\text{Na}_2\text{B}_{12}\text{H}_{11}\text{SH}$

Denise J. Noonan

and

J.L. Russell, Jr.

Georgia Institute of Technology, Atlanta, GA 30332

Introduction

While the basic concept of Neutron Capture Therapy (NCT) is quite simple, the large number of variables which must be specified for a given course of therapy makes its practical application one of the more complex procedures of medicine. These variables include choice of the specific boron-carrying compound; the schedule and dosage of the compound; composition, spectrum and geometry of the beam; radiation dosages and schedule; and options of use of chemical radiation protectors, blood exchange and many possible adjuvant therapies. The difficulty of the task of finding an optimum regimen in the midst of this overabundance of options is perhaps one of the reasons for the agonizingly slow pace of the process of bringing NCT from the laboratory to the patients in need. Clearly, it will be necessary to resort to mathematical modelling, where applicable, and animal modelling to explore the range and quality of the effects of the many variables in order to reduce the scope of random human trials to reasonable proportions. However, there is no way to avoid extensive human experimentation if NCT is ever to become clinically available.

This paper is a progress report on a broad-scale attack on many (certainly not all) of the above problems being conducted at the Frank H. Neely Nuclear Research Center at Georgia Institute of Technology. Much of this International Conference on NCT is devoted to the problem of choice of boron compound so that subject will not be addressed in this paper. Considerations in this paper will be arbitrarily limited to the use of  $\text{Na}_2\text{B}_{12}\text{H}_{11}\text{SH}$ .

Work to date has included design and preparation of an epithermal neutron beam that is remarkably free of fast neutrons, yet has adequate intensity for therapy. Parameters addressed are beam composition, spectrum and geometry as they relate to penetration, skin sparing, dose schedule (fractionation) and possibility of repeat therapy. Physical and biological dosimetry provide the information to mathematically model radiation-dose schedule.

A rat model has been developed for exploring the distribution of boron, the many possible combinations of boron-dose-schedule and radiation-dose-schedule, and such supplementary procedures as blood exchange and the use of chemical radiation protectors.

Behind the immediate objectives of the current research is the general goal of helping to bring to fruition the great promises of NCT: 1) Certainly one of the first is the promise of treatment of brain cancer without surgery. The epithermal beam with its skin-sparing property may avoid the need for surgical reflection of the skin of the scalp during irradiation. The deep penetration of the epithermal beam is also important. Another consideration is the effect of suddenly killing a large tumor mass in the brain. In particular, the vasculature of the suddenly necrotic tumor may hemorrhage before the

body has time to dissolve the tumor mass and re-route the blood supply. Conventional wisdom suggests that fractionation of dose (perhaps once or twice per week for two to four weeks) would give the body time to accommodate a more slowly dying tumor. 2) A second great promise would be the possibility of a second or even a third course of treatment in the event that a first remission did not prove to be permanent. The significance of this can only be appreciated when compared with the conventional approaches of radiation therapy. In these, the radiation dose is chosen to be the maximum which can be tolerated by the patient. If this is sufficient to kill the cancer, fine. However, if it is not, there is no recourse.

The possibility of very high  $^{10}\text{B}$  concentrations in the tumor (~ 100 ppm) results in a relatively small neutron dose required for tumor lethality. Combined with a high boron ratio of tumor to surrounding tissue, this leads to the concept of delivering only enough radiation to kill the tumor, since more radiation would only further damage normal tissue. Calculations based on favorable assumptions suggest that an optimum treatment would leave the patient with the reserve to be able to withstand one or more further courses of treatment if required. This possibility could be further enhanced by the use of chemical radiation protectors such as SOD and corticosteroids, and inclusion of plasma replacement in the protocol as discussed in the animal model below. 3) Finally, the greatest promise is the generalization of NCT to treat other types of cancer, especially lung cancer. Multiple lobe involvement precludes lung surgery and the poor tolerance of lung tissue for radiation usually precludes more than palliative radiation therapy. The deeply penetrating epithermal neutron beam, combined with the above approaches maximizing the tumor-to-normal tissue radiation-dose ratio, suggest that NCT may someday provide an effective treatment for this scourge which kills some 120,000 people per year in the U.S. alone.

#### Physical Considerations

An epithermal neutron beam approach to BNCT has been taken at Georgia Tech. These intermediate energy neutrons have long been advocated for NCT, not only for their added penetration, but also for the lower fluence-to-kerma factors than both thermal and fast neutrons, and the potential for skin-sparing (1).

An epithermal neutron beam has been built at the 5 MW Georgia Tech Research Reactor using aluminum and sulfur filters (2). These two elements share the unusual property of total cross sections which are greater for fast than for intermediate or thermal neutrons, allowing the preferential transmission of lower energy radiation in a mixed radiation field.

20 cm of aluminum and 25 cm of sulfur were placed in a tangential beam port in the reactor (Figure 1). A 60 cm graphite plug scatters mixed energy neutrons from the core down the port to a 0.63 cm thick Boral cup which filters out the thermal neutrons, minimizing activation in the subsequent filters. The aluminum and sulfur filter out the fast neutrons, allowing the thermal and epithermal neutrons to pass down the tube to an 0.08 cm thick cadmium sheet. The cadmium removes any neutrons thermalized within the filters or scattered into the beam from the sides. An additional 25 cm of lead rings block the gammas streaming between the filters and beam tube.

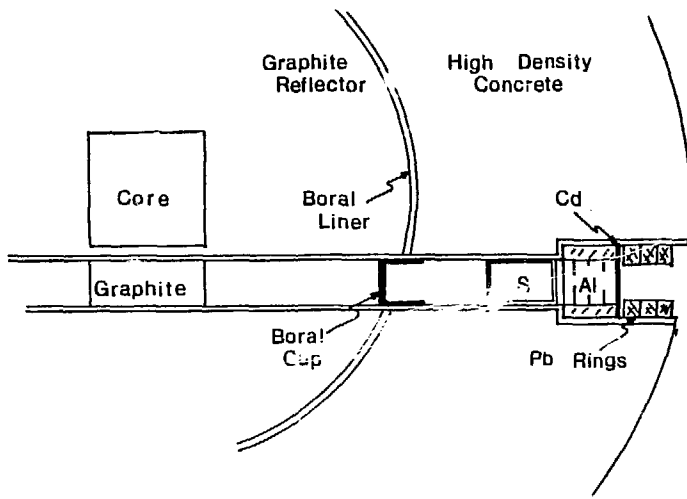


Figure 1: Filter configuration for the epithermal neutron beam

Spectral measurements of the transmitted flux indicate that the beam is strongly epithermal, spanning over four energy decades, with less than 4% of the total flux due to fast neutrons (3) (Figure 2). The peaks at 20 and 70 keV originate from deep minima in the cross sections of aluminum and sulfur, respectively. At the lower end of the spectrum, the thermal flux drops off sharply below 10 eV.

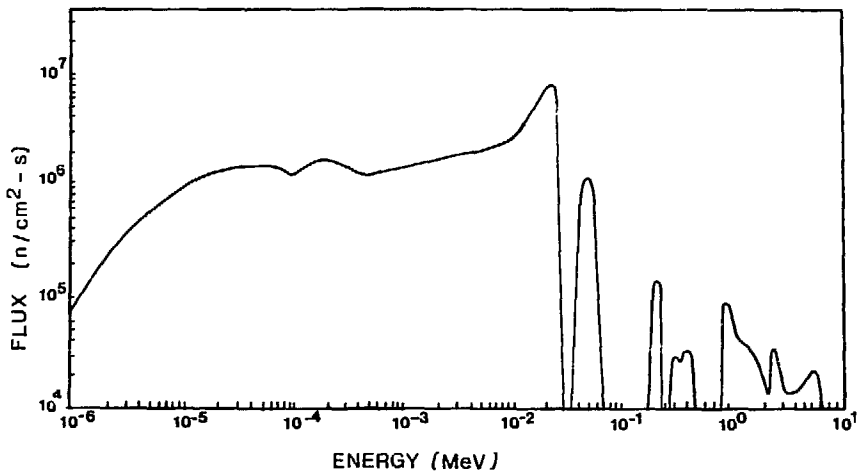


Figure 2: Neutron transmission spectrum of the filtered beam at 5 MW

Beam penetration and skin-sparing have been demonstrated in a 15 cm diameter polyethylene head phantom placed in the center of the beam, 47 cm from the face of the reactor (Figure 3). The thermal neutron flux peaks at  $3 \times 10^8 \text{ n/cm}^2/\text{s}$  at 5 MW, several centimeters within the phantom for a peak-to-incident thermal flux ratio of 4.5. The thermal flux drops off thereafter, yet remains above the incident flux to a depth of seven centimeters. For this flux, delivery of 2000 rads via the  $^{10}\text{B}(\text{n},\alpha)^{7}\text{Li}$  reaction to a tumor located three centimeters within the head and containing 100 ppm  $^{10}\text{B}$  would be complete in 2.5 hours.

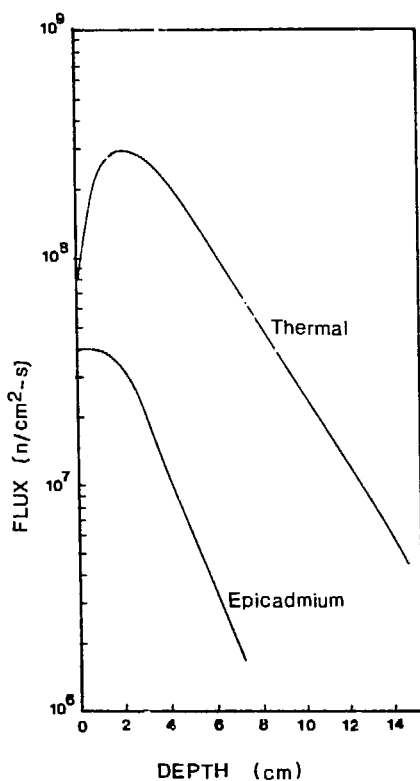


Figure 3: Thermal & epicadmium fluxes generated in a 15 cm diameter polyethylene head phantom, 50 cm from the beam port at 5 MW.

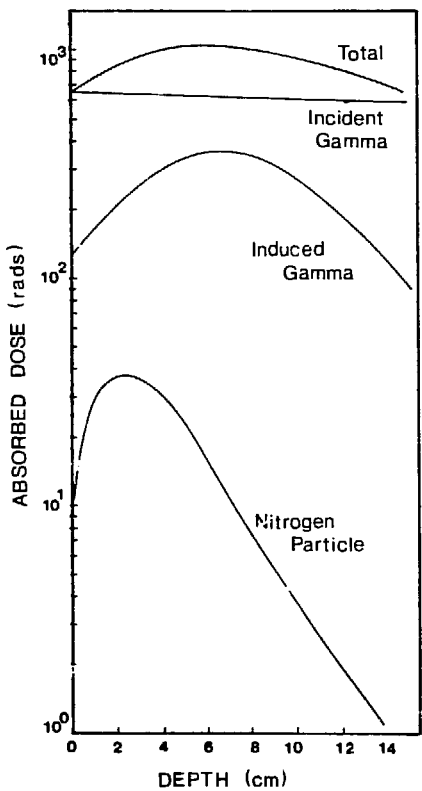


Figure 4: Depth dose distributions in a head phantom 47 cm from the epithermal port.

For comparison with other facilities, the absorbed dose delivered by the various radiations in the beam was plotted against depth in the head for the 2.5 hour irradiation (Figure 4). The nitrogen particle dose was calculated for 1.9% by weight  $^{14}\text{N}$  content in the brain (4), for a fluence-to-kerma factor of  $1.58 \times 10^{-11} \text{ rads/n/cm}^2$ . The fast neutrons were neglected as they represent only 8% of the neutron dose and less than 3% of the total dose at a three centimeter depth.

The plot demonstrates the excellent skin-sparing potential of the beam if the incident photon contamination can be reduced. As the facility is the

first of its kind, built only for a feasibility study, several options remain for reducing this contamination by at least a factor of three. Thus, in terms of the physical parameters of beam penetration, skin-sparing, and absorbed dose, the epithermal neutron beam provides a viable approach to BNCT.

#### Biological Investigations

The advantages and parameters described above are physical considerations only, dealing with the amount and location of energy deposition in the head. Very little information is available on the biological effects of epithermal neutrons. Biological investigations were therefore directed in three areas:

1) determining whether the overall biologically equivalent dose delivered during a 2.5 hour patient irradiation remains below the 1400 R tolerance limit of the brain beyond which radiation necrosis begins to appear (5), 2) whether the skin-sparing predicted by physical considerations is retained in the biological realm, and 3) the establishment of an animal tumor model to test the combined effects of the boron and the beam.

A. RBE,  $^{60}\text{Co}$ -Equivalent Dose, and Skin-Sparing. The RBE and equivalent dose were evaluated using radiation-induced chromosome aberration frequencies in the pollen nuclei of the plant, Tradescantia paludosa (spiderwort) as the biological endpoint (6). Dicentrics and centric rings were scored; both are the result of lesions in two chromosome arms within the pollen nucleus and their subsequent rearrangement. Individual inflorescences from these plants were irradiated in the pre-DNA duplication stage of interphase of the first post-meiotic division. Aberration production was scored four days later during metaphase when the six large chromosomes were in their most constricted phase, facilitating spotting of the aberrations.

The dosimeter was calibrated in a  $^{60}\text{Co}$  field up to 300 rads, at approximately the same intensity (12.5 rads/min) as the photons present in the epithermal beam. At this intensity, the aberration yield was found to increase as the 1.53 power of the dose. Tradescantia inflorescences were then irradiated at three positions in the filtered beam: directly in the beam 50 cm from the biological shielding, and on the front face and several centimeters within a head phantom placed in a corresponding position to evaluate skin-sparing.

The irradiations were run at low doses (200-300 rads) to avoid saturation of the dosimeter (6). The individual contributions to the aberration frequency from the gammas, thermal neutrons, and epithermal neutrons were separated, based on photon dose and thermal flux measurements. The values were then extrapolated to the higher doses incurred during a 2.5 hour treatment, linearly for the neutrons and to the 1.53 power for the photons.

The photon intensity in the beam fell slightly short of that in the calibration curve. At low intensities, the yield of photon-induced dicentrics and centric rings becomes more linear (6). Therefore, a 'worst possible case' was designed in which the photon contribution to the aberration frequency was extrapolated to the 1.2 power of the dose.

The RBEs and  $^{60}\text{Co}$ -equivalent doses calculated for the three positions in the filtered beam are listed in Table 1 for both the 1.53 and the 1.2 exponents. Thus, the mixed radiation field at the peak of the thermal flux in the phantom delivers a dose which is biologically equivalent to 1368 rads ( $x = 1.53$ ) or a maximum dose of 1895 rads ( $x = 1.2$ ). The front face receives

a biologically equivalent dose between 1091 and 1578 rads. Hence, 20-25% skin-sparing is retained in the epithermal beam.

Table 1. Biological Effectiveness of the Filtered Beam

	$x = 1.53$ $^{60}\text{Co}$ -equiv(rads)	$x = 1.2$ $^{60}\text{Co}$ -equiv(rads)
RBE	RBE	
Phantom	1.2	1368
Face	1.3	1091
Beam	1.2	1135

The  $^{60}\text{Co}$ -equivalent dose in the phantom approaches, and in the worst case exceeds, the 1400 R tolerance limit for the brain. However, over 800 rads of this 1368-1895 rads stems directly from photon contamination in the beam. If only 500 of this 800 rads were eliminated by refining the beam, the equivalent dose at all three positions would drop below the cutoff point.

Similarly, the RBE values of 1.2-1.7 listed in the table are low primarily because of the large photon contribution to the dose. Thus, not only is skin-sparing retained in the biological context, but the overall equivalent dose is potentially low enough for clinical applications of the epithermal beam.

B. The Animal Tumor Model. The remaining test of the epithermal beam involves the combined effects of the radiation and the  $\text{Na}_2\text{B}_{12}\text{H}_{11}\text{SH}$  compound. To evaluate this effect and the efficacy of various dose-modifying factors in the treatment regimen, an animal tumor model was established. Small pieces of an adenocarcinoma tumor line are transplanted into the hind feet of 150-160 gram female F344 Fisher rats. The tumors are allowed to grow to approximately one cubic centimeter before the animal is anesthetized and placed in a shielded restrainer for the irradiation (Figure 5).

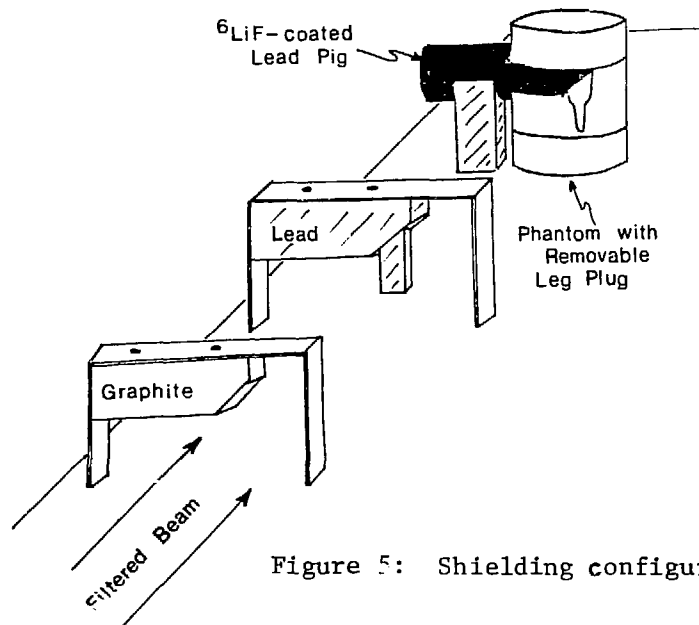


Figure 5: Shielding configuration for the rat irradiations

To demonstrate the penetrating power of the epithermal neutrons, the rat is placed in a  $^6\text{LiF}$ -coated lead pig with its tumor-bearing leg splinted and extending out of the cylinder into a polyethylene head phantom. The leg is positioned so that it lies three centimeters from the front face of the phantom, simulating treatment of a brain tumor at the peak thermal flux.

The epithermal beam presents a unique shielding problem in that the neutrons are moderated to thermal energies within several centimeters. Therefore a rat injected with boron and placed in the lead pig will receive a prohibitively large dose to its midline, i.e., the radiation-sensitive intestinal tract, if large amounts of boron are retained in the intestinal epithelium. To alleviate this problem, graphite blocks were placed between the rat restrainer and the reactor face to moderate and capture the epithermal neutrons before reaching the animal. An additional lead brick with an extension for the rat's leg was added to shield the rat from the large photon contamination in the beam.

The shielding configuration reduces the peak thermal flux in the phantom and hence at the tumor to  $2 \times 10^8 \text{ n/cm}^2/\text{s}$  at 5 MW. The thermal intensity at the midline of the rat is a factor of ten lower. To deliver 2000 rads to a tumor containing 100 ppm  $^{10}\text{B}$ , nearly four hours of irradiation is required. The total gamma dose delivered to the leg and intestines during this time are 420 and 175 rads, respectively.

Two rats have been irradiated in the beam without the boron injection to test the shielding. The irradiation was divided into three fractions of 80 minutes each, 3-4 days apart, further reducing the effective photon dose to the leg to 250 rads, according to the Ellis equation (7). The tumor regressed slightly after the first two treatments, but continued to grow thereafter until the animal was sacrificed. Both rats tolerated the procedure well, with no gross observable changes in their health.

It remains yet to irradiate a rat injected with  $\text{Na}_2\text{B}_{12}\text{H}_{11}\text{SH}$  in the epithermal beam. Whereas fractionation reduces the effective photon dose, it will have little effect on the large neutron dose delivered to the intestinal area by the capture of thermalized neutrons in the boron residing therein. Further moderation and shielding of the epithermal neutrons would reduce the thermal flux in the rat, but would also cut the intensity at the tumor. Therefore a plasma exchange is being explored as a potential route for reducing the free boron in the rat's system while maintaining a therapeutically significant amount in the tumor.

Studies by Tolpin, et al (8) indicate that nearly 85% of the boron injected as  $\text{Na}_2\text{B}_{12}\text{H}_{11}\text{SH}$  and residing in the bloodstream is associated with the plasma. If a 50% exchange of plasma is performed, nearly half of the boron in the blood should be eliminated. At the same time, the poorer circulation, large extracellular space, and binding of the compound in the tumor may retain the boron for a long enough period for a significant differential to be built up between the tumor and the blood.

To test the idea, catheters have been implanted in the left common carotid artery and the right internal jugular vein of the rats. The catheters remain open up to a month if flushed daily with diluted heparin (0.5 ml in 30 ml saline). Prior to the exchange, the rat is injected with an anti-inflammatory corticosteroid, methylprednisolone sodium succinate. One milliliter fractions of blood are withdrawn from the carotid and spun down. The

boronated plasma is then replaced with fresh plasma and the blood reinjected into the vein while withdrawing the next milliliter fraction from the artery. Up to three exchanges have been performed on one rat, following the same schedule as the irradiation fractionation experiments described earlier. The rats tolerate the procedure well and are up and eating within several hours.

Boron distribution studies are currently being run to test the efficacy of the plasma exchange. Six rats bearing tumors were catheterized and injected with 200 ppm  $^{10}\text{B}$  in the form of  $\text{Na}_2\text{B}_{12}\text{H}_{11}\text{SH}$  at the rate of 0.1 ml/min. One hour was allowed to pass for uptake of the compound in the rat's system. Two rats were then given plasma exchanges, taking one hour each, and sacrificed immediately thereafter. Tissue samples of the blood, tumor, liver, kidneys, skin, intestine and muscle were taken and frozen for analysis.

Two other rats served as controls and were sacrificed two hours after receiving the boron injection. Plasma exchanges were run on the final two rats, followed by a two-hour interval before sacrifice to test the retention of the compound in the organs. Based on the amount and retention of boron in the tumor, the time of the final irradiation in the epithermal beam will be calculated.

#### Summary

Several aspects of the problem of bringing the use of epithermal beam NCT from the laboratory to clinical trials are being investigated at the Frank H. Neely Nuclear Research Center at the Georgia Institute of Technology. An epithermal beam has been prepared based on sulfur, aluminum and boron filtration. This approach reduces the fast neutron dose to acceptable levels while maintaining adequate intensity for therapy. Using Tradescantia as a biological dosimeter the skin-sparing effect of the beam has been verified and it has been shown that it is possible to hold the total effective dose to normal tissue below the tolerance limit for the brain. A rat tumor has been developed to test various dose modifying or protective factors such as plasma exchange, fractionation of radiation delivery, chemoprotectors and other variables.

#### References

1. Zamenhof, R.G., Murray, B.W., Brownell, G.L., Wellum, G.R., Tolpin, E.I., Med. Phys. 2 (1975) 47-60.
2. Block, R.C., Brugger, R.M., Neutron Physics and Nuclear Data in Science and Tech. 2, Pergamon Press, 1983.
3. Noonan, D.J., Russell, J.L., Brugger, R.M., Paper to 26th Annual Health Physics Society Meeting, June 23, 1981, Louisville, KY.
4. Ritts, J.J., Solomito, M., Stevens, P.N., Nucl. Applic. & Tech. 7 (1969) 89-99.
5. Lindgren, M., Acta. Radiol. (Suppl.) 170 (1958).
6. Savage, J.R.K., Rad. Bot. 15 (1975) 88-140.
7. Ellis, F., Clin. Radiol. 20 (1969) 1-7.
8. Tolpin, E.I., Wellum, G.R., Dohan, F.C., Kornblith, P.L., Zamenhof, R.G., Oncology 32 (1975) 223-246.

TESTING BORON-CONTAINING ESTROGENS  
ON HUMAN BREAST CANCER CELLS IN A NEUTRON BEAM

Frederick Sweet, Ming-Shian Kao, Alice Williams, and Leili Khachatrian  
Washington University School of Medicine, St. Louis, MO 63110

and

Barry Wessels and John Kirsch  
Massachusetts Institute of Technology, Cambridge, MA 02139

ABSTRACT

Of the several boron-containing estrogen derivatives synthesized by us, we found that  $17\alpha$ -carboranyestradiol (*Carbestrol*) had estrogenic potency equal to natural estradiol both in female rats and also in human breast cancer cells (cell line MCF-7, estrogen sensitive). The therapy neutron beam from the MITR II nuclear reactor was trained on the MCF-7 cells which had been pre-incubated with various concentrations of *Carbestrol*. Control cells contained correspondingly equal concentrations of estradiol, or *o*-carborane plus estradiol. The neutron fluence measured by the gold foil method was  $4 \times 10^{12}$  n/cm<sup>2</sup>. The background  $\gamma$ -radiation was 300 rads. Both the test cells and also the control cells were markedly damaged by the irradiation. Under similar experimental conditions, 300 rads of  $\gamma$ -radiation from a calibrated cesium source were found to produce about half of the cell damage observed in the neutron irradiation experiments. Experiments involving the treatment of estrogen-sensitive cancer cells with a boron-containing estrogen may be more productive when the non-selectively destructive  $\gamma$ -radiation is removed from the neutron beam and also by enriching *Carbestrol* with <sup>10</sup>B.

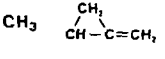
INTRODUCTION

In 1964, Soloway was first to suggest that the carbon-containing, boron-cage structured group called carborane be considered for attachment to biologically active compounds intended for BNCT (1). Compared with other boron-containing substances, carborane was exceptionally stable in aqueous media which approximated biological fluids. Also, derivatives of carborane were practically non-toxic in contrast with analogous compounds containing other boron groups.

By 1980, ours and Kahl's group had successfully attached the carborane group to estradiol (2,3,5). Working independently, we prepared appropriate acetylenic derivatives of estradiol, then reacted these compounds with decaborane to directly form the carborane moiety on the estrogen. Kahl's approach was to activate a suitable carborane derivative and attach it to a modified form of estradiol (5,6). Testing the first generation of our carborane-containing estrogens (3-O-carboranylmethylestradiol) in female rats showed that it was stable and non-toxic. However, it also had greatly reduced biological potency (2,3).

The exact location of a substituent group added to estradiol is known to be critical for both estrogenic potency and also the estrogen receptor-binding affinity of estradiol analogs (Table 1). This is true for the effects of the hormone analog on estrogen-sensitive normal and cancerous tissues. Therefore, to improve the boron-containing estrogen for BNCT it had to contain the carborane group at the 17 $\alpha$  position of estradiol. Accordingly, we synthesized 17 $\alpha$ -carb-

TABLE 1. Location of substituents versus biological activities of estradiol derivatives (from the data of D.J. Ellis, ref. 8)

R <sup>1</sup>	R <sup>2</sup>	% Relative Binding Activity	% Estrogenic Activity
H	H	100	100
CH <sub>3</sub>	H	0.004	10-50
CH <sub>3</sub>	C≡CH	0.130	436
CH <sub>3</sub>	CH <sub>2</sub> C≡CH	0.014	22
CH <sub>3</sub>	CH <sub>3</sub>	0.030	3
H	CH <sub>3</sub>	18	25
CH <sub>3</sub>	CH <sub>2</sub> CH <sub>3</sub>	0.001	—
CH <sub>3</sub>		0.004	8
CH <sub>3</sub>		0.400	87

(David Ellis, Report No. 11)

oranylestadiol (*Carbestrol*) by methods similar to those used for preparing our first-generation compounds (4). Kahl and coworkers also concentrated their efforts on making 17-position and D-ring, carborane-substituted estradiol analogs (5,6). Later, Hadd's group reported a synthesis of  $17\alpha$ -carboranylestadiol 17-acetate by using our approach (7,12). This compound was probably produced as an intermediate or an impurity during our earlier synthesis of *Carbestrol*.

*Carbestrol* was tested in female rats and shown to be equal in estrogenic potency to the natural hormone, estradiol (4). Hence this compound appeared suitable for experiments with human estrogen-sensitive cancer cells in culture. The present report describes the results from our experiments with the estrogen-sensitive cells from an human breast adenocarcinoma. *Carbestrol* was tested in the cells for growth stimulation. This system was irradiated with a thermal neutron beam to examine its potential for boron neutron capture therapy.

#### MATERIALS AND METHODS

*Carbestrol* was synthesized, purified, and characterized according to our previously reported method (4). The human breast MCF-7 cancer cells were the kind gift of Dr. E.M. Jensen of the Mason Research Institute in Rockville, MD. We cultured and characterized the MCF-7 cells according to established methods (9,10). Incubation of the cancer cells was carried out in sterile, 5%  $\text{CO}_2$ /air, in a water saturated atmosphere at 37 °C.

*Neutron Irradiation Experiments.* The MCF-7 were passaged and then plated at a density of  $5 \times 10^5$  cells/flask (25 mL culture flasks) in 4 mL of DMEM-calf serum (CS). After 5 hr of cell attachment, the medium was aspirated and the cells were rinsed with an additional 4 mL of DMEM-CS. Then the cells were fed with either 4 mL of medium alone (control) or with one of these substances added: *Carbestrol* ( $10^{-8}$  M); estradiol ( $10^{-8}$  M); *o*-carborane ( $10^{-8}$  M) plus estradi-

ol ( $10^{-8}$  M). For each substance tested and the control, 24 flasks were prepared. The MCF-7 cells were incubated for 15 h and then divided into two groups for either neutron irradiation or to serve as the non-irradiated controls. The flasks containing MCF-7 cells for neutron irradiation had gold foils attached to them and then they were arranged doubly stacked, in a circular array on a 3-m-diameter circular plywood platform which was mounted on a Rototorque rotating apparatus (by Cole-Parmer Instrument Co.). The flasks thus arranged were placed in the center of the vertical beam port (therapy neutron beam) of the MITR II reactor, such that the center of a flask coincided with the center of the beam port<sup>1</sup>. Rotating the platform at 15 cpm, and with the reactor operating at a level of 4.68 megawatts, the cells were irradiated for 5.7 h. These conditions provided a total average neutron dose of  $4.8 \times 10^{12}$  n/cm<sup>2</sup>, calculated from the gold foil measurements by an established method (11). Immediately after irradiation, the medium in each flask was exchanged with 4 mL of the appropriate medium<sup>2</sup> and the flasks were replaced in an incubator. The cells were harvested in triplicate on the days indicated in Fig. 2 (day of plating was taken as Day 0).

*Gamma-Irradiation Experiments:* The measured dose of background  $\gamma$ -radiation during the neutron irradiation experiment was 300 rads/5.7 h. Therefore, flasks of MCF-7 cells under conditions exactly corresponding to those described above were subjected to irradiation from a calibrated cesium  $\gamma$ -source in the Mallinckrodt Institute of Radiology at Washington University School of Medicine. The measured rate of  $\gamma$ -ray emission was 9.3 rads/min. The MCF-7 cells were variously exposed to doses of 50, 100, 150, or 300 rads of  $\gamma$ -radiation. The cells exhibited a typical radiation dose-response to irradiation. The effects of 300 rads

---

<sup>1</sup>Clearance between flask and beam port was 1 cm. <sup>2</sup>Containing Carbestrol, etc.

of  $\gamma$ -radiation on two groups of MCF-7 cells are compared with the effects on these cells of  $4.8 \times 10^{12}$  n/cm<sup>2</sup> thermal neutrons plus 300 rads of  $\gamma$ -radiation (Panel B, Fig. 2).

## RESULTS AND DISCUSSION

Human breast adenocarcinoma cells of the established cell line MCF-7 were tested for growth stimulation by the natural estrogen estradiol, Carbestrol, and 3-carboranyl methyl estradiol. The MCF-7 cells exhibited dose-dependent growth stimulation as represented in Fig. 1. Earlier, we found that in experiments with female rats treated by a classical protocol designed to measure hormone activity (by stimulation of uterine growth) 3-O-carboranylestradiol had 1/60 the potency of estradiol (2) but Carbestrol was practically equal to estradiol in potency (4). Thus the consistency in this pattern of biological activity observed in the present *in vitro* experiments is both interesting and also reassuring. Because the sub-cellular mechanism of estrogen growth stimulation of both rat uterine and also human breast cancerous tissues is now known to be strikingly similar we can be assured that, like estradiol, the boron-containing estradiol analogs are transported into the cell nuclei. This is encouraging because for BNCT to do the most good the  $^{10}\text{B}(\text{n},\alpha)^7\text{Li}$  reaction must occur where it can do the most damage to the cancer cells: inside the cell nucleus.

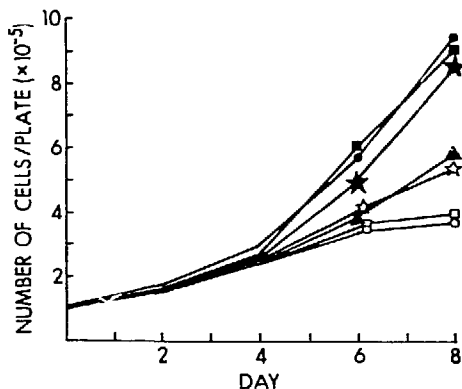
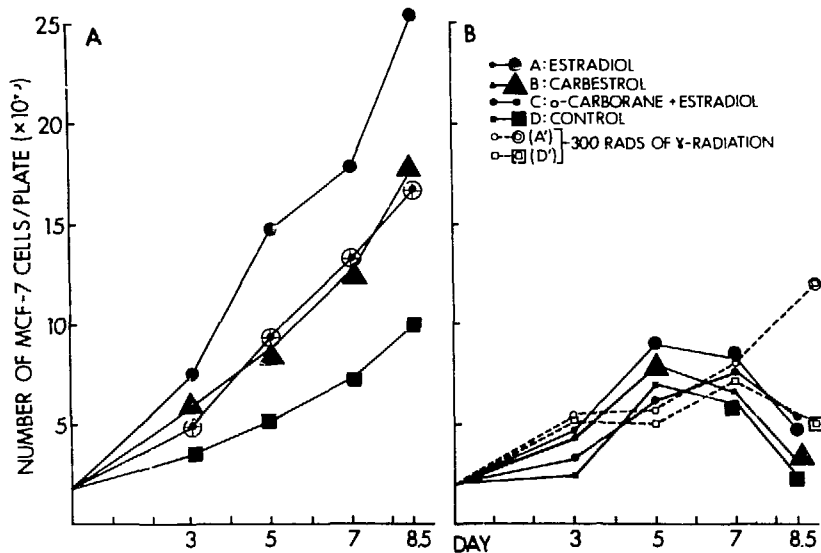


Fig. 1. Growth stimulation of MCF-7 cells by Carbestrol (■,  $10^{-8}\text{M}$ ), estradiol (●,  $10^{-8}\text{M}$ ), and 3-O-carboranylestradiol (★,  $10^{-6}\text{M}$ ) compared to the control group (▲). At concentrations of  $10^{-9}\text{M}$  growth stimulation due to Carbestrol and estradiol was about half of that shown, while at  $10^{-10}\text{M}$  it was near the control level. 3-O-Carboranylestradiol at  $10^{-8}\text{M}$  (★) had no effect on cell growth. However,  $10^{-6}\text{M}$  of either Carbestrol (□) or estradiol (○) caused inhibition of cell growth.

**Neutron and  $\gamma$ -Radiation Experiments.** Following a 15 h preincubation of the MCF-7 cells with Carbestrol, estradiol, or *o*-carborane plus estradiol, the cells were irradiated for 5.7 h in the therapy neutron beam of the MITR II reactor. The conditions of these experiments are described under MATERIALS AND METHODS. The results of these experiments are represented by the tracings in Fig. 2. At the same time, control groups of MCF-7 cells were subjected to similar conditions of transportation and temperature but kept shielded from radiation (Panel A, Fig. 2). All of the MCF-7 cells which were irradiated with the thermal neutrons were markedly damaged as evidenced by their substantial growth inhibition at Day 8.5 (Panel B, Fig. 2). No selectivity in the growth inhibition was evident among the various groups of cells which had been irradiated. The control



**Fig. 2. Neutron irradiation of MCF-7 cancer cells pretreated with Carbestrol.** Panel A. The non-irradiated control groups of cells were pretreated with: A, estradiol( $10^{-8}M$ , ●); B, Carbestrol( $10^{-8}M$ , ▲); C, *o*-carborane( $10^{-8}M$ ) plus estradiol( $10^{-8}M$ ), ◎; D, control with medium alone, ■. Panel B. The neutron irradiated MCF-7 cells were preincubated with the same media containing the substances detailed in Panel A. Note that C, ◎ in Panel A, corresponds to C, ◎ in Panel B. The results from the cesium  $\gamma$ -irradiation experiments are represented as A', ◎, and D', □, which correspond to cells under conditions A and D, respectively. Details of these experiments are discussed under MATERIALS AND METHODS.

cells were seemingly more damaged than the boron containing cells. However, the presence of the growth stimulators in the media during the days following neutron irradiation accounts for these differences.

The results from the cesium source  $\gamma$ -irradiation experiments are interesting. As shown in *Panel B*, Fig. 2, both the estrogen-stimulated cancer cells (A') and the unstimulated control cells (D') had their growths inhibited by over 50% as a result of receiving 300 rads of  $\gamma$ -irradiation. The background  $\gamma$ -radiation which accompanied the thermal neutrons during irradiation of the MCF-7 cells was at the same dose during 5.7 h of irradiation. We surmise that at least 50% of the cell damage observed as cell growth inhibition was due to this background radiation.

The present results have shown that to make further progress with the techniques described here the background  $\gamma$ -radiation must be more efficiently filtered. Then the biological effects of thermal neutron irradiation of MCF-7 cells in culture can be reliably assessed. Furthermore, to provide the possibility of observing a selective BNCT effect on the cancer cells which have been treated with Carbestrol, the boron-containing estrogen must be enriched with  $^{10}\text{B}$ . The carborane group on Carbestrol contains ten boron atoms. Therefore, enriching this group with  $^{10}\text{B}$  to about 99% can potentially enhance the molecular neutron capture cross-section of Carbestrol by an approximate factor of five. When all of this has been accomplished we hope to observe the successful and selective destruction of these cancer cells.

## ACKNOWLEDGEMENTS

The generous support of this research by the Cancer Committee of the Fraternal Order of Eagles (*Missouri Chapter*) is gratefully acknowledged. The authors wish to acknowledge the encouragement and enlightening discussions given us by Drs. James C. Warren, Gordon L. Brownell, Nicholas Tsoufanidis, Albert H. Soloway, Ralph G. Fairchild, and Stephen B. Kahl. Assistance with the  $\gamma$ -irradiation experiments was kindly provided by Dr. Hsiu-san Lin of the Radiation Oncology and Cancer Biology Division, Mallinckrodt Institute of Radiology.

## REFERENCES and NOTES

1. Soloway, A. (1964) in Steinberg, H. and McCloskey, A.L. (ed.) *Progress in Boron Chemistry*, New York, Macmillan Company, p. 227.
2. Sweet, F. (1981) *Steroids* 37, 223-238.
3. Sweet, F. (1981) *Abstracts of the 63rd Annual Meeting of The Endocrine Society*, Cincinnati. abstr. 670, p. 250.
4. Sweet, F., and Samant, B.R., (1983) *Proceedings of the International Symposium on Synthesis and Applications of Isotopically Labeled Compounds* (6-11 June 1982, Kansas City) Duncan, W.P., and Susan, A.B. (eds.) Amsterdam, Elsevier Scientific Publishing Company, pp. 175-180.
5. Kahl, S.B., and Wolff, M.E. (1980) *Abstracts of the Semi-Annual Meeting of The American Chemical Society*, Las Vegas. Medi. abstr. 108.
6. Kahl, S.B. (1983) *Proceedings of the International Symposium on Synthesis and Applications of Isotopically Labeled Compounds* (6-11 June 1982, Kansas City) Duncan, W.P., and Susan, A.B. (eds.) Amsterdam, Elsevier Scientific Publishing Company, pp. 181-186.
7. Hard, H.E., Brunson, K.W., and Kokosa, J.M. (1982) *Abstracts of the 64th Annual Meeting of The Endocrine Society*, San Francisco. abstr. 68.
8. These data were generously provided to one of the authors (F.S.) by Dr. David J. Ellis of the Institute of Clinical Medicine, Syntex Research, Palo Alto, CA.
9. Soule, H.D., Vazquez, J., Long, A., Albert, S., and Brennan, M. (1973) *J. Natl. Cancer Inst.* 51, 1409.
10. Horwitz, K.B., Kostlow, M.E., and McGuire, W.I. (1975) *Steroids* 26, 785.
11. ORTEC (1976) *Report AN-34: Experiments in Nuclear Science*, pp. 92-95.
12. Hadd, H.E. (1983) *See Paper V-11 in this Symposium.*

Combined Action of Thermal Neutron Irradiation and Boron-10-Amino acid Analogs on a Solid Experimental Tumor (EO771 C57 Bl/6J)

W. Porschen, J. Marx, H. Mühlensiepen, L.E. Feinendegen  
Institute of Medicine, Nuclear Research Center Jülich GmbH.,  
D-5170 Jülich, Federal Republic of Germany

F. Dallacker, H. Mückter, W. Müllners, Th. Böhmel  
Rheinisch-Westfälische Technische Hochschule Aachen,  
D-5100 Aachen, Federal Republic of Germany

ABSTRACT

If a tumor can be preferentially loaded with a suitable  $^{10}\text{B}$ -compound and irradiated with thermal neutrons, malignant cells can be selectively destroyed via the reaction  $^{10}\text{B}(\text{n},\alpha)^7\text{Li}$ ; both the  $\alpha$  particle and the  $^7\text{Li}$  nucleus have a high LET and an OER of about one; the combined range of the two particles amounts to about 14  $\mu\text{m}$  in water.

Two boron-amino acid analogs were synthesized with enriched boron (90%  $^{10}\text{B}$ ): (a) The compound Trimethylamine-carboxyborane (Mol weight: 116.2) contains 8.7% boron, and (b) Amine-carboxyborane (Mol weight: 74.1) contains 13.6% boron and shows a good solubility in water. The solid Adenocarcinoma EO 771 on C57 Bl/6J mice was used as test object.

The tumor-bearing animals were irradiated in a thermal column of the swimming-pool type reactor FRJ-1 (MERLIN); the bodies were shielded against thermal neutrons by a boron carbide-plastic mixture. The thermal neutron flux was  $2.3 \cdot 10^{10} \text{n/cm}^2 \text{ sec.}$  at the tumor.

Boron concentrations in tumor, liver, muscle and in blood were analysed by emission spectroscopy. The effects of the tumor treatment were evaluated by tumor volume measurements. Cell cycle changes were analysed by means of flow cytometry using the ICP-22 from Phywe.

INTRODUCTION

Clinical experience with neutron capture therapy since 1968 in Japan has been partially successful (1). But the full benefits of this unique therapy scheme can only be gained with better compounds of the third generation (2) characterized by selective binding to the tumor and biological half-lives in the order of days. Aminoacids are of interest since protein constitutes about 15% of tissue and turnover is rapid. Different boron-amino acid analogs have been reported; Trimethylamine-carboxyborane (A<sub>3</sub>) and Amine-carboxyborane (A<sub>7</sub>) were of specific interest (3).

## MATERIAL AND METHODS

### $^{10}\text{B}$ -Compounds

The organic  $^{10}\text{B}$ -compound Trimethylamine-carboxyborane  
 $(\text{CH}_3)_3 \text{NBH}_2 \text{COOH}$

(Molecular weight: 116.9) ( $\text{A}_3$ ) was synthesized either with natural boron (20%  $^{10}\text{B}$ ) or with enriched boron (90%  $^{10}\text{B}$ ). This betain analog contains 9.24% boron or 8.7% boron in the enriched compound.  $\text{A}_3$  shows a very low toxicity with a  $\text{LD}_{50}$  i.p. of about 1700 mg/kg in healthy mice. 0.5 mg/g were injected i.p. (3). Later, Amine-carboxyborane ( $\text{A}_7$ ) (Molecular weight: 74.8) was synthesized with natural boron or with 90% enriched boron-10. This boron analog of glycine contains 14.4% boron or 13.6% boron in the enriched compound and shows a good solubility in water. 1.0 mg  $\text{A}_7$ /g were injected i.p. 30 min. before irradiation.

### Mice and tumors

The adenocarcinoma EO 771 was used as transplantable tumor in mice. It originated in a mammary gland of a C57 Bl/6J mouse in 1940 and now appears as an undifferentiated, monomorphic neoplasm. The  $\text{TD}_{50}$  is about 24 cells\* (4). Autoradiographic experiments with a seven-day-old tumor yielded a growth fraction of about 90 percent and a cell cycle time of 19 hours with  $\text{G}_1$ : 8.5 hrs,  $\text{S}$ : 8.2 hrs,  $\text{G}_2+\text{M}$ : 2.3 hrs. The tumor is serially passed every week by injecting approximately  $1.75 \cdot 10^5$  viable cells in physiological saline (0.1 ml) into the right hind leg of male C57 Bl/6J mice, 8 to 12 weeks old, weighing 25 to 30 g (Zentralinstitut für Versuchstierzucht, Hannover-Linden, F.R. Germany). The tumor cell suspension was obtained by dissecting seven-day-old tumors with scissors and gently grinding the tumor pieces in a mortar, followed by sieving; the resulting cell suspension was diluted to the required cell number (4). Tumor growth was assayed by measuring diameters with a caliper and the tumor volume is read off from a calibration curve.

It is important to normalize the experimental conditions and the standard tumor is characterized by the following parameters: Tumor diameter: about 9-10 mm; Tumor volume: about 400-500 mm<sup>3</sup>; Growth fraction: 70%; Percentage of necrotic cells: 0%; Tumor doubling time: 48 hrs.; Number of Passages: 900; Spontaneous Regression: 0%.

### Influence of tumor treatment

Tumor growth was studied after giving thermal neutron irradiation and/or  $\text{A}_3$  or  $\text{A}_7$  respectively. Tumor growth delay represents the time delay between the treated and non-treated tumors with respect to volume doubling. This tumor is very radiation resistant and 40 Gy gamma rays result in a growth delay of about 5 days.

\* $\text{TD}_{50}$  cell no. = av. no. of cells per tumour implant that give 50% take probability.

### Irradiation facility FRJ-1 (MERLIN)

The tumor-bearing animals were irradiated at the research reactor FRJ-1 (MERLIN) in Jülich. MERLIN is a swimming-pool type reactor with 10 MW power and a maximum thermal neutron flux of  $2 \cdot 10^{14} \text{n/cm}^2$ . The reactor has two thermal columns BE-14 and BE-15. BE-15 was equipped with a facility for neutron capture therapy of mice in 1965 (5) but it is no longer in use now as a result of interference with other nuclear physics experiments. The central channel in BE-14 covers a wide range of thermal neutron fluxes ( $10^9$ - $10^{11} \text{n/cm}^2 \text{sec}$ ). The neutron flux density and the neutron spectrum depends on the  $\gamma$ -radiation position. In the standard position (60 cm from the reactor bound face) the following values were measured: thermal neutron flux density at the tumor:  $2 \cdot 10^{10} \text{n/cm}^2 \text{sec}$ .; thermal neutron flux density inside the shielding:  $7 \cdot 10^8 \text{n/cm}^2 \text{sec}$ .; fast neutron flux density ( $E > 1 \text{ MeV}$ ):  $2 \cdot 10^7 \text{n/cm}^2 \text{sec}$ .; cadmium ratio: 80 (gold foils); gamma dose rate: 30 Gy/h. During irradiation the tumor-bearing animals are shielded by a small container made of boron carbide plastic mixture with a wall thickness of 2 cm so that only the tumor is exposed. The animals are loaded and unloaded with the reactor in operation with minimal stress.

### Flow cytometry

Cell cycle changes were analysed using flow cytometry with a flow cytometer ICP 22 from Phywe, Göttingen. A cell suspension of the tumor cells from the adenocarcinoma EO 771 was prepared in PBS (phosphate buffer solution) with a concentration of about  $10^7$  cells per ml, fixed in alcohol and kept at 4 - 6°C until further use. For the analysis the cell suspension was stained with a mixture of ethidium bromide (Serva No. 21238) and mithramycin (Serva No. 34803) 1:1 and measured 10-30 minutes later. The distribution of the fluorescence intensity of the nuclear DNA was displayed as analog-print-out from the multichannel (Canberra 8100-MCA). The percentage of cells in the different phases:  $G_1$ , S and ( $G_2+M$ ) was evaluated from the area under the DNA histogram using background and aggregates correction (6, 7).

## RESULTS

### Boron analysis

Following intraperitoneal injection into tumor-bearing mice, boron concentration in tumor, liver, muscle and blood were analysed by emission spectroscopy (ICP) in the Institute for Chemical Analysis (Prof. Sansoni). The results are indicated in Fig. 1 and 2.

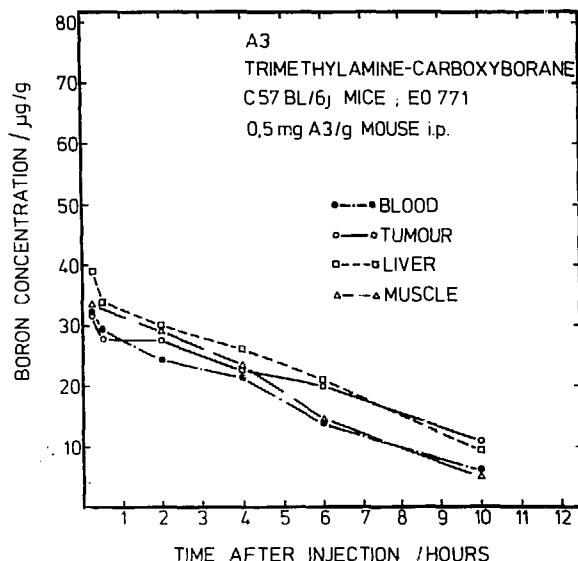


Fig. 1: Boron concentration ( $\mu\text{g/g}$ ) in blood, tumor, liver and muscle analysed at different times (15 min., 30 min., 2, 4, 6 and 10 hrs) following intraperitoneal injection of 0.5 mg/g Trimethylamine-carboxyborane (A<sub>3</sub>) into tumor-bearing animals (9 mm Adenocarcinoma EO 771 on C57 BL/6J mice).

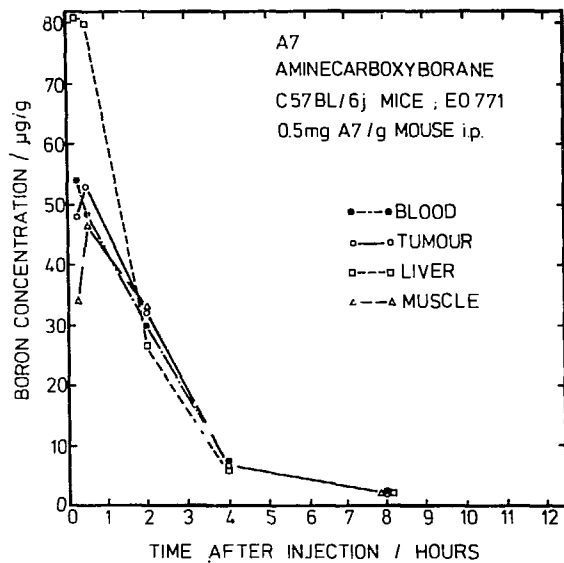


Fig. 2: Boron concentration ( $\mu\text{g/g}$ ) in blood, tumor, liver and muscle analysed at different times (15 min., 30 min., 2, 4 and 8 hours) following intraperitoneal injection of 0.5 mg/g Amine-carboxyborane (A<sub>7</sub>) into tumor-bearing animals (9 mm Adenocarcinoma EO 771 on C57 BL/6J mice).

### A<sub>3</sub> Trimethylamine-carboxyborane (Fig. 1)

6 hours after intraperitoneal injection of 0.5 mg/g A<sub>3</sub> a tumor to blood ratio of 1.3 was registered. The boron concentration in the tumor diminished with an effective half-life of about 6 hours.

### A<sub>7</sub> Amine-carboxyborane (Fig. 2)

A<sub>7</sub> shows a different time pattern of concentration. 30 min. after intraperitoneal injection of 1 mg/g A<sub>7</sub> a very high concentration of boron in the liver is registered (about 80  $\mu$ g/g). The boron concentration in the tumor diminishes with an effective half-life of about 2 hours.

#### Growth Delay - Flow Cytometry (A<sub>3</sub>)

A<sub>3</sub> was injected intraperitoneally at a concentration of 0.5 mg/g mouse. The analysis of the toxicity with normal mice without irradiation had demonstrated that A<sub>7</sub> shows a lower toxicity (LD<sub>50</sub> : 2500 mg/kg) than A<sub>3</sub> (LD<sub>50</sub> : 1700 mg/kg). Therefore only a limited number of experiments with A<sub>3</sub> was arranged and the main experimental effort was concentrated in the reaction from A<sub>7</sub> injected at a concentration of 1 mg/g for tumor bearing mice.

A<sub>3</sub> (90% <sup>10</sup>B) was injected 6 hours before neutron irradiation: A<sub>3</sub> injection alone or irradiation with thermal neutrons in the fluence range from  $4.3 \cdot 10^{11}$  -  $1.3 \cdot 10^{12}$  n/cm<sup>2</sup> produced a growth delay for tumor doubling of only 1 day to 2 days, but 0.5 mg A<sub>3</sub>/g and  $8.6 \cdot 10^{11}$  n/cm<sup>2</sup> resulted in a growth delay of 3.5 days (Fig. 3). Flow cytometry demonstrated a pronounced G<sub>2</sub> arrest after the combination, namely 24% cells in G<sub>2</sub> + M, whereas the neutrons alone or A<sub>3</sub> alone showed smaller effects, between 10% and 15%.

#### Growth Delay (A<sub>7</sub>)

a) The boron-glycine analog alone has no significant effect on tumor volume growth (Fig. 4) of the system EO 771 on C57 black mice.

b) Thermal neutron irradiation alone results in minimal growth delay in the range of 0.5 up to 1 day (Fig. 4.1 - 4.4) depending on neutron fluence.

c) The alpha particles from the boron-10 reaction produce growth delay depending on neutron fluence and boron-10 concentration.

In Fig. 4.1 and Fig. 4.2 the effects are comparatively small for a neutron fluence of  $1.9 \cdot 10^{12}$  or  $3.1 \cdot 10^{12}$  n/cm<sup>2</sup> and no difference is seen for A<sub>7</sub> with 20% or 90% <sup>10</sup>B.

In Fig. 4.3 and Fig. 4.4 the effect of boron 10 concentration is clearly demonstrated and a growth delay of 6 to 7 days is demonstrated for fluence values of 4.5 up to  $6 \cdot 10^{12}$  n/cm<sup>2</sup> in the case of A<sub>7</sub> with 90% <sup>10</sup>B. In contrast, the same fluence values after i.p. injection of A<sub>7</sub> (20%) results in growth delay of only 1-2 days (Table I).

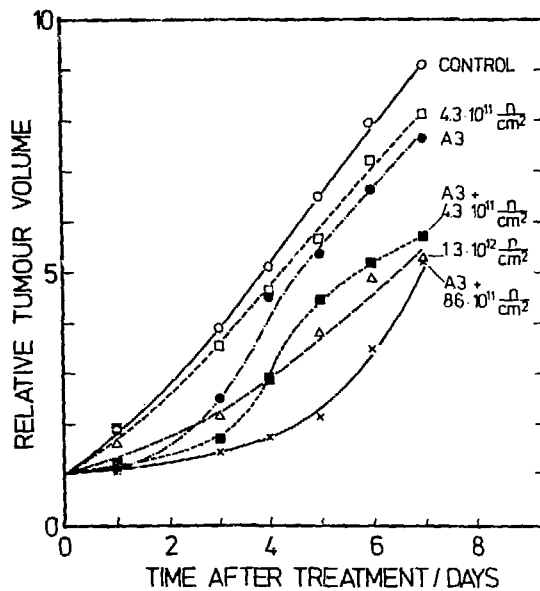


Fig. 3: Relative tumor volume of the Adenocarcinoma EO 771 following neutron capture therapy with  $A_3$  (90%  $^{10}B$ ) 0.5 mg  $A_3/g$  6 hrs before irradiation. Thermal neutron fluence:  $4.3 \cdot 10^{11} - 1.3 \cdot 10^{12} n/cm^2$ .

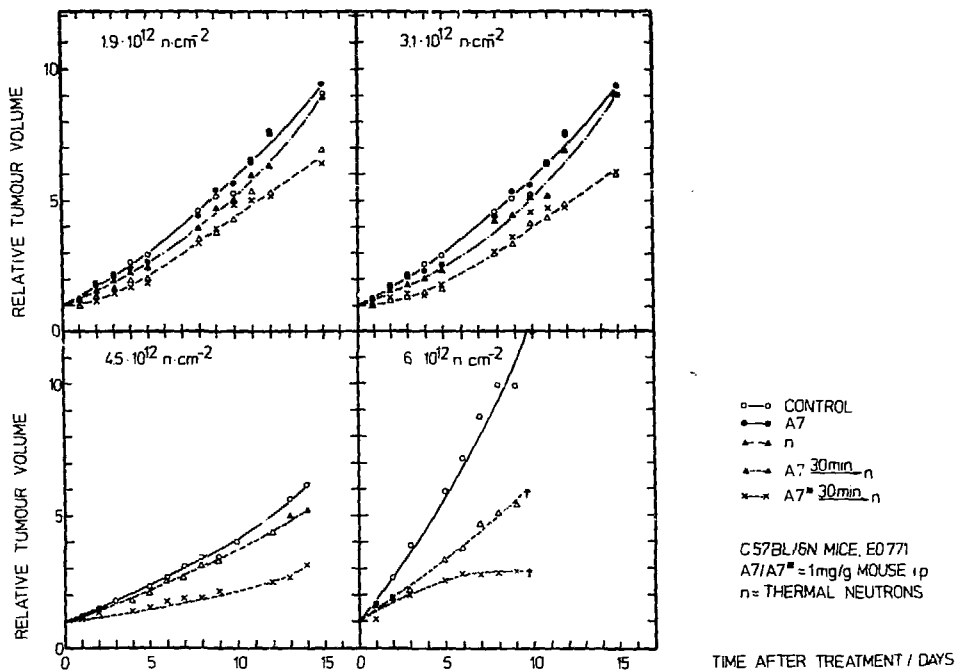


Fig. 4: Relative tumor volume of the Adenocarcinoma EO 771 following neutron capture therapy with  $A_7$  (20%  $^{10}B$ ) +  $A_7^*$  (90%  $^{10}B$ ) 1 mg/g, 30 minutes before irradiation; thermal neutron fluence:  $1.9 - 3.1 - 4.5 - 6 \cdot 10^{12} n/cm^2$ .

Table I. Growth Delay (days)

	$A_7$ (20% $^{10}\text{B}$ )	$A_7$ (90% $^{10}\text{B}$ )
$1.9 \cdot 10^{12} \text{n/cm}^2 \text{sec}$	0.7	1.5
$3.1 \cdot 10^{12} \text{n/cm}^2 \text{sec}$	1.0	2.5
$4.5 \cdot 10^{12} \text{n/cm}^2 \text{sec}$	0.5	1.0
$6.0 \cdot 10^{12} \text{n/cm}^2 \text{sec}$	1.0	2.0
		6.5

Flow Cytometry ( $A_7$ )

Changes in the cell cycle distribution were analyzed using flow cytometry as described above under material and methods.

The experiments focussed on the treatment with  $A_7$  (Amine-carboxyborane) alone or in combination with thermal neutrons. The compound  $A_7$  was synthesized either with natural boron (20%  $^{10}\text{B}$ ) or enriched  $^{10}\text{B}$  (90%). The results are shown in Fig. 5. The percentage figures are the corrected values (7). Different experimental conditions were analysed 6 hrs or 24 hrs after treatment: Untreated control animals; intraperitoneal injection of 1 mg  $A_7$ /g mice; irradiation with  $1.9 \cdot 10^{12} \text{n/cm}^2$ ,  $3.1 \cdot 10^{12} \text{n/cm}^2$  and  $6 \cdot 10^{12} \text{n/cm}^2$  thermal neutrons.

Treatment with 1 mg  $A_7$ /g and  $1.9 \cdot 10^{12}$ ,  $3.1 \cdot 10^{12}$  and  $6 \cdot 10^{12} \text{n/cm}^2$  thermal neutrons.

From the analysis of the diagram certain conclusions can be deduced taking into account the great difficulties in analysing the heterogeneous cell population of a solid tumor. After treatment with neutrons and in combination with a glycine-analogue, the biochemical pathways are influenced in multiple ways, resulting in a severe disturbance of cell cycle kinetics.

From Table II the following trends may be observed with respect to the percentage of tumor cells in (G2 + M) phase:

- a) Amine-carboxyborane ( $A_7$ ) alone, or irradiation with thermal neutrons alone, produces only minor accumulation in (G2 + M).
- b) The alpha particles from the boron-10 reaction result in a stronger accumulation, most pronounced in the case of 90% enriched boron-10 and  $6 \cdot 10^{12} \text{n/cm}^2$ . 52% of all tumor cells are found in (G2 + M) 24 hours after treatment. These results are in good agreement with the experimental findings of Lücke-Huhle (8).

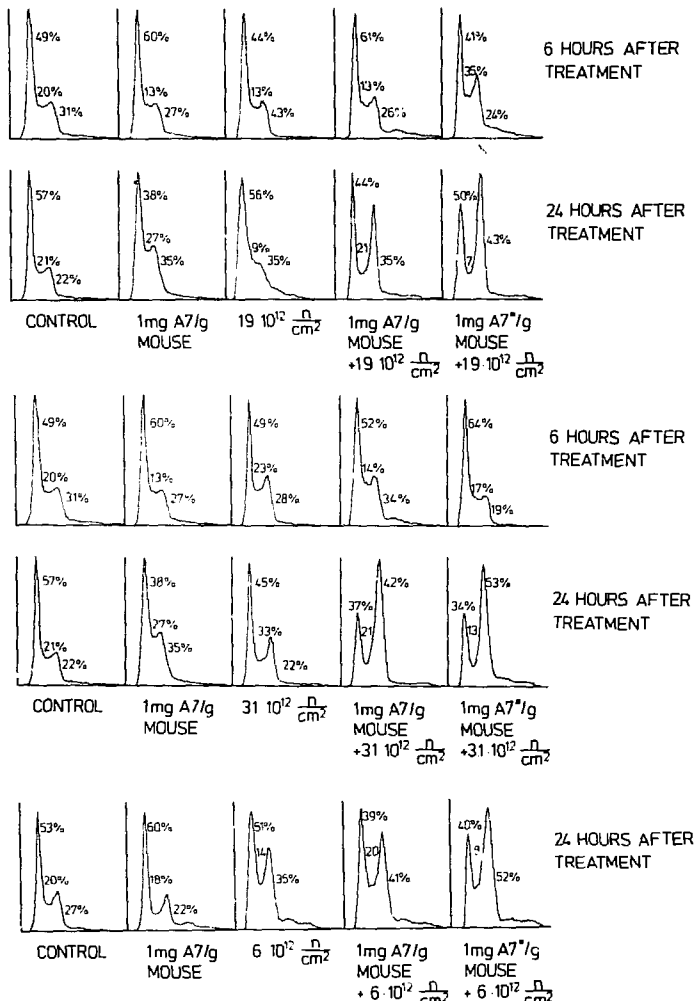


Fig. 5: Cell kinetic analysis of the cell cycle distribution of the Adenocarcinoma EO 771 (diameter about 9-10 mm) using flow cytometry (ICP-22). Cell cycle kinetics were analysed at 6 hrs or 24 hrs respectively after treatment with different schemes: Control animals; A<sub>7</sub> alone; neutrons alone, and the combination of A<sub>7</sub> and thermal neutron irradiation with different fluence values in the range from  $1.9 \cdot 10^{12}$  up to  $6 \cdot 10^{12} n/cm^2$ .

Table II. Cells in (G2+M) Phase (S.E. ~ 5%)

Treatment	Hours after treatment	
	6	24
Control	31%	22%
1 mg A <sub>7</sub> /g mouse	27%	35%
$1.9 \cdot 10^{12} \text{n/cm}^2$	43%	35%
$3.1 \cdot 10^{12} \text{n/cm}^2$	28%	22%
$6.0 \cdot 10^{12} \text{n/cm}^2$	-	35%
1 mg A <sub>7</sub> /g (20% <sup>10</sup> B)		
$+1.9 \cdot 10^{12} \text{n/cm}^2$	26%	35%
$+3.1 \cdot 10^{12} \text{n/cm}^2$	34%	42%
$+6.0 \cdot 10^{12} \text{n/cm}^2$	-	41%
1 mg A <sub>7</sub> * /g (90% <sup>10</sup> B)		
$+1.9 \cdot 10^{12} \text{n/cm}^2$	24%	43%
$+3.1 \cdot 10^{12} \text{n/cm}^2$	19%	53%
$+6.0 \cdot 10^{12} \text{n/cm}^2$	-	52%

## DISCUSSION

In contrast to glycine revealing a tumor/normal tissue ratio of 5 to 10 (9) the borated analogs of glycine A<sub>3</sub> (n-Trimethyl-amine-carboxyborane and A<sub>7</sub> (Amine-carboxyborane) surprisingly do not show increased uptake in tumor analogues over that of glycine. Therefore our experiments have the interesting result, that only such amino acid analogs may have beneficial effects in neutron capture therapy, which possess a low toxicity and a high percentage of <sup>10</sup>B. Of the so far described amine-carboxyboranes and derivatives only A<sub>3</sub> and A<sub>7</sub> with highly enriched boron-10 (90% <sup>10</sup>B or more) fulfil these conditions.

The analysis of the observed effect is difficult. The cell damage in the tumor after combined treatment results from the following components:

Cytotoxic effects under the influence of either amine-carboxyborane or trimethylamine-carboxyborane as a result of the depression of DNA synthesis, protein synthesis, RNA synthesis (3).

Cell damage as a result of the neutron flux and gamma irradiation in the thermal column and from the gamma component from the <sup>10</sup>B(n,α)<sup>7</sup>Li reaction.

Cell damage as a result of the internal irradiation with alpha particles from the <sup>10</sup>B(n,α)<sup>7</sup>Li reaction. The additional effect from the alpha particle is most clearly demonstrated after i.p. injection of enriched boron-10 (see Fig. 4.3 and 4.4) and this alpha component produces an additional growth delay of about 5 days if one compares the two curves in Fig. 4.3 and 4.4 either

with natural boron (20%  $^{10}\text{B}$ ) or enriched boron (90%  $^{10}\text{B}$ ).

The increment in growth delay of about 5 days (7 days - 2 days) may be attributed to the increment in the dose resulting from the increase in the alpha-particle dose as a result of the higher number of alpha particles from  $\text{A}_7$  (90%) in comparison to  $\text{A}_7$  (20%).

The additional alpha-particle dose may be estimated from the formula:

$$D = \frac{\mu\text{g}}{\text{g}} ({}^{10}\text{B}) \cdot \frac{F}{10^{12}} \cdot 0.09 \text{ Gy} \quad (5)$$

resulting in  $D = 38 \text{ Gray}$  ( $F = \text{neutron fluence, n/cm}^2$ ).

#### SUMMARY

a) Either Trimethylamine-carboxyborane ( $\text{A}_3$ ) injection alone or thermal neutron irradiation alone produced a growth delay of only 1 day to 2 days. b) 0.5 mg  $\text{A}_3/\text{g}$  plus  $8.6 \cdot 10^{11} \text{n/cm}^2$  resulted in a growth delay of 4 - 5 days. c) Flow cytometry demonstrated a pronounced G2 arrest after the combination (24%) whereas the neutrons alone or  $\text{A}_3$  alone showed smaller effects. d) Similar results were observed with Amine-carboxyborane ( $\text{A}_7$ ), both for the volume effect and for the cell cycle changes. The percentage of cells in (G2 + M) 24 hours after treatment were: Normal tumor: 22%; following  $\text{A}_7$ -treatment: 35%; following neutrons: 35%; combination: 43-53%. e) The most pronounced effect was clearly demonstrated after  $\text{A}_7^*$  (90%  $^{10}\text{B}$ ) and  $6 \cdot 10^{12} \text{n/cm}^2$  thermal neutrons (growth delay 6 - 7 days). f) The additional alpha-particle dose after  $\text{A}_7^*$  (90%  $^{10}\text{B}$ ) compared with  $\text{A}_7$  (20%  $^{10}\text{B}$ ) and  $6 \cdot 10^{12} \text{n/cm}^2$  was 38 Gy.

#### LITERATURE

1. H. Hatanaka, In: *Synthesis and Application of Isotopically Labeled Compounds, Proceedings* (W.P. Duncan and A.B. Susan, Eds.), Elsevier Scient. Publ. Comp., 167-174, 1983.
2. R.G. Fairchild and V.P. Bond, *New Compounds for Neutron Capture Therapy (NCT) and their Significance, presented at: Biological Individualization of Cancer Therapy*. Inst.of Med., Nucl.Res.Ctr., Germany, Apr. 1982.
3. I.H. Hall, C.O. Starnes, B.F. Spielvogel, P. Wisian-Neilson, M.K. Das and L. Wojmowich, *J. Pharm. Sci.*, 68, 685-688 (1979).
4. R. Porschen, W. Porschen, H. Mühlensiepen, L.E. Feinendegen, *Cell Tiss. Kinet.* 16, 549-556 (1983).
5. W. Porschen, F. Ritzl, G. Siebers, W. Stockhausen, I. Witt, *Strahlentherapie* 135, 575-585 (1968)
6. H.P. Beck, *Cell Tiss. Kinet.* 13, 173-181 (1980).
7. H. Baisch, *Cell Tiss. Kinet.* 15, 235-249 (1982).
8. Ch. Lücke-Huhle, *Rad. Res.* 89, 298-308 (1982).
9. R.G. Fairchild, In: *Synthesis and Applications of Isotopically Labeled Compounds, Proceedings* (W.P. Duncan and A.B. Susan, Eds.), Elsevier Scient. Publ. Comp., 155, 1983.

In Vitro and In Vivo Studies in Boron Neutron  
Capture Therapy of Malignant Melanoma

B.J. Allen

Australian Atomic Energy Commission Research Establishment  
Lucas Heights Research Laboratories  
Private Mail Bag, Sutherland, NSW 2232, Australia

ABSTRACT

A multidisciplinary research project in boron neutron capture therapy of malignant melanoma is under consideration by the Australian Atomic Energy Commission. This paper reviews the biochemistry of melanoma and the properties of some melanoma-affined radiopharmaceuticals and their boron analogues. Human cell lines are being used for in vitro tests of uptake and incorporation of some of these compounds, and selected lines will then be implanted in nude mice for in vivo distribution studies. The fidelity of human melanoma xenografts in nude mice has been well studied, and results are reviewed in this paper. Boron concentration will be measured directly by plasma arc emission spectroscopy or liquid scintillation counting with  $^{14}\text{C}$ -labelled boron analogues. Track-etch techniques will be used for the microscopic determination of boron in tumour sections. Neutron irradiation and radiobiology experiments are outlined.

1. INTRODUCTION

Melanoma is a cancer associated with the melanocyte (melano = black, cyte = cell), which produces the suntan that shields skin against strong sunlight. Often, melanocytes form moles, one in a million of which may produce a cancer. If the cancer is malignant, it has the potential to spread to other parts of the body.

The likelihood of spreading is dependent on the depth to which the melanoma has grown under the skin. For deep melanomas, metastases will often occur in the lymph glands, situated in the groin, armpit, and neck. These glands act as filters against infection or cancer. It is not possible to detect the early presence of metastases in the lymph glands.

The three main types of melanoma, in order of superior prognosis, are Hutchinson's melanotic freckle (HMF), superficial spreading melanoma (SSM), and nodular melanoma (NM). Lymph node metastases occur earliest with NM and are rare with HMF. The thickness of the lesion (i.e. penetration through the skin) is a reliable and most important determinant of prognosis and therapy, invasion of the subcutaneous tissues being highly lethal.

Australia has a high incidence of malignant melanoma, the state of Queensland having the highest incidence in the world at 34 cases per 100 000; the lowest incidence is 0.05 per 100 000 in Uganda. Most cases occur in the coastal districts, and it is apparent that solar exposure and race are important causal factors. New South Wales has about half the incidence rate of Queensland, with about 230 deaths ascribed to malignant melanoma each year.

The New South Wales mortality rate is 19% for women and 38% for men, and 30% of deaths result from multiple node metastases to the brain. Early detection is a major factor in survival. During the last two decades, the incidence of melanoma has doubled in New South Wales and Queensland and increased markedly all over the world.

Meticulous surgical management of primary melanoma is advocated, with prophylactic (preventative) lymph node dissection for tumours of thickness greater than 2 mm. Disseminated melanoma is, in general, resistant to radiotherapy and chemotherapy. Immunotherapy is in the experimental stage and so far has yielded disappointing results.

It is therefore appropriate and timely for the Australian Atomic Energy Commission to investigate a research program in boron neutron capture therapy of malignant melanoma. The program consists of the following:

- (a) Production of appropriate boron compounds for uptake by melanomas.
- (b) Maintenance of human melanoma cell line cultures.
- (c) Demonstration of uptake and incorporation of boron compounds in human melanoma cell cultures.
- (d) In vitro neutron irradiation of boron-loaded cell cultures for determination of relative biological effectiveness (RBE).
- (e) Xenografting human melanomas in nude mice and studies of the uptake of boron compounds.
- (f) Design and construction of a nude mouse boron neutron capture therapy facility on the AAEC's 100-kW reactor Moata.
- (g) Radiobiology and pathology of irradiated tumours and growth delay studies.

Once this program has been accomplished and satisfactory results obtained, clinical oncologists would be expected to take advantage of the facilities. It is envisaged that topics (b), (c), and (d) will be undertaken in collaboration with the Queensland Institute of Medical Research.

## 2. MELANIN CONTENT IN MELANOTIC AND AMELANOTIC MELANOMA IN MICE, HAMSTERS, AND HUMANS

Melanoma is one of a number of cancers having cellular functional differentiation, synthesizing a specific protein, melanin. As malignant transformation occurs, these tumours usually acquire increased mitotic activity and often retain their melanin synthesizing ability.

Melanin content has been determined by Watts et al. (1) for pigmented and nonpigmented tissues of Syrian golden hamsters bearing Greene melanoma, B-16 melanoma in C57 mice, Harding-Passey (HP) in BALB/C mice, KHDD in C3H mice, and nine human melanomas, as well as selected normal tissues.

Well-pigmented animal melanomas contained 0.3 to 0.8 wt% melanin, whereas human melanomas varied from 0.1 to 0.9 wt% (average 0.35 wt%). With the exception of skin, other tissues were lower in content by a factor of 30 or more.

Clinically, melanin content is described by the terms "deeply," "heavily," or "lightly" pigmented, or amelanotic (no visible pigmentation). Well-pigmented human melanomas have an average concentration of 0.35 wt%, very similar to the average for the Greene and HP models. This result is unexpected, for the rapid doubling time of the Greene ( $\sim 2$  d) and HP ( $\sim 4$  d) melanomas suggests a lower content relative to the slower growth period (6 to 7 weeks) for human melanoma (2). Human melanomas often show large areas of

necrosis (up to 90%), but no correlation has been found between gross pigment content and viable tumour fraction.

Amelanotic animal models had concentrations from 0.003 to 0.02 wt%, i.e. about 10 to 80 times less than the well-pigmented melanomas. These results are generally in agreement with those of earlier workers, other than Borovansky (3), who found about half the melanin content of melanotic lines for amelanotic melanomas.

Of the tissues showing a high incidence of metastatic melanoma, heart (41%) and liver (77%) have been reported at 0.05 wt% of melanin in tissue, about five times as high as that observed by Watts et al. (1). The difference in melanin concentration between most tissues and melanotic melanoma (30 to 50 times) indicates a high efficacy for preformed melanin-affined compounds such as chlorpromazine (CPZ).

A significant variation in the melanin content of several metastases was found within the same patient; this variation is well known in human and animal melanoma models. However, pigmentation may be regained or stimulated through the introduction of such chemicals as 1- $\beta$ -D-arabinofuranosylcytosine (4), theophyllin (5), or cytarabine (6).

Most primary malignant melanomas have a dark colour because of melanin, which is formed as the result of a long chain of chemical changes, beginning with phenylalanine (see Figure 1). Blois and Kallman (7) investigated the precursors of melanin by incorporating  $^{14}\text{C}$ -labelled 3,4-dihydroxyphenylalanine into the melanin of a mouse melanoma. The precursor chain includes a side branch, which is also shown in Figure 1.

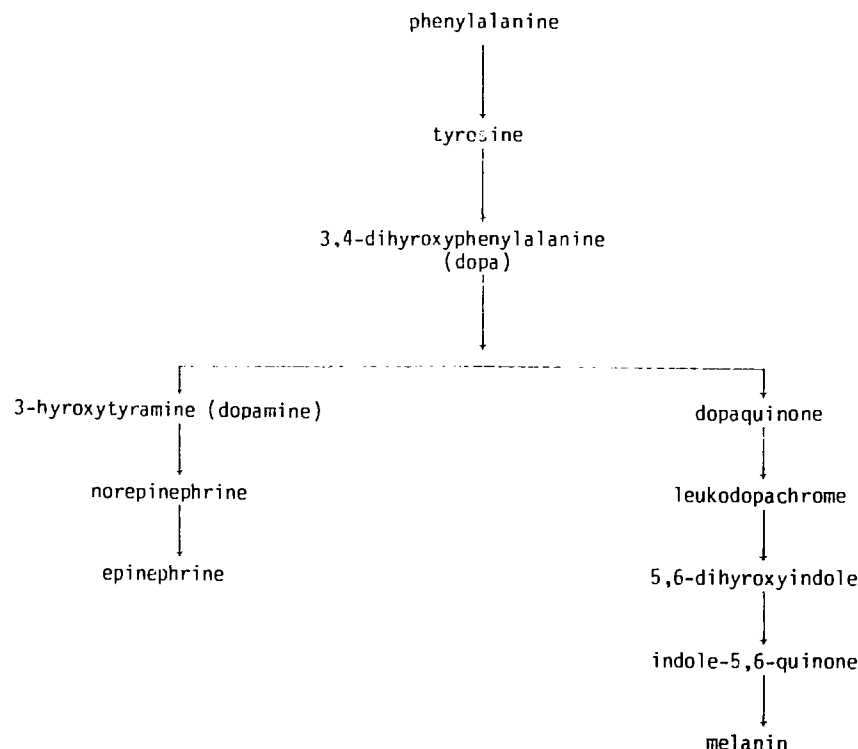


Figure 1. Biosynthetic pathway of melanin and epinephrin (7).

Melanin is an irregular, three-dimensional, heteropolymer composed of dopaquinone, 5,6-dihydroxyindole, and 5,6-dihydroxyindole 2-carboxylic acid units with free radicals trapped in segments of the structure (8), as shown in Figure 2. Brown to black melanins are of high molecular weight, relatively insoluble, of polymer nature, and resistant to chemicals (9). Melanin is rich in such metals as Zn, Cu, Fe, and Mn (10).

Melanin can act as a free electron acceptor, but within cells it is bound to protein, which blocks the free radical sites. The proportion of free radical sites may be critical to radiopharmaceutical uptake, especially where trace metal binding is involved.

Melanin-bearing tissues are found in the skin, mucous membranes, eye, inner ear, meninges (membranes of the brain and cord), and the neuro-melanin of the brain stem. The origin of the melanin of the central nervous system is

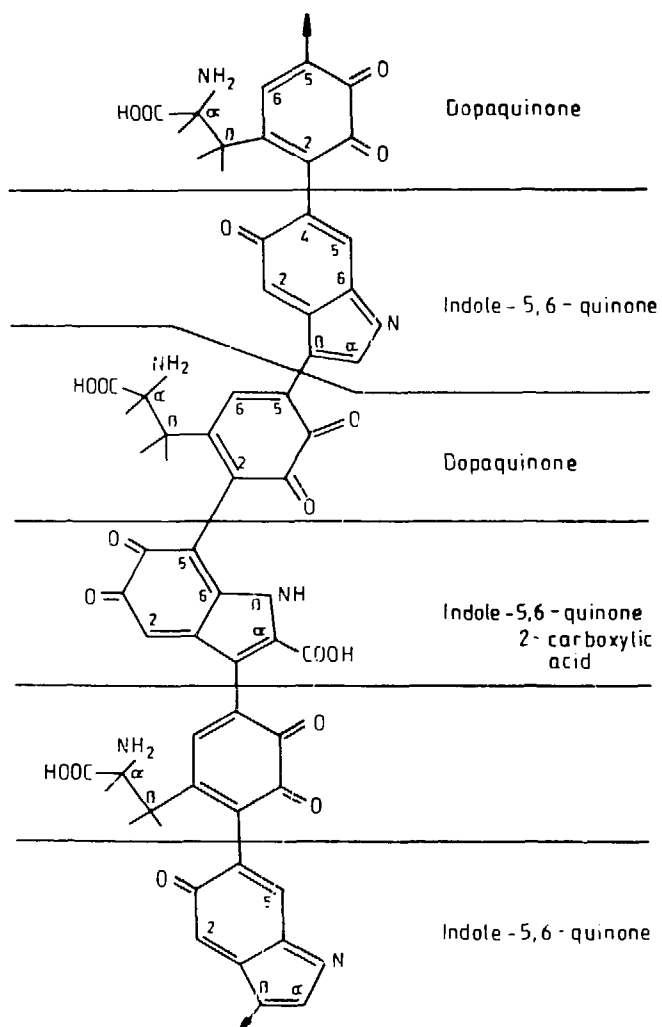


Figure 2. Hypothetical structure for melanin in Harding-Passey melanoma (8).

thought to be correlated with a tyrosinase-independent biochemical pathway. The skin and melanoma melanins are synthesised through the tyrosinase-dependent pathway.

Melanin content and tyrosinase activity may vary markedly between human and murine melanomas. Furthermore, there may be histological and pathological differences which could further influence uptake of the boron compounds needed for neutron capture therapy. The B-16 melanoma has not only a very low melanin content but also a poor record for predicting the sensitivity of human cell lines to cytotoxic chemotherapy (A. Coates, priv. comm.). Consequently, successful experiments with murine melanomas must be reproduced on human melanomas before clinical application is authorised. Moreover, antibodies are specific only to human melanomas. It is therefore not only cost effective but in some cases essential to use human melanoma for in vitro and in vivo experiments.

### 3. MELANOMA-AFFINED COMPOUNDS

The potential use of most melanoma-affined agents for tumour scanning and therapy is based on the specific function of the tumour to produce melanin. Following the systemic injection, the agent arrives at the site of the melanoma and, depending on blood flow and microcirculation within the tumour, accumulates at the melanoma cell membrane. There the agent must affix to the cell and either remain attached to the membrane or be transported into the cell. The receptor sites may be immunologically specific or chemically selective. The cell surface is usually negatively charged; positively charged agents accumulate at the surface, and the electrical charge increases with malignancy (11). Once in the cell, the agent may be incorporated into the melanin synthesis or it may react with melanin or melanoproteins. The interactions may be biochemical, physiological, or immunological.

The uptake of many agents in the melanoma can be classified as follows:

- (a) Interaction with preformed melanin.
- (b) Physiological precursors in melanin polymerization.
- (c) False precursors.
- (d) Interaction with membrane antigens.

A brief description of the outstanding melanoma-affined compounds, chlorpromazine, iodo- $\alpha$ -methyltyrosine, boronophenylalanine, and thiouracil, follows.

#### A. Chlorpromazine (CPZ)

CPZ gives tumour/blood ratios of 150 for a single dose and 630 for a sequence of doses (12). The worst ratio, for the liver, is in the range 12 to 16. Compared with a non-specific compound, a boron analogue synthesized and tested in cell culture (13) yielded a concentration factor of only 4.5 for cell killing and 9 for  $\alpha$ -track counting. In vivo studies in hamsters showed tumour growth suppression for 18 days after irradiation, but complete eradication could not be achieved. A  $^{10}\text{B}$  content of 45 to 62  $\mu\text{g}$   $^{10}\text{B}/\text{g}$  tumour is possible if  $^{10}\text{B}_{12}$ -CPZ has the same uptake in melanoma as CPZ alone. Further in vivo research is needed on both  $^{10}\text{B}_{12}$ -CPZ uptake and the derivative 7-OH CPZ (14).

## B. Iodo- $\alpha$ -methyltyrosine (IMT)

In the L-optical isomer configuration, the uptake ratio of iodo- $\alpha$ -methyltyrosine accumulation per gram for melanoma/kidney is 7; for melanoma/liver, 69; and for melanoma/blood, 46, at 24 h after administration (15). However, this compound was not taken up by the hamster melanoma, and the iodine-labelled version reduced the precursor role of the compound. Other labelled versions should therefore be investigated.

## C. Boronophenylalanine (BPA)

Whereas dopa borate has no effect for *in vitro* survival, BPA gives an elevenfold enhanced incorporation and a  $D_0$  of  $\sim 10^{12}$  neutrons  $\text{cm}^{-2}$  (down by  $\times 3$  from that for thermal neutrons alone) for  $4.3 \mu\text{g}^{10}\text{B/g}$  wet cells (16). No data are yet available on the *in vivo* uptake of this boron compound.

## D. Thiouracil (TU)

Fairchild et al. (17) found uptake ratios for tumour/blood, 77; for tumour/muscle, 417; and for tumour/kidney, 70. Up to  $300 \mu\text{g/g}$  tumour uptakes are possible; this corresponds to  $26 \mu\text{g}^{10}\text{B/g}$  if one boron atom is attached, and  $312 \mu\text{g}^{10}\text{B/g}$  if a  $\text{B}_{12}$  cage is added.

These boron concentrations are more than adequate for neutron capture therapy if uptakes similar to those of the parent compound can be achieved for the boron analogue. However, further research is needed for each compound to determine its efficacy in neutron capture therapy. Some compounds labelled with  $^{35}\text{S}$  or  $^{123}\text{I}$  could also play a useful diagnostic or therapeutic role.

## E. Monoclonal Antibodies

The malignant transformation of cells is associated with functional and structural changes to their membranes. Of particular relevance is the appearance of tumour-associated antigens, to which tumour-specific antibodies may respond. Problems relating to the production of specific xenoantisera appear to have been overcome by the development of the hybridoma technique (18), a method which can continuously produce monoclonal antibodies of defined specificity. Experiments strongly suggest that monoclonal antibodies to human tumour-associated antigens may be used to localise human primary tumours and metastases. Imai et al. (19) have developed monoclonal antibodies to human melanoma-associated antigens (MAA). Hybridoma lines have high but variable reactivity *in vitro* to human melanoma cell cultures compared with lymphoid cells, carcinomas, sarcomas, and foetal fibroblasts.

Studies have shown that the injection of monoclonal antibodies to MAA in nude mice with human melanoma xenografts inhibits tumour growth. This may result from an antibody-dependent, cell-mediated cytotoxicity reaction, or the coating of cells with antibodies may inhibit mitotic activity. The data strongly suggest that monoclonal antibodies to MAA can bind to melanoma cells

in vivo and, when suitably labelled, may have a role in imaging and therapy of melanoma.

#### 4. SYNTHESIS OF BORON ANALOGUE OF THIOURACIL

Although thiouracil has excellent properties for incorporation in melanotic melanomas, a boron analogue has not yet been synthesized. One approach may be via *n*-alkylthiouracil in which the alkyl group carries the boron cage (J. Wilson, priv. comm.). The boron can be incorporated early in the synthesis because the chemical stability of the carborane moiety would ensure its survival in subsequent reactions. After synthesis of 1-bromomethylcarborane (compound I, Figure 3), the synthesis of 3-(carboranyl methyl)thiouracil (CMT, compound II) should proceed according to the sequence of well-known reactions shown in Figure 3.

It would be useful to have  $^{14}\text{C}$ -labelled CMT available for in vitro and in vivo uptake studies, but several factors need to be considered:

(a) The labelling of one of the carbons ( $\alpha$ ,  $\beta$ ,  $\gamma$ ) of the alkyl side-chain carrying the boron cage would initially require a  $^{14}\text{C}$ -labelled propargyl derivative. These are commercially unavailable.

(b) To incorporate the label at position 2 in the pyrimidine ring would require  $^{14}\text{C}$ -labelled thiocyanate for the preparation of the intermediate thiourea. This too is unobtainable.

(c) Uracil (compound III in Figure 3,  $R = \text{H}$ ) universally labelled with  $^{14}\text{C}$  at positions 2, 4, 5, and 6 is commercially available and could provide a suitable intermediate stage. Availability is due to the recent synthesis of thiouracil substituted with alkyl groups at position 1; this derivative is based on the ability of dimethyl uracil (compound III,  $R = \text{Me}$ ), to react with 1-alkylthioureas to give 1-alkyl substituted thiouracils by an exclusive process in which the 1,2,3-urea fragment of dimethyl uracil is exchanged for the corresponding thiourea. Calculations based, *inter alia*, on a four-step synthesis of compound I, starting from the reaction that provides the  $^{14}\text{C}$  incorpora-

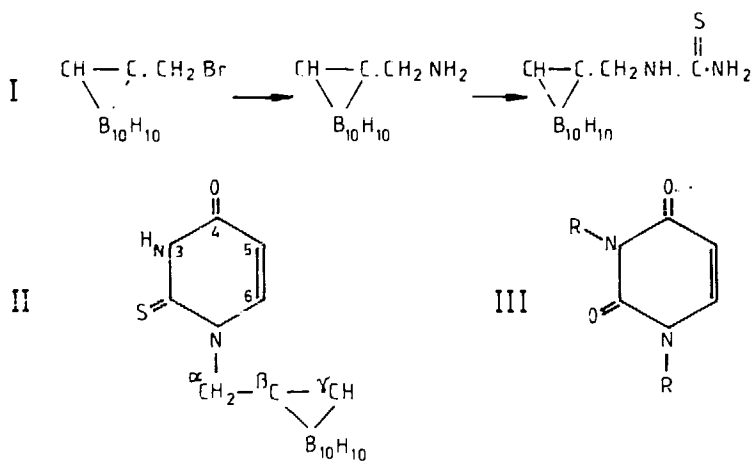


Figure 3. Proposed synthesis of 3-(carboranyl methyl)thiouracil.

tion and the necessary loss of one quarter of the activity due to loss of carbon-14 by the uracil, indicate that 100  $\mu$ Ci of  $^{14}\text{C}$ -labelled uracil would be required to synthesize a working amount of compound I.

### 5. UPTAKE AND INCORPORATION STUDIES IN HUMAN MALIGNANT MELANOMA CELL CULTURES

The Queensland Institute for Medical Research maintains a library of human melanoma cell cultures obtained from the Queensland Melanoma Project. The cell lines vary in melanin content and tyrosinase activity and have been classified according to responses to numerous chemical tests (P. Parsons, priv. comm.).

Initial uptake and incorporation studies are underway using  $^{14}\text{C}$ -labelled CPZ and TU compounds, to establish benchmarks for comparison with boron analogues and to provide a direct check against in vitro studies on murine melanomas. The most responsive melanoma lines will then be chosen for in vitro RBE measurements, using the appropriate boron compounds, and for xeno-grafts in nude mice.

Preliminary results have been obtained for HeLa cells and three human melanoma lines. Uptake (after two quick washes with cold buffer) and incorporation (i.e. as an acid-insoluble label) of  $^{14}\text{C}$ -CPZ and  $^{14}\text{C}$ -TU were measured after an 18-h incubation; both uptakes were similar for all lines. After application of a tyrosinase inhibitor it was observed that CPZ incorporation is not tyrosinase-dependent. As was expected, the high tyrosinase line showed a marked incorporation of TU.

### 6. FIDELITY OF HUMAN MELANOMA XENOGRAFTS IN NUDE MICE

A detailed examination of the fidelity of a human melanoma metastasis passaged in nude mice was made by Fogh et al. (20). When cultivated in MEM medium with 15% calf serum, the cell line grew as a monolayer with fibroblastic morphology. Subcutaneous inoculation of  $2 \times 10^7$  cultured cells was applied to the dorsal region of nude mice (Rex/Trembler origin back-crossed three times to a Swiss strain). The developing tumour was excised under sterile conditions after 31 days, minced with scalpels, and treated with 0.25% trypsin. From the beginning, these cultured cells maintained a cell morphology and ultrastructure similar to that of the original line: similar characteristics were found for growth pattern, cell viability, shape, and size; nuclei shape, size, chromatic pattern, and nucleoli; cytoplasmic organelles; cell membrane; mitosis; cellular cannibalism; and cell membrane junctions. In vitro cell doubling time for passage cells 19 and 5 was 57.7 h, and the mitotic indexes were 1.54 and 1.55 respectively.

In vivo tumour growth was studied on inocula from  $(2.5 \text{ to } 16) \times 10^6$  cells. Tumours grew at all levels of inocula, the larger tumours appearing earlier at the higher levels. No difference in the tumour-producing capacity was found for the original and passage cell lines. However, variations in tumour volume suggest differences in susceptibility for individual mice. The original line was susceptible to polio virus type 1, and similar cytopathic effects were observed for passage cell lines.

Chromosome analysis showed that both lines contained human chromosomes, with a modal number of 44. Although abnormalities were not observed in the passage cell line and a few metaphases contained a higher number of chromosomes, Fogh et al. (20) concluded that the chromosomal pictures of the two lines were very similar. Further, the isozyme analyses of both lines were almost identical, indicating that there was no evidence of mouse cell contamination.

Sharkey et al. (21) examined six melanomas (one primary, four metastatic, and one recurrent) and also observed a striking similarity in histological appearance of the passage cell tumours to the original human material, e.g. similar amounts of small nevoid, epithelioid and giant cells, melanin production, and pleiomorphism spindling.

Forty-six melanoma cell lines, mainly from metastatic tumours, were grafted in nude mice by Hajdu and Fogh (22). For 26 cases pathological specimens of the original tumours were available for review. The histological grade of these neoplasms and that of the corresponding nude mice tumours were similar in 22 cases; of the others, two were more differentiated and two were less. However, intracytoplasmic melanin pigment (i.e. melanin granules), although identified in most surgical specimens and cultures, was present in less than half of the nude mice tumours. Demoplastic changes were seen occasionally in the human tumours, but not in the mouse tumours in the nude host.

Overall, there is little change in the characteristics of malignant melanoma after passage through the nude mouse. An exception to this is the decrease in metastatic behaviour observed in the nude mouse host.

## 6.1 Metastasis of Tumour Xenografts

Although the fidelity of passage cell tumours is high, there is a discrepancy between the invasive and metastatic capacities of tumours in their natural hosts and those in the nude mouse. The majority of primary and metastatic human tumours grown successfully as subcutaneous xenografts in the nude mice (or in immuno-depressed hosts) exhibited few metastases. Experience with xenogeneic metastases is rather limited and conflicting, and has been reviewed by Sordat et al. (23).

Giovanella et al. (24) investigated the metastatic spread of three amelanotic melanomas to the regional lymph nodes, with one line also disseminating to the lymphatics in the lungs. A study of additional cell lines indicated that the frequency of metastases was as low as 10%, i.e. 4/40 mice had macroscopic evidence of growth in the lymph nodes. These mice were maintained under specific pathogen-free (SPF) conditions and received diverse combinations of antibiotics. However, for mice maintained conventionally, no metastases were found in a number of earlier and later studies.

Sharkey and Fogh (25) studied 106 different human tumours in more than 1000 outbred nude mice and found an incidence of metastases of only 1.7%. Three of eleven tumours (all carcinomas) demonstrated repeated metastases. However, they observed that original metastatic tumours were no more likely to disseminate than primaries. For subcutaneous grafts of 66 different tumours on 534 BALB/C SPF nude mice (20), metastases were observed in 5.6% of cases.

Inoculation route, cell dose, and cell type are important for the establishment of *in vivo* tumour grafts. The majority of tumour cells introduced into the circulation of the nude mouse are effectively destroyed, mainly after trapping in the lungs. Under these conditions, few cells can escape to establish secondary growths.

## 6.2 Chemotherapy

For the past seven years, the melanoma unit at the Fox Chase Cancer Centre, Philadelphia, has been testing chemotherapeutic agents in patients with metastatic melanoma. To alleviate patient morbidity and occasional mortality, a secondary screen for chemotherapeutic agents is planned with the nude mouse--human melanoma model. Bellet and Mastrangelo (26) have evaluated the chemosensitivity of this model for agents of known clinical activity and found it to be consistent with clinical experience.

## 6.3 Radiotherapy

Extensive *in vitro* and *in vivo* radiobiological studies have been carried out by Rofstad (27) for a human melanoma line taken from a lymph node metastasis. For these experiments, mice were loaded into Perspex tubes, the tumour projecting through a hole in the side of the tube. A 14x14-mm brass collimator set in an 8-cm-thick lead block was used as the defining aperture. Doses up to 25 Gy of cobalt-60 gamma rays were applied for periods up to 20 min. The mice were not anaesthetized because of the need to maintain natural respiration for aerobic conditions. The tumour and lower body of the mouse were immersed in water which was maintained at 30°C.

To enable hypoxic tumour studies, the mice were killed 15 min before irradiation. In this work EE melanoma was found to be 5 to 10% hypoxic, whereas Guichard et al. (28) reported 85% hypoxicity for a Nall malignant melanoma.

The use of misonidazole (a hypoxic cell radiosensitizer) gave an enhancement ratio of 1.5 (i.e. 12 Gy + misonidazole  $\equiv$  19 Gy). When tumours were left *in situ* after irradiation, single cell survival was higher than if they were immediately removed, because of the repair of potentially lethal damage (PLD). However, the misonidazole enhancement ratio, calculated as the ratio of  $D_{0}$  values, showed no misonidazole enhancement for PLD repair. This is contrary to the observation by Guichard et al. (28) that in the Nall melanoma PLD was suppressed by misonidazole.

Clearly, different melanoma lines can have quite different responses to chemo- and radiotherapy. It is apparent, therefore, that potential therapeutic modalities must be tested over the widest possible range of melanomas.

The AAEC is the major producer of nude mice in New South Wales, servicing the Ludwig Institute for Cancer Research and a number of hospitals in New South Wales. The mice, bred under SPF conditions, are of good health and provide an important resource for an *in vivo* research program with human tumour xenografts.

## 7. THE CONCENTRATION OF BORON COMPOUNDS IN MELANOMAS

Subcutaneous injection of equal numbers of cultured human melanoma cells at the same time will ensure the uniform development of tumours in a given batch. The inoculated mice are then maintained in a laminar flow cabinet under biohazard conditions.

Intravenous injection of the boron compound would take place after adequate tumour growth (about 14 days). The mice are then sacrificed at different time intervals after injection and dissected for the determination of boron in the tumour, blood, and vital organs.

The spatial distribution of boron compounds in the tumour can be obtained by freeze-drying tumour sections and sandwiching them under vacuum between CR-39 slides. This forms a solid state detector (29) which, under thermal neutron irradiation, produces sub-microscopic tracks of the  $^{7}\text{Li}$  and alpha particles. When etched with 2.25 to 6.25 N NaOH at  $60^{\circ}\text{C}$ , these tracks are readily observed by light or electron microscopy. The 5- $\mu\text{m}$ -thick tumour section is stained and overlapped with the etched film to determine the spatial distribution of  $^{10}\text{B}$  at the cellular level. This is of particular importance when determining the absorption of  $^{10}\text{B}$  in endothelial cells in the normal vasculature. Further, the effectiveness of boron neutron capture therapy (BNCT) is markedly dependent on whether the boron loading is intra- rather than inter-cellular. Kobayashi and Kanda (30) have estimated that significant variations in sensitivity can result from the location of the boron.

The time-dependent uptake distribution of boron in the tumour and the skin, eye, and sensitive organs of the nude mouse can be determined by dissolution of the tissue sample for boron counting in a plasma arc emission spectrometer having a sensitivity of better than  $10^{-7}$  (i.e. 0.1  $\mu\text{g B/mL}$ ). Alternatively, if the boron compound can be labelled with  $^{14}\text{C}$ , the addition of a scintillant and quencher will allow liquid scintillator counting.

## 8. NEUTRON IRRADIATION

An accessible thermal neutron source is readily available at the AAEC's 100-kW light water reactor Moata. At 88 kW, a core flux of  $1.2 \times 10^{12}$  neutrons  $\text{cm}^{-2} \text{ s}^{-1}$  can be scaled down to fluxes of  $10^9$  to  $10^{10}$  neutrons  $\text{cm}^{-2} \text{ s}^{-1}$  in the thermal column. However, the present  $\gamma$ -dose is very high ( $\sim 10^6$  cGy  $\text{h}^{-1}$ ) and Pb core screens are needed to reduce this by a factor of 1000. A bismuth- $^{6}\text{LiH}$  biological shield is being designed to permit mouse irradiations. Prolonged irradiation of the nude mouse poses other constraints on bacterial isolation, temperature control, and anaesthesia.

Fluxes of better than  $10^9$  neutrons  $\text{cm}^{-2} \text{ s}^{-1}$  with accompanying  $\gamma$ -doses less than 100 cGy  $\text{h}^{-1}$  should be achievable. The neutron fluence is now measured by Au foil activation techniques and the  $\gamma$ -dose is monitored by thermoluminescence detectors (TLDs).

In vivo measurements with nude mice can proceed on the basis of satisfactory boron incorporation in human melanoma xenografts.

## 9. RADIOBIOLOGY OF IRRADIATED CELL CULTURES AND TUMOURS

Cell survival data are needed for  $^{10}\text{B}$  doped and undoped cell lines and tumour sections. After irradiation, cells can be plated in triplicate and incubated for 7 days at 37°C in a humidified atmosphere containing 5%  $\text{CO}_2$ . The number of colonies having more than 50 cells are counted to obtain the exponential dose-survival curves as a function of neutron dose (D), i.e. surviving fraction  $\text{SF} = \exp(-D/D_0)$ .

The  $D_0$  value is found for each fluence/ $^{10}\text{B}$  concentration/cell line variation. Ichihashi et al. (16) noted that for  $^{10}\text{B}_1\text{-BPA}$ ,  $D_0 \approx 1 \times 10^{12}$  neutrons  $\text{cm}^{-2}$ , which is about one third the value for neutrons only ( $D_0 = 2.8 \times 10^{12}$  neutrons  $\text{cm}^{-2}$ ), at a concentration of 10  $\mu\text{g/mL}$  (i.e. 0.44  $\mu\text{g}^{10}\text{B}/\text{mL}$ ).

Melanoma is a radiation-resistant tumour, possibly because of its capability to repair potentially lethal damage (PLD). For in vitro BNCT experiments it is preferable, therefore, to irradiate the cells in their stationary or density inhibited phase, and grow colonies at different times after the irradiation to investigate the PLD repair effect. Other aspects to be investigated include oxygen enhancement, cell cycle, and split-dose repair effects.

The RBE of reactor beams in BNCT can be determined for melanomas by comparison of orthovoltage x rays at different survival levels. Ujimo et al. (31) used the tumour volume method, following whole-body irradiation of mice with inoculated B-16 melanoma, to determine a thermal neutron RBE of 2.22 for 10% survival, in good agreement with the value of 2.25 measured by Nakanishi et al. (13). Because the thermal neutron RBE value is so well known, BNCT-RBE measurements can be made relative to it.

The  $^{7}\text{Li}$  and  $^{4}\text{He}$  particles are high linear energy transfer (LET) radiations and, as such, cause "single hit" cell death. The Japanese cell survival data (13,16) did not exhibit a shoulder either for thermal neutrons alone or for  $^{11}\text{B}_1\text{-BPA}$  and  $^{10}\text{B}_1\text{-BPA}$  preincubations, indicating the absence of sublethal damage at low dose levels.

Relative biological effectiveness values for mammalian cells have not been well determined in the low keV neutron energy range. The  $^{14}\text{N}(\text{n},\text{p})$  reaction gives way to hydrogen recoils at 100 eV, and the recoil proton energy reaches its maximum energy loss at  $E = 30$  to 100 keV. The variation of RBE with energy from 0.1 to 10 keV is unknown, and irradiations at a 3-MV Van de Graaff accelerator are needed to improve tissue dose-depth calculations (32).

## 10. CONCLUSIONS

Prospects for the boron neutron capture therapy of malignant melanoma are promising. Some melanoma-affined compounds have been synthesized (13,16) and others are under investigation. Human melanoma xenografts in the nude mouse model provide an efficient vehicle for determining the potential efficacy of BNCT. If results are sufficiently encouraging, thermal neutron beams with low  $\gamma$ -dose components can be readily applied for the therapy of advanced primary and recurrent melanomas in patients. The aim is, of course, the elimination of metastases; this may be facilitated by the development of more penetrating neutron beams and the synthesis of boron derivatives of monoclonal antibodies.

## 11. ACKNOWLEDGEMENTS

The author is grateful for the encouragement of Dr. W. McCarthy (Sydney Melanoma Clinic) and Dr. G.R.C. McCleod (Queensland Melanoma Project) and for specialist advice of Dr. J.G. Wilson, Mr. D.J. Wilson, Mr. D.J. Maddalena, Mr. J.R. McNeil and Mr. J.K. Brown of the AAECC. The valuable collaboration of Dr. P. Parsons (Queensland Institute of Medical Research) is gratefully acknowledged.

## 12. REFERENCES

1. Watts, K.P., Fairchild, R.G., Slatkin, D.N., Greenberg, D., Packer, S., Atkins, H.L., and Hannon, S.J. (1981). Melanin content of hamster tissues, human tissues and various melanomas. *Cancer Res.* 41, 467.
2. Kitano, Y. and Hu, F. (1970). Proliferation and differentiation of pigment cells in vitro. *J. Invest. Dermatol.* 55, 444.
3. Borovansky, J. (1978). Quantitative parameters of melanoma differentiation. *Neoplasma (Bratislava)* 25, 349.
4. Lee, T.H., Lee, M.S., and Lu, M. (1972). Effects of  $\alpha$ -MSH on melanogenesis and tyrosinase of B-16 melanoma. *Endocrinol.* 91, 1180.
5. Steinberg, M.L. and Whittaker, J.R. (1976). Stimulation of melanotic expression in a melanoma cell line by theophylline. *J. Cell Physiol.* 87, 265.
6. Silagi, S. (1969). Control of pigment production in mouse melanoma cells in vitro. *J. Cell. Biol.* 43, 263.
7. Blois, M.S. and Kallman, R.F. (1964). The incorporation of  $^{14}\text{C}$  from 2,4-dihydroxyphenylalanine-2'- $\text{C}^{14}$  into the melanin of mouse melanoma. *Cancer Res.* 24, 863.
8. Hemple, K. (1966). Investigation of the structure and formation of melanin in malignant melanoma with  $^3\text{H}$ - and  $^{14}\text{C}$ -dopa labelled at different positions. In Structure and Control of the Melanocyte, G. Della Porta and O. Muehlbock, Eds., p. 162, Springer, Berlin.
9. Nicholaus, R.A. (1968). Melanins in Humans. Paris, 1968.
10. Dryja, T.P., O'Neil-Dryja, M., and Albert, D.M. (1979). Elemental analysis of melanins in bovine hair, iris, choroid and retinal pigment epithelium. *Invest. Ophthalmol.* 18, 231.
11. Purdon, L. and Ambrose, E.J. (1958). A correlation between electrical charge and some biological characteristics during the stepwise progression of a mouse sarcoma. *Nature* 181, 2586.
12. Fairchild, R.G., Greenberg, D., Watts, K.P., Packer, S., Atkins, H.L., Som, P., Hannon, S.J., Brill, A.B., Fand, I., and McNally, W.P. (1982a). Chlorpromazine distribution in hamsters and mice bearing transplantable melanoma. *Cancer Res.* 42, 556.
13. Nakanishi, T., Ichihashi, M., Mishima, Y., Motsuzawa, T., and Fukuda, H. (1980). Thermal neutron capture therapy of malignant melanoma: in vitro radiobiological analysis. *Int. J. Radiat. Biol.* 37, 573.
14. Damsker, J.I., Macklis, R., and Brady, L.W. (1978). Radiosensitization of malignant melanoma. I. *Int. J. Radiat. Oncol. Biol. Phys.* 4, 821.

15. Kloss, G. and Leven, M. (1979). Accumulation of radioiodinated tyrosine derivatives in the adrenal medulla and in melanomas. *Eur. J. Nucl. Med.* 4, 179.
16. Ichihashi, M., Nakanishi, T., and Mishima, Y. (1982). Specific killing effect of  $^{10}\text{B}_1$ -para-boronophenylalanine in thermal neutron capture of malignant melanoma: *in vitro* radiobiological evaluation. *J. Invest. Dermatol.* 78, 215.
17. Fairchild, R.G., Packer, S., Greenberg, D., Som, P., Brill, A.B., Fand, I., and McNally, W.P. (1982b). Thioouracil distribution in mice carrying transplantable melanoma. *Cancer Res.* 42, 5126.
18. Kohler, G. and Milstein, C. (1975). Continuous cultures of fused cells secreting antibodies of predefined specificity. *Nature* 256, 495.
19. Imai, K., Yachi, A., and Ferrone, S. (1982). Preparation and characterization of monoclonal antibodies to human melanoma associated antigens. In Tumor Imaging, S.W. Burchiel et al., Eds., p. 141, Masson Publishing USA Inc.
20. Fogh, J., et al. (1978). Comparison of a tumour cell line before and after growth in the nude mouse. In The Nude Mouse in Experimental and Clinical Research, J. Fogh and B.C. Giovanella, Eds., p. 215, Academic Press.
21. Sharkey, F.E., et al. (1978). Experience in surgical pathology with human tumour growth in the nude mouse. *Ibid.*, p. 187.
22. Hajdu, S.I. and Fogh, J. (1978). The nude mouse as a diagnostic tool in human tumour cell research. *Ibid.*, p. 235.
23. Sordat, B.C.M., Ueyama, Y., and Fogh, J. (1982). Metastasis of tumour xenografts in the nude mouse. *Ibid.*, Vol. 2, p. 95.
24. Giovanella, B.C., Stehlin, J.S., and Williams, L.J. (1974). *J. Nat. Cancer Inst.* 52, 921.
25. Sharkey, F.E. and Fogh, J. (1979). *Int. J. Cancer* 24, 733.
26. Bellet, R.E. and Mastrangelo, M.J. (1982). Malignant melanoma: investigations in the nude mouse. In The Nude Mouse in Experimental and Clinical Research, J. Fogh and B.C. Giovanella, Eds., Vol. 2, p. 511, Academic Press.
27. Rofstad, E.K. (1982). Radiobiological studies using the nude mouse. *Ibid.*, p. 401.
28. Guichard, M., de Langen-Omri, F., and Malaise, E. (1979). *Int. J. Radiat. Oncol. Biol. Phys.* 5, 487.
29. Wong, C.F. (1982). The use of nuclear track detectors in radiation protection, a review. *Aust. Phys. Eng. Sci. Med.* 5, 75.
30. Kobayashi, T. and Kanda, K. (1982). Analytical calculation of boron-10 dosage in cell nucleus for neutron capture therapy. *Radiat. Res.* 91, 77.
31. Ujimo, Y., Takimoto, K., Kanda, K., Kobayashi, T., and Ono, K. (1981). RBEs of nuclear reactor beams and thermal neutrons in responses of B-16 melanoma. *Strahlentherapie* 157, 682.
32. McGregor, B.J. and Allen, B.J. (1983). Filtered-beam dose distributions for boron neutron capture therapy of brain tumours. See paper in this Symposium.

Cure of Malignant Melanoma by Single Thermal Neutron Capture Treatment  
Using Melanoma-Seeking Compounds:  
 $^{10}\text{B}$ /Melanogenesis Interaction to In Vitro/In Vivo  
Radiobiological Analysis to Preclinical Studies

Yutaka Mishima, Masamitsu Ichihashi, Takafumi Nakanishi,  
Masayuki Tsuji, Masato Ueda, Toshio Nakagawa

Dept. of Dermatology, Kobe University School of Medicine, Kobe 650, Japan  
and

Tatsuo Suzuki

School of Veterinary Medicine, Azabu University, Sagamihara 229, Japan

Melanoma is the highly lethal cancerous growth of the pigment cells which have the specific function of synthesizing melanin from dopa and tyrosine by the action of tyrosinase.

As malignant transformation occurs in the pigment cells, they usually acquire accentuated activity of the melanogenic enzyme, tyrosinase. Melanoma cells have the characteristic properties of increased amount not only of tyrosinase but also of its product, melano-protein, in numerous melanosomes which encircle individual target nuclei within melanoma cells. Therefore biological and non-surgical treatment of melanoma could be achieved by utilizing these specific cellular properties.

It was around 1972 that it occurred to me that, by using such melanogenic activity, the  $^{10}\text{B}(\text{n},\alpha)^7\text{Li}$  reaction could be powerful for melanoma therapy. Thermal neutrons taken from an atomic reactor are absorbed easily by the non-radioactive isotope,  $^{10}\text{B}$ , and this absorption results in the emission of  $\alpha$  particles and lithium atoms sharing between them an average total kinetic energy of 2.33 MeV, which is transferred totally to the tissues. Because of the limited travelling range of both these charged particles, the resulting primary radiation injury is confined to a distance of .0 to 14  $\mu$  from the location of the neutron activated boron atom. Since this distance is almost equal to the diameter of individual melanoma cells, if we can selectively accumulate  $^{10}\text{B}$  in cancer cells we can destroy them without serious injury to the surrounding normal tissue. Therefore I developed a different method of neutron capture treatment from the previous one used for brain tumours, which depended on the loss of their blood/brain barrier. Thus, since 1972 our idea has been to synthesize new tumour-seeking  $^{10}\text{B}$ -compounds which themselves possess selective affinity for the specific metabolic activity of the target cancer cells (1,2). Since not only malignant melanomas but also many kinds of human cancers, for example thyroid cancer and squamous cell carcinoma, synthesize their specific protein, our aim is to establish selective thermal neutron capture treatment of malignant melanoma as a prototype of such cancer cells. Once we achieve success in this positive type of capture therapy, it would have many applications.

## $^{10}\text{B}$ CHLORPROMAZINE COMPOUNDS

$^{35}\text{S}$ -labelled CPZ was shown by Blois (3) to bind selectively with melanin, presumably by forming a charge-transfer complex with an indole nucleus of melanin, thus highly localizing in melanoma and eyes, as also confirmed by Dr. Fairchild recently (10). This can still be seen in the tissues three days after systemic administration.

Taking into account all these data, we decided to synthesize molecular hybrid compounds of  $^{10}\text{B}$ -chlorpromazine. First we were able to synthesize  $^{10}\text{B}_{12}$ -chlorpromazineborane and found this compound promising, but it had limited effect. Thus we looked for  $^{10}\text{B}$ -chlorpromazine compounds having a higher boron content and good water solubility. To fulfill these requirements my associate, Dr. Nakagawa, and I synthesized two newer compounds,  $^{10}\text{B}$  sodium chlorpromazine undecahydrododecaborate, referred to as  $^{10}\text{B}_{12}$ -CPZ, and subsequently sodium chlorpromazine nonahydrodecaborate,  $^{10}\text{B}_{10}$ -CPZ, which contain twelve and ten boron atoms per molecule respectively (4). These compounds have unique polyhedron structures having a  $^{10}\text{B}$  atom on every apex, and were synthesized from 2-chloro-10-(3-bromopropyl)-phenothiazine and ammoniumundecahydrodecaborate or 2-ammonioronahydrodecaborate.

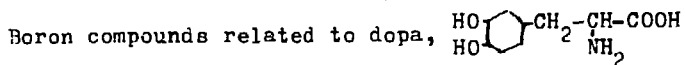
Prior to the in vitro irradiation experiments, the affinity of CPZ for melanotic melanoma cells was tested. Cultured melanotic and amelanotic B-16 melanoma cells were incubated with  $^{35}\text{S}$ -labelled CPZ for 24 hr at 0.1  $\mu\text{Ci}/\text{ml}$  medium concentration. Thereafter the medium was replaced with normal fresh medium after varying time intervals, and the  $^{35}\text{S}$ -labelled CPZ uptake of the melanoma cells was measured. Incorporated  $^{35}\text{S}$ -CPZ in cultured melanoma cells decreased to 50% during the first 30 min of the post-incubation period, but thereafter its value remained constant for over 24 hr. On the other hand, the accumulation of CPZ in amelanotic cells was extremely small, indicating the specific affinity and binding of CPZ to melanotic melanoma cells. As we have already demonstrated in a Greene's hamster melanoma in-vivo system, this  $^{10}\text{B}_{12}$ -CPZ pre-incubation provides a distinct enhancement of the killing effect of neutron irradiation. To obtain the same killing effect using a non-specific  $^{10}\text{B}$ -compound, such as  $^{10}\text{B}$ -boric acid, 5  $\mu\text{g}$   $^{10}\text{B}/\text{ml}$  must be present during irradiation, which is more than 4 times the amount of  $^{10}\text{B}$  required in the form of  $^{10}\text{B}_{12}$ -CPZ (5).

## $^{10}\text{B}_1$ -PARA-BORONOPHENYLALANINE

While we were working with  $^{10}\text{B}$ -chlorpromazines, we also thought of making compounds which would specifically accumulate in melanoma cells with little or melanin content but having tyrosinase activity, particularly young post-mitotic melanoma cells. Melanin is formed from tyrosine or dopa by the action of tyrosinase. If boron-labelled dopa is administered, the boron uptake is proportional to the rate of melanin synthesis.

Thus, with Nakagawa and further cooperation with Drs. Kakihana, Okamoto, and Yoshino, we have synthesized four hybrid compounds of  $^{10}\text{B}$  and the enzyme substrate dopa (Fig. 1). Among these,  $^{10}\text{B}_1$ -para-boronophenylalanine hydrochloride, called  $^{10}\text{B}_1$ -BPA, is the most promising. Our recent findings include the marked melanoma-killing effect of  $^{10}\text{B}_1$ -BPA revealed by in vitro radiobiological systems and in vivo experiments using Greene's melanoma proliferating

in Syrian golden hamsters, as well as our pre-clinical therapeutic experiments which led to our first success in mid-1981, followed by our second success in February 1983, in curing naturally occurring malignant melanoma in Duroc pig skin by a single thermal neutron irradiation. We used the thermal columns of the Kyoto University nuclear reactor (KUR) heavy water facility and of the Musashi Institute of Technology reactor (MITR). Prior to irradiation the neu-



Chemical structure Customary name	Abbreviation	MW	10B per cent Natural abund.	10B abund.	Melanoma killing effect
	Dopa borate	263.00	0.729	3.512	
Dopa borate neutralized with sodium hydroxide					
	Dopeba	209.01	0.917	4.423	
	(hydrochloride)	245.48	0.781	3.764	
		181.99	1.054	5.082	
		n=1.1 162.17	1.182	5.706	
3,4-Dihydroxyphenylethylboronic acid					
	Amino-dopeba	197.00	0.973	4.693	
	beta-Borono-dopa	241.01	0.796	3.834	
beta-Borono-dopa					

Fig. 1. Molecular hybrid compounds of 10B and dopa. We have synthesized the first four and are working on the synthesis of the last two.

tron field was modified for medical and biological purposes by the development of a bismuth scatterer by Drs. Kanda, Kobayashi, and other physicists of our group (6). This reduced the gamma-to-neutron ratio by one order of magnitude.

The next point was to evaluate in cooperation with our physicists the iso-dose distribution of radiation energy within a human body. Therefore, an acrylic lifesize model of a thigh was made, containing a ping-pong ball to represent the melanoma at the subcutaneous level. Rossi's tissue equivalent solution was put into both, with additions of up to 40  $\mu\text{g/g}$  of  $^{10}\text{B}$  in the melanoma model. An iso-dose distribution curve was formulated of irradiation energy after irradiation with the KUR operated at 1000 kW for 30 min, with a dosage of  $5 \times 10^8 \text{ n/cm}^2/\text{sec}$  on the surface. The dose distribution at the surface of the melanoma was 2.5 to 4 times that at the surface of the thigh. The absorbed dose in the  $^{10}\text{B}$ -containing melanoma model is much higher than that in the surrounding normal tissue equivalent solution.

#### In Vitro Studies

Prior to in vivo experiments, an in vitro radiobiological analysis was carried out to evaluate the specific enhanced melanoma cell killing effect of  $^{10}\text{B}_1\text{-BPA}$  in capture therapy. The cultured B-16 melanoma cells were pre-incubated for 20 hr with and without  $^{10}\text{B}_1\text{-BPA}$ , and then each group was irradiated on parallel graphite tables at different distances from the bismuth surface of the reactor. As shown in Fig. 2a, cell survival curves were then formulated. As compared to neutron irradiation alone, shown on the right, the two curves on the left reveal the enhanced marked specific killing effect obtained by pre-incubating with 10  $\mu\text{g}$  of  $^{10}\text{B}_1\text{-BPA}$ , containing 0.44  $\mu\text{g}$   $^{10}\text{B}$  per ml of medium, followed by 1-hr (line on extreme left) or 6-hr post-incubation in fresh medium before irradiation (7). The same amount, 10  $\mu\text{g}$ , of  $^{n}\text{B}_1\text{-BPA}$  compound produced a distinctly lower killing effect, indicating that the main factor is a different density of  $n,\alpha$  reactions, since  $^{10}\text{B}_1\text{-BPA}$  contains approximately 5 times as much  $^{10}\text{B}$  as  $^{n}\text{B}_1\text{-BPA}$ , which contains natural boron.

#### $^{10}\text{B}$ Dosimetry in Melanoma

In order to cure melanoma, the assay of  $^{10}\text{B}$  in various organs in relation to their melanogenic activity and to kinds of  $^{10}\text{B}$  compounds is necessary. We determined the boron concentration by colorimetric assay (8) in melanoma, blood, and other organs at various intervals after injection. At 28 hr after administration, the melanoma-to-blood ratio of  $^{10}\text{B}$  is 11.5 and the melanoma-to-liver ratio is 15, indicating an optimum time for neutron capture. Furthermore, in cooperation with Drs. Kanda and Kobayashi, we have become able to examine the in vivo  $^{10}\text{B}$  concentration and its time course in situ without removing target tissue (Fig. 2b).

#### In Vivo Studies

On the basis of the above, we have tested the in vivo therapeutic effects of  $^{10}\text{B}_1\text{-BPA}$  using melanoma-bearing hamster and found a heretofore unobserved

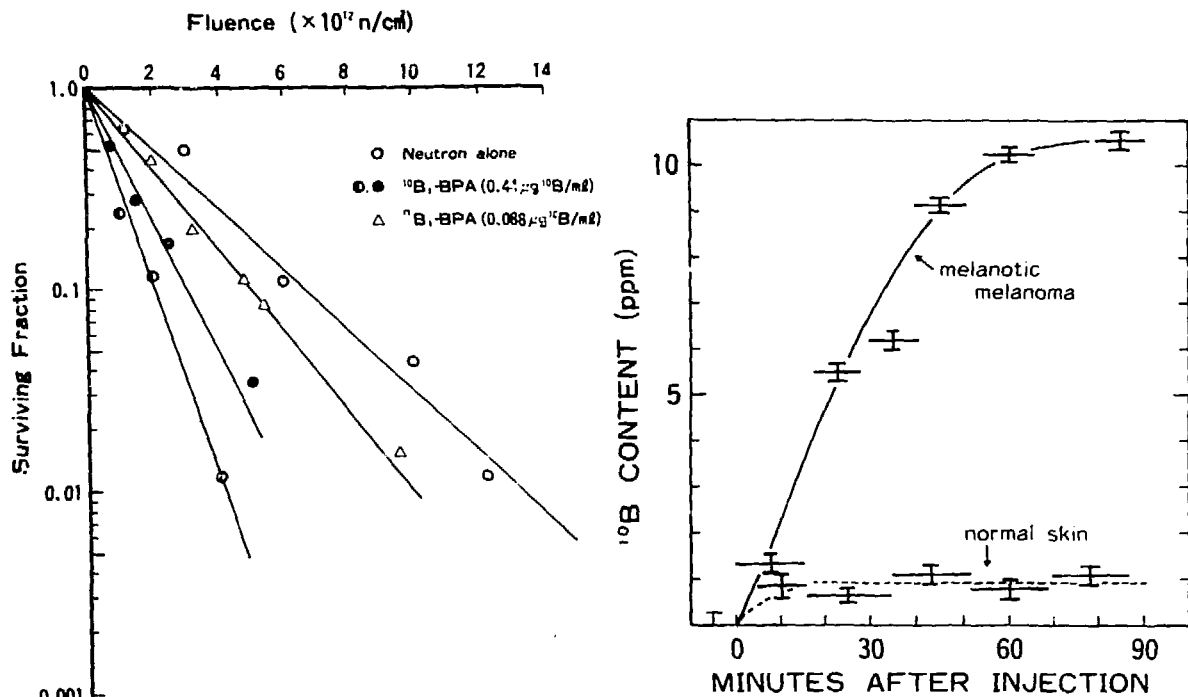


Fig. 2a. Surviving fraction of cells irradiated with or without  $^{10}\text{B}_1\text{-BPA}$  or  $^{10}\text{B}_1\text{-BPA}$  after 20-hr pre-incubation followed by 6-hr (●) or 1-hr (○) post-incubation with fresh normal medium, and of cells pre-incubated with  $^{10}\text{B}_1\text{-BPA}$  (Δ). The number of colonies was counted to obtain the dose survival curve. Each point represents the mean value of triplicate plates; the standard errors ranged from 2.2 to 9.5%.

Fig. 2b. In vivo time course of selective  $^{10}\text{B}$  accumulation in melanotic malignant melanoma proliferating in hamster's subcutaneous tissue revealed by prompt gamma-ray spectrometry of Kanda and Kobayashi.

marked killing effect. Figure 3 shows the growth curves of six Greene's melanomas in the control unirradiated hamster group G III. Figure 4 shows the melanoma growth curves of hamster group G II, irradiated for 2 hr without prior administration of  $^{10}\text{B}_1\text{-BPA}$ . Figure 5 shows the tumour growth curves of group G I, six hamster melanomas treated with the same dosage of neutron irradiation and intramuscular administration of 40 mg of  $^{10}\text{B}_1\text{-BPA}$  8 hr before irradiation.

#### Preclinical Studies

These results led us to start preclinical therapeutic experiments using spontaneously occurring malignant melanoma in Duroc pig skin. General anesthesia, controlled from a distance, is used to keep the subject in front of the reactor. After six experiments (9) we finally cured melanoma in a pig with a single irradiation of  $1.56 \times 10^{13} \text{ n/cm}^2$  and a 6-g  $^{10}\text{B}_1\text{-BPA}$  peri-lesional

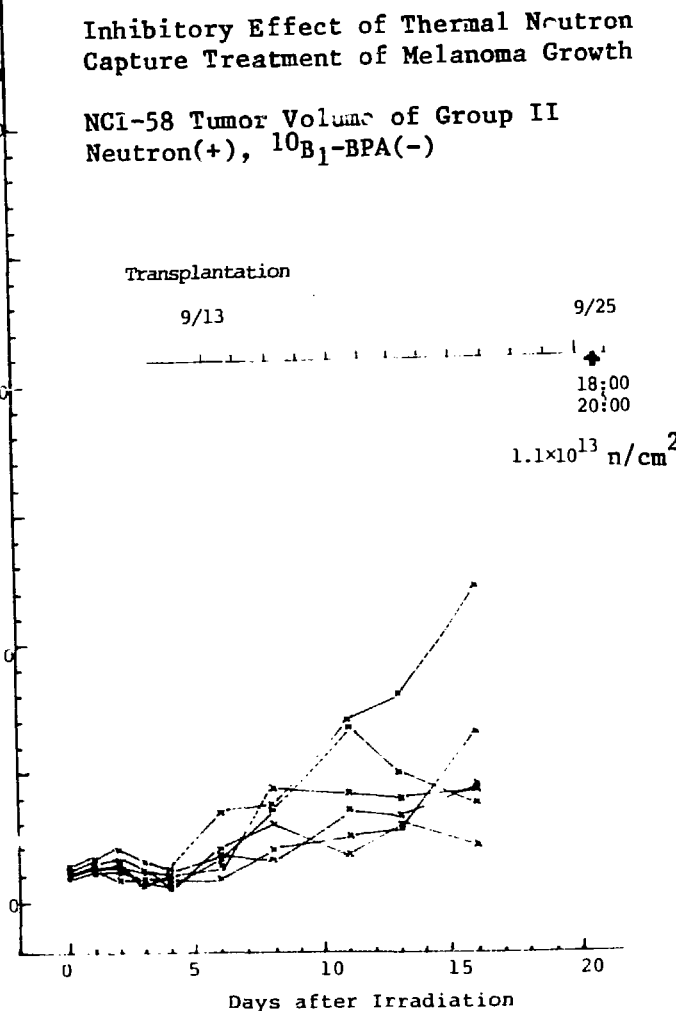
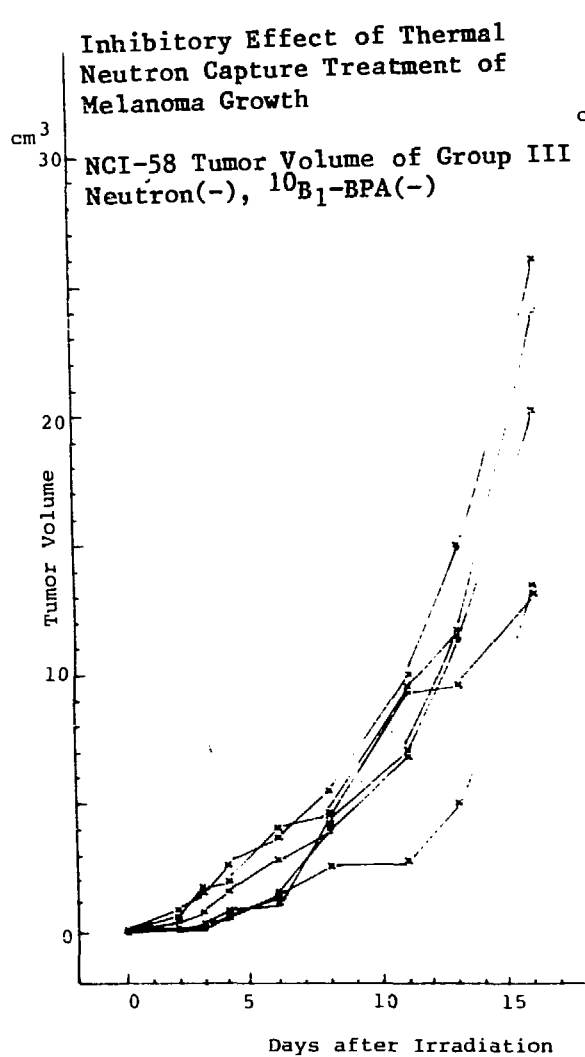


Fig. 3. Growth curves of Greene's melanoma transplanted into subcutaneous tissue of Syrian (golden) hamsters. Control unirradiated group.

injection. The sequential curve of the tumor size shows a marked killing effect leading to a cure at 65 days after irradiation. In order to confirm the cure we continued to observe the pig for 174 days, and then did an autopsy and microscopic examination. No melanoma cells were visible, even when the specimens were viewed microscopically.

In order to evaluate the actually induced  $(n,\alpha)$  reaction within melanoma, we used the  $\alpha$ -track method. The number of pits produced on special film by  $\alpha$  particles and lithium atoms is proportional to the melanogenic status of melanoma and to various standard  $^{10}\text{B}$  concentrations. Using this  $\alpha$ -track

Fig. 4. Growth curves of Greene's melanoma transplanted into subcutaneous tissue of Syrian (golden) hamsters. Thermal neutron irradiation  $(1.1 \times 10^{13} \text{ n/cm}^2)$ , only group.

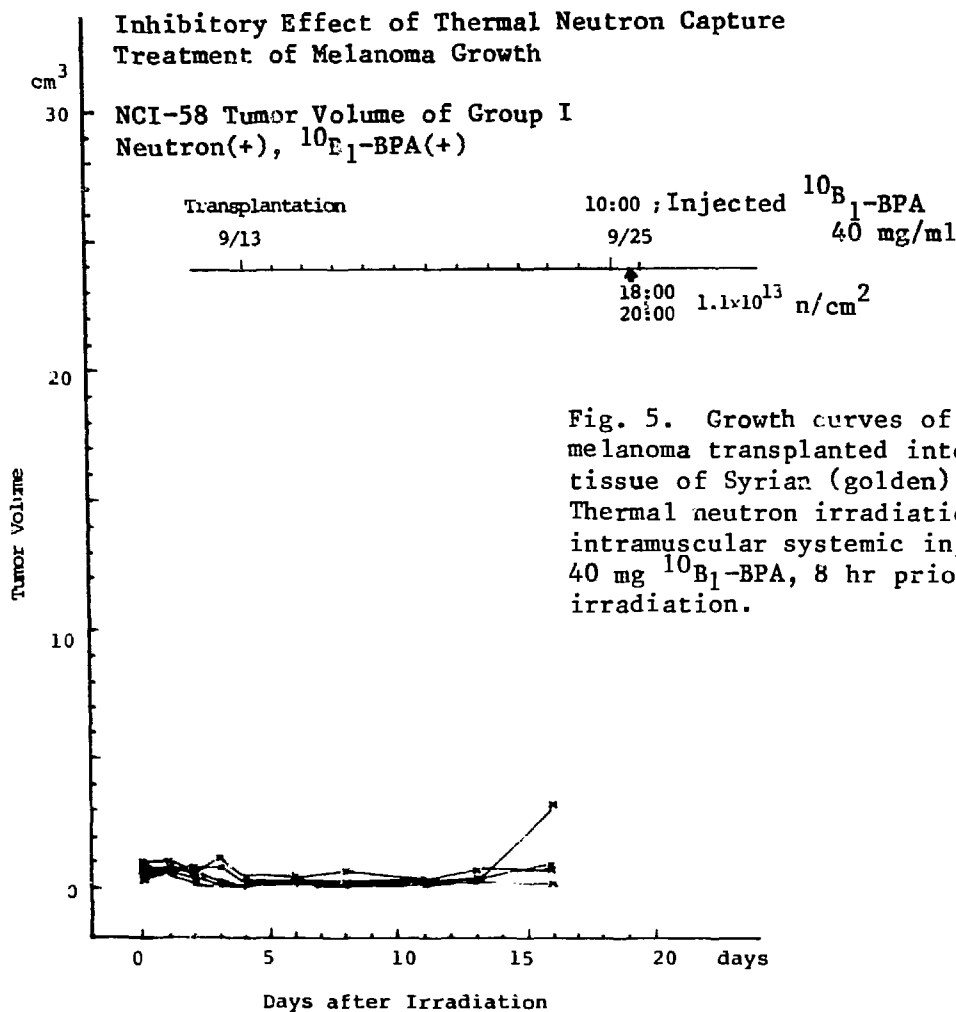


Fig. 5. Growth curves of Greene's melanoma transplanted into subcutaneous tissue of Syrian (golden) hamsters. Thermal neutron irradiation with intramuscular systemic injection of 40 mg  $^{10}\text{B}_1\text{-BPA}$ , 8 hr prior to irradiation.

method, we found the selective distribution and the concentration of  $(n,\alpha)$  reaction actually induced within the pig melanoma to be 27  $\mu\text{g}$  of  $^{10}\text{B}/\text{g}$  melanoma.

We had a second success in curing melanoma in a pig irradiated on November 5, 1982. This melanoma (Fig. 6) was 10 times as large as that in the first cured case, being 12 cm in diameter. It was found occurring naturally on the right lateral abdomen of a 2-year-old female pig. We gave her two peri-lesional injections of 5 g each of  $^{10}\text{B}_1\text{-BPA}$ , one 19 hr and the other 20 min prior to the commencement of a single irradiation which lasted for 4 hr at 100 kW. Figure 7 shows the actually measured dose distribution of neutron and  $\gamma$ -ray irradiation energy on melanoma and surrounding, as well as distant, body surfaces. As in the previous case, ulceration was observed 14 days later. Figure 8 is the clinical appearance of the pig 115 days after irradiation, showing complete disappearance of melanoma with depigmentation in February 1983. She is still under my care in the hospital and has shown no sign of recurrence. Figure 9 shows the melanoma regression curve. No obvious



Fig. 6. Clinical appearance of naturally occurring malignant melanoma in the skin of Duroc pig before treatment.

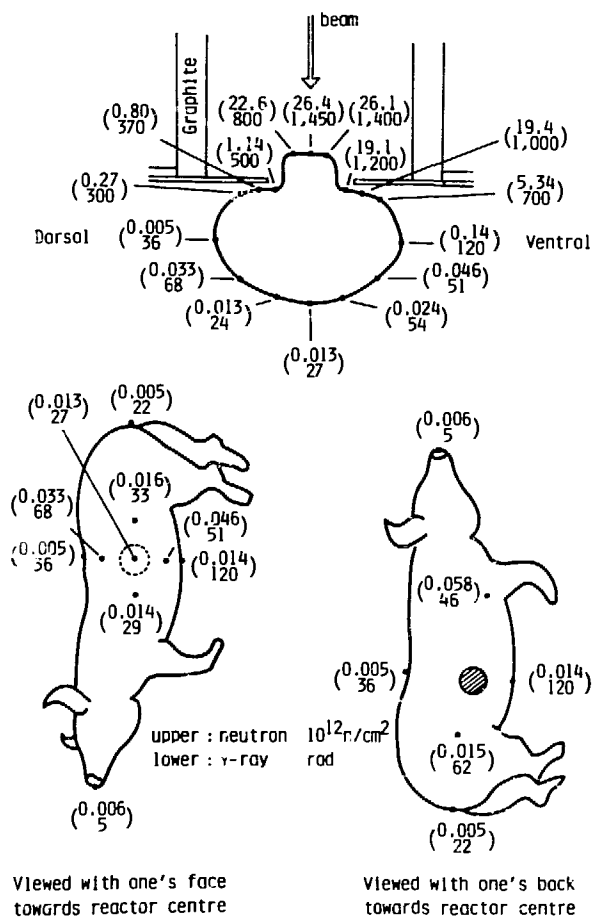


Fig. 7. Measured dose distribution of neutron and  $\gamma$ -ray irradiation energy on melanoma and surrounding, as well as distant, body surface of the treated pig shown in Fig. 8. (Work done in cooperation with K. Sato and H. Fukuda.)

Fig. 8. Clinical appearance of pig, showing complete disappearance of melanoma with depigmentation on 2/28/83. No recurrence of the melanoma has been seen up to 10/8/83. The capture treatment was carried out on 11/5/92.

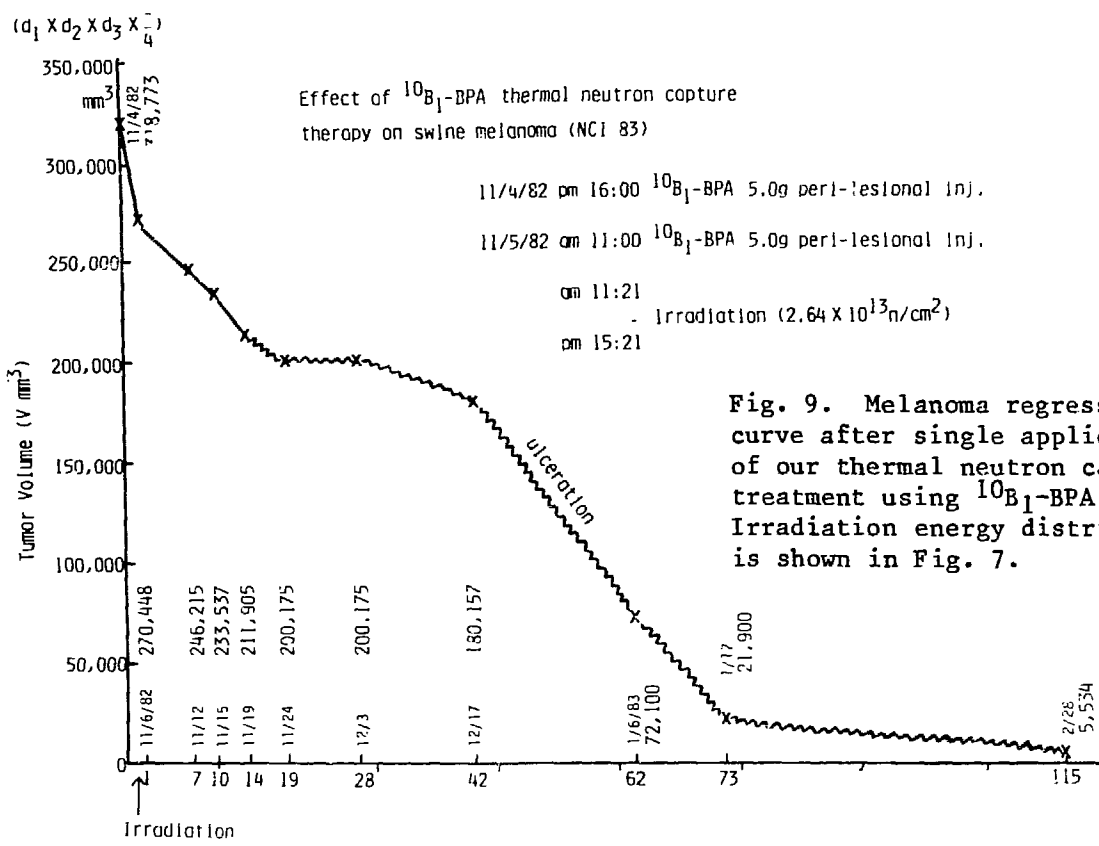


Fig. 9. Melanoma regression curve after single application of our thermal neutron capture treatment using  $^{10}\text{B}_1$ -BPA. Irradiation energy distribution is shown in Fig. 7.

side effects have been observed, and the blood count and liver function have been found to be essentially normal after the treatment.

Establishment of a clinical therapeutic method for curing human melanoma without failure is underway by correlating biophysical, biochemical, biological, and therapeutic data analysis.

Before closing, I should like to mention that recently we have been working also to develop neutron capture therapy of melanoma using  $^{10}\text{B}$ -monoclonal antibodies in cooperation with Professor Taniguchi's group. We were able to make a  $^{10}\text{B}$  conjugate with the specific M259-0 antibody (11). However, we have found that substantial specific enhanced killing effect, compared with that of neutron irradiation alone, could not be obtained so far, despite remaining antibody activity of these conjugates, because of the limitation of antibody-binding sites. We are currently working on ways to increase the  $^{10}\text{B}$  per antibody.

#### ACKNOWLEDGMENTS

This work was supported by Grants-in-Aid #401052, #50/010048, and #58010052 to Prof. Y. Mishima for Cancer Research from the Ministry of Education, Science and Culture, Japan. This work was done under the visiting Researcher's programs of Kyoto University Research Reactor Institute and of Atomic Energy Research Laboratory, Musashi Institute of Technology. We are indebted to nuclear physicists Drs. K. Kanda, T. Kobayashi, S. Shibata, K. Sato, and K. Ono (KURRI) and O. Aizawa and T. Nozaki (MITR), as well as nuclear chemists Drs. H. Kakihana, M. Okamoto, and K. Yoshino (Tokyo Institute of Technology) for their kind cooperation.

#### REFERENCES

1. Y. Mishima: *Pigment Cell* (Karger, Basel), 1:215, 1973.
2. Y. Mishima and T. Shimakage: *Pigment Cell* (Karger, Basel), 2:394, 1976.
3. M.S. Blois: *J. Invest. Dermatol.* 45:475, 1965.
4. T. Nakagawa and K. Ono: *Chem. Pharm. Bull.* 24:778, 1976.
5. T. Nakanishi, M. Ichihashi, Y. Mishima, T. Matsuzawa, and H. Fukuda: *Int. J. Radiat. Biol.* 37:573, 1980.
6. K. Kanda, T. Kobayashi, K. Ono, T. Sato, T. Shibata, Y. Ueno, Y. Mishima, H. Hatanaka, and Y. Nishiwaki: in IAEA-SM-193/68:205, International Atomic Energy Agency (Vienna), 1975.
7. M. Ichihashi, T. Nakanishi, and Y. Mishima: *J. Invest. Dermatol.* 78:215, 1982.
8. K. Yoshino, M. Kobata, M. Okamoto, and H. Kakihana: *Bull. Chem. Soc. Jap.* 52:3005, 1979.
9. Y. Mishima, M. Ichihashi, T. Nakanishi, and T. Nakagawa: KURRI-TR-195:3, 1980.
10. R.G. Fairchild, S. Packer, D. Greenberg, P. Som, A.B. Brill, I. Fand, and W.P. McNally: *Cancer Res.* 42:5126, 1982.
11. S. Wakabayashi, M. Taniguchi, T. Tokuhisa, H. Tomioka, and S. Okamoto: *Nature* 294:748, 1981.

## NEUTRON CAPTURE USING BORONATED POLYCLONAL AND MONOCLONAL ANTIBODIES

Rolf F. Barth, Albert H. Soloway, Fazlul Alam, Walter E. Carey, Cathy Andrews, Barbara Holman, Carol W. Johnson, Jeanette Mohammed, and Joseph Talnagi, Jr.

The Ohio State University, Columbus, Ohio 43210  
and

Zenon Steplewski  
The Wistar Institute, Philadelphia, PA 19104

### INTRODUCTION

The success of boron neutron capture therapy (BNCT) for the treatment of cancer ultimately is dependent upon the selective delivery of a sufficient number of boron-10 ( $^{10}\text{B}$ ) atoms to tumor target cells. In the past, efforts have been directed towards the development of compounds that might have tumor localizing properties (1-9). This eventually lead to the synthesis (10) and subsequent clinical use by Hatanaka et al. (11,12) of the polyhedral borane,  $\text{Na}_2\text{B}_{12}\text{H}_{11}\text{SH}$ . Although impressive clinical results have been obtained using this compound as the capture agent for the treatment of patients with glioblastoma (13,14), it is clear that more selective delivery will be required.

With the advent of hybridoma technology and the development of monoclonal antibodies that recognize tumor-associated antigens, a new avenue of approach has been opened up. The linkage of  $^{10}\text{B}$  containing compounds to antibody molecules theoretically might provide a means for specifically delivering the capture agent to tumor cells (15). As shown in Fig. 1, these antibodies would

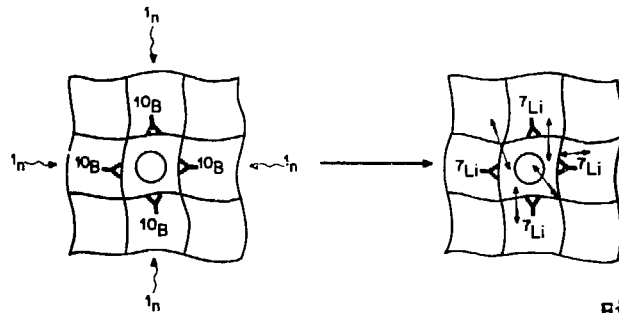
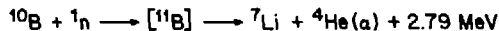


Figure 1.

bind to surface membrane antigens, and following neutron irradiation and the subsequent capture reaction, would yield high LET alpha particles and recoiling  $^7\text{Li}$  nuclei. Since the path of the alpha particles is random and limited to a distance of approximately  $10 \mu$ , adjacent cells also might sustain a lethal hit. The present study has been directed towards defining the feasibility of using a combination of capture agents consisting of boronated antibodies and  $^{10}\text{B}$ -enriched boric acid ( $^{10}\text{B}-\text{H}_3\text{BO}_3$ ) for the delivery of  $^{10}\text{B}$ . Two systems have been investigated, one employing polyclonally derived horse anti-human thymocyte globulin, and the other a monoclonal antibody directed against human colorectal cancer associated antigen. The data presented indicate that

antibodies can be used to deliver  $^{10}\text{B}$  to target cells, and that in combination with a non-selective agent, it is possible to sustain a lethal  $n,\alpha$  reaction at the cellular level.

#### MATERIALS AND METHODS

**Antibodies.** Purified horse anti-human thymocyte globulin (ATGAM<sup>R</sup>) was kindly provided by the Upjohn Co., Kalamazoo, Michigan. This was a polyclonally derived antibody that was produced by repeatedly immunizing horses with human thymocytes, and its production and characterization have been described in detail elsewhere (16). It cannot, however, be considered specific for human T lymphocytes, and in fact, also was reactive with the human colon cancer cell line, SW 1116, that also was used in the present study.

Monoclonal anti-colorectal cancer antibody 17-1A was produced by Steplewski et al. (17,18) and has binding specificity for surface membrane antigens of colonic adenocarcinoma cells, including SW 1116.

**Boronation of Antibodies.** The method employed for boronating both ATG and monoclonal 17-1A antibodies has been described in detail in another report presented at this symposium (19). Briefly, the cesium salt of undecahydro-mercaptopclos-o-dodecaborate ( $\text{Cs}_2\text{B}_{12}\text{H}_{11}\text{SH} \cdot 2\text{H}_2\text{O}$ ) was reacted in acetonitrile with the heterobifunctional reagent N-succinimidyl-3-(2-pyridyldithio)-propionate (SPDP, Pharmacia, Piscataway, NJ). The reaction was allowed to proceed overnight yielding the cesium salt of N-succinimidyl-3-(undecahydro-clos-o-dodecaboranyldithio)-propionate (SBDP). This compound was reacted with antibody at varying molar ratios ranging from 200:1 to 1300:1. After 1 hr at ambient temperature and overnight at 4°C, the boronated antibody was separated from the reaction mixture by sequential filtration through Sephadex G25 columns.

**Cells.** Peripheral blood lymphocytes (PBL) were isolated from 30-60 ml of heparinized blood obtained from healthy donors by means of the Ficoll-Hypaque density gradient separation technique as described by Bøyum (20). The cells were washed twice in RPMI 1640 with Hepes buffer, resuspended in medium, counted, and adjusted to a final concentration of  $8 \times 10^6$  per ml.

SW 1116 colorectal cancer cells (18) were propagated in Liebovitz's medium supplemented with 10% fetal calf serum, non-essential amino acids and L-glutamine in a humidified incubator at 37°C.

**Reactor Description and Determination of Flux Profile.** The Ohio State University Research Reactor (OSURR) is a swimming pool-type reactor fueled with fully enriched, flat-plate MTR-type fuel. It is licensed to operate at steady state power levels up to a maximum of 10 kilowatts thermal power. A variety of instrumentation channels are available for power monitoring. The reactor control system allows reproducibility of power levels to within 5%.

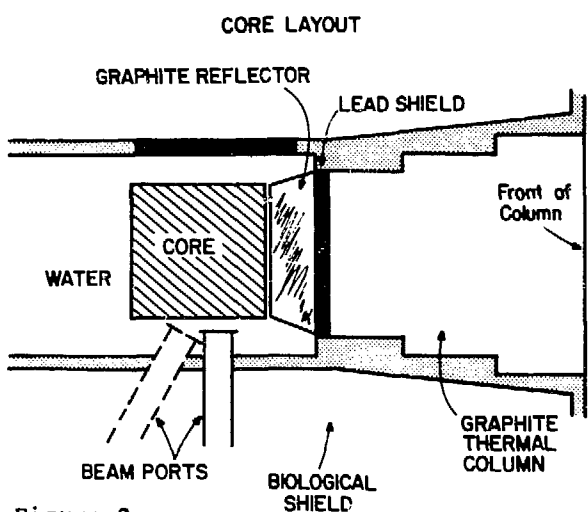


Figure 2.

Figure 2 shows a top view of the core and several irradiation facilities, including two beam ports and a graphite thermal column. Irradiations were conducted in the thermal column. A graphite reflector serves as the end cap of the thermal column at the reactor core. Next, there is a 4-inch lead shield to reduce the gamma-ray flux directly streaming from the core. The column itself is composed of removable graphite stringers. Each stringer is 4" wide and 4" high, with a length dependent upon its position in the column. The total distance from the lead shield to the end of the column is 56". Irradiations were carried out in the space occupied by stringer G-7, which is at the geometric center of the column.

This position allows placement at the peak of the neutron flux as a function of horizontal and vertical position. Knowledge of the radiation environment was a necessary part of this study. Specification of the radiation environment required measurement of the neutron and gamma-ray components of the radiation field. Gamma dose rates were measured using an ionization chamber, while neutron flux was measured by means of flux wire and foil activities.

Gamma dose rates were measured with a calibrated ionization chamber whose output current was directly proportional to gamma-ray intensity. Dose rates were measured at various positions along the length of stringer position G-7, starting at the lead shield and moving away from the core to the end of the column. Gamma dose rate as a function of reactor power level also was measured at each position.

The relative neutron flux profile was determined by measuring the neutron-induced activity of a copper wire placed along the length of stringer position G-7. The wire was cut into 1" segments and the activity of each was measured using a germanium-lithium detector-based gamma-ray spectrometer. Measured activities were corrected for variations in wire mass. A normalized flux profile was obtained by dividing all wire segment activities by the maximum activities for the 0-inch position adjacent to the lead shield.

Copper flux wires also were used to determine the neutron flux profile along the vertical and horizontal lengths of stringer position G-7. Since these distances were only 4", the flux wires were sectioned into 1/2" segments. The linear dependence of the neutron flux on reactor power level also was verified.

Absolute determination of the energy-dependent neutron flux was accomplished by the method of multiple foil activation. Activation foils were placed at the 0-inch position of stringer location G-7. Reactor power level was 10 kilowatts. Foil activities were determined using the Ge(Li)-based

gamma-ray spectrometer. The neutron energy spectrum was calculated from the measured foil activities using the SAND-II neutron spectrum unfolding code (21).

Radiation. Lymphocytes at a concentration of  $\sim 8 \times 10^6$  per ml were added to an appropriate volume of  $^{10}\text{B}$ -ATG to reach the final desired dilution either alone or in the presence of varying molar concentrations of  $^{10}\text{B}$  enriched boric acid ( $^{10}\text{B}-\text{H}_3\text{BO}_3$ ), kindly provided by Dr. James Blue, NASA/CSF Neutron Therapy Facility, Cleveland, OH. Following 30 minutes incubation at ambient temperature the cells were taken to The Ohio State University Research Reactor and irradiated with neutron fluences ranging from  $10^{11}$  to  $10^{13}$  n/cm<sup>2</sup>. The cells then were sedimented by centrifugation in a Beckman microfuge, washed once, and resuspended in RPMI 1640 supplemented with 15% human AB serum.

A similar procedure was employed for the treatment and irradiation of SW 1116 cells, except that boronated 17-1A antibody ( $^{10}\text{B}-17-1\text{A}$ ) was used instead of the  $^{10}\text{B}$ -ATG.

$^{125}\text{I}$ -Binding Assay. Non-boronated and boronated ATG were iodinated using the iodogen method (22) at a ratio of 1  $\mu\text{Ci}$  of  $^{125}\text{I}$ -NaI per  $\mu\text{g}$  of protein. Separation of free  $^{125}\text{I}$ -NaI was carried out by passage through a Sephadex G-25 column loaded with horse IgG. The binding assay itself was performed by adding 10  $\mu\text{g}$  of  $^{125}\text{I}$ -ATG to increasing numbers of lymphocytes ranging from  $5 \times 10^5$  to  $5 \times 10^6$  cells, allowing them to incubate for 2 hrs at ambient temperature with occasional mixing, and then terminating the reaction by adding 1 ml of cold washing solution. The cells were sedimented, washed two times, and the pellets counted for  $^{125}\text{I}$  in a Tracor Analytic model 1185 gamma scintillation counter.

Blastogenic Assay. Assays were carried out in Costar Microtest plates (#3596, Costar, Cambridge, MA) using quadruplicate samples. Phytohemagglutinin (PHA, Difco, Detroit, MI) was diluted 1:20 with RPMI 1640. Concanavalin A (Con A, Difco) was dissolved in RPMI 1640 to give a concentration of 200  $\mu\text{g}/\text{ml}$ . To each well were added 150  $\mu\text{l}$  of RPMI 1640 supplemented with 15% human AB serum and  $10^5$  lymphocytes, and 50  $\mu\text{l}$  of a 1:5 dilution of either PHA or Con A. Cultures were maintained at 37°C in a humidified incubator containing 5% CO<sub>2</sub> for 72 hrs before being pulsed with 1  $\mu\text{Ci}$  of  $^3\text{H}$ -thymidine ( $^3\text{H}$ -TdR, specific activity, 40-60  $\mu\text{Ci}/\text{mM}$ , Amersham, Arlington Heights, IL). After 16 hrs the cultures were harvested by means of an automatic sample harvester (model CH 103, Dynatech, Alexandria, VA), discs were allowed to dry, placed in scintillation minivials to which 4.5 ml of #3a20 scintillation fluid (Research Products Intl., Elk Grove Village, IL) were added, and then counted in a Searle Analytic liquid scintillation counter. Replicate samples showed close agreement with one another and usually varied less than  $\pm 20\%$ .

Clonogenic Assay. SW 1116 cells, at a concentration of 5,000 per 5 ml of Liebovitz's medium, were added to 100-mm petri dishes (Corning Glass Works, Corning, NY) and placed in a humidified incubator at 37°C for 17 days. At termination, the cells were fixed with 5 ml of 37% formaldehyde for 10 minutes, dishes were dumped, gently washed with tap water, rinsed with distil-

led water, again dumped, and allowed to air dry. They were stained with a saturated solution of crystal violet, rinsed with water and allowed to dry. Colonies were enumerated by means of an Artek Counter, model 880 (Artek Systems Corp., Farmingdale, NY).

A short-term microassay was carried in parallel with the clonogenic assay.

To each well of a microtest plate were added 150  $\mu$ l of Liebovitz's medium and 50  $\mu$ l of 5,000 SW 1116 cells. Following 72 hrs incubation in a humidified incubator at 37°C, the cells were pulsed with 1  $\mu$ Ci per well of  $^3$ H-TdR and allowed to incubate for an additional 16 hrs. Following this, medium was aspirated from the wells, washed 3X with PBS, allowed to air dry, spray-fixed with Fluoro-glide spray adhesive (Chemplast, Inc., Wayne, NJ), allowed to dry, the wells punched out, and discs added to minivials containing 4.5 ml of #3a20 scintillation cocktail.

## RESULTS

Reactivity of Non-Boronated and Boronated Antibodies. The binding of  $^{125}$ I-labeled ATG and  $^{10}$ B-ATG to increasing numbers of lymphocytes is presented in Figs. 3 and 4. Boronated and non-boronated ATG were almost identical in their

binding to lymphocytes, and the percent bound increased exponentially as a function of the number of cells (Fig. 3). When extrapolating from the curve,  $B_{max}$  has a value of ~4%; when plotted as  $(\text{Bound})^{-1}$  as a function  $(\text{Free})^{-1}$ , straight lines were obtained. Binding also was demonstrated by means of membrane immunofluorescence, and when corrected for dilution, an endpoint titer of 1:1250 was obtained for the  $^{10}$ B-ATG compared to 1:10,000 for non-boronated ATG. The binding of monoclonal antibody 17-1A with SW 1116 cells was determined by membrane immunofluorescence. Although membrane binding was demonstrable, there was a loss in reactivity, as determined by fluorescent endpoint titers. These were 1:6,400 for the non-boronated antibody and 1:640 for the boronated antibody, when corrected for dilution.

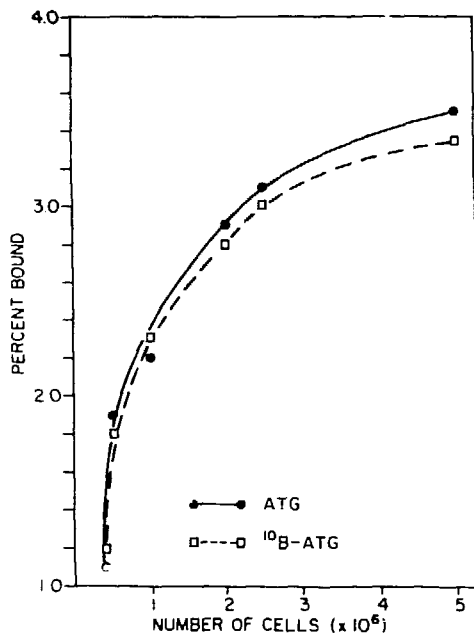
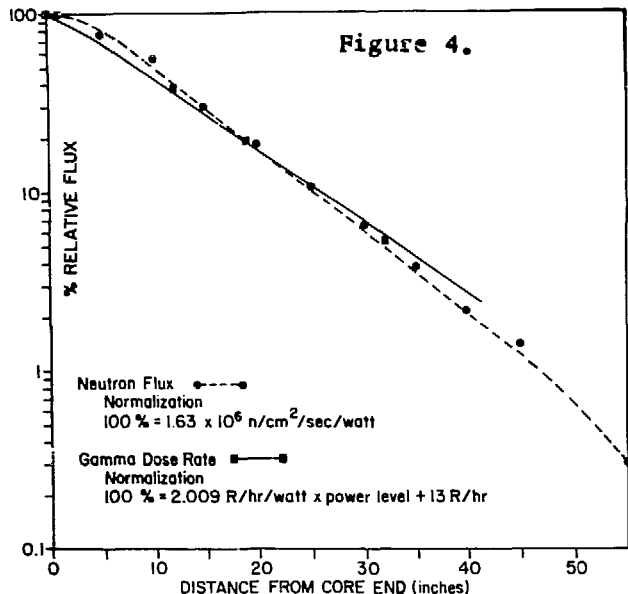


Figure 3.

Determination of Neutron Profile Results of the gamma ray dose rate and neutron flux profile are shown in Figure 4. This figure also shows the normalization factors for both the gamma-ray dose rate and neutron flux, and, as expected, there was an exponential dependence on position for both quantities. Furthermore, the normalization factors indicated a linear dependence on reactor power. Measurement of the neutron flux profile along the 4" horizontal and vertical dimensions of stringer position G-7 demonstrated a "flat" profile. That is, the neutron flux did not vary more than 5% along either of

these distances. The majority of the total neutron flux (64%) was in the thermal energy range. The shape of this neutron energy distribution was assumed to be invariant with reactor power. However, as the power level was changed, the magnitude of the energy-dependent flux for a given neutron energy varied directly with reactor power.



From Figure 4, it is evident that a significant component of the overall dose resulted from gamma rays. This "contamination" of the radiation field by gamma rays is a major concern in this study. For example, using Figure 4 and data from neutron energy spectrum measurements (not shown) and assuming a reactor power level of 10 kilowatts, an irradiation time of 10.22 minutes, and a thermal neutron fluence-to-dose equivalent of  $268 \text{ n/cm}^2/\text{sec/mrem/hr}$ , the following dose rate and fluences were obtained:

$$\begin{aligned} \text{total neutron fluence} &= 1 \times 10^{13} \text{ n/cm}^2 \\ \text{thermal neutron fluence} &= 6.44 \times 10^{12} \text{ n/cm}^2 \\ \text{thermal neutron dose equivalent} &= \\ &6.67 \times 10^3 \text{ R} \\ \text{gamma dose equivalent} &= 3.42 \times 10^3 \text{ R} \end{aligned}$$

Thus, of the total soft-tissue equivalent dose, about 34% results from gamma radiation.

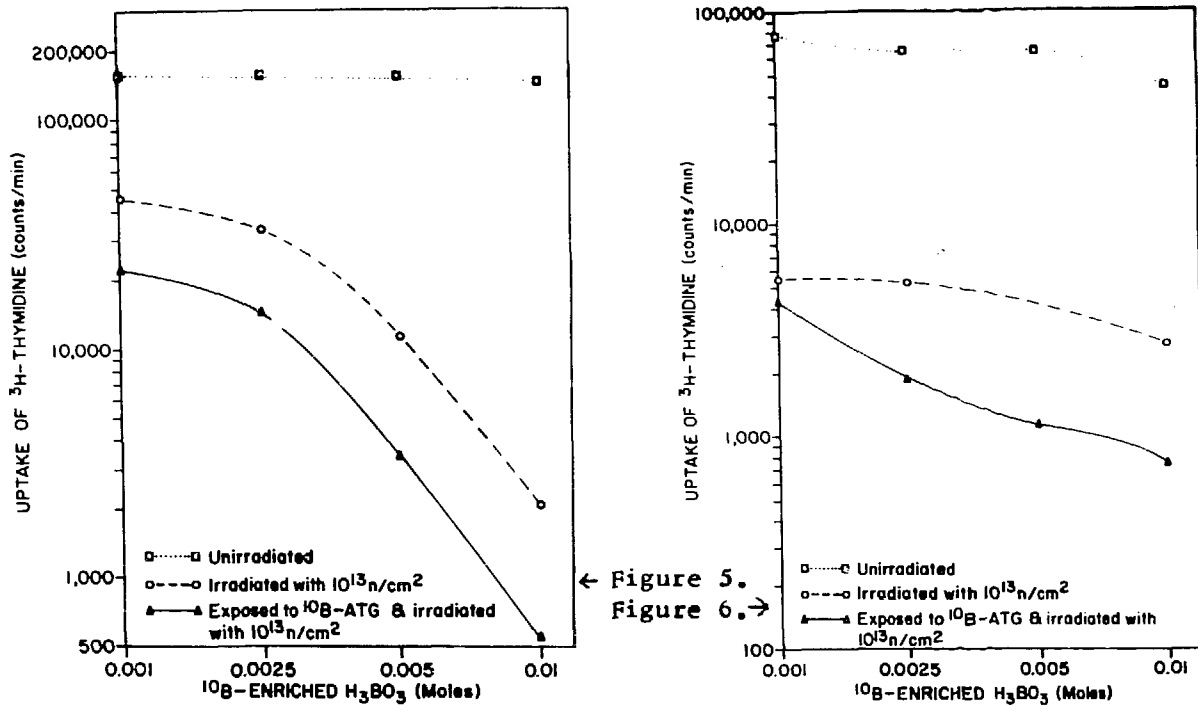
Neutron Radiation of Lymphocytes. The effects of neutron irradiation and  $^{10}\text{B}$ -neutron capture on the ability of peripheral blood lymphocytes to respond to PHA and Concanavalin A are summarized in Table 1 and Figures 5 and 6.

Table 1. Mitogenic Responses of Lymphocytes to PHA and Con A

Treatment	Irradiation	Uptake of Radioactivity (c.p.m. + S.E.)	
		PHA	Con A
None	None	197,893 + 19,536	69,733 + 3,809
0.01M $^{10}\text{B-H}_3\text{BO}_3$	None	207,567 + 7,477	91,975 + 7,825
$^{10}\text{B-ATG}$	None	125,782 + 10,391	43,405 + 6,257
None	$10^{13} \text{ n/cm}^2$	43,005 + 2,389	4,498 + 441
$^{10}\text{B-ATG}$	$10^{13} \text{ n/cm}^2$	11,087 + 167	706 + 137

Unirradiated cells exposed to 0.01M  $^{10}\text{B-H}_3\text{BO}_3$  and stimulated with either PHA or Con A gave responses (207,000 and 92,000 cpm) that were similar in magnitude to those of untreated, unirradiated controls (198,000 and 70,000 cpm). Responses of unirradiated cells exposed to  $^{10}\text{B-ATG}$  were reduced by approximately 33% and untreated irradiated cells by 80%. The latter effect was attributed to the gamma dose of 3,425 R that was delivered at a fluence of  $10^{13} \text{ n/cm}^2$ . Cells exposed to  $^{10}\text{B-ATG}$  and irradiated showed a 95% reduction in responsiveness (11,000 cpm), indicating that the antibody was capable of delivering enough  $^{10}\text{B}$  to sustain a lethal  $n,\alpha$  reaction.

Blastogenic responses in the presence of 0.001 to 0.01 M  $^{10}\text{B-H}_3\text{BO}_3$  either alone or in combination with  $^{11}\text{B-ATG}$  are presented in Figures 5 (left) and 6 (right). The addition of  $^{11}\text{B-ATG}$  consistently reduced responses to both PHA and Con A compared to those seen in the presence of  $^{10}\text{B-H}_3\text{BO}_3$  alone. Cells



treated with a mixture of  $^{11}\text{B-ATG} + 10^{-2}\text{M H}_3\text{BO}_3$ , for example, showed a >99% reduction in responsiveness compared to irradiated controls. This augmentation is attributed to the specific delivery of  $^{10}\text{B}$  by antibody.

Neutron Radiation of Colorectal Carcinoma Cells. The effects of radiation with  $10^{11}$ ,  $10^{12}$  and  $10^{13}\text{n/cm}^2$  on SW 1116 cells are presented in Figure 7. Varying doses between  $10^{11}$  and  $10^{12}\text{n/cm}^2$  had little effect on the surviving fraction. Irradiation with  $5 \times 10^{12}\text{n/cm}^2$  reduced the S.F. to 0.035 and with  $10^{13}\text{n/cm}^2$  this decreased to 0.0025. The associated gamma doses were 199 R at  $5 \times 10^{11}\text{n/cm}^2$ , 688 R at  $10^{12}$ , 1,468 R at  $5 \times 10^{12}$ , and 3,425 R at  $10^{13}\text{n/cm}^2$ . We previously had shown that gamma doses up to 700 R had minimal effects on SW 1116, but higher doses drastically reduced the S.F. The survival of cells radiated with  $10^{12}\text{n/cm}^2$  in the presence of varying concentrations of  $^{10}\text{B-H}_3\text{BO}_3$  ranging from 0.0001 to 0.01 M is presented in Figure 8. Little effect was seen with concentrations in the range of 0.0001 to 0.001 M. A break in the curve was seen with 0.002 M  $^{10}\text{B-H}_3\text{BO}_3$  at which concentration the S.F. was 0.37. This decreased to 0.055 at 0.04 M and to 0.015 at 0.08 M. These data clearly indicate that molar concentrations of  $^{10}\text{B-H}_3\text{BO}_3$  in excess of 0.002 M were capable of supporting a lethal  $n,\alpha$  reaction. Recently obtained data indicate that boronated 17-1A either alone or in combination with  $10^{-4}\text{M}$   $^{10}\text{B-H}_3\text{BO}_3$  is capable of delivering  $^{10}\text{B}$  to SW 1116 cells. Although the effect was relatively modest, the data clearly indicate a reduction in S.F. following exposure to  $^{10}\text{B-17-1A}$ .

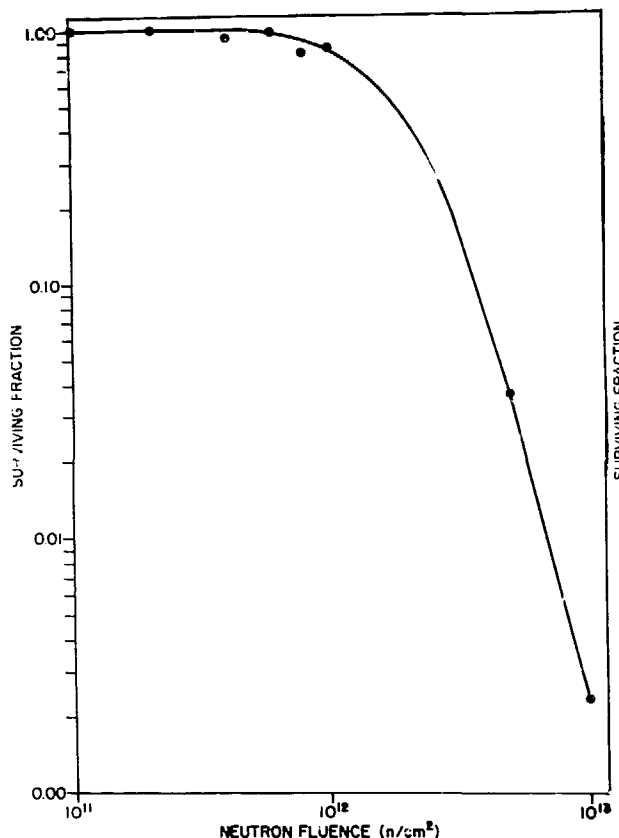


Figure 7.

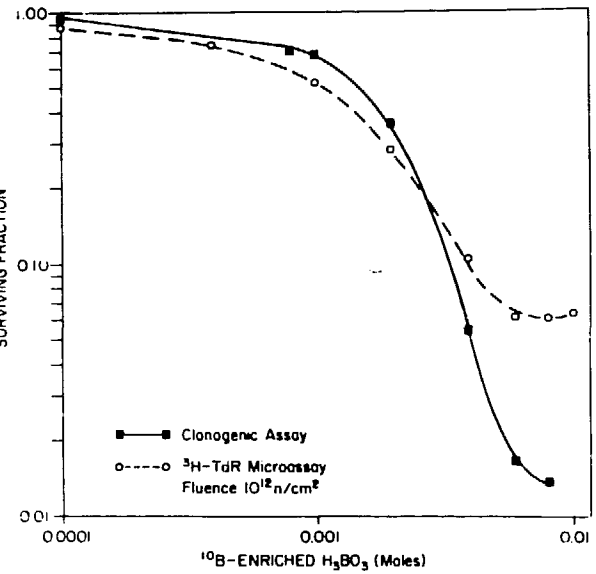


Figure 8.

### Discussion

In the present study we have shown that polyclonally derived horse anti-human thymocyte globulin can be used to deliver  $^{10}\text{B}$  to lymphoid target cells. As reported by us elsewhere in this symposium (19), the ATG had approximately  $4.8 \times 10^2$  atoms of natural boron ( $^{n}\text{B}$ ) per molecule of antibody, and the monoclonal 17-1A had  $1.3 \times 10^3$  atoms. These numbers represent an average, and in reality there may have been considerable variation in the degree of boronation of individual antibody molecules. Boronation of the ATG did not result in a reduction in binding, as determined by a quantitative  $^{125}\text{I}$  binding assay, although a decrease in fluorescent endpoint titers of both ATG and  $^{10}\text{B}$ -17-1A were observed. Although the track etching technique can be used to detect  $n,\alpha$  reactions (23,24), there is no method currently available to quantify the amount of  $^{10}\text{B}$  at the cellular level. Consequently, we do not know the exact number of boron atoms that were delivered to each target cell. The data presented in Table 1, however, show that lymphocytes exposed to  $^{n}\text{B}$ -ATG and irradiated with  $10^{13} \text{ n/cm}^2$  had a 75% reduction in  $^3\text{H}$ -TdR uptake compared to untreated, irradiated cells. Furthermore, the data presented in Figs. 5 and 6 indicate that treatment of lymphocytes with a mixture of  $^{n}\text{B}$ -ATG and  $^{10}\text{B}$ - $\text{H}_3\text{BO}_3$  resulted in up to a 99% reduction in  $^3\text{H}$ -TdR uptake compared to irradiated cells. Since on a molar basis the amount of  $^{10}\text{B}$  linked to the ATG was

$0.00003M$  ( $2.1 \times 10^{-5}M$ ), the non-specific contribution of the  $^{11}B$ -ATG was insignificant. From this it can be concluded that the effect of the  $^{11}B$ -ATG was attributable to specific delivery to the target lymphocytes. Antibody alone produced an effect equivalent to a  $5 \times 10^{-3}M$  concentration of  $^{10}B-H_3BO_3$ . In other words, specific delivery of  $^{10}B$  at a concentration of  $2.1 \times 10^{-5}M$  was equivalent to a  $5 \times 10^{-3}M$  concentration delivered non-selectively. On a mole per mole basis therefore, boronated antibody was approximately 240 times ( $5 \times 10^{-3}M/2.1 \times 10^{-5}M$ ) more efficient than non-selective delivery by  $^{10}B-H_3BO_3$ . These calculations clearly indicate the theoretical superiority of targeted versus non-targeted delivery of  $^{10}B$ .

If specific delivery is so superior to non-selective delivery, why then was the  $^{11}B$ -ATG incapable of producing the same effect as a  $10^{-2}M$  solution of  $^{10}B-H_3BO_3$ ? The answer to this question can be seen from our own data. A  $10^{-3}M$  solution of  $^{10}B-H_3BO_3$ , which was equivalent to  $1.2 \times 10^{17}$  atoms of  $^{10}B/ml$ , had no significant effect compared to radiation alone (43,000 vs 45,048 c.p.m.). On the other hand, a  $10^{-2}M$  solution ( $1.2 \times 10^{18}$  atoms of  $^{10}B/ml$ ) had a profound effect (2,092 c.p.m.). In other words, within the range of one log unit, there was a 95% reduction in responsiveness. Assuming negligible differences in Poisson distribution statistics, this would lead us to predict that with a small increase in the amount of  $^{10}B$  per antibody molecule, we would expect to see an effect comparable to that achieved non-selectively with a  $10^{-2}M$  solution of  $^{10}B-H_3BO_3$ . The compound that we used to boronate antibody was not enriched in  $^{10}B$ . If  $^{10}B$  enriched material had been employed, this would have automatically increased the amount of  $^{10}B$  per antibody molecule fivefold. If one could further increase the amount of  $^{10}B$  twofold, for example by more heavily boronating the antibody, this theoretically should provide an amount of  $^{10}B$  equivalent to  $10^{-2}M$   $^{10}B-H_3BO_3$ . By linking a boronated polymer to antibody molecules, this goal should be attainable.

Data have been obtained on the radiation profile of the O.S.U. Research Reactor. As seen in Fig. 4, there was significant gamma contamination of the neutron beam. This problem will be solved by inserting a bismuth filter into the beam port, as described by Kanda et al. (25) in the remodeling of the Musashi Institute of Technology Reactor in Japan. We were able to partially circumvent the problem by virtue of the fact that lymphocytes were relatively radioresistant compared to tumor cells. SW 1116 cells, on the other hand, were less resistant and fluences greater than  $10^{12} n/cm^2$  could not be used because of the high contaminating gamma dose. Even with this limitation, it still was possible to obtain preliminary data indicating that monoclonal 17-1A was capable of specifically delivering  $^{10}B$  to SW 1116 target cells. Other data would lead us to predict that once we have reduced or eliminated the contaminating gamma radiation, it should be possible to achieve a uniformly lethal  $n,\alpha$  reaction.

The data that we have presented establish the feasibility of using antibodies for the delivery of  $^{10}B$ . Problems that must be faced include 1) preservation of antibody activity following boronation, 2) antigenic receptor site density of the target cells, and 3) delivery of a critical number of  $^{10}B$  atoms per cell. Each of these has been addressed. The linkage of a heavily boronated polymeric species to antibody by means of a single functional group should allow for the delivery of a large number  $^{10}B$  atoms per antibody molecule without a significant reduction in affinity. Both the ATG and the mono-

clonal 17-1A recognize antigens that are expressed with a density of approximately  $10^6$  epitopes per cell. There is no reason, however, why mixtures of boronated antibodies could not be used, each recognizing a different set of epitopes, the sum total of which could far exceed  $10^6$  per cell. Finally, the major concept that we would like to advance is that just as effective cancer chemotherapy is based on the use of a combination of drugs, similarly a combination of compounds could be employed to deliver the requisite amount of  $^{10}\text{B}$  to tumor target cells. This could include compounds such as  $\text{Na}_2\text{B}_{12}\text{H}_{11}\text{SH}$ , used by Hatanaka et al. (13,14),  $^{10}\text{B}$ -chlorpromazine, used by Mishima et al. (26), or other compounds described elsewhere in this symposium, together with boronated antibodies directed against tumor-associated antigens.

#### Summary

The present study was undertaken to determine the feasibility of using a combination of capture agents consisting of boronated antibodies and  $^{10}\text{B}$  enriched boric acid ( $^{10}\text{B}-\text{H}_3\text{BO}_3$ ) for the delivery of boron-10 to tumor and non-tumor target cells. Two model systems have been studied, the first employing polyclonally derived horse anti-human thymocyte globulin, and the second monoclonal mouse anti-human colorectal cancer antibody 17-1A. Antibodies were boronated with the cesium salt of undecahydro-mercapto-closo-dodecaborate ( $\text{Cs}_2\text{B}_{12}\text{H}_{11}\text{Si} \cdot 2\text{H}_2\text{O}$ ) using the heterobifunctional reagent N-succinimidyl-3-(2-pyridyldithio)-propionate (SPDP).

The effects of boronated ATG ( $^{11}\text{B}$ -ATG) on the ability of human peripheral blood lymphocytes (PBL) to respond to phytohemagglutinin (PHA) have been investigated. PBL were exposed to  $10^{-2}$  to  $10^{-4}\text{M}$  concentrations of  $^{10}\text{B}-\text{H}_3\text{BO}_3$ ,  $^{11}\text{B}$ -ATG, or a mixture of  $^{11}\text{B}$ -ATG +  $^{10}\text{B}-\text{H}_3\text{BO}_3$  and irradiated with a neutron fluence of  $10^{13}/\text{cm}^2$ . Irradiated PBL, either untreated or exposed to  $^{11}\text{B}$ -ATG or  $10^{-3}\text{M}$   $^{10}\text{B}-\text{H}_3\text{BO}_3$ , showed ~70-75% reduction in responsiveness. Irradiated cells treated with a  $10^{-2}\text{M}$   $^{10}\text{B}-\text{H}_3\text{BO}_3$  had a 95% reduction, while those exposed to a mixture of  $^{11}\text{B}$ -ATG +  $10^{-2}\text{M}$   $\text{H}_3\text{BO}_3$  showed ~99% reduction.

The effects of neutron irradiation alone or in combination with  $^{10}\text{B}-\text{H}_3\text{BO}_3$  and boronated monoclonal 17-1A ( $^{10}\text{B}-17-1\text{A}$ ) on the survival of SW 1116 cells were studied. Doses up to  $10^{12}\text{ n/cm}^2$  had no effect on the surviving fraction (S.F.), but with  $10^{13}\text{ n/cm}^2$  the S.F. was reduced to 0.0025. This effect was largely attributable to gamma photon contamination of the neutron beam. Molar concentrations of  $^{10}\text{B}-\text{H}_3\text{BO}_3$  in excess of 0.01 M were capable of supporting a  $n,\alpha$  reaction with >99% lethality. Boronated 17-1A appeared to be capable of supporting a lethal  $n,\alpha$  reaction, but at a lower level.

The major concept that we would like to advance is that by using a combination of agents such as non-selective delivery via  $^{10}\text{B}-\text{B}_{12}\text{H}_{11}\text{SH}^{2-}$ , together with targeted delivery via boronated antibody, it should be possible to deliver a sufficient amount of  $^{10}\text{B}$  to sustain an  $n,\alpha$  reaction that will have >99% lethality.

#### ACKNOWLEDGEMENTS

This work was supported by grants PDT-197 from the American Cancer Society, contract DE-AC02-82ER60040 from the Department of Energy, and U.S. Public Health Service grant P-30-CA-16508-09 from the National Cancer Institute. We thank Mrs. Jacqui Roberts for secretarial assistance.

#### REFERENCES

1. Soloway, A.H. *Science* 128:1572, 1958.
2. Soloway, A.H., Whitman, B., and Messner, J.R. *J. Med. Pharm. Chem.* 5:191, 1962.
3. Nyilas, E. and Soloway, A.H. *J. Amer. Chem. Soc.* 81:2681, 1961.
4. Easterday, O.D. and Farr, L.E. *J. Pharm. Exptl. Therap.* 132:392, 1961.
5. Snyder, R.R. and Meisel, S.L. *J. Amer. Chem. Soc.* 70:774, 1948.
6. Lenarz, W.J. and Snyder, H.R. *J. Amer. Chem. Soc.* 82:2172, 1960.
7. Schleppnik, A.A. and Gutsche, C.D. *J. Org. Chem.* 25:1378, 1960.
8. Matteson, D.S. and Peacock, K. *J. Amer. Chem. Soc.* 82:5759, 1960.
9. Matteson, D.S. *J. Org. Chem.* 27:275, 1962.
10. Soloway, A.H., Hatanaka, H., and Davis, M.A. *J. Med. Chem.* 10:714, 1967.
11. Hatanaka, H. *J. Neurol.* 209:81, 1975.
12. Hatanaka, H., Amano, K., Kamano, S., Fankhouser, H., Hanamura, T., and Sano, K. *Acta Neurochirurgica* 42:57, 1978.
13. Hatanaka, H., Amano, K., Kamano, S., et al. *Mod. Neurosurg.* 1: , 1981.
14. Hatanaka, H., *See paper VII-3 in this Symposium.*
15. Barth, R.F., Johnson, C.W., Wei, W-Z., et al. *Cancer Det. and Preven.* 5:315, 1983.
16. Wechter, W.J., Nelson, J.W., Perper, R.J. et al. *Transplant.* 28:303, 1979.
17. Steplewski, Z. *Transpl. Proc.* 12:384, 1980.
18. Herlyn, M., Steplewski, Z., Herlyn, D. and Koprowski, H. *Proc. Natl. Acad. Sci. USA* 76:1438, 1979.
19. Alam, F., Soloway, A.H., Barth, R.F., Johnson, C.W., and Carey, W.E. *See paper V-4 in this Symposium.*
20. Bøyum, A. *Scand. J. Immunol.* 5(Suppl.)9, 1976.
21. McElroy, W.N., Berg, S., Crockett, T. and Hawkins, R.G. *AFWL-TR-67-41.* 1967. Air Force Weapons Laboratory, Kirtland AFB, New Mexico.
22. Markwell, M.A.K. and Fox C.F. *Biochemistry* 17:4807, 1978.
23. Fews, A.P. and Henshaw, D.L. *Phys. Med. Biol.* 28:459, 1983.
24. Kirsch, J.E. and Brownell, G.L. *See paper IV-4 in this Symposium.*
25. Aizawa, O., Kanda, K., Nozaki, T., and Matsumoto, T. *Nuclear Technol.* 48:150, 1980.
26. Mishima, Y., and Shimakage, T. *Pigment Cell* 2:394, 1976.

Practical Problems of the Past in the Use of Boron--Slow Neutron Capture Therapy in the Treatment of Glioblastoma Multiforme

William H. Sweet, M.D., D.Sc., D.H.C.

Massachusetts General Hospital, Ambulatory Care Center 312, Boston, MA 02114

After over a decade of chemical and animal studies, a series of 19 boron-10--slow neutron capture irradiations was carried out on 18 patients from 1959 to 1961. The treatments were given in the surgical operating room especially constructed for this purpose beneath the core of the nuclear reactor at the Massachusetts Institute of Technology.

The preoperative diagnosis was glioblastoma multiforme in the 16 patients with a supratentorial tumor. All patients had had a craniectomy at which the diagnosis was established; at that time as much tumor was resected as was feasible--usually a grossly total removal--and specimens of normal brain, blood, and tumor were taken for analysis of boron content. (The boron compound was given at about the start of the operation.) A previous study by Soloway, De Rougemont, and Sweet (4) had shown that the canine blood-brain barrier around the site of a partial cerebral lobectomy requires 3 weeks to recover fully after the operation. Hence the second human operation due now at the MIT reactor was deferred for at least 3 weeks. At this procedure, scalp, bone flap, and dura were reflected. A series of earlier irradiations of patients with gliomas at the 20-MW reactor at Brookhaven National Laboratory by Farr, Sweet, and others, reported in 1954 (2), had demonstrated that even pre-radiation occlusion of external carotid arteries and tight bandages of the scalp had not precluded the development of non-healing painful ulcers after radiation through intact scalp. Other lessons from the Brookhaven experience leading to the methods used at MIT have been described by Farr et al. (2) and Goodwin et al. (3). In the MIT series the cerebrospinal fluid was kept sucked out of the lobectomy site, and an air-filled balloon was placed in the operative cavity to prevent normal brain from sagging into it. Scalp and orbit were protected by boron-free plastic and small bags filled with lithium fluoride. Paracarboxybenzene boronic acid synthesized with the  $^{10}\text{B}$  isotope was given intravenously to 16 patients; 2 received sodium perhydrodecaborate ( $\text{Na}_2\text{B}_{10}\text{H}_{10}$ ) via the ipsilateral carotid artery. Further details have been recorded by Soloway et al. (5) and Asbury et al. (1). In the latter paper the pathologic studies in the 14 post-mortem experiences are described. All the patients died within 10 days to 11.5 months after the radiation.

We have carried out no more such treatments in man despite the fact that the more promising compound  $\text{Na}_2\text{B}_{12}\text{H}_{11}\text{SH}$  was developed in our laboratories by Dr. Albert Soloway.

The patient who died in 10 days proved to have much more boron in her bloodstream than we had calculated by extrapolation from the boron concentrations at her first operation. She received much more than the planned radiation dose and died of massive cerebral edema. At that time the fastest method of determining boron concentration in tissue required many hours. The crucial determinant of the radiation time, i.e. the boron concentration in normal brain and blood, needed to be ascertained, preferably by an on-line  $\alpha$ -particle detector recording from the normal brain throughout the period of radiation. This ideal desideratum has not yet been met, but the practically useful solution of a prompt determination of boron content at the start of the radiation

has been achieved by Fairchild and colleagues. A measurement of the prompt gamma radiation accompanying the disintegration of  $^{10}\text{B}$  to an  $\alpha$  particle and  $^7\text{Li}$  is the basis for this rapid determination (see paper I-12 by Kanda et al. and paper I-13 by Fairchild and Gabel in this Symposium).

Two other major problems were brought to light by Asbury et al. in the postmortem slices. Whole-brain sections were studied, and the histologic appearances correlated with the neutron flux data obtained by measurements in all segments of the tiny gold wires inserted into the brain and gold discs placed on the brain throughout the radiation. The neutron flux fell off rapidly with depth as expected, and in accordance with this decline there were zones of residual tumor in 10 of the 11 glioblastomas. Although there were minor nests in most of the patients, the cause of death was considered to be due primarily to recurrent tumor in one of the cases and to a combination of extensive tumor recurrence and radiation necrosis in another. Had the patients lived longer, the tumor nests might have become a lethal problem. It was puzzling that at times the islands of glioma were in the main path of the radiation beam, even close to the resection margin at times. It will be noted that we sought to eliminate all solid and liquid matter between the radiation portal and the face of remaining brain containing the tumor remnants we hoped to kill. Thus we sought to maximize the penetration of slow neutrons. Since this is one of the principal weaknesses of the method, we suggest this tactic be pursued even when epithermal beams are utilized.

However, the disconcerting and unexpected finding and easily the main cause of death in 8 of the glioblastomas and the lone medulloblastoma of the posterior fossa was a special form of radiation necrosis--a "coagulation necrosis." In broad fields there was "disappearance of all recognizable parenchymal elements save for the skeletons of thickened blood vessels and gnarled remains of astrocytic processes." Hematoxylin-stained fragments of countless cell nuclei, mainly polymorphonuclear leucocytes, generously sprinkled these necrotic zones. There was only minor phagocytic activity, and fat stains of frozen sections showed almost no sudanophilia. But it was the blood vessel changes which were distinctive. In the patient who died at 10 days there was an acute necrotizing lesion of vessels of all sizes. Fibrin and polymorphonuclear leucocytes impregnated the vessel walls; the endothelial nuclei were swollen; many of the vessels were thrombosed. In later cases adventitial proliferation was added to the inflammatory reaction and fibrin exudate. Still later, connective tissue in the media and adventitia was more prominent, and the infiltrate was primarily lymphocytic. In the patient surviving 11.5 months the blood vessel walls showed extreme thickening and fibrosis. The radiation necrosis was most intense at the site of the highest neutron flux, the brain surface. The high concentration of the  $^{10}\text{B}$  in the blood, the sensitivity of the endothelial cells to radiation, and the short range of the heavy particles released appeared to have killed the brain by choking off its blood supply.

The necessity 1) for developing a boron compound which would eventually attain a much higher concentration in tumor than blood and 2) for developing a major epithermal component of the incident beam of slow neutrons seemed to us imperative.

Important advances in the last decade or so which contribute to the solution of the problems include 1) the better control of cerebral edema by large doses of dexamethasone and hyperosmotic agents; 2) the ease of injections into the internal carotid and/or vertebral arteries by retrograde femoral

catheterization to get the boron compound exactly where one wants it; 3) the ability to culture endothelial cells to determine their uptake of the boron compound; 4) the development of track-etching techniques to determine the precise cell of origin of  $\alpha$  particles and hence the site of the disintegrating boron atom. Other factors leading to renewed enthusiasm for this approach to gliomas are the relatively poor prognosis despite widespread intensive efforts of various combinations of photon radiation and chemotherapy. These modes of management have yet to yield any case approaching Hatanaka's patient who now, 11 years after boron--slow neutron therapy of his grade IV glioblastoma of the dominant hemisphere's central gyri, has no neurological sequel and is leading a normal life at the age of 61 years. The vast strides in immunochemistry will surely yield a specific antibody whose binding sites will not be impaired by the addition of the stable boron cage if simpler chemical substances incorporating the  $B_{10}$  or  $B_{12}$  cage cannot be found to yield uniformly satisfactory results.

#### ACKNOWLEDGMENT

The author wishes to express his gratitude to the Neuro-Research Foundation for its support in the preparation of this manuscript.

#### REFERENCES

1. A.K. Asbury, R.G. Ojemann, S.L. Nielsen, and W.H. Sweet. Neuropathologic study of fourteen cases of malignant brain tumor treated by boron-10--slow neutron capture radiation. *J. Neuropathol. Exp. Neurol.* 31:278-303, 1972.
2. L.E. Farr, W.H. Sweet, J.S. Robertson, C.G. Foster, H.B. Locksley, D.L. Sutherland, M.L. Mendelsohn, and E.E. Stickley. Neutron capture therapy with boron in the treatment of glioblastoma multiforme. *Am. J. Roentgenol.* 71:279-93, 1954.
3. J.T. Godwin, L.E. Farr, W.H. Sweet, and J.S. Robertson. Pathological study of eight patients with glioblastoma multiforme treated by neutron capture therapy using boron-10. *Cancer* 8:601-15, 1955.
4. A.H. Soloway, J.G. De Rougemont, and W.H. Sweet. The re-establishment in dogs of the blood-brain barrier to tri-iso-propanolamine borate. *Neurochirurgia* 3:1-5, 1960.
5. A.H. Soloway, G.L. Brownell, R.G. Ojemann, and W.H. Sweet. Boron slow neutron capture therapy: Present status. In *Preparation and Biomedical Application of Labeled Molecules* (Proc. Int. Symp., Venice, 1964), pp. 383-403, J. Sirchis, Ed., Euratom, Brussels, 1964.

# Monoclonal Antibodies to Cell Surface Antigens of Human Melanoma\*

Ingegerd Hellström, Karl Erik Hellström, Joseph P. Brown  
Oncogen, Seattle, Washington 98121, and Departments of Microbiology/Immunology  
and Pathology, University of Washington, Seattle, WA 98199

Steven M. Larson, J.A. Carrasquillo

Veterans Administration Medical Center, Seattle, Washington 98144;  
and Departments of Radiology and Laboratory Medicine,  
University of Washington, Seattle, Washington 98195

and G. Goodman

Tumor Institute, Swedish Hospital Medical Center, Seattle, Washington 98124

## ABSTRACT

Our group has worked with three human melanoma antigens which have been defined by monoclonal mouse antibodies: p97, a glycoprotein that is structurally related to transferrin, a proteoglycan, and a GD3 ganglioside that is slightly different from the GD3 of normal brain. All three antigens can be detected in frozen sections of melanoma, using immunohistological techniques. Antibodies and Fab fragments, specific for either p97 or the proteoglycan antigen, have been radiolabelled with  $^{131}\text{I}$  and successfully used for tumor imaging, and Phase I therapeutic trials are underway, using  $^{131}\text{I}$ -labelled Fab fragments, specific for p97 or the proteoglycan antigen, to localize a potentially therapeutic dose of radiation into tumors. It may be feasible to use the same monoclonal antibodies, or antibody fragments, as carriers of neutron capturers, such as boron, for possible use in tumor therapy. The initial experiments on this are best carried out by using nude mice (or rats) carrying human melanoma xenografts.

## INTRODUCTION

Melanomas belong to the human tumors that have been studied the most with the monoclonal antibody technique (1). As a result of these studies, it has become apparent that there are several cell surface antigens that are more strongly expressed by melanomas than by other tumors or by normal tissues. None of these antigens appear to be entirely specific for melanoma, since small amounts of the respective antigens can be detected in various normal cells, if highly sensitive assays are used (2,3). Nevertheless, there are good reasons to believe that some of the melanoma antigens can be used as diagnostic markers, e.g., for

---

\*This work has been supported by grants CA 19148, CA 19149, CA 26939, and CA 34777 from the National Institutes of Health; and IM 241 from the American Cancer Society. The work described in this article was performed when the 3 senior authors were Members of the Fred Hutchinson Cancer Research Center, Seattle, Washington.

tumor imaging by radiolabelled antibodies (or antibody fragments) and they may probably be useful also as therapeutic targets.

We shall here discuss some of our experience from the melanoma system as it relates to the topic of this symposium. We do so for two reasons. First, we believe that existing monoclonal antibodies to melanoma-associated antigens can be useful to work out procedures for the targeting of a variety of agents into tumor tissues. Second, it is likely that what is being learned about melanomas will prove applicable to other solid tumors as well.

### THREE ANTIGENS OF RELATIVELY HIGH MELANOMA SPECIFICITY

Our group has taken a particular interest in three melanoma-associated antigens, which we believe have sufficient degree of melanoma specificity to be useful as diagnostic markers and therapeutic targets. These antigens are p97, a proteoglycan and a GD3 ganglioside. We shall briefly discuss each of these antigens.

p97 is a phosphorylated sialoglycoprotein which has approximately the same molecular weight as rabbit phosphorylase b, that is around 97,000, and forms an integral part of the cell membrane (4,5, and unpublished findings). While most melanomas express 50,000-400,000 p97 molecules per cell, non-melanoma tumors generally have less than about 20,000 molecules per cell and normal adult tissues less than about 8,000 molecules per cell, the highest normal tissue levels being seen have been in smooth muscle (3,5, and unpublished findings). A partial amino acid sequencing of the N-terminal end has shown p97 to be structurally related to transferrin (6) and, like transferrin, p97 can bind iron. The gene for p97 has been assigned to chromosome 3 (7) which is the same chromosome that carries the gene for the transferrin receptor, a molecule different from p97, and probably also for transferrin. Many monoclonal antibodies to p97 are available, defining 5 different epitopes (5).

The proteoglycan antigen, to which our group has developed several monoclonal antibodies, including 48.7, was first discovered by Reisfeld's (8) and Ferrone's (9) groups. It is strongly expressed in most melanomas and much more weakly in other tumors (10). Small amounts of the antigen can be detected in some endothelial cells, while other normal cells have not been positive when tested in frozen sections, with immunohistological techniques.

The GD3 antigen, as defined by our antibody 4.2 (11,12) is very similar to an antigen defined by antibody R<sub>23</sub>, as described by Old's group (13,14). It has a very high degree of specificity for melanomas as compared to other tumors. Although our original antibody 4.2 reacted also with some cells in normal brain, a more recent antibody, 2B2, does not. As shown by Nudelman *et al.* (12), the fatty acids of the melanoma-associated GD3 are longer than those of the brain, which may explain why brain is not stained by antibody 2B2.

All three antigens are expressed in melanomas *in vivo*, as best shown by using immunohistological techniques on frozen sections. They are also expressed in benign nevi, while normal, resting skin melanocytes have been negative (15, unpublished findings). Using immunohistological techniques, every melanoma so far tested has stained for at least one of the 3 antigens, and 96% have stained for 2 of them. While no non-melanoma tumors so far tested have expressed all 3 antigens, approximately 60% of melanomas do.

The three antigens are expressed in human melanomas growing in nude mice and antibodies to them (radiolabelled or unlabelled) will localize into such tumors, when injected intravenously (16, and I. Hellström, unpublished findings). Antibody 2B2, specific for the GD3 antigen, shows strong lymphocyte-dependent antibody activity *in vitro* in the presence of human lymphocytes and can strongly inhibit the growth of human melanomas in nude mice, providing further evidence that the antibodies can target to tumor (I. Hellström, unpublished data). Since both melanomas and other types of tumors with ability to grow in nude mice and a known degree of expression of the three antigens are available, the nude mouse model should be useful to assess the tumor targeting of antibodies conjugated, for example, with a neutron capturer.

#### LOCALIZATION OF ANTI-MELANOMA ANTIBODIES IN HUMAN PATIENTS

We have studied whether antibodies to p97 and to the proteoglycan antigen can localize into metastatic melanoma in human patients. This has been done in two ways. First, we have given either whole antibody or Fab fragments, after they have been labelled with  $^{131}\text{I}$ . Both by using imaging techniques and by measuring the relative uptake of specific versus control antibody in tumors and normal tissues, we could show that the specific antibodies were selectively taken up in tumors (16-18). Second, we have given large doses (up to 224 mg of each antibody over a 10-day period) of a mixture of unlabelled antibodies specific for either p97 or the proteoglycan, and tested, by immunohistological techniques on frozen tumor sections, whether the injected antibodies could be detected in tumor and, if so, for how long. We found that the injected antibodies did, indeed, localize to tumor cells, as compared to surrounding normal stroma cells. This localization was throughout the tumor tissue and not just confined to the areas closest to large blood vessels. The antibodies remained at the tumor cell surface up to around 80 hours after the last injection (Goodman *et al.*, unpublished findings).

We have not observed the formation of anti-mouse antibodies in the four patients receiving large doses of the mouse immunoglobulin and followed over a 6-week period. On the other hand, such antibodies occur early and regularly in patients receiving only a few mg of mouse antibodies and more infrequently in patients receiving Fab fragments (16). Perhaps the large doses of whole antibody can induce a temporary state of immunological nonreactivity.

#### IMPLICATIONS OF THESE FINDINGS FOR STUDIES ON THE TARGETING OF ANTI-TUMOR ANTIBODIES CONJUGATED, FOR EXAMPLE, WITH A BORON COMPOUND

Antibodies to the three melanoma antigens described offer promise for studies on tumor using, for example, boron compounds for conjugation with the antibody. The problem will rather be the extent to which antigen-binding tumor-seeking conjugates can be made and what biological activity they will have. There are several reliable, highly sensitive assays by which antibody binding to cultured cells (19) and tissue sections (15) can be detected. It is possible, therefore, to follow how antibody conjugation with, for example, a boron compound will interfere with its ability to bind to antigen. Tumor lines with different degrees of expression of the target antigens can be grown in nude mice to study the targeting

of intravenously injected antibody-conjugate into tumor, its degree of tumor-antigen specificity and the therapeutic potential of the tumor targeting. Since mouse antibodies to the two antigens that have been tested will localize into metastatic melanomas in patients and can be given without much complication, it should be possible to conduct clinical trials when tumor-targeting compounds have been found that bind to tumor cells in vitro and localize into tumor tissues in vivo in nude mice.

It may be a good strategy to carry out the melanoma studies in parallel with studies in a syngeneic animal tumor model, for example using mouse bladder carcinomas as described in a separate presentation (20).

#### References

1. Reisfeld, R.A. *Nature* 298: 325-326, 1982.
2. Hellström, K.E, Hellström, I., and Brown, J.P. In: Monoclonal Antibodies and Cancer, G.L. Wright, ed., Marcel Dekker, Inc., N.Y., in press.
3. Brown, J.P., Woodbury, R.G., Hart, C.E., Hellström, I., and Hellström, K.E. *Proc. Natl. Acad. Sci. USA* 78: 539-543, 1981.
4. Woodbury, R.G., Brown, J.P., Yeh, M.-Y., Hellström, I., and Hellström, K.E. *Proc. Natl. Acad. Sci. USA* 77: 2183-2186, 1980.
5. Brown, J.P., Nishiyama, K., Hellström, I., and Hellström, K.E. *J. Immunol.* 127: 539-546, 1981.
6. Brown, J.P., Hewick, R.M., Hellström, I., Hellström, K.E., Doolittle, R.F., and Dreyer, W.J. *Nature* 296: 171-173, 1982.
7. Plowman, G.D., Brown, J.P., Enns, C.A., Schröder, J., Nikinmaa, B., Sussman, H.H., Hellström, K.E., and Hellström, I. *Nature* 303: 70-72, 1983.
8. Bumol, T.F., and Reisfeld, R.A. *Proc. Natl. Acad. Sci. USA* 79: 1245-1249, 1982.
9. Imai, K., Molinaro, C.A., and Ferrone, S. *Transplantation Proc.* 12: 380, 1980.
10. Hellström, I., Garrigues, H.J., Cabasco, L., Mosely, G.H., Brown, J.P., and Hellström, K.E. *J. Immunol.* 130: 1467-1472, 1983.
11. Yeh, M.-Y., Hellström, I., Abe, K., Hakomori, S., and Hellström, K.E. *Int. J. Cancer* 29: 269-275, 1982.
12. Nudelman, E., Hakomori, S., Kannagi, R., Levery, S., Yeh, M.-Y., Hellström, K.E., and Hellström, I. *J. Biol. Chem.* 257: 12752-12756, 1982.
13. Dippold, W.G., Lloyd, K.O., Li, L.T.C., Iieda, H., Oettgen, H.F., and Old, L.J. *Proc. Natl. Acad. Sci. USA* 77: 6114-6118, 1980.

14. Pukel, C.S., Lloyd, K.O. Trabassos, L.R., Dippold, W.G., Oettgen, H.F., and Old, L.J. *J. Exp. Med.* 155: 1133-1147, 1982.
15. Garrigues, H.J., Tilgen, W., Hellström, I., Franke, W., and Hellström, K.E. *Int. J. Cancer* 29: 511-515, 1982.
16. Larson, S.M., Brown, J.P., Wright, P.W., Carrasquillo, J.A., Hellström, I., and Hellström, K.E. *J. Nuclear Med.* 24: 123-129, 1983.
17. Larson, S.M., Carrasquillo, J.A., Krohn, K.A., Brown, J.P., McGuffin, R.W., Ferens, J.M., Graham, M.M., Hill, L.D., Beaumier, P.L., Hellström, K.E., and Hellström, I. *J. Clin. Invest.*, in press.
18. Larson, S.M., Carrasquillo, J.A., Krohn, K.A., McGuffin, R.W., Hellström, I., Hellström, K.E., and Lyster, D. *J. Amer. Med. Assoc.* 249: 811-812, 1983.
19. Brown, J.P., Hellström, K.E., and Hellström, I. *Methods Enzymol.* 92: 160-168, 1983.
20. Hellström, K.E., Hellström, I., Kohwi, Y., and Lee, V.K. See paper IV-7 in this Symposium.

Clinical Experience of Boron Neutron Capture Therapy  
for Malignant Brain Tumors

Hiroshi Hatanaka, M.D., D.Sc.,

Department of Neurosurgery, Teikyo University, Kaga, Itabashi-ku, Tokyo, Japan

The ancient Chinese sage, Confucius, said in four words, "On-ko-chi-shin," which means "By studying the old, one can discover the new." I would like to start this talk by briefly reviewing the history of Slow-Neutron Capture Therapy.

Review of the past

The first man who discussed the possibility of neutron capture therapy was Gordon L. Locher, a physicist at the Bartol Foundation of Swarthmore College. Unfortunately I could not track him down, although I was able to meet one of his former colleagues. Locher discussed the possibility of applying neutron capture reaction to cancer therapy in a review paper entitled "Biological effects and therapeutic possibilities of neutrons" which was published in 1936 in the American Journal of Roentgenology. In this article, he said, "Research covering these fields might well be expected to occupy the entire time of many workers for many years. Yet, if they led to the eradication of a single disease, or to a better understanding of biological processes involved in disease, so that the way to cure was made clearer, the effort would be justified." His prediction proved to be true. It took almost 40 years before the first glioblastoma patient could be successfully cured by this therapy.

The first problem was how to obtain a large flux of neutrons. It was only after atomic reactors were built that a sufficiently large amount of thermal neutrons became available.

The second problem was the choice of nuclide to be used as neutron-capturing material. Among lithium-6, boron-10, uranium-235, and other heavy particle emitters by neutron capture reaction, boron-10 was selected first for various biological reasons. Boron-10 has been attractive to chemists, because of its vast potential for synthesizing new compounds (Soloway). Initially a large part of boron chemistry was kept classified as boron was one of the possible candidates for space fuel, but after the 1960's, it was declassified. Only 18% of natural boron is boron-10. To improve the effect of therapy, it is more efficient to use enriched boron-10. The method of enriching such an isotope involves technology similar to that required in enriching uranium-235. Hence, boron-10 was expensive 20 to 30 years ago, when a large amount of boron-10 was required for clinical trials, although not so much was needed for animal experiments. One gram of boron-10 was priced at 25 dollars in those days. It is amazing that a dose of boron-10 compound for one patient's treatment could be available now at a much cheaper price, if it were on the market, than that of an ordinary antitumor drug dispensed in a course of therapy.

Selection and synthesis of boron compounds was, and even now is, one of

the crucial problems. Such compounds should penetrate into the malignant tissue, but should not remain in the normal cells. It was Dr. William Sweet, a neurosurgeon, who introduced the idea of taking advantage of the Blood-Brain Barrier to treat brain tumors. The Blood-Brain Barrier is not really an anatomical structure, but is a physiological phenomenon encountered in the brain that does not allow free penetration of substances into the brain matter. Even glucose or water, which are physiologically consumed by the brain, cannot enter the brain matter in excessive amounts. It is well known that oil-soluble compounds can easily cross the Blood-Brain Barrier, but that water-soluble compounds cannot cross so easily. For this reason, many oil-soluble boron compounds have been found inadequate for neutron capture therapy. On the contrary, tumors are usually so "hungry" that they are easily penetrated by almost any substance. Dr. Sweet and his colleagues at his laboratory at Massachusetts General Hospital had studied the Blood-Brain Barrier by using P-32 and other newly available isotopes in the 1950's. This background was naturally helpful in starting a Boron-10 uptake study.

The ratio of Boron concentration in tumor(T) to Boron concentration in normal tissue(N) was the initial interest for Sweet and his chemist collaborator, Albert H. Soloway. Boron compounds which would yield high T/N ratio were enthusiastically sought. Paracarboxyphenylboronic acid or perhydrodecaborate was actually used for human treatment in the 1960 and 1961 series.

My knowledge of the clinical studies conducted between 1953 and 1961 at Brookhaven National Laboratory reactor and at MIT reactor is rather incomplete. Some of my knowledge of Dr. Sweet's past experience I learned directly from Dr. Sweet himself, but a lot more was learned indirectly from his earlier collaborators including Janette Robinson Messer, Manucher Javid, Lucas Yamamoto, Arthur Asbury, Al Soloway, and Gordon Brownell. Because Dr. Sweet was such a busy director of the neurosurgical service, it was not always possible to catch up with him. Consequently, my knowledge of his past experience may not be totally correct.

Brain tumors have almost constantly been the primary target of neutron capture therapy for these reasons: 1) The brain is such an unreplaceably important organ that it is particularly for brain tumors that we want such a highly specific therapy as boron neutron capture therapy. For other tumors, quite often surgical extirpation is simple and effective, but for brain tumors a radical surgery is usually impossible; 2) It is relatively easy to obtain an appreciably high Tumor-to-Normal ratio of boron-10 concentration in the case of brain tumors, thanks to the Blood-Brain Barrier. For other tumors such a high T/N ratio cannot be obtained so simply, unless boron chemistry or boron immunochemistry makes further advances; 3) Brain tumor is such a fatal tumor, and thus is most challenging. It was reported that, in the year 1975, in the U.S.A., there were 5,000 new glioma patients and that, in the same year, there was a glioma death toll of 5,000. Even for non-glioma brain tumors, which are sometimes called benign brain tumors, in the year 1975, there were 5,700 new patients and 3,500 dead. This means that even for the so-called benign tumors, 60% are fatal.

Dr. Sweet's clinical series was discontinued in 1961. The mean survival of glioblastoma patients treated at MIT reactor was 5.5 months after neutron capture therapy. The cause of failure was reported to be excessive radiation of cerebral vascular walls by the neutron capture reaction which occurred between neutrons and the excessive boron-10 in the circulating blood. His

clinical result has always been described as "a failure." However, I do not think it was. The reasons are: 1) Many of his 18 cases treated at MITR were not really fresh cases. Many had been operated on by other surgeons before BNCT. As my clinical experience indicates, the patients who undertook their first tumor extirpation with me and then BNCT ("Consistent BNCT cases") do far better than the other patients who were treated by BNCT only after surgery by other neurosurgeons ("Inconsistent BNCT cases"). The average survival of the Consistent BNCT cases is 3 times longer than the Inconsistent BNCT cases. The main reason for this difference in survival is that BNCT is a Primary Radio-surgery, and not an Adjuvant Therapy as is conventional radiotherapy, chemotherapy or immunotherapy. It is no wonder that Dr. Sweet's cases did not do very well; 2) When I scrutinized his series, I wondered at first if the neutron fluence delivered to the patient's brain might have been too large. The MITR in those days yielded a flux of  $1 \times 10^{10}$  at the surface of the brain, according to a document which I had a chance to read. Neutrons of  $1.8 \times 10^{13}$  in n.v.t. were supposed to have been delivered. This fluence was once considered too much, but later neutron capture radiation tolerance studies at MITR or at HTR and KUR indicated that the animal brains could tolerate even more. As for human brains, from my clinical experience, I have some opinions about human brain tolerance, but it is premature to discuss them for the moment; 3) It has been my feeling that the brain capillary vessels might have tolerated the radiation better, even in the MITR series. In 1965-66, I reenacted Dr. Sweet's MITR series in 6 cats, using the same boron compound and radiating by the same regimen as in 1960-1961. I was able to demonstrate serious vascular endothelial damage at an electron microscope level. It consisted of swelling of the endothelial cells, disruption of the cell membranes, clumping of ribosomes, and, above all, dissolution of the cristae of the mitochondria in the endothelial cells. These changes were almost unrecognized after a large dose of adrenocorticosteroid had been administered. Using large doses of steroid hormone to protect the Blood-Brain Barrier was a relatively new concept which was proved by me, using I-135-labelled human gamma globulin in 1962 and 63 - after the MIT-series was discontinued; 4) Recently after the introduction of computerized tomography of the brain (the so-called CT-scans), the discrete expansion of a glioma has been more clearly recognized. Dr. Sweet irradiated through craniectomized windows in the skull, by shielding the rest of the head so that the scalp, which contains some amount of boron, would not be radiated with neutrons. I followed his procedure from 1968 until a few years ago, when I realized this method is far from satisfactory, because a large tumor bed, which can sometimes be more than 10 cm in diameter may well escape the neutron beam. Indeed common practice in conventional radiotherapy has been to fashion a large radiation field of 10 or 12 cm square, or even to radiate the whole brain. Why should not BNCT do the same? As a matter of fact whole-brain radiation yields an effect that multiplies the central radiation dose, as in the case of rotating or multiportal irradiation, because the slow neutrons do not always travel straight. My idea was endorsed by experimental data offered by Aizawa and Nozaki. Through a large aperture of 22 cm, which is about the size of the head, the neutron flux at the depth of 8-10 cm from the brain surface is more than 10-fold as compared to the delivery of neutrons through a conventional craniotomy bone window. It can be easily imagined that owing to this small radiation field, Dr. Sweet's patients did not always receive theoretically curative doses as

was true of some of my own cases; 5) Dr. Sweet started neutron delivery within 30 minutes after intravenous injection of boron. This certainly may have contributed to the serious damage to the brain capillaries due to high concentration of boron in the circulating blood. Now it is generally accepted that neutron should be delivered only after waiting a certain number of hours.

When reviewing Dr. Sweet's series today, I have to conclude that his failure before 1961 was not really a failure at all in regard to the basic principles of BNCT, but was merely a reflection of our limited knowledge 20 years ago. Everything in neurosurgery has made great advances in the past 20 years, except for brain tumor treatments. Aneurysm, which causes subarachnoid hemorrhage, was treated 20 years ago by only ligating major arteries in order to minimize the direct blood flow to the aneurysm. Direct intervention was tried only by professors, and with poor results. By now aneurysms are no longer monopolized by professors of neurosurgical departments. It is everybody's operation. It is such a simple operation that I can ride a motorcycle to a distant rural hospital and operate without any assistant and with only 4% operative mortality. Treatment of brain tumors should no longer be allowed to lag behind so much. In August, this year, there was a Klaas Breuer Memorial Lecture by Dr. John F. Fowler, a British radiologist, at the 2nd Annual Meeting of the European Society for Therapeutic Radiology and Oncology. In this lecture he emphasized Patients and Patience for clinical trials. He quoted the case of Hodgkin's disease as one of the best examples of the improvement in treatment of cancer by radiotherapy and a multi-disciplinary approach. In 1940 this disease was regarded as inevitably fatal with a 5-year survival of 5%. Twenty years later in 1960, 250 KV X-ray apparatus could assure a 5-year survival of 35%. In 1980 supravoltage machines and chemotherapy yielded an 80% 5-year survival. This situation resembles the situation of our BNCT. By conventional radiotherapy for grade III-IV gliomas, which approximates the term glioblastoma, a 5-year survival of 5.7% was reported (by Mayo people). By the present technique of BNCT, the 5-year survival of the cases treated before 1979 reached 33%, 20 years after Dr. Sweet's initial series. I am convinced that in another twenty years we too will be able to achieve an 80% 5-year survival, but only if a good collaborative study can be organized.

As Confucius said 2,500 years ago, "By studying the old, one can discover the new." In reviewing what Dr. Sweet had done, I concluded that it was not a failure but the first bold step on the long road to success. He is entitled to be called the Patriarch of Neutron Capture Therapy, although I am not sure if he will recognize me as his legitimate heir.

#### Preclinical or Paraclinical Studies for the Clinical Trials of BNCT in Japan

In the present symposium, some preclinical or paraclinical studies were presented by my colleagues. These studies are largely classified as follows:

- 1) Medicinal studies on boron compounds. (Synthesis, distribution study by quantitative chemical analysis, distribution study by autoradiography, toxicological study, etc.)
- 2) Physics studies. (Neutron beam port, phantom study for dosimetry, elimination of gamma ray, simultaneous monitoring system, etc.)
- 3) Therapy for tumor-bearing animals. (Survival, pathological appraisal, etc.)
- 4) Studies of normal tissue tolerance.

It is important to note that by our relatively large series of human brain tumor studies of boron-10 uptake, it became clear that the previously hypothesized concept of "large Tumor-to-Blood ratio" is almost obsolete. Indeed some patients have proved that their brain well tolerated small Tumor-to-Blood ratio (smaller than unity), without any neurological deterioration.

Besides the earlier concept of large T/B ratio, there was a classical belief that we need at least 50ug boron-10/gram of tumor to destroy tumors. These concepts are certainly nice and naive, but I must say these concepts are no longer absolutely important, as clinical experience does not necessarily indicate them.

#### Clinical experience

In August, 1968, after spending nearly 10 months on dosimetry and remodeling of the thermal column at HTR (100 KW), Kawasaki, and after going through some tough questions by committees of specialists, the author was granted permission to use the reactor by the Atomic Energy Commission and eventually by the Prime Minister. The questions were tough, because the proposal was filed after a similar treatment had been discontinued in the United States. These meetings discussed not only technical aspects but also ethical problems. Engineers of the Hitachi Shipbuilding Company and the Hitachi Training Reactor were able to somehow arrange the reactor room for human treatment. Financial aid from the shipbuilding company was crucial. Shionogi Pharmaceutical Company launched research and production of therapeutically employable amounts of boron-10 compound at the urge of the author. Mercaptoundecahydrododecaborate, which was originally studied by Soloway, Hatanaka, and Davis, has been clinically used since 1968.

Since larger research reactors are located in distant countrysides, HTR and MuITR (Hitachi Training Reactor and Musashi Institute of Technology Reactor, both of 100 KW) were used for all except two of the 60 cases. There was no treatment performed for almost 3 years between 1974 and 1977 as HTR was closed for good in 1974. At MuITR, elimination of core gamma with a bismuth layer, by Kanda, Aizawa, et al., made it possible to yield a higher neutron flux.

From 1968 until 1971 only cases which had already undergone Cobalt-60 radiotherapy were treated by neutron capture (9 cases). Besides these nine, another case with a deep-seated glioma was treated by combining neutron capture with Photon. It was only after 1972 that patients without any previous intervention could be treated by neutron capture alone. For the 30 patients treated between 1972 and 1979, the 5-year survival was 33.3% (10/30). As mentioned before, there was no treatment in 1974-76, for almost 5 years.

For grade III-IV malignant gliomas (even though grade I II gliomas are also fatal as long as they cannot be totally excised), the control group treated by the so-called multimodality treatment of chemo-/immuno-radiotherapy with Cobalt-60 or Linear accelerator, died out before 3 years after treatments. The 5-year survival was naturally 0%. As historical controls I can quote, as an impressive report, the one by Mayo Clinic people who reported 5.7% 5-year survival with grade III-IV. The mean survival of the author's control group was  $11.5 \pm 1.3$  months. By neutron capture therapy, the 5-year survival was 33.3% and the mean survival was  $36.9 \pm 14.8$  months, as of June 30, 1983. The longest surviving glioblastoma patient is now 61 years old, 11 years after the

neutron capture treatment, and is in perfect working condition. His original tumor with a size of 6 x 5.5 x 4.5 cm, was located in the motor and speech area in the left posterior frontal lobe, and before neutron treatment 20 gram had been excised by the author's operation. BNCT was performed against the considerably large tumor residue. Tumor-to-Blood ratio was 0.5, but there was no neurological deterioration by BNCT. He is even now right-handed, and can speak or can calculate correctly. It should be noted that the literature reporting the rare long survival of glioblastoma patients have dealt with cases in which radical surgical excision could have been conducted.

12 autopsied cases were reviewed and it was learned that the tumor tissue irradiated with more than 1000 rad or 3000 rem-equivalent dose had been destroyed by a single treatment. The cause of failure in unsuccessful cases was attributable either to an inadequate field of radiation resulting from the small conventional craniotomy bone window through which neutron had been introduced, or to an insufficient penetration of neutron flux. (International Congress of Neuropathology, Vienna, 1982)

Since 1982, the results of work done by Aizawa and Nozaki in 1976 have been put into routine use. Instead of irradiating through a small window in the skull, the whole head is irradiated by exposing the skull by a cross incision. This easily multiplies the neutron flux at such a depth of 8-10 cm from the cerebral surface by 10-fold. This approach has eliminated the nuisance of putting a void such as a balloon or a pingpong ball in the tumor cavity which was a practice by Sweet until 1961 and by Hatanaka after then. Deep-seated tumors such as those of the pons or medulla can now be even more sufficiently treated than in the past when they somehow responded to neutron capture treatment fairly well. (A case of astrocytoma of the medulla whose respiration had been paralyzed was taken to the reactor supported on a respirator and after treatment recovered spontaneous breathing within a few days. Another case with a recurrent pons tumor recovered from coma after neutron capture and survived 5 years.) Thanks to the new practice, further improvement in survival rate is anticipated. If epithermal neutron beam becomes available, as Fairchild predicted as early as in 1964, the efficiency of BNCT will be greatly improved.

If the present modest clinical success of this therapy can give an impetus to studies in physics and boron chemistry or immunochemistry, there could be a real breakthrough in brain tumor treatment which is presently in a grim state. The author's colleagues in surgery and pathology are interested in boronating antitumor antibodies. If this idea is feasible, we may be able to treat such incurable tumors as pancreas cancers without radiating other abdominal viscera.

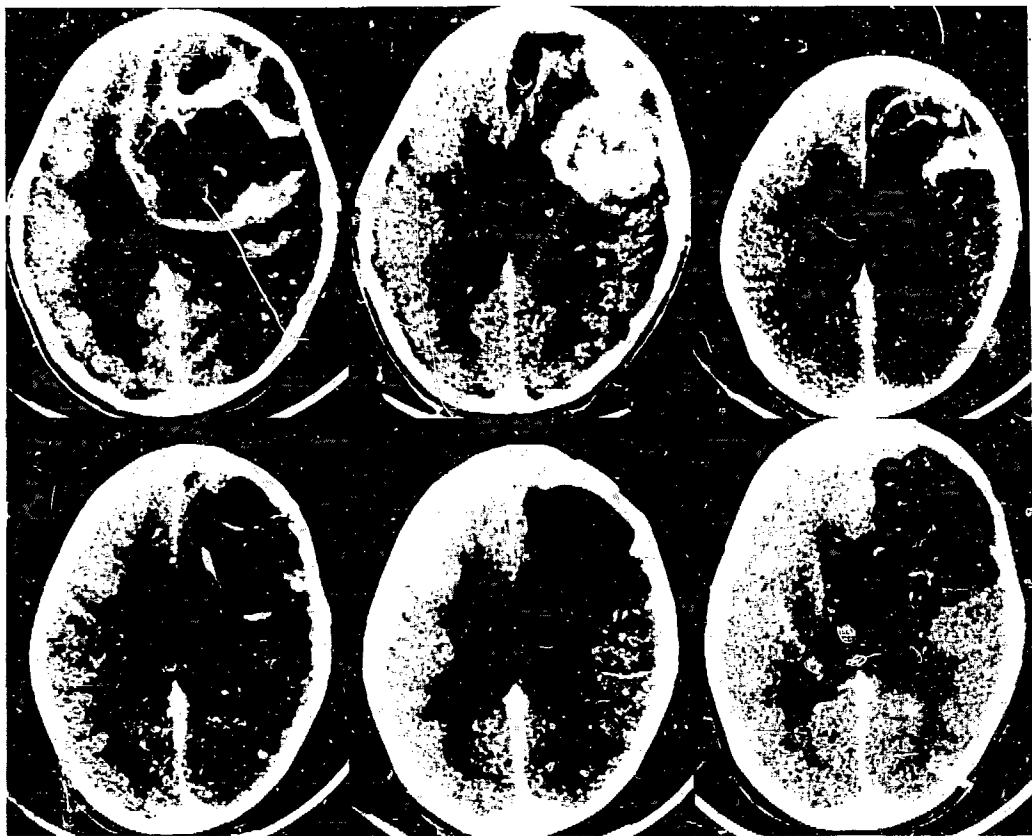
Although many other anti-cancer therapies are being intensively studied, neutron capture therapy has a definite advantage over the others in cellular-level specificity and lethality. This therapy will have a much higher future potential, because the present modestly encouraging clinical data have been achieved only with very limited resources.

Table 1.  $^{10}\text{B}$  in brain tumor and blood at therapeutic hours after infusion

( As of October, 1982 )

	Glioma (Astrocyt-, Glioblast-, Medulloblastomas)	Non-gliomas (Meningioma, sarcoma and metastases)
Tumor $^{10}\text{B}$	$\mu\text{g}^{10}\text{B/g}$ $25.4 \pm 2.4$ [104.7 - 5.0] (n=53)	$\mu\text{g}^{10}\text{B/g}$ $34.2 \pm 9.7$ [90.4 - 11.2] (n=7)
Blood $^{10}\text{B}$	$\mu\text{g}^{10}\text{B/g}$ $23.2 \pm 1.5$ [44.5 - 5.0] (n=51)	$\mu\text{g}^{10}\text{B/g}$ $15.4 \pm 2.9$ [27.7 - 7.3] (n=6)
T/B ratio	$1.5 \pm 0.2$ [8.7 - 0.26] (n=51)	$2.7 \pm 1.1$ [8.95 - 0.713] (n=6)
Dose	$\text{mg}^{10}\text{B/kg}$ $10.4 \pm 2.3$ [79 - 30] (n=29)	$\text{mg}^{10}\text{B/kg}$ $14.8 \pm 2.1$ [52 - 40] (n=6)
Hours (after infusion)	hrs $13.2 \pm 0.14$ [19.5 - 3.5] (n=53)	hrs $16.7 \pm 2.5$ [28 - 11.2] (n=6)

Specimens were obtained at the time of the 2nd or 3rd craniotomy which was assigned to neutron irradiation — only after a good tumor bulk reduction by the previous craniotomy which should have reduced the intracranial pressure and displacement of the brain and which should have restored good blood circulation to the brain as well as to the brain tumor bed. Naturally the tumor uptake data thus obtained should be higher than the tumor uptake data obtained at the 1st craniotomy when the tumor bulk is being reduced. Normal brain specimen was not obtained for chemical analysis, because it is not ethically permissible to obtain a large brain tissue when boron-10 concentration in the normal brain tissue is unmeasurably low. ( below 0.3 $\mu\text{g/g}$  ). The blood concentration is obviously related to the functions of kidney, heart, liver and other organs. Although not tabulated here, there was a tendency of more rapid excretion into urine of boron in younger individuals. It is important that high T/B ratio did not necessarily guarantee good clinical result. As described in the text, the patient now 62 years old who has survived 11.5 years yielded a T/B ratio of only 0.5 when he was treated by NCT. His pre-operative right-sided hemiparesis and speech disturbance disappeared.



Example of tumor dissolution after neutron capture therapy. A case of 11-year-old girl with a huge malignant glioma (diameter ca. 8-9 cm) in the right frontal lobe. From top left to bottom right. CT scans obtained on:

1) September 11, 1981, 7 days before an attempt by a neurosurgeon to excise the tumor; 2) September 29, 1981, 11 days after partial excision, and 10 days before NCT; 3) October 26, 1981, 17 days after NCT; 4) 6 months after NCT. Tumor tissue has been fairly well dissolved, but its periphery is still suspiciously contrast-medium stained; 5) 12 months after NCT. Tumor tissue has been almost totally dissolved; and 6) 18 months after NCT (April 7, 1983). This patient, now an 8th grader, is enjoying her school life, without any neurological deficit. Academic score is not at the bottom of the class, if not at the top.

All the tumors treated by NCT in 1982 and 1983 by the new method of whole-brain irradiation to increase the depth dose of neutrons showed such complete dissolution of the CT-scan tumors, except one who obviously had disseminating tumor cells. (Patients who died within a month for hepatitis or hemorrhage into the tumor are excluded. Also patients treated in the latter half of the year 1983 are excluded, as it is too premature.)

## REFERENCES

- 1) Abe, M., Kitamura, K., Amano, K., Hatanaka, H.: Tissue distribution of  $^{10}\text{B}$  compound in ENU-induced tumor-carrying rats and transplanted brain tumor-carrying rats. 39th Annual Meeting of the Japanese Neurosurgical Society, Oct. 16, 1980.
- 2) Aizawa, O., Kanda, K., Nozaki, T., Matsumoto, T.: Remodeling and dosimetry on the neutron irradiation facility of the Musashi Institute of Technology Reactor for Boron Neutron Capture Therapy. *Nuclear Technology* 48, 150-163 (1980).
- 3) Al-Sarraj, S.F., Hatanaka, H., Takeuchi, A.: Electron microscopic study on the response of the normal canine brain to Boron Neutron Capture Therapy. *Gann* 66, 663-672 (1975).
- 4) Amano, K., Sweet, W.H.: Alpha-autoradiography of  $^{10}\text{B}$  compound distribution in tissue by use of superimposition technique. *Nippon Acta Radiol.* 33, 267-272 (1973).
- 5) An, S., Furuhashi, A., Oka, Y., Akiyama, M., Kuga, H., Tanaka, H.: Development studies regarding the construction of epithermal-enriched neutron field for medical purposes at the University of Tokyo Yayoi Fast Reactor. *Nuclear Technology* 48, 204-215 (1980).
- 6) Brownell, G.L., Zamenhof, R.G., Murray, B.W., Wellum, G.R.: Boron Neutron Capture Therapy. In: *Therapy in Nuclear Medicine*. Spencer, R.P. (ed.), pp. 205-222. New York, San Francisco, London: Grune & Stratton 1978.
- 7) Fairchild, R.G.: Development and dosimetry of an 'epithermal' neutron beam for possible use in neutron capture therapy. *Physics in Medicine and Biology* 10, 491-503 (1965).
- 8) Hatanaka, H., Sano, K.: A revised boron neutron capture therapy for malignant brain tumors. In: *Present Limits of Neurosurgery*. Fusek, I., Kunc, A. (eds), pp. 83-85. Prague: Avicenum, Czechoslovak Medical Press 1972.
- 9) Hatanaka, H., Sweet, W.H.: Slow-neutron capture therapy for malignant tumors. Its history and recent development. In: *Biomedical Dosimetry*. pp. 147-178. Vienna: International Atomic Energy Agency 1975.
- 10) Hatanaka, H. et al.: Boron Neutron Capture Therapy vs. photon beam for malignant brain tumors - 12 years experience. In: Brock ed., *Modern Neurosurgery*. Heidelberg, Springer. pp. 122-135 (1982).
- 11) Hayakawa, Y., Harasawa, S., Nakamoto, A., Amano, K., Hatanaka, H., Egawa, J.: Simultaneous monitoring system of thermal neutron flux for Boron Neutron Capture Therapy. *Radiation Research* 75, 243-251 (1978).
- 12) Jellinger, K., Kothbauer, P., Volc, D., Vollmer, R., Weiss, R.: Combination chemotherapy (COMP protocol) and radiotherapy of anaplastic supratentorial gliomas. *Acta Neurochirurgica* 51, 1-13 (1979).
- 13) Kitao, K.: A method for calculating the absorbed dose near interface from  $^{10}\text{B}$  ( $n, \alpha$ )  $^7\text{Li}$  Reaction. *Radiation Research* 61, 304-315 (1975).
- 14) Matsuoka, O., Hatanaka, H., Miyamoto, M.: Neutron capture whole body autoradiography of  $^{10}\text{B}$  compounds. *Acta Pharmacologica et Toxicologica* 41, (Suppl. 1), 56-57 (1977).
- 15) Schoene, W.C., Murray, B.W., Rumbaugh, C.L., Shalev, M., Kleinman, G., Zamenhof, R.G., Wellum, G.R., Murphy, J.C., Brownell, G.L.: Morphological assessment of Boron Neutron Capture Therapy (BNCT) effectiveness on experimental brain tumors. 56th Annual Meeting of the American Association of Neuropathologists. June 13-15, 1980. *J. Neuropathology Exp. Neurol.*

39, 388-389 (1980).

- 16) Soloway, A.H.: Boron compounds in cancer therapy. In: Progress in Boron Chemistry, pp. 203-234. New York: Pergamon Press 1964.
- 17) Soloway, A.H., Hatanaka, H., Davis, M.A.: Penetration of brain and brain tumor. VII. Tumor-binding sulfhydryl boron compounds. J. Med. Chemistry 10, 714-717 (1967).
- 18) Sweet, W.H., Javid, M.: The possible use of neutron-capturing isotopes such as Boron-10 in the treatment of neoplasms. I. Intracranial tumor. J. Neurosurg. 9, 200-209 (1952).

## AUTHOR INDEX

Abe, M., 155  
 Aizawa, O., 44  
 Alam, F., 207, 229, 365  
 Allen, B.J., 14, 341  
 Amano, K., 155, 159  
 An, S., 57  
 Andrews, C., 365  
 Aoki, K., 99  
 Ashtari, M., 88, 304  
  
 Barth, R.F., 207, 229, 365  
 Böhmel, T., 331  
 Bond, V.P., 1  
 Borg, D.C., 237  
 Brown, J.P., 379  
 Brownell, G.L., 88, 164, 304  
 Brugger, R.M., 26  
 Buraggi, G., 174  
  
 Callegaro, L., 174  
 Carey, W.E., 207, 229, 365  
 Carlsson, J., 140  
 Carrasquillo, J.A., 379  
 Crawford, J.F., 35  
  
 Dallacker, F., 331  
 Drescher, K., 128  
  
 Elmore, J.J., Jr., 237  
 Epenetos, A.A., 184  
  
 Fairchild, R.G., 1, 106, 113, 245,  
     260, 266  
 Feinendegen, L.E., 114, 331  
 Ferrone, S., 174  
 Forrest, M., 88  
  
 Gabel, D., 106, 128, 140, 225, 237,  
     266, 276  
 Giacomini, P., 174  
 Glass, J., 255  
 Goldenberg, D.M., 215  
 Goodman, G., 379  
 Greenberg, D., 106  
  
 Hadd, H.E., 281  
 Hall, I.H., 245  
 Harasawa, S., 77  
 Hatanaka, H., 77, 155, 384  
  
 Hawthorne, M.F., 215  
 Hayakawa, Y., 77  
 Hechter, O., 197  
 Hellström, I., 193, 379  
 Hellström, K.E., 193, 379  
 Hillman, M., 266  
 Hocke, I., 225  
 Holman, B., 365  
  
 Ichihashi, M., 355  
 Inada, T., 77  
  
 Johnson, C.W., 229, 365  
  
 Kahl, S.B., 294  
 Kanda, K., 44, 99, 120  
 Kao, M.-S., 323  
 Kawecka, B., 114  
 Khachatrian, L., 323  
 Kirsch, J.E., 164, 304, 323  
 Kiszenick, W., 106  
 Kitamura, K., 155  
 Knot, W.H., 229  
 Kobayashi, T., 44, 99, 120  
 Kohwi, Y., 193  
  
 Larson, S.M., 379  
 Larsson, B., 34, 35, 128, 140  
 Laster, B.H., 106, 260  
 Lee, V.K., 193  
  
 Marx, J., 331  
 McGregor, B.J., 14  
 McPhail, A.T., 245  
 Micca, P.L., 106, 237, 245  
 Mishima, Y., 355  
 Mizusawa, E., 215  
 Mohammed, J., 365  
 Morsttin, K., 114  
 Mückter, H., 331  
 Mühlensiepen, H., 331  
 Müllners, W., 331  
 Murphy, J.C., 304  
  
 Nakagawa, T., 355  
 Nakanishi, T., 355  
 Natali, P.G., 174  
 Noonan, D., 315

Oká, Y., 44, 57

Forschen, W., 331

Prusoff, W.H., 260

Riesenbergs, H., 225

Rosa, U., 174

Rosander, K., 134

Rowe, W.R., 128

Ruiter, D., 174

Rumbaugh, C., 304

Russell, J.L., Jr., 315

Sasuga, N., 67

Schinazi, R.F., 260

Schoene, W.C., 304

Schwartz, I.L., 197

Serino, A.J., 215

Sharkey, R.M., 215

Slatkin, D.N., 134

Soloway, A.H., 207, 229, 365

Spielvogel, B.F., 245

Steplewski, Z., 365

Stoner, R.D., 134

Suzuki, T., 355

Sweet, F., 323

Sweet, W.H., 376

Talnagi, J.W., Jr., 365

Tateishi, J., 155

Tsuji, M., 355

Ueda, M., 355

Wakabayashi, H., 44, 67

Walczyna, R., 225

Watts, K., 266

Wellman, F., 225, 276

Wellum, G.R., 13, 304

Wessels, B., 323

Williams, A., 323

Yanagi, H., 67

Yosii, K., 67

Zamenhof, R.G., 13

## PARTICIPANTS

Dr. Rushdy Abadir  
Radiation Oncology  
U. of Missouri, Hospital and Clinics  
Columbia, MO 65212

Dr. Rolf F. Barth  
Dept. of Pathology  
Ohio State U.  
Columbus, OH 43210-1239

Dr. Masamitsu Abe  
Saga Medical School,  
Kyushu U. and Teikyo U.  
Tokyo 173, Japan

James J. Benedict  
Proctor & Gamble Co.  
Cincinnati, OH 45247

Dr. Christopher Adams  
Dept. of Neurosurgery  
Radcliffe Infirmary  
Oxford, United Kingdom

Dr. Rodney E. Bigler  
Memorial Sloan-Kettering Cancer Center  
New York, NY 10021

S.J. Adelstein  
Nuclear Medicine Dept.  
Harvard Medical School  
Boston, MA 02115

James W. Blue  
NASA/CCF Neutron Therapy Facility  
Lewis Research Center  
Cleveland, OH 44135

Dr. Fazlul Alam  
College of Pharmacy  
Ohio State U.  
Columbus, OH 43210-1291

Dr. Donald C. Borg  
Chairman, Medical Dept.  
Brookhaven National Lab.  
Upton, NY 11973

Dr. Barry J. Allen  
Australian Atomic Energy Commission  
Research Establishment  
Lucas Heights Research Lab.  
Sutherland NSW 2232, Australia

Dr. A. Bertrand Brill  
Medical Dept.  
Brookhaven National Lab.  
Upton, NY 11973

Dr. Kazuyoshi Amano  
Dept. of Neurosurgery  
Teikyo U. School of Medicine  
Tokyo 173, Japan

Dr. Robert J. Brotherton  
Manager, Chemical Research  
U.S. Borax Corp.  
Anaheim, CA 92801

Dr. Manzar Ashtari  
Dept. of Radiation Medicine  
Albert Chandler Medical Center  
U. of Kentucky  
Lexington, KY 40536-0084

Dr. Gordon L. Brownell  
Director, Physics Research Lab.  
Massachusetts General Hospital  
Boston, MA 02114

Dr. Frank M. Bacon  
Sandia Labs.  
Albuquerque, NM 87185

Dr. Robert M. Brugger  
Research Reactor Facility  
U. of Missouri  
Columbia, MO 65211

Dr. Nathaniel Barr  
U.S. Dept. of Energy  
Washington, DC 20545

Dr. Walter E. Carey  
Nuclear Engineering Program  
Ohio State U.  
Columbus, OH 43085

J. Chu  
Dept. of Radiation Therapy  
U. of Pennsylvania  
Philadelphia, PA 19184

Dr. G. Constantine  
Materials Physics Division  
HERE Harwell  
Oxfordshire, England

Dr. J.F. Crawford  
S.I.N.  
Villigen, Switzerland CH-5234

Ms. Margaret Dienes  
Technical Information Division  
Brookhaven National Lab.  
Upton, NY 11973

Dr. William P. Duncan  
Midwest Research Institute  
Kansas City, MO 64110

Dr. Keith Durrant  
Churchill Hospital  
John Radcliffe Hospital  
Oxford, United Kingdom

Dr. John J. Elmore, Jr.  
Medical Dept.  
Brookhaven National Lab.  
Upton, NY 11973

Dr. Agamemnon A. Epenetos  
Dept. of Medical Physics  
Royal Postgraduate Medical School  
Hammersmith Hospital  
London W12 OHS, U.K.

Dr. Ralph G. Fairchild  
Medical Dept.  
Brookhaven National Lab.  
Upton, NY 11973

Irwin Fand  
SUNY at Stony Brook  
Stony Brook, NY 11545

Dr. Ludwig F. Feinendegen  
Director, Inst. of Medicine  
Kernforschungsanlage Jülich GmbH  
D-5170 Jülich, West Germany

Dr. Soldano Ferrone  
Dept. of Pathology  
College of Physicians and Surgeons  
Columbia U.  
New York, NY 10032

Dr. Peter Fessenden  
Dept. of Radiology  
Stanford U. Medical Center  
Stanford, CA 94305

Dr. Detlef Gabel  
Medical Dept.  
Brookhaven National Lab.  
Upton, NY 11973  
(Chem. Dept., U. of Bremen  
D-2800 Bremen 33, West Germany)

Mrs. Lillian Gille  
Gustaf Werner Institute  
University of Uppsala  
Uppsala, Sweden S-75121

Dr. John D. Glass, Jr.  
Medical Dept.  
Brookhaven National Lab.  
Upton, NY 11973

D.M. Goldenberg  
Center for Molecular Medicine  
and Immunology  
Newark, NJ 07103

Dr. Harry E. Hadd  
Northwest Center for Medical Education  
Indiana U.  
Gary, IN 46408

Dr. Hiroshi Hatanaka  
Dept. of Neurosurgery  
Teikyo U. School of Medicine  
Tokyo 173, Japan

Dr. M. Frederick Hawthorne  
Dept. of Chemistry  
U. of California, Los Angeles  
Los Angeles, CA 90024

Dr. Yoshinori Hayakawa  
Inst. for Basic Medical Sciences  
U. of Tsukuba  
Ibaraki 305, Japan

Dr. Oscar M. Hechter  
Dept. of Physiology  
Northwestern U. Medical School  
Chicago, IL 60611

Dr. Ingegerd Hellström  
Fred Hutchinson Cancer Research Center  
Seattle, WA 98104

Dr. Karl Erik Hellström  
Fred Hutchinson Cancer Research Center  
Seattle, WA 98104

Dr. Manny Hillman  
Dept. of Energy and Environment  
Brookhaven National Lab.  
Upton, NY 11973

Dr. Walter L. Hughes  
Brookhaven National Lab.  
Upton, NY 11973

Ms. Linda Jansen  
Callery Chemical Company  
Callery, PA 16059

Dr. Les Jones  
Monsanto Research Corp.  
Dayton, Ohio 45407

Dr. Stephen B. Kahl  
Dept. of Pharmacological Chemistry  
U. of California, San Francisco  
San Francisco, CA 94143

Dr. Keiji Kanda  
Research Reactor Institute  
Kyoto U.  
Osaka 590-04, Japan

Dr. Amin I. Kassis  
Harvard Medical School  
Boston, MA 02115

Dr. John E. Kirsch  
Physics Research Lab.  
Massachusetts General Hospital  
Boston, MA 02114

Dr. Tooru Kobayashi  
Research Reactor Institute  
Kyoto U.  
Osaka 590-04, Japan

Dr. L. Koester  
FRM Reaktor Station Garching  
Technische Universität  
D-8046 München, West Germany

Dr. David L. Krohn  
NYU Medical Center  
New York, NY 10016

Dr. Börje Larsson  
Gustaf Werner Institute  
U. of Uppsala  
S-751 21 Uppsala, Sweden

Ms. Brenda H. Laster  
Medical Dept.  
Brookhaven National Lab.  
Upton, NY 11973

Dr. Fang-Jen Lin  
Director of Radiation Oncology  
Chang Gung Memorial Hospital  
Taipei, Taiwan

Dr. John Little  
Callery Chemical Company  
Callery, PA 16024

F.J. Mahoney  
National Cancer Institute  
Rockville, MD 20854

Samuel McCalmont  
Callery Chemical Co.  
Callery, PA 16024

Mrs. Janette R. Messer  
Massachusetts General Hospital  
Boston, MA 02114

Ms. Peggy L. Micca  
Medical Dept.  
Brookhaven National Lab.  
Upton, NY 11973

Dr. Yutaka Mishima  
Dept. of Dermatology  
Kobe U. School of Medicine  
Kobe 650, Japan

Ms. Denise J. Noonan  
Georgia Institute of Technology  
Atlanta, GA 30332

Dr. Robin E. Offord  
U. de Genève  
Dept. de Biochimie Médical  
Centre Médical Universitaire  
1211 Geneve 4, Switzerland

Dr. Yoshiaki Oka  
Nuclear Engineering Research Lab.  
U. of Tokyo  
Tokai-Mura, Ibaraki 319-11 Japan

Dr. Donald Picker  
Johnson Mitthey  
West Chester, PA 19380

Dr. Walter Porschen  
Inst. of Medicine  
Kernforschungsanlage Jülich GmbH  
D-5170 Jülich, West Germany

Dr. Chris H. Poynton  
M.D. Anderson Hospital  
Houston, Texas 77030

Richard Radomski  
Callery Chemical Co.  
Callery, PA 16024

Dr. Horst H. Riesenbergs  
Medical Dept.  
Brookhaven National Lab.  
Upton, NY 11973

Ms. Kerstin Rosander  
Gustaf Werner Inst.  
Uppsala U.  
S-75121 Uppsala, Sweden

Dr. John L. Russell, Jr.  
School of Nuclear Engineering  
Georgia Inst. of Technology  
Atlanta, GA 30332

Dr. Raymond F. Schinazi  
Dept. of Pediatrics  
Emory U. School of Medicine  
Atlanta, GA 30303

Dr. Irving L. Schwartz  
Mount Sinai Medical Center  
New York, NY 10029

Carl Seidel  
New England Nuclear  
North Billerica, MA 01862

Anthony J. Serino  
Dept. of Chemistry & Biochemistry  
UCLA  
Los Angeles, CA 90024

Siamak Shababi  
Medical Physics  
Tufts New England Medical Center  
Boston, MA 02111

Robert M. Sharkey  
Center for Molecular Medicine and  
Immunology  
UMDNJ  
Newark, NJ 01703

Dr. A.B. Shenvi  
Dupont Experimental Station 328/107  
Wilmington, DE 19898

Dr. Daniel N. Slatkin  
Medical Dept.  
Brookhaven National Lab.  
Upton, NY 11973

Larry G. Sneddon  
Dept. of Chemistry  
U. of Pennsylvania  
Philadelphia, PA 19104

Dr. Albert H. Soloway  
Dean, College of Pharmacy  
Ohio State U.  
Columbus, OH 43210-1291

Dr. Bernard F. Spielvogel  
Chief, Inorganic & Analytical Branch  
Chemical & Biological Sciences Division  
Division of the Army  
Research Triangle Park, NC 27709

Dr. Ralph J. Starks  
Eagle-Picher Company  
Miami, OK 74355

Dr. Fredrick Sweet  
Dept. of Obstetrics and Gynecology  
Washington U. School of Medicine  
St. Louis, MO 63110

Dr. William H. Sweet  
Ambulatory Care Center  
Massachusetts General Hospital  
Boston, MA 02114

Dr. Akira Takeuchi  
Dept. of Veterinary Surgery  
Faculty of Agriculture, U. of Tokyo  
Tokyo 113, Japan

Dr. Marcia Urie  
Dept. of Radiation Biophysics  
Massachusetts General Hospital  
Boston, MA 02114

Dr. Hiroaki Wakabayashi  
Nuclear Engineering Research Lab.  
U. of Tokyo  
Tokai-Mura, Ibaraki 319-11, Japan

Bernard Wehring  
U. of Illinois  
Urbana, IL 61801

Folkert Wellmann  
Chemistry Dept.  
U. of Bremen  
D-2800 Bremen 33, West Germany

Lucian Wielopolski  
Brookhaven National Lab.  
Upton, NY 11973

Dr. Henry Wolfe  
U.S. Dept. of Energy  
Washington, DC 20545

Dr. Robert G. Zamenhof  
Medical Physics Div.  
Tufts-New England Medical Center  
Boston, MA 02111